frontiers | Research Topics

Targeting redox regulation and autophagy systems for cancer therapy

Edited by
Junmin Zhang, Abdelhabib Semlali, Paola Maycotte and Luciano Saso

Published in
Frontiers in Oncology

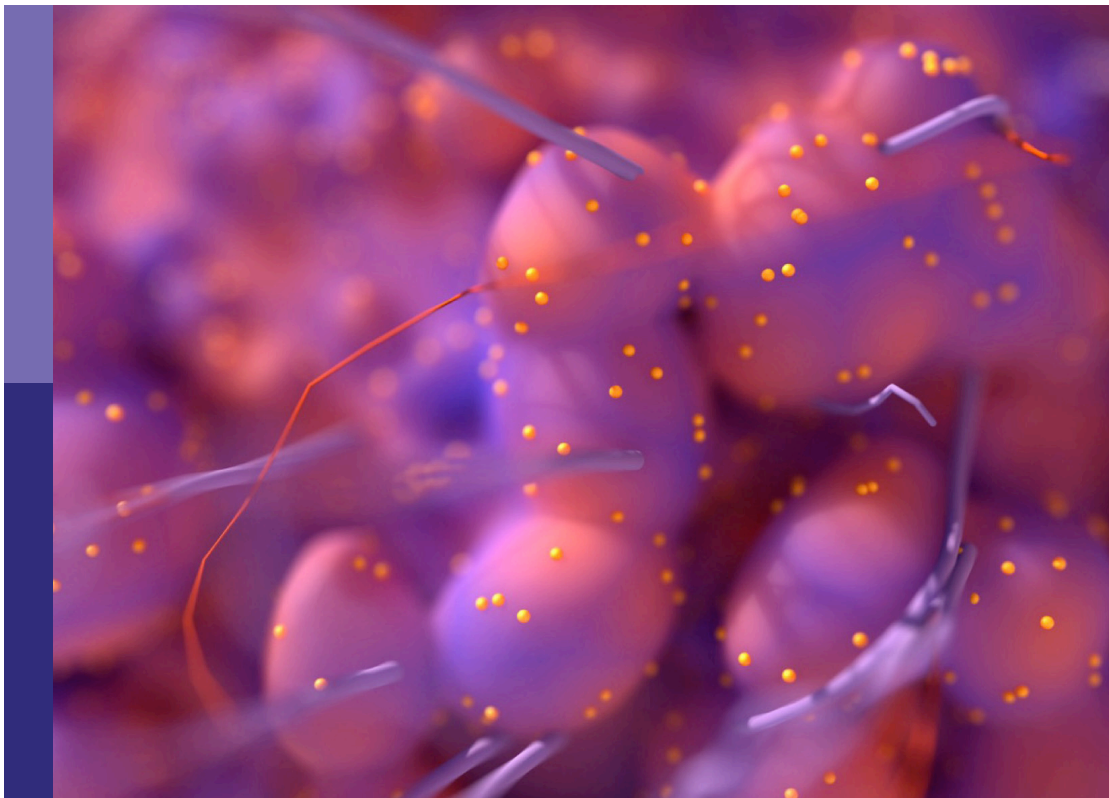

ISSN 1664-8714
ISBN 978-2-83251-668-3
DOI 10.3389/978-2-83251-668-3

About Frontiers

Frontiers is more than just an open access publisher of scholarly articles: it is a pioneering approach to the world of academia, radically improving the way scholarly research is managed. The grand vision of Frontiers is a world where all people have an equal opportunity to seek, share and generate knowledge. Frontiers provides immediate and permanent online open access to all its publications, but this alone is not enough to realize our grand goals.

Frontiers journal series

The Frontiers journal series is a multi-tier and interdisciplinary set of open-access, online journals, promising a paradigm shift from the current review, selection and dissemination processes in academic publishing. All Frontiers journals are driven by researchers for researchers; therefore, they constitute a service to the scholarly community. At the same time, the *Frontiers journal series* operates on a revolutionary invention, the tiered publishing system, initially addressing specific communities of scholars, and gradually climbing up to broader public understanding, thus serving the interests of the lay society, too.

Dedication to quality

Each Frontiers article is a landmark of the highest quality, thanks to genuinely collaborative interactions between authors and review editors, who include some of the world's best academicians. Research must be certified by peers before entering a stream of knowledge that may eventually reach the public - and shape society; therefore, Frontiers only applies the most rigorous and unbiased reviews. Frontiers revolutionizes research publishing by freely delivering the most outstanding research, evaluated with no bias from both the academic and social point of view. By applying the most advanced information technologies, Frontiers is catapulting scholarly publishing into a new generation.

What are Frontiers Research Topics?

Frontiers Research Topics are very popular trademarks of the *Frontiers journals series*: they are collections of at least ten articles, all centered on a particular subject. With their unique mix of varied contributions from Original Research to Review Articles, Frontiers Research Topics unify the most influential researchers, the latest key findings and historical advances in a hot research area.

Find out more on how to host your own Frontiers Research Topic or contribute to one as an author by contacting the Frontiers editorial office: frontiersin.org/about/contact

Targeting redox regulation and autophagy systems for cancer therapy

Topic editors

Junmin Zhang — Lanzhou University, China

Abdelhabib Semlali — Laval University, Canada

Paola Maycotte — Centro de Investigacion Biomedica de Oriente, Instituto Mexicano del Seguro Social, Mexico

Luciano Saso — Sapienza University of Rome, Italy

Citation

Zhang, J., Semlali, A., Maycotte, P., Saso, L., eds. (2023). *Targeting redox regulation and autophagy systems for cancer therapy*. Lausanne: Frontiers Media SA.

doi: 10.3389/978-2-83251-668-3

Table of contents

frontiers | Frontiers in Oncology

TYPE Editorial
PUBLISHED 31 January 2023
DOI 10.3389/fonc.2023.1146670

OPEN ACCESS

EDITED AND REVIEWED BY
Massimo Broggini,
Mario Negri Institute for Pharmacological Research (IRCCS), Italy

*CORRESPONDENCE
Junmin Zhang
zhangjunmin@lzu.edu.cn
Abdelhabib Semlali
abdelhabib.semlali@greb.ulaval.ca
Paola Maycotte
paola.maycotte@imss.gob.mx
Luciano Saso
luciano.saso@uniroma1.it

SPECIALTY SECTION
This article was submitted to Cancer Molecular Targets and Therapeutics, a section of the journal Frontiers in Oncology

RECEIVED 17 January 2023
ACCEPTED 20 January 2023
PUBLISHED 31 January 2023

CITATION
Zhang J, Semlali A, Maycotte P and Saso L (2023) Editorial: Targeting redox regulation and autophagy systems for cancer therapy. *Front. Oncol.* 13:1146670. doi: 10.3389/fonc.2023.1146670

Editorial: Targeting redox regulation and autophagy systems for cancer therapy

Junmin Zhang[1]*, Abdelhabib Semlali[2]*, Paola Maycotte[3]* and Luciano Saso[4]*

[1]School of Pharmacy and State Key Laboratory of Applied Organic Chemistry, Lanzhou University, Lanzhou, China, [2]Groupe de Recherche en Écologie Buccale, Faculté de Médecine Dentaire, Université Laval, Quebec, QC, Canada, [3]Centro de Investigación Biomédica de Oriente, Instituto Mexicano del Seguro Social, Puebla, Mexico, [4]Department of Physiology and Pharmacology "Vittorio Erspamer", Sapienza University of Rome, Rome, Italy

KEYWORDS

redox regulation, reactive oxygen species, oxidative stress, redox-active compounds, autophagy, apoptosis, ferroptosis, cancer therapy

Editorial on the Research Topic
Targeting redox regulation and autophagy systems for cancer therapy

Autophagy and increased ROS production are important contributors to cancer metabolic remodeling (1, 2), and an interplay between both processes has been described with important consequences on cancer cell survival and death (3). Both ROS production and autophagy have a context and stage-dependent role on tumorigenesis and cancer progression. For instance, autophagy is a tumor suppressor pathway but can promote cancer cell survival under diverse stress conditions (4). Similarly, increased ROS have been implicated in tumorigenesis caused by diverse infectious or environmental agents as well as in the maintenance of cancer cell signaling pathways (5, 6), but have been suggested to limit metastasis formation (7, 8). Thus, a detailed study of the role of ROS and autophagy is needed, to understand their role in cancer initiation and progression and to design effective therapies targeting these mechanisms.

This issue includes manuscripts covering diverse aspects of ROS and autophagy in cancer progression and therapy. The review by Hasan et al., describes the close interplay between ROS and autophagy in cancer cells and the complexity involved in designing anticancer therapies targeting these processes. In a different review, Roy et al. describe the diverse roles of autophagy in response to cancer radiotherapy (RT), outlining the role of autophagy in deciding the cellular fate upon exposure to radiation, in cancer stem cell (CSC) maintenance and the radiation-induced bystander effect as well as its contribution to cell survival or death and its interplay with radiation-induced ROS. The authors emphasize the role of autophagy inhibitors and inducers in radiosensitization and, they refer to studies where autophagy markers were related to a poor therapeutic outcome in patients treated with RT or chemo-radiotherapy (CRT). The authors also mention clinical trials using autophagy inhibitors as adjuvant to CRT in glioblastoma with promising results as well as another one in pancreatic cancer patients where no significant improvement in survival was observed. They conclude that an encouraging clinical response using autophagy regulators is needed to incorporate them as adjuvant to current RT or CRT regimens.

Two interesting manuscripts describe gene signatures related to autophagy modulation. The first one, by Wu et al. describes a gene signature with prognostic significance consisting of genes participating in autophagy in lung adenocarcinoma (LUAD), with functions in immune and tumor-related pathways. The second manuscript by Liu et al., describes a gene signature consisting of three autophagy-related long noncoding RNAs (lncRNAs) in cholangiocarcinoma (CCA), with prognostic potential, and whose lncRNAs were found to be increased in CCA tissue when compared to normal tissue. Importantly, in both papers, the authors found differences in the enrichment scores for immune cells between low and high-risk groups, as well as different expression levels of checkpoint inhibitors in Wu et al., suggesting an important role for the expression of genes participating in autophagy, or regulating autophagy in the definition of the immune landscape in LUAD and CCA. Another interesting paper using data analysis is the one by Zhu et al. In this manuscript, the authors analyzed BNIP3, an apoptosis regulator and mitophagy receptor in scRNA-seq datasets, identifying cancer cell subpopulations characterized by high BNIP3 levels in most epithelial malignancies characterized by NRF2 signaling, HIF1A, wound response, metabolic reprogramming, high ROS-related pathways, oxidative phosphorylation and MYC targets. Also, high BNIP3 mRNA was a worse prognostic factor for cervical squamous cell carcinoma, endocervical adenocarcinoma, cholangiocarcinoma, sarcoma and breast cancer and BNIP3 was overexpressed in liver cancer organoids. This study emphasizes the role of the BNIP3-high cellular population in defining the prognosis of certain cancer types. Also relating to autophagy and cancer therapy, the manuscript by Karim et al., describes a phase I clinical trial to determine the maximum tolerated dose (MTD) of chloroquine (CQ) or hydroxychloroquine (HCQ), two of the most widely used autophagy inhibitors, in combination with carboplatin and gemcitabine in heavily pre-treated patients with advanced solid tumors. The authors found a MTD of HCQ of 100 mg when given in combination with carboplatin and gemcitabine, a lower than previously reported MTDs, probably due to the myelosuppressive nature of gemcitabine. The overall response rate was 71% and limiting factors were neutropenia and thrombocytopenia. The authors also observed that patients receiving subsequent immunotherapy after participating in this clinical trial had excellent clinical outcomes, suggesting a promising response, and warranting progression to a phase II clinical trial.

Regarding potential therapeutic interventions for different cancer types, Zhu et al. describe the use of elaiophylin, a macrodiolide antibiotic isolated from *Streptomyces melanosporus* which can function as a late-stage autophagy inhibitor in uveal melanoma cell lines. The authors found that elaiophylin induced cell death by inducing oxidative stress, mitochondrial dysfunction, regulating SIRT1, FoxO3a, and decreasing mitophagy. Similar results were found in a xenograft model, implying the use of elaiophylin for the treatment of this rare, but deadly cancer. Another study using a natural compound is the one by Alsamri et al., where the authors use carnosol, a phenolic compound against breast cancer cell lines. The authors found that carnosol triggered a ROS-dependent endoplasmic reticulum (ER)-stress response, p38-dependent autophagy, activation of ATF6 and IRE-1a and mTOR degradation in the proteasome. This study adds up carnosol to natural compounds known to trigger a ROS-dependent ER-stress mediated cell death emphasizing its potential use for breast cancer therapy. Regarding differentiation therapies, the manuscript by Benjamin et al. describes the use of valproic acid (VPA), an autophagy inducer, in all-*trans*-retinoic acid (ATRA) resistant acute promyelocytic leukemia (APL), a type of acute myeloid leukemia (AML). The authors describe a key role for autophagy in the differentiation of APL cells induced by ATRA and VPA combination treatment and implying a potential use for autophagy inducers in this type of therapy. Another therapeutic intervention is presented in the manuscript by Semlali et al., which describes the use of rapamycin for oral cancer treatment. Rapamycin induced cell death in oral cancer cells when compared to controls involving total ROS and mitochondrial ROS production, DNA damage, MAPK, NFkB and Wnt/b-catenin pathway inhibition. Interestingly, antioxidants in combination with an autophagy inhibitor decreased cancer cell death suggesting both mechanisms participate in cell death induction by rapamycin. Another study by Park et al. describes an association between nuclear factor erythroid 2-like 2 (NRF2), a master transcriptional factor for antioxidant response genes and the CSC marker CD133 in colon cancer stem cells. The authors found that CD133 controls NRF2 expression levels by regulating Akt and GSK-3β phosphorylation. These results support an important role for ROS detoxifying mechanisms in supporting the aggressive phenotype of CSCs. Finally, the study by Ling et al., describes the use of a superoxide dismutase 1 (SOD1) inhibitor (LCS-1) for glioma treatment. The authors found increased SOD1 levels in grade III and IV gliomas as well as SOD1/2 expression in glioma cell lines, where LCS-1 induced ROS-dependent, p53- and caspase-independent cell death with PARP and BRCA1/2 degradation. LCS-1 also decreased tumor growth in a mouse xenograft model highlighting the potential use of LCS-1 or ROS-inducing agents for the treatment of this deadly disease.

Altogether, this collection of manuscripts covers aspects of the ROS-autophagy-cancer interplay, discussing novel therapeutic targets for different cancer types. We hope you enjoy them.

Author contributions

All authors listed have made a substantial, direct, and intellectual contribution to the work and approved it for publication.

Conflict of interest

The authors declare that the research was conducted in the absence of any commercial or financial relationships that could be construed as a potential conflict of interest.

Publisher's note

References

1. Ferro F, Servais S, Besson P, Roger S, Dumas JF, Brisson L. Autophagy and mitophagy in cancer metabolic remodelling. *Semin Cell Dev Biol* (2020) 98:129–38. doi: 10.1016/j.semcdb.2019.05.029

2. DeBerardinis RJ, Chandel NS. Fundamentals of cancer metabolism. *Sci Adv* (2016) 2 (5):e1600200. doi: 10.1126/sciadv.1600200

3. Redza-Dutordoir M, Averill-Bates DA. Interactions between reactive oxygen species and autophagy: Special issue: Death mechanisms in cellular homeostasis. *Biochim Biophys Acta Mol Cell Res* (2021) 1868(8):119041. doi: 10.1016/j.bbamcr.2021.119041

4. Liu J, Debnath J. Chapter one - the evolving, multifaceted roles of autophagy in cancer. In: Tew KD, Fisher PB, editors. *Advances in cancer research* UK: Academic Press (2016) 130:1–53.

5. Sarmiento-Salinas FL, Perez-Gonzalez A, Acosta-Casique A, Ix-Ballote A, Diaz A, Trevino S, et al. Reactive oxygen species: Role in carcinogenesis, cancer cell signaling and tumor progression. *Life Sci* (2021) 284:119942. doi: 10.1016/j.lfs.2021.119942

6. Zhang J, Duan D, Song ZL, Liu T, Hou Y, Fang J. Small molecules regulating reactive oxygen species homeostasis for cancer therapy. *Medicinal Res Rev* (2021) 41(1):342–94. doi: 10.1002/med.21734

7. Le Gal K, Ibrahim MX, Wiel C, Sayin VI, Akula MK, Karlsson C, et al. Antioxidants can increase melanoma metastasis in mice. *Sci Trans Med* (2015) 7(308):308re8. doi: 10.1126/scitranslmed.aad3740

8. Piskounova E, Agathocleous M, Murphy MM, Hu Z, Huddlestun SE, Zhao Z, et al. Oxidative stress inhibits distant metastasis by human melanoma cells. *Nature.* (2015) 527 (7577):186–91. doi: 10.1038/nature15726

frontiers in Oncology

ORIGINAL RESEARCH
published: 02 December 2021
doi: 10.3389/fonc.2021.780601

Identification and Validation of Three Autophagy-Related Long Noncoding RNAs as Prognostic Signature in Cholangiocarcinoma

Ya Jun Liu[1], Alphonse Houssou Hounye[2], Zheng Wang[2,3], Xiaowei Liu[1], Jun Yi[1] and Min Qi[4]**

[1] Department of Gastroenterology, Xiangya Hospital Central South University, Changsha, China, [2] School of Mathematics and Statistics, Central South University, Changsha, China, [3] Information Science and Engineering School, Hunan First Normal University, Changsha, China, [4] Department of Plastic Surgery, Xiangya Hospital Central South University, Changsha, China

OPEN ACCESS

Edited by:
Abdelhabib Semlali, Laval University, Canada

Reviewed by:
Rachid El Fatimy, Mohammed VI Polytechnic University, Morocco
Giovanni Brandi, University of Bologna, Italy

***Correspondence:**
Jun Yi
junyee1989@csu.edu.cn
Min Qi
qimin05@csu.edu.cn

Specialty section:
This article was submitted to Cancer Molecular Targets and Therapeutics, a section of the journal Frontiers in Oncology

Received: *21 September 2021*
Accepted: *10 November 2021*
Published: *02 December 2021*

Citation:
Liu YJ, Hounye AH, Wang Z, Liu X, Yi J and Qi M (2021) Identification and Validation of Three Autophagy-Related Long Noncoding RNAs as Prognostic Signature in Cholangiocarcinoma. Front. Oncol. 11:780601. doi: 10.3389/fonc.2021.780601

Cholangiocarcinoma (CCA) is featured by common occurrence and poor prognosis. Autophagy is a biological process that has been extensively involved in the progression of tumors. Long noncoding RNAs (lncRNAs) have been discovered to be critical in diagnosing and predicting various tumors. It may be valuable to elaborate autophagy-related lncRNAs (ARlncRNAs) in CCA, and indeed, there are still few studies concerning the role of ARlncRNAs in CCA. Here, a prognostic ARlncRNA signature was constructed to predict the survival outcome of CCA patients. Through identification, three differentially expressed ARlncRNAs (DEARlncRNAs), including CHRM3.AS2, MIR205HG, and LINC00661, were screened and were considered predictive signatures. Furthermore, the overall survival (OS) of patients with high-risk scores was significantly lower than that of patients with low scores. Interestingly, the risk score was an independent factor for the OS of patients with CCA. Moreover, receiver operating characteristic (ROC) curve analysis showed that the screened and constructed prognosis signature for 1 year (AUC = 0.884), 3 years (AUC =0.759), and 5 years (AUC = 0.788) presented a high score of accuracy in predicting OS of CCA patients. Gene set enrichment analysis (GSEA) revealed that the three DEARlncRNAs were significantly enriched in CCA-related signaling pathways, including "pathways of basal cell carcinoma", "glycerolipid metabolism", etc. Quantitative real-time PCR (qRT-PCR) showed that expressions of CHRM3.AS2, MIR205HG, and LINC00661 were higher in CCA tissues than those in normal tissues, similar to the trends detected in the CCA dataset. Furthermore, Pearson's analysis reported an intimate correlation of the risk score with immune cell infiltration, indicating a predictive value of the signature for the efficacy of immunotherapy. In addition, the screened lncRNAs were found to have the ability to modulate the expression of mRNAs by

interacting with miRNAs based on the established lncRNA-miRNA-mRNA network. In conclusion, our study develops a novel nomogram with good reliability and accuracy to predict the OS of CCA patients, providing a significant guiding value for developing tailored therapy for CCA patients.

Keywords: autophagy, long noncoding RNAs, cholangiocarcinoma, The Cancer Genome Atlas, prognostic signature, Gene Expression Omnibus

INTRODUCTION

Cholangiocarcinoma (CCA) is such a dangerous malignancy originating from biliary epithelium that carries increasing morbidity and mortality currently (1, 2). There is a great difficulty in the early diagnosis of CCA owing to the occult location of bile duct system anatomically, and hence a majority of patients may loss the opportunity of radical surgery. The major therapeutic approaches for its treatment include interventional therapy, radiotherapy, targeted therapy, etc., which, however, have a limited curative effect and can lead to poor prognosis of patients with CCA (3–5). For instance, Rizzo et al. demonstrated that adding EGFR-mAbs to gemcitabine-based first-line chemotherapy could not significantly improve the overall survival rate of patients with advanced CCA, nor the objective response rate, and even lead to hematological and cutaneous adverse drug events (6). In addition, a more recent study by Rizzo et al. revealed that the role of adjuvant systemic chemotherapy is still the object of debate and controversy in the medical community of resected biliary tract cancer (BTC) (7). Considering the absence of efficient diagnostic tools in the early stage and available therapeutics at present, patients who enter the advanced stage may have a low 5-year survival rate of <5% (8). Currently, some molecular markers have been confirmed to provide explanation for the poor prognosis and tumor progression of CCA. For instance, high EGFR expression may predict postoperative CCA recurrence independently (9), and inducible nitric oxide synthase (iNOS) is involved in the pathogenesis of CCA in an inflammation-dependent manner (5). Unfortunately, CCA is indeed a disease with strong genetic heterogeneity, and there is so far poor understanding of its molecular mechanisms, resulting in a relatively low application of the majority of the identified markers in clinical data. It in turn highlights the importance of clarifying potential molecular mechanisms and cellular signaling pathways of CCA as well as finding new biomarkers with prognostic value, so as to benefit early detection of CCA and improvement of its prognosis.

Despite an initial recognition as "transcriptional noise" due to the absence of protein-coding capacity, long noncoding RNAs (lncRNAs; >200 nucleotides in length) have now been widely accepted to be a series of RNA molecules with critical functions (10, 11). Large numbers of novel lncRNAs have been identified with the development of sequencing technologies. Based on their regulatory roles of gene expressions at transcriptional, posttranscriptional, and translational levels, lncRNAs play biological functions in many cellular activities (12, 13). It is now accepted commonly that tumor progression can be partially explained by abnormal expression or dysfunction of lncRNAs, highlighting their key roles in tumor diagnosis and prognosis prediction in the oncology field. Cheng et al. (14), for example, found that lncRNA AC125603.2 had a promoting role in the biological activities of colon cancer cells and predicted a poor prognosis of colorectal cancer. Jia et al. (15) confirmed that lncRNA AC005229.4 could be regarded as a prognostic biomarker of hepatoma. However, the mechanism of lncRNAs in tumors has not been fully clarified due to the complexity of tumor physiological mechanisms and individual differences. It remains to be improved with respect to the accuracy of lncRNAs in predicting cancer prognosis, and further systematic studies are required to identify and explain multiple lncRNAs.

Autophagy is the main metabolic pathway in cells. It can decompose damaged proteins and organelles for energy recycling, and can participate in aging and various physiological and pathological processes related to aging. Autophagy can participate in maintaining the stability of the internal environment of life, whose function depends largely on the involvement of autophagy-related signaling pathways (16, 17). Under normal conditions, autophagy provides necessary circulating metabolites for cell survival and maintains cell homeostasis. However, autophagy can be abnormally activated in human malignancies, and exert different roles in different stages of tumors (18, 19). Nowadays, the importance of autophagy-related pathways has been paid much attention to, with the aim to search for novel targets to formulate targeted therapies for tumors. For example, Hector collected clinical evidence of autophagy imbalance during CCA and found autophagy dysfunction in the initial stage of CCA development, accompanied by increased expressions of autophagy markers in established tumors and invasive phenotypes. Furthermore, autophagy regulators could promote CCA cell death and reduce its invasive ability (20). In addition, lncRNAs have been disclosed to be possibly responsible for the autophagy of tumor cells. For instance, Luan et al. (21) reported 10 autophagy-related lncRNAs (ARlncRNAs) in predicting the prognosis of glioma and in regulating glioma biology. Deng et al. (22) also reported the value of LINC01559 for reliable prognostic prediction and individualized therapy development of pancreatic cancer patients. Given the current clinical status of CCA and considering the critical roles of ARlncRNAs, it may be a valuable direction of research to explore the role of ARlncRNAs in CCA, and indeed, there is still few study related to this topic. Here, our study attempts to establish an ARlncRNA signature, with emphasis placed on the identification of potential ARlncRNAs and exploration of their clinical significance in CCA, so as to

assist the prediction of CCA patients' prognosis and facilitate future drug selection.

MATERIALS AND METHODS

Data Acquisition

Data of sequencing and survival that were specific to CCA were acquired from The Cancer Genome Atlas (TCGA) dataset (https://portal.gdc.cancer.gov/, RNAseq, I llumina). These data consisted of 36 CCA tissues and 9 adjacent normal biliary tissues, which were used as the test set. Clinical data were also extracted from this database, including age, gender and pathological stages. Simultaneously, the Human Autophagy Database (HADb) was also searched through visiting https://www.Autophagy.lu/index.html, with 232 autophagy gene datasets obtained. GSE107943 was downloaded from the Gene Expression Omnibus (GEO) database and contained data on 57 patients with CCA and their associated clinical information, which was selected as the validation cohort in this experiment.

Identification and Construction of ARlncRNAs in CCA and Normal Tissues

The transcriptome sequencing data consisted of the following two parts: (1) protein-encoding mRNA (including autophagy-related gene (ARG) expression data); and (2) lncRNA expression data. By using R language, EdgeR package was utilized to analyze the differentially expressed autophagy-related genes (DEARGs) and differentially expressed lncRNAs (DElncRNAs) (|log2 Fold Change (FC)| > 1, adjusted p-value <0.05). After screening in the former step, the "ggplot2" package was applied for generating volcano plots, with corresponding heatmaps plotted by using R heatmap package.

Coexpression Network Construction

Our study constructed the gene coexpression network (Cytoscape 3.8.2) to further investigate the differentially expressed ARlncRNAs (DEARlncRNAs). Furthermore, the correlations of DEARGs with DElncRNAs in CCA and normal tissues were disclosed by using Pearson's correlation analysis. DEARlncRNAs were confirmed from the screened DElncRNAs with Pearson's correlation coefficient (PCC) |R2| >0.3 and p < 0.001. Moreover, the coefficient of variation (CV) was also selected to get more available information in gene coexpression network analysis. The formula of CV can be described as follows: CV = σ/μ (σ and μ standard deviation, and mean of the subject of interest, respectively).

Construction and Validation of Prognostic DEARlncRNA Signatures

Firstly, the ARlncRNA expression matrix was integrated with survival data. Then, the "survival" R package was used to identify ARlncRNAs showing intimate association with the overall survival (OS), with $p < 0.01$ indicating a statistically significant difference. Subsequently, the significant OS-related ARlncRNAs were further screened based on LASSO regression analysis by the "glmnet" package to avoid excessive overfitting of the signature model. The optimal value of the penalization coefficient lambda (λ) was obtained through cross-validation with 1,000 iterations to prevent overfitting. Eligible lncRNAs with the greatest suitability for building the signature were screened out finally based on the generated minimum λ. Next, the ARlncRNAs obtained from LASSO regression analysis were involved in subsequent multivariate Cox regression analysis. The signatures were constructed through different combination of lncRNAs, accompanied by the calculation of the Akaike information criterion (AIC) value for each independent lncRNA. Afterwards, the optimal prognosis signature was generated according to the minimum AIC value which had the goodness of fit. Risk scores were calculated based on $RiskScore = \sum_{i=1}^{n} \beta_i gene_i(expression)$, where, β_i is the coefficient of each gene expression, and gene (expression) represents DEARlncRNA expression. Two subgroups were divided based on the median value of the calculated risk scores, those who had high scores were classified into the high-risk group, and those with low scores into the low-risk group. The survival analysis for the different groups was realized by using the Kaplan-Meier (K-M) survival curve analysis and log-rank test by using the "survminer" R package. In addition, the specificity and sensitivity of the constructed prognostic signature were further calculated based on the area under the dynamic time-dependent receiver operating characteristic (ROC) curve (AUC) and the concordance index (C-index).

Analysis of Risk Scores and Clinical Characteristics of CCA Patients

Patients' clinical characteristics from TCGA were integrated with the risk score file by using "ggplot2" package to determine the presence of significant differences in risk scores. Univariate and multivariate Cox regression analyses based on clinical characteristics were then made to clarify whether the DEARlncRNA could predict patient prognosis independently. Subsequently, K-M analysis was used to identify the existence of significant differences in OS between groups when both groups shared common clinical characteristics. Gene set enrichment analysis (GSEA) could identify the significant enrichment of target gene set in some functional pathways. In this study, functional annotation was realized on the basis of GO and KEGG enrichment analyses by using the "clusterProfiler" package with NES >1 and FDR <0.05 ($p < 0.01$) to benefit subsequent pathway analysis of target mRNAs. The principal component analysis (PCA) was utilized for evaluating samples and expression patterns between high- and low-risk groups. In order to further investigate the discrimination among the prognostic values, the signature was then involved in assessing the relationship of the expression patterns with OS in tumor and normal tissues.

Nomogram Based on the Signature of DEARlncRNAs for Prognostic Prediction in CCA Patients

For a quantitative prediction of the survival probability (1, 3, and 5 years) of CCA patients, a prognosis nomogram was established

using the ARlncRNAs identified in our study and the clinical factors based on risk scores and other clinical characteristics by using the "survival" and "rms" packages of R language. The consistency of the prediction and actual outcomes was assessed based on C-index and displayed by calibration curves. Finally, the AUC values were evaluated to be associated with the depiction of the ROC curves of the nomogram. All the analyses were conducted in the test and validation cohorts.

Regulatory Network Construction

DIANA Tools Online Suite was used to further identify the miRNAs related to lncRNAs, with a threshold preset at 0.9. Moreover, for a better understanding of the interaction between lncRNAs and miRNAs, this regulatory network was constructed with Cytoscape (version 3.8.2).

Predictive Efficacy of Immunotherapy With the Established Signature

By using "CIBERSORT," our study measured the infiltration expressions of different immune cells (n = 22) in CCA. In addition, the correlation between risk score and targeted therapeutic molecules was assessed for further clarification of the clinical value of the signature we constructed.

Clinical CCA Sample Collection

The clinical samples used for experimental validation were CCA surgery-treated patients in Xiangya Hospital of Central South University from July 2020 to July 2021. The CCA samples and paired adjacent samples were collected intraoperatively and frozen immediately in liquid nitrogen for subsequent storage at −80°C. None of the patients received preoperative anticancer treatment. Written consent from each patient was provided before the surgery, with approval obtained as well by the Ethics Committee of our hospital.

Quantitative Real-Time PCR

Collected tissues were subjected to the extraction of total RNA using Total RNA Kit II (Omega BioTek, Norcross, GA, USA). The quantity and quality of RNA were assessed by ultraviolet absorption spectrometry. Based on the manufacturer's instructions, cDNA was synthesized from total RNA (1 μg) using the Quantscript RT Kit. qPCR was performed using the iQ SYBR Green Supermix on a CFX96 System (Bio-Rad Laboratories Inc., Hercules, CA,USA). Products were amplified using primers that recognized MIR205HG [ATCTCTCAA GTACCCATCTTGGA (forward); GGCCTCATGGTTGT CAGCTC (reverse)], LINC00661 [CTGTCCTGCGTACCT CCTCTGG (forward), CACTGCCTGCTGAGAAGTTGGATG (reverse)], CHRM3.AS2 [CATGCTGGCTGTGCTAGT TCTATCC (forward); GGCCCGTGATAATTCTCAG CAGAAC (reverse)], and GAPDH [CGTGCCGCCT GGAGAAACCTG (forward), AGAGTGGGAGTTGCTGTT GAA (reverse)]. A threshold cycle value (Ct) of each gene was produced and normalized to corresponding GAPDH in the same sample by processing the raw fluorescence data. Identical results were obtained with at least three repeated procedures independently.

Statistical Analysis

Figure 1 summarized the flowchart of this study. R software (version 4.1.0) was the primary statistical tool for analysis. Cox regression analyses were performed for screening survival-related DEARlncRNAs and establishing the risk score model. K-M analysis was used for analyzing survivals, and the differences in survivals were evaluated by log-rank test. ROC curve and AUC were displayed by using "Survival ROC" package in R language. $p < 0.05$ was preset to determine the statistical difference during statistical analysis.

RESULTS

Identification of DEARlncRNA Based on TCGA Data

Through searching TCGA, RNA-seq and clinical follow-up data (tumor, n = 36; normal, n = 9) were obtained as the test set. Among the 232 ARGs downloaded from HADb, there were 219 DEARGs in CCA. Consequently, a total of 13 DEARGs and 108 DElncRNAs were screened (|log2F C| >1 and FDR <0.05). The expressions of DEARGs and DElncRNAs between CCA and normal tissues were then identified based on the plotted volcano plot and heatmap (**Figures 2A–E**). A total of 92 DElncRNAs were identified to be statistically significant (PPC >0.3 and $p < 0.001$) and were hence selected as the DEARlncRNAs for subsequent validation.

Establishment of Prognostic DEARlncRNA Signature for CCA Patients

As shown in **Figure 3A**, 59 lncRNAs were further identified from the 92 DEARlncRNAs screened above (all $p < 0.05$). When minimum λ = 0.0345, four DEARlncRNAs were obtained, which could reduce the overfitting of the signature (**Figure 3B**). Based on AIC = 94.89, these DEARlncRNAs were then selected for multivariate analysis. Finally, three DEARlncRNAs (CHRM3.AS2, MIR205HG, and LINC00661) were identified (**Figure 3C**) for subsequent construction of a predictive model. Furthermore, MIR205HG was identified to have a high hazard ratio (HR = 1.055, p = 0.0056) and was defined as high-risk factor, whereas CHRM3.AS2 and LINC00661 were identified to have low hazard ratios (HR = 0.877, p = 0.0432 and HR = 0.771, p = 0.008) and were defined as low-risk factor. A formula of the risk model was established by exploring the best three DEARlncRNAs based on the prognosis signature. The formula can be given as follows: Risk score = −(0.1309 * CHRM3.AS2) + (0.1833 * MIR205HG) − (0.2603 * LINC00661). The risk score of each patient was then determined on the basis of the detected expressions of CHRM3.AS2, MIR205HG, and LINC00661. As described previously, patients (test set) were grouped into high-risk (n = 18) and low-risk (n = 18) groups when median risk score = 0.896. **Figure 3D** shows a gradual elevation of the score from left to right. **Figure 3E** displays the survival of each CCA patient. **Figure 3F** shows the heatmap of CHRM3.AS2, MIR205HG, and LINC00661 expression profiles in both groups (**Figure 3F**). Furthermore, compared with low-risk group, the three DEARlncRNAs were observed to be highly expressed in the high-risk group, and

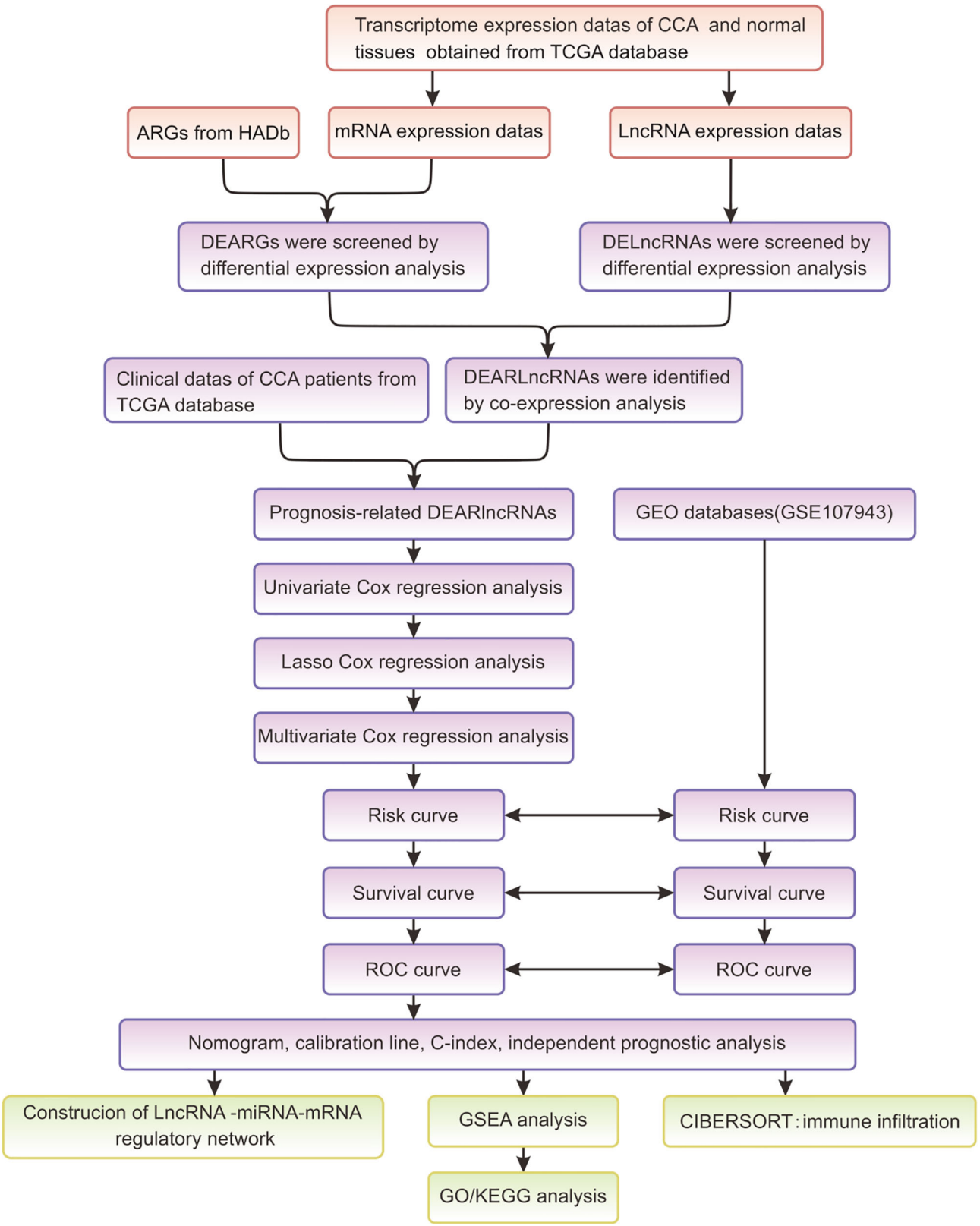

FIGURE 1 | The flowchart of this study.

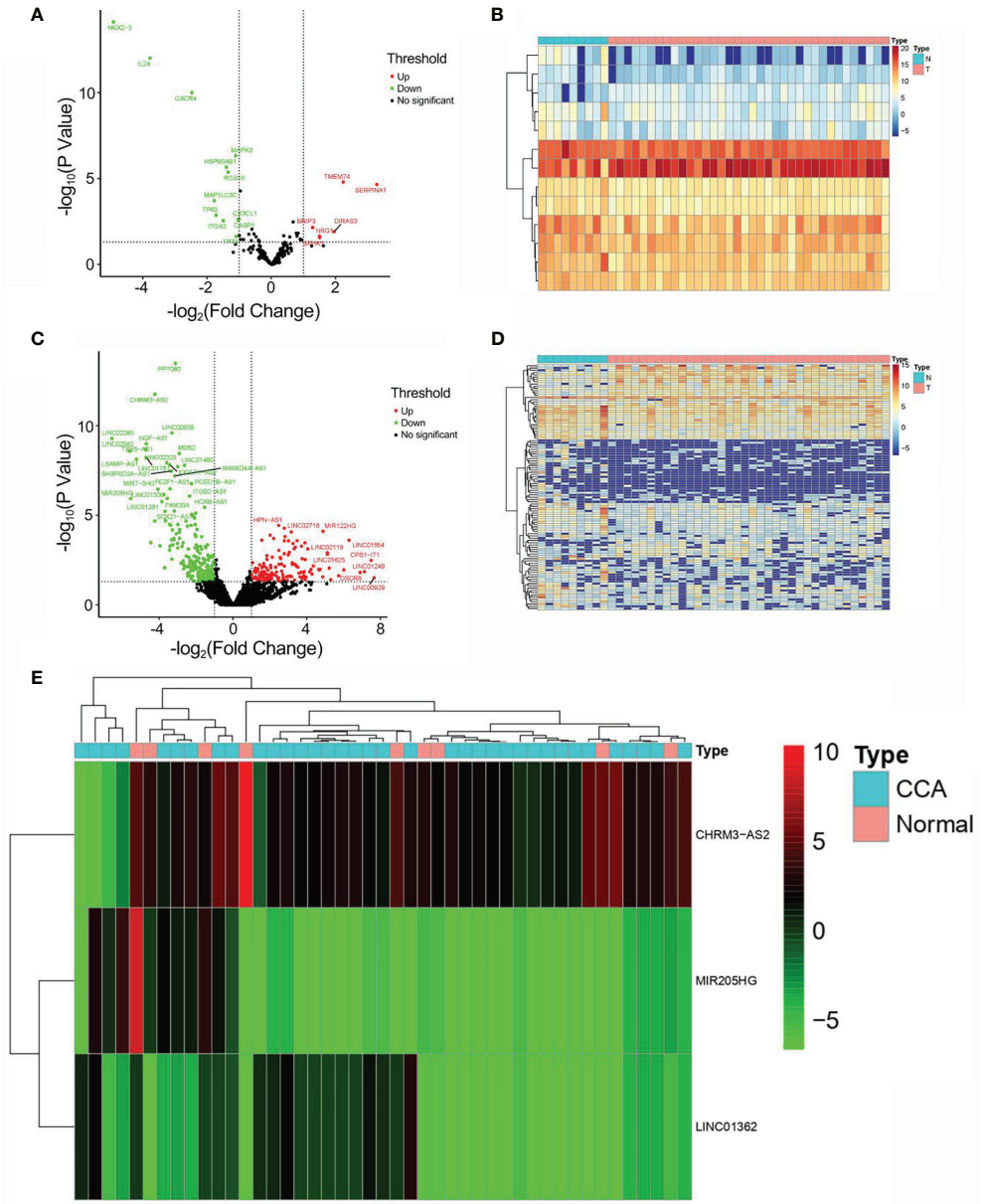

FIGURE 2 | Identification of DEARGs and DElncRNAs. **(A)** Volcano plot of DEARG distribution (n = 13; red dots, upregulated; green dot, downregulated). **(B)** Heatmap of DEARG expression profiles. **(C)** Volcano plot of DElncRNA distribution (n = 108; red dots, upregulated ARGs; green dot, downregulated ARGs). **(D)** Heatmap of DElncRNA expression profiles. **(E)** Heatmap of the expression profiles of CHRM3.AS2, MIR205HG, and LINC00661 in CCA patients and normal controls.

corresponding expression profiles had differences significantly, as evidenced by PCA in **Figure 3G**. Moreover, coexpression network analysis revealed the relationship between DElncRNAs and DEARGs with consistent prognosis signature using the threshold PCC >0.3 and $p < 0.001$ (**Figure 3H**).

Verification of the Predictive Ability of the Three DEARlncRNA Prognostic Signatures

Further verification was promoted to confirm the predictive ability of the three DEARlncRNAs identified above. Firstly, patients in the high-risk group were observed to have shorter OS time than those in the low-risk group, as revealed by K-M analysis in **Figure 4A**, similarly to the trends described before. With another validation of the role of risk scores, patients were then divided based on the quartiles (Q). Again and similarly, a worse OS was noticed in those with high scores relative to those with low scores (**Figure 4B**). Furthermore, as presented in **Figures 4C, D**, both pathological stage and risk scores were confirmed to be effective prognosis factors for CCA patients ($p <$ 0.001). Moreover, the ROC curve analysis showed a high

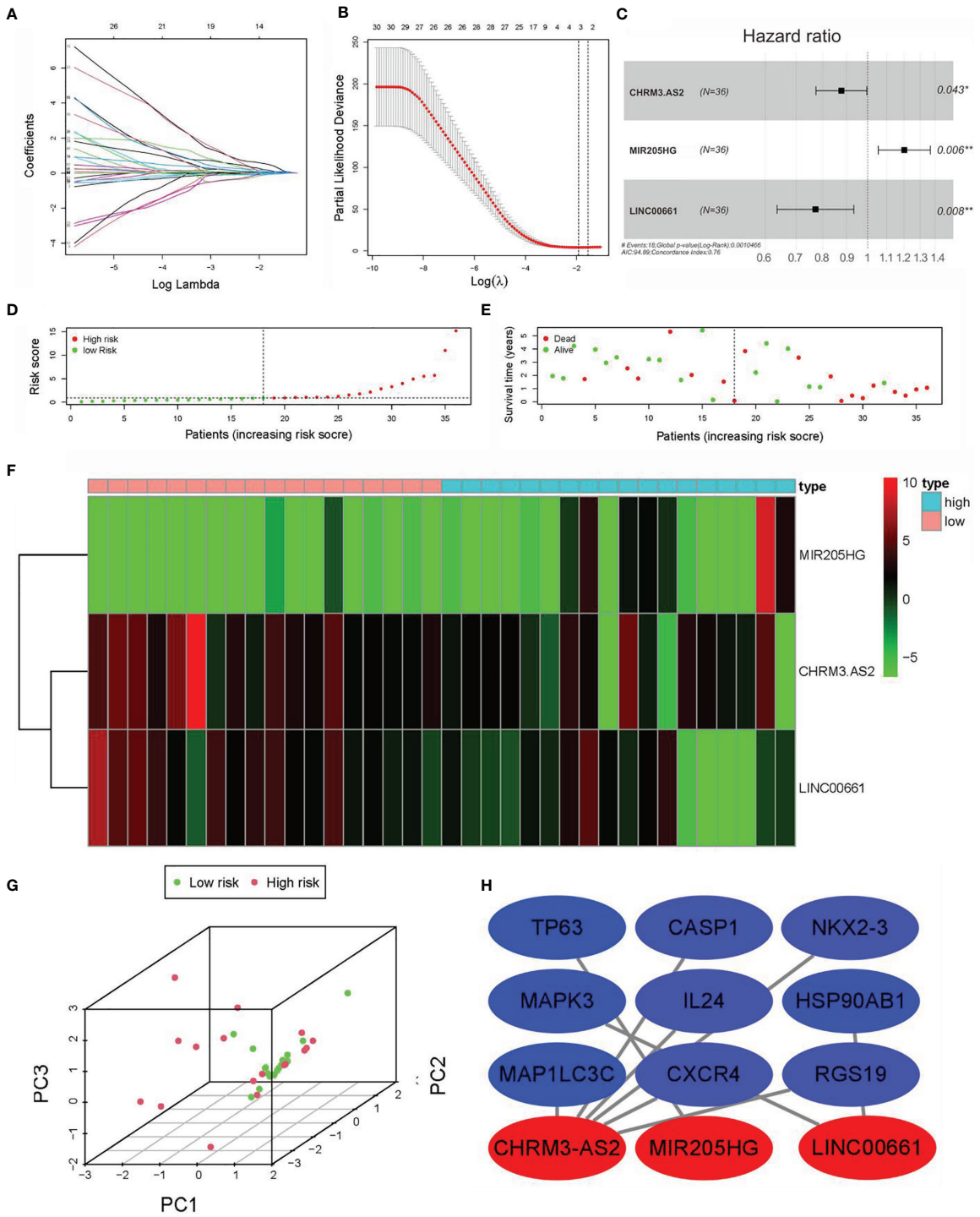

FIGURE 3 | Construction of prognostic DEARlncRNA signatures for CCA patients based on TCGA data. **(A)** univariate Cox regression analysis. **(B)** LASSO-penalized Cox regression analysis. **(C)** Multivariate Cox regression analysis. **(D)** Distribution of CCA patients with high and low risk based on TCGA data. **(E)** Survival status of CCA patients with high and low risk based on TCGA data. **(F)** The heatmap of the three DEARlncRNAs expression profiles in high- and low-risk CCA patients. **(G)** PCA of the expression profiles of CHRM3.AS2, MIR205HG, and LINC00661. **(H)** Coexpression relationship of CHRM3.AS2, MIR205HG, and LINC00661 with corresponding ARGs (*P < 0.05, **P < 0.01).

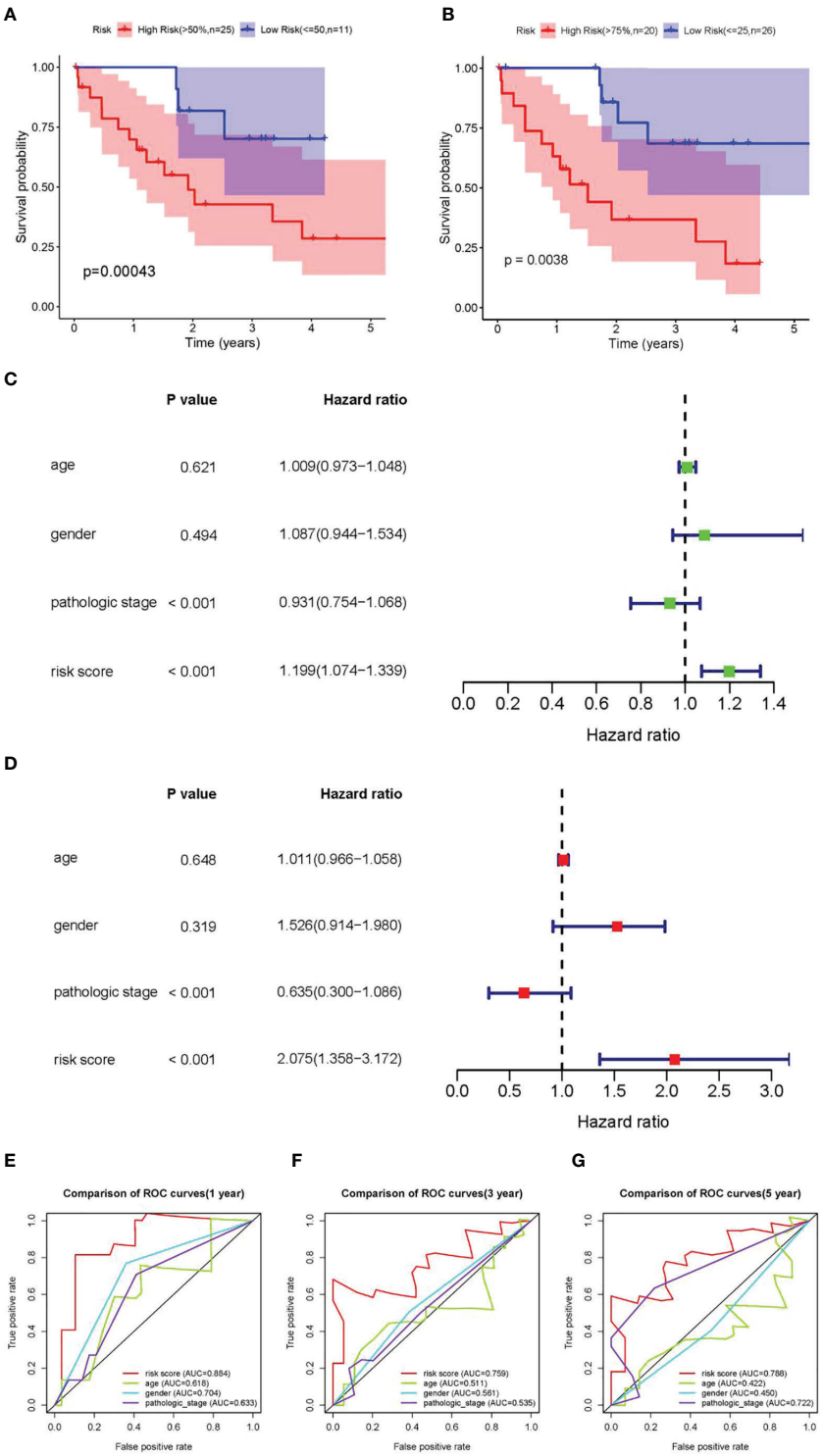

FIGURE 4 | Validation of the prognostic DEARlncRNA signatures of CHRM3.AS2, MIR205HG, and LINC00661. **(A)** The K-M curve analysis in high-risk (>50%) and low-risk (≤50%) patients. **(B)** The K-M curve analysis in high-risk (>75%) and low-risk (≤25%) patients. **(C)** Relationship of clinical characteristics and risk scores with OS of CCA patients presented by forest plot. **(D)** Relationship of clinical characteristics and risk scores with OS of CCA patients presented by forest plot. The 1-year (AUC = 0.884) **(E)**, 3-year (AUC = 0.759) **(F)**, and 5-year (AUC = 0.788) **(G)** time-dependent ROC curves.

prediction accuracy of patient survival, demonstrating good agreement, sensitivity, and specificity of the risk score. The AUC of 1-, 3-, and 5-year time-dependent ROC curves were 0.884, 0.759, and 0.788, respectively (**Figures 4E–G**).

Verification of the Predictive Ability of Prognostic Signatures in the Test Set (GSE107943)

For the validation of the predictive power of CHRM3.AS2, MIR205HG, and LINC00661, dataset GSE107943 containing 57 samples (tumors, n = 32 and normal tissues, n = 25) was used for validation. Based on the same processing on the TCGA database, 30 samples were obtained after combining the DEARlncRNAs with clinical follow-up data. Two groups were also set, with 15 cases in each group (median risk score = 1.031). **Figures 5A, B** shows the distribution of the risk score and survival status of each patient. The results were consistent with that obtained on the TCGA database. However, neither the heatmap nor the PCA showed a clear distinction between patients with high- and low-risk scores (**Figures 5C, E**), which was possibly attributed to the limited sample size of the available TCGA dataset. Fortunately, patients in the high-risk group (n = 15) were observed to have shorter OS time than those in the low-risk group (n = 15) by K-M analysis, supporting the predictive power of the proposed signature (**Figure 5D**). Further ROC curve analysis revealed that the AUC for 1-, 3-, and 5-year time-dependent ROC curve were 0.742, 0.776, and 0.699, respectively (**Figures 5F–H**), confirming the consistency described on CCA datasets in the TCGA database (**Figure 5C**).

Correlation Analysis of the Risk Scores With Clinical Characteristics of CCA Patients

We firstly compared the impact of clinical characteristics on each patient with CCA in high- and low-risk groups. Despite with no obvious correlation found with gender and age (both $p > 0.05$) (**Figures 6A, B**), the risk score indicated an evident correlation with pathological grade (e.g., stage I vs. stages III–IV; stage II vs. stage IV) (both $p < 0.05$) (**Figures 6E–H**). These results showed that there might be a higher risk score as the pathological grade increased, which might indicate a worse prognosis. However, no statistical difference was noticed in patients with stage II vs. stage III ($p > 0.05$). Furthermore, the high-risk score was significant correlations with pathological stage, N stage, and survival status (**Figures 6C, D**).

Construction and Validation of the Nomogram

A nomogram was established and validated using data from TCGA (**Figure 7D**) and GEO (**Figure 7E**) respectively to determine the survival rate of CCA patients conveniently. As a result, the calibration plots had excellent prediction accuracy, showing an approximately similar trend of the predicted survival to that of the actual results (**Figure 7A**). Furthermore, the ROC curve confirmed that the predictive ability of the nomogram has good accuracy for 1-, 3-, and 5-year OS, with corresponding AUC of 0.884, 0.759, and 0.788, respectively (**Figure 7B**). Interestingly, the calibration curve of the nomogram based on GEO data also demonstrated a good accuracy of the 1- and 3-year predictive survival rates (**Figure 7C**). Calibration curves showed that the nomogram had a superior agreement between the predicted and actual OS in both cohorts (**Figures 7D, E**).

Validation of the Expressions of LncRNAs in CCA Samples

As mentioned previously, the expressions of CHRM3.AS2, MIR205HG, and LINC00661 from the TCGA and GEO databases were remarkably upregulated in tumor tissues compared with those in normal tissues. In view of the above results, six paired CCA samples and matching adjacent nontumor tissues obtained clinically were used for examining the mRNA levels of CHRM3.AS2, MIR205HG, and LINC00661 *via* quantitative real-time PCR (qRT-PCR). Corresponding results were consistent with the trends reported based on data from the TCGA and GEO databases (**Figure 7F**) (all $p < 0.05$).

Regulatory Network Construction

LncRNAs could have a regulatory role in the biological features of cancers based on a network of lncRNA-miRNA-mRNA through interacting with miRNAs to modulate mRNA expression, and hence mediating the initiation of malignant tumor development. In order to explore the regulation of these screened lncRNAs, our study further established a regulatory network including 16 lncRNAs, 52 miRNAs, and 156 mRNAs (**Figure 7G**).

Functional Analysis of the Signature

A hypothesis was proposed that the predictive performance of the constructed prognostic DEARlncRNA signature based on CHRM3.AS2, MIR205HG, and LINC00661 relied on the biological functions of lncRNAs in CCA. In order to explore the potential mechanism, GSEA was performed to identify the enrichment of KEGG and GO pathways in the high-risk group. In **Figures 8A, C**, the top 4 KEGG pathways were "pathways of basal cell carcinoma", "glycerolipid metabolism", "glycerophospholipid metabolism", and "regulation of autophagy", respectively. Moreover, five GO signaling pathways were significantly altered (**Figures 8B, D**), including "positive regulation of macroautophagy", "organelle localization", "lymphocyte activation", "cell signaling", and "autophagy of mitochondrion".

The Relationship of Signature and Immunity in CCA Tissues

It is common knowledge that the tumor mutation burden (TMB) can be associated with the clinical efficacy of immunotherapy (23). **Figures 9A, B** shows that macrophages M0, T-cell regulatory (Tregs), and plasma cells were increased evidently in the high-risk group, yet with an obvious decrease in monocytes and other protective immune cells. Accordingly, our study evaluated the TMB of CCA patients to explore the value of the signature established in our study for efficacy prediction.

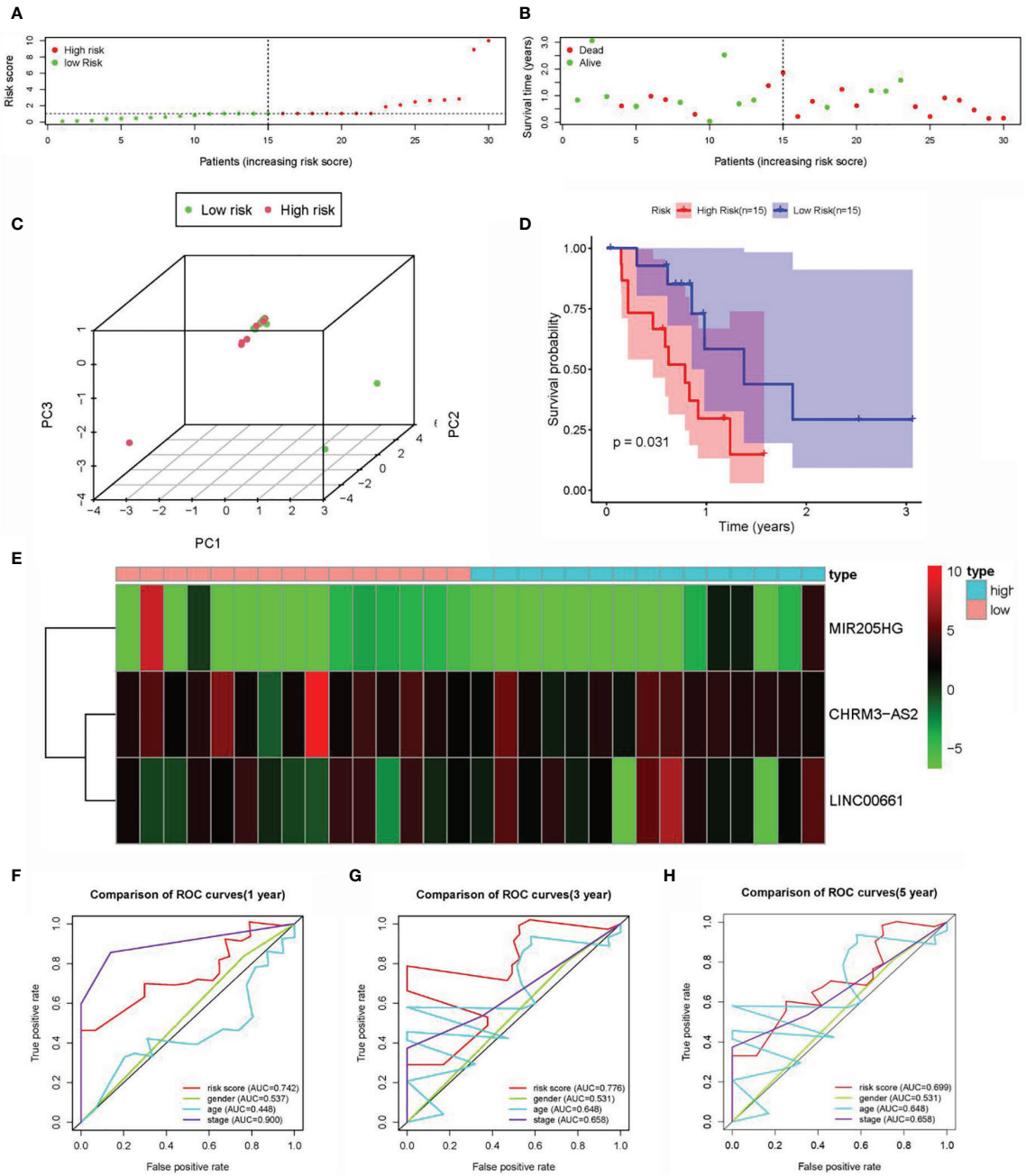

FIGURE 5 | Construction of the prognostic DEARlncRNA signatures for CCA patients using GEO datasets. **(A)** Distribution of CCA patients with high- and low-risk scores. **(B)** Survival status of CCA patients with high- and low-risk scores. **(C)** PCA of the expression profiles of CHRM3.AS2, MIR205HG, and LINC00661. **(D)** The K-M curve analysis in high-risk (n = 15) and low-risk (n = 15) patients. **(E)** The heatmap of the expression profiles of CHRM3.AS2, MIR205HG, and LINC00661. **(F)** The 1-year time-dependent ROC curve. **(G)** The 3-year time-dependent ROC curve. **(H)** The 5-year time-dependent ROC curve.

Asshown in **Figure 9C**, patients in high-risk group had higher TMB, implying the potential effective outcome of immunotherapy. Furthermore, a close correlation of the score was found with PD-L1 (cor = 0.055, p = 0.0074), VEGFR3 (cor = 0.258, p = 0.00128), EGFR (cor = −0.058, p = 0.00737), FLT3 (cor = −0.062, p = 0.0072), KIT (cor = 0.3, p = 0.00075), and MET (cor = −0.036, p = 0.00083) (**Figure 9D**).

DISCUSSION

CAA has been recognized as the second most commonly diagnosed primary liver tumor (24). It results from cholangiocyte differentiation and can be developed from any part of the biliary tree (25). Current data support that it has rising morbidity and mortality, difficulty in the early diagnosis, and

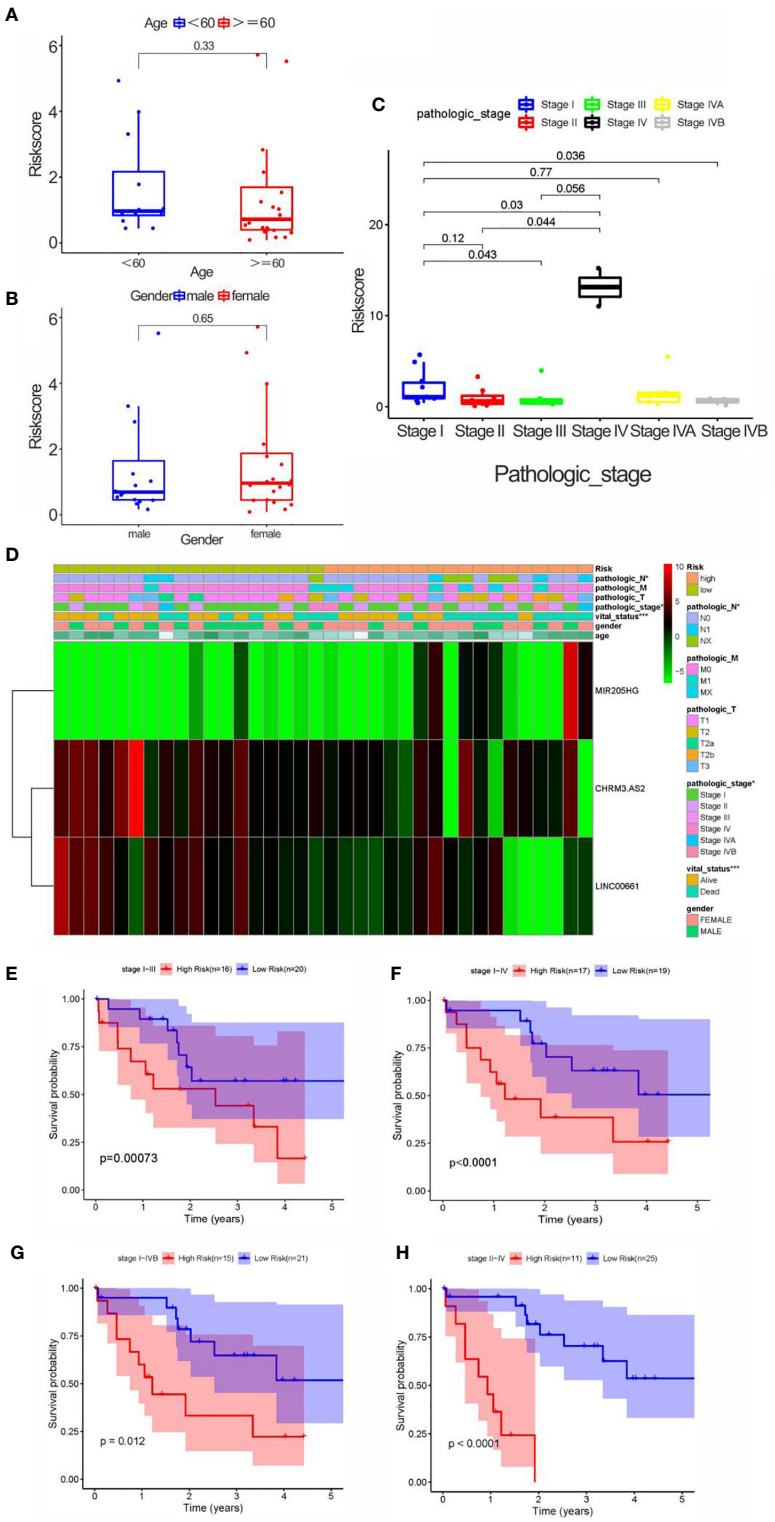

FIGURE 6 | Correlation analysis between clinical characteristics and risk scores. **(A)** Correlation between age and risk score, without significant difference (<60, and 60 years old). **(B)** Correlation between gender and risk score, without significant difference. **(C)** The correlation between pathological stage and risk score. **(D)** Heatmap of three key prognostic DEARlncRNA in the correlation of risk group and clinical traits. **(E)** K-M curve based on pathological stage (stages I and III). **(F)** K-M curve based on pathological stage (stages I and IV). **(G)** K-M curve based on pathological stage (stages I and IVB). **(H)** K-M curve based on pathological stage (stages II and IV).

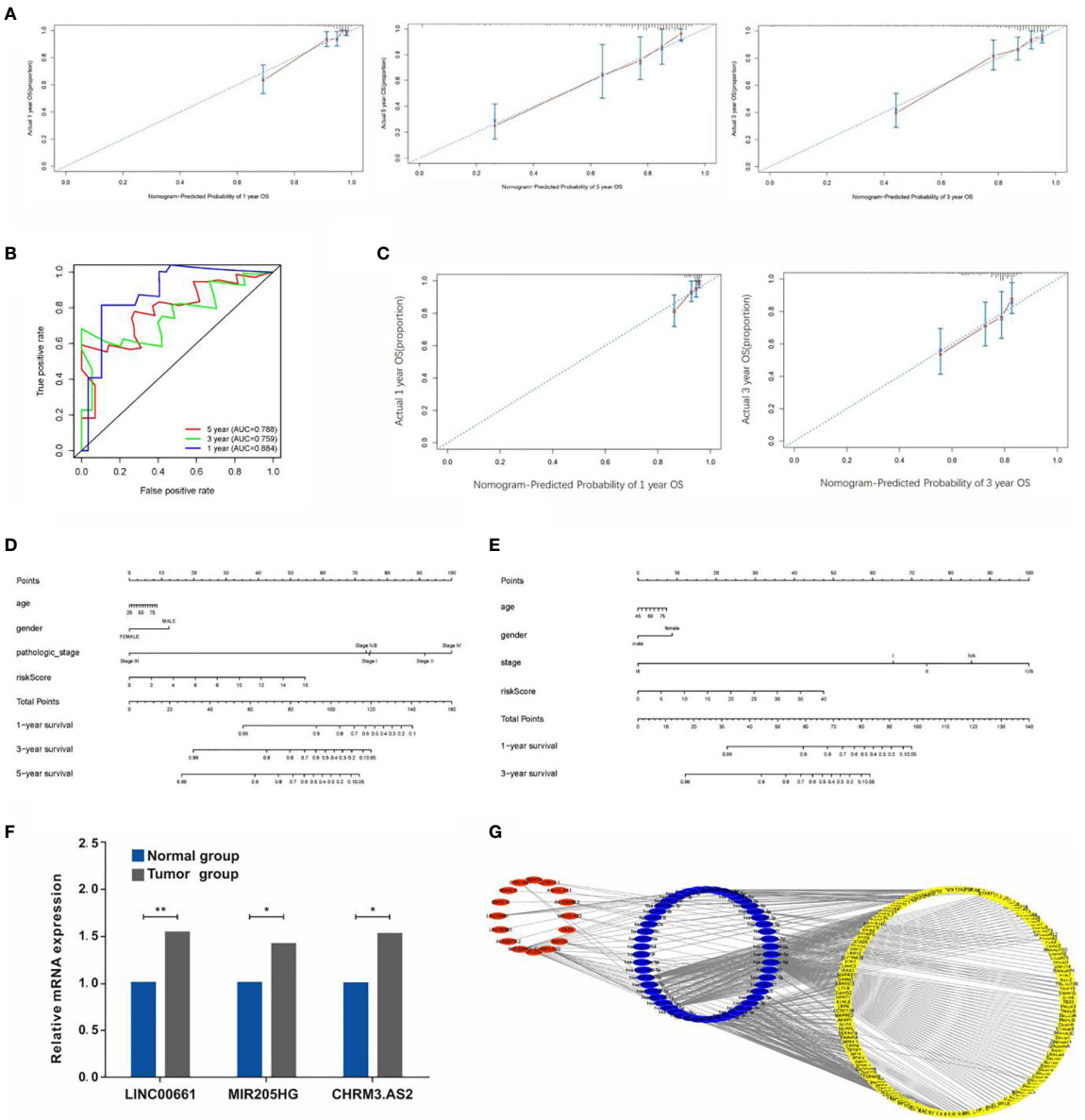

FIGURE 7 | **(A)** Calibration plots of the predictive accuracy of the nomogram for 1, 3, and 5 years in TCGA data. **(B)** Time-dependent ROC curve in TCGA data. **(C)** Calibration plots based on the GEO data. **(D)** Nomogram based on the signature and clinical information in the TCGA data. **(E)** Nomogram based on the signature and clinical information in the GEO data. **(F)** qRT-PCR detection of the expressions of LINC00661, MIR205HG, and CHRM3.AS. **(G)** Construction of lncRNA-miRNA-mRNA regulatory network (*P < 0.05, **P < 0.01).

unsatisfied therapeutic outcome, resulting in a poor prognosis of this cancer that has attracted the special attention of the medical community (1, 26, 27). Its overall 5-year survival is estimated to be less than one-third in patients undergoing radical surgery (28). The etiology of CCA is related to a strong genetic heterogeneity, and there is an absence of comprehensive cognition of the pathogenesis of CCA at present (29, 30). It is still controversial with regard to the genetic changes involved in CCA initiation, progression, and prognosis. At present, there is a relatively low clinical applicability of the available biomarkers although they are valuable to predict, diagnose, or provide a therapeutic effect on CAA, e.g., mucin antigen MUC1, fascia, and EGFR (31–33). So far, there are still many gaps in the research of valuable biomarkers for CAA with high practicability. As we have described before, autophagy has a role in CCA, and there is a dysfunction of autophagy in the initial stage of CCA development. In addition, autophagy modulators can promote CCA cell death and reduce the invasiveness capacity of tumor cells (34, 35). Thus, there may be a great significance to identify potential autophagy-related molecules for predicting CCA

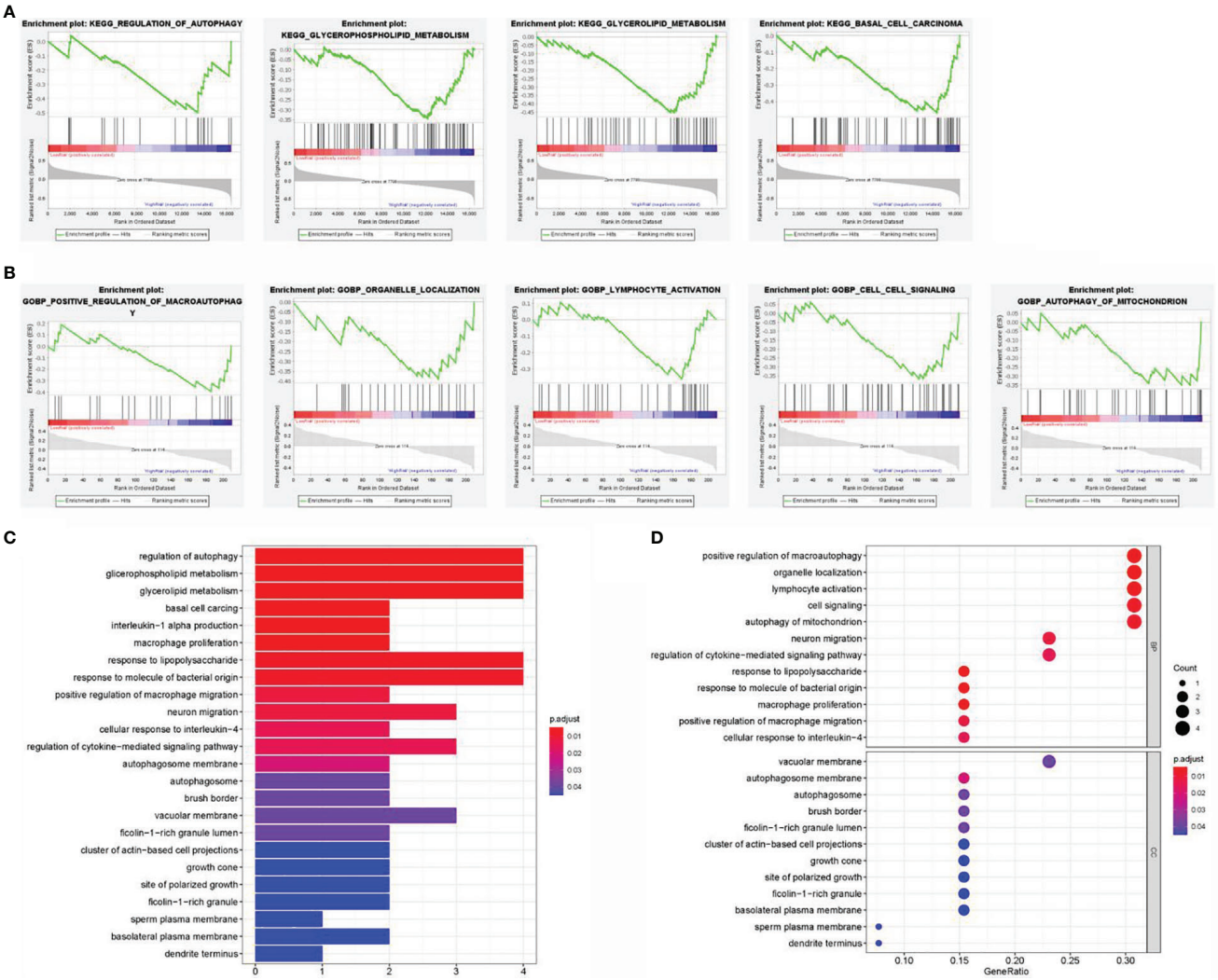

FIGURE 8 | Gene set enrichment analysis (GSEA) of the high- and low-risk groups. **(A)** Enrichment analysis of KEGG pathway. **(B)** Enrichment analysis of GO pathway. **(C)** Barplot graph for KEGG pathways. **(D)** Bubble graph for GO enrichment.

prognosis. Here, on the basis of development in genomics, our study constructed a reliable prognostic ARlncRNA signature for CCA.

In this study, the TCGA and GEO were retrieved for data collection to explore the prognosis of ARlncRNAs for CCA. Our study initiated from the analysis of the transcriptome and clinical data of CCA patients in TCGA, followed by identifying 108 ARlncRNAs through the lncRNA-autophagy gene coexpression analysis. Subsequently, a signature based on CHRM3.AS2, MIR205HG, and LINC00661 was constructed for OS prediction. The constructed prognosis signature was useful for risk score calculation separately for each case, which was evaluated in the test set. Our study indicated a low survival and thus a worse prognosis in patients with high-risk scores. The detection results were found to be similar with those in validation cohort. Meanwhile, the risk score was also confirmed to have a significant correlation with tumor pathological grade. It is speculated that patients with higher tumor pathological grades may have higher scores and thus poor prognosis. Therefore, a hypothesis was proposed in our study that the prognostic DEARlncRNA signatures of CHRM3.AS2, MIR205HG, and LINC00661 might be responsible partially for CCA progression. Further analysis of the 1-, 3-, and 5-year time-dependent ROC curves of CCA patients revealed that the prognostic signature was found to have good sensitivity and specificity, suggesting good reliability in prediction. Furthermore, a nomogram was established, and the calibration plot showed that the predicted survival was in good agreement with that of the actual situation, which in turn confirms the good predictive performance of the nomogram constructed in our study. Finally, the expressions of CHRM3.AS2, MIR205HG, and LINC00661 were identified in clinical samples, with similar

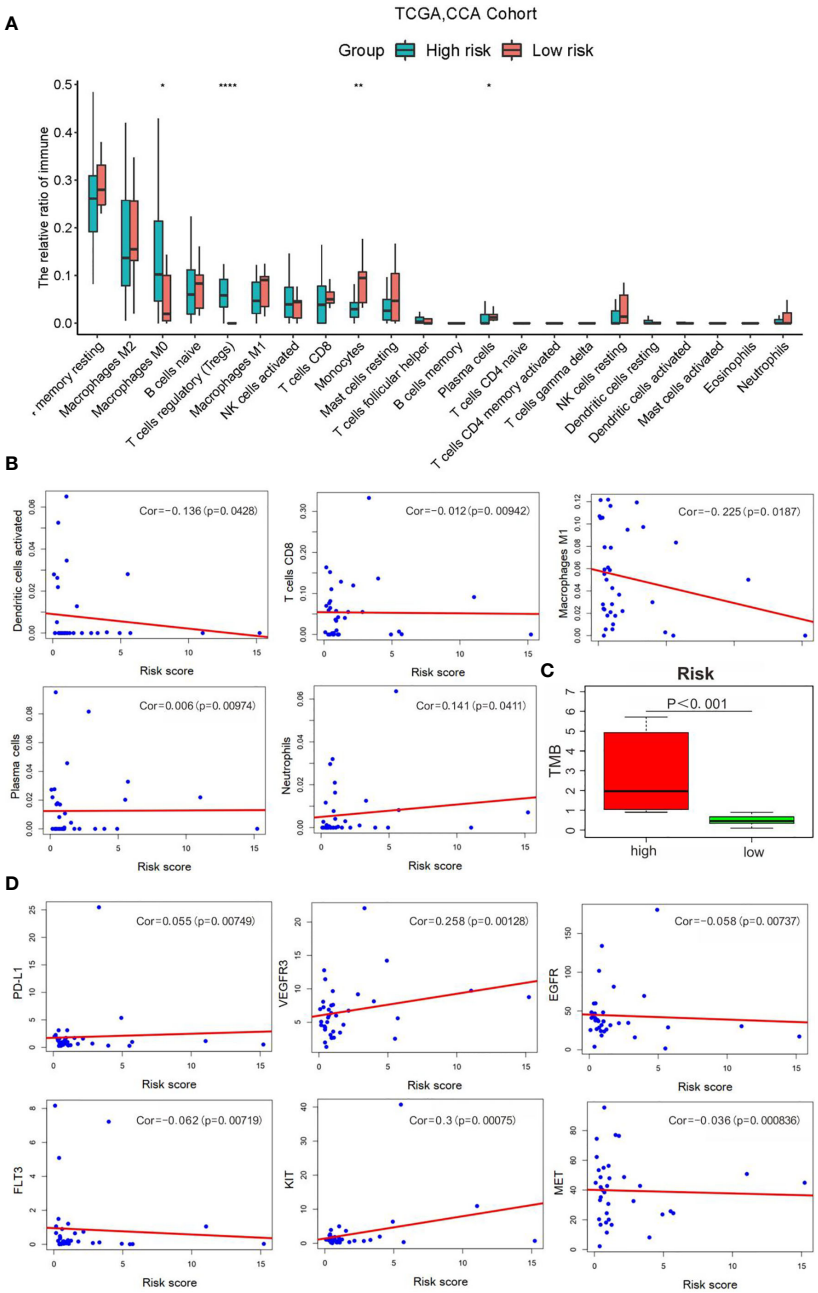

FIGURE 9 | Correlation analysis of risk scores with the clinical characteristics, immune cells and therapy targets. **(A)** Relative infiltration expression of 22 immune cells between different risk groups. (*P < 0.05, **P < 0.01, ****P < 0.0001); **(B)** Correlation of with immune cells; **(C)** TMB evaluation; **(D)** Correlation with therapy targets.

trends based on database analyses. Collectively, CHRM3.AS2, MIR205HG, and LINC00661 may be considered wonderful predictors in CCA prognosis and can be regarded as powerful indicators for patients with CCA in clinical practice.

The function of autophagy in reducing DNA damage and oxidative stress in cells in the early stage of tumors is well known. Nevertheless, autophagy can also promote tumor progression by providing sufficient energy to tumor cells under various adverse environments. Whereas, the pathological role of autophagy and its therapeutic potential in CCA are still unclear. Importantly, the prognostic significance of autophagy-related markers, emphasizing the importance of this process in tumors has been identified. It has been documented that regulating autophagy-related signaling pathways, such as PI3K/Akt/mTOR, p53and JAK/STAT, can significantly affect epithelial-mesenchymal transition, which may be drivers of tumor aggravation, and

thus may result in adverse outcomes in tumor growth and metastasis, and even drug resistance (36). Moreover, past research has verified the potential prognostic value of Beclin1 for CCA (37). Interestingly, Beclin1 plays an important role in linking autophagy, apoptosis, and differentiation. In addition, He et al. demonstrated that cellular autophagy can be promoted through modulating FOXO1 expression and transcriptional activity. Through acetylation, FOXO1 can interact with ATG7 to regulate basal and starvation-induced autophagy in CCA cells (38). The present study intended to construct a prognostic DEARlncRNA signature for CCA in view of the importance of autophagy and the lack of study of related lncRNAs for the disease we studied.

Among the three selected DEARlncRNAs, Yan et al. identified the prognostic significance of CHRM3.AS2 in ovarian carcinoma, with possible association with hedgehog pathway, basal cell carcinoma, Wnt signaling pathway, etc. (39). Interestingly, CHRM3.AS2 was a risk-associated gene in our study, which was highly expressed in CCA. Moreover, as for MIR205HG, Li et al. demonstrated that MIR205HG could exert roles on cell cycle, migration, and apoptosis of esophageal squamous cell carcinoma by mediating miR-214 negatively and regulating SOX4 as a molecular sponge, which can be regarded as a novel candidate for the diagnosis and treatment of that tumor (40). In another recent study, Liu and colleagues demonstrated that by acting as a competing endogenous RNA, MIR205HG could accelerate lung squamous cell carcinoma development *via* mediating the molecular axis of miR-299-3p/MAP 3 K2 (41). Furthermore, MIR205HG could also target SRSF1 and modulate KRT17 to mediate biological activities of cervical cancer cells (42). In our study,the expressions of CHRM3.AS2, MIR205HG, and LINC00661 were significantly increased in tumor tissues of CCA patients, further verifying the prognostic prediction value of the established signatures for CCA.

The effective prognostic prediction of the three ARlncRNAs could be interrelated with the biological functions of the lncRNAs in CCA. However, there is a lack of report on the biological functions of CHRM3.AS2, MIR205HG, and LINC00661 in our signature previously. Therefore, to determine the underlying mechanism, GSEA revealed patients with high-risk scores showed enrichment of "pathways of basal cell carcinoma", 5"glycerolipid metabolism", "positive regulation of macroautophagy", and "organelle localization". The significant enrichment results suggest a higher risk of developing CCA under the aforementioned conditions. These results indicate the association of high scores with autophagy modulation, and also provide potential therapeutic targets for patients with CCA. Furthermore, autophagy is complicated with the involvement of multiple ARGs and signaling pathways, forming a huge and complex regulatory network to mediate the activities of tumor cells. Hence, a lncRNA-miRNA-mRNA regulatory network was constructed in our study that benefits the understanding of the potential biological mechanism of ARlncRNAs. In addition, immunotherapy may be effective for treating CCA patients with high-risk scores. Also, the risk score was positively correlated with macrophages M0, Tregs, and plasma cells, as suggested by the immune cell infiltration analysis. These findings suggested that these DEARlncRNA signatures screened in our study may be closely related to immune microenvironment and classical signaling pathways. Collectively, CHRM3.AS2, MIR205HG, and LINC00661 may regulate autophagy through the above various pathways, leading to differences in survival outcomes according to prognostic characteristics of CCA patients with high- and low-risk scores. Furthermore, similar studies may have been reported, for example, Cao et al. (43) reported most recently in May 2021 a similar exploration of DEG signature related to TME for CCA patients' prognosis prediction. Their study emphasized on TME and DEGs, while our study focused on autophagy and DEARlncRNAs, both of which deserve affirmation with positive and promising results generated. Importantly, there are some highlights in this study; to be specific, our study discloses the significance of three ARlncRNAs with differential expressions in predicting the prognostic outcomes of CCA based on abundant data assessment, accompanied by experimental verification, which, of course, remains to be explored comprehensively in the future.

Inevitably, there are several limitations in our current study which shall be taken into consideration in a cautious manner. Firstly, the sample size of the CCA TCGA database is relatively small that may affect the reliability and accuracy of the predictive model, which constitutes the main disadvantage of this study. Secondly, some of the findings in our research were obtained based on speculation and assumptions from bioinformatics analysis, with lack of support from our own experiments and of larger sample scales for confirmation. Further confirmation based on our own sufficient experiments will contribute a lot to improve the reliability of our study, which is the major direction of our research. In addition, considering the emergence of bioinformatics analysis for the screening of molecular or drug targets and analysis of functional pathways, there may be some methodological overlaps. Anyway, findings based on these analyses are valuable for further screening and references on the basis of prospective analysis combined with retrospective designs jointly. Significantly and specifically, concerning the potential direction of research based on our exploration, the expression of the three DEARlncRNAs can be further knocked out in CCA cells *in vitro* by transfection technology to explore the effects of silencing the three DEARlncRNAs level on the proliferation, migration, and invasion of CCA cells. In addition, a syngeneic mouse model of CCA can be further established to analyze the expression of the three DEARlncRNAs in various carcinogenic development stages and their correlation with immunity, so as to further verify which autophagy markers can benefit from the inhibition or activation of autophagy. Finally, the roles of three DEARlncRNAs in autophagy, chemotherapy resistance, and targeted therapy are also worthy of further exploration, which is a promising strategy to improve the therapeutic expectation of CCA patients.

In conclusion, our study constructs an ARlncRNA coexpression network and identifies a signature of three DEARlncRNAs with prognostic value for CCA patients. This study also identifies and validates a novel and robust nomogram

combining the signature and clinical characteristics to predict the 1-, 3-, and 5-year OS rates of CCA patients. Findings in this study may contribute to the formulation of individualized therapies for CCA patients and may provide a therapeutic reference for other tumors. Meanwhile, considering the existence of certain deficiencies in this analysis, further investigation is scheduled by our research team to confirm the exact roles of CHRM3.AS2, MIR205HG, and LINC00661 and corresponding utility in the clinical setting based on more *in vivo* and *in vitro* experiments rather than bioinformatic analysis primarily.

DATA AVAILABILITY STATEMENT

The datasets presented in this study can be found in online repositories. The names of the repository/repositories and accession number(s) can be found in the article/**Supplementary Material**.

ETHICS STATEMENT

Ethics committee approval and written informed consents were obtained from participants. The study was performed based on standard principles of ethical principles and professional conduct.

AUTHOR CONTRIBUTIONS

YL drafted the manuscript. AH collected and carried out data. ZW and MQ designed the study and critically revised the manuscript. JY provided general advice and supervised the whole process of this study. All authors contributed to the article and approved the submitted version.

FUNDING

This work was supported by the National Natural Science Foundation of China (No. 81770584 and No. 82000502), Natural Science Foundation of Hunan Province (No. 2020SK2068 and No. 2020JJ5941), and the Projects of the National Social Science Foundation of China (grant number No. 82073019 and No. 82073018).

SUPPLEMENTARY MATERIAL

The Supplementary Material for this article can be found online at: https://www.frontiersin.org/articles/10.3389/fonc.2021.780601/full#supplementary-material

REFERENCES

1. Banales JM, Cardinale V, Carpino G, Boberg KM, Marin JJ, Alvaro D, et al. Expert Consensus Document: Cholangiocarcinoma: Current Knowledge and Future Perspectives Consensus Statement From the European Network for the Study of Cholangiocarcinoma (ENS-CCA). *Nat Rev Gastroenterol Hepatol* (2016) 13(5):261–80. doi: 10.1038/nrgastro.2016.51
2. Bergquist A, Von Seth E. Epidemiology of Cholangiocarcinoma. *Best Pract Res Clin Gastroenterol* (2015) 29(2):221–32. doi: 10.1016/j.bpg.2015.02.003
3. Ikeno Y, Seo S, Uemoto S. Preoperative Metabolic Tumor Volume of Intrahepatic Cholangiocarcinoma Measured by 18F-FDG-PET Is Associated With the KRAS Mutation Status and Prognosis. *J Transl Med* (2018) 16:95. doi: 10.1186/s12967-018-1475-x
4. Fairweather M, Balachandran VP, D'Angelica MI. Surgical Management of Biliary Tract Cancers. *Chin Clin Oncol* (2016) 5:63. doi: 10.21037/cco.2016.10.03
5. Ghouri YA, Mian I, Blechacz B. Cancer Review: Cholangiocarcinoma. *J Carcinog* (2015) 14:1. doi: 10.4103/1477-3163.151940
6. Rizzo A, Frega G, Brandi G. Anti-EGFR Monoclonal Antibodies in Advanced Biliary Tract Cancer: A Systematic Review and Meta-Analysis. *In Vivo* (2020) 34(2):479–88. doi: 10.21873/invivo.11798
7. Rizzo A, Brandi G. Pitfalls, Challenges, and Updates in Adjuvant Systemic Treatment for Resected Biliary Tract Cancer. *Expert Rev Gastroenterol Hepatol* (2021) 15(5):547–54. doi: 10.1080/17474124.2021.1890031
8. Khan SA, Taylor-Robinson SD, Thomas HC. Changing International Trends in Mortality Rates for Liver, Biliary and Pancreatic Tumours. *J Hepatol* (2002) 37:806–13. doi: 10.1016/S0168-8278(02)00297-0
9. Andersen JB, Spee B, Barbour A, Roberts LR, Factor VM, Thorgeirsson SS, et al. Genomic and Genetic Characterization of Cholangiocarcinoma Identifies Therapeutic Targets for Tyrosine Kinase Inhibitors. *Gastroenterology* (2012) 142:1021–31.e15. doi: 10.1053/j.gastro.2011.12.005
10. Li Y, Li W, Huang H, Liang B, Li SH, Wang L, et al. Identification of Cancer Risk lncRNAs and Cancer Risk Pathways Regulated by Cancer Risk lncRNAs Based on Genome Sequencing Data in Human Cancers. *Sci Rep* (2016) 6:39294. doi: 10.1038/srep39294
11. Mercer TR, Dinger ME, Mattick JS. Long Non-Coding RNAs: Insights Into Functions. *Nat Rev Genet* (2009) 10:155. doi: 10.1038/nrg2521
12. Chen YG, Satpathy AT, Chang HY. Gene Regulation in the Immune System by Long Noncoding RNAs. *Nat Immunol* (2017) 18:962. doi: 10.1038/ni.3771
13. Bian EB, Li J, Zhao B. LncRNAs: New Players in Gliomas, With Special Emphasis on the Interaction of lncRNAs With Ezh2. *J Cell Physiol* (2015) 230:496–503. doi: 10.1002/jcp.24549
14. Cheng L, Han T, Pen W. Identification and Validation of Six Autophagy-Related Long Non-Coding RNAs as Prognostic Signature in Colorectal Cancer. *Int J Med Sci* (2021) 18: (1):88–98. doi: 10.7150/ijms.49449
15. Jia Yu, Chen Y, Liu J. Prognosis-Predictive Signature and Nomogram Based on Autophagy-Related Long Non-Coding RNAs for Hepatocellular Carcinoma. *Front Genet* (2020) 11:608668. doi: 10.3389/fgene.2020.608668
16. Saha S, Panigrahi DP, Patil S. Autophagy in Health and Disease: A Comprehensive Review. *Biomed Pharmacother* (2018) 104:485–95. doi: 10.1016/j.biopha.2018.05.007
17. Zhao YG, Zhang H. Core Autophagy Genes and Human Diseases. *Curr Opin Cell Biol* (2019) 61:117–25. doi: 10.1016/j.ceb.2019.08.003
18. White E. Deconvoluting the Context-Dependent Role for Autophagy in Cancer. *Nat Rev Cancer* (2012) 12(6):401–10. doi: 10.1038/nrc3262
19. Hsu P, Shi Y. Regulation of Autophagy by Mitochondrial Phospholipids in Health and Diseases. *Biochim Et Biophys Acta Mol Cell Biol Lipids* (2016) 1862 (1):114–29. doi: 10.1016/j.bbalip.2016.08.003
20. Montoyo HP. Therapeutic Potential of Autophagy Modulation in Cholangiocarcinoma. *Cells* (2020) 9(3):614. doi: 10.3390/cells9030614
21. Luan F, Chen W, Mo L. An Autophagy-Related Long Non-Coding RNA Signature for Glioma. *FEBS Open Bio* (2019) 9(4):653–67. doi: 10.1002/2211-5463.12601
22. Deng Z, Li X, Wang J. A Novel Autophagy-Related IncRNAs Signature for Prognostic Prediction and Clinical Value in Patients With Pancreatic Cancer. *Front Cell Dev Biol* (2020) 8:606817. doi: 10.3389/fcell.2020.606817
23. Cao D, Xu H, Xu X, Guo T, Ge W. High Tumor Mutation Burden Predicts Better Efficacy of Immunotherapy: A Pooled Analysis of 103078 Cancer Patients. *Onco Immunol* (2019) 8(9):1–12. doi: 10.1080/2162402X.2019.1629258
24. Li H, Long J, Xie F, Kang K, Shi Y, Jin G, et al. Transcriptomic Analysis and Identification of Prognostic Biomarkers in Cholangiocarcinoma. *Oncol Rep* (2019) 42(5):1833–42. doi: 10.3892/or.2019.7318
25. Hill MA, Alexander WB, Guo B, Kato Y, Patra K, Hezel AF, et al. Kras and Tp53 Mutations Cause Cholangiocyte- and Hepatocyte-Derived

Cholangiocarcinoma. *Cancer Res* (2018) 78(16):4445–51. doi: 10.1158/0008-5472.CAN-17-1123
26. Tyson GL, Ilyas JA, Duan Z, Green LK, Younes M, El-Serag HB, et al. Secular Trends in the Incidence of Cholangiocarcinoma in the USA and the Impact of Misclassification. *Dig Dis Sci* (2014) 59:3103–10. doi: 10.1007/s10620-014-3276-2
27. Banales JM, Cardinale V, Fouassier L, Boberg KM, Marin JG, Alvaro D, et al. Expert Consensus Document: Cholangiocarcinoma: Current Knowledge and Future Perspectives Consensus Statement From the European Network for the Study of Cholangiocarcinoma (ENS-CCA). *Nat Rev Gastroenterol Hepatol* (2016) 13:261–80. doi: 10.1038/nrgastro.2016.51
28. Tashiro S, Tsuji T, Miyake H, Sumise Y, Takai S, Yoshioka K, et al. Strategy for Improving the Prognosis of Patients With Intrahepatic Cholangiocarcinoma by Surgical Treatment: Considerations Based on Experience and a Literature Review. *J Med Invest* (2021) 68(1.2):15–21. doi: 10.2152/jmi.68.15
29. Hu J, Yin B. Advances in Biomarkers of Biliary Tract Cancers. *BioMed Pharmacother* (2016) 81:128–35. doi: 10.1016/j.biopha.2016.02.045
30. Jusakul A, Cutcutache I, Yong CH, Lim JQ, Huang MN, Padmanabhan N, et al. Whole-Genome and Epigenomic Landscapes of Etiologically Distinct Subtypes of Cholangiocarcinoma. *Cancer Discov* (2017) 7:1116–35. doi: 10.1158/2159-8290.CD-17-0368
31. Xu F, Liu F, Zhao H, An G, Feng G. Prognostic Significance of Mucin Antigen Muc1 in Various Human Epithelial Cancers: A Meta-Analysis. *Med (Baltimore)* (2015) 94(50):e2286. doi: 10.1097/MD.0000000000002286
32. Zhao H, Yang F, Liu J. Fascin Overexpression Promotes Cholangiocarcinoma RBE Cell Proliferation, Migration, and Invasion. *Technol Cancer Res Treat* (2016) 15(2):322–33. doi: 10.1177/1533034615580696
33. Padthaisong S, Thanee M, Namwat N, Khuntikeo N, Titapun A, Loilome W, et al. A Panel of Protein Kinase High Expression Is Associated With Postoperative Recurrence in Cholangiocarcinoma. *BMC Cancer* (2020) 20 (1):154. doi: 10.1186/s12885-020-6655-4
34. Pietrocola F, Pol J, Kroemer G. Autophagy Induction for the Treatment of Cancer. *Autophagy* (2016) 12:1962–4. doi: 10.1080/15548627.2016.1214778
35. Chude CI, Amaravadi RK. Targeting Autophagy in Cancer: Update on Clinical Trials and Novel Inhibitors. *Int J Mol Sci* (2017) 18:1279. doi: 10.3390/ijms18061279
36. Chen HT, Liu H, Shan H, Liu Y, Shan H, Jiang GM, et al. Crosstalk Between Autophagy and Epithelial-Mesenchymal Transition and Its Application in Cancer Therapy. *Mol Cancer* (2019) 18:101. doi: 10.1186/s12943-019-1030-2
37. Dong LW, Hou YJ, Wang HY. Prognostic Significance of Beclin 1 in Intrahepatic Cholangiocellular Carcinoma. *Autophagy* (2011) 7:1222–9. doi: 10.4161/auto.7.10.16610
38. He W, Zhang A, Chen J. FOXO1, a Potential Therapeutic Target, Regulates Autophagic Flux, Oxidative Stress, Mitochondrial Dysfunction, and Apoptosis in Human Cholangiocarcinoma QBC 939 Cells. *Cell Physiol Biochem* (2018) 45:1506–14. doi: 10.1159/000487576
39. Li Y, Huo FF, Jiang M, Wen YY, Jiang M. Screening and Identification of an Immune-Associated lncRNA Prognostic Signature in Ovarian Carcinoma: Evidence From Bioinformatic Analysis. *BioMed Res Int* (2021) 2021:6680036. doi: 10.1155/2021/6680036
40. Li H, Jia J, Chu J, He F, Yin H, Wan J, et al. LncRNA MIR205HG Drives Esophageal Squamous Cell Carcinoma Progression by Regulating miR-214/SOX4 Axis. *Onco Targets Ther* (2020) 13:13097–1310. doi: 10.2147/OTT.S286627
41. Liu L, Li Y, Wei Y, Zhang RF, Li C, Xiong J, et al. MIR205HG Acts as a ceRNA to Expedite Cell Proliferation and Progression in Lung Squamous Cell Carcinoma via Targeting miR-299-3p/MAP3K2 Axis. *BMC Pulm Med* (2020) 20(1):163. doi: 10.1186/s12890-020-1174-2
42. Dong M, Dong Z, Song L, Zhu XY, Zhang YH, Song L, et al. Long Non-Coding RNA MIR205HG Regulates KRT17 and Tumor Processes in Cervical Cancer via Interaction With SRSF1. *Exp Mol Pathol* (2019) 111:104322. doi: 10.1016/j.yexmp.2019.104322
43. Cao J, Chen X, Lu G, Wang HW, Zhang XY, Bai Y, et al. Identification of Prognostic Gene Signature Associated With Tumor Microenvironment of Cholangiocarcinoma. *Res Sq* (2021). doi: 10.21203/rs.3.rs-524410/v1

Conflict of Interest: The authors declare that the research was conducted in the absence of any commercial or financial relationships that could be construed as a potential conflict of interest.

Publisher's Note: All claims expressed in this article are solely those of the authors and do not necessarily represent those of their affiliated organizations, or those of the publisher, the editors and the reviewers. Any product that may be evaluated in this article, or claim that may be made by its manufacturer, is not guaranteed or endorsed by the publisher.

frontiers in Oncology

ORIGINAL RESEARCH
published: 25 January 2022
doi: 10.3389/fonc.2021.799759

Development and Validation of a Prognostic Index Based on Genes Participating in Autophagy in Patients With Lung Adenocarcinoma

Zi-Xuan Wu[1], *Xuyan Huang*[1], *Min-Jie Cai*[2], *Pei-Dong Huang*[3*] *and Zunhui Guan*[4]

[1] Guangzhou University of Chinese Medicine, Guangzhou, China, [2] Shantou Health School, Shantou, China, [3] Yunnan University of Chinese Medicine, Kunming, China, [4] Kunming Municipal Hospital of Traditional Chinese Medicine, Kunming, China

Background: Lung adenocarcinoma (LUAD) is a deadly respiratory system malignancy with poor prognosis. Autophagy is essential for the beginning, development, and therapy resistance of cancer. However, the expression of genes participating in autophagy in LUAD and their associations with prognosis remain unclear.

Methods: Predictive genes participating in autophagy in LUAD samples from The Cancer Genome Atlas (TCGA) and Gene Expression Omnibus (GEO) datasets were investigated. TCGA and GEO cohorts were divided into two risk groups, while the low-risk group having a longer overall survival (OS) time. This article aims to point out the interaction between genes participating in autophagy and immune function, immune checkpoints, and m^6a in LUAD. The prediction model was designed for exploring least absolute shrinkage and selection operator (LASSO) regression. It has been revealed that gene expression and autophagy are inextricably connected.

Results: Genes participating in autophagy were shown to be somewhat overexpressed in the high-risk group even though no different clinical symptoms were present, indicating that they might be used in a model to predict LUAD prognosis. The majority of genes participating in autophagy prognostic signatures controlled immunological and tumor-related pathways, according to gene set enrichment analysis (GSEA). *KRT6A*, *KYNU*, *IGFBP1*, *DKK1*, *PKP2*, *PLEK2*, *GAPDH*, *FLNC*, and *NTSR1* might be related to the oncology process for LUAD patients. *CERS4*, *CMAHP*, and *PLEKHB1* have been identified as being associated with low risk in patients with LUAD. Furthermore, the immune function and m^6a gene expression differed significantly between the two groups.

Conclusions: Genes participating in autophagy are connected to the development and progression of LUAD. LUAD patients' prognoses are often foreseen utilizing matched prognostic models. Genes participating in autophagy in LUAD may be therapeutic targets that ought to be investigated more.

Keywords: lung adenocarcinoma (LUAD), TCGA and GEO dataset, immunity, m^6a, and immune checkpoint, bioinformatics analysis, genes participating in autophagy

OPEN ACCESS

Edited by:
Paola Maycotte, Instituto Mexicano del Seguro Social, Mexico

Reviewed by:
Marina Mendiburu-Eliçabe, Centro de Investigación del Cancer, Spain
Federico Centeno, Instituto Nacional de Medicina Genómica (INMEGEN), Mexico

***Correspondence:**
Pei-Dong Huang
yeruyun@163.com

Specialty section:
This article was submitted to Cancer Molecular Targets and Therapeutics, a section of the journal Frontiers in Oncology

Received: *22 October 2021*
Accepted: *22 December 2021*
Published: *25 January 2022*

Citation:
Wu Z-X, Huang X, Cai M-J, Huang P-D and Guan Z (2022) Development and Validation of a Prognostic Index Based on Genes Participating in Autophagy in Patients With Lung Adenocarcinoma. Front. Oncol. 11:799759. doi: 10.3389/fonc.2021.799759

INTRODUCTION

Lung adenocarcinoma (LUAD) may be a leading reason for cancer-related death globally. LUAD is classified into two categories in microscopic anatomy, which differ clinically (1, 2). Significantly, more than half of LUAD patients had metastases at the time of diagnosis. Despite this, the absence of precise biomarkers for early tumor identification, likewise as restricted preclinical models, has obstructed prospering LUAD treatment (3, 4). To avoid the onset and development of LUAD, more molecular identification is essential for its fundamental and clinical research, likewise as the identification of novel and effective LUAD prognostic indicators.

Autophagy can be a cell-renewal mechanism that depends on the breakdown of cytoplasmic proteins or lysosome organelles. As a sort of death, it has received loads of attention and dialogue in recent years (5, 6). Yoshinori Ohsumi (7) highlighted the essential principle: autophagy is essential for eliminating "garbage" from cells, preventing aberrant death and protecting traditional cell functioning. It is a cell self-defense and self-renewal method that depends on lysosomes to destroy their organelles or proteins (8, 9). A growing variety of studies have discovered that autophagy is crucial in maintaining the intracellular environment's integrity and participates in cellular processes (10). In distinction, alternative investigations have discovered that many diseases, including cancer and respiratory organ malady, are joined to enhance or reduce the levels of autophagy (11). Despite contradictory evidence showing that autophagy is thought to promote oncogenesis and cancer spread. Rare sequence-based studies on aberrant gene expression and its relationship to overall survival (OS) in LUAD patients with autophagy were conducted.

Immune checkpoint-related gene (ICRG) profiles in LUAD patients may facilitate determining, evaluating, and predicting treatment responses (12, 13). Despite the very fact that there has been very little analysis on the link between genes participating in autophagy and LUAD, it is very essential to study the interaction between genes participating in autophagy, immunity, immunological checkpoints, and m^6a with LUAD clinicopathological tumor options. At this time, the cause and mechanism of LUAD's abnormal organic phenomenon and autophagy are unknown. Transcriptions of genes participating in autophagy alterations in LUAD patients are needed to perceive the genes participating in autophagy pathways that influence the prognosis of LUAD patients. In LUAD patients, ICRG profiles may be utilized to predict medical care response, quantify risk, and predict OS. Understanding, however, the impact of genes participating in autophagy on LUAD development may invent a biomarker that might be utilized as a therapeutic target The strategy of genes participating in autophagy is shown in **Figure 1**.

This study aimed to form a prognostic model for LUAD prognosis prediction by spotting genes participating in autophagy expression related to LUAD patient prognosis. By better understanding the invasion of genes participating in autophagy and their associated targets, the innovative LUAD therapeutic targets and pharmacologic approaches will be facilitated developing.

Abbreviations: LUAD, lung adenocarcinoma; GO, Gene Ontology; AUC, area under the curve; MF, molecular functions; ICIs, immune checkpoint inhibitors; ROC, receiver operating characteristic; GSEA, gene set enrichment analysis; KEGG, Kyoto Encyclopedia of Genes and Genomes; TCGA, The Cancer Genome Atlas; ICRG, immune checkpoint-related gene; BP, biological processes; CC, cellular components; OS, overall survival; GEO, Gene Expression Omnibus; DEGs, differentially expressed genes.

MATERIALS AND METHODS

Datasets and Genes Participating in Autophagy

LUAD gene expression patterns and clinical data were collected from The Cancer Genome Atlas (TCGA) (14). In October 21, 2021, the expression patterns of 535 instances of LUAD and 59 cases of normal tissues were enrolled in TCGA. The Gene Expression Omnibus (GEO) was searched for micro data on mRNA expression. Series: GSE68465. Platform: GPL570. The GEO was used to maintain the expression patterns of 462 LUAD cases. **Table 1** summarized the clinical features of the patients. In addition, 139 genes participating in autophagy in total were identified from KEGG (https://www.kegg.jp/kegg/) (**Table S1**).

Annotation of Genes

Transcription data and human configuration files were matched and sorted by Perl to obtain the precise mRNA gene expression data. Using information from the ensemble database, the gene IDs were transformed into gene names. The R4.1.0 Limma was used to retrieve the genes participating in autophagy expression data.

Identification of Participating in Autophagy Differentially Expressed Genes and Their Mutation Rate Analysis

False discovery rate (FDR) <0.05 and |log2FC| ≥0.585 were used to evaluate a significant difference in genes participating in autophagy expression. First, the functions of differential genes participating in autophagy that were both upregulated and downregulated [differentially expressed genes (DEGs)] were looked into. The genetic changes of these genes were investigated because of the significant clinical consequences of these genes participating in autophagy. DEG mutation rates were examined using Cbioportal (http://www.cbioportal.org/).

Tumor Classification Based on the Differentially Expressed Genes

First, the prognosis-related genes participating in autophagy were classified into two groups: cluster 1 and cluster 2. Survminer was used to explore the survival of genes participating in autophagy subtypes, and survival was used to evaluate genes participating in autophagy predictive value. The pheatmap was used to construct a heatmap showing the differential expression of genes participating in autophagy in each cluster, and the relationship

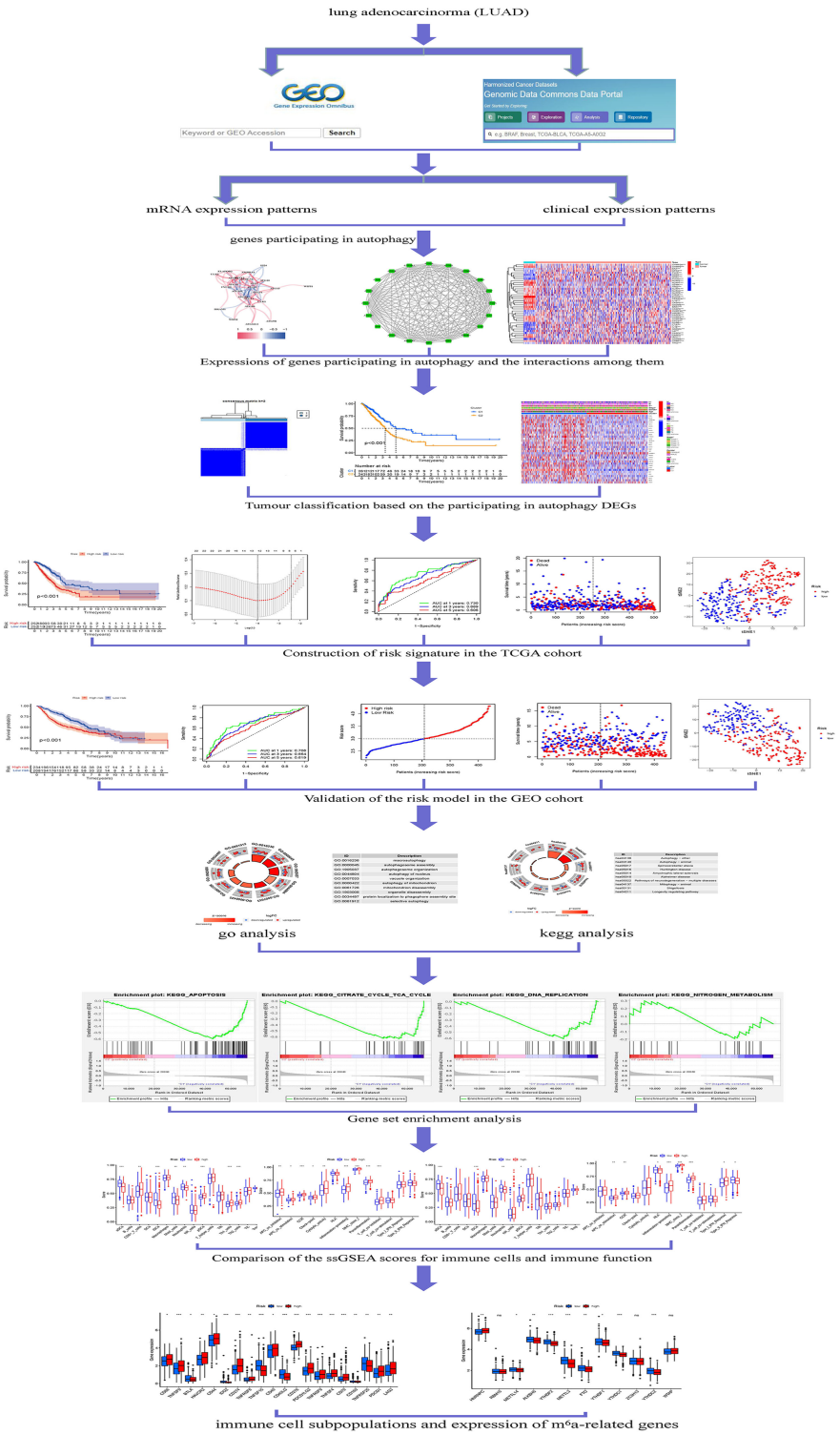

FIGURE 1 | Framework based on an integration strategy of genes participating in autophagy. The data of LUAD patients were obtained from TCGA and GEO databases, and then the autophagy-related genes were matched to carry out difference analysis and risk model construction, respectively. TCGA dataset was used as the main body and GEO dataset was used to verify the model with good grouping, and genes participating in autophagy related to the prognosis of LUAD patients were obtained. Then, Gene Ontology (GO), Kyoto Encyclopedia of Genes and Genomes (KEGG), and gene set enrichment analysis (GSEA) were performed with multiple databases to obtain the functions related to genes participating in autophagy. Last, the immune cells and function were analyzed. *P < 0.05; **P < 0.01; ***P < 0.001.

TABLE 1 | The clinical characteristics of patients.

TCGA		GEO	
Variables	**Number of samples**	**Variables**	**Number of samples**
Gender		Gender	
Male/female	242/280	Male/female/NA	223/220/19
Age at diagnosis		Age at diagnosis	
≤65/>65/NA	241/262/19	≤65/>65	231/212
Stage		Stage	
I/II/III/IV/NA	279/124/85/26/8	I/II/III/IV/NA	Unknown
T		T	
T1/T2/T3/T4/NA	172/281/47/19/3	T1/T2/T3/T4	Unknown
M		M	
M0/M1/NA	353/25/144	M0/M1/NA	Unknown
N		N	
N0/N1/N2/N3/NA	335/98/75/2/12	N0/N1/N2/N3	Unknown

GEO, Gene Expression Omnibus; TCGA, The Cancer Genome Atlas; T, T stage; M, M stage; N, N stage.

between genes participating in autophagy and clinicopathological features was examined. Limma was used to identify differences in the expression of target genes from the appropriate subtypes and tissue types. To explore the gene connection between LUAD target genes and prognostic genes participating in autophagy, Limma and corrplot were employed.

Development of Genes Participating in Autophagy Prognostic Signature

The risk score of every LUAD patient was additionally assessed. The DEGs were split into two classes that supported the median score: low-risk and high-risk. Least absolute shrinkage and selection operator (LASSO) regression was shown to be related to the low- and high-risk classes. Following the image, the boldness interval and risk ratio were computed, and therefore the forest diagram was created. Survival curves for the two groups were generated and compared. To evaluate the accuracy of this model for predicting survival in LUAD, the time dependent receiver operating characteristic curve (timeROC) was used to provide a comparable receiver operating characteristics (ROC) curve. For the chance curve bestowed by the risk score, genes participating in autophagy risk and survival status were examined. The nursing independent prognostic study was carried out to confirm that this model was unaffected by different clinical factors. The relationship between clinical characteristics and risk prediction model was determined, also the relationship between 2 genes participating in autophagy patients. Analyses of risk and clinical relationships were distributed. Additionally, principal component analysis (PCA) and t-distributed stochastic neighbor embedding (T-SNE) were investigated to analyze whether the prognostic model might properly categorize patients into two risk teams. By desegregation of the prognosticative signals, a representation was developed to predict the 1-, 2-, and 3-year OS of LUAD patients.

Functional Enrichment of the Differentially Expressed Genes Participating in Autophagy

The biological pathways associated with TCGA DEGs were then examined using GO. Biological processes (BP), molecular functions (MF), and cellular components (CC) controlled by the DEGs participating in autophagy were further investigated using R software, clusterProfiler, org.Hs.eg.db, enrichplot, and ggplot2 package based on KEGG data.

Gene Set Enrichment Analysis and the Predictive Nomogram

GSEA was used to find related functions and pathway variations in several samples, and Perl was used to import information. The associated score and graphs were wont to verify whether the functions and routes within the numerous risk groups were dynamic. Every sample was classified as "H" or "L" depending on whether it had been a high-risk cluster of prognosis-related genes participating in autophagy.

Comparison of the Immune Activity Between Subgroups

The analysis of single sample gene set enrichment analysis (ssGSEA) was flexible. The enrichment score of immune cells and immune-related activities in the two groups were examined in each TCGA and GEO cohort. Additionally, the connections between genes participating in autophagy, checkpoints, and m^6a were investigated, since these genes participating in autophagy have significant therapeutic implications.

RESULTS

Twenty-five participating in autophagy DEGs similarly to 12 risk genes participating in autophagy were found. GSEA was used to uncover latent signaling pathways involved within the development and progression of LUAD, and LASSO regression was accustomed to build an appropriate prediction model.

Differentially Expressed Genes Participating in Autophagy

Twenty-five DEGs associated with autophagy (17 upregulated, 8 downregulated; **Table S2**) were found (**Figure 2A**). To further examine the interactions of these genes participating in autophagy, a protein–protein interaction (PPI) analysis was

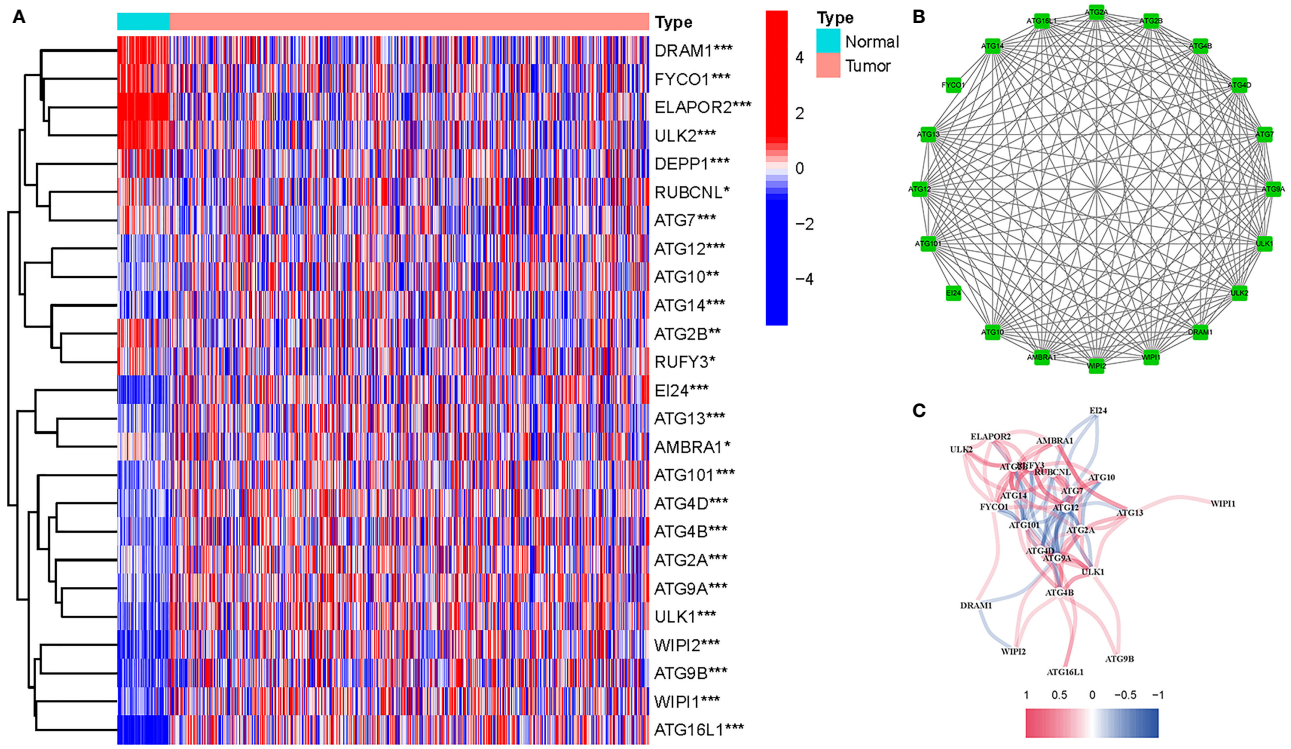

FIGURE 2 | Expressions of the 25 genes participating in autophagy and the interactions among them. **(A)** Heatmap (green: low expression level; red: high expression level) of the genes participating in autophagy between the normal (N, brilliant blue) and the tumor tissues (T, red). P values were shown as *P < 0.05; **P < 0.01; ***P < 0.001. **(B)** PPI network showing the interactions of the genes participating in autophagy (interaction score = 0.4). **(C)** The correlation network of the genes participating in autophagy (red line: positive correlation; blue line: negative correlation. The depth of the colors reflects the strength of the relevance).

conducted, and the results were given in **Figure 2B**. By putting the lowest required interaction value at 0.4, it was found that *ATG14*, *ATG101*, *AMBRA1*, *WIPI1*, *ATG10*, *ULK1*, *ATG7*, *ATG16L1*, *ULK2*, *ATG12*, and *ATG13* were hub genes (**Table S3**). These genes, which comprised all DEGs detected in normal and tumor tissues, may be found to be independent LUAD prognostic indicators. The correlation network, including all genes participating in autophagy, was depicted in **Figure 2C**. It was observed that truncating and missense mutations were the two most prevalent types of mutations (**Figure 3**). A total of nine genes showed a 3% mutation rate, with *WIPI2* being the most often changed (6%).

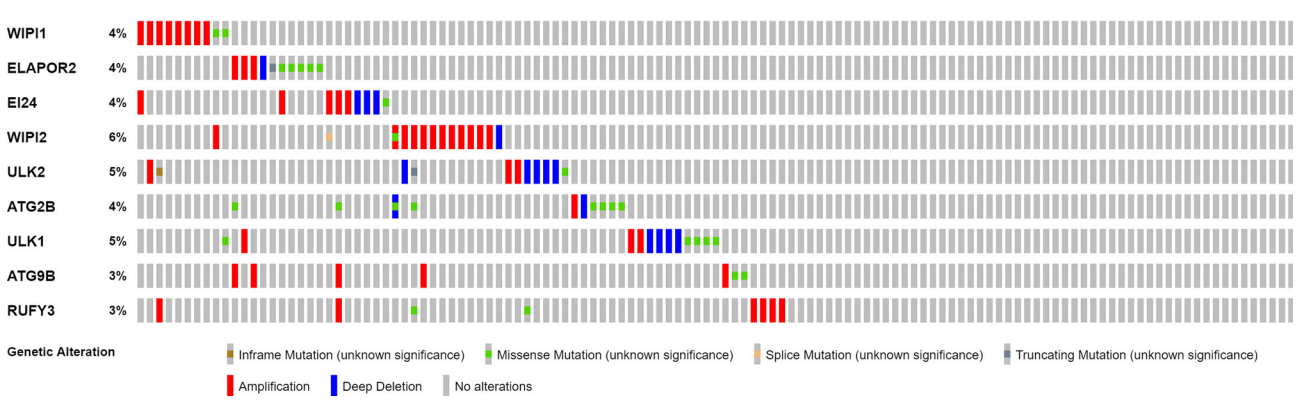

FIGURE 3 | Mutations in genes participating in autophagy. A total of 10 genes have a mutation rate ≥3%.

Tumor Classification Based on the Differentially Expressed Genes

To investigate the links between ATG gene expression and LUAD subtypes, a consensus clustering analysis on all 535 LUAD patients were performed in TCGA dataset. It was discovered that when the clustering variable (k) was set to 2, the intragroup correlations were the highest and the intergroup correlations were the lowest, indicating that the 535 LUAD patients could be separated into two groups based on the genes participating in autophagy (**Figure 4A**). The gene expression profiles and clinical features were shown using a heatmap (**Figure 4B**). A survival study was undertaken to examine the predictive value of genes participating in autophagy utilizing PRG subtypes, and cluster 1 had a higher survival rate ($P < 0.001$), as shown in **Figure 4C**.

Development of a Prognostic Gene Model in The Cancer Genome Atlas Cohort

Here, 22 major genes participating in autophagy were identified throughout the univariate Cox investigation. These genes participating in autophagy were discovered as independent LUAD prognostic markers (*GJB3*, *KRT6A*, *IRX5*, *RGS20*, *ARNTL2*, *CERS4*, *SLC2A1*, *KYNU*, *IGFBP1*, *RHOF*, *CMAHP*, *DKK1*, *FOSL1*, *PKP2*, *PLEK2*, *GAPDH*, *VEGFC*, *LYPD3*, *FLNC*, *TNS4*, *NTSR1*, *PLEKHB1*) (**Figure 5A**). A gene signature was created using the LASSO Cox regression analysis and the optimal value (**Figures 5B, C**). Employing a risk survival standing plot, it was tended to discover that a patient's risk score was negatively connected to LUAD patients' survival. The presence of high-risk PRG signatures were linked with a decreased chance of survival ($P < 0.001$; **Figure 5E**). For 1-, 2-, and 3-year survival rates, the AUC predictive value of the unique NRG signature was 0.730, 0.689, and 0.606, respectively (**Figure 5F**). PCA and t-SNE results showed that patients with varying risks were divided into two groups (**Figures 5G, H**).

External Validation of the Risk Signature

A total of 462 LUAD patients from a GEO cohort were enclosed within the validation group. It was tended to discover that a patient's risk score was negatively associated with LUAD patients' survival. Amazingly, similar with TCGA findings, the bulk of the novel genes participating in autophagy discovered during this study was adversely linked with this risk model (**Figure 6A**). High-risk PRG signatures were joined with a lower probability of survival ($P < 0.001$; **Figure 6B**). The AUC predictive value of the distinctive genes participating in autophagy signature was 0.708, 0.664, and 0.619 for 1-, 2-, and 3-year survival rates, respectively (**Figure 6C**). The results of PCA and t-SNE discovered that patients with varied risks were well divided into two groups (**Figures 6D, E**).

Independent Prognostic Value of the Risk Model

In TCGA cohort, Cox analysis demonstrated that the genes participating in autophagy signature [hazard ratio (HR): 2.696, 95% CI: 2.001–3.632] were primarily independent predictive variables for the OS of LUAD patients (**Figures 7A, B**). In the GEO cohort, Cox analysis demonstrated that the genes participating in autophagy signature (HR: 1.921, 95% CI:

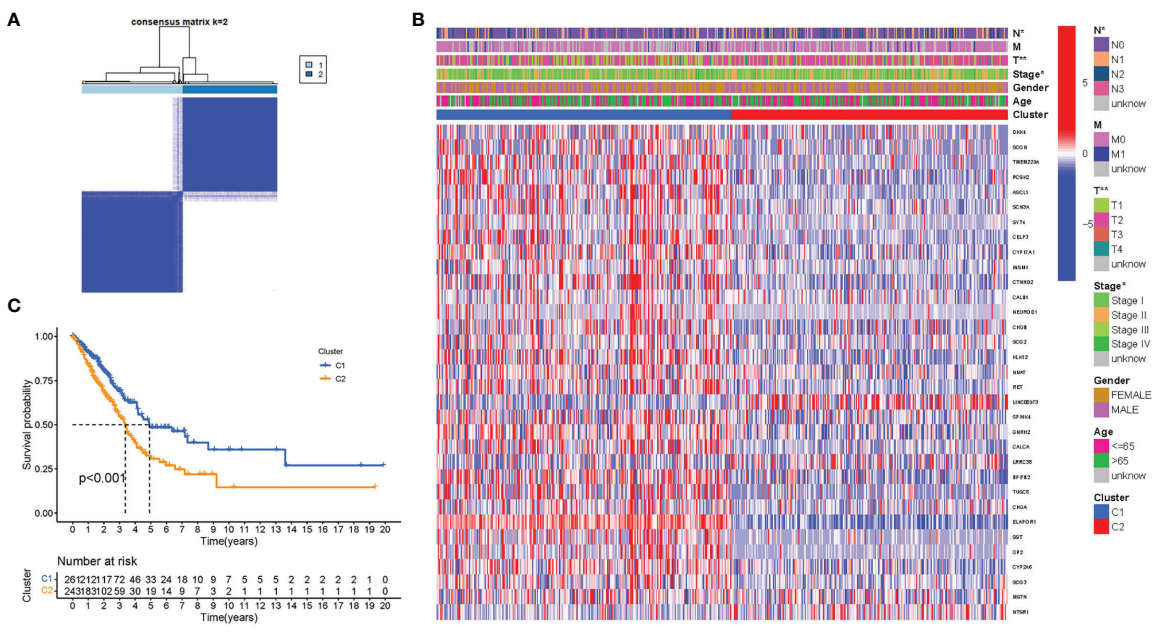

FIGURE 4 | Tumor classification based on the participating in autophagy DEGs. **(A)** Here, 535 LUAD patients were grouped into two clusters according to the consensus clustering matrix (k = 2). **(B)** Heatmap. Heatmap and the clinicopathologic characters of the two clusters classified by these DEGs (T, N, and Stage are the degree of tumor differentiation. **(C)** Kaplan–Meier OS curves for the two clusters.

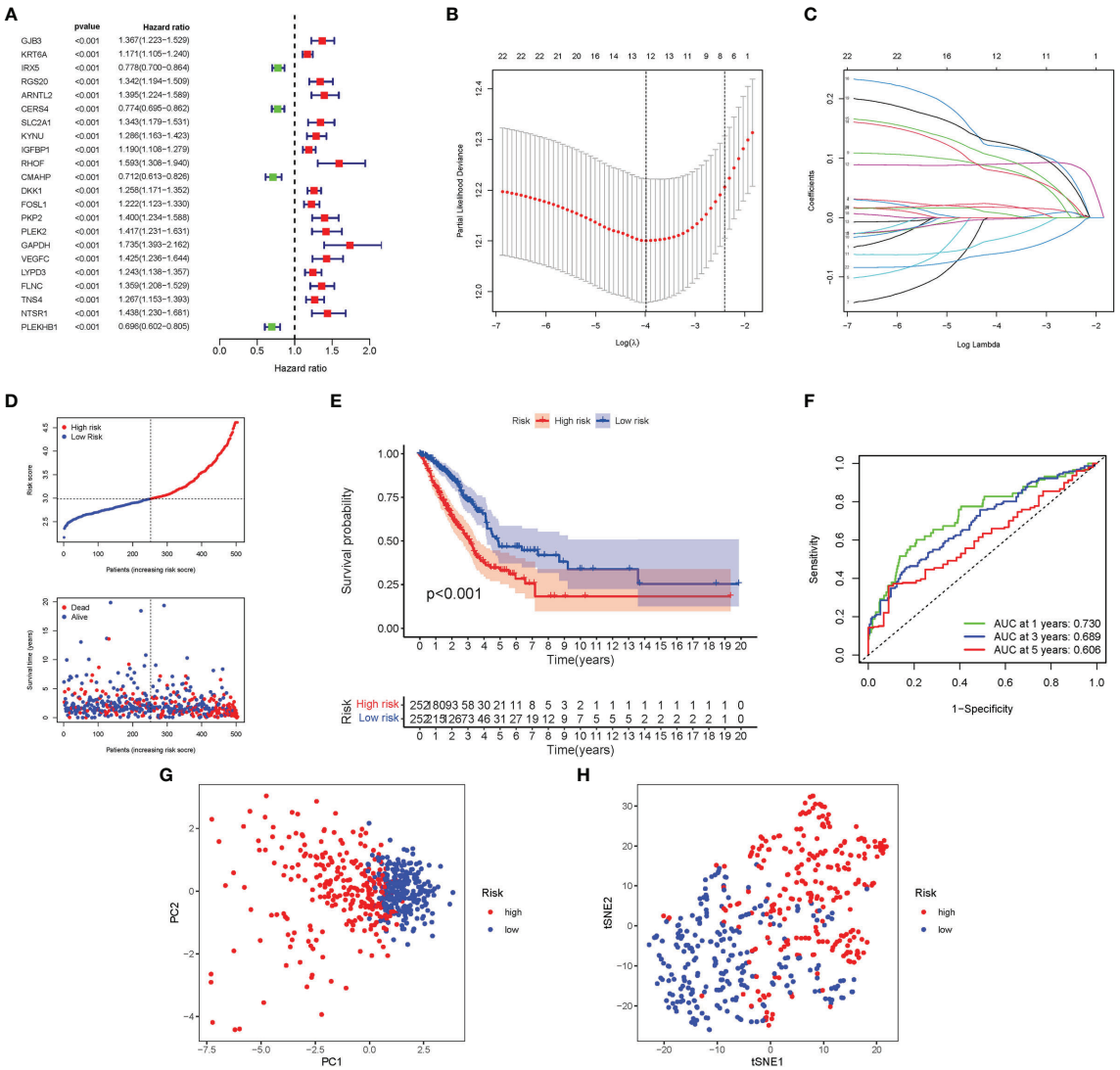

FIGURE 5 | Construction of risk signature in the TCGA cohort. **(A)** A univariate Cox regression analysis of OS for each participating in autophagy gene and 22 genes with P < 0.01. **(B)** LASSO regression of the 22 OS-related genes. **(C)** Cross-validation for tuning the parameter selection in the LASSO regression. **(D)** The survival status for each patient (low-risk population: on the left side of the dotted line; high-risk population: on the right side of the dotted line). **(E)** Kaplan–Meier curves for the OS of patients in the high- and low-risk groups. **(F)** The AUC of the prediction of 1-, 2-, 3-year survival rate of LUAD. **(G)** PCA plot for LUADs based on the risk score. **(H)** t-SNE plot for LUADs based on the risk score.

1.455–2.537), age (HR: 1.029, 95% CI: 1.016–1.043), and gender (HR: 0.761, 95% CI: 0.587–0.987) were primarily independent predictive variables (**Figures 7C, D**). In addition, for TCGA cohort, a heatmap of clinical characteristics was constructed (**Figure 7E** and **Table S4**).

Enrichment Analysis of Genes Participating in Autophagy

In TCGA cohort, 25 DEGs were discovered between the two groups. GO enrichment analysis revealed 91 core targets, including BP, MF, and CC. The MF mainly involved phospholipid binding (GO:0005543), phosphatidylinositol binding (GO:0035091), and protein serine kinase activity (GO:0106310). The CC mainly involved vacuolar membrane (GO:0005774), endocytic vesicle (GO:0030139), and extrinsic component of membrane (GO:0019898). The BP mainly involved response to extracellular stimulus (GO:0009991), cell growth (GO:0016049), and response to nutrient levels (GO:0031667). In addition, the main signaling pathways were identified by KEGG enrichment analysis, revealing that the overexpressed genes were mainly involved in pathways of neurodegeneration-multiple diseases (hsa05022), amyotrophic lateral sclerosis (hsa05014), autophagy-other (hsa04136), and autophagy-animal (hsa04140) (**Figure 8** and **Table S5**).

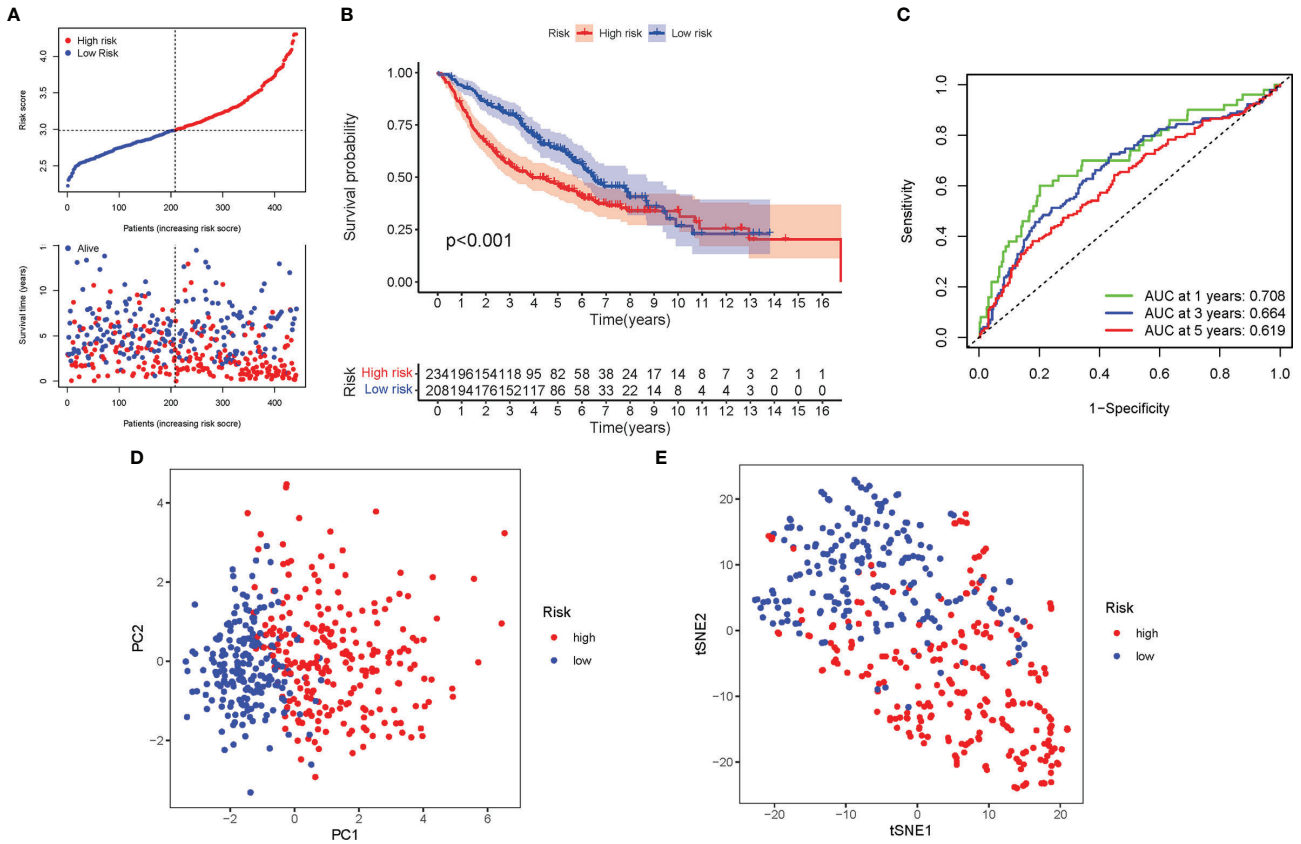

FIGURE 6 | Validation of the risk model in the GEO cohort. **(A)** The survival status for each patient (low-risk population: on the left side of the dotted line; high-risk population: on the right side of the dotted line). **(B)** Kaplan–Meier curves for the OS of patients in the high- and low-risk groups. **(C)** The AUC of the for the prediction of 1-, 2-, 3-year survival rate of LUAD. **(D)** PCA plot for LUADs based on the risk score. **(E)** t-SNE plot for LUADs based on the risk score.

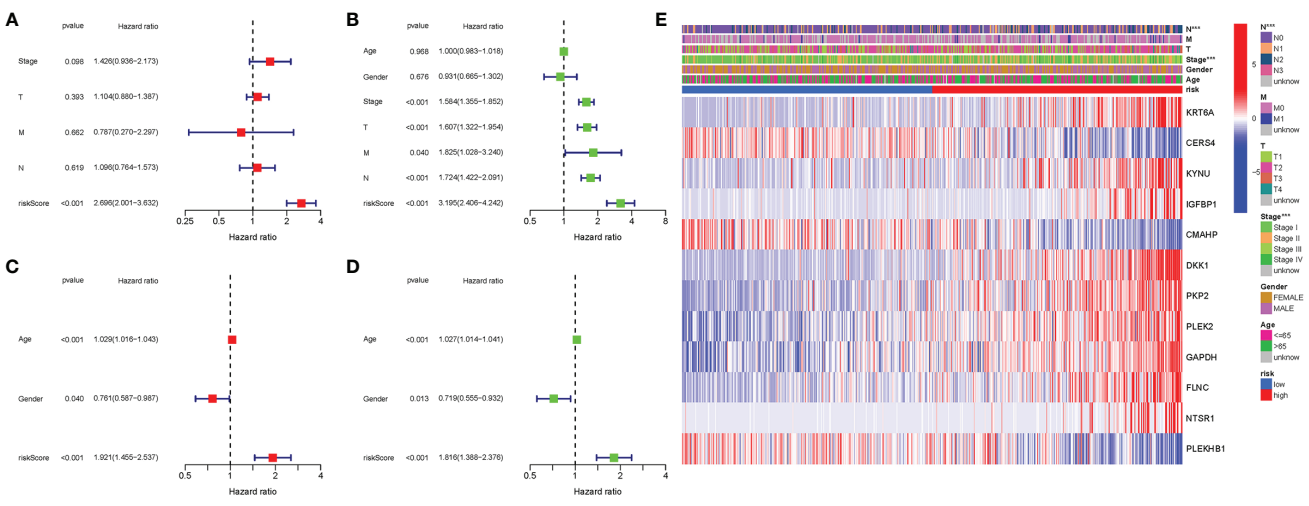

FIGURE 7 | Univariate and multivariate Cox regression analyses. **(A)** Multivariate analysis for TCGA cohort. **(B)** Univariate analysis for TCGA cohort (T, M, N, Stage: the degree of tumor differentiation). **(C)** Multivariate analysis for the GEO cohort. **(D)** Univariate analysis for the GEO cohort (Age, Gender). **(E)** Heatmap (green: low expression; red: high expression) for the connections between clinicopathologic features and the risk groups. ***P < 0.001.

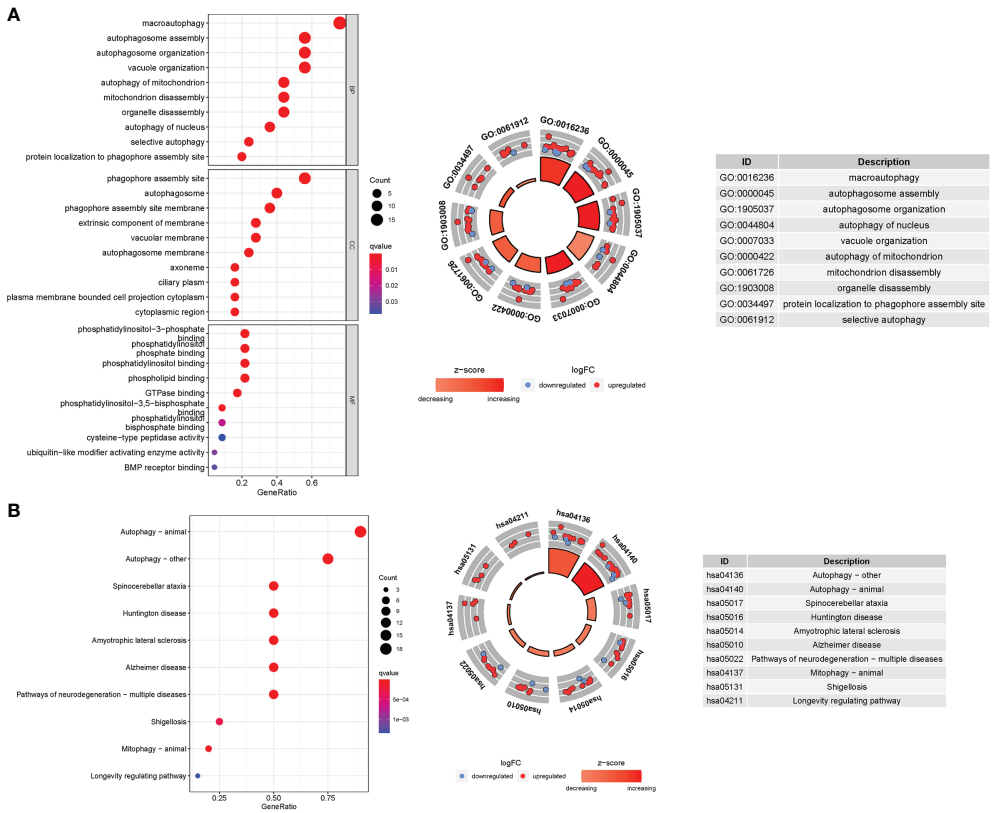

FIGURE 8 | GO and KEGG analyses for genes participating in autophagy. **(A)** Bubble graph for GO enrichment (the bigger bubble means the more genes enriched, and the increasing depth of red means the differences were more obvious; q-value: the adjusted P value). The GO circle shows the scatter map of the logFC of the specified gene. **(B)** Barplot graph for KEGG pathways (the longer bar means the more genes enriched, and the increasing depth of red means the differences were more obvious). The KEGG circle shows the scatter map of the logFC of the specified gene. The higher the Z-score value indicated, the higher expression of the enriched pathway.

Gene Set Enrichment Analyses

According to GSEA, the majority of genes participating in autophagy prognostic signature regulated immune and tumor-related pathways such as glycosaminoglycan biosynthesis chondroitin sulfate, extracellular matrix (ECM) receptor interaction, allograft rejection, Hedgehog (Hh) signaling pathway, and notch signaling pathway. The top 6 enriched functions or pathways for each cluster were shown in **Figure 9** and **Table S6**. The "hedgehog signaling pathway" was the most enriched, and some of the genes were positively correlated with H or L.

Comparison of the Immune Activity Between Subgroups

The enrichment scores of 16 kinds of immune cells and the activity of 13 immune-related functions across the low- and high-risk groups in two cohorts (ssGSEA) were evaluated. *aDCs*, *iDCs*, *Neutrophils*, *pDCs*, and *Tfh* infiltrated at a greater rate in the high-risk subgroup (**Figure 10A**). APC costimulation, CCR, HLA, Inflammation-promoting, MHC class I, Parainflammation, Type I IFN Response, and Type II IFN Response were usually more significant in the high-risk group (**Figure 10B**). Similar findings were reached when examining the immunological state of the GEO cohort (**Figures 10C, D**).

Analysis of the Correlation Between Genes Participating in Autophagy With Immune Checkpoints and m^{6}a

Given the importance of checkpoint inhibitor-based immunotherapies, it was considered whether there were any changes in immune checkpoint expression between the two groups. The expression of *TNFSF9*, *IDO2*, *CD274*, *TNFSF15*, *CD40LG*, *CD276*, and other genes differed significantly between the two patient groups (**Figure 11A**). When PRG expression was examined, the relationship of m^{6}a and genes participating in autophagy, *YTHDF2*, *METTL3*, *YTHDC1*, *YTHDC2*, *HNRNPC*, *METTL14*, *ALKBH5*, *FTO*, and *YTHDF1*, was substantially more significant in the high-risk group (**Figure 11B**).

DISCUSSION

LUAD therapy may be a significant therapeutic downside due to its severe condition and poor prognosis (15, 16). The molecular

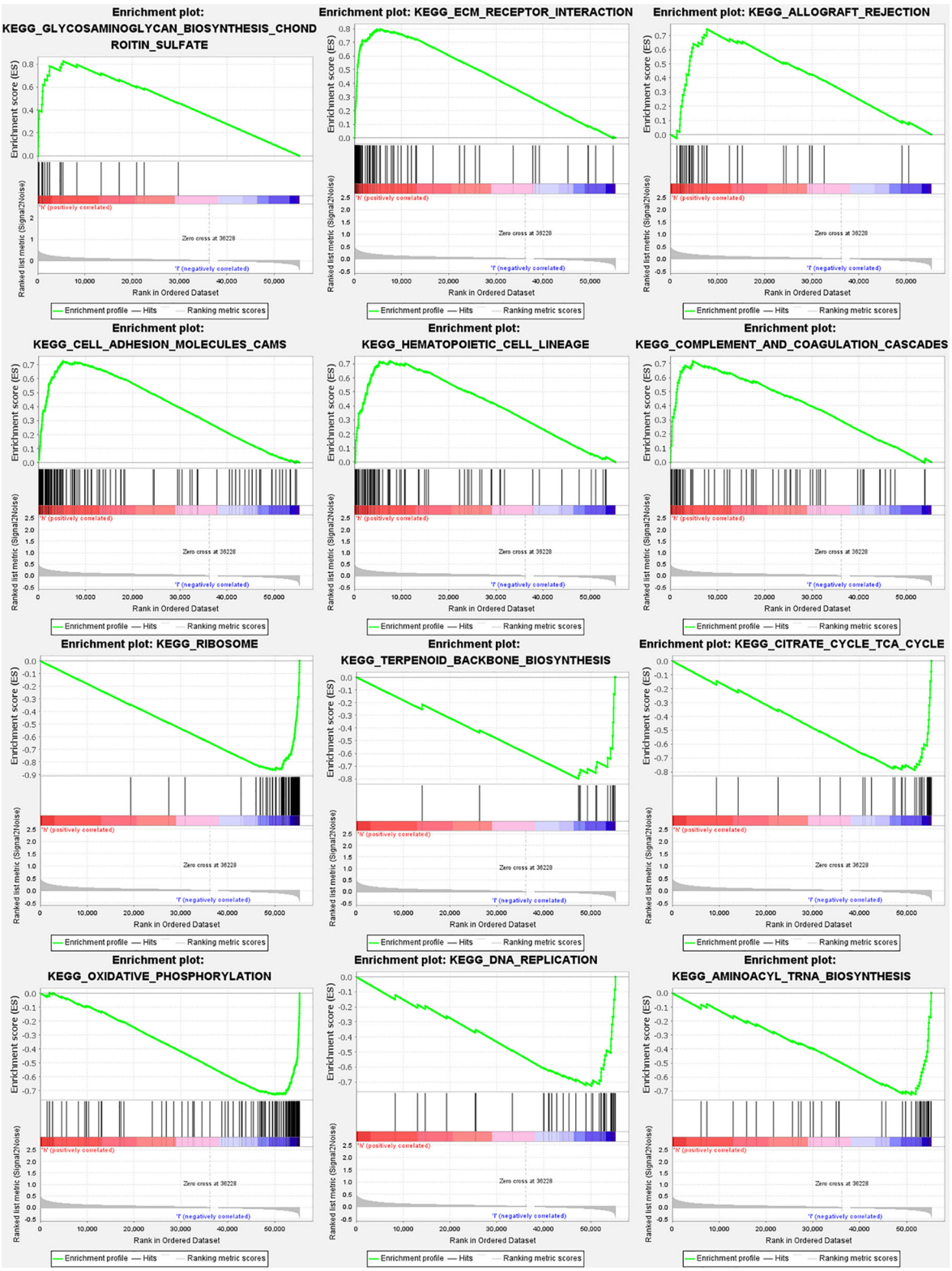

FIGURE 9 | Gene set enrichment analyses for genes participating in autophagy. To clarify the difference of related function or pathway in different samples, the top 6 enriched functions or pathways of each cluster were listed. The most enriched pathway was the Hedgehog signaling pathway. Both FDR q-value and FWER P value were <0.05.

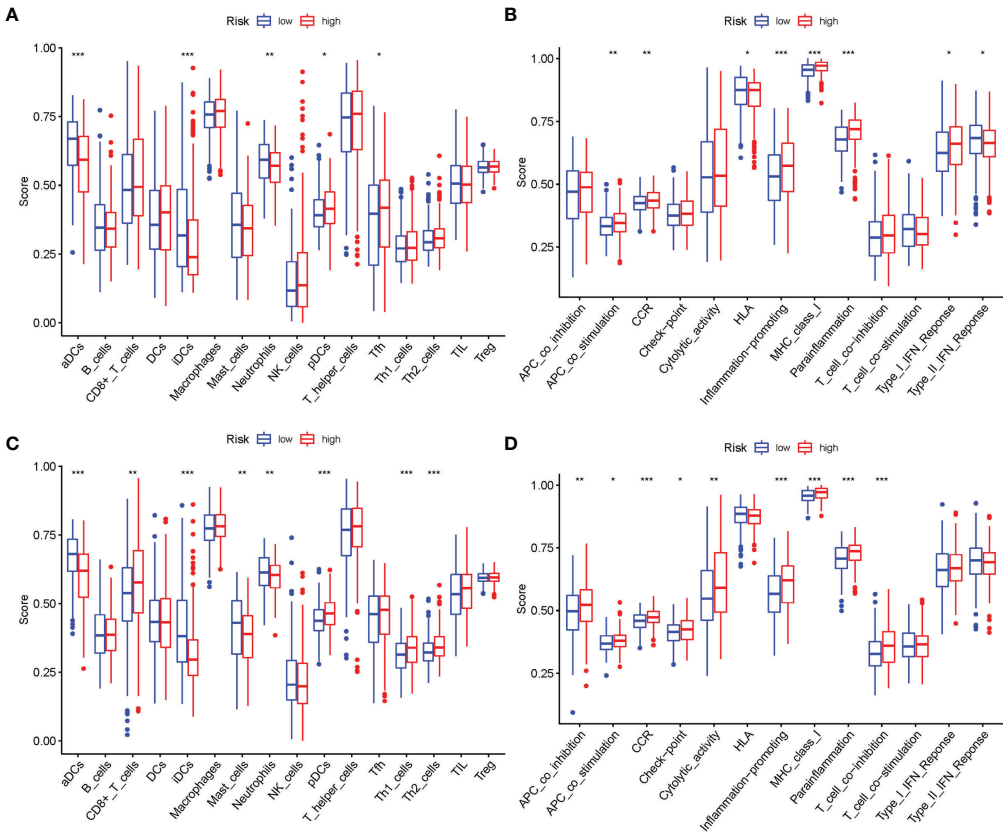

FIGURE 10 | Comparison of the ssGSEA scores. **(A, B)** Comparison of the enrichment scores of 16 types of immune cells and 13 immune-related pathways between low-risk (green box) and high-risk (red box) group in TCGA cohort. **(C, D)** Comparison of the tumor immunity between low-risk (blue box) and high-risk (red box) group in the GEO cohort. *P < 0.05; **P < 0.01; ***P < 0.001.

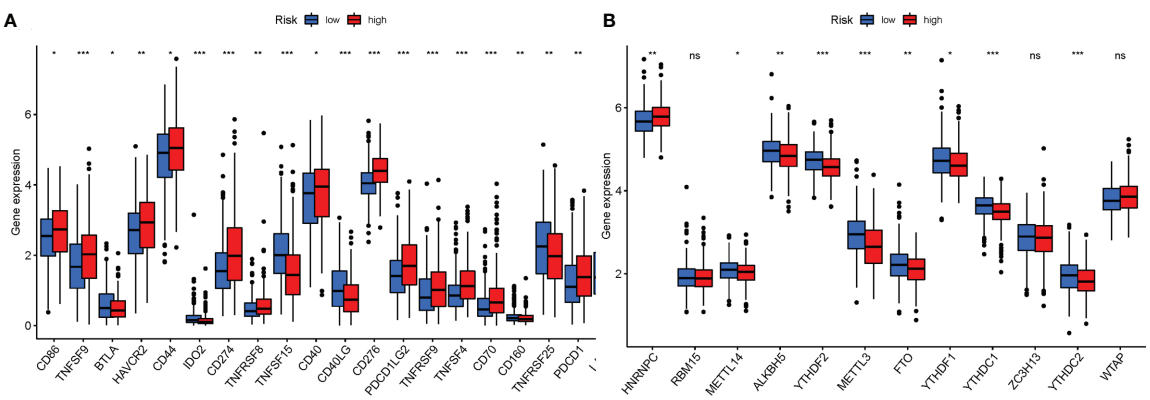

FIGURE 11 | **(A)** Expression of immune checkpoints among high and low LUAD risk groups. **(B)** The expression of m^6a-related genes between high and low LUAD risk groups. P values were shown as ns, not significant; *P < 0.05; **P < 0.01; ***P < 0.001.

identification of diagnostic biomarkers and treatment targets for LUAD ought to be promoted at all times. Previous studies have shown that autophagy is concerned with the abnormal cell death related to LUAD (17, 18). Genes participating in autophagy can perform as a tumor suppressor, making them a promising cancer medical care approach (19). It is unknown, however, how it affects LUAD formation *via* dominant genes participating in autophagy. This study aimed to develop a predictive model by

identifying genes participating in autophagy with expressions connected to LUAD patient prognosis.

Several RNAs in LUAD were found to be related to autophagy during this investigation. Following that, 25 DEGs coupled to autophagy were tended to know. Using the information on prognosis-related genes, the confidence interval and HR were calculated to examine their potential roles in LUAD. In a univariate Cox regression analysis, genes participating in autophagy were shown to be considerably associated with LUAD prognosis. The researchers identified 12 prognostic genes participating in autophagy that expressed differentially in different groups. Some genes participating in autophagy were discovered to be overexpressed at high risk. Others, on the other hand, were overexpressed in low risk ($P < 0.05$). It was tended to investigate a lot of into the role of genes participating in autophagy in LUAD. The prognostic significance of genes participating in autophagy was determined by employing a survival analysis supported gene subtypes. *KRT6A*, *KYNU*, *IGFBP1*, *DKK1*, *PKP2*, *PLEK2*, *GAPDH*, *FLNC*, and *NTSR1* were all overexpressed in insecure areas people, indicating that they may be related to the oncology process for LUAD patients; they seemed to be cancer-promoting genes. Our results on the above genes provide some insights for further research, but there is still no conclusive evidence that they are involved in the expression of specific transcription factors related to autophagy regulation, such as TFEB, HSF1, and FOXO3, which requires further investigation. *CERS4*, *CMAHP*, and *PLEKHB1* were found to be considerably expressed in low-risk people, suggesting that they are associated with a low risk in LUAD patients. The previously discovered genes participating in autophagy may be used as a therapeutic target for LUAD. Furthermore, within the LUAD analysis, genes participating in autophagy were coupled to patient outcomes. The OS and ROC analysis of the GSE68465 Kaplan–Meier curves indicated that a participating in autophagy signature might be an independent prognostic predictor. Solely a little amount of study has been conducted on the cistron alterations related to autophagy. Many more studies are needed to comprehend the NRG alteration and identification method and to validate the findings in this study.

Following that, KEGG analysis revealed that the genes were primarily concerned in amyotrophic lateral sclerosis, autophagy-other, and autophagy-animal. As a result, autophagy plays a vital role in LUAD. The Hh signal pathway was discovered to be the significant well-enriched route in GSEA. In invertebrates, the Hh pathway regulates sophisticated biological processes. As a result of the abnormal Hh pathway, activation is chargeable for carcinogenesis and cancer maintenance during a type of malignancies; addressing this provides a viable therapeutic opportunity (20). The Hh sign has been shown to suppress autophagy in normal and cancer cells from various tissue sources (21, 22) and has been shown in many investigations to activate autophagy. The Hh antagonist cyclopamine, for instance, reserved autophagy activation within the neuroblastoma cell line SHSY5Y (23). By bidirectionally regulation autophagy, the Hh sign influences a range of tissue origins. The findings listed above were under consideration. Genes participating in autophagy could influence LUAD cell migration and proliferation *via* modulating the Hh signaling pathway. Furthermore, methods in this study can accurately predict the survival of LUAD patients. An increase within the risk score is related to a rise in mortality and high-risk ratio. The conception could be utilized in a variety of therapeutic contexts. Genes participating in autophagy seem to be a potential biomarker for predicting LUAD patient outcomes, supporting literature findings and information.

Furthermore, the connections between genes participating in autophagy, immune cells, immunological function, immune checkpoints, and m^6a were investigated and examined. Recent studies have discovered an affiliation between completely different cell death mechanisms and anticancer immunity (24, 25). Within the recent decade, immune checkpoint inhibitors (ICIs) have transformed cancer treatment. They are monoclonal antibodies, and those targeting programmed death 1 (PD-1) or PD-1 ligand (PD-L1) are accustomed treat LUAD (26). In ICI-resistant tumors, activating pyroptosis, ferroptosis, and necroptosis in conjunction with ICIs resulted in synergistically increased anticancer effectiveness (27, 28). By targeting Atg5 and Atg7 within the m^6a-YTHDF2-dependent mechanism, FTO Alpha-Ketoglutarate Dependent Dioxygenase (FTO) plays a conservative and vital function in promoting autophagy and adipogenesis (29). A microscopic investigation of the connection between ICI, m^6a, and pyrolysis has been conducted. Even though there has been very little analysis on genes participating in autophagy and LUAD, supported by the information presented above, it could be concluded that ARG alterations were associated with the onset and development of LUAD.

Although it is offered for theoretical underpinnings and analysis recommendations, this study has its limitations. First, it was tended to develop a validated genes participating in autophagy prediction signature exploitation of TCGA and GEO datasets. We tend to be unable to gather sufficient external information from different publicly offered sources to evaluate the model's dependableness. Second, we tend to center on the signature's 12 risk genes participating in autophagy in the early expression study. Despite this, no additional functional or mechanical analysis was conducted. Finally, no LUAD studies were conducted to substantiate the link between prognostic genes and shift. However, to completely grasp the facts declared above, we tend to conduct additional analysis.

CONCLUSIONS

In conclusion, 12 expected genes participating in autophagy were found in LUAD patients as part of the autophagy regulation. It provides LUAD with a high degree of predictability. These findings contribute to an improved understanding of the connection between immunological, m^6a, and autophagy, maybe paving the way for new therapeutic targets and prognostic indicators. It is hoped that the findings will aid in discovering genes participating in autophagy that promote LUAD growth, permitting us to learn additional concerning their potential role within the development and progression.

DATA AVAILABILITY STATEMENT

The original contributions presented in the study are included in the article/**Supplementary Material**. Further inquiries can be directed to the corresponding author.

ETHICS STATEMENT

This article is not a clinical trial; hence, the ethics approval and consent to participation are not applicable.

AUTHOR CONTRIBUTIONS

ZX-W drafted and revised the article. XH and M-JC were in charge of data collection. P-DH conceived and designed this article, was in charge of syntax modification, and revised the article. ZG revised the article. All the authors have read and agreed to the final version of the article.

FUNDING

This work was supported by the Health and Health Commission of Yunnan Province 2020 High-level TCM Reserve Talents Incubation Project (Yunwei TCM Development [2021] No. 1); The second round of construction project of The National Traditional Chinese Medicine School Heritage Studio of the State Administration of Traditional Chinese Medicine (National Traditional Chinese Medicine Teaching Letter [2019] 62); and Scientific and Technological Innovation Team of Acupuncture and Moxibustion Prevention and Treatment of Mental Disorders in Yunnan Colleges and Universities (No.: 2019YGC04).

ACKNOWLEDGMENTS

Thanks to Professor Huang for his strict guidance on this paper and thanks to Miss Huang and Miss Cai for their support on this paper. Thanks to the reviewers and editors for their sincere comments.

SUPPLEMENTARY MATERIAL

The Supplementary Material for this article can be found online at: https://www.frontiersin.org/articles/10.3389/fonc.2021.799759/full#supplementary-material

REFERENCES

1. Wu G, Jochems A, Refaee T, Ibrahim A, Yan C, Sanduleanu S, et al. Structural and Functional Radiomics for Lung Cancer. *Eur J Nucl Med Mol Imaging* (2021) 48(12):3961–74. doi: 10.1007/s00259-021-05242-1
2. Rodriguez-Canales J, Parra-Cuentas E, Wistuba II. Diagnosis and Molecular Classification of Lung Cancer. *Cancer Treat Res* (2016) 170:25–46. doi: 10.1007/978-3-319-40389-2_2
3. Pennell NA, Arcila ME, Gandara DR, West H. Biomarker Testing for Patients With Advanced Non-Small Cell Lung Cancer: Real-World Issues and Tough Choices. American Society of Clinical Oncology Educational Book. *Am Soc Clin Oncol Annu Meeting* (2019) 39:531–42. doi: 10.1200/EDBK_237863
4. van de Ven M, Koffijberg H, Retèl V, Monkhorst K, Smit E, van Harten W, et al. Real-World Utilization of Biomarker Testing for Patients With Advanced Non-Small Cell Lung Cancer in a Tertiary Referral Center and Referring Hospitals. *J Mol Diag* (2021) 23(4):484–94. doi: 10.1016/j.jmoldx.2021.01.004
5. Song B, Yan X, Li R, Zhang H. Ghrelin Ameliorates Chronic Obstructive Pulmonary Disease-Associated Infllammation and Autophagy. *Biotechnol Appl Biochem* (2020) 68(2):356–65. doi: 10.1002/bab.1933
6. Zhao H, Wang Y, Qiu T, Liu W, Yao P. Autophagy, an Important Therapeutic Target for Pulmonary Fibrosis Diseases. *Clinica Chimica Acta; Int J Clin Chem* (2020) 502:139–47. doi: 10.1016/j.cca.2019.12.016
7. Ohsumi Y. Yoshinori Ohsumi: Autophagy From Beginning to End. Interview by Caitlin Sedwick. [Interview]. *J Cell Biol* (2012) 197(2):164–5. doi: 10.1083/jcb.1972pi
8. May AI, Prescott M, Ohsumi Y. Autophagy Facilitates Adaptation of Budding Yeast to Respiratory Growth by Recycling Serine for One-Carbon Metabolism. *Nat Commun* (2020) 11(1):5052. doi: 10.1038/s41467-020-18805-x
9. Adachi A, Koizumi M, Ohsumi Y. Autophagy Induction Under Carbon Starvation Conditions Is Negatively Regulated by Carbon Catabolite Repression. *J Biol Chem* (2017) 292(48):19905–18. doi: 10.1074/jbc.M117.817510
10. Liao SX, Sun PP, Gu YH, Rao XM, Zhang LY, Ou-Yang Y. Autophagy and Pulmonary Disease. *Ther Adv Respir Dis* (2019) 13:1023341718 doi: 10.1177/1753466619890538
11. Sun S, Shen Y, Wang J, Li J, Cao J, Zhang J. Identification and Validation of Autophagy-Related Genes in Chronic Obstructive Pulmonary Disease. *Int J Chronic Obstruct Pulmon Dis* (2021) 16:67–78. doi: 10.2147/COPD.S288428
12. Jain P, Jain C, Velcheti V. Role of Immune-Checkpoint Inhibitors in Lung Cancer. *Ther Adv Respir Dis* (2018) 12:1825482181. doi: 10.1177/1753465817750075
13. Maung TZ, Ergin HE, Javed M, Inga EE, Khan S. Immune Checkpoint Inhibitors in Lung Cancer: Role of Biomarkers and Combination Therapies. *Cureus* (2020) 12(5):e8095. doi: 10.7759/cureus.8095
14. Wang Z, Jensen MA, Zenklusen JC. A Practical Guide to The Cancer Genome Atlas (TCGA). *Methods Mol Biol (Clifton NJ)* (2016) 1418:111–41. doi: 10.1007/978-1-4939-3578-9_6
15. Nasim F, Sabath BF, Eapen GA. Lung Cancer. *Med Clinics North America* (2019) 103(3):463–73. doi: 10.1016/j.mcna.2018.12.006
16. D'Amico AG, Maugeri G, Rasà DM, Reitano R, Saccone S, Federico C, et al. Modulatory Role of PACAP and VIP on HIFs Expression in Lung Adenocarcinoma. *Peptides* (2021) 146:170672. doi: 10.1016/j.peptides.2021.170672
17. Liu G, Pei F, Yang F, Li L, Amin AD, Liu S, et al. Role of Autophagy and Apoptosis in Non-Small-Cell Lung Cancer. *Int J Mol Sci* (2017) 18(2). doi: 10.3390/ijms18020367
18. Liu Y, Wu L, Ao H, Zhao M, Leng X, Liu M, et al. Prognostic Implications of Autophagy-Associated Gene Signatures in Non-Small Cell Lung Cancer. *Aging* (2019) 11(23):11440–62. doi: 10.18632/aging.102544
19. Chen X, Mao R, Su W, Yang X, Geng Q, Guo C, et al. Circular RNA Circhipk3 Modulates Autophagy *via* MIR124-3p -STAT3-PRKAA/Ampkα Signaling in STK11 Mutant Lung Cancer. *Autophagy* (2019) 16(4):659–71. doi: 10.1080/15548627.2019.1634945
20. Zeng X, Ju D. Hedgehog Signaling Pathway and Autophagy in Cancer. *Int J Mol Sci* (2018) 19(8). doi: 10.3390/ijms19082279
21. Jimenez-Sanchez M, Menzies FM, Chang Y-Y, Simecek N, Neufeld TP, Rubinsztein DC. The Hedgehog Signalling Pathway Regulates Autophagy. *Nat Commun* (2012) 3(1):1200. doi: 10.1038/ncomms2212

22. Rouschop KMA, van den Beucken T, Dubois L, Niessen H, Bussink J, Savelkouls K, et al. The Unfolded Protein Response Protects Human Tumor Cells During Hypoxia Through Regulation of the Autophagy Genes MAP1LC3B and ATG5. *J Clin Invest* (2010) 120(1):127–41. doi: 10.1172/JCI40027
23. Milla LA, González-Ramírez CN, Palma V. Sonic Hedgehog in Cancer Stem Cells: A Novel Link With Autophagy. *Biol Res* (2012) 45(3):223–30. doi: 10.4067/S0716-97602012000300004
24. Kuo C-J, Hansen M, Troemel E. Autophagy and Innate Immunity: Insights From Invertebrate Model Organisms. *Autophagy* (2018) 14(2):233–42. doi: 10.1080/15548627.2017.1389824
25. Pardoll DM. The Blockade of Immune Checkpoints in Cancer Immunotherapy. *Nat Rev Cancer* (2012) 12(4):252–64. doi: 10.1038/nrc3239
26. Sławiński G, Wrona A, Dąbrowska-Kugacka A, Raczak G, Lewicka E. Immune Checkpoint Inhibitors and Cardiac Toxicity in Patients Treated for Non-Small Lung Cancer: A Review. *Int J Mol Sci* (2020) 21(19):7195. doi: 10.3390/ijms21197195
27. Tang R, Xu J, Zhang B, Liu J, Liang C, Hua J, et al. Ferroptosis, Necroptosis, and Pyroptosis in Anticancer Immunity. *J Hematol Oncol* (2020) 13(1):110. doi: 10.1186/s13045-020-00946-7
28. Hsu SK, Li C, Lin IL, Syue WJ, Chen YF, Cheng KC, et al. Inflammation-Related Pyroptosis, a Novel Programmed Cell Death Pathway, and Its Crosstalk With Immune Therapy in Cancer Treatment. *Theranostics* (2021) 11(18):8813–35. doi: 10.7150/thno.62521
29. Wang X, Wu R, Liu Y, Zhao Y, Bi Z, Yao Y, et al. m6A mRNA Methylation Controls Autophagy and Adipogenesis by Targeting Atg5 and Atg7. *Autophagy* (2020) 16(7):1221–35. doi: 10.1080/15548627.2019.1659617

Conflict of Interest: The authors declare that the research was conducted in the absence of any commercial or financial relationships that could be construed as a potential conflict of interest.

frontiers in Oncology

ORIGINAL RESEARCH
published: 26 January 2022
doi: 10.3389/fonc.2021.808300

Role of CD133/NRF2 Axis in the Development of Colon Cancer Stem Cell-Like Properties

Jimin Park[1], *Seung Ki Kim*[1], *Steffanus Pranoto Hallis*[1], *Bo-Hyun Choi*[2] *and Mi-Kyoung Kwak*[1,3,4*]

[1] Department of Pharmacy and BK21FOUR Advanced Program for SmartPharma Leaders, Graduate School of The Catholic University of Korea, Gyeonggi-do, South Korea, [2] Department of Pharmacology, School of Medicine, Daegu Catholic University, Daegu, South Korea, [3] Integrated Research Institute for Pharmaceutical Sciences, The Catholic University of Korea, Gyeonggi-do, South Korea, [4] College of Pharmacy, The Catholic University of Korea, Gyeonggi-do, South Korea

Cancer stem cells (CSCs) exhibit intrinsic therapy/stress resistance, which often cause cancer recurrence after therapy. In this study, we investigated the potential relationship between the cluster of differentiation (CD)-133, a CSC marker of colon cancer, and nuclear factor erythroid 2-like 2 (NFE2L2; NRF2), a master transcription factor for the regulation of multiple antioxidant genes. In the first model of CSC, a sphere culture of the colorectal cell line HCT116, showed increased levels of CD133 and NRF2. Silencing of *CD133* reduced the levels of CSC markers, such as Kruppel-like factor 4 (KLF4) and ATP-binding cassette subfamily G member 2 (ABCG2), and further suppressed the expression levels of NRF2 and its target genes. As a potential molecular link, CD133-mediated activation of phosphoinositide 3-kinase/serine-threonine kinase (PI3K/AKT) signaling appears to increase the NRF2 protein levels *via* phosphorylation and the consequent inhibition of glycogen synthase kinase (GSK)-3β. Additionally, *NRF2*-silenced HCT116 cells showed attenuated sphere formation capacity and reduced CSC markers expression, indicating the critical role of the NRF2 pathway in the development of CSC-like properties. As a second model of CSC, the $CD133^{high}$ cell population was isolated from HCT116 cells. CSC-like properties, including sphere formation, motility, migration, colony formation, and anticancer resistance, were enhanced in the $CD133^{high}$ population compared to $CD133^{low}$ HCT116 cells. Levels of NRF2, which were elevated in $CD133^{high}$ HCT116, were suppressed by *CD133*-silencing. In line with these, the analysis of The Cancer Genome Atlas (TCGA) database showed that high levels of CD133 expression are correlated with increased NRF2 signaling, and alterations in *CD133* gene or expression are associated with unfavorable clinical outcome in colorectal carcinoma patients. These results indicate that the CD133/NRF2 axis contributes to the development of CSC-like properties in colon cancer cells, and that PI3K/AKT signaling activation is involved in CD133-mediated NRF2 activation.

Keywords: CD133, cancer stem cell, NRF2, PI3K/AKT/GSK-3β, sphere formation, colorectal cancer

OPEN ACCESS

Edited by:
Junmin Zhang,
Lanzhou University, China

Reviewed by:
Jiwei Yu,
Shanghai Jiao-Tong University, China
Mirna Jovanovic,
University of Belgrade, Serbia

***Correspondence:**
Mi-Kyoung Kwak
mkwak@catholic.ac.kr

Specialty section:
This article was submitted to Cancer Molecular Targets and Therapeutics, a section of the journal Frontiers in Oncology

Received: *03 November 2021*
Accepted: *27 December 2021*
Published: *26 January 2022*

Citation:
Park J, Kim SK, Hallis SP, Choi B-H and Kwak M-K (2022) Role of CD133/NRF2 Axis in the Development of Colon Cancer Stem Cell-Like Properties. Front. Oncol. 11:808300. doi: 10.3389/fonc.2021.808300

INTRODUCTION

Cancer stem cell (CSC) is a subpopulation of tumor cells, which is known to account for 1–2% of tumors. Initially, Dick and colleagues identified the leukemia-initiating cluster of differentiation (CD)-34^+ $CD38^-$ cells from acute myeloid leukemia (AML) and showed that these cell fractions have differentiation and self-renewal capacities using serial transplantation in immunodeficient mice (1). CSCs share several common characteristics with normal stem cells, including self-renewal capacity, asymmetric division, and differentiation potential (2–4). In addition, CSCs attribute core characteristics to aggressive cancers due to their intrinsic resistance to anticancer treatment. Upregulation of drug efflux transporters, increased expression of the reactive oxygen species (ROS) scavenging system, and promotion of DNA damage repair are observed in CSCs, which enhance their survival in response to chemo- and radiotherapy (5–9). Several cell surface molecules, such as CD44, CD133, and ATP-binding cassette subfamily G member 2 (ABCG2), and transcription factors, such as Kruppel-like factor 4 (KLF4) and octamer-binding transcription factor 4 (OCT4), have been used to isolate and characterize CSCs (2, 8, 10, 11)

CD133 (Prominin-1) is a transmembrane penta-span glycoprotein localized in cholesterol-based lipid rafts in the plasma membrane (12). It has two large extracellular loops, an N-terminal extracellular domain and a C-terminal intracellular domain, and eight glycosylation sites. Since its first identification in human hematopoietic stem cells (13), CD133 has been recognized as a marker of CSCs (14). The CD133-positive population was identified as 2.5% of the total tumor cells from colon cancer tissues and reproduced original tumors in immunodeficient mice (15). In an animal model of renal capsule transplantation, all colon cancer-initiating cells were CD133-positive, while CD133-negative cells, which comprised majority of cancer specimens, were not able to initiate tumorigenesis (16). High CD133 expression in colorectal cancer is correlated with low survival of patients with cancer (17). Furthermore, CD133 expression is associated with an aggressive cancer phenotype. CD133 overexpression in pancreatic cancer cells induced epithelial-mesenchymal transition (EMT) and enhanced cancer metastasis in athymic mice (18). CD133-positive cells from primary non-small cell lung cancer (NSCLC) specimens exhibited higher levels of genes associated with stemness, migration, and drug efflux than CD133-negative cells (19). Additionally, cisplatin treatment in primary tumor xenografts showed that the CD133-positive population survived after therapy. Suppression of ABCG2 in CD133-positive colon cancer cells enhances their apoptotic response to chemotherapy (20).

Nuclear factor erythroid 2-like 2 (NFE2L2/NRF2) is a cap'n'collar (CNC) transcription factor containing a basic leucine zipper (bZip) domain. Under normal conditions, NRF2 binds to the cytoplasmic protein, Kelch-like ECH-associated protein (KEAP1) and is subjected to proteasomal degradation *via* the formation of the KEAP1/Cul3/Rbx1 E3 ligase complex (21). In the presence of oxidative/electrophilic stress, NRF2 is liberated from KEAP1 and translocated into the nucleus where it binds to the antioxidant response element (ARE) of the promoter regions of an array of genes (22, 23). These genes encode various cytoprotective proteins, including detoxifying enzymes (e.g., NAD(P)H: quinone oxidoreductase-1 [NQO1], aldo-keto reductase 1C1 [AKR1C1]), antioxidant proteins (*e.g.*, glutamate-cysteine ligase catalytic subunit [GCLC], glutathione peroxidase 1 [GPX1]), heme metabolizing enzymes (*e.g.*, heme oxygenase-1 [HO-1]), and drug efflux transporters (*e.g.*, breast cancer resistance protein [BCRP/ABCG2], multi-drug resistance-1 [MDR1/ABCB1]) (21, 23, 24). NRF2 is accepted as a critical component of cellular defense systems that cope with oxidative and environmental stress by removing intracellular ROS/electrophiles, thereby maintaining cellular redox homeostasis (25, 26). In addition to KEAP1, glycogen synthase kinase-3β (GSK-3β), a Ser/Thr kinase, also participates in NRF2 regulation (27, 28). GSK-3β phosphorylates NRF2 and promotes β-transducin repeat-containing protein (β-TRCP)-dependent ubiquitination and subsequent proteasomal degradation (27, 29). Since GSK-3β activity is inhibited by phosphoinositide 3-kinase (PI3K)/protein kinase B (AKT)-mediated phosphorylation, PI3K/AKT activation results in the blockade of β-TRCP-dependent NRF2 degradation (27, 30).

Although NRF2 shows protective roles in normal cells under stressful conditions, elevated levels of NRF2 in cancers promote cancer cell survival and facilitate tumor growth, cancer progression, and development of resistance to therapy (31–33). In particular, there is evidence that NRF2 signaling is upregulated in several types of CSC models, such as tumor spheres, $CD44^{high}$ cells, and aldehyde dehydrogenase $(ALDH)^{high}$ cancer cells. Additionally, this upregulation was responsible for the development of CSC-like properties, including therapy resistance, spheroid growth, enhanced migration capacity, and facilitated tumor growth (34–39). In the present study, we investigated the potential relationship between CSC markers, CD133 and NRF2, in colon cancer cells and demonstrated the role of the CD133/NRF2 axis in the development of CSC-like properties using two CSC models of spheroid culture system and $CD133^{high}$ subpopulation system.

MATERIALS AND METHODS

Materials

Doxorubicin, 3-(4,5-dimethylthiazol-2-yl)-2,5-diphenyltetrazolium bromide (MTT), and LY294002 were purchased from Sigma-Aldrich (St. Louis, MO, USA). Lipofectamine RNA iMAX was purchased from Invitrogen Life Technologies (Carlsbad, CA, USA). Agarose was purchased from Promega Corp. (Madison, WI, USA). Antibodies recognizing NRF2 (sc-13032), NQO1 (sc-16464), and glyceraldehyde 3-phosphate dehydrogenase (GAPDH; sc-47724) were obtained from Santa Cruz Biotechnology (Dallas, TX, USA). Antibodies against AKT (#4691S), p-AKT (S473; #4060S), GSK-3β (#9315S), p-GSK-3β (S9; #9336S), KLF4 (#4038S), ABCG2 (#4477S), and CD133 (#5860S) were purchased from Cell Signaling Technology (Danvers, MA, USA). Anti-AKR1C1 (H00001645-B01P), anti-GCLC (ab207777), and anti-HO-1

(ADI-SPA-896) antibodies were purchased from Abnova (Walnut, CA, USA), Abcam (Cambridge, UK), and Enzo Life Sciences (Farmingdale, NY, USA), respectively. Allophycocyanin (APC)-conjugated CD133 (25-110-963-110-963) antibody and its control IgG (25-113-434-113-434) were purchased from Miltenyi Biotec (Bergisch Gladbach, NW, Germany). TB Green Premix Ex Taq was obtained from Takara Bio (Kusatsu, Shiga, Japan). Ultra-low attachment culture dishes or 6-well plates for sphere culture were obtained from Corning Costar Corp. (Cambridge, MA, USA). Gene-specific small interfering RNAs (siRNAs), CD133 siRNA, NRF2 siRNA, and non-specific scrambled control siRNA, were obtained from Bioneer Corp. (Daejeon, Republic of Korea).

Cell Culture

The human colorectal carcinoma cell line, HCT116, was purchased from the American Type Culture Collection (Rockville, MD, USA). Cells were cultured in Dulbecco's modified Eagle's medium (DMEM; Welgene Inc., Daegu, Republic of Korea) and Nutrient Mixture F-12 medium (Welgene Inc.) supplemented with 10% fetal bovine serum (FBS; Corning Costar Corp.) and 1% penicillin/streptomycin (Welgene Inc.). The cells were grown at 37°C in a humidified atmosphere containing 5% carbon dioxide (CO_2). Colorectal cancer cell line Colo205, pancreatic carcinoma cell line PANC-1 and MIA PaCa-2, and breast carcinoma cell line MCF-7 were purchased from ATCC, and were grown in RPMI1640 (Colo205) and DMEM (PAC-1, MIA PaCa-2, MCF-7).

Sphere Culture

Cells were plated at a density of 1×10^5 cells/mL in ultralow attachment 100 mm plates or 6-well plates. The cells were grown in serum-free DMEM and Nutrient Mixture F-12 medium supplemented with B27 (Life Technologies), 20 ng/mL epithelial growth factor, 20 ng/mL basic fibroblast growth factor (R&D Systems, Minneapolis, MN, USA), 5 mg/mL bovine insulin (Cell Applications Inc., San Diego, CA, USA), 0.5 mg/mL hydrocortisone (Sigma-Aldrich), and penicillin/streptomycin. In sphere culture conditions, HCT116 cells were grown for 3–6 d and then harvested as described previously (37). The sphere number and size were counted using ToupView software (ToupTek, Hangzhou, Zhejiang, China).

siRNA Transfection

Cells were seeded at a density of 2×10^5 cells in a 60 mm dish and grown for 2 d. The medium was changed to antibiotic-free DMEM and Nutrient Mixture F-12 medium with 10% FBS. The cells were transfected with final concentration of 10 nmol predesigned *CD133*-specific siRNA (3′-GUCUACAAGGA CUUUCCAA-5′ and 3′-UUGGAAAGUCCUUGUAGAC-5′) or *NRF2*-specific siRNA (3′-GAGACUACCAUGGUUCCAA-5′ and 3′-UUGGAACCAUGGUAGUCUC-5′), or scrambled control siRNA using (1:3) volume ratio of Lipofectamine RNAiMAX reagent (Invitrogen Life Technologies) according to manufacturer's protocol. After 24 h, the transfection complex-containing medium was removed, and the cells were further cultured for 24 h for recovery in complete medium (36).

Immunoblotting Analysis

Whole lysates were prepared by adding 5X sample buffer containing 250 mM Tris-HCl (pH 6.8), 10% sodium dodecyl sulfate (SDS; Biosesang, Gyeonggi-do, Korea), 30% glycerol, 0.25% bromophenol blue, and 5% β-mercaptoethanol (Sigma-Aldrich, Co.). Protein samples were separated in 8–10% SDS-polyacrylamide gels and then transferred to nitrocellulose membranes (Whatman GmbH, Dassel, Germany). The membranes were blocked with 5% skim milk for 1 h and then incubated with the primary antibody in 3% bovine serum albumin (BSA) overnight. After incubation with the secondary antibody, chemiluminescent images were detected using a LAS-4000 mini-imager (GE Healthcare Life Sciences, Piscataway, NJ, USA). The loading control was detected after antibodies removal using stripping buffer (Restore Western blot stripping buffer; Thermo Fischer Scientific Inc., Waltham, MA, USA) followed by membrane blocking, primary and secondary antibodies incubation, and chemiluminescent detection as described previously.

Total RNA Extraction and Real-Time Reverse Transcription-Polymerase Chain Reaction (RT-PCR) Analysis

Total RNA was isolated using TRIzol reagent (Thermo Fisher Scientific Inc., Waltham, MA, USA) and processed for cDNA synthesis. RT reactions were performed by incubating 200 ng of total RNA with a reaction mixture containing oligo (dT), Go script 5X buffer, $MgCl_2$ (25 mM), and dNTP (2 mM) (Promega Corp.). Relative quantification of real-time RT-PCR was carried out using a Roche Light Cycler (Mannheim, Germany) with the Takara TB Premix ExTaq System (Otsu, Japan) as described previously (40). Primers were synthesized by Bioneer Corp., and the primer sequences for human genes were as follows: Hypoxanthine phosphoribosyltransferase-1 (*HPRT1*), 5′-TGGCGTCGTGATTAGTGATG-3′ and 5′-GCTACAATG TGATGGCCTCC-3′, 5′-CCTGGCGTCGTGATTAGTGA-3′ and 5′-GCTACAATGTGATGGCCTCC-3′, 5′-TGACACTGG CAAAACAATGC-3′ and 5′-CAAATCCAACAAAGTCTGGC-3′; *ABCG2*, 5′-CACAACCATTGCATCTTGGCTG-3′ and 5′-TGAGAGATCGATGCCCTGCTTT-3′; *KLF4*, 5′-ACACTTG TGATTACGCGGGCTGC-3′ and 5′-GGCGAATTTCCATCC ACAGCCG-3′; *CD133*, 5′-CCGCAGGAGTGAATCTTTTA-3′ and 5′-CTATAGGAAGGACTCGTTGC-3′; *NRF2*, 5′-TAGCA ATGAAGACTGGGCTC-3' and 5′-CCAGTGGATCTGC CAACTAC-3′; *NQO1*, 5′-CAGTGGTTTGGAGTCCCTGCC-3' and 5′-TCCCCGTGGATCCCTTGCAG-3′; *AKR1C1*, 5′-GAAAGAAACATTTGCCAGCC-3' and 5′-TGAGCAGAAT CAATATGGCG-3′; *GCLC*, 5′-TGAAGGGACACCAGGAC AGCC-3' and 5′-GCAGTGTGAACCCAGGACAGC-3′; *HO-1*, 5′-GCTGCTGACCCATGACACCAAGG-3′ and 5′-AAGGAC CCATCGGAGAAGCGGAG-3′; *GPx1*, 5′-TTCCCGTGCAAC CAGTTTG-3′ and 5′-TTCACCTCGCACTTCTCGAA-3′.

Flow Cytometry and Cell Sorting

Approximately 1×10^6 HCT116 cells were harvested and incubated in 2 μL CD133/1-APC staining dye (Miltenyi Biotec)

with 98 μL buffer containing 2 mM ethylenediaminetetraacetic acid (EDTA) and 2% FBS for 40 min. IgG control samples were incubated with 2 μL REA control (S)-APC staining dye (Miltenyibiotec Korea) with 98 μL of buffer. The fluorescence intensity of the stained cells was analyzed using an FACS Aria III cell sorter flow cytometer (BD Biosciences, Franklin Lakes, NJ, USA), and $CD133^{high}$ and $CD133^{low}$ subpopulations were sorted as described previously (35).

MTT Assay

Cells were plated at a density of 3×10^3 cells/well in a 96-well plate and incubated with doxorubicin for 24 h. After the addition of MTT solution (2 mg/mL), the cells were further incubated for 4 h. The MTT solution was removed, 100 μL/well of dimethyl sulfoxide (DMSO; Sigma-Aldrich Co.) was added, and the absorbance was measured at 540 nm using SpectraMax (Molecular Devices, San Jose, CA, USA) (41).

Wound Healing Assay

To determine cell motility, $CD133^{high}$ and $CD133^{low}$ cells were plated in a 12-well plate at a density of 2.5×10^5 cells/well. When 95–100% confluency was achieved, a straight scratch was made on the surface using a pipette tip. Then, the cells were grown for 24 or 48 h in serum-free medium, and the migration of cells into the wounded area was photographed using a JULI^{TM} Smart fluorescent cell analyzer (Digital Bio source, Seoul, Korea). The wound closure rate was determined using the initial and final wound widths, and the wound closure percentage was calculated by dividing the change in wound width by the initial wound width, as described previously (40).

Soft Agar Colony Formation Assay

Soft agar colony formation assay was performed to evaluate the anchorage-independent growth ability of the cells. Approximately 5×10^3 cells were suspended in the top soft agar layer (0.35% soft agar) and seeded into 6-well plates, which were pre-coated with 0.5% base agar. Colonies were allowed to grow at 37°C in a 5% CO_2 incubator for 2–3 weeks, and colony numbers were counted using an ECLIPSE Ti inverted microscope and the NIS-Elements AR (V. 4.0) computer software program (NIKON Instruments Korea, Seoul, Republic of Korea), as described previously (35).

Correlation of CD133/NRF2 With Colorectal Cancer Prognosis

We used gene expression data of colorectal adenocarcinoma patients (n=526) available at the Cancer Genome Atlas (TCGA) Pan-Cancer Atlas data set. Analyzed data were visualized using the cBioPortal (http://cbioportal.org) to investigate the gene expression levels of NRF2, NQO1, and PIK3CA depending CD133 mRNA levels. Levels of mRNA are presented as RSEM processed using the RNA-Seq by Estimation Maximization (RSEM) algorithm in log2 scale. In addition, we examined the overall survival rates depending on CD133 expression levels and genetic alterations in *CD133* and *NRF2*. These Kaplan-Meier survival estimates were generated by log-rank nonparametric test in the cBioPortal. P-values are derived from student t-test, and q-values are obtained from Benjamini-Hochberg procedure.

Statistical Analysis

We conducted multiple comparison tests for different treatment groups using histomorphometric analysis. The data were analyzed using one-way analysis of variance (ANOVA) followed by Tukey's multiple comparison test to determine which pairs of groups were significantly different. Statistical analyses were conducted using GraphPad Prism 5 (GraphPad Software, Inc., La Jolla, CA, USA). Differences were considered statistically significant at $P < 0.05$.

RESULTS

High CD133 Levels Are Associated With Facilitated Sphere Growth and CSC Marker Expression

To examine the relationship between CD133 and CSC-like properties, we first examined the expression levels of CD133 in different carcinoma cell lines. When the basal levels of CD133 were determined in colorectal carcinoma cell line HCT116 and Colo205, pancreatic carcinoma cell line PANC-1 and MIA PaCa-2, and breast carcinoma cell line MCF7, HCT116 showed the highest level of CD133 (**Supplementary Figures 1A, B, 2B**). FACS analysis with CD133-specific antibody showed that 79.8% of HCT116 total cell fraction expressed CD133 (**Figure 1A**). In an attempt to investigate the role of CD133 in CSC-like property development, we used a sphere culture system, which was shown to be a CSC-enriched system (42). When HCT116 cells were cultured in ultra-low attachment plates, the transcript level of CD133 increased 3.16-fold in HCT116 spheres and CD133 protein levels were also elevated (**Figures 1B, C**). Whereas, sphere culture of Colo205, PANC-1, and MIA-PaCa-2 did not show the elevations in CD133, which shows that HCT116 can be used as our experimental model (**Supplementary Figures 2A, B**). In accordance with CD133 elevation, levels of CSC markers, including KLF4 and ABCG2, were significantly increased in HCT116 colonospheres (**Figures 1D, E**). We then assessed the association of CD133 with CSC-like properties by silencing *CD133* in HCT116 (**Figure 1F**). The *CD133*–silenced colonospheres expressed lower levels of KLF4 and ABCG2 than the nonspecific siRNA-transfected colonospheres (**Figure 1G**). In addition, the number of spheres with a diameter greater than 70 μm was markedly diminished by *CD133* silencing (**Figure 1H**). These results showed the critical contribution of CD133 to the development of CSC-like properties in colon cancer cells.

NRF2 Elevation Is Mediated by CD133 in Sphere Cultured Colon Cancer Cells

In HCT116 colonospheres, transcription levels of NRF2 and its target genes, such as *GCLC*, *AKR1C1*, and *NQO1* were all increased compared to the HCT116 monolayer (**Figure 2A**). Increased protein levels of NRF2, GCLC, AKR1C1, and NQO1

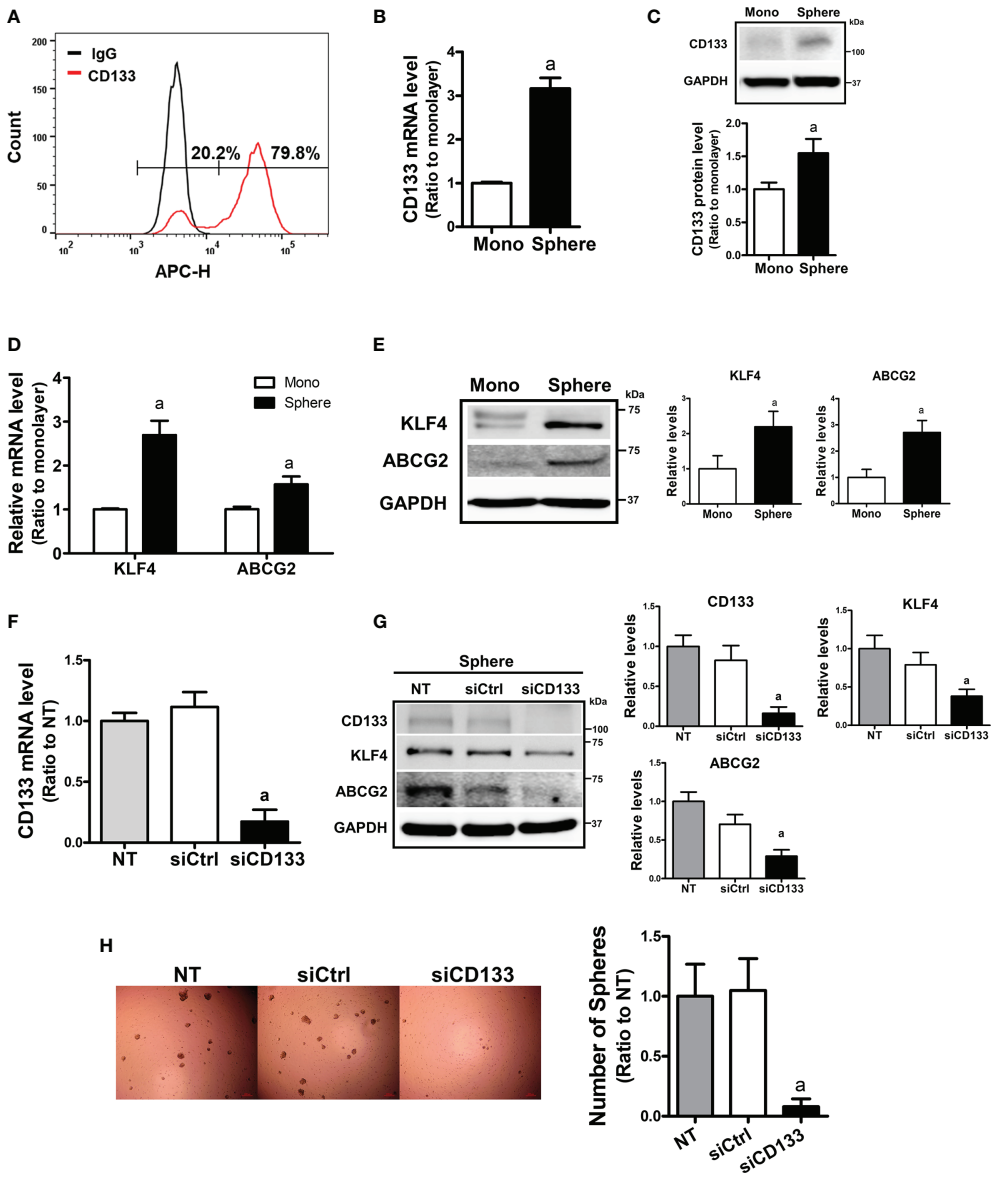

FIGURE 1 | Enhanced CD133 levels in sphere cultured HCT116 cells and their involvement in sphere formation. **(A)** The presence of CD133-positive cell population in monolayer-cultured HCT116 cells was analyzed using allophycocyanin (APC)-fluorescence-based fluorescence-activated cell sorting method. **(B, C)** Transcript **(B)** and protein levels **(C)** of CD133 were assessed in monolayer and sphere cultured HCT116 cells using relative quantitative reverse transcription-polymerase chain reaction (qRT-PCR) analysis and western blotting. Bar graph represents quantified protein levels from at least three experiments. $^{a}P < 0.05$ compared with the monolayer HCT116. **(D, E)** The transcript **(D)** and protein levels **(E)** of Kruppel-like factor 4 (KLF4) and ATP-binding cassette subfamily G member 2 (ABCG2) in monolayer and sphere HCT116 cells were assessed. Bar graph represents quantified protein levels from at least three experiments. $^{a}P < 0.05$ compared with the monolayer HCT116 cells. **(F)** Transcript levels of CD133 in the non-transfected (NT), non-specific small interfering RNA (siRNA) (siCtrl)- or CD133-specific siRNA (siCD133)-transfected HCT116 cells. $^{a}P < 0.05$ compared with the siCtrl group. **(G)** HCT116 cell with either the non-specific siRNA (siCtrl) or CD133-specific siRNA (siCD133) transfection, were grown in sphere culture systems and the protein levels of CD133, KLF4, ABCG2 were examined. Bar graph represents quantified protein levels from at least three experiments. **(H)** Sphere formation was assessed in the non-transfected (NT), non-specific siRNA (siCtrl)- or CD133-specific siRNA (siCD133)-transfected HCT116 cells. Number of spheres over 70 μm diameter was counted using an image processing ToupView software. $^{a}P < 0.05$ compared with the siCtrl group. Quantification results of western blotting were relative values to the loading control GAPDH. All values represent the mean ± standard error of the mean (SEM) of more than three experiments.

were also confirmed by western blotting (**Figure 2B**). Next, we tested the potential involvement of CD133 in NRF2 signaling activation by silencing *CD133* in colonospheres. When *CD133*-silenced HCT116 was cultured in sphere conditions, the elevations in NRF2 and its targets GCLC, AKR1C1, and NQO1 were attenuated when compared to the control siRNA-transfected spheres (**Figures 2C, D**). Whereas, NRF2 mRNA levels, which were elevated in spheres, were not significantly

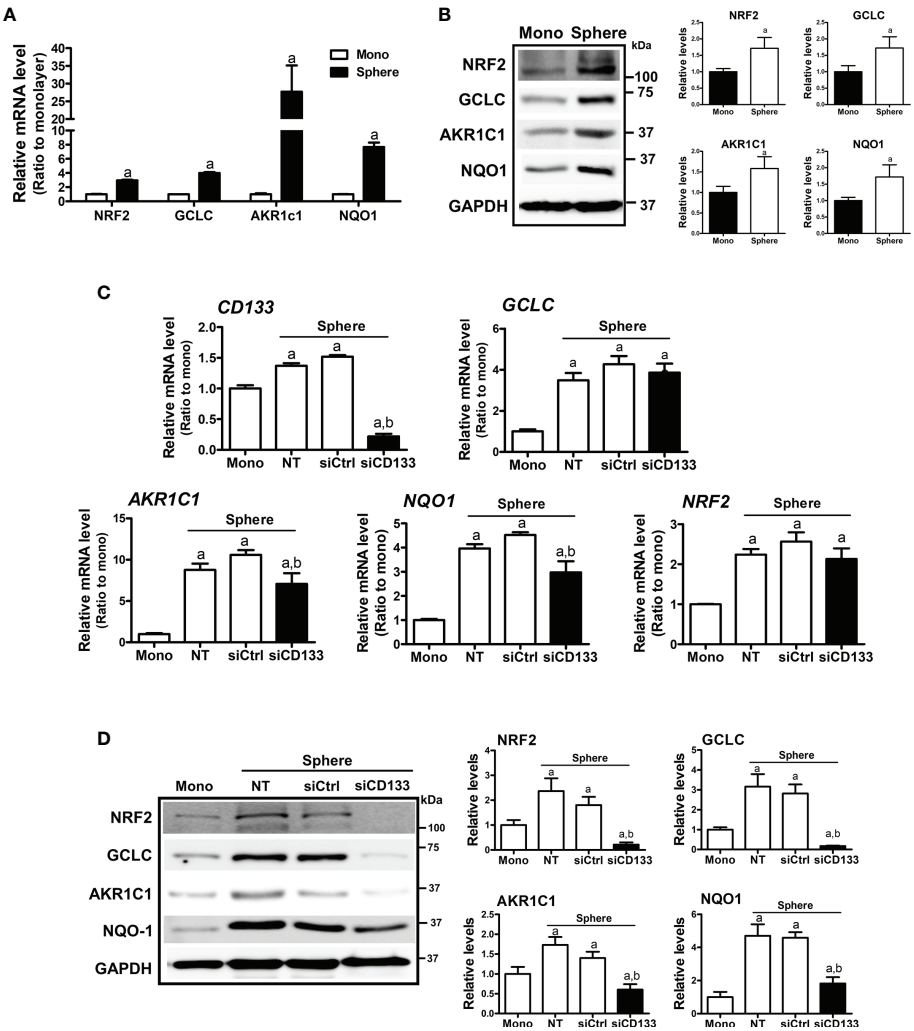

FIGURE 2 | Association of CD133 with NRF2 upregulation in HCT116 spheres. **(A)** Transcript levels of *NRF2*, *GCLC*, *AKR1C1*, and *NQO1* were measured in monolayer and sphere HCT116 cells using a relative qRT-PCR analysis. [a]P < 0.05 compared with the monolayer group. **(B)** Protein levels of NRF2, GCLC, AKR1C1 and NQO1 were assessed in monolayer and sphere HCT116 cells. Bar graph represents quantified protein levels from at least three experiments. [a]P < 0.05 compared with the monolayer group. **(C)** HCT116 with either the non-transfection (NT), non-specific siRNA (siCtrl) or CD133-specific siRNA (siCD133) transfection were grown in the sphere culture system, and transcript levels of *CD133*, *GCLC*, *AKR1C1*, *NQO1*, and *NRF2* were measured. [a]P < 0.05 compared with the monolayer. [b]P < 0.05 compared with the siCtrl group. **(D)** Protein levels for NRF2, GCLC, AKR1C1, and NQO1 were monitored in sphere cultured HCT116 cells with either the non-specific siRNA (siCtrl) or CD133-specific siRNA (siCD133) transfection. Bar graph represents quantified protein levels from at least three experiments. Quantification results of western blotting were relative values to the loading control GAPDH. [a]P < 0.05 compared with the monolayer. [b]P < 0.05 compared with the siCtrl group. NT, non-transfection group.

reduced by *CD133* silencing. These results showed that the high NRF2 level in sphere-cultured HCT116 cells was attributed to CD133.

Activation of PI3K/AKT Signaling Is Involved in CD133-Mediated Elevation of NRF2

There have been reports showing that CD133 induces PI3K/AKT signaling activation in colon cancer cells as well as glioma stem cells (43, 44). In addition, AKT-mediated GSK-3β phosphorylation stabilizes NRF2 (27). Based on these results, we monitored the activation levels of AKT/GSK-3β using western blotting to elucidate the molecular events involved in CD133-mediated NRF2 elevation in colonospheres. The level of phosphorylated AKT (p-AKT) at Ser473 was higher in colonospheres than in monolayer HCT116 cells, implying the activation of PI3K (**Figure 3A**). Subsequently, the level of phosphorylated GSK-3β (Ser9), an inactive form of proteasomal NRF2 degradation, was elevated in sphere-cultured HCT116 cells. These results show that CD133-mediated PI3K/AKT activation and resultant GSK-3β inactivation could be a cause of NRF2 elevation in colonospheres. Indeed, when *CD133* was silenced, levels of p-AKT and p-GSK-3β were reduced in colonospheres (**Figure 3B**), and treatment with the PI3K inhibitor LY294002

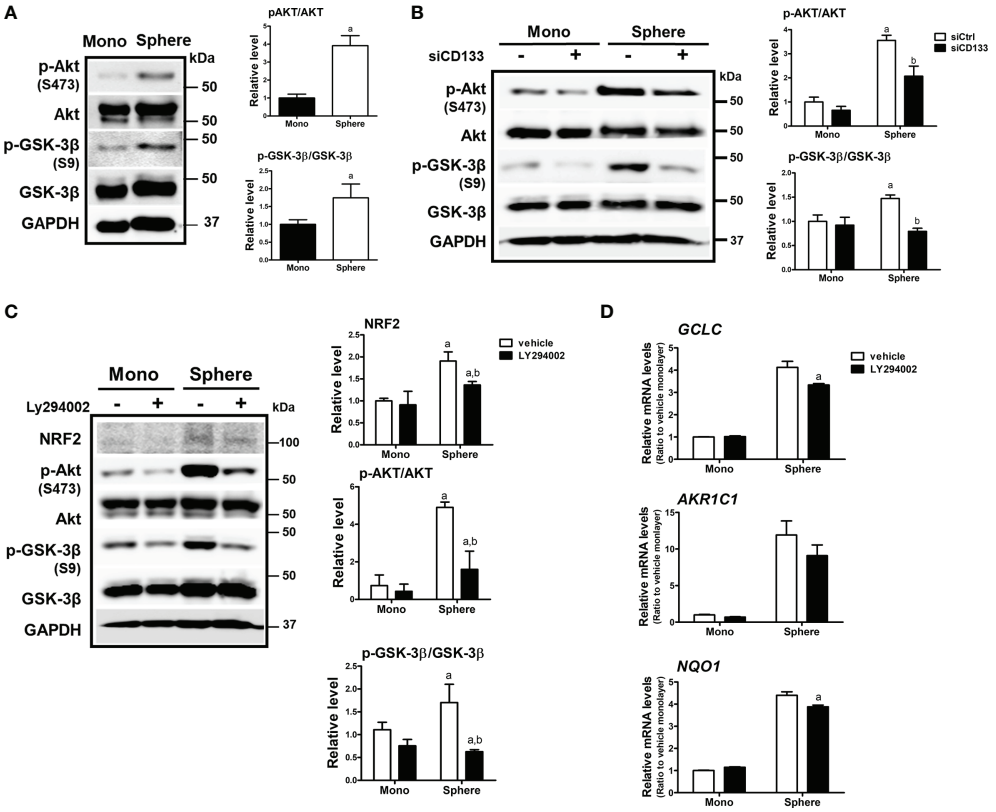

FIGURE 3 | Involvement of PI3K/AKT/GSK-3β signaling in NRF2 activation in HCT116 spheres. **(A)** Protein levels of p-AKT (S473), total AKT, p-GSK-3β (S9), and total GSK-3β were determined in monolayer and sphere HCT116 cells. Bar graph represents quantified protein levels from at least three experiments. $^{a}P < 0.05$ compared with the monolayer group. **(B)** HCT116 cells were transfected with the non-specific siRNA (siCtrl) or CD133-specific siRNA (siCD133) and grown in either monolayer or sphere culture system. Protein levels for p-AKT (S473), AKT, p-GSK-3β (S9), and GSK-3β were assessed using western blotting. Bar graph represents quantified protein levels from at least three experiments. $^{a}P < 0.05$ compared with the monolayer group. **(C)** LY294002 (10 μM), a pharmacological inhibitor of PI3K, was incubated in monolayer and sphere HCT116 cells for 24 h, and protein levels of NRF2, p-AKT (S473), AKT, p-GSK-3β (S9), and GSK-3β were determined. Bar graph represents quantified protein levels from at least three experiments. $^{a}P < 0.05$ compared with the monolayer vehicle group. $^{b}P < 0.05$ compared with the sphere vehicle group. **(D)** Transcript levels of *GCLC AKR1C1*, and *NQO1* were measured using a relative qRT-PCR analysis in vehicle- or LY294002-treated cells. $^{a}P < 0.05$ compared with the vehicle-treated sphere group. Quantification results of western blotting were relative values to the loading control GAPDH. Values represent the mean ± SEM of more than three experiments.

(10 μM) repressed these elevations (**Figure 3C**). Additionally, PI3K inhibitor treatment diminished NRF2 levels and target gene expression levels in HCT116 spheres (**Figures 3C, D**). These results showed that CD133 contributes to NRF2 upregulation *via* PI3K/AKT activation and subsequent inhibition of p-GSK-3β.

NRF2 Contributes to Facilitated Sphere Formation and CSC Marker Elevation

In order to assess the role of NRF2 in colonosphere formation, *NRF2*-silenced HCT116 was cultured in sphere culture condition (**Figure 4A**). *NRF2*-silencing affected the sphere-forming capacity of HCT116 cells, and the sphere number was reduced (**Figure 4B**). In line with this, the levels of CSC markers KLF4 and ABCG2 were significantly lower in the *NRF2*-silenced colonospheres than in the control siRNA-transfected colonospheres (**Figure 4C**). These results confirmed the functional contribution of NRF2 to the sphere-forming capacity.

$CD133^{high}$ HCT116 Cells Display Enhanced CSC-Like Properties and NRF2 Activation

To confirm the relationship between CD133/NRF2 and CSC-like properties, we isolated CD133-positive and CD133-negative cell fractions from total HCT116 cells, and established $CD133^{low}$ and $CD133^{high}$ cell lines (**Figure 5A**). These cell lines were cultured for up to 1 month, and high CD133 expression was maintained along with elevated ABCG2 and KLF4 levels (**Figure 5B**). As phenotypic characteristics, the cell growth rate of $CD133^{high}$ HCT116 cells was higher than that of $CD133^{low}$ cells (**Figure 5C**), and anchorage-independent colony formation was enhanced (**Figure 5D**). In addition, cell motility in the wound healing assay (**Figure 5E**) and sphere forming capacity (**Figure 5F**) were higher in $CD133^{high}$ HCT116 cells than in $CD133^{low}$ cells. In line with these CSC-like properties, the cytotoxic response to anticancer treatment was determined using doxorubicin. We observed that 0.5 to 1 μM doxorubicin treatment for 24 h showed similar rates of growth inhibition, and

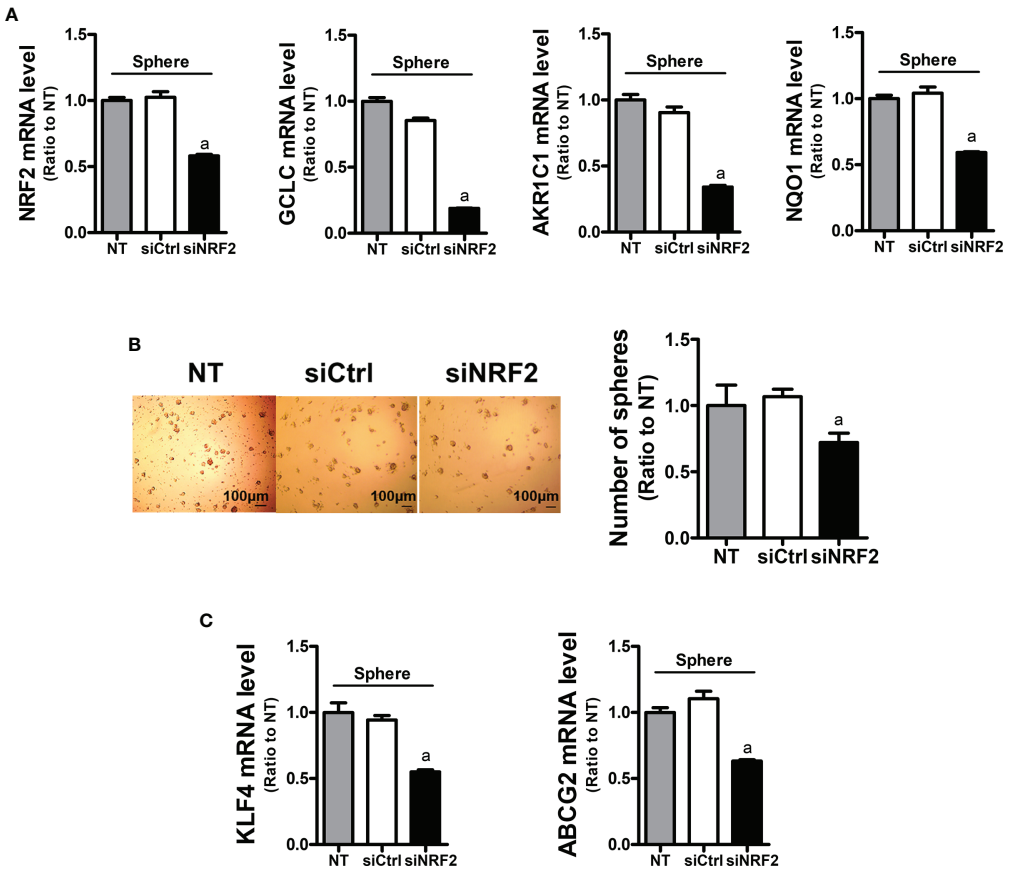

FIGURE 4 | Inhibition of sphere formation and CSC marker levels in *NRF2*-silenced HCT116 cells. **(A)** HCT116 cells were transfected with the non-specific siRNA (siCtrl) or *NRF2*-specific siRNA (siNRF2) and grown for 3 days in sphere culture condition. Levels of *NRF2, GCLC, AKR1C1,* and *NQO1* mRNAs were determined in the siCtrl and siNRF2 spheres. $^{a}P < 0.05$ compared to the siCtrl group. **(B)** The siCtrl and siNRF2 HCT116 were grown in sphere culture condition, and sphere formation was assessed. Number of spheres over 70 μm diameter was counted using an image processing ToupView software. Values represent the mean ± SEM from three independent experiments. $^{a}P < 0.05$ compared to the siCtrl group. **(C)** Levels of *KLF4* and *ABCG2* mRNA were assessed in the siCtrl and siNRF2 spheres. $^{a}P < 0.05$ compared to the siCtrl group. All values in RT-PCR analysis represent the mean ± SEM from at least three independent experiments. NT, non-transfection group.

the cell growth inhibition by 0.5 μM doxorubicin treatment was alleviated in $CD133^{high}$ HCT116 cells (**Figure 5G**). When CD133 levels were silenced in $CD133^{high}$ HCT116 cells, the levels of the CSC markers ABCG2 and KLF4, which were elevated in this cell line, were diminished (**Figure 5H**). Additionally, the levels of NRF2 and NQO1 were higher in $CD133^{high}$ HCT116 cells than in $CD133^{low}$ cells and were repressed by *CD133* silencing (**Figure 5H**). These results provide direct evidence that the CD133-enriched population exhibited enhanced colony formation, cell migration, colony formation, and drug resistance, which is accompanied by NRF2 activation.

CD133 Alterations Are Associated With NRF2 Elevation and Poor Clinical Outcome in Patients With Colorectal Cancer

In an attempt to investigate the clinical implication of the linkage between CD133 and NRF2, we analyzed clinical data from the TCGA Pan-Cancer Atlas database using the cBioPortal interface. A total of 526 gene expression data from colorectal adenocarcinoma patients were available in the TCGA Pan-Cancer Atlas database, and 17 cases showed genetic alterations in *CD133* gene (missense mutation, 15; frameshift deletion, 1; splice, 1). In *CD133*-altered group, 11.8% of patient samples demonstrated *NRF2* gene alteration, whereas only 1.4% of samples showed *NRF2* alteration in *CD133*-unaltered group (data not shown). First, the clinical relationship between *CD133* gene alteration (n=17) and colorectal cancer patients survival was assessed by Kaplan-Meier estimate analysis. It revealed shorter overall survival rate in patients with altered *CD133* gene (median survival months=41.36) compared to unaltered *CD133* patients (median survival months=83.24) (**Figure 6A**). Additionally, patients whose tumors have *NRF2* or *CD133* gene alteration showed shorter overall survival estimates (median survival months=51.48) than patients with unaltered *CD133* gene groups (median survival months=83.24) (**Figure 6B**). These imply the potential correlation between *CD133* gene alteration and clinical outcome of colorectal cancer patients.

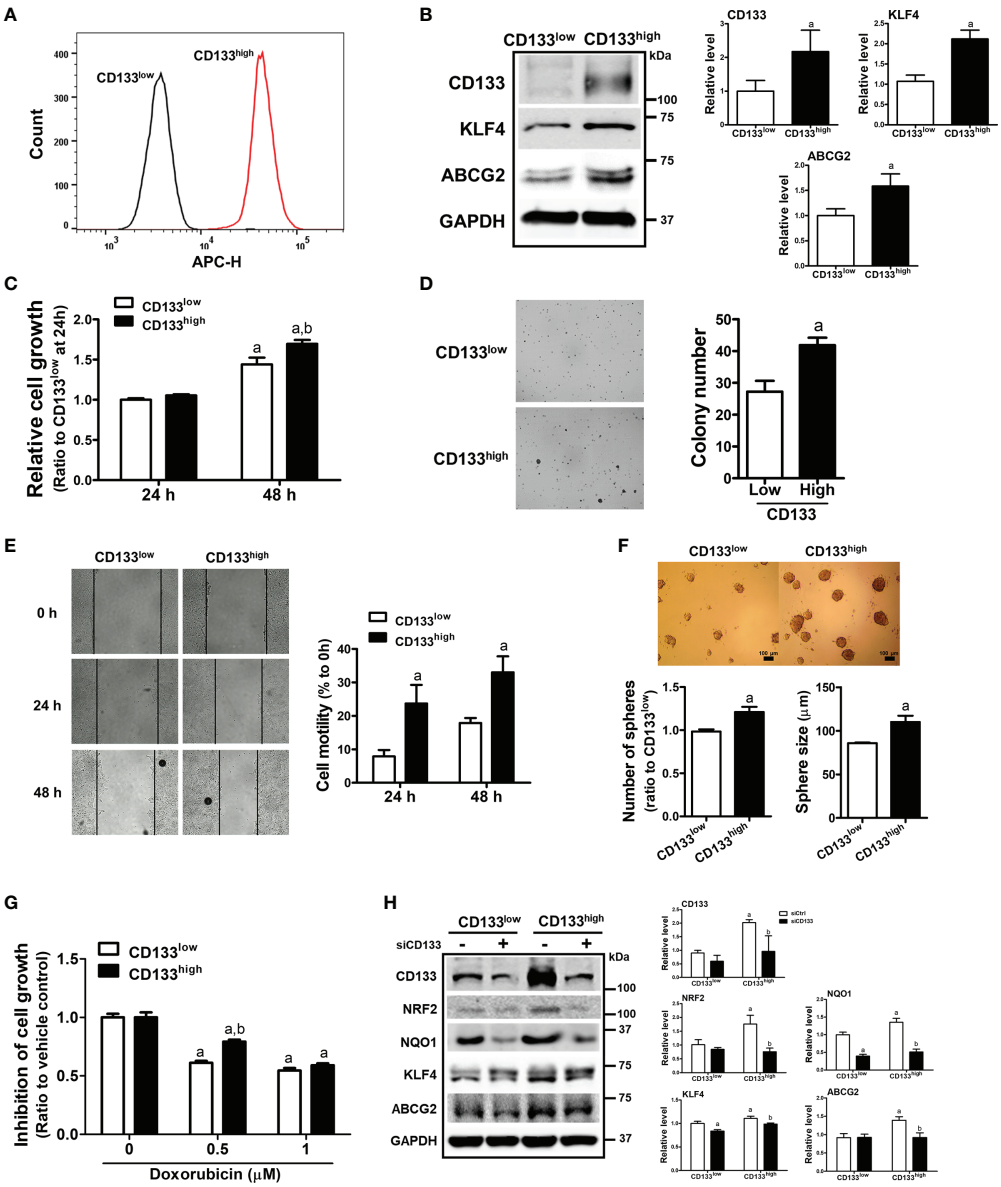

FIGURE 5 | Enhanced CSC-like properties and NRF2 levels in CD133^{high} HCT116 fraction. **(A)** CD133-positive and CD133-negative cell fractions were isolated using FACS analysis, and the CD133^{high} and CD133^{low} HCT116 cell lines were established. CD133-positive cell fraction in the CD133^{high} and CD133^{low} HCT116 cell lines was assessed following maintenance for 2 weeks. **(B)** Protein levels of CD133, KLF4, and ABCG2 were determined in established CD133^{high} and CD133^{low} HCT116 cells. Bar graph represents quantified protein levels from at least three experiments. $^{a}P < 0.05$ compared with the CD133^{low} cell line. **(C)** The CD133^{high} and CD133^{low} HCT116 cells were grown in the absence of fetal bovine serum (FBS) and relative cell growth was assessed using MTT assay after 24 h and 48 h of plating. $^{a}P < 0.05$ compared to each 24 h group. $^{b}P < 0.05$ compared to CD133^{low} HCT116 cells. **(D)** The CD133^{high} and CD133^{low} HCT116 cells were suspended in the top soft agar layer (0.35% soft agar) and anchorage-independent growth was monitored for 2 weeks. Colony number was counted using an ECLIPSE Ti inverted microscope and the NIS-Elements AR (V. 4.0) software. Bar graph represents quantified results from at least three experiments. $^{a}P < 0.05$ compared to the CD133^{low} HCT116 cells. **(E)** Cell migration ability was assessed in the CD133^{high} and CD133^{low} HCT116 cells using a wound-healing assay for 24 h and 48 h. Bar graph represents quantified results from at least three experiments. $^{a}P < 0.05$ compared to the CD133^{low} HCT116 cells. **(F)** CD133^{high} and CD133^{low} HCT116 cells were grown in sphere culture condition, and sphere formation capacity was assessed by measuring the number and average size of the spheres. Bar graph represents quantified results from at least three experiments. $^{a}P < 0.05$ compared to the CD133^{low} HCT116 cells. **(G)** Inhibition of cell growth was monitored following doxorubicin (0.5 and 1 μM) incubation for 24 h using MTT assay. Values represent the mean ± SEM from four independent experiments. $^{a}P < 0.05$ compared to the doxorubicin-treated CD133^{low} group. **(H)** CD133^{high} and CD133^{low} HCT116 cells were transfected with *CD133* siRNA and protein levels of CD133, NRF2, NQO1, KLF4, and ABCG2 were determined. Bar graph represents quantified protein levels from at least three experiments. Quantification results of western blotting were relative values to the loading control GAPDH. All values represent the mean ± SEM from three independent experiments. $^{a}P < 0.05$ compared with the CD133^{low} siCtrl group. $^{b}P < 0.05$ compared with the CD133^{high} siCtrl group.

Among 526 colorectal cancer patients, 52 patients exhibited higher *CD133* mRNA levels when compared to unaltered CD133 mRNA group (n=474). The Kaplan-Meier survival analysis showed that the median survival month of patients with high CD133 expression is 81.37 month, which is lower than that of patients with unaltered CD133 expression (83.24 month), although no statistical significance obtained (**Figure 6C**). In addition, CD133 mRNA levels were associated with increased mRNA levels of NRF2 and NQO1 in these patients. Mean log2 mRNA expressions of NRF2 were 10.79, 11.21, and 11.28 in CD133-low, unaltered, and CD133-high group, respectively (**Figure 6D**). NQO1 levels were increased depending on CD133 levels (**Figure 6D**). PIK3CA mRNA levels were also relatively high in CD133-high group when compared to unaltered group (**Figure 6F**). These results indicate that CD133 expression is associated with NRF2 signaling activation in colorectal cancers, and further suggested the correlation of

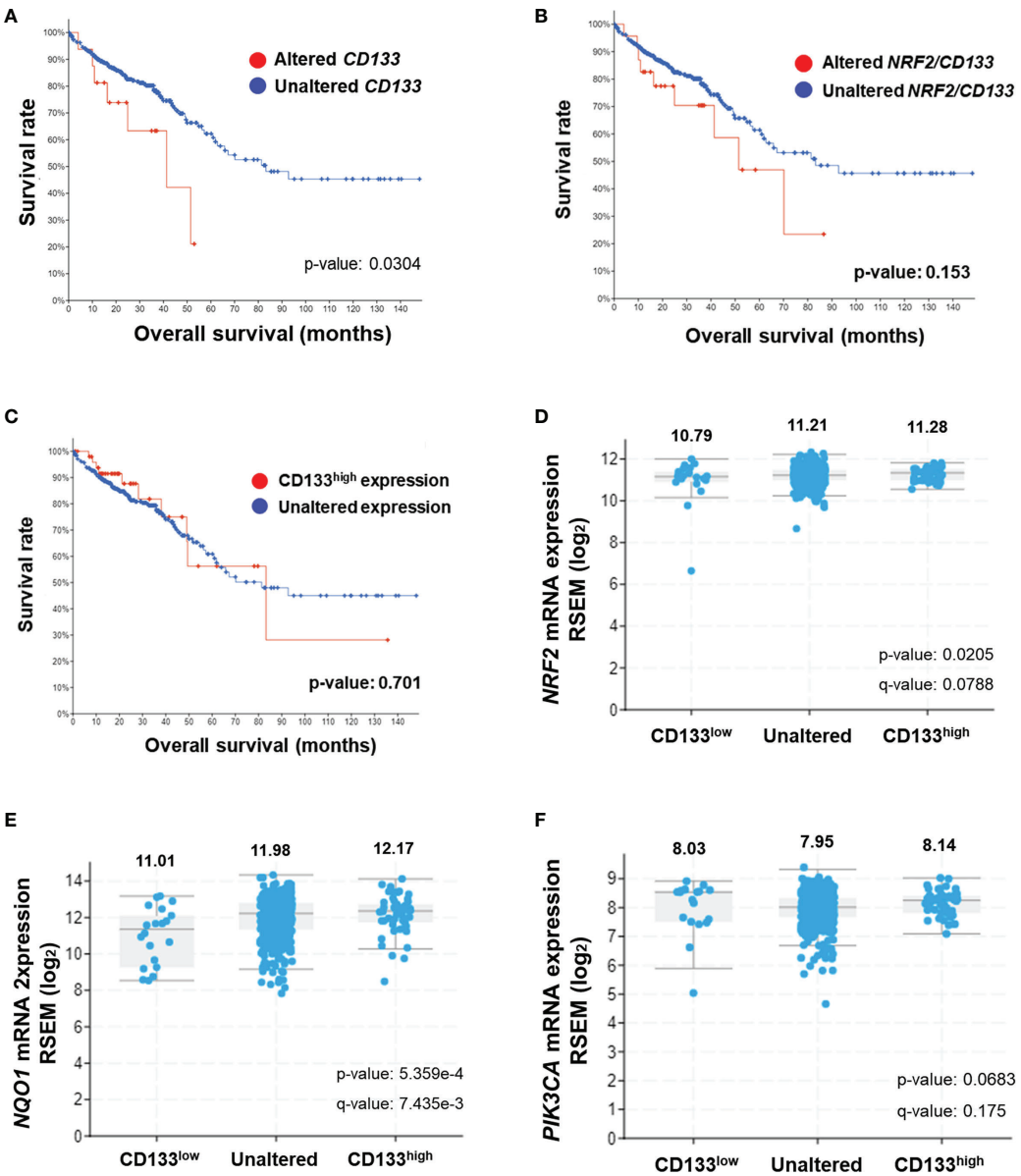

FIGURE 6 | Association of CD133 with NRF2 and clinical outcome of colorectal cancer patients. **(A)** Overall survival rates of colorectal patients with altered (n = 17) *vs* unaltered (n = 509) *CD133* gene. **(B)** Overall survival rates of colorectal patients with altered (n = 24) vs unaltered (n = 502) *NRF2* or *CD133* gene. **(C)** Overall survival rates of colorectal patients with high CD133 (n = 52) *vs* unaltered (474) mRNA levels. Plots generated by cBioPortal were modified. **(D–F)** Correlation of CD133 mRNA levels (high CD133, n = 52; unaltered CD133, n = 454; low CD133, n = 20) with NRF2 **(D)**, NQO1 **(E)**, and PIK3CA **(F)** mRNA levels in colorectal tumors. Values are given in (RNA Seq V2 RSEM) in log2. Plots generated by cBioPortal were modified.

CD133 alteration (mutation and increased expression) with unfavorable clinical outcome.

DISCUSSION

The major characteristics of CSCs, which include refractory response to conventional chemotherapy and radiotherapy, can be explained by the elevation of drug efflux transporters, enhanced DNA repair ability, and activation of the ROS defense system. The side population of cancer cells, which excludes the fluorescent dye Hoechst 33342, expresses a high level of ABCG2 (BCRP) and displays chemoresistant phenotypes (45). The CD133-high fraction from glioma cells was more resistant to radiotherapy than the CD133-negative fraction, and CD133-high cells activated the molecular event for the DNA damage checkpoint and enhanced DNA repair capacity following radiotherapy (46). The $CD44^+/CD24^-$ cell fraction was found to be resistant to radiation, and maintenance of low ROS levels was associated with radioresistance (47). CSCs from human breast tumors exhibited less DNA damage and a higher rate of survival after irradiation compared to non-CSCs, and low levels of ROS in CSCs were attributed to increased expression levels of ROS detoxifying systems, such as glutamate-cysteine ligase and GSH synthetase (9). In leukemia with a high frequency of stem cells, ROS levels were low and ROS-scavenging GPX3 levels were high compared to leukemia with a low frequency of stem cells (48). Leukemic stem cells exhibited high levels of FoxoO3a expression, and deletion of foxO blocked the initiation of myeloid leukemia in a mouse model (49). In head and neck squamous cell carcinoma, a CSC marker CD44 variant was found to directly bind to the cystine/glutamate antiporter xCT, thereby increasing GSH synthesis, which is involved in therapy resistance (50). These reports consistently support the importance of the ROS detoxifying system in CSCs for maintaining low ROS levels and high survival under therapy stress.

In the current study, we demonstrated a positive linkage between CD133 and NRF2 in CSC-like properties using the colonosphere culture system and the $CD133^{high}$ subpopulation. Sphere culture of the colorectal cell line HCT116 led to an increase in CD133 expression along with elevated CSC markers, such as KLF4 and ABCG2. *CD133*-silencing suppressed sphere-forming capacity and expression of KLF4 and ABCG2, which indicates the critical role of CD133 in CSC-like properties development. NRF2 signaling was also upregulated in colonospheres and partly responsible for CSC marker elevation and sphere-forming capacity. Notably, NRF2 activation in colonospheres was CD133-dependent: *CD133*-silencing inhibited NRF2 elevation and attenuated the expression of GCLC, AKR1C1, and NQO1. The relationship between CD133 and NRF2 was confirmed in an isolated $CD133^{high}$ subpopulation from HCT116 cells. Established $CD133^{high}$ cell line showed higher doxorubicin resistance, colony formation, sphere formation, and migration capacity than $CD133^{low}$ cell line, and *CD133*-silencing in $CD133^{high}$ cells suppressed NRF2 activation and KLF4 elevation. These *in vitro* results were supported by clinical relationship between CD133 and NRF2, which were obtained from ATCG database. In colorectal carcinoma patients, overall survival rates were diminished by *CD133* and *CD133/NRF2* gene alterations, and high CD133 mRNA levels also showed a relationship with reduced overall survival rates. Additionally, high CD133 mRNA levels in colorectal carcinoma showed positive correlations with high transcript levels of NRF2 and NQO1. Taken together, these results suggest that CD133 mediates the activation of NRF2 signaling, which in turn contributes to the CSC-like properties of $CD133^{high}$ colon cancers.

As a molecular event for CD133-mediated NRF2 activation, we suggest the involvement of PI3K/AKT/GSK-3β. Multiple reports have suggested the activation and contribution of PI3K/AKT signaling in CD133-positive CSCs. Microarray analysis revealed that expression of genes related to the PI3K/AKT signaling pathway was elevated in sphere-cultured $CD133^+/CD44^-$ prostate CSCs, and knockdown of phosphatase and tensin homolog (PTEN) stimulated sphere formation by inhibiting PI3K/AKT signaling (51). Phosphorylation of Tyr828 residue in the cytoplasmic domain of CD133 mediates binding with PI3K, and subsequently activates PI3K/AKT signaling for self-renewal and tumorigenicity of glioma stem cells (44). In line with these findings, an inhibitor of PI3K/AKT suppressed the proliferation and stemness of colon CSCs (52). In our colonosphere system, activation of the PI3K/AKT axis and consequent phosphorylation of GSK-3β at Ser9 were observed. Since AKT-mediated phosphorylation inhibits GSK-3β activity for β-TCRP-dependent degradation of NRF2, activated PI3K/AKT signaling is often associated with NRF2 activation in multiple types of cancers. In breast cancers with oncogenic PI3K/AKT activation, NRF2-driven GSH biosynthesis is stimulated, which is required for oxidative stress resistance, tumor spheroid formation, and colony formation. In addition, elevation of NRF2 targets showed a positive correlation with mutation status in the PI3K/AKT pathway (53). In the absence of *KEAP1*, the deletion of *PTEN* could further elevate NRF2 levels, which accompanied GSK-3β inactivation *via* PI3K/AKT activation (8, 54). In our study with colonospheres, *CD133*-silencing reduced phosphorylation of AKT/GSK-3β, and the PI3K inhibitor LY294002 blocked AKT-mediated GSK-3β phosphorylation and attenuated NRF2 target genes expression. These results suggested that CD133 activates PI3K/AKT signaling, which in turn stabilizes NRF2 protein *via* GSK-3β inhibition in colonospheres. Of note, we observed that transcript levels of NRF2 were also higher in colonospheres than those in monolayer cultured cells (**Figures 2A, C**). As NRF2 transcription is regulated by its 5-flanking upstream ARE as a positive feedback loop (55), it can be plausible that PI3K/AKT-mediated NRF2 stabilization elevates NRF2 transcription.

Several reports have demonstrated that NRF2 signaling plays a role in CSC maintenance and therapy resistance. In primary glioma stem cells from human glioblastoma tissues, NRF2 knockdown disrupts self-renewal and pluripotency (38). NRF2 signaling is elevated in spheroid cultured breast cancer cells, and

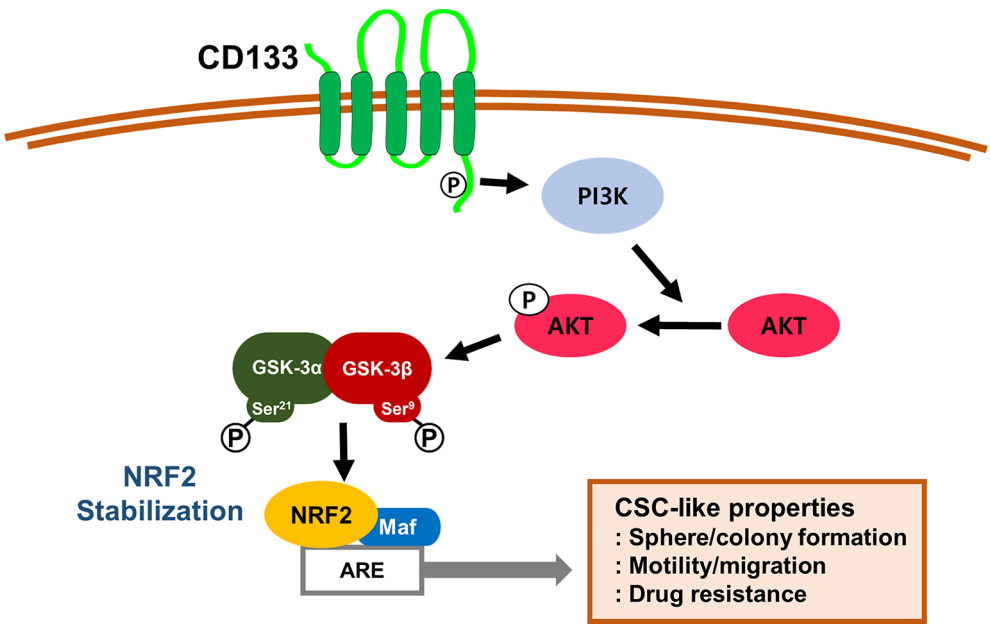

FIGURE 7 | A schematic diagram of the activation of NRF2 signaling and the development of CSC-like properties in CD133-enriched cancer cells. In colonospheres and the CD133-positive cell fraction, high CD133 levels induce PI3K/AKT activation and subsequently inactivate GSK-3β to stabilize NRF2 protein, which results in the acquisition of CSC-like properties, including anchorage-independent growth, sphere formation, facilitated migration, and resistance to anticancer drugs.

high NRF2 levels are required for the maintenance of low ROS levels and taxol resistance (56). Similarly, NRF2 elevation in mammospheres resulted in high levels of drug efflux transporters and antioxidant genes, and NRF2-silencing blocked sphere growth and induced chemosensitization (37). Approximately 3.1% of cervical CSCs were isolated from tumor specimens, NRF2 was aberrantly upregulated, and NRF2 silencing could sensitize cervical CSCs to DNA damage-induced apoptosis (34). $CD133^{+}/CD44^{+}$ colon CSCs express high levels of ABCB1 *via* NRF2 elevation, which is associated with doxorubicin resistance (57). In our previous study, $CD44^{high}CD24^{low}$ breast CSCs exhibited high levels of NRF2 signaling, and NRF2-silencing led to retarded tumor growth, suppression of sphere formation and invasion capacity, and anticancer sensitization (36). The ovarian CSC fraction with high ALDH1 retained low levels of ROS, which was accompanied by NRF2 signaling activation (35). These results suggested a critical role of NRF2 signaling in CSC maintenance and tumor resistance/recurrence and support our current observation of the association between CD133 and NRF2.

Taken together, our results indicate that CD133, a molecular marker of colon CSCs, leads to PI3K/AKT-associated NRF2 activation (**Figure 7**). High NRF2 levels in spheroid cultured HCT116 cells and the $CD133^{high}$ subpopulation contributed to the aggressive CSC phenotypes, including anticancer resistance, sphere formation, anchorage-independent colony formation, and migration potential. Therefore, the NRF2 axis might be a promising target for the inhibition of therapeutic resistance and enhancement of survival capacity under stress conditions in $CD133^{high}$ CSCs.

DATA AVAILABILITY STATEMENT

The original contributions presented in the study are included in the article/**Supplementary Material**. Further inquiries can be directed to the corresponding author.

AUTHOR CONTRIBUTIONS

JP carried out the experiment with support from SKK and SPH. SKK and SPH contributed to sample preparation, data analysis, and figure preparation. JP and MKK wrote the manuscript with the help from SKK and SPH. BHC contributed to data analysis and figure preparation. MKK conceived the original idea and supervised the project. All authors provided critical feedback and helped shape the research, analysis and manuscript preparation. All authors contributed to the article and approved the submitted version.

FUNDING

This work was supported by the National Research Foundation of Korea (NRF) grant funded by the Korean government (MSIT) (2018R1A2A1A05078894, 2018R1A6A1A03025108).

SUPPLEMENTARY MATERIAL

The Supplementary Material for this article can be found online at: https://www.frontiersin.org/articles/10.3389/fonc.2021.808300/full#supplementary-material

REFERENCES

1. Bonnet D, Dick JE. Human Acute Myeloid Leukemia is Organized as a Hierarchy That Originates From a Primitive Hematopoietic Cell. *Nat Med* (1997) 3(7):730–7. doi: 10.1038/nm0797-730
2. Huang R, Rofstad EK. Cancer Stem Cells (CSCs), Cervical CSCs and Targeted Therapies. *Oncotarget* (2017) 8(21):35351–67. doi: 10.18632/oncotarget.10169
3. Chen W, Dong J, Haiech J, Kilhoffer M-C, Zeniou M. Cancer Stem Cell Quiescence and Plasticity as Major Challenges in Cancer Therapy. *Stem Cells Int* (2016) 2016:1740936–. doi: 10.1155/2016/1740936
4. Shahriyari L, Komarova NL. Symmetric vs. Asymmetric Stem Cell Divisions: An Adaptation Against Cancer? *PloS One* (2013) 8(10):e76195. doi: 10.1371/journal.pone.0076195
5. Khan AQ, Ahmed EI, Elareer NR, Junejo K, Steinhoff M, Uddin S. Role of miRNA-Regulated Cancer Stem Cells in the Pathogenesis of Human Malignancies. *Cells* (2019) 8(8):840. doi: 10.3390/cells8080840
6. Zhao J. Cancer Stem Cells and Chemoresistance: The Smartest Survives the Raid. *Pharmacol Ther* (2016) 160:145–58. doi: 10.1016/j.pharmthera.2016.02.008
7. Tan BT, Park CY, Ailles LE, Weissman IL. The Cancer Stem Cell Hypothesis: A Work in Progress. *Lab Invest* (2006) 86(12):1203–7. doi: 10.1038/labinvest.3700488
8. Abdullah LN, Chow EK-H. Mechanisms of Chemoresistance in Cancer Stem Cells. *Clin Trans Med* (2013) 2(1):3–. doi: 10.1186/2001-1326-2-3
9. Diehn M, Cho RW, Lobo NA, Kalisky T, Dorie MJ, Kulp AN, et al. Association of Reactive Oxygen Species Levels and Radioresistance in Cancer Stem Cells. *Nature* (2009) 458(7239):780–3. doi: 10.1038/nature07733
10. Villodre ES, Kipper FC, Pereira MB, Lenz G. Roles of OCT4 in Tumorigenesis, Cancer Therapy Resistance and Prognosis. *Cancer Treat Rev* (2016) 51:1–9. doi: 10.1016/j.ctrv.2016.10.003
11. Yu F, Li J, Chen H, Fu J, Ray S, Huang S, et al. Kruppel-Like Factor 4 (KLF4) is Required for Maintenance of Breast Cancer Stem Cells and for Cell Migration and Invasion. *Oncogene* (2011) 30(18):2161–72. doi: 10.1038/onc.2010.591
12. Weigmann A, Corbeil D, Hellwig A, Huttner WB. Prominin, a Novel Microvilli-Specific Polytopic Membrane Protein of the Apical Surface of Epithelial Cells, is Targeted to Plasmalemmal Protrusions of non-Epithelial Cells. *Proc Natl Acad Sci USA* (1997) 94(23):12425–30. doi: 10.1073/pnas.94.23.12425
13. Miraglia S, Godfrey W, Yin AH, Atkins K, Warnke R, Holden JT, et al. A Novel Five-Transmembrane Hematopoietic Stem Cell Antigen: Isolation, Characterization, and Molecular Cloning. *Blood* (1997) 90(12):5013–21. doi: 10.1182/blood.V90.12.5013
14. Aghajani M, Mansoori B, Mohammadi A, Asadzadeh Z, Baradaran B. New Emerging Roles of CD133 in Cancer Stem Cell: Signaling Pathway and miRNA Regulation. *J Cell Physiol* (2019) 234(12):21642–61. doi: 10.1002/jcp.28824
15. Ricci-Vitiani L, Lombardi DG, Pilozzi E, Biffoni M, Todaro M, Peschle C, et al. Identification and Expansion of Human Colon-Cancer-Initiating Cells. *Nature* (2007) 445(7123):111–5. doi: 10.1038/nature05384
16. O'Brien CA, Pollett A, Gallinger S, Dick JE. A Human Colon Cancer Cell Capable of Initiating Tumour Growth in Immunodeficient Mice. *Nature* (2007) 445(7123):106–10. doi: 10.1038/nature05372
17. Horst D, Kriegl L, Engel J, Kirchner T, Jung A. CD133 Expression is an Independent Prognostic Marker for Low Survival in Colorectal Cancer. *Br J Cancer* (2008) 99(8):1285–9. doi: 10.1038/sj.bjc.6604664
18. Nomura A, Banerjee S, Chugh R, Dudeja V, Yamamoto M, Vickers SM, et al. CD133 Initiates Tumors, Induces Epithelial-Mesenchymal Transition and Increases Metastasis in Pancreatic Cancer. *Oncotarget* (2015) 6(10):8313–22. doi: 10.18632/oncotarget.3228
19. Bertolini G, Roz L, Perego P, Tortoreto M, Fontanella E, Gatti L, et al. Highly Tumorigenic Lung Cancer CD133+ Cells Display Stem-Like Features and are Spared by Cisplatin Treatment. *Proc Natl Acad Sci USA* (2009) 106(38):16281–6. doi: 10.1073/pnas.0905653106
20. Ma L, Liu T, Jin Y, Wei J, Yang Y, Zhang H. ABCG2 is Required for Self-Renewal and Chemoresistance of CD133-Positive Human Colorectal Cancer Cells. *Tumour Biol* (2016) 37(9):12889–96. doi: 10.1007/s13277-016-5209-5
21. Baird L, Yamamoto M. The Molecular Mechanisms Regulating the KEAP1-NRF2 Pathway. *Mol Cell Biol* (2020) 40(13):e00099–20. doi: 10.1128/mcb.00099-20
22. Cho HY, Kleeberger SR. Mitochondrial Biology in Airway Pathogenesis and the Role of NRF2. *Arch Pharm Res* (2020) 43(3):297–320. doi: 10.1007/s12272-019-01182-5
23. Otsuki A, Yamamoto M. Cis-Element Architecture of Nrf2-Smaf Heterodimer Binding Sites and its Relation to Diseases. *Arch Pharm Res* (2020) 43(3):275–85. doi: 10.1007/s12272-019-01193-2
24. Hayes JD, Dinkova-Kostova AT. The Nrf2 Regulatory Network Provides an Interface Between Redox and Intermediary Metabolism. *Trends Biochem Sci* (2014) 39(4):199–218. doi: 10.1016/j.tibs.2014.02.002
25. Shaw P, Chattopadhyay A. Nrf2-ARE Signaling in Cellular Protection: Mechanism of Action and the Regulatory Mechanisms. *J Cell Physiol* (2020) 235(4):3119–30. doi: 10.1002/jcp.29219
26. Cuadrado A, Rojo AI, Wells G, Hayes JD, Cousin SP, Rumsey WL, et al. Therapeutic Targeting of the NRF2 and KEAP1 Partnership in Chronic Diseases. *Nat Rev Drug Discov* (2019) 18(4):295–317. doi: 10.1038/s41573-018-0008-x
27. Chowdhry S, Zhang Y, McMahon M, Sutherland C, Cuadrado A, Hayes JD. Nrf2 is Controlled by Two Distinct Beta-TrCP Recognition Motifs in its Neh6 Domain, One of Which can be Modulated by GSK-3 Activity. *Oncogene* (2013) 32(32):3765–81. doi: 10.1038/onc.2012.388
28. Salazar M, Rojo AI, Velasco D, de Sagarra RM, Cuadrado A. Glycogen Synthase Kinase-3β Inhibits the Xenobiotic and Antioxidant Cell Response by Direct Phosphorylation and Nuclear Exclusion of the Transcription Factor Nrf2. *J Biol Chem* (2006) 281(21):14841–51. doi: 10.1074/jbc.M513737200
29. Cuadrado A. Structural and Functional Characterization of Nrf2 Degradation by Glycogen Synthase Kinase 3/β-TrCP. *Free Radical Biol Med* (2015) 88:147–57. doi: 10.1016/j.freeradbiomed.2015.04.029
30. Rojo AI, Sagarra M, Cuadrado A. GSK-3β Down-Regulates the Transcription Factor Nrf2 After Oxidant Damage: Relevance to Exposure of Neuronal Cells to Oxidative Stress. *J Neurochem* (2008) 105(1):192–202. doi: 10.1111/j.1471-4159.2007.05124.x
31. Choi B-H, Kim JM, Kwak M-K. The Multifaceted Role of NRF2 in Cancer Progression and Cancer Stem Cells Maintenance. *Arch Pharmacal Res* (2021) 44(3):263–80. doi: 10.1007/s12272-021-01316-8
32. Rojo de la Vega M, Chapman E, Zhang DD. NRF2 and the Hallmarks of Cancer. *Cancer Cell* (2018) 34(1):21–43. doi: 10.1016/j.ccell.2018.03.022
33. Torrente L, DeNicola GM. Targeting NRF2 and Its Downstream Processes: Opportunities and Challenges. *Annu Rev Pharmacol Toxicol* (2022) 62:279–300. doi: 10.1146/annurev-pharmtox-052220-104025
34. Jia Y, Chen J, Zhu H, Jia ZH, Cui MH. Aberrantly Elevated Redox Sensing Factor Nrf2 Promotes Cancer Stem Cell Survival *via* Enhanced Transcriptional Regulation of ABCG2 and Bcl-2/Bmi-1 Genes. *Oncol Rep* (2015) 34(5):2296–304. doi: 10.3892/or.2015.4214
35. Kim D, Choi BH, Ryoo IG, Kwak MK. High NRF2 Level Mediates Cancer Stem Cell-Like Properties of Aldehyde Dehydrogenase (ALDH)-High Ovarian Cancer Cells: Inhibitory Role of All-Trans Retinoic Acid in ALDH/NRF2 Signaling. *Cell Death Dis* (2018) 9(9):896. doi: 10.1038/s41419-018-0903-4
36. Ryoo IG, Choi BH, Ku SK, Kwak MK. High CD44 Expression Mediates P62-Associated NFE2L2/NRF2 Activation in Breast Cancer Stem Cell-Like Cells: Implications for Cancer Stem Cell Resistance. *Redox Biol* (2018) 17:246–58. doi: 10.1016/j.redox.2018.04.015
37. Ryoo I-G, Choi B-H, Kwak M-K. Activation of NRF2 by P62 and Proteasome Reduction in Sphere-Forming Breast Carcinoma Cells. *Oncotarget* (2015) 6(10):8167–84. doi: 10.18632/oncotarget.3047
38. Zhu J, Wang H, Sun Q, Ji X, Zhu L, Cong Z, et al. Nrf2 is Required to Maintain the Self-Renewal of Glioma Stem Cells. *BMC Cancer* (2013) 13(1):380. doi: 10.1186/1471-2407-13-380
39. Wu T, Harder BG, Wong PK, Lang JE, Zhang DD. Oxidative Stress, Mammospheres and Nrf2-New Implication for Breast Cancer Therapy? *Mol Carcinog* (2015) 54(11):1494–502. doi: 10.1002/mc.22202
40. Ryu D, Lee JH, Kwak MK. NRF2 Level is Negatively Correlated With TGF-β1-Induced Lung Cancer Motility and Migration *via* NOX4-ROS Signaling. *Arch Pharm Res* (2020) 43(12):1297–310. doi: 10.1007/s12272-020-01298-z

41. Choi JH, Jin SW, Lee GH, Cho SM, Jeong HG. Orostachys Japonicus Ethanol Extract Inhibits 2,4-Dinitrochlorobenzene-Induced Atopic Dermatitis-Like Skin Lesions in NC/Nga Mice and TNF-α/IFN-γ-Induced TARC Expression in HaCaT Cells. *Toxicol Res* (2020) 36(2):99–108. doi: 10.1007/s43188-019-00026-0
42. Hubert CG, Rivera M, Spangler LC, Wu Q, Mack SC, Prager BC, et al. A Three-Dimensional Organoid Culture System Derived From Human Glioblastomas Recapitulates the Hypoxic Gradients and Cancer Stem Cell Heterogeneity of Tumors Found *In Vivo*. *Cancer Res* (2016) 76(8):2465–77. doi: 10.1158/0008-5472.Can-15-2402
43. Shimozato O, Waraya M, Nakashima K, Souda H, Takiguchi N, Yamamoto H, et al. Receptor-Type Protein Tyrosine Phosphatase Kappa Directly Dephosphorylates CD133 and Regulates Downstream AKT Activation. *Oncogene* (2015) 34(15):1949–60. doi: 10.1038/onc.2014.141
44. Wei Y, Jiang Y, Zou F, Liu Y, Wang S, Xu N, et al. Activation of PI3K/Akt Pathway by CD133-P85 Interaction Promotes Tumorigenic Capacity of Glioma Stem Cells. *Proc Natl Acad Sci USA* (2013) 110(17):6829–34. doi: 10.1073/pnas.1217002110
45. Hadnagy A, Gaboury L, Beaulieu R, Balicki D. SP Analysis may be Used to Identify Cancer Stem Cell Populations. *Exp Cell Res* (2006) 312(19):3701–10. doi: 10.1016/j.yexcr.2006.08.030
46. Bao S, Wu Q, McLendon RE, Hao Y, Shi Q, Hjelmeland AB, et al. Glioma Stem Cells Promote Radioresistance by Preferential Activation of the DNA Damage Response. *Nature* (2006) 444(7120):756. doi: 10.1038/nature05236
47. Phillips TM, McBride WH, Pajonk F. The Response of CD24(-/Low)/CD44+ Breast Cancer-Initiating Cells to Radiation. *J Natl Cancer Inst* (2006) 98 (24):1777–85. doi: 10.1093/jnci/djj495
48. Herault O, Hope KJ, Deneault E, Mayotte N, Chagraoui J, Wilhelm BT, et al. A Role for GPx3 in Activity of Normal and Leukemia Stem Cells. *J Exp Med* (2012) 209(5):895–901. doi: 10.1084/jem.20102386
49. Naka K, Hoshii T, Muraguchi T, Tadokoro Y, Ooshio T, Kondo Y, et al. TGF-Beta-FOXO Signalling Maintains Leukaemia-Initiating Cells in Chronic Myeloid Leukaemia. *Nature* (2010) 463(7281):676–80. doi: 10.1038/nature08734
50. Ishimoto T, Nagano O, Yae T, Tamada M, Motohara T, Oshima H, et al. CD44 Variant Regulates Redox Status in Cancer Cells by Stabilizing the xCT Subunit of System Xc(-) and Thereby Promotes Tumor Growth. *Cancer Cell* (2011) 19(3):387–400. doi: 10.1016/j.ccr.2011.01.038
51. Dubrovska A, Kim S, Salamone RJ, Walker JR, Maira SM, García-Echeverría C, et al. The Role of PTEN/Akt/PI3K Signaling in the Maintenance and Viability of Prostate Cancer Stem-Like Cell Populations. *Proc Natl Acad Sci USA* (2009) 106(1):268–73. doi: 10.1073/pnas.0810956106
52. Chen J, Shao R, Li F, Monteiro M, Liu JP, Xu ZP, et al. PI3K/Akt/mTOR Pathway Dual Inhibitor BEZ235 Suppresses the Stemness of Colon Cancer Stem Cells. *Clin Exp Pharmacol Physiol* (2015) 42(12):1317–26. doi: 10.1111/1440-1681.12493
53. Lien EC, Lyssiotis CA, Juvekar A, Hu H, Asara JM, Cantley LC, et al. Glutathione Biosynthesis is a Metabolic Vulnerability in PI(3)K/Akt-Driven Breast Cancer. *Nat Cell Biol* (2016) 18(5):572–8. doi: 10.1038/ncb3341
54. Mitsuishi Y, Taguchi K, Kawatani Y, Shibata T, Nukiwa T, Aburatani H, et al. Nrf2 Redirects Glucose and Glutamine Into Anabolic Pathways in Metabolic Reprogramming. *Cancer Cell* (2012) 22(1):66–79. doi: 10.1016/j.ccr.2012.05.016
55. Kwak MK, Itoh K, Yamamoto M, Kensler TW. Enhanced Expression of the Transcription Factor Nrf2 by Cancer Chemopreventive Agents: Role of Antioxidant Response Element-Like Sequences in the Nrf2 Promoter. *Mol Cell Biol* (2002) 22(9):2883–92. doi: 10.1128/mcb.22.9.2883-2892.2002
56. Wu T, Harder BG, Wong PK, Lang JE, Zhang DD. Oxidative Stress, Mammospheres and Nrf2–new Implication for Breast Cancer Therapy? *Mol Carcinog* (2014) 54(11):1494–502. doi: 10.1002/mc.22202
57. Goto S, Kawabata T, Li TS. Enhanced Expression of ABCB1 and Nrf2 in CD133-Positive Cancer Stem Cells Associates With Doxorubicin Resistance. *Stem Cells Int* (2020) 2020:8868849. doi: 10.1155/2020/8868849

Conflict of Interest: The authors declare that the research was conducted in the absence of any commercial or financial relationships that could be construed as a potential conflict of interest.

Publisher's Note: All claims expressed in this article are solely those of the authors and do not necessarily represent those of their affiliated organizations, or those of the publisher, the editors and the reviewers. Any product that may be evaluated in this article, or claim that may be made by its manufacturer, is not guaranteed or endorsed by the publisher.

frontiers in Oncology

ORIGINAL RESEARCH
published: 24 February 2022
doi: 10.3389/fonc.2022.848517

All-*Trans*-Retinoic Acid Combined With Valproic Acid Can Promote Differentiation in Myeloid Leukemia Cells by an Autophagy Dependent Mechanism

Dalyia N. Benjamin[1,2,3†], Tracey R. O'Donovan[1†], Kristian B. Laursen[3], Nina Orfali[4], Mary R. Cahill[5], Nigel P. Mongan[3,6], Lorraine J. Gudas[3] and Sharon L. McKenna[1]*

[1] Cancer Research, University College Cork, Cork, Ireland, [2] Department of Haematology, Tallaght University Hospital, Dublin, Ireland, [3] Department of Pharmacology, Weill Cornell Medical College of Cornell University, New York, NY, United States, [4] Department of Haematology, St James's Hospital, Dublin, Ireland, [5] Department of Haematology, Cork University Hospital, Cork, Ireland, [6] Faculty of Medicine and Health Science, Biodiscovery Institute, University of Nottingham, Nottingham, United Kingdom

OPEN ACCESS

Edited by:
Tomofusa Fukuyama, The University of Tokyo, Japan

Reviewed by:
Ewa Teresa Marcinkowska, University of Wrołław, Poland
Shinichiro Takahashi, Tohoku Medical and Pharmaceutical University, Japan

***Correspondence:**
Sharon L. McKenna
s.mckenna@ucc.ie

†These authors have contributed equally to this work

Specialty section:
This article was submitted to Cancer Molecular Targets and Therapeutics, a section of the journal Frontiers in Oncology

Received: *04 January 2022*
Accepted: *26 January 2022*
Published: *24 February 2022*

Citation:
Benjamin DN, O'Donovan TR, Laursen KB, Orfali N, Cahill MR, Mongan NP, Gudas LJ and McKenna SL (2022) All-Trans-Retinoic Acid Combined With Valproic Acid Can Promote Differentiation Nottingham, in Myeloid Leukemia Cells by an Autophagy Dependent Mechanism. Front. Oncol. 12:848517. doi: 10.3389/fonc.2022.848517

Acute myeloid leukemia (AML) is an aggressive blood cancer with an overall survival of 30%. One form of AML, acute promyelocytic leukemia (APL) has become more than 90% curable with differentiation therapy, consisting of all-*trans*-retinoic acid (ATRA) and arsenic trioxide (ATO). Application of differentiation therapy to other AML subtypes would be a major treatment advance. Recent studies have indicated that autophagy plays a key role in the differentiation of ATRA-responsive APL cells. In this study, we have investigated whether differentiation could be enhanced in ATRA resistant cells by promoting autophagy induction with valproic acid (VPA). ATRA sensitive (NB4) and resistant leukemia cells (NB4R and THP-1) were co-treated with ATRA and valproic acid, followed by assessment of autophagy and differentiation. The combination of VPA and ATRA induced autophagic flux and promoted differentiation in ATRA-sensitive and -resistant cell lines. shRNA knockdown of ATG7 and TFEB autophagy regulators impaired both autophagy and differentiation, demonstrating the importance of autophagy in the combination treatment. These data suggest that ATRA combined with valproic acid can promote differentiation in myeloid leukemia cells by mechanism involving autophagy.

Keywords: APL, AML, ATRA, valproic acid, autophagy, differentiation, TFEB, ATG7

Abbreviations: AML, acute myeloid leukaemia; APL, acute promyelocytic leukaemia; ATG, autophagy related; ATO, arsenic trioxide; ATRA, All-*trans*-retinoic acid; BECN1, BCL-2-interacting coiled-coil protein or Beclin 1; BFA, brefeldin A; CEPBe, CCAAT enhancer-binding protein; CQ, chloroquine; CTSD, cathepsin D; ER, endoplasmic reticulum; GABARAP, gamma-aminobutyric-acid-type-A-receptor-associated protein; GCSFR, granulocyte colony-stimulating factor receptor; HATS, histone acetyltransferases; HDAC, histone deacetylase; HDACi, histone deacetylase inhibitor; hnRNPL, heterogeneous nuclear ribonucleoprotein L; HPRT, hypoxanthine phosphorybosyl transferase; HSP, heat shock protein; HSPC, heamatopoietic stem and progenitor cells; ID2, inhibitor of DNA binding family member; LC3, microtubule-associated protein 1α/β-light chain 3; LDAC, low-dose cytarabine; MDS, Myelodysplastic syndrome; PE, phosphatidylethanolamine; RARE's, retinoic acid response elements. Scr, off-target scrambled shRNA; TFEB, transcription factor EB; VPA, valproic acid.

INTRODUCTION

Acute myeloid leukemia (AML) is a group of haematopoietic disorders characterised by a failure of differentiation in myeloid progenitor cells. The clonal expansion of immature cells impairs critical aspects of haematopoiesis and requires urgent intervention. Prognosis depends on multiple factors including age, patient co-morbidity and the presence of cytogenetic and genetic abnormalities in leukemic clones (1). The outcome for adults with AML remains poor with a 5-year survival rate of ~40% for younger patients (18–60 years) and until recently was as low as ~10% for patients above the age of 60 years (2, 3). While therapies have advanced in the last 5 years (4), there remains an urgent need for better, well tolerated, outpatient-based management strategies in older adults. One particular subgroup of AML, acute promyelocytic leukemia (APL), which represents about 5-10% of cases, has undergone a radical improvement in treatment outcomes in the last 30 years with the advent of differentiation therapy. Current chemotherapy-free treatment regimens for low to intermediate-risk APL, based on all-*trans*-retinoic acid (ATRA) and arsenic trioxide (ATO), achieve complete remission rates exceeding 90% and overall survival of 85-99% (5).

Most APL cells have a specific cytogenetic abnormality involving a translocation between chromosomes 15 and 17 t (15,17), leading to the formation of an abnormal fusion gene *PML/RARα*. The PML-RARα oncoprotein binds to retinoic acid response elements (RAREs) on retinoid target gene promoters and has a high affinity for co-repressor histone deacetylases (HDACs) (6, 7). This leads to repressive epigenetic changes that inhibit the transcription of RARα target genes required for differentiation (8). In addition, PML-RARα disrupts the organisation of nuclear PML bodies (9). When ATRA binds to PML/RARα, co-repressors are released and co-activators including histone acetyltransferases (HATS) are recruited to decompress chromatin and initiate transcription (10, 11). ATRA also influences the stability of the PML-RARα oncoprotein by promoting its degradation through co-operating proteolytic mechanisms [reviewed in (12)]. The introduction of arsenic trioxide (ATO) into the protocol can eliminate the leukemic stem cell, generating a lasting cure (13).

The evolution of APL therapy away from chemotherapy has been a remarkable achievement and the application of this approach to other forms of AML would be hugely advantageous, particularly for older patients, who are often ineligible for intensive chemotherapy due to co-morbidities. However, despite an increased understanding of the molecular abnormalities in other AML subtypes, no targeted agent has been developed that can overcome the repression of differentiation to the extent achieved with ATRA in APL. One approach has been to globally release the repression of gene expression using inhibitors of epigenetic regulators. Several epigenetic drugs have either been approved for AML or are in clinical development [reviewed in (14)]. It is currently unclear how much of their anti-leukemic activity is related to effects on differentiation – as direct induction of apoptosis and cell cycle arrest are also reported activities of these agents (15).

Autophagy has now been identified as a key component of differentiation in myeloid leukemia cells. Canonical autophagy is a highly conserved catabolic process in which cells self-digest organelles and other macromolecular complexes by forming a double-membraned vesicle around sequestered cytoplasmic material, termed the autophagosome. Fusion of the autophagosome with a lysosome generates an autolysosome, which facilitates the degradation and recycling of macromolecules back to the cytoplasm for anabolic activities. At least two forms of alternative autophagy have been characterised, mainly through autophagy gene knockouts in mouse embryonic fibroblasts. These include (i) BECN1-independent autophagy and (ii) ATG5- and ATG7-independent autophagy. In conventional autophagy, autophagosome biogenesis is initiated at various intracellular membranes such as the ER and mitochondria, whereas in alternative autophagy, the Golgi is the primary membrane source for autophagosomes. Both forms of alternative/non-canonical autophagy are inhibited by the Golgi inhibitor and anti-viral agent, brefeldin A (BFA) (16–18).

Autophagy is important for various aspects of haematopoiesis including the cellular remodelling involved in differentiation (19). A compelling role for autophagy in the development of AML has come from knockout studies of key autophagy genes. Loss of either ATG7 or ATG5 in haematopoietic stem and progenitor cells (HSPC) leads to a lethal pre-leukemic phenotype in mice (20, 21). In addition, heterozygous loss of ATG5 in a MLL-ENL murine model of AML led to a more aggressive leukemic phenotype (21). These studies indicate that effective autophagy will protect against leukemic transformation and is consistent with other studies suggesting compromised autophagy in AML (22, 23).

We and others have demonstrated the importance of autophagy in ATRA-induced differentiation (24). We subsequently conducted RNAseq analysis following ATRA treatment of APL cells and found that 84 genes implicated in autophagy were differentially expressed. One of these genes was *TFEB*, a master regulator of autophagy and lysosome biogenesis. shRNA-mediated depletion of TFEB impacted both autophagy and expression of differentiation associated genes. Interestingly, inhibition of alternative autophagy with BFA also impeded ATRA-induced autophagy and differentiation suggesting more than one autophagy pathway is likely to be involved in differentiation (25).

In the current paper we investigate the possibility of enhancing differentiation through the promotion of autophagy. To this end, we sought a clinically approved agent with (i) a reasonable toxicity profile and (ii) reported activity in the induction of both autophagy and differentiation. Valproic acid (VPA), is a HDAC inhibitor with activity against Type I and IIa histone deacetylases (15). It has been used safely for decades to treat epilepsy and bipolar disorder and is well tolerated by cancer and leukemia patients (26, 27). VPA has previously been reported to have anti-leukemic effects and to promote differentiation in the presence of ATRA (28, 29). It has also been demonstrated to induce autophagy (30–33). It is not known whether these activities are directly or indirectly linked. It is also not known whether autophagy is important for the activity of the

combination treatment, as the HDAC inhibitory activity of VPA may induce several co-operating pathways.

We have therefore examined VPA as a co-agent with ATRA, for the treatment of sensitive and resistant APL (NB4 and NB4R cells) and non-APL AML leukemia cells (THP-1 cells), which are differentiation resistant. We have evaluated both differentiation and autophagy induced by the compounds alone and in combination. We have demonstrated the importance of autophagy in this drug combination through shRNA knockdown of the ATG7 and TFEB autophagy regulators in NB4 cells. In addition, BFA treatment inhibits VPA and ATRA induced autophagy, indicating the possibility of alternative autophagy pathways playing a role in the differentiation induced. These data suggest that the induction of autophagy is a key component of an effective differentiation-inducing regimen in myeloid leukemia cells.

MATERIALS AND METHODS

Cell Culture and Drug Treatments

NB4 human APL cells were a gift from Dr. David Scheinberg (Memorial Sloan Kettering Institute, New York, NY, USA). The ATRA-resistant NB4R cell line was a gift from Prof. Pier Paolo-Pandolfi (Beth Israel Deaconess Cancer Centre, Boston, MA, USA). Cells were cultured at 37°C, 5% CO_2 in HyClone RPMI 1640 medium (GE Healthcare Life Sciences SH30027), supplemented with 10% foetal calf serum (Sigma-Aldrich, F7524) and 1% penicillin/streptomycin (Invitrogen, 10378-016). THP-1 cells (monocytic-lineage) were from the American Type Culture Collection (ATCC). Cells were cultured in RPMI 1640 (1x) medium (Gibco by Life technologies, 21870-076), supplemented with 10% foetal calf serum and 1% penicillin/streptomycin. Cells were seeded at $5x10^4$ cells/ml prior to treatment. ATRA (Sigma-Aldrich, R2625) was used to induce differentiation at 1 μM, diluted from a 1 mM stock in 100% ethanol (EtOH). Control populations were treated with 0.1% v/v EtOH. Valproic acid (Sigma-Aldrich, P4543) was used at 1 mM concentration, diluted from a 500mM stock in H_20.

RNA Extraction, Reverse Transcription, Quantitative PCR (RT-qPCR)

Total cellular RNA was harvested using TriZol (Invitrogen, 15596-018), according to the manufacturer's protocol. Total RNA (1μg) was reverse transcribed using qScript (Quanta Biosciences, 95047) as per product protocol at a final reaction volume of 20μL and the resulting cDNA was diluted 1:10 in H_2O. Subsequent qRT-PCR reactions were carried out using 2μL of template together with 1x SYBR Green Supermix (Quanta Biosciences, 84091), forward and reverse primers at 0.25uM and 2.5μL H_2O in a final reaction volume of 15μL. Reactions were run on a Bio-Rad MyiQ™ Single Colour Real-time PCR detection system with each cycle including a 94°C x 20sec denaturation step, 60°C x 20sec annealing step and a 72°C x 30sec extension step. Primer pairs are listed in **Table 1**. The transcript levels in biological replicates (n=6) were normalized to *HPRT* transcript levels and relative differences were calculated using the Pfaffl method (34). Graphical displays and measurements of statistical significance were performed on GraphPad Prism software.

Morphology

Cells were cytospun onto glass slides and stained with Rapi-Diff (Braidwood Laboratories, 22007, 22008, 22009) according to product guidelines. Granulocytic differentiation was assessed by light microscopy using an Olympus DP70 digital microscope (Mason Technology, Ireland). Cells with lobular/sub-divided nuclei were scored as differentiated.

Western Blotting

Cells were lysed in modified RIPA buffer (50 mM TrisHCl - pH 7.4, 150 mM NaCl, 0.25% sodium deoxycholate, 1% Igepal, 1 mM EDTA, 1x Pefabloc, 1x Protease inhibitor cocktail, 1 mM Na_3VO_4, 1 mM NaF). Protein samples were separated on NuPAGE 4-12%, Bis-Tris gels (Invitrogen, NP0322) and electrophoretically transferred onto PVDF membranes (Invitrogen, IB401001). Membranes were incubated with anti-LC3 (MBL, PD014) antibody, diluted 1/500 in 5% milk overnight, at 4°C and with ß-actin (loading control) (Sigma-Aldrich, A5441) for 1 hour at room temperature. Proteins were visualized using relevant IR-DYE secondary antibodies and quantified on the Odyssey IR imaging system (Li-Cor, Cambridge, UK). All bands were quantified, normalised to ß-actin and presented as integrated intensities, with all bands normalised to untreated control cells. For all western blots, integrated intensities shown are representative of three independent experiments.

TABLE 1 | List of Primer pairs used.

	Gene Name	Forward Primer	Reverse Primer
Differentiation associated	CD11β	ATGGAGTTCAATCCCAGGGAAG	GAGTCCAGAGCCAGGTCATAAG
	ID2	CACTGTGTGGCTGAATAAGCGGTGT	GTAAGAGAACACCCTGGGAAGATG
	GCSFR	ATCCTGGACTGCGTGCCCAAG	AGCATGGGGGGCTCCAGTTTCA
	CEBP	ACAATCCCCTGCAGTACCAAG	ACTGCCTTCTTGCCCTTGTG
Autophagy associated	*CTSD*	TGCTCAAGAACTACATGGACGC	CGAAGACGACTGTGAAGCACT
	GABARAP	GGGCGAGAAGATCCGAAAGA	TCCAGGTCTCCTATCCGAGC
	TFEB	AAGCGAGAGCTCACAGATGC	TGAGGATGGTGCCCTTGTTC
	ATG16L1	TTGCAAGCCGAATCTGGACTGT	GGTCGTGACTTCCTGAGACAAT
Control	*HPRT*	TGCTCGAGATGTGATGAAGG	TCCCCTGTTGACTGGTCATT

Flow Cytometry

Live cells were incubated for 30 min with PE-conjugated anti-CD11b antibody (eBioscience, 12-0118) in 1% albumin/phosphate buffered saline (PBS), and washed with PBS prior to analysis. Fluorescence was detected using a BD-LSRII flow cytometer (BD Biosciences, Oxford, UK). Data analysis and histogram overlays were performed on FlowJo software.

ATG7 and TFEB knockdown cells. ATG7 and TFEB knockdown cell lines were previously generated using shRNA vectors targeting ATG7 and TFEB and non-gene targeting scrambled controls (Scr). Gene expression levels and effect on downstream targets is detailed in previous publications (24, 25).

Statistical Analysis

Statistical analysis was carried out using GraphPad Prism 5 software. Means were compared using independent student t-tests (unpaired). The p-value was considered statistically significant when it was *p < 0.05, **p < 0.005, ***p < 0.0005.

RESULTS

VPA Promotes ATRA-Mediated Differentiation in ATRA Sensitive and Resistant Cell Lines

We investigated whether valproic acid (VPA) alone and in combination with all-*trans*-retinoic acid (ATRA) could induce differentiation in ATRA sensitive and resistant acute promyelocytic leukemia (APL) cell lines (NB4, NB4R) (**Figure 1** and **Supplementary Figure 1**) and in a non-APL, differentiation resistant myeloid leukemia cell line (THP-1) (**Supplementary Figures 2A, B**). Cells were treated with VPA (1 mM) or ATRA (1 μM) alone or in combination for 72 hours. For clarity, the combination treatment is referred to in the figures as "VPA & ATRA". Expression levels of four known markers of myeloid differentiation were evaluated by RT-qPCR. Data for *CD11β* and granulocyte colony-stimulating factor receptor (*GCSFR*) are shown in **Figure 1A**, with additional differentiation markers, *CEPBε* and *ID2*, shown in **Supplementary Figure 1**. In NB4 cells, expression of (i) *CD11β* and (ii) *GCSFR* was significantly increased in the combination treatment compared to treatment with either agent alone (p = 0.0077 and p = 0.0197 respectively). In the ATRA-resistant NB4R cells, ATRA alone had no significant effect on transcript levels, but the combination of VPA and ATRA induced a significant increase in both differentiation markers [**Figure 1A (iii) and (iv)**] (p < 0.0001). Similar to the NB4R cells, THP-1 cells displayed little or no *CD11β* or *GCSFR* expression in response to ATRA alone, but we observed a significant increase in the combination treated cells (**Supplementary Figure 2A**) (p < 0.0001 and p = 0.0071 respectively).

Surface expression of CD11β protein was also examined by flow cytometry (**Figure 1B**). As shown previously (24), surface CD11β expression is significantly elevated in response to ATRA alone (red histogram overlay) in NB4 cells (p < 0.0001) and this was not further enhanced by the addition of VPA (blue overlay) [**Figure 1B (i)**]. The NB4R cells however, display a significant increase in surface CD11β in combination treated cells (blue overlay) when compared to either ATRA (red overlay) (p < 0.0001) or VPA alone (green overlay) (p = 0.0011) [**Figure 1B (ii)**]. In THP-1 cells, surface CD11β is also significantly enhanced in the combination treated cells compared to ATRA (p = 0.0014) or VPA alone (p = 0.004) (**Supplementary Figure 2B**).

Morphological assessment shows granulocytic differentiation in ATRA-treated and combination treated NB4 cells (denoted with red arrows) [**Figure 1C (i)**]. In the ATRA resistant NB4R cells, differentiation is only evident with the combination of VPA and ATRA [**Figure 1C (ii**), lower right panel]. In THP1 cells, morphological features of differentiation were also only observed with the combination treatment (**Supplementary Figure 2C**).

VPA Promotes ATRA-Induced Autophagy in ATRA Sensitive and Resistant Cell Lines

We and others have previously shown that ATRA induces autophagy in the APL NB4 cell line (24). Here, we investigate whether VPA can enhance the autophagy induced by ATRA in NB4 cells and whether it can help to initiate autophagy in the ATRA-resistant NB4R and THP-1 cells. Cells were treated with VPA (1 mM) or ATRA (1 μM) alone or in combination for 72 hours. Induction of autophagy was initially examined by RT-qPCR assessment of key autophagy genes, identified from our previous RNAseq analysis as induced in ATRA sensitive cells (25). Expression of both *TFEB* and *ATG16L* increased in response to ATRA or VPA alone in ATRA-sensitive NB4 cells, with a further significant increase in cells treated with the combination [**Figure 2A (i, ii)**] (p = 0.0013, 0.0078 respectively). ATRA alone had no significant effect on *TFEB* and *ATG16L* transcript levels in NB4R cells, but the addition of VPA to ATRA induced a significant increase in expression of both *TFEB* and *ATG16L* [**Figure 2A (iii, iv)**] (p < 0.0001, = 0.0001 respectively). Additional autophagy associated genes *GABARAP* and *CTSD* are shown in **Supplementary Figure 3**.

The presence of autophagosomes was then quantified by flow cytometry, using the fluorescent autophagosome marker Cyto-ID (**Figure 2B**). ATRA treatment induced autophagosome accumulation in the NB4 cell line (red overlay), which was significantly increased by the addition of VPA (blue overlay) (p = 0.0208), [**Figure 2B (i)**]. VPA alone induced a backward shift (green overlay), indicating that less autophagosomes accumulate in the presence of VPA [**Figure 2B (i)**]. This suggests that VPA is either inhibiting autophagy or promoting faster turnover of autophagosomes. To distinguish this, cells were treated with the lysosome inhibitor, chloroquine (CQ), (10 μM) for two hours prior to the addition of VPA, ATRA or VPA with ATRA. CQ raises lysosomal pH, inhibiting autophagosome-lysosome fusion. CQ treatment alone will therefore cause an increase in fluorescence due to a block in the turnover of existing/basal autophagosomes. In cells co-treated with another agent, accumulation of autophagosomes beyond that observed with CQ alone represents new autophagosome production.

In **Figure 2B (ii, iv)**, all cells are treated with CQ. In NB4 cells, the addition of CQ caused a shift of the grey histogram to the right [**Figure 2B (ii)**], (compared to the grey histogram in

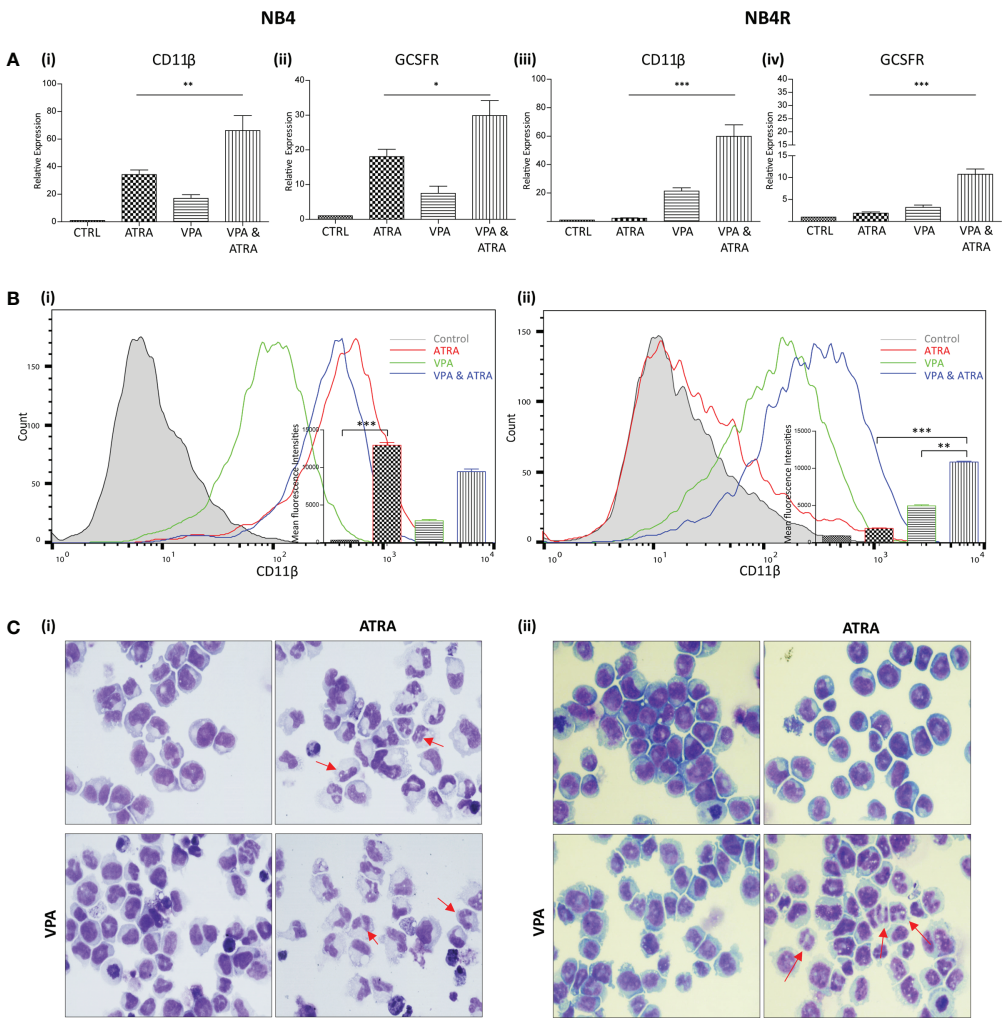

FIGURE 1 | Valproic acid (VPA) promotes all-*trans*-retinoic acid (ATRA)-mediated myeloid differentiation in ATRA sensitive and ATRA resistant, acute promyelocytic leukemia (APL) cell lines (NB4 and NB4R). NB4 and NB4R cell lines were treated with either ATRA (1 μM) or VPA (1mM) alone or in combination for 72 hours. Induction of differentiation was assessed by measuring **(A)** expression levels of known differentiation genes CD11β **(i, iii)** and GCSFR **(ii, iv)** by RT-qPCR. Raw Ct values were normalised to a housekeeping gene and data are shown as n-fold induction compared to untreated controls (n = 3). **(B)** Expression of surface CD11β (eBioscience antibody) by flow cytometry was assessed in NB4 **(i)** and NB4R **(ii)** cells. Colours are as follows: control untreated (grey histogram), ATRA (red overlay), VPA (green overlay) and VPA&ATRA treated cells (blue overlay). A single representative histogram is shown, with mean fluorescence intensity ± SEM presented in the inset graph (n = 4). ***p < 0.0005, **p < 0.005, *p < 0.05. **(C)** Morphological features of granulocytic differentiation were assessed by light microscopy (400x) in NB4 **(i)** and NB4R **(ii)** cells. Red arrows indicate cells with lobular/sub-divided nuclei, a feature of granulocytic differentiation.

[**Figure 2B(i)**], indicative of a block in the turnover of basal autophagy. Interestingly, VPA also demonstrated increased autophagosome accumulation in the presence of CQ (green histogram). This indicates that VPA is an inducer of autophagy, and that the backward shift in fluorescence with the VPA treatment noted above [**Figure 2B (i)**] is likely to be due to enhanced lysosomal processing of autophagosomes. It is possible that valproic acid may enhance the delivery to lysosomes, or increase the availability of lysosomes for autophagosome turnover. Indeed, the increased expression of TFEB (a master regulator of lysosome biogenesis), in response to VPA (shown in **Figure 2A**), may contribute to this effect.

Further autophagosomes accumulated in NB4 cells in the presence of ATRA and CQ (red overlay) and this was again enhanced by the VPA&ATRA combination [**Figure 2B (ii)**, blue overlay] ($p = 0.005$), demonstrating that autophagic flux is significantly induced by the combination treatment.

In the NB4R cells, autophagy was only evident when CQ was added, with a significant increase seen in the combination of VPA and ATRA [**Figure 2B (iv)**, blue overlay], compared to CQ, or ATRA and CQ ($p = 0.017$ and 0.0229 respectively.)

Induction of autophagy was also confirmed by examining the levels of a known autophagy marker, LC3. LC3I becomes conjugated to phosphatidylethanolamine (PE), to form LC3II,

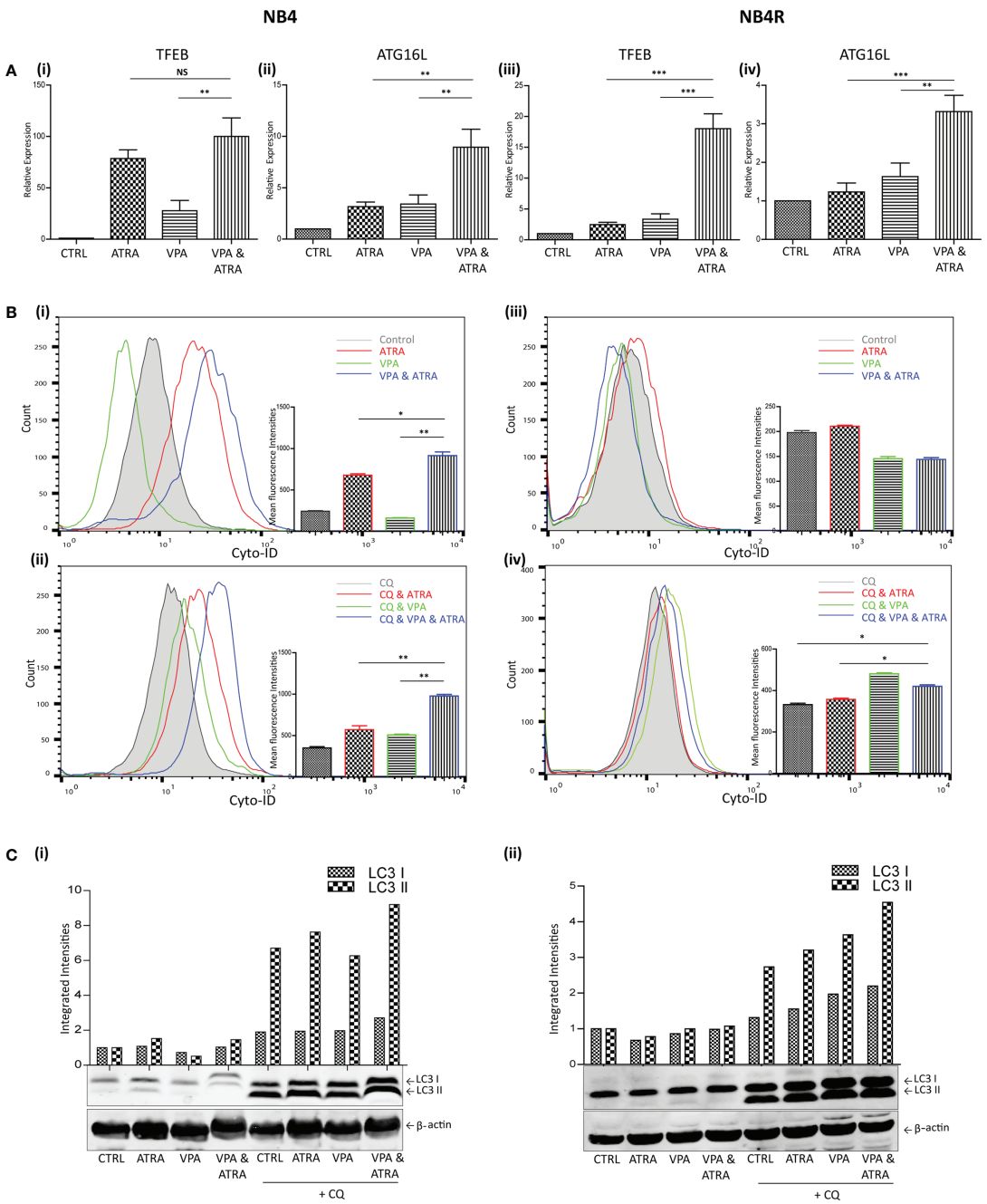

FIGURE 2 | Valproic acid (VPA) promotes all-*trans*-retinoic acid (ATRA)-induced autophagy in ATRA sensitive and ATRA resistant, acute promyelocytic leukemia (APL) cell lines (NB4 and NB4R). NB4 and NB4R cell lines were treated with either ATRA (1 μM) or VPA (1mM) alone or a combination of both for 72 hours. To assess autophagy flux, chloroquine (CQ) (10 μM) was added 2 hours prior to the addition of ATRA, VPA or combination treatment. Autophagy induction was assessed by measuring **(A)** mRNA expression of autophagy regulators, TFEB **(i, iii)** and ATG16L **(ii, iv)** by RT-qPCR. Raw Ct values were normalised to a housekeeping gene and data are shown as n-fold induction compared to untreated controls (n = 3). **(B)** Cyto ID was used to assess autophagosome formation in NB4 **(i)** and NB4R **(iii)** cells in response to ATRA (red overlay), VPA (green overlay) and VPA&ATRA (blue overlay) relative to untreated controls (grey histogram). Flux was analysed in NB4 **(ii)** and NB4R **(iv)** cells with the addition of CQ to all treatments, which are then assessed relative to CQ alone-control cells (grey histogram). Data from three independent experiments is presented in the inset graph as mean fluorescence intensities ± SEM ***$p < 0.0005$, **$p < 0.005$, *$p < 0.05$. **(C)** Autophagic flux was assessed by western blot analysis of LC3II levels in NB4 **(i)** and NB4R **(ii)** cells, following treatment with ATRA, VPA or a combination of both, in the absence (lanes 1-4) and presence of chloroquine (CQ) (lanes 5-8). An increase in LC3II in cells treated with VPA, ATRA & CQ (lane 8), beyond that induced with chloroquine alone (lane 5) is indicative of flux. All bands were quantified using the Odyssey Infrared Imaging System (Li-COR), normalised to ß-actin and presented as integrated intensities, with all bands normalised to untreated control cells (lane 1). For all western blots, integrated intensities are representative of three independent experiments (n = 3). NS, not significant.

which is incorporated into forming autophagosome membranes. Accumulation of LC3II was assessed by western blot (**Figure 2C**). Both NB4 and NB4R cell lines demonstrated basal autophagy flux with the addition of CQ (lane 5 (i) and (ii)), with an increased accumulation in VPA&ATRA treated cells (lane 8), beyond that observed with CQ or ATRA and CQ (lanes 5 & 6).

In a similar pattern to NB4R cells, THP-1 cells displayed little or no difference in transcript levels of either *TFEB* or *ATG16L* in response to ATRA alone, with a significant increase observed with the addition of VPA to ATRA [**Supplementary Figure 2D (i, ii)**], (p = 0.0131, 0.0127). Evidence of autophagy flux was only obvious when CQ was added [**Supplementary Figure 2E (ii, iii)**], noted in both Cyto-ID and western blot analysis (suggesting rapid autophagosome turnover), with significantly higher levels of autophagosomes in the combination treatment (blue overlay and lane 8), compared to ATRA alone (red overlay and lane 5) (p = 0.0144).

Collectively these data demonstrate that VPA promotes both ATRA-induced myeloid differentiation and autophagy in ATRA sensitive and ATRA resistant, APL and non-APL cell lines.

shRNA-Mediated Depletion of ATG7 Attenuates VPA and ATRA-Induced Autophagy and Differentiation in APL Cells

We have previously demonstrated the importance of the autophagy regulator ATG7, in ATRA-induced differentiation (24). Here we have investigated whether ATG7 is also important for autophagy and differentiation induced by the combination of ATRA and VPA. ATG7 was depleted by lentivirus-mediated shRNA knockdown in NB4 cells, as previously described and validated in (24). Following treatment with either VPA (1 mM) or ATRA (1 μM) alone or in combination for 72 hours, autophagy levels were compared in scrambled (Scr) and the ATG7 KD clone. Basal autophagy was significantly reduced in the ATG7 KD clone [**Figure 3A (i)** black overlay] compared to the Scr control cells (grey filled overlay) (p = 0.0031). Triplicate data is graphed in **Figure 3A (ii)**. In addition, the loss of ATG7 completely reduced autophagy induced by the VPA and ATRA combination (blue overlay), compared to Scr control cells (red overlay) (p < 0.0001). The loss of ATG7 also significantly reduced ATRA-induced and VPA-induced autophagy [**Supplementary Figure 4A (i, ii)**, pink and blue overlay respectively]. Western blot analysis of LC3II confirmed these data, with significant reduction in LC3II levels in ATRA and combination treated ATG7 KD clones (**Figure 3B**, lanes 4 and 8).

The loss of ATG7 however, induced a significant increase in basal expression of surface CD11β [**Figure 3C (i, ii)** black overlay] compared to Scr control cells (grey filled overlay) (p = 0.0074). Despite this increase in basal expression, VPA and ATRA-induced CD11β expression was significantly reduced in the ATG7 clone (blue overlay) (p = 0.0014) compared to the scramble control treated clone (red overlay). The loss of ATG7 also attenuated ATRA-induced CD11β expression [**Supplementary Figure 4B (i, ii)** pink overlay] with no change in VPA-induced expression [**Supplementary Figure 4B (i, ii)**, blue overlay]. We cannot rule out the possibility that autophagy may be involved in the stability or degradation of CD11β. Expression of CD11β might then be elevated by depletion of ATG7. Nevertheless, loss of ATG7 still reduces the significant enhancement of CD11β expression induced by the ATRA VPA combination treatment (blue and red histogram overlays) suggesting that autophagy plays a role in the promotion of differentiation by this treatment.

shRNA-Mediated Depletion of TFEB Attenuates VPA and ATRA-Induced Autophagy and Differentiation in APL Cells

We have previously demonstrated the significant role that TFEB plays in ATRA-induced autophagy and differentiation (25). We therefore investigated whether TFEB is also involved in the autophagy and granulocytic differentiation induced by the combination treatment in NB4 cells. As previously described (25), TFEB was depleted by lentivirus-mediated shRNA knockdown in NB4 cells. Following treatment with either VPA or ATRA alone or in combination for 72 hours, expression levels of TFEB were assessed by RT-qPCR, in wild type (green bars), scrambled control (Scr) (blue bars) and a TFEB KD clone (red bars). A significant reduction of TFEB expression was evident in all treatments of the TFEB KD clone (red histograms), relative to the Scr and Wild Type (**Figure 4A**) (p = 0.0013). Expression levels of additional transcripts, identified as important for autophagy and induced by ATRA, in our previous RNAseq analysis were also examined (25). *ATG16L*, *CTSD* and *GABARAP* mRNA levels were all reduced in the TFEB KD clone following treatment [**Supplementary Figure 5A (i-iii)**].

Unlike the ATG7 KD, the loss of TFEB induced an increase in basal autophagosome levels (black overlay) compared to Scr controls (filled grey overlay) (p = 0.0088). However, loss of TFEB still significantly reduced the autophagy induced by the combination of VPA & ATRA (blue overlay) compared to the Scr control treated clone (red overlay) [**Figure 4B (i, ii)**] (p = 0.049). The loss of TFEB also reduced ATRA-induced and VPA-induced autophagy [**Supplementary Figure 5B (i, ii)**, pink and blue overlay respectively].

Expression levels of *CD11β* and *GCSFR* as determined by RT-qPCR, again showed a marked reduction in the TFEB knockdown clone [**Figure 4C (i, ii)** red bars], following treatment with ATRA, VPA or the combination (p < 0.0001, 0.0001).

Similar to ATG7 knockdown clones, the loss of TFEB induced a significant increase in basal expression of surface CD11β (black overlay) compared to scramble controls (grey histogram) [**Figure 4D (i, ii)**] (p = 0.0027). Yet, again there was still a significant reduction in the VPA & ATRA-induced CD11β expression (blue overlay) in the TFEB knockdown clone, as compared to the Scr control treated clone (red overlay) (p = 0.0231). The loss of TFEB also significantly reduced the ATRA-induced CD11β expression [**Supplementary Figure 5C (i, ii)**, pink overlay] with an increase in VPA-induced expression [**Supplementary Figure 5C (i, ii)**, blue overlay].

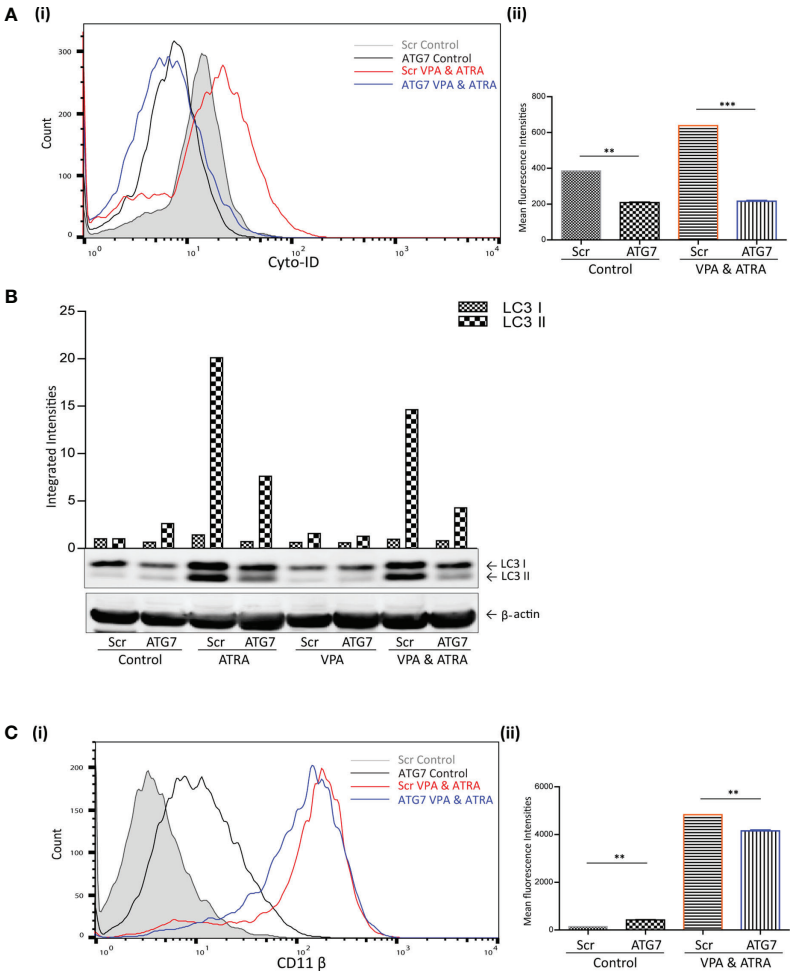

FIGURE 3 | ATG7 knockdown attenuated valproic acid (VPA) & all-*trans*-retinoic acid (ATRA)-induced autophagy and differentiation. ATG7 was knocked down in NB4 cells using lentiviral transduction of target-specific short hairpin (sh)RNA (ATG7). NB4 cells were also transduced with an off-target scrambled shRNA (Scr). Both cell lines were treated with either ATRA (1 μM) or VPA (1mM) alone or a combination of both for 72 hours. **(A) (i)** Cyto-ID was used to assess autophagosome content in control untreated Scr (grey histogram), untreated ATG7 knockdown (black overlay), VPA&ATRA treated Scr (red overlay) and ATG7 knockdown (blue overlay) cell lines. **(ii)** Data from three independent experiments is presented in the graph to the right, as mean fluorescence intensities ± SEM ***p < 0.0005, **p < 0.005. **(B)** Western blot analysis of LC3II levels in Scr and ATG7 knockdown cells, following treatment with ATRA, VPA or a combination of both. All bands were quantified using the Odyssey Infrared Imaging System (Li-COR), normalised to ß-actin and presented as integrated intensities, with all bands normalised to Scr untreated control cells (lane 1). For all western blots, integrated intensities are representative of three independent experiments (n = 3). **(C) (i)** The induction of differentiation was assessed by measuring expression of surface CD11β by flow cytometry in untreated Scr (grey histogram), untreated ATG7 KD (black overlay), and VPA&ATRA treated Scr (red overlay) and ATG7 KD (blue overlay) cells. A single representative histogram is shown, with mean fluorescence intensity ± SEM presented in graph to the right **(ii)** (n = 4) **p < 0.005.

Together, these data demonstrate that loss of either autophagy regulators, ATG7 or TFEB, impedes granulocytic differentiation induced by ATRA and VPA co-treatment, demonstrating the importance of autophagy in the activity of this combination.

Brefeldin A (BFA) Augmented the Effects of ATG7 and TFEB Depletion on VPA and ATRA-Induced Autophagy and Differentiation in APL Cells

TFEB is only one of several transcription factors known to influence autophagy and alternative mechanisms of autophagy have been described which do not require all of the canonical components of autophagy initiation complexes (16). We previously showed that ATRA could induce autophagy that was independent of TFEB (25). This alternative ATRA-induced autophagy was sensitive to the Golgi inhibitor BFA, which disrupts an autophagy pathway that originates at the Golgi (17). We therefore examined if BFA-sensitive autophagy might contribute to the autophagy induced by the combination of ATRA and VPA in the ATG7 and TFEB KD cells. Scramble, ATG7 and TFEB KD clones were treated with ATRA (1 μM) and VPA (1 mM) for 72 hours, and 24 hours prior to analysis, BFA (10 μM) was added to inhibit Golgi-initiated autophagy.

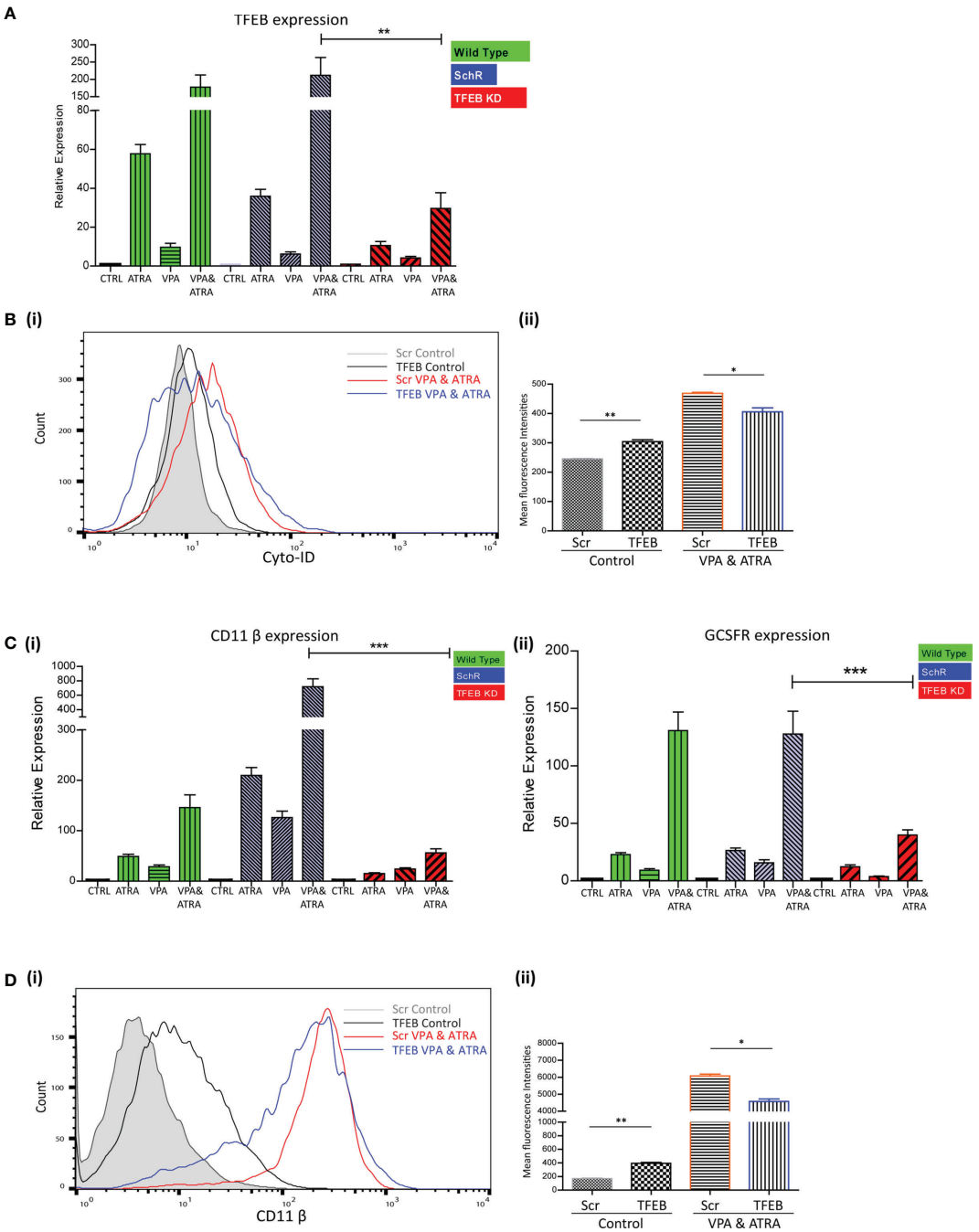

FIGURE 4 | TFEB knockdown attenuated valproic acid (VPA) & all-*trans*-retinoic acid (ATRA)-induced autophagy and differentiation. TFEB was knocked down in NB4 cells using lentiviral transduction of target-specific short hairpin (sh)RNA (TFEB). NB4 cells were also transduced with an off-target scrambled shRNA (Scr). Both cell lines were treated with either ATRA (1 μM) or VPA (1mM) alone or a combination of both for 72 hours. **(A)** Expression levels of TFEB were assessed by RT-qPCR, in wild type (green bars), Scr (blue bars) and TFEB KD (red bars) cell lines. Raw Ct values were normalised to a housekeeping gene and data are shown as n-fold induction compared to untreated controls for each cell line (n = 3) $^{**}p < 0.005$. **(B) (i)** Cyto-ID was used to assess autophagosome formation in untreated Scr (grey histogram), untreated TFEB knockdown (black overlay), VPA&ATRA treated Scr (red overlay) and TFEB knockdown (blue overlay) cell lines. **(ii)** Data from three independent experiments is presented in the graph to the right, as mean fluorescence intensities ± SEM $^{**}p < 0.005$, $^{*}p < 0.05$. **(C)** Expression levels of known differentiation genes CD11β **(i)** and GCSFR **(ii)** were assessed by RT-qPCR, in wild type (green bars) Scr (blue bars) and TFEB KD (red bars) cells. Raw Ct values were normalised to a housekeeping gene and data are shown as n-fold induction compared to untreated controls for each cell line (n = 3) $^{***}p < 0.0005$. **(D) (i)** The induction of differentiation was assessed by measuring expression of surface CD11β by flow cytometry in untreated Scr (grey histogram), untreated TFEB KD (black overlay), and VPA&ATRA treated Scr (red overlay) and TFEB KD (blue overlay) cells. A single representative histogram is shown, with mean fluorescence intensity ± SEM presented in the graph to the right **(ii)** (n = 4) $^{**}p < 0.005$, $^{*}p < 0.05$.

The addition of BFA to the combination treated scramble cells (Scr VPA&ATRA, red overlay) significantly reduced autophagosome accumulation relative to combination treated Scr cells (grey histogram) ($p = 0.0026$ and $p = 0.001$, respectively) [**Figure 5A (i, ii)**)] Knockdown of ATG7 or TFEB also significantly reduced the level of autophagosomes induced by the combination treatment of VPA and ATRA (black overlays) relative to their scramble control cells (grey histogram) ($p < 0.0001$ and $p = 0.049$, respectively). Importantly, autophagosome levels were then further reduced by the addition of BFA in both Atg7 ($p = 0.0012$) and TFEB ($p = 0.0017$) knockdown clones (**Figure 5A** blue overlays versus black).

LC3II levels were assessed for the same treatments by Western blot analysis [**Figure 5B (i)**]. These are graphed separately [**Figure 5B (ii, iii)**] for each knockdown cell line for clarity. These data indicate that the addition of BFA significantly reduced LC3II levels in VPA & ATRA treated clones [**Figure 5B (ii, iii)**]. It has been reported that LC3II is not necessarily required for alternative autophagy (16, 18), but here we notice an impact on LC3II in response to the presence of BFA. This may be a result of an overlap between pathways or effects of BFA on overall protein synthesis.

Disruption of this alternative, Golgi-derived autophagy with BFA resulted in a corresponding reduction of VPA&ATRA-induced differentiation in both clones [**Figure 5C (i, ii)**, blue overlays versus black] ($p = 0.0005$ and $p = 0.0027$ respectively).

These data were combined as triplicate mean fluorescence intensities, normalised to combination treated scramble clones. Taken together these data highlight the effect of ATG7 and TFEB silencing on VPA&ATRA-induced autophagy and differentiation, an effect that is further enhanced by BFA treatment. These experiments do not allow us to differentiate between a reduction in surface CD11β due to inhibition of an alternative autophagy pathway or due to impaired Golgi trafficking. More selective inhibitors of alternative autophagy pathways should help to address this question in future studies.

DISCUSSION

This study has shown that VPA can promote autophagy and differentiation in ATRA treated APL cells and in ATRA resistant APL and non-APL myeloid leukemia cells. Autophagy is important for differentiation as shRNA knockdown of the key autophagy regulators, ATG7 or TFEB, impedes both autophagy and differentiation. The mechanism by which autophagy is induced by VPA is currently unknown and may be related to its activity as a HDAC inhibitor.

As HDAC enzymes contribute to the repressive effects of PML-RARα, a combination of a ATRA and a HDAC inhibitor is a logical approach to improve efficacy. VPA has shown activity in inducing apoptosis, arrest or differentiation in a variety of cell line models (reviewed in (27) and primary AML blasts (35). Several phase I/II clinical trials have been conducted in the last decade with myelodysplastic syndrome (MDS) or AML using VPA as a monotherapy or in combination with ATRA. Activity was modest and disappointing overall, as complete or partial remissions were rarely observed [reviewed in (27)]. Trials with other HDAC agents as single agents have also shown modest hematologic improvements in a subset of patients (15). Further combination strategies to improve efficacy have been evaluated, such as combining a demethylating agent to help release transcriptional repression. A recent Phase I/II trial combined 5-azacytidine with VPA and ATRA, with impressive results. The overall response rate was 42% and in previously untreated older patients, the response rate was 52% which is favourable for an out-patient based therapy (36); (https://clinicaltrials.gov/ct2/show/NCT00326170). These data compare advantageously to trials with 5-aza-2'-deoxycytidine (decitabine) and 5-azacytidine as single agents, but a randomised trial would be required to establish this. Four biomarkers were evaluated in this trial: VPA levels, histone acetylation, global DNA hypomethylation and induction of p21 and p15 expression. Higher VPA levels were found in patients who responded, versus those who did not, which implies that a more potent HDAC inhibitor may improve the activity of the protocol. However, while histone acetylation was observed, this was not associated with response, nor were VPA levels associated with histone acetylation. In addition, there was no correlation between clinical response and induction of hypomethylation, or expression of *p21* and *p15* mRNA. Other molecular effects may therefore contribute to the efficacy of this drug combination in these patients.

Several studies have now demonstrated that acetylation regulates many non-histone targets (37). Class II HDAC inhibitors have been shown to target p53 and HIF1α and have cytoplasmic targets, including a-tubulin, HSP70 and HSP90 [reviewed in (15)]. Analysis of VPA targets in CML cells identified several acetylated cytoplasmic proteins including HSP90 and hnRNPL (38). Recent advances in mass spectrometry proteomic approaches have identified thousands of novel acetylation sites, with most on non-nuclear proteins. Acetylation was particularly widespread in the mitochondrial proteome and metabolic enzymes (39). It is therefore possible that the key targets of successful HDAC inhibitors have yet to be discovered and current markers of activity are therefore unable to represent efficacy of these agents.

Our data suggest that autophagy is important for the differentiation induced by the combination of VPA and ATRA. Autophagy has previously been shown to be induced by VPA, but the mechanism is poorly understood. It is possible that autophagy genes are epigenetically silenced in these cells and this is relieved by VPA. Epigenetic regulation of autophagy has been well described (40, 41). However, it is also possible that autophagy is promoted by non-epigenetic mechanisms. Acetylation of cytoplasmic autophagy regulators ULK1, TFEB and ATG proteins has been reported (42–44). It is also interesting that tubulin acetylation is essential for fusion of autophagosomes to lysosomes (45). A HDACi may therefore improve this trafficking of autophagosomes to lysosomes and therefore reduce the overall cellular content of autophagosomes, due to more efficient turnover. This is also consistent with an unexplained feature in **Figure 2B (i)**, where VPA reduced the

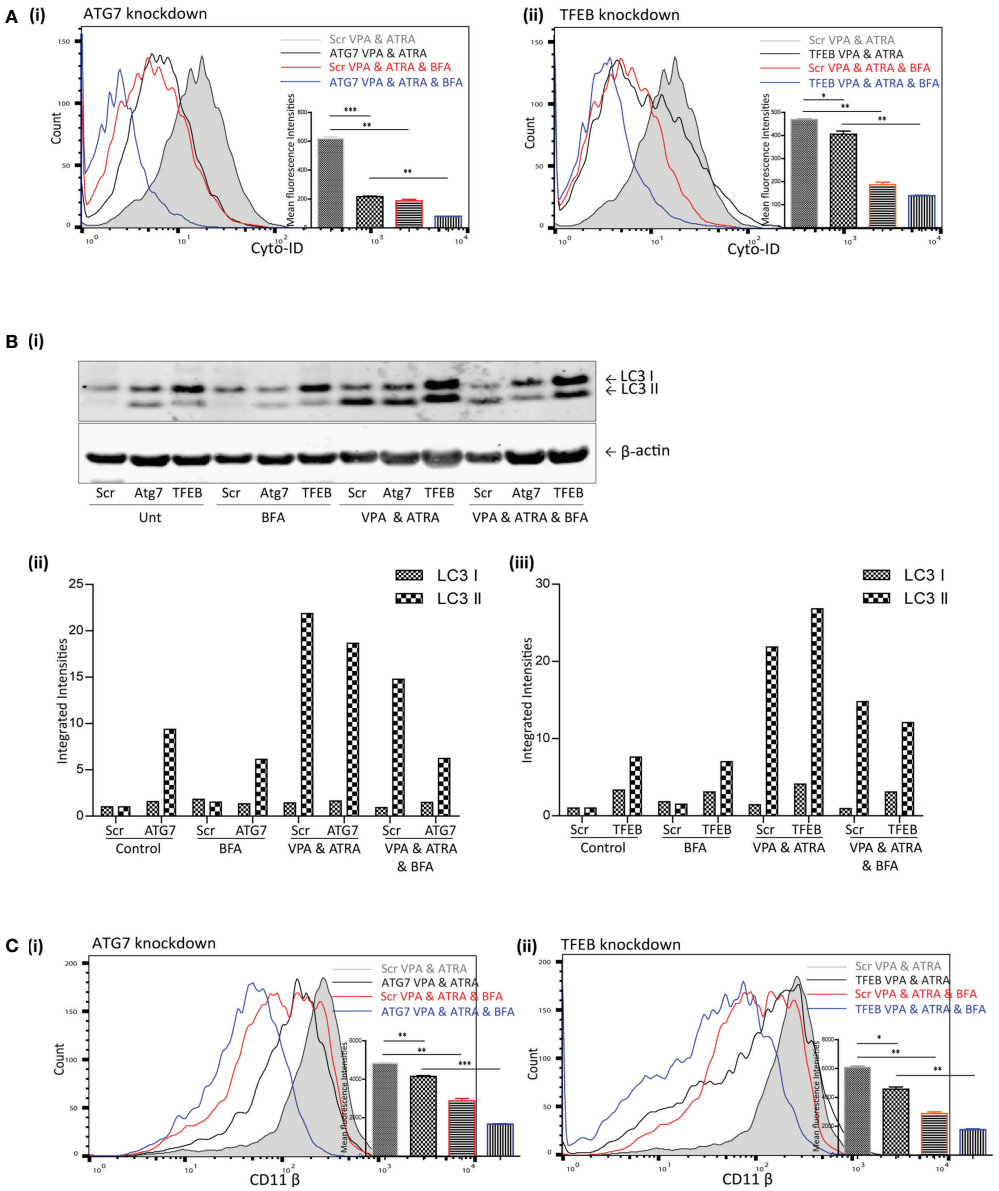

FIGURE 5 | Brefeldin A (BFA) augmented the effects of ATG7 and TFEB depletion on VPA & ATRA-induced autophagy and differentiation. NB4 cells expressing non-targeting shRNA (Scr) or shRNA targeting ATG7 or TFEB were treated with a combination of VPA (1mM) & ATRA (1 μM) for 72 hours. To assess the effects of BFA on VPA&ATRA-induced autophagy and differentiation, cells were treated with BFA (10 μM) for 24 hours prior to analysis. **(A)** Cyto-ID was used to assess autophagosome formation in ATG7 knockdown **(i)** or TFEB knockdown **(ii)** cell lines; VPA&ATRA treated Scr (grey histograms), VPA&ATRA treated knockdown clones (black overlays), VPA&ATRA&BFA treated Scr (red overlays) and knockdown clones treated with VPA&ATRA&BFA (blue overlays). Data from three independent experiments is presented in the inset graph, as mean fluorescence intensities ± SEM ***$p < 0.0005$, **$p < 0.005$, *$p < 0.05$. **(B)** Western blot analysis of LC3II levels in Scr, ATG7 and TFEB knockdown cells, following treatment with VPA and ATRA in the absence or presence of BFA **(i)**. All bands were quantified using the Odyssey Infrared Imaging System (Li-COR), normalised to ß-actin and presented here as separate integrated intensities for each knockdown cell line – Atg7 **(ii)** and TFEB **(iii)**, with all bands normalised to Scr untreated control cells (lane 1). **(C)** The induction of differentiation was assessed by measuring expression of surface CD11β in in ATG7 knockdown **(i)** or TFEB knockdown **(ii)** cell lines; VPA&ATRA treated Scr (grey histograms), VPA&ATRA treated knockdown clones (black overlays), VPA&ATRA&BFA treated Scr (red overlays) and knockdown clones treated with VPA&ATRA&BFA (blue overlays). Data from three independent experiments is presented in the inset graph, as mean fluorescence intensities ± SEM ***$p < 0.0005$, **$p < 0.005$, *$p < 0.05$.

basal autophagosome content (measured with Cyto-ID), an effect that was abolished by inhibiting the lysosome with chloroquine, **Figure 2B (ii)**. Further studies are now required to properly evaluate the key targets of VPA and other HDAC inhibitors, so that better markers for clinical trials can be established. Our data would suggest that where induction of differentiation is the objective of treatment, a marker of autophagy induction could be useful.

Our data with BFA indicates that non-canonical/alternative autophagy may also play a significant role in differentiation in AML cells. Further knockdown studies with genes specific for this pathway would be needed to confirm this. Interestingly, another study has suggested that haematopoietic stem cells rely on ATG7-dependant canonical autophagy, whereas more differentiated myeloid cells can use either pathway (46). Beclin1 independent autophagy has also been recently reported during ATRA induced differentiation of APL cells (23). Undoubtedly further insights are into the diverse mechanisms of autophagy regulation and the importance of specific pathways are required so that autophagy can be more selectively modulated for clinical benefit.

The Bcl-2 inhibitor Venetoclax has recently emerged as a new treatment option for older adults with AML and may become the benchmark for testing new developments. As a single agent it has modest anti-leukemic activity (47), however combinations with hypomethylating agents (HMAs) azacitidine/decitabine or with low-dose cytarabine (LDAC) have shown activity and were FDA approved in 2018 for AML [reviewed in (48)]. Further studies are however required on the molecular determinants of response. Venetoclax is only modestly efficacious in relapsed/refractory or secondary AML and AML patients with adverse cytogenetics and high risk mutations continue to have poorer outcomes [reviewed in (49)]. The full extent of its mechanisms of action, including possible actions on autophagy, remain to be defined. The expression levels of Bcl-2 alone do not seem to be predictive of response, rather the expression of interacting Bcl-2 family members, such as Bax and Bad and upregulation of other anti-apoptotic family members such as Mcl-1 and Bcl-xL are thought to be more relevant (47, 49). It is notable that one of the key interacting partners of Bcl-2 is the autophagy regulator Beclin-1. Beclin-1 has a BH3 domain that can interact with Bcl-2 or Bcl-xL (50). It is interesting in this regard that many BH3 mimetics have been shown to induce autophagy (51, 52), including venetoclax (53, 54). It would be interesting to assess whether venetoclax can influence autophagy and ATRA induced differentiation in AML cells.

The overall concept of differentiation therapy is particularly apposite given recent experience with the global COVID-19 pandemic, when hospital resources have never been scarcer and the need to avoid profound immunosuppression in patients with blood cancers is a high priority. Re-examination of inexpensive, low toxicity compounds such as VPA is more relevant now than ever before. It is hoped that new strategies will emerge for the potential treatment of AML patients, particularly aimed at reducing the complexity of clinical care and improving quality of life.

CONCLUSIONS

This study has shown that a combination of valproic acid and ATRA can induce differentiation in myeloid leukemia cells. shRNA knockdown of ATG7 or TFEB autophagy regulators impaired both autophagy and differentiation, indicating the importance of autophagy in this combination treatment. In addition, impeding non-canonical/alternative autophagy with brefeldin A (BFA), was found to further inhibit VPA and ATRA induced autophagy and differentiation in the knockdown cells, suggesting the involvement of more than one autophagy pathway. These data support accumulating evidence that autophagy is a key component of an effective differentiation-inducing regimen in myeloid leukemia cells.

Other clinical studies would suggest that additional compounds are likely to be needed to comprise a clinically efficacious regimen. Our data would suggest that new combination strategies should consider the impact of modulation of autophagy on the compounds being tested. Further interrogation of the mechanistic interplay between autophagy pathways and differentiation in leukemia is warranted to improve therapeutic regimes in the future

DATA AVAILABILITY STATEMENT

The original contributions presented in the study are included in the article/**Supplementary Material**. Further inquiries can be directed to the corresponding author.

AUTHOR CONTRIBUTIONS

Conceptualization; SLM, LJG, NPM, TOD and MRC. Methodology; TOD, DNB, KBL, NO. Data curation and analysis, TOD, DNB, KBL. Construction and validation of ATG7 and TFEB knockdown cell lines, NO and TOD. Preparation of manuscript; SLM and TOD. Review and editing; SLM, TOD, MRC, LJG, KBL and NM. Supervision, SLM, LJG, and NPM. All authors have read and agreed to the published version of the manuscript.

FUNDING

DB was funded by the Haematology Education and Research Trust (HERO) and Breakthrough Cancer Research (BCR). TO'D was funded by BCR. This research was also supported by the National Institutes of Health (CA043796) (LG.) and by Weill Cornell funds. The financial support of the University of Nottingham, University College Cork and Higher Education Authority of Ireland is gratefully acknowledged.

SUPPLEMENTARY MATERIAL

The Supplementary Material for this article can be found online at: https://www.frontiersin.org/articles/10.3389/fonc.2022.848517/full#supplementary-material

Supplementary Figure 1 | VPA promotes ATRA-mediated myeloid differentiation in ATRA sensitive and ATRA resistant, acute promyelocytic leukemia (APL) cell lines

(NB4 and NB4R). NB4 and NB4R cell lines were treated with either ATRA (1 μM) or VPA (1mM) alone or a combination of both for 72 hours. The induction of differentiation was assessed by measuring expression levels of additional differentiation genes CEBP and ID2 by RT-qPCR. Raw Ct values were normalised to a housekeeping gene and data are shown as n-fold induction compared to untreated controls (n = 3). Expression levels of ID2 were significantly enhanced by the addition of VPA to ATRA in the ATRA-resistant NB4R cells. CEBPε was not significantly induced in NB4R cells relative to ATRA alone. Expression levels were not increased in ATRA-sensitive NB4 cells – which are already sensitive to ATRA. ***p < 0.0005, **p < 0.005, *p < 0.05.

Supplementary Figure 2 | Valproic acid (VPA) promotes all-*trans*-retinoic acid (ATRA)-mediated differentiation and autophagy in ATRA resistant, non-APL THP-1 cells. The THP-1 cell line was treated with either ATRA (1 μM) or VPA (1mM) alone or a combination of both for 72 hours. Induction of differentiation was assessed by measuring **(A)** expression levels of known differentiation genes **(i)** CD11β and **(ii)** GCSFR by RT-qPCR. Raw Ct values were normalised to a housekeeping gene and data are shown as n-fold induction compared to untreated controls (n = 3). **(B)** Expression of surface CD11β by flow cytometry was assessed. Control untreated (grey histogram), ATRA (red overlay), VPA (green overlay) and VPA&ATRA treated cells (blue overlay). A single representative histogram is shown, with mean fluorescence intensity ± SEM presented in the graph to the right (n = 4). **(C)** Morphological features of granulocytic differentiation were assessed by light microscopy (400x) in THP-1 cells. Red arrows indicate cells with features of granulocytic differentiation. Autophagy induction was assessed by measuring **(D)** expression levels of genes, important for autophagy, **(i)** TFEB and **(ii)** ATG16L by RT-qPCR. Raw Ct values were normalised to a housekeeping gene and data are shown as n-fold induction compared to untreated controls (n = 3). **(E) (i)** Cyto ID was used to assess autophagosome formation in response to ATRA (red overlay), VPA (green overlay) and VPA&ATRA (blue overlay) relative to untreated controls (grey histogram). **(ii)** Flux was analysed with the addition of CQ to treated cells, relative to CQ alone control cells (grey histogram). Data from three independent experiments is presented in the inset graph as mean fluorescence intensities ± SEM. **(iii)** Western blot analysis of LC3II levels in the absence (lanes 1-4) and presence of chloroquine (CQ) (lanes 5-8). An increase in LC3II in cells treated with VPA&ATRA & CQ (lane 8), beyond that induced with chloroquine alone (lane 5) is indicative of flux. All bands were quantified using the Odyssey Infrared Imaging System (Li-COR), normalised to ß-actin and presented as integrated intensities, with all bands normalised to untreated control cells (lane 1) ***p < 0.0005, **p < 0.005, *p < 0.05. For all western blots, integrated intensities are representative of three independent experiments (n = 3).

Supplementary Figure 3 | Valproic acid (VPA) promotes all-*trans*-retinoic acid (ATRA)-mediated autophagy in ATRA sensitive and ATRA resistant, acute promyelocytic leukemia (APL) cell lines (NB4 and NB4R). NB4 and NB4R cell lines were treated with either ATRA (1μM) or VPA (1mM) alone or a combination of both for 72 hours. Induction of autophagy was assessed by measuring expression levels of additional autophagy genes GABARAP and CTSD by RT-qPCR. Raw Ct values were normalised to a housekeeping gene and data are shown as n-fold induction compared to untreated controls (n = 3). Expression levels of both additional markers were enhanced by the addition of VPA to ATRA in the ATRA-resistant NB4R cells. Levels were not significantly different from ATRA alone in the ATRA-sensitive NB4 cells ***p < 0.0005, **p < 0.005.

Supplementary Figure 4 | ATG7 knockdown attenuated valproic acid (VPA) and all-*trans*-retinoic acid (ATRA)-induced autophagy and acute promyelocytic leukemia (APL) cell differentiation. ATG7 was knocked down in NB4 cells using lentiviral transduction of target-specific short hairpin (sh)RNA (ATG7). NB4 cells were also transduced with an off-target scrambled shRNA (Scr). Both cell lines were treated with either ATRA (1μM) or VPA (1mM) alone for 72 hours. **(A) (i)** Cyto-ID was used to assess autophagosome formation in control untreated Scr (grey histogram), untreated ATG7 knockdown (black overlay), ATRA treated Scr (red overlay) and ATG7 knockdown (pink overlay) and VPA treated Scr (green overlay) and ATG7 knockdown (blue overlay) cell lines. **(ii)** Data from three independent experiments is presented in the graph to the right, as mean fluorescence intensities ± SEM. **(B) (i)** Expression of surface CD11β was assessed in control untreated Scr (grey histogram), untreated ATG7 knockdown (black overlay), ATRA treated Scr (red overlay) and ATG7 knockdown (pink overlay) and VPA treated Scr (green overlay) and ATG7 knockdown (blue overlay) cell lines. A single representative histogram is shown, with mean fluorescence intensity ± SEM presented in graph to the right (n = 4).

Supplementary Figure 5 | TFEB knockdown attenuated VPA and ATRA-induced autophagy and differentiation. TFEB was knocked down in NB4 cells using lentiviral transduction of target-specific short hairpin (sh)RNA (TFEB). NB4 cells were also transduced with an off-target scrambled shRNA (Scr). Both cell lines were treated with either ATRA (1μM) or VPA (1mM) alone for 72 hours. **(A)** Expression levels of additional genes, identified as important for autophagy were examined. Expression levels of **(i)** ATG16L, **(ii)** CTSD and **(iii)** GABARAP were reduced in the TFEB clone, following treatment (red bars). **(B) (i)** Cyto-ID was used to assess autophagosome formation in control untreated Scr (grey histogram), untreated TFEB knockdown (black overlay), ATRA treated Scr (red overlay) and TFEB knockdown (pink overlay) and VPA treated Scr (green overlay) and TFEB knockdown (blue overlay) cell lines. **(ii)** Data from three independent experiments is presented in the graph to the right, as mean fluorescence intensities ± SEM (* **). **(C) (i)** Expression of surface CD11β was assessed. Control untreated Scr (grey histogram), untreated TFEB knockdown (black overlay), ATRA treated Scr (red overlay) and TFEB knockdown (pink overlay) and VPA treated Scr (green overlay) and TFEB knockdown (blue overlay) cell lines. A single representative histogram is shown, with mean fluorescence intensity ± SEM presented in graph to the right (n = 4) ***p < 0.0005, **p < 0.005, *p < 0.05.

REFERENCES

1. Döhner H, Estey E, Grimwade D, Amadori S, Appelbaum FR, Büchner T, et al. Diagnosis and Management of AML in Adults: 2017 ELN Recommendations From an International Expert Panel. *Blood* (2017) 129:424–47. doi: 10.1182/blood-2016-08-733196
2. Döhner H, Weisdorf DJ, Bloomfield CD. Acute Myeloid Leukemia. *N Engl J Med* (2015) 373(12):1136–52. doi: 10.1056/NEJMra1406184
3. Wang ES. Treating Acute Myeloid Leukemia in Older Adults. *Hematol (U States)* (2014) 2014(1):14–20. doi: 10.1182/asheducation-2014.1.14
4. Short NJ, Konopleva M, Kadia TM, Borthakur G, Ravandi F, DiNardo CD, et al. Advances in the Treatment of Acute Myeloid Leukemia: New Drugs and New Challenges. *Cancer Discov* (2020) 10(4):506–25. doi: 10.1158/2159-8290.CD-19-1011
5. Thomas X. Acute Promyelocytic Leukemia: A History Over 60 Years—From the Most Malignant to the Most Curable Form of Acute Leukemia. *Oncol Ther* (2019) 7(1):33–65. doi: 10.1007/s40487-018-0091-5
6. Lin RJ, Nagy L, Inoue S, Shao W, Miller J, Evans RM. Role of the Histone Deacetylase Complex in Acute Promyelocytic Leukaemia. *Nature* (1998) 391 (6669):811–4. doi: 10.1038/35895
7. Di Croce L, Raker VA, Corsaro M, Fazi F, Fanelli M, Faretta M, et al. Methyltransferase Recruitment and DNA Hypermethylation of Target Promoters by an Oncogenic Transcription Factor. *Sci (80-)* (2002) 295 (5557):1079–82. doi: 10.1126/science.1065173
8. Grignani F, De Matteis S, Nervi C, Tomassoni L, Gelmetti V, Cioce M, et al. Fusion Proteins of the Retinoic Acid Receptor-α Recruit Histone Deacetylase in Promyelocytic Leukaemia. *Nature* (1998) 391(6669):815–8. doi: 10.1038/35901
9. de Thé H, Le Bras M, Lallemand-Breitenbach V. Acute Promyelocytic Leukemia, Arsenic, and PML Bodies. *J Cell Biol* (2012) 198(1):11–21. doi: 10.1083/jcb.201112044
10. Fazi F, Travaglini L, Carotti D, Palitti F, Diverio D, Alcalay M, et al. Retinoic Acid Targets DNA-Methyltransferases and Histone Deacetylases During APL Blast Differentiation *In Vitro* and *In Vivo*. *Oncogene* (2005) 24(11):1820–30. doi: 10.1038/sj.onc.1208286
11. Gudas LJ. Retinoids Induce Stem Cell Differentiation via Epigenetic Changes. *Semin Cell Dev Biol* (2013) 24:701–5. doi: 10.1016/j.semcdb.2013.08.002
12. Orfali N, McKenna SL, Cahill MR, Gudas LJ, Mongan NP. Retinoid Receptor Signaling and Autophagy in Acute Promyelocytic Leukemia. *Exp Cell Res* (2014) 324:1–12. doi: 10.1016/j.yexcr.2014.03.018

13. Zheng X, Seshire A, Rüster B, Bug G, Beissert T, Puccetti E, et al. Arsenic But Not All-Trans Retinoic Acid Overcomes the Aberrant Stem Cell Capacity of PML/Rarα-Positive Leukemic Stem Cells. *Haematologica* (2007) 92(3):323–31. doi: 10.3324/haematol.10541
14. Bewersdorf JP, Shallis R, Stahl M, Zeidan AM. Epigenetic Therapy Combinations in Acute Myeloid Leukemia: What Are the Options? *Ther Adv Hematol* (2019) 10:1–19. doi: 10.1177/2040620718816698
15. José-Enériz ES, Gimenez-Camino N, Agirre X, Prosper F. HDAC Inhibitors in Acute Myeloid Leukemia. *Cancers* (2019) 11:1–24. doi: 10.3390/cancers11111794
16. Shimizu S. Biological Roles of Alternative Autophagy. *Mol Cells* (2018) 41:50–4. doi: 10.14348/molcells.2018.2215
17. Grose C, Klionsky DJ. Alternative Autophagy, Brefeldin A and Viral Trafficking Pathways. *Autophagy* (2016) 12:1429–30. doi: 10.1080/15548627.2016.1203489
18. Arakawa S, Honda S, Yamaguchi H, Shimizu S. Molecular Mechanisms and Physiological Roles of Atg5/Atg7-Independent Alternative Autophagy. *Proc Japan Acad Ser B: Phys Biol Sci* (2017) 93:378–85. doi: 10.2183/pjab.93.023
19. Riffelmacher T, Simon AK. Mechanistic Roles of Autophagy in Hematopoietic Differentiation. *FEBS J* (2017) 284:1008–20. doi: 10.1111/febs.13962
20. Mortensen M, Soilleux EJ, Djordjevic G, Tripp R, Lutteropp M, Sadighi-Akha E, et al. The Autophagy Protein Atg7 is Essential for Hematopoietic Stem Cell Maintenance. *J Exp Med* (2011) 208(3):455–67. doi: 10.1084/jem.20101145
21. Watson AS, Riffelmacher T, Stranks A, Williams O, De Boer J, Cain K, et al. Autophagy Limits Proliferation and Glycolytic Metabolism in Acute Myeloid Leukemia. *Cell Death Discov* (2015) 1:1–10. doi: 10.1038/cddiscovery.2015.8
22. Evangelisti C, Evangelisti C, Chiarini F, Lonetti A, Buontempo F, Neri LM, et al. Autophagy in Acute Leukemias: A Double-Edged Sword With Important Therapeutic Implications. *Biochim Biophys Acta - Mol Cell Res* (2015) 1853:14–26. doi: 10.1016/j.bbamcr.2014.09.023
23. Jin J, Britschgi A, Schläfli AM, Humbert M, Shan-Krauer D, Batliner J, et al. Low Autophagy (ATG) Gene Expression Is Associated With an Immature AML Blast Cell Phenotype and can be Restored During AML Differentiation Therapy. *Oxid Med Cell Longev* (2018) 2018:1–17. doi: 10.1155/2018/1482795
24. Orfali N, O'Donovan TR, Nyhan MJ, Britschgi A, Tschan MP, Cahill MR, et al. Induction of Autophagy Is a Key Component of All-Trans-Retinoic Acid-Induced Differentiation in Leukemia Cells and a Potential Target for Pharmacologic Modulation. *Exp Hematol* (2015) 43(9):781–93.e2. doi: 10.1016/j.exphem.2015.04.012
25. Orfali N, O'Donovan TR, Cahill MR, Benjamin D, Nanus DM, McKenna SL, et al. All-Trans Retinoic Acid (ATRA)-Induced TFEB Expression Is Required for Myeloid Differentiation in Acute Promyelocytic Leukemia (APL). *Eur J Haematol* (2020) 104(3):236–50. doi: 10.1111/ejh.13367
26. David KA, Mongan NP, Smith C, Gudas LJ, Nanus DM. Phase I Trial of ATRA-IV and Depakote in Patients With Advanced Solid Tumor Malignancies. *Cancer Biol Ther* (2010) 9(9):678–84. doi: 10.4161/cbt.9.9.11436
27. Kuendgen A, Gattermann N. Valproic Acid for the Treatment of Myeloid Malignancies. *Cancer* (2007) 110:943–54. doi: 10.1002/cncr.22891
28. Cimino G, Lo-Coco F, Fenu S, Travaglini L, Finolezzi E, Mancini M, et al. Sequential Valproic Acid/All-Trans Retinoic Acid Treatment Reprograms Differentiation in Refractory and High-Risk Acute Myeloid Leukemia. *Cancer Res* (2006) 66(17):8903–11. doi: 10.1158/0008-5472.CAN-05-2726
29. Fredly H, Gjertsen BT, Bruserud Ø. Histone Deacetylase Inhibition in the Treatment of Acute Myeloid Leukemia: The Effects of Valproic Acid on Leukemic Cells, and the Clinical and Experimental Evidence for Combining Valproic Acid With Other Antileukemic Agents. *Clin Epigenet* (2013) 5:12. doi: 10.1186/1868-7083-5-12
30. Torgersen ML, Engedal N, Bøe SO, Hokland P, Simonsen A. Targeting Autophagy Potentiates the Apoptotic Effect of Histone Deacetylase Inhibitors in T (8,21) AML Cells. *Blood* (2013) 122(14):2467–76. doi: 10.1182/blood-2013-05-500629
31. Ji MM, Wang L, Zhan Q, Xue W, Zhao Y, Zhao X, et al. Induction of Autophagy by Valproic Acid Enhanced Lymphoma Cell Chemosensitivity Through HDAC-Independent and IP3-Mediated PRKAA Activation. *Autophagy* (2015) 11(12):2160–71. doi: 10.1080/15548627.2015.1082024
32. Xia Q, Zheng Y, Jiang W, Huang Z, Wang M, Rodriguez R, et al. Valproic Acid Induces Autophagy by Suppressing the Akt/mTOR Pathway in Human Prostate Cancer Cells. *Oncol Lett* (2016) 12(3):1826–32. doi: 10.3892/ol.2016.4880
33. Wang Y, Hao CL, Zhang ZH, Wang LH, Yan LN, Zhang RJ, et al. Valproic Acid Increased Autophagic Flux in Human Multiple Myeloma Cells *In Vitro*. *BioMed Pharmacother* (2020) 127:1–6. doi: 10.1016/j.biopha.2020.110167
34. Pfaffl MW. A New Mathematical Model for Relative Quantification in Real-Time RT-PCR. *Nucleic Acids Res* (2001) 29(9):e45. doi: 10.1093/nar/29.9.e45
35. Göttlicher M, Minucci S, Zhu P, Krämer OH, Schimpf A, Giavara S, et al. Valproic Acid Defines a Novel Class of HDAC Inhibitors Inducing Differentiation of Transformed Cells. *EMBO J* (2001) 20(24):6969–78. doi: 10.1093/emboj/20.24.6969
36. Soriano AO, Yang H, Faderl S, Estrov Z, Giles F, Ravandi F, et al. Safety and Clinical Activity of the Combination of 5-Azacytidine, Valproic Acid, and All-Trans Retinoic Acid in Acute Myeloid Leukemia and Myelodysplastic Syndrome. *Blood* (2007) 110(7):2302–8. doi: 10.1182/blood-2007-03-078576
37. Narita T, Weinert BT, Choudhary C. Functions and Mechanisms of Non-Histone Protein Acetylation. *Nat Rev Mol Cell Biol* (2019) 20:156–74. doi: 10.1038/s41580-018-0081-3
38. Buchi F, Pastorelli R, Ferrari G, Spinelli E, Gozzini A, Sassolini F, et al. Acetylome and Phosphoproteome Modifications in Imatinib Resistant Chronic Myeloid Leukaemia Cells Treated With Valproic Acid. *Leuk Res* (2011) 35(7):921–31. doi: 10.1016/j.leukres.2011.01.033
39. Choudhary C, Weinert BT, Nishida Y, Verdin E, Mann M. The Growing Landscape of Lysine Acetylation Links Metabolism and Cell Signalling. *Nat Rev Mol Cell Biol* (2014) 15:536–50. doi: 10.1038/nrm3841
40. Peixoto P, Grandvallet C, Feugeas JP, Guittaut M, Hervouet E. Epigenetic Control of Autophagy in Cancer Cells: A Key Process for Cancer-Related Phenotypes. *Cells* (2019) 8:1–30. doi: 10.3390/cells8121656
41. Baek SH, Kim K. Epigenetic Control of Autophagy: Nuclear Events Gain More Attention. *Mol Cell* (2017) 65:781–5. doi: 10.1016/j.molcel.2016.12.027
42. Webster BR, Scott I, Traba J, Han K, Sack MN. Regulation of Autophagy and Mitophagy by Nutrient Availability and Acetylation. *Biochim Biophys Acta - Mol Cell Biol Lipids* (2014) 1841:525–34. doi: 10.1016/j.bbalip.2014.02.001
43. Li YT, Yi C, Chen CC, Lan H, Pan M, Zhang SJ, et al. A Semisynthetic Atg3 Reveals That Acetylation Promotes Atg3 Membrane Binding and Atg8 Lipidation. *Nat Commun* (2017) 8:1–9. doi: 10.1038/ncomms14846
44. Zhang J, Wang J, Zhou Z, Park JE, Wang L, Wu S, et al. Importance of TFEB Acetylation in Control of its Transcriptional Activity and Lysosomal Function in Response to Histone Deacetylase Inhibitors. *Autophagy* (2018) 14(6):1043–59. doi: 10.1080/15548627.2018.1447290
45. Xie R, Nguyen S, McKeehan WL, Liu L. Acetylated Microtubules Are Required for Fusion of Autophagosomes With Lysosomes. *BMC Cell Biol* (2010) 11:1–12. doi: 10.1186/1471-2121-11-89
46. Cao Y, Zhang S, Yuan N, Wang J, Li X, Xu F, et al. Hierarchal Autophagic Divergence of Hematopoietic System. *J Biol Chem* (2015) 290(38):23050–63. doi: 10.1074/jbc.M115.650028
47. Konopleva M, Pollyea DA, Potluri J, Chyla B, Hogdal L, Busman T, et al. Efficacy and Biological Correlates of Response in a Phase II Study of Venetoclax Monotherapy in Patients With Acute Myelogenous Leukemia. *Cancer Discov* (2016) 6(10):1106–17. doi: 10.1158/2159-8290.CD-16-0313
48. Lachowiez C, DiNardo CD, Konopleva M. Venetoclax in Acute Myeloid Leukemia – Current and Future Directions. *Leuk Lymphoma* (2020) 61(6):1313–22. doi: 10.1080/10428194.2020.1719098
49. Konopleva MY. Mechanisms for Resistance in AML Insights Into Molecular Pathways Mediating Resistance to Venetoclax. *Best Pract Res: Clin Haematol* (2021) 34:101251. doi: 10.1016/j.beha.2021.101251
50. Maiuri MC, Le Toumelin G, Criollo A, Rain JC, Gautier F, Juin P, et al. Functional and Physical Interaction Between Bcl-XL and a BH3-Like Domain in Beclin-1. *EMBO J* (2007) 26(10):2527–39. doi: 10.1038/sj.emboj.7601689
51. Maiuri MC, Criollo A, Tasdemir E, Vicencio JM, Tajeddine N, Hickman JA, et al. BH3-Only Proteins and BH3 Mimetics Induce Autophagy by Competitively Disrupting the Interaction Between Beclin 1 and Bcl-2/Bcl-Xl. *Autophagy* (2007) 3(4):374–6. doi: 10.4161/auto.4237

52. Opydo-Chanek M, Gonzalo O, Marzo I. Multifaceted Anticancer Activity of BH3 Mimetics: Current Evidence and Future Prospects. *Biochem Pharmacol* (2017) 136:12–23. doi: 10.1016/j.bcp.2017.03.006
53. Bodo J, Zhao X, Durkin L, Souers AJ, Phillips DC, Smith MR, et al. Acquired Resistance to Venetoclax (ABT-199) in T (14,18) Positive Lymphoma Cells. *Oncotarget* (2016) 7(43):70000–10. doi: 10.18632/oncotarget.12132
54. Alhoshani A, Alatawi FO, Al-Anazi FE, Attafi IM, Zeidan A, Agouni A, et al. BCL-2 Inhibitor Venetoclax Induces Autophagy-Associated Cell Death, Cell Cycle Arrest, and Apoptosis in Human Breast Cancer Cells. *Onco Targets Ther* (2020) 13:13357–70. doi: 10.2147/OTT.S281519

Conflict of Interest: The authors declare that the research was conducted in the absence of any commercial or financial relationships that could be construed as a potential conflict of interest.

Publisher's Note: All claims expressed in this article are solely those of the authors and do not necessarily represent those of their affiliated organizations, or those of the publisher, the editors and the reviewers. Any product that may be evaluated in this article, or claim that may be made by its manufacturer, is not guaranteed or endorsed by the publisher.

frontiers in Oncology

REVIEW
published: 10 March 2022
doi: 10.3389/fonc.2022.852424

Crosstalk Between ROS and Autophagy in Tumorigenesis: Understanding the Multifaceted Paradox

Adria Hasan[1,2], *Suroor Fatima Rizvi*[1,2], *Sana Parveen*[1,3], *Neelam Pathak*[4], *Aamir Nazir*[5] *and Snober S. Mir*[1,2*]

[1] Molecular Cell Biology Laboratory, Integral Information and Research Centre-4 (IIRC-4), Integral University, Lucknow, India, [2] Department of Bioengineering, Faculty of Engineering, Integral University, Lucknow, India, [3] Department of Biosciences, Faculty of Science, Integral University, Lucknow, India, [4] Department of Biochemistry, Dr. RML Avadh University, Faizabad, India, [5] Laboratory of Functional Genomics and Molecular Toxicology, Division of Neuroscience and Ageing Biology, CSIR-Central Drug Research Institute, Lucknow, India

OPEN ACCESS

Edited by:
Abdelhabib Semlali, Laval University, Canada

Reviewed by:
Sujit Kumar Bhutia, National Institute of Technology Rourkela, India
Paola Maycotte, Instituto Mexicano del Seguro Social, Mexico

***Correspondence:**
Snober S. Mir
smir@iul.ac.in
mirssnober@gmail.com

Specialty section:
This article was submitted to Cancer Molecular Targets and Therapeutics, a section of the journal Frontiers in Oncology

Received: *11 January 2022*
Accepted: *14 February 2022*
Published: *10 March 2022*

Citation:
Hasan A, Rizvi SF, Parveen S, Pathak N, Nazir A and Mir SS (2022) Crosstalk Between ROS and Autophagy in Tumorigenesis: Understanding the Multifaceted Paradox. Front. Oncol. 12:852424. doi: 10.3389/fonc.2022.852424

Cancer formation is a highly regulated and complex process, largely dependent on its microenvironment. This complexity highlights the need for developing novel target-based therapies depending on cancer phenotype and genotype. Autophagy, a catabolic process, removes damaged and defective cellular materials through lysosomes. It is activated in response to stress conditions such as nutrient deprivation, hypoxia, and oxidative stress. Oxidative stress is induced by excess reactive oxygen species (ROS) that are multifaceted molecules that drive several pathophysiological conditions, including cancer. Moreover, autophagy also plays a dual role, initially inhibiting tumor formation but promoting tumor progression during advanced stages. Mounting evidence has suggested an intricate crosstalk between autophagy and ROS where they can either suppress cancer formation or promote disease etiology. This review highlights the regulatory roles of autophagy and ROS from tumor induction to metastasis. We also discuss the therapeutic strategies that have been devised so far to combat cancer. Based on the review, we finally present some gap areas that could be targeted and may provide a basis for cancer suppression.

Keywords: autophagy, ROS, tumor microenvironment, epithelial–mesenchymal transition, metastasis, anticancer therapy resistance

INTRODUCTION

Autophagy, meaning "self-eating," is a catabolic process where cytoplasmic organelles, proteins, and other macromolecules are degraded during starvation or other types of stress (1–3). It is vital in maintaining cellular homeostasis, helps eliminate pathogens, and is regulated by the autophagy-related (ATG) genes. The molecules/cargo to be degraded are sequestered in double-membrane vesicles (autophagosomes). Autophagosomes fuse to lysosomes, forming autolysosomes that lead to cargo degradation. The degraded molecules provide energy that can be used in anabolic and bioenergetic pathways (4). Apart from macroautophagy, there are two other forms of autophagy:

microautophagy and chaperone-mediated autophagy (5). Any disruption in autophagic pathways has been shown to play a significant role in different diseases such as neurodegeneration, atherosclerosis, and cancer (6, 7).

Usually, autophagy acts as a tumor suppressor during initiation but promotes cancer cell proliferation in established tumors (8). Autophagy can be regulated by several factors, including starvation, infections, drugs, hypoxia, ATP/AMP ratio, and reactive oxygen species (ROS) levels (9). Cancer cells also exhibit high ROS levels (10) due to increased metabolism rate, incomplete oxidative phosphorylation, mitochondrial dysfunction, low nutrient levels, hypoxia, and low pH in their microenvironment (11–13). Under normal conditions, low ROS levels are generated to regulate signaling pathways, including autophagy, to maintain cellular homeostasis (14–16). Moreover, starvation conditions known to upregulate autophagy can also induce ROS. Consistently, studies have shown ROS-mediated regulation of autophagy as ROS scavengers or high expression of antioxidants can block stress-induced autophagy (17, 18).

ROS-induced autophagy can lead to cell death or survival (17, 19). High ROS levels can also activate several oncogenic pathways, such as mitogen-activated protein kinase (MAPK) and nuclear factor (NF)-κB signaling pathways. Contrarily, increased ROS can also promote cell death by activating the tumor suppressor p53 or apoptosis caused by excessive mitochondrial and DNA damage (20). Thus, an intricate cellular balance between autophagy and ROS is required to maintain cellular redox balance in normal and disease-related physiological conditions. Therefore, the exact role of autophagy and ROS in cancer cells is context-dependent and varies in different cancer phenotypes (21–24). This review describes the role of autophagy and ROS as tumor promoters and suppressors. We further discuss the intricate crosstalk between autophagy and ROS that can regulate tumor promotion, metastasis, and response to therapy and may ultimately decide the fate of cancer cells.

REGULATION OF AUTOPHAGY

Autophagy is moderately active at the basal level but becomes highly activated due to different cellular stresses, including chemotherapeutics and radiotherapy (25–27). To date, 35 different *ATG* genes have been identified in yeast that are also conserved in higher eukaryotes (28–31). The autophagy pathway can be divided into several steps: (a) initiation and nucleation, (b) autophagosome closure, (c) maturation through autophagosome–lysosome fusion, and (d) cargo degradation through lysosomal enzymes. Autophagy is regulated through a series of proteins, including mammalian target of rapamycin (mTOR) and 5' adenosine monophosphate-activated protein kinase (AMPK). Activated mTOR negatively regulates autophagy through phosphorylation of the Atg proteins. However, during stress conditions, mTOR is inhibited, and autophagy is enhanced. Conversely, AMPK negatively regulates mTOR and induces the autophagic process (32; 33). After mTOR inhibition, the Unc-51-like autophagy-activating kinase (ULK) complex is activated (34), which in turn activates the class III phosphoinositide 3 kinase (PI3K) (35). The class III PI3K complex consists of several proteins including VPS34, p150, Atg14, and Beclin-1, which initiates autophagosome formation. Beclin-1, a primary autophagy regulator, recruits different proteins involved in the maturation and elongation of the autophagosome. Subsequently, Atg9 protein mediates the trafficking of the source membrane for autophagosome elongation. These may include the Golgi complex, mitochondria, endoplasmic reticulum, endosome, and plasma membrane (36). The primary component required for autophagosome maturation is the ubiquitin-like protein lipidation system that conjugates phosphatidylethanolamine to the C terminus of Atg8 (LC-3) protein, thereby facilitating the incorporation of Atg8 protein into autophagosomal membranes (37, 38). The proteins Atg7 and Atg10 help in conjugating Atg12 protein to Atg5 protein. The Atg12–Atg5 protein complex then conjugates with Atg16L1 protein to promote Atg8 protein lipidation. Atg8 protein is present in the inactive pro-Atg8 form but is cleaved by Atg4B protein, leaving a C-terminal glycine residue (39). The lipidated form of Atg8 protein is strongly associated with the autophagosomal membranes. Yeast contain a single Atg8 protein, while mammals have seven Atg8 proteins in two structurally related subfamilies (MAP1LC3A, B, C and GABARAP, GABARAPL1, and GABARAPL2), signifying a complex diversification of their functions (37). During autophagy induction, damaged organelles, protein aggregates, and ubiquitinated proteins are sorted to the phagophore for degradation. The Atg5–Atg12–Atg16L protein complex localizes to the phagophore, forming a cup-shaped structure, and dissociates when LC3-II localizes to the phagophore to complete the autophagosome formation. The cargo adaptor proteins like p62, NBR1, or NIX are further recruited on the autophagosome to target ubiquitinated protein aggregates and damaged organelles for degradation (40–42). Furthermore, the autophagosome fuses with the lysosomes forming autolysosomes to degrade targeted contents (**Figure 1**). This fusion is mediated by lysosomal-associated membrane protein 2 (LAMP2), the small GTPase RAB7A and UVRAG. Finally, lysosomal hydrolases and cathepsins degrade the targeted proteins, while cathepsins degrade LC3-II on the inner autophagosomal surface (43).

REACTIVE OXYGEN SPECIES AND AUTOPHAGY

ROS include a reactive group of molecules such as hydroxyl radical, superoxide anion (O_2^-), and hydrogen peroxide (H_2O_2) (44). During normal physiological conditions, most intracellular ROS are produced in the mitochondria during oxidative phosphorylation due to the leaking of electrons from the electron transport chain (45, 46). However, an increase in intracellular ROS levels can promote mitochondrial dysfunction by accumulating high ROS levels, oxidation of lipids, proteins, and DNA damage (**Table 1**) (56, 57). The

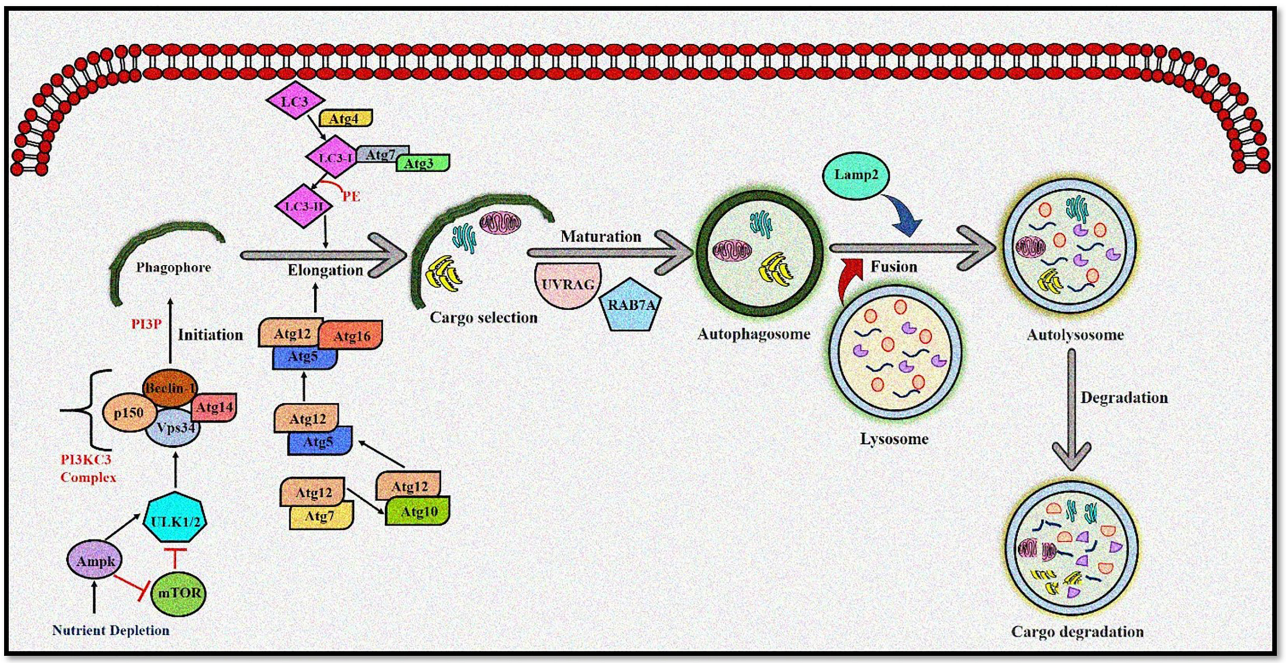

FIGURE 1 | The autophagy pathway. AMPK and ULK1 kinase complex initiates autophagy. mTOR inhibition promotes phagophore formation through class III PI3K and Beclin 1 complex formation. Atg5-12 complex and LC3 are required to complete the autophagosome. After maturation, autophagosomes fuse with lysosomes to form autolysosomes where cargo degradation occurs. UVRAG, RAB7A, and LAMP2 mediate autophagosome maturation and fusion with lysosomes. AMPK, 5' adenosine monophosphate-activated protein kinase; ULK1, Unc-51 Like Autophagy Activating Kinase 1; mTOR, mammalian target of rapamycin; PI3K, phosphoinositide 3-kinase; ATG, Autophagy related; LC3, Microtubule-associated protein 1A/1B-light chain 3; UVRAG, UV radiation resistance-associated gene protein; RAB7A, Ras-related protein Rab-7a; LAMP2, lysosomal-associated membrane protein 2.

TABLE 1 | Role of different reactive oxygen species in cancer.

ROS	Roles in Cancer	References
1 Generic ROS	• Activation of oncogenes. • Activate oncogenic signals including Ras, Bcr-Abl, c-Myc, which hyperactivates cell proliferation. • Inactivation of tumor suppressors, promoting angiogenesis, and mitochondrial dysfunction. • Induction of Wnt/β-catenin pathway which increases metastatic potential. • High expression of MMPs. • Matrix metalloproteinases (MMPs) trigger epithelial-mesenchymal transition (EMT) • MMPs inhibitor or ROS inhibitor may be useful in the reversal of EMT or the killing of cancer stem cells. • Regulation of NF-κB pathways • Contribution to drug resistance such as through high mutagenic rates	(47–49)
2 Hydrogen Peroxide (H_2O_2)	• Promotes phosphoinositide 3 kinases (PI3Ks)/RAC-alpha serine/threonine-protein kinase (Akt) survival pathway. • Enhanced MAPK and ERK signaling pathway. • Oxidative modification of PTEN • Oncogenic stabilization of hypoxia-inducible factor (HIF)-1α; conversion to hydroxyl radical	(50; 51, 52)
3 Hydroxyl radical (•OH)	• Initiates lipid peroxidation • promotes DNA mutagenesis	(53, 54)
4 Hypochlorous acid (HOCl)	• Induces mutations in mitochondrial DNA with age	(54)
5 Superoxide anion (O_2^-)	• Conversion to H_2O_2, peroxynitrite • Stimulates AMPK activity to induce metastasis. • Oncogenic stabilization of HIF-1α	(51, 55)

Ras, Rat sarcoma virus; Bcr-Abl, breakpoint cluster region protein -v-abl Abelson murine leukemia viral oncogene; c-Myc, Cellular myelocytomatosis oncogene; MAPK, Mitogen-activated protein kinase; ERK, extracellular-signal-regulated kinase; PTEN, Phosphatase and Tensin Homolog deleted on Chromosome 10; DNA, deoxyribonucleic acid; H2O2, Hydrogen peroxide; AMPK, 5' adenosine monophosphate-activated protein kinase; ROS, reactive oxygen species; NF-κB, Nuclear factor kappa B.

selective removal of damaged mitochondria by autophagy is called mitophagy. It is mediated by two signaling pathways, namely, NIX/BNIP3L and PARKIN (PARK2)/phosphatase and tensin homolog (PTEN)-induced putative kinase 1 (PINK1) (58–61). Targeting mitochondria toward mitophagy requires interaction between Nix/BNIP3L and GABARAP at the autophagosome (41, 62). PARKIN/PINK1 help remove dysfunctional mitochondria in response to ROS-induced mitochondrial membrane depolarization (63). Furthermore, the redox balance in a cell is maintained through the antioxidant defense system consisting of glutathione peroxide (GPx), catalase, glutathione reductase, glutathione S-transferase (GST), superoxide dismutase (SOD), and glutathione (64). Intracellular H_2O_2 is generated by SOD-catalyzed dismutation from O_2^- formed within the mitochondria (46). Increased H_2O_2 levels were observed during tumorigenesis due to increased ROS production, high SOD levels, and inactivation of H_2O_2-scavenging enzymes (48). High H_2O_2 levels induce autophagic cell death in glioma cells after treatment with the polycyclic ammonium ion sanguinarine, which increases electron leakage from mitochondria and induces NADPH oxidases (NOXs) (65). NOXs, a membrane-bound enzyme complex, is another source of extracellular ROS (49) and are abnormally upregulated in cancer cells (66).

Studies have demonstrated that several oncogenes, including *K-RAS* and *c-MYC*, induce intracellular ROS to promote cancer cell proliferation (67, 68). *K-RAS* also promotes extracellular ROS generation by increasing the activity of NOXs on the tumor cell membrane (69). In this regard, a study reports the tumor-promoting effect of autophagy in K-Ras [K-Ras(V12)]-induced malignant cell transformation, where inhibiting ROS with antioxidants reduced K-RasV12-induced induction of Atg5 protein and Atg7 protein, autophagy, and cancer growth (70). However, another study reports that rapamycin, an mTOR inhibitor, combined with (Hsp90) inhibitor IPI-504, causes tumor regression by promoting mitochondrial damage, oxidative stress, and autophagy in Kras/p53 mutant lung cancer and Nf1-deficient *RAS*-driven tumors (71).

Following another mechanism of action, ROS can also regulate autophagy through AMPK. AMPK induces autophagy during hypoxia or nutrient starvation by inhibiting mammalian target of rapamycin complex 1 (mTORC1 (72, 73). AMPK is phosphorylated by AMP-activated protein kinase kinase (AMPKK) following the accumulation of H_2O_2, which promotes its activation and autophagy induction (74). Inactivation of Atg4 protein increases autophagosomes and ATM-mediated oxidation of AMPK that inhibits mTORC1 in a H_2O_2-dependent manner (26, 75, 76). ROS can also mediate the induction of autophagy genes, including Beclin-1 or SQSTM1/p62, by regulating the activity of NF-κB in cancer cells (77–79).

The redox regulation of the proto-oncogene Akt provides another crucial point in the ROS-mediated regulation of autophagy. A well-described Akt-activating mechanism is PTEN oxidation (80, 81). In this regard, ROS production due to the growth factor stimulation promotes PTEN inactivation by forming a disulfide bridge between a cysteine in the catalytic site with a proximal cysteine residue. Consequently, Akt is activated due to increased PtdIns(3,4,5)P_3 levels (81). However, disruption of mitochondrial membrane potential by an increase in H_2O_2 levels inhibits Akt, an upstream activator of mTOR, and induces autophagy (82; 83). This ROS-mediated signal transduction mechanism may also have a critical physiological role, as it may block catabolic pathways, like autophagy, in the presence of growth factors and may also induce the process of tumorigenesis.

Although ROS can promote autophagy induction, autophagy can also modulate ROS production. It was observed that caspase 8 inhibition and subsequent activation of JNK1 led to Atg6-Atg7 protein-dependent cell death when apoptosis was impaired (84). Moreover, caspase 8 inhibition promotes selective catalase degradation *via* autophagy that results in increased lipid peroxidation and autophagic cell death (85). Thus, it can be hypothesized that autophagy-mediated removal of catalase creates a self-sustaining loop, in which increased production of H_2O_2 by mitochondria may promote aberrant activation of autophagy, ultimately leading to autophagic cell death. However, catalase degradation was not observed under starvation conditions stimulating cytoprotective autophagy.

Furthermore, superoxides also modulate autophagy, as starvation-induced autophagy, mitochondrial electron transfer chain inhibitors, and the addition of exogenous H_2O_2 correlate with increased superoxide production and reduced H_2O_2 levels. Thus, overexpression of the SOD2 [manganese superoxide dismutase (Mn-SOD)] scavenges the superoxides, inhibits autophagy, and promotes H_2O_2 levels and starvation-induced cell death. In contrast, increasing superoxide levels by using the mitochondrial electron transfer chain inhibitors combined with SOD inhibitor 2-methoxyestradiol (2-ME) promoted both autophagy and cell death (86).

Thus, it can be concluded that autophagy and ROS-generating agents work in an unprecedented complex manner, as ROS-induced autophagy and *vice versa* can either be a cytoprotective mechanism that reduces oxidative stress or a self-destructing process promoting autophagic cell death (**Figure 2**). A clearer understanding of this intricate crosstalk between autophagy and ROS can help develop therapeutic strategies and open several opportunities to target the disease development process.

AUTOPHAGY AND REACTIVE OXYGEN SPECIES IN CANCER: A PROMOTER OR SUPPRESSOR

Autophagy usually acts as a survival pathway in normal and cancer cells exposed to various stresses like hypoxia, nutrient deprivation, or chemotherapeutics. These stress conditions also promote ROS generation that could aid in autophagy-mediated cell survival (25, 86). Indeed, ROS accumulation can activate several transcription factors like p53, hypoxia-inducible factor-1

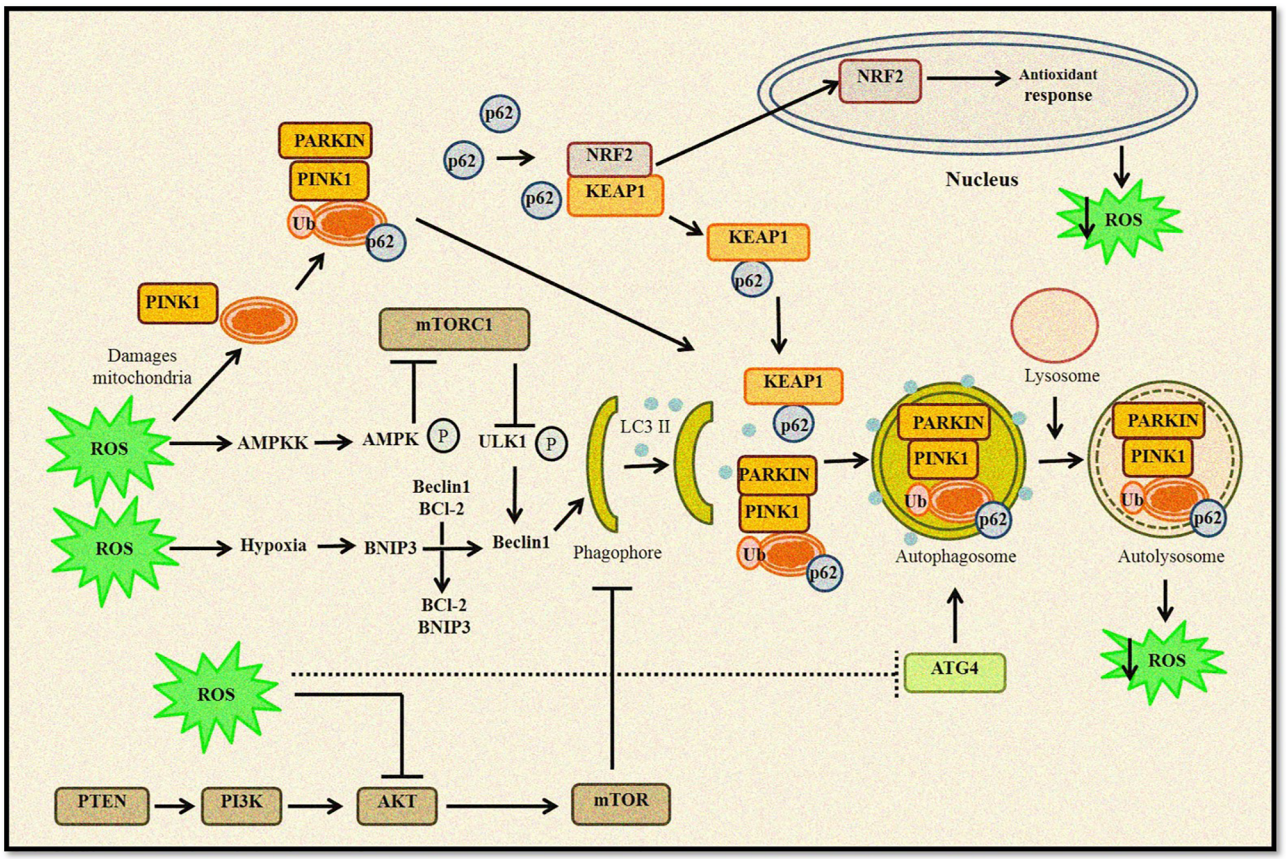

FIGURE 2 | Relationship between ROS and autophagy. Increased ROS levels lead to oxidation of Atg4, which triggers autophagosome formation. ROS can regulate autophagy through AMPK activation that in turn phosphorylates ULK1 complex and promotes autophagy induction. Furthermore, disruption of Beclin 1–Bcl2 complex also induces autophagy. Any change in mitochondrial homeostasis promote ROS accumulation inducing mitophagy and removal of damaged mitochondria. Kelch-like ECH-associated protein 1 (KEAP1) degradation by p62-mediated selective autophagy leads to Nrf2-regulated antioxidant production and reduction in ROS levels. ROS can also inhibit the Akt/mTOR signaling cascade to induce autophagy.

(HIF-1), nuclear factor (erythroid-derived 2)-like 2 (NRF2), and forkhead box transcription factors (FOXO3), which can increase the transcription of several proteins involved in autophagy (87). The initial connection between autophagy and cancer was established when studies demonstrated that Beclin-1 is mono-allelically deleted in approximately 50% of breast, ovarian, and prostate cancers (88, 89). Other studies revealed that mice hemizygous for Beclin-1 show a high incidence of lymphoma, liver, and lung cancer (90, 91).

Thus, it was believed that autophagy acts as a tumor suppressor. It removes damaged mitochondria through mitophagy and prevents ROS accumulation, therefore limiting the tumor-promoting effect of ROS (92). Consequently, autophagy inhibition promotes ROS production, mitochondrial impairment, and DNA damage, all potentially pro-tumorigenic during tumor initiation (6) but deleterious at later stages (75, 93). Studies have shown that autophagy loss causes genomic instability and aneuploidy (94, 95). Furthermore, autophagy dysfunction can promote tumor cell-extrinsic effects, including a pro-tumorigenic inflammatory microenvironment (25).

ROS are also induced by several tumor-associated immune cells in the tumor microenvironment (TME) (96) that may trigger altered activation of macrophages and immunosuppression (97). Macrophages are the first host cells to enter the TME to kill cancer cells (98). However, tumor-associated macrophages (TAMs) infiltrate into the tumors and differentiate into mature pro-tumor macrophages (M1 and M2 macrophages) mediated by cytokines in the TME (99–101). Although the pro-tumorigenic role of M1 is context dependent based on tumor microenvironmental cues (102, 103). Macrophages also show phagocytotic activity toward damaged tumor cells (104). However, macrophages are recruited through chemokines during cancer initiation, amplifying an inflammatory response. Macrophages also produce redoxosomes (exosomes containing functional NOX complexes) in the TME, which generates extracellular ROS and is incorporated into neighboring cells through endocytosis (105). Thus, a supportive TME is essential for tumorigenesis, wherein ROS plays a significant role in creating immunosuppressive TME for cancer growth and metastasis. Hence, it is plausible that autophagy inhibition may promote

pro-tumorigenic ROS, since dysregulated autophagy leads to mitochondrial damage and high ROS levels, and oxidative stress, all potentially pro-tumorigenic.

Several studies have demonstrated that dysregulated autophagy due to the deletion of proteins such as Atg16L1, Beclin-1, or LC-3B promotes the accumulation of damaged mitochondria and mitochondrial ROS. It also promotes inflammation linked to increased levels of IL-1β and IL-18 (106–109). ROS can also be induced by IL-1, whose high expression has been associated with a poor cancer prognosis (110). Moreover, increased ROS levels also activate pro-inflammatory factors such as the pyrin domain-containing 3 (NLRP3) inflammasome (109). Inflammation aids in cancer initiation and survival through vascularization and stimulating the TME through the IL-1 and IL-18 pathway. Inflammatory cells further produce ROS or reactive nitrogen species (RNS) *via* iNOS, xanthine oxidase (XO), nicotinamide adenine dinucleotide phosphate (NADPH) oxidase, and myeloperoxidase (MPO). These oxidant-generating enzymes may promote damage to DNA damage. (111). Autophagy also plays a crucial role in inflammation by regulating the homeostasis, development, and survival of inflammatory cells (112). Inflammatory cells also release cytokines, activating NF-κB. NF-κB can help generate excess ROS or RNS by stimulating COX_2, lipoxygenase (LOX), and inducible nitric oxide synthase (iNOS), that in turn may stimulate several oncogenes such as c-Jun and c-Fos and initiate tumorigenesis (113).

Another major regulator of both autophagy and ROS is the tumor suppressor p53 that plays a contrasting role in autophagy based on its subcellular localization (114). Nuclear p53 is suggested to activate autophagy through several transcriptional mechanisms. Many autophagy genes are said to be direct interacting partners of p53, and that autophagy helps in p53-dependent apoptosis and cancer suppression (115). In the nucleus, p53 activates the transcription of pro-autophagic molecules such as AMPK, damage-regulated autophagy modulator (DRAM), death-associated protein kinase 1 (DAPK-1), pro-apoptotic Bcl-2 proteins, sestrin 2, and Tuberous Sclerosis Complex 2 (TSC2) (116–120). However, cytoplasmic p53 inhibits autophagy, primarily through interactions with autophagic proteins (114). Cytoplasmic p53 mediates mitochondrial outer membrane permeabilization, promoting apoptosis and inhibiting autophagy (121, 122). Although the mechanism of cytoplasmic p53-mediated autophagy inhibition is not well elucidated, it was observed that cytoplasmic p53 inhibits AMPK and activates mTOR, leading to autophagy suppression (123).

p53 also can regulate autophagy by modulating ROS levels. During oxidative stress, basal p53 induces several antioxidants such as GPx1, MnSOD, ALDH4, and TPP53INP1 to remove oxidative stress (124–127). Additionally, p53 also exerts antioxidant effects by upregulating the expression of several p53 target genes in response to DNA damage and oxidative stress. This leads to inhibition of mTORC1 activity and autophagy induction. Sestrin1 and sestrin2 are the links between p53 activation and mTORC1 activity (119). Sestrins also regulate ROS (128) and inhibit mTORC1 activity by inducing the expression of the pro-autophagic AMPK, TSC1, and TSC2 (119).

However, p53 can also induce ROS. A study observed that silibinin, an active constituent extracted from *Silybum marianum* (milk thistle), induced ROS-mediated autophagy and apoptosis in HeLa cells (129). Furthermore, another study by the same group demonstrated that silibinin promotes p53-mediated ROS in HeLa cells. The study also observed that p53 inhibition decreased ROS generation and reversed silibinin's growth-inhibitory effect. Moreover, silibinin was not able to induce ROS in the epithelial carcinoma cells (A431), as they lack p53 activity (p53His273mutation) (130). Another study reports that silibinin may upregulate p53-mediated autophagy by inhibiting MAPK and PI3K/Akt pathways and activating ROS/p38 and JNK pathways (131). Furthermore, upregulation in PI3K and AKT or downregulation in PTEN activates mTOR and inhibits autophagy. Thus, these oncogenic alterations suggest the importance of autophagy suppression during tumor initiation (132, 133).

Other studies also demonstrated that any defect in the autophagic machinery promotes tumor initiation, including liver and breast (114, 134). Tang etal. (114) demonstrated that low expression of Beclin-1 suggested poor prognosis in Her2, basal-like, and p53-mutant breast cancer. Autophagy also acts as a tumor suppressor through its role in cellular senescence, where cells undergo growth arrest (135). Kang etal. (136) demonstrated that GATA Binding Protein 4 (GATA4), a transcription factor regulating senescence, is degraded by p62-selective autophagy. Autophagic adapters, p62/SQSTM1, act as cargo receptors for autophagic degradation of ubiquitinated targets (137). p62 is upregulated under various stresses, including ROS, where ROS-induced p62 gene expression is mediated by NRF2. Furthermore, p62 protein activates NRF2 by interacting with the Nrf2-binding site on Keap1, a component of Cullin 3 (CUL3)-based E3 ubiquitin ligase for Nrf2, resulting in stabilization of Nrf2 and transcriptional activation of its target genes (138, 139). Another major autophagy regulator, Atg5 protein, also plays a dual role in the regulation of autophagy and apoptosis. Studies have indicated that overexpression of Atg5 protein can sensitize tumor cells to chemotherapy. In contrast, silencing the *ATG5* gene with short interfering RNA made tumor cells partially resistant to chemotherapy. Atg5 protein is cleaved by calpains, a family of Ca2+-dependent cysteine proteases, producing an amino-terminal cleavage product. Calpain induction and subsequent Atg5 protein cleavage appear to be universal phenomena in apoptotic cells (140). Similarly, the Atg12 protein also has a dual function, participating in both autophagy and apoptosis, and is necessary for caspase activation in response to a range of apoptotic stress inducers. Non-conjugated Atg12 protein can bind to and inhibit Mcl-1 and Bcl-2 by a BH3-like motif, inducing mitochondria-dependent apoptosis (141). Knockout of *ATG12* gene prevents Bax activation and cytochrome c in apoptotic cells.

Although autophagy functions as a tumor suppressor during the initiation of tumorigenesis (6), other studies have revealed that autophagy can also act as a tumor promoter (132; 142). Furthermore, autophagy can also promote resistance to many anticancer therapies (27). The pro-survival role of autophagy can

be seen during stress conditions, including hypoxia and nutrient deprivation. Autophagy rapidly degrades unfolded proteins during stress and provides the substrate for ATP production (143, 144). Thus, autophagy is generally upregulated in hypoxic regions of a tumor and promotes cell survival (25).

During later stages of tumor initiation, autophagy is required for cell transformation by the RAS oncogene to promote cell tolerance to stress A high basal level of autophagy is observed in RAS-mutated cancers, including lung, colon, and pancreatic (145, 146). Furthermore, mutations in the RAS genes promote uncontrollable cell proliferation and apoptosis inhibition (147, 148). Herein, autophagy promotes cancer cell survival by providing nutrients during starvation or other stress conditions (149). Consequently, autophagy inhibition increases the accumulation of damaged mitochondria and promotes cell death (150). Thus, tumor cells utilize autophagy to survive metabolic stress, and autophagy mitigates cellular damage (151). Autophagy inhibition leads to slower tumor growth and increased sensitivity to cancer treatments. This has led researchers to assess the efficacy of autophagy inhibitors combined with chemotherapy to increase therapeutic responses in cancers.

Consistently, autophagy inhibition reduced malignant transformation and proliferation of mouse embryonic fibroblasts (MEFs) transformed with Harvey Rat Sarcoma Virus (HRAS) and MDA-MB-231 breast cancer cells presenting with KRAS expression (152). Other studies have shown that model systems such as immortalized baby mouse kidney (iBMK), MCF-10A, and pancreatic ductal adenocarcinoma (PDAC) cell lines harboring ectopic expression of the oncogenic KRAS has high basal autophagy levels. However, inhibiting autophagy by deleting the gene *ATG5* or *ATG7* prevented RAS-mediated cancer cell proliferation (145; 70, 153). It can be stated that mitochondrial respiration is required for RAS-induced tumorigenesis, and active autophagy maintains cellular homeostasis (154). Thus, RAS-mediated cancers are addicted to autophagy for survival, and dysregulated autophagy in these cancer types is proportional to decreased cancer cell survival, accumulation of damaged mitochondria, and oxidative stress that may ultimately promote cell death (155; 25). Furthermore, p62/SQSTM1 deficiency also reduces tumorigenicity and increases ROS levels following RAS activation (145, 156, 157). Another study also states that autophagy inhibition by FIP200 (FAK family-interacting protein of 200 kDa) deletion suppressed the breast cancer initiation *in vivo* driven by the polyoma virus middle T (*PyMT*) oncogene. The study demonstrated that FIP200 ablation promoted accumulation of p62/SQSTM1, ubiquitinated protein aggregates, and deficient LC3 conversion with an increased number of abnormal mitochondria confirming the pro-tumorigenic role of autophagy (158). Interestingly, FIP200 deletion did not affect apoptosis but significantly reduced the proliferation of breast cancer cells or Ras-transformed MEFs.

Taken together, these studies confirm the complex and paradoxical role of autophagy and ROS in cancer initiation and progression (**Figure 3**). However, this dual role also provides several therapeutic windows that could be exploited to develop targeted anticancer therapies.

ROLE OF AUTOPHAGY AND REACTIVE OXYGEN SPECIES IN EPITHELIAL TO MESENCHYMAL TRANSITION AND CANCER METASTASIS

Metastasis is a complex mechanism in which cancer cells undergo epithelial to mesenchymal transition (EMT) and spread from the tissue of origin to distant organs. It is the main reason behind high cancer mortality (159–161). EMT promotes contact inhibition in cancer cells, leading to invasive tumor epithelial phenotype (162). EMT can be regulated by several mechanisms, including epigenetics, transcriptional control, miRNAs, protein stability, alternative splicing, ROS, and autophagy (163, 164).

A study by Avivar-Valderas etal. (165) observed that in mammary tumor cells, autophagy was induced due to matrix detachment or integrin blockade in response to ROS-dependent upregulation of protein kinase R-like ER kinase (PERK1). Consistently, autophagy or PERK inhibition during matrix detachment or integrin signaling blockade induced cell death and reduced clonogenic recovery following detachment, highlighting the role of PERK-induced autophagy in mammary tumor cell survival during matrix detachment (165, 166). Furthermore, hepatocellular carcinoma and melanoma cells also require autophagy to survive following matrix detachment, leading to increased lung colonization during metastasis (167–169). Moreover, high ROS levels induced by matrix detachment may further promote autophagy activation through direct activation of Atg4 protein (26, 170).

One of the major contributors of EMT is transforming growth factor-beta 1 (TGF-β1) (171). Exogenous TGF-β1 regulates urokinase-type plasminogen activator (uPA) and Matrix metalloproteinase 9 (MMP9) to promote cell migration and invasion by activating NF-κB *via* the Rac1-NOXs-ROS-dependent mec`ism (172). ROS also regulates EMT *via* the non-canonical TGF-β1–TGF-β-activated kinase 1 (TAK1) pathway. TAK1 deficiency promotes integrin:Rac-induced ROS, further accelerating the EMT process. Consistently, low TAK1 expression was observed in invasive squamous cell carcinoma (SCC) but not in benign SCCs (173). ROS-mediated activation of Nrf2 also promotes Notch signaling and EMT induction (174). ROS can also activate TGF-β1 in response to ionizing radiation (175). Thus, these studies significantly highlight the role of ROS in EMT induction. Moreover, it is well characterized that cancer cells have a high metabolic rate. Therefore, to fulfill the bioenergetic needs of the cancer cells, an increase in ATP production and tricarboxylic acid (TCA) cycle is required. In turn, ROS is accumulated due to increased oxidative metabolism, disturbing the cellular homeostasis, dysregulating autophagy, inducing EMT, and promoting cancer cell survival and metastasis (6, 176, 177).

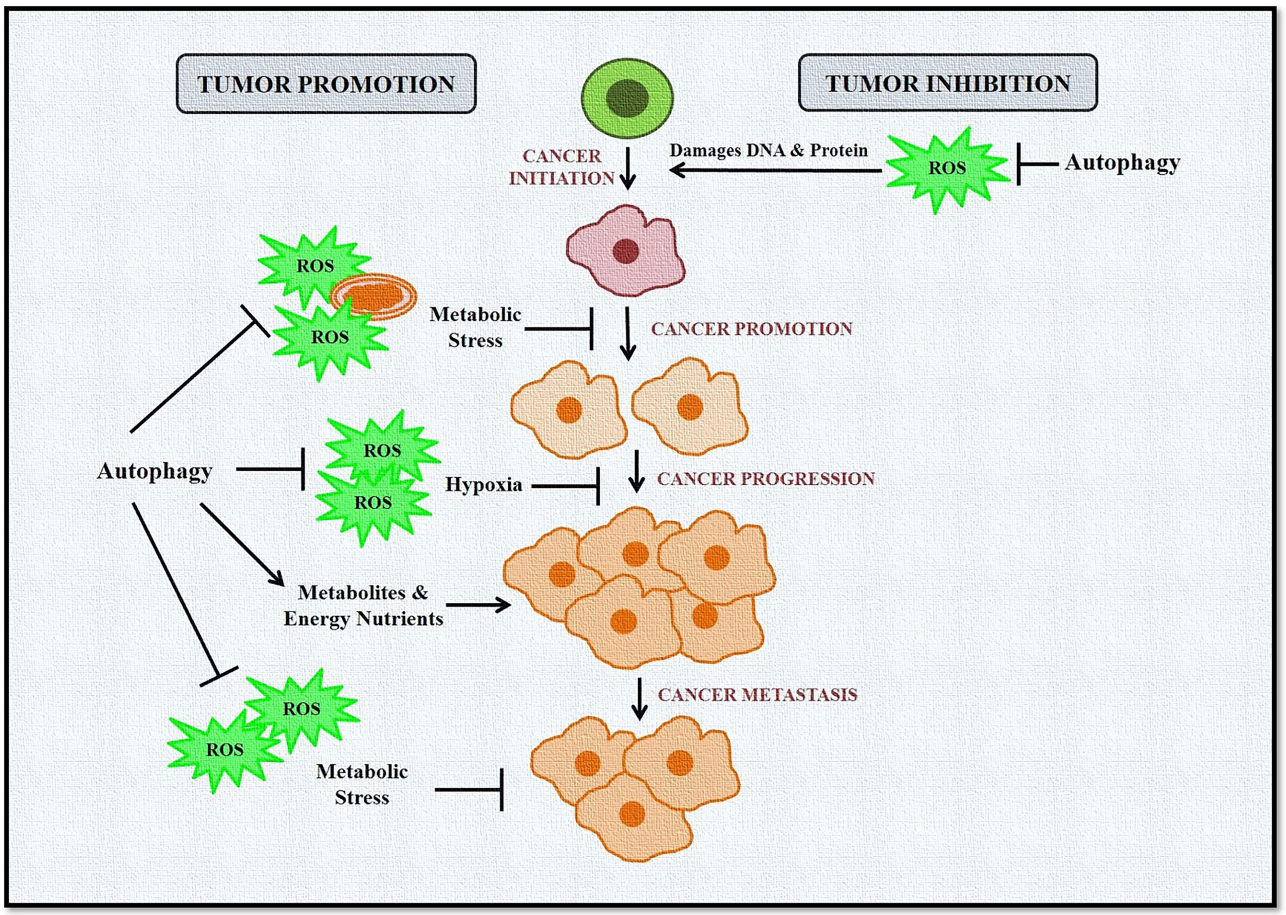

FIGURE 3 | Role of autophagy and ROS in cancer promotion and suppression. Autophagy in cancer works in a context-dependent manner based on tumor type and stage. It acts as a suppressor during tumor initiation but plays a protective role in established tumors. During tumor initiation, autophagy targets ROS-damaged organelles, DNA, and protein toward degradation, leading to inhibition of tumorigenesis. Autophagy eliminates ROS-induced stress during tumor progression and metastasis and provides much-needed nutrients to cells, including cancer cells. ROS is also induced in cancer cells during hypoxic conditions, activating autophagy in stromal cells. These cells then provide high-energy nutrients for cancer cell survival.

Furthermore, self-aggregation of TGF-β1-induced antiapoptotic factor (TIAF1) was observed in the cancer stroma and peritumor capsules of solid tumors, which is indicative of aggregation-dependent control of cancer progression and metastasis (178).

Autophagy also helps tumor cells adapt to hypoxic conditions before vascularization during *in vivo* tumor formation (179). High autophagy levels were observed in the hypoxic regions of the tumors. Autophagy can also be activated by ischemia to promote cancer cell survival and growth (25, 94, 95). Moreover, hypoxia can also induce ROS and stabilizes HIF-1α, the primary regulator of oxygen homeostasis (180). HIF-1α induces mitophagy *via* Bcl-2/adenovirus E1B 19-kDa-interacting protein 3 (BNIP3), along with a constitutive expression of Beclin-1 and Atg5 protein promotes cell survival during prolonged hypoxia by preventing increased ROS levels (181). BNIP3, a target gene for HIF-1α, induces autophagy by disrupting the Beclin 1–Bcl2 interaction (182). Autophagy dysregulation due to *BECLIN-1*, *ATG5* gene, or *ATG7* gene knockdown promotes hypoxia-induced cell death. Indeed, BNIP3-induced autophagy is required to prevent aberrant ROS levels during hypoxia and thus presents a survival mechanism (183–185). Autophagy is also induced in a HIF-1α-independent manner *via* AMPK and unfolded protein response (UPR) during hypoxia (186, 187).

Starvation-induced autophagy can also induce EMT and is required for HepG2 and BEL7402 HCC cell invasion *in vitro*. Thus, knockdown of autophagy genes like *ATG7* or *ATG3* in these cells suppressed EMT and invasion and decreased the expression of Fibronectin 1 (FN1), TGF-β1, and activated SMAD family member 3 (SMAD3) (188). Kim etal. (189) observed that another autophagy regulator, Unc-51 Like Autophagy Activating Kinase 2 (ULK2), promotes EMT by downregulating E-cadherin and increasing the invasiveness of lung cancer cells *in vitro*. Increased autophagy also promotes mesenchymal stem-like phenotype and invasion/migration of glioblastoma stem cell

lines. Hence, autophagy dysregulation *via ATG12* gene knockdown or p62/SQSTM1 deficiency reduced invasion and migration phenotypes in glioblastoma cells (190, 191).

Contrarily, another study argues that autophagy reduces migration of glioblastoma tumor cells *via* SNAIL and SLUG inhibition (192). Similarly, in hepatocytes, autophagy inhibition *via* liver-specific knockout of *ATG7* gene (*Alb-Cre*;$Atg7^{fl/fl}$) promoted the expression of vimentin and SNAIL. The study further reports that autophagy degraded Snail in a p62/SQSTM1-dependent manner. Moreover, treating wild-type MMH (murine hepatocytes) with TGF-β1 suppressed autophagy, whereas starvation-induced autophagy inhibited TGF-β1-mediated EMT (193).

Low basal autophagy levels also correlate with an increased propensity for migration and invasion in Skov-3 ovarian cancer cells compared to cells with high basal autophagy. Furthermore, a decrease in migration, invasion, and expression of the mesenchymal markers was observed due to starvation-induced autophagy, which was reversed following siRNA-mediated knockdown of *ATG7* gene. Moreover, EMT transition in these cells was regulated *via* increased ROS and heme oxygenase 1 (HMOX1), highlighting a role of autophagy in the ROS–HMOX1–EMT signaling axis (194). Similarly, autophagy can also inhibit EMT by degrading SNAIL and TWIST, two major mesenchymal markers that promote the invasion phenotype in cancer cells (195). Apart from TGF-β1, EMT is also induced by IL-1, IL-6 that regulate SNAIL or TWIST. ROS also induces HIF-1α and lysyl oxidase (LOX), decreasing E-Cadherin levels and activating EMT and cancer cell migration. Thus, it is plausible that autophagy may also be detrimental to EMT by inhibiting inflammation and removing ROS (196).

The autophagy receptor p62/SQSTM1 stabilizes the transcription factor TWIST and induces EMT (197, 198). Autophagy inhibition also promotes p62/SQSTM1 accumulation and contributes to tumorigenesis. Autophagy loss promoted the expression of TWIST in a p62-dependent manner, where it directly binds to TWIST and prevents its proteasomal degradation, promoting EMT and metastasis *in vivo* (197). Another study also demonstrated that accumulation of p62/SQSTM1 stabilizes TWIST and activates TGF-β1–SMAD signaling, further promoting EMT-associated junction remodeling (198).

It is evident that a complex link exists between autophagy, ROS, and EMT (**Figure 4**). Thus, to design better treatment modalities, extensive knowledge of the interlinked cellular events would be necessary to regulate cellular homeostasis.

ROLE OF AUTOPHAGY AND REACTIVE OXYGEN SPECIES IN CANCER THERAPY

For the past two decades, autophagy has been an attractive target for researchers to develop better anticancer therapies. Several cancer drugs either induce cytoprotective autophagy or promote autophagic cell death or autophagy-mediated apoptosis in cancer cells. Indeed, the cytoprotective role of autophagy was observed against temozolomide (199), tamoxifen (200), the histone deacetylase inhibitor SAHA (201), cyclophosphamide (27), irradiation (202), imatinib mesylate (203), and cisplatin (204). Thus, autophagy inhibitors such as hydroxychloroquine were used combined with standard chemotherapeutics in clinical trials to increase the therapeutic potential of the drugs (205). However, it should be noted that the stage at which autophagy is inhibited may alter drug sensitivity and plays a critical role in deciding the fate of cancer cells.

Certain anticancer treatments also promote ROS-induced autophagy that can promote drug resistance. In this case, using autophagy inhibitors with the chemotherapy agents may help restore the sensitivity to the treatment. Moreover, the type and dosage of drugs used, along with the cancer genotype, are other factors that may decide the outcome of autophagy activation. Consistently, Beclin-1-dependent protective autophagy was induced when pancreatic cancer cells were exposed to sorafenib, a pan-kinase inhibitor combined with HDACI, a histone deacetylase inhibitor. However, Bcl-2 knockdown or inhibition conditioned Beclin 1-dependent autophagy to promote apoptosis into a toxic pathway promoting intrinsic apoptosis (206). Another study demonstrated that ROS-mediated activation of c-Jun N-terminal kinase (JNK) induced cytoprotective autophagy when human rhabdomyosarcoma (Rh30 and RD) cells were treated with ciclopirox olamine (CPX). However, inhibiting autophagy *via* chloroquine (CQ) promoted CPX-induced cell death (207).

Hahm et al. (208) reported that honokiol, derived from the bark of *Magnolia officinalis*, induced ROS-induced cytoprotective autophagy and promoted drug resistance in prostate cancer. However, inhibiting autophagy *via* 3-methyladenine (3-MA) or *ATG5* gene siRNA sensitized cancer cells to apoptosis (208). Moreover, exposing breast and glioblastoma cancer cells to mitoquinone and quercetin, respectively, also promoted cytoprotective autophagy (209, 210). Hence, it can be hypothesized that any changes in the mitochondrial homeostasis would induce ROS and autophagy, which may lead to cell survival by autophagy-mediated degradation of damaged mitochondria. Therefore, autophagy inhibitors or siRNA-mediated silencing of *ATG* genes can turn protective ROS deleterious to cancer cells and promote apoptosis.

Another study showed that using 3-bromopyruvate (3-BrPA), a hexokinase II inhibitor, induced autophagy in breast cancer cells (MDA-MB-231435 and MDA-MB-435). However, ROS-mediated cell death was observed when 3-BrPA was used in combination with chloroquine, an autophagy inhibitor. The authors also concluded that autophagy induction was not dependent on ROS accumulation (211). Similar results were observed when A549 lung cancer cells were exposed to artemisinin, an antimalarial drug. Treatment with artemisinin induced autophagy that was attenuated by chloroquine. Autophagy inhibition promoted the accumulation of damaged mitochondria and ROS generation, resulting in apoptosis. Furthermore, apoptosis was ROS-dependent, as using a ROS scavenger N-acetyl-cysteine (NAC) rescued A549 cells from apoptosis *via* caspase-3 inhibition (212).

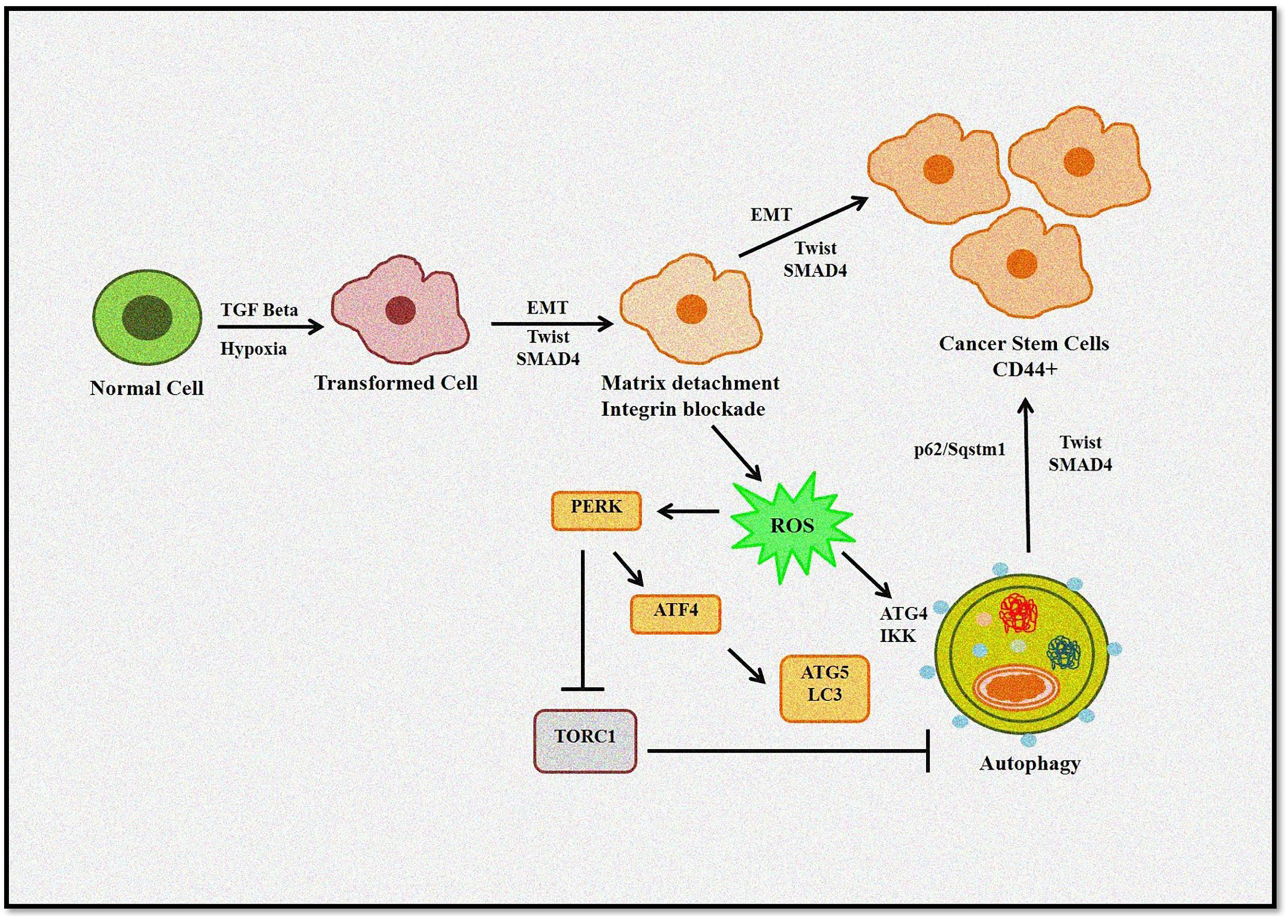

FIGURE 4 | Role of autophagy and ROS in the EMT process. Autophagy induces tumor invasiveness by promoting stem cell phenotype linked to hypoxia and TGF-β. Matrix detachment leads to ROS-induced EMT transition and autophagy induction. Furthermore, p62/Sqstm1 autophagy cargo adapter interacts with Twist, an EMT regulator, preventing its proteasomal degradation and promoting invasion.

However, autophagy-induced apoptosis has also been reported. Carnosol, a polyphenol, inhibited the cell viability in MDA-MB-231 breast cancer cells. The study reported that carnosol caused DNA and mitochondrial damage and promoted ROS-dependent early autophagy and late apoptosis (213). Thus, this could be another mechanism of action that a drug could follow to induce cancer cell death. Some chemotherapy agents like 2-methoxyestradiol (2-ME) and arsenic trioxide (As_2O_3) also promote oxidative stress-mediated autophagic cell death (214). Nevertheless, ROS is essential for As_2O_3-mediated autophagic cell death in glioma cells (215). 2-ME also upregulates ROS levels by inhibiting complex I of the mitochondrial electron transport chain and mitochondrial SOD (77, 216, 217). Furthermore, 2-ME, a ROS-generating agent, induced autophagic cell death in a transformed cell line HEK293 and the cancer cell lines HeLa and U87 (77). However, both 2-ME and As_2O_3 can induce autophagy and apoptosis (17, 215).

Autophagy-induced apoptosis was also observed in A375, HT144, and Hs294T cells treated with the H1 histamine receptor antagonist terfenadine, which may increase ROS depending on culture condition (218). Similarly, in melanoma cancer cells (A375 and BLM), bortezomib, a proteasome inhibitor, at least in part *via* ROS-mitochondrial dysregulation-associated pathways (219). Another study revealed that sasanquasaponin III (SQS III) inhibited the viability of A375 cells by inducing apoptosis and autophagy. The authors further observed that both, apoptosis as well as autophagy induction was ROS dependent. (220). Moreover, resveratrol and psoralidin promoted ROS-triggered autophagy induction followed by apoptosis in colon and lung cancer cell death, respectively (221, 222).

Other studies also highlight the role of autophagy and ROS levels in cancer treatment. It was shown that 2-deoxy-D-glucose (2DG), when combined with cisplatin or staurosporine, promoted apoptosis but promoted cytoprotective autophagy and decreased ROS levels when combined with pyrimethamine. Moreover, 2DG alone promoted protective autophagy, inhibited ROS levels, and increased mitochondrial membrane potential in melanoma cells (8863 and 501) (223, 224).

Thus, several treatment studies can be used to induce cancer cell death. As cancer develops high resistance against apoptosis, causing autophagic cell death could be an option. Moreover,

TABLE 2 | ROS-inducing or -inhibiting chemotherapeutic agents and their effect on autophagy.

	Drug	Cancer type	Mechanism of action	Reference
1	Arsenic trioxide	Ovarian cancer cells (HEY, OVCA429, and SKOV3)	Induced Beclin 1-independent autophagic pathway by modulating SnoN/SkiL expression and altering TGFβ signaling *via* ROS generation	(225)
2	Artemisinin	Different cancer cells	Weakens the levels of glutathione, elevates ROS levels, and Self-amplification of oxidative stress Induces cytoprotective autophagy	(212, 226)
3	Buthionine sulfoximine	Phase I/II studies Cancer cells (Human gallbladder cancer (GBC-SD), human cholangiocarcinoma (RBE) and osteosarcoma cells (DLM8 and K7M3)	Inhibitor of GSH synthesis Depletes intracellular GSH; increased apoptosis may affect the STAT3 pathway, induces oxidative stress and autophagy	(227, 228) (226, 229, 230)
4	b-Lapachone (ARQ501)	Pancreatic cancers, squamous cell carcinoma and glioma cells	Produces ROS by undergoing futile redox-cycles catalyzed by NQO1 Induces autophagic cell death in glioma cells	(231–233)
5	Chloroquine	Cancer cells (MCF-7, HT29, U373)	Inhibition of autophagy; increased ROS generation and subsequent cell death	(183)
6	Cisplatin	Head and neck cancer patients Bladder cancer cells	Induced ROS levels and DNA damage Induces cytoprotective autophagy	(234, 235)
7	Curcumin	Colon cancer cells (HCT116)	Induced ROS production and autophagic cell death	(236)
8	Daunorubicin	T-lymphoblastic leukemia cells (CCRF-CEM and MOLT-4), B-lymphoblastic leukemia cells (SUP-B15) and Chronic myelogenous leukemia (K562 cells)	Increased expression of SOD2 and lower ROS production Induces cytoprotective autophagy	(237, 238)
9	Doxorubicin (Adriamycin)	Different cancers	Cell death through multiple intracellular targets: ROS generation, DNA adduct formation, topoisomerase II inhibition, histone eviction, $Ca^{2+,}$ and iron hemostasis regulation, and ceramide overproduction. Inhibits autophagy to induce cancer cell death	(239, 240)
10	Diphenylene iodonium	Pancreatic cancer Colon cancer cells (HT-29), colon cancer cells (HCT-116) Macrophages	Jak/STAT pathway inhibited dephosphorylation of AKT/ASK1 pathway and low ROS levels promotes apoptosis Inhibit ROS level Inhibits autophagy in macrophages	(241–243)
11	Disulfiram	Advanced non-small lung cancer carcinoma, Metastatic melanoma cells (c81-46A, c81-61, and c83-2C) Lung cancer Pancreatic, breast and colorectal cancer cells	Inhibitor of cytosolic SOD1 Induces cytoprotective autophagy in lung cancer Induces autophagy-dependent apoptosis in pancreatic and breast cancer cells Induces autophagic cell death in colorectal cancer cells	(244–248)
12	Fullerene C60 (Nano-C60)	Normal and drug-resistant cancer cells MCF-7 and HeLa)	Induced autophagy and sensitizes chemotherapeutic agents to kill drug-resistant cancer cells in a ROS-dependent and photo-enhanced fashion	(249)
13	Gemcitabine	Head and neck cancer, pancreatic cancer Triple-negative breast cancer cells (TNBC), bladder cancer	Activate antioxidant agents, suppress Nox4, block ROS-related signaling pathways Induces cytoprotective autophagy in TNBC, pancreatic cancer, and bladder cancer	(234, 250–253)
14	Idarubicin (IDR)	Breast cancer, cardiac muscle cell (HL-1) Leukemia (K562 cells)	Induces ROS, oxidative DNA damage, and apoptosis Induces autophagy and promotes apoptosis in leukemia	(254–256)
15	Imexon	Phase I/II studies leukemia	Binds to thiol to disrupt GSH activity elevate oxidative stress and stimulate apoptosis in cancer cells.	(257, 258)
16	Itraconazole	Liver cancer, glioblastoma, colon cancer	Increases ROS and activates apoptosis in liver cancer Induces autophagic cell death in glioblastoma Induces autophagy-mediated apoptosis in colon cancer	(259–261)
17	Mangafodipir	Cancer cell line (CT26, Hepa1.6, and A549)/ Phase II studies in combination with chemotherapy in liver cancer	Increased H_2O_2 levels, specifically in cancer cells. SOD, catalase, and GSH reductase mimetic	(262)
18	Medroxyprogesterone	Head and neck cancer Glioblastoma	Induction of 15d-PGJ2-ligand of PPAR, increased ROS and Induced apoptosis Induces autophagy in C6 glioma cells when used in combination with tibolone or temozolomide	(234, 263, 264)
19	Metformin	Colorectal, Pancreatic cancer, Hepatocellular carcinoma, preneoplastic JB6 Cl 41-5a cells	Increases ROS production Induces autophagy to promote cell death in pancreatic, hepatocellular carcinoma and preneoplastic cells	(265–268)

(Continued)

TABLE 2 | Continued

	Drug	Cancer type	Mechanism of action	Reference
20	Motexafin gadolinium (gadolinium texaphyrin)	Hematological malignancies	Inducer of superoxide by futile redox cycling, an inhibitor of Trx, induces apoptosis in lymphoma cells.	(269; 144)
21	OSU-03012 (celecoxib derivative)	Hepatocellular carcinoma	Caused ROS accumulation and subsequent autophagic cell death	(270)
22	Panitumumab (EGFR antibody)	EGFR-expressing metastatic colorectal carcinoma	ROS accumulation and autophagic cell Death	(271)
23	Proton pump inhibitor esomeprazole	Melanoma	Induced ROS and protective autophagy	(272)
24	Photodynamic therapy (PDT)	Head and neck, brain, lung, bile duct, esophagus, bladder, ovarian, skin, ophthalmic, pancreatic, cervical, colorectal, and bladder carcinoma	Photochemical generation of cytotoxic ROS through the light-activation of a photosensitizer accumulated in cancer cells or tumor vasculature Induces cytoprotective autophagy	(273–277)
25	Proscillaridin A (PSD-A)	Breast cancer, colorectal cancer	ROS generation, Ca^{2+} Oscillation, inhibits STAT3 activation, induces apoptosis and Autophagy	(278)
26	Recombinant human HMGB1	Glioblastoma Pancreatic cancer	Activate MAPK and NF-κB, release cytokines, and induce NADPH oxidase to produce ROS. Induces cytoprotective autophagy in pancreatic cancer	(279–281)
27	Resveratrol	Colon cancer cells	Induced ROS and subsequent cytotoxic autophagy	(222)
28	Ruthenium(II) complexes	Cancer cells	Induced ROS and subsequent protective autophagy along with apoptosis	(282)
29	Suberoylanilide hydroxamic acid (Zolinza, Vorinostat)	Cutaneous T-cell lymphoma	Induced ROS and autophagy, prosurvival	(283, 284)
30	Sulforaphane	Therapy-resistant pancreatic carcinoma cells	Promoted mitochondria-derived ROS to initiate diverse cellular responses, including protective autophagy	(285, 286)
31	Sulindac	colon and lung cancer	mitochondrial damage, elevate ROS production and induces cytoprotective autophagy	(287, 288)
32	Tamoxifen	Breast cancer cells (MCF-7)	Induced ROS and subsequent protective autophagy	(289)
33	Temozolomide	Human glioblastoma cell lines (U87 MG, GBM8401, and GBM-SKH)	Induced ROS/ERK-mediated autophagy, protected glioma cells from apoptosis	(290)
34	Tetrathiomolybdate (ATN-224)	Phase II studies in myeloma, melanoma, prostate, and breast carcinoma	Inhibitor of cytosolic SOD1 copper chelation *via* tetrathiomolybdate induces cytoprotective autophagy in pancreatic cancer cells	(291–293)
35	Valproic acid	Glioma cells	Oxidative stress activated the ERK1/2 pathway, autophagic cell death	(294)
36	Vitamin A	Testis tumor Leydig cell lines	Modulated antioxidant enzyme activities, induced protective autophagy or apoptosis at different doses	(295)
38	2-Methoxyestradiol	Phase II studies in different tumors, Chondrosarcoma	Generates superoxide by inhibition of SOD Induces autophagy in chondrosarcoma whose inhibition promotes apoptosis	(296, 297)
39	7-formyl-10-methylisoellipticine	Acute myeloid leukemia	Increase mitochondrial ROS production and apoptosis induction	(298)

combining ROS and autophagy-inducing agents could also promote cancer cell death. Other strategies include combining apoptosis inducers with autophagy inhibitors in cancer cells harboring protective autophagy (**Table 2**). Taken together, choosing correct cancer treatment strategies is highly complex and should be based on tumor phenotype and genotype.

CONCLUSION

Thus, it can be concluded that ROS and autophagy work in a tight regulation with each other to maintain cellular homeostasis. They can either help cancer cells adapt to severe stress, which may otherwise be detrimental to cells, or induce cell death. This paradoxical role of ROS and autophagy in cancer is mainly dependent on the cancer types and their microenvironment. Therefore, it is imperative to decipher the crosslinked mechanisms in tumorigenesis with respect to ROS and autophagy so that autophagy modulators may be designed to target cancer.

This review highlights the role of ROS and autophagy in cancer survival and suppression mechanisms. The major mechanisms include response to hypoxia, turnover of antioxidant enzymes, oxidative damage-induced protein aggregation of regulatory molecules like TGF-β1, p53, enhanced survival in RAS-mutated cancers, EMT transition, and drug resistance. However, consistent with the role of autophagy and ROS in cancer, they provide large windows of opportunities to develop better treatment strategies that may help fulfill the unmet needs of cancer patients.

A better understanding of the molecular and chemical mechanisms of the redox regulation of autophagy is required. There are still some unanswered questions like 1) How does

autophagy modulate the turnover of regulatory enzymes required for maintaining redox potential? 2) How do autophagy and ROS regulate the posttranslational modifications of specific tumor suppressors? 3) How does excessive ROS impair autophagy and dysregulate the cellular microenvironment to promote invasive phenotype? Answer to these questions may help develop better anticancer treatment options.

AUTHOR CONTRIBUTIONS

AH: conceptualization, writing—original draft, writing—review and editing. SFR: preparation of figures. SP: preparation of tables. NP: critical revision of the article. AN: critical revision of the article. SSM: conceptualization, supervision, writing—original draft, writing—review and editing, critical revision of the article. All authors contributed to the article and approved the submitted version.

ACKNOWLEDGMENTS

The authors are thankful to Honorable Vice-Chancellor, Integral University, Lucknow, for providing infrastructural support and Dean Office, R&D, Integral University for providing article communication number (IU/R&D/2022-MCN0001357).

REFERENCES

1. De Duve C, Wattiaux R. Functions of Lysosomes. *Annu Rev Physiol* (1966) 28:435–92. doi: 10.1146/annurev.ph.28.030166.002251
2. Rikiishi H. Novel Insights Into the Interplay Between Apoptosis and Autophagy. *Int J Cell Biol* (2012) 2012:317645. doi: 10.1155/2012/317645
3. Hu CAA, White K, Torres S, Ishak MA, Sillerud L, Miao Y, et al. Apoptosis and Autophagy: The Yin–Yang of Homeostasis in Cell Death in Cancer. In: *Autophagy: Cancer, Other Pathologies, Inflammation, Immunity, Infection, and Aging*. Academic Press (2015). p. 161–81. doi: 10.1016/B978-0-12-801043-3.00010-8
4. Mizushima N, Komatsu M. Autophagy: Renovation of Cells and Tissues. *Cell* (2011) 147(4):728–41. doi: 10.1016/j.cell.2011.10.026
5. Li WW, Li J, Bao JK. Microautophagy: Lesser-Known Self-Eating. *Cell Mol Life Sci* (2012) 69(7):1125–36. doi: 10.1007/s00018-011-0865-5
6. White E. The Role for Autophagy in Cancer. *J Clin Invest* (2015) 125(1):42–6. doi: 10.1172/JCI73941
7. White E. Deconvoluting the Context-Dependent Role for Autophagy in Cancer. *Nat Rev Cancer* (2012) 12(6):401–10. doi: 10.1038/nrc3262
8. Chavez-Dominguez R, Perez-Medina M, Lopez-Gonzalez JS, Galicia-Velasco M, Aguilar-Cazares D. The Double-Edge Sword of Autophagy in Cancer: From Tumor Suppression to Pro-Tumor Activity. *Front Oncol* (2020) 10:578418. doi: 10.3389/fonc.2020.578418
9. Weidberg H, Shvets E, Elazar Z. Biogenesis and Cargo Selectivity of Autophagosomes. *Annu Rev Biochem* (2011) 80:125–56. doi: 10.1146/annurev-biochem-052709-094552
10. Carew JS, Huang P. Mitochondrial Defects in Cancer. *Mol Cancer* (2002) 1:9. doi: 10.1186/1476-4598-1-9
11. Pelicano H, Carney D, Huang P. ROS Stress in Cancer Cells and Therapeutic Implications. *Drug Resist Updat* (2004) 7(2):97–110. doi: 10.1016/j.drup.2004.01.004
12. Jin S, White E. Role of Autophagy in Cancer: Management of Metabolic Stress. *Autophagy* (2007) 3(1):28–31. doi: 10.4161/auto.3269
13. Vander Heiden MG, Cantley LC, Thompson CB. Understanding the Warburg Effect: The Metabolic Requirements of Cell Proliferation. *Science (New York N Y)* (2009) 324(5930):1029–33. doi: 10.1126/science.1160809
14. Finkel T. Oxidant Signals and Oxidative Stress. *Curr Opin Cell Biol* (2003) 15(2):247–54. doi: 10.1016/s0955-0674(03)00002-4
15. Hamanaka RB, Chandel NS. Mitochondrial Reactive Oxygen Species Regulate Cellular Signaling and Dictate Biological Outcomes. *Trends Biochem Sci* (2010) 35(9):505–13. doi: 10.1016/j.tibs.2010.04.002
16. Scherz-Shouval R, Elazar Z. Regulation of Autophagy by ROS: Physiology and Pathology. *Trends Biochem Sci* (2011) 36(1):30–8. doi: 10.1016/j.tibs.2010.07.007
17. Chen Y, McMillan-Ward E, Kong J, Israels SJ, Gibson SB. Mitochondrial Electron-Transport-Chain Inhibitors of Complexes I and II Induce Autophagic Cell Death Mediated by Reactive Oxygen Species. *J Cell Sci* (2007) 120(Pt 23):4155–66. doi: 10.1242/jcs.011163
18. Park SH, Chi GY, Eom HS, Kim GY, Hyun JW, Kim WJ, et al. Role of Autophagy in Apoptosis Induction by Methylene Chloride Extracts of Mori Cortex in NCI-H460 Human Lung Carcinoma Cells. *Int J Oncol* (2012) 40(6):1929–40. doi: 10.3892/ijo.2012.1386
19. Klionsky DJ, Emr SD. Autophagy as a Regulated Pathway of Cellular Degradation. *Science (New York N Y)* (2000) 290(5497):1717–21. doi: 10.1126/science.290.5497.1717
20. Wu WS. The Signaling Mechanism of ROS in Tumor Progression. *Cancer Metastasis Rev* (2006) 25(4):695–705. doi: 10.1007/s10555-006-9037-8
21. Farkas T, Daugaard M, Jäättelä M. Identification of Small Molecule Inhibitors of Phosphatidylinositol 3-Kinase and Autophagy. *J Biol Chem* (2011) 286(45):38904–12. doi: 10.1074/jbc.M111.269134
22. Zhuang W, Li B, Long L, Chen L, Huang Q, Liang Z. Induction of Autophagy Promotes Differentiation of Glioma-Initiating Cells and Their Radiosensitivity. *Int J Cancer* (2011) 129(11):2720–31. doi: 10.1002/ijc.25975
23. Bae H, Guan JL. Suppression of Autophagy by FIP200 Deletion Impairs DNA Damage Repair and Increases Cell Death Upon Treatments With Anticancer Agents. *Mol Cancer Res* (2011) 9(9):1232–41. doi: 10.1158/1541-7786.MCR-11-0098
24. Chen S, Rehman SK, Zhang W, Wen A, Yao L, Zhang J. Autophagy Is a Therapeutic Target in Anticancer Drug Resistance. *Biochim Biophys Acta* (2010) 1806(2):220–9. doi: 10.1016/j.bbcan.2010.07.003
25. Degenhardt K, Mathew R, Beaudoin B, Bray K, Anderson D, Chen G, et al. Autophagy Promotes Tumor Cell Survival and Restricts Necrosis, Inflammation, and Tumorigenesis. *Cancer Cell* (2006) 10(1):51–64. doi: 10.1016/j.ccr.2006.06.001
26. Scherz-Shouval R, Elazar Z. ROS, Mitochondria and the Regulation of Autophagy. *Trends Cell Biol* (2007) 17(9):422–7. doi: 10.1016/j.tcb.2007.07.009
27. Amaravadi RK, Yu D, Lum JJ, Bui T, Christophorou MA, Evan GI, et al. Autophagy Inhibition Enhances Therapy-Induced Apoptosis in a Myc-Induced Model of Lymphoma. *J Clin Invest* (2007) 117(2):326–36. doi: 10.1172/JCI28833
28. Kabeya Y, Mizushima N, Ueno T, Yamamoto A, Kirisako T, Noda T, et al. LC3, a Mammalian Homologue of Yeast Apg8p, Is Localized in Autophagosome Membranes After Processing. *EMBO J* (2000) 19(21):5720–8. doi: 10.1093/emboj/19.21.5720
29. Mizushima N, Noda T, Yoshimori T, Tanaka Y, Ishii T, George MD, et al. A Protein Conjugation System Essential for Autophagy. *Nature* (1998) 395(6700):395–8. doi: 10.1038/26506
30. Levine B, Kroemer G. Autophagy in the Pathogenesis of Disease. *Cell* (2008) 132(1):27–42. doi: 10.1016/j.cell.2007.12.018
31. Klionsky DJ, Cregg JM, Dunn WAJr., Emr SD, Sakai Y, Sandoval IV, et al. A Unified Nomenclature for Yeast Autophagy-Related Genes. *Dev Cell* (2003) 5(4):539–45. doi: 10.1016/s1534-5807(03)00296-x
32. Scott RC, Schuldiner O, Neufeld TP. Role and Regulation of Starvation-Induced Autophagy in the Drosophila Fat Body. *Dev Cell* (2004) 7(2):167–78. doi: 10.1016/j.devcel.2004.07.009
33. Kim J, Kundu M, Viollet B, Guan KL. AMPK and mTOR Regulate Autophagy Through Direct Phosphorylation of Ulk1. *Nat Cell Biol* (2011) 13(2):132–41. doi: 10.1038/ncb2152
34. Torii S, Yoshida T, Arakawa S, Honda S, Nakanishi A, Shimizu S. Identification of PPM1D as an Essential Ulk1 Phosphatase for Genotoxic

Stress-Induced Autophagy. *EMBO Rep* (2016) 17(11):1552–64. doi: 10.15252/embr.201642565
35. Itakura E, Kishi C, Inoue K, Mizushima N. Beclin 1 Forms Two Distinct Phosphatidylinositol 3-Kinase Complexes With Mammalian Atg14 and UVRAG. *Mol Biol Cell* (2008) 19(12):5360–72. doi: 10.1091/mbc.e08-01-0080
36. Papinski D, Schuschnig M, Reiter W, Wilhelm L, Barnes CA, Maiolica A, et al. Early Steps in Autophagy Depend on Direct Phosphorylation of Atg9 by the Atg1 Kinase. *Mol Cell* (2014) 53(3):471–83. doi: 10.1016/j.molcel.2013.12.011
37. Slobodkin MR, Elazar Z. The Atg8 Family: Multifunctional Ubiquitin-Like Key Regulators of Autophagy. *Essays Biochem* (2013) 55:51–64. doi: 10.1042/bse0550051
38. Klionsky DJ, Schulman BA. Dynamic Regulation of Macroautophagy by Distinctive Ubiquitin-Like Proteins. *Nat Struct Mol Biol* (2014) 21(4):336–45. doi: 10.1038/nsmb.2787
39. Noda NN, Inagaki F. Mechanisms of Autophagy. *Annu Rev Biophys* (2015) 44:101–22. doi: 10.1146/annurev-biophys-060414-034248
40. Pankiv S, Clausen TH, Lamark T, Brech A, Bruun JA, Outzen H, et al. P62/SQSTM1 Binds Directly to Atg8/LC3 to Facilitate Degradation of Ubiquitinated Protein Aggregates by Autophagy. *J Biol Chem* (2007) 282 (33):24131–45. doi: 10.1074/jbc.M702824200
41. Sandoval H, Thiagarajan P, Dasgupta SK, Schumacher A, Prchal JT, Chen M, et al. Essential Role for Nix in Autophagic Maturation of Erythroid Cells. *Nature* (2008) 454(7201):232–5. doi: 10.1038/nature07006
42. Johansen T, Lamark T. Selective Autophagy Mediated by Autophagic Adapter Proteins. *Autophagy* (2011) 7(3):279–96. doi: 10.4161/auto.7.3.14487
43. Mizushima N, Levine B. Autophagy in Mammalian Development and Differentiation. *Nat Cell Biol* (2010) 12(9):823–30. doi: 10.1038/ncb0910-823
44. Gough DR, Cotter TG. Hydrogen Peroxide: A Jekyll and Hyde Signalling Molecule. *Cell Death Dis* (2011) 2(10):e213. doi: 10.1038/cddis.2011.96
45. St-Pierre J, Buckingham JA, Roebuck SJ, Brand MD. Topology of Superoxide Production From Different Sites in the Mitochondrial Electron Transport Chain. *J Biol Chem* (2002) 277(47):44784–90. doi: 10.1074/jbc.M207217200
46. Murphy MP. How Mitochondria Produce Reactive Oxygen Species. *Biochem J* (2009) 417(1):1–13. doi: 10.1042/BJ20081386
47. Kumari S, Badana AK, Murali Mohan G, Shailender G, Malla R. Reactive Oxygen Species: A Key Constituent in Cancer Survival. *Biomark Insights* (2018) 13:1177271918755391. doi: 10.1177/1177271918755391
48. Moloney JN, Cotter TG. ROS Signalling in the Biology of Cancer. *Semin Cell Dev Biol* (2018) 80:50–64. doi: 10.1016/j.semcdb.2017.05.023
49. Prasad S, Gupta SC, Tyagi AK. Reactive Oxygen Species (ROS) and Cancer: Role of Antioxidative Nutraceuticals. *Cancer Lett* (2017) 387:95–105. doi: 10.1016/j.canlet.2016.03.042
50. Chan JS, Tan MJ, Sng MK, Teo Z, Phua T, Choo CC, et al. Cancer-Associated Fibroblasts Enact Field Cancerization by Promoting Extratumoral Oxidative Stress. *Cell Death Dis* (2017) 8(1):e2562. doi: 10.1038/cddis.2016.492
51. Ježek J, Cooper KF, Strich R. Reactive Oxygen Species and Mitochondrial Dynamics: The Yin and Yang of Mitochondrial Dysfunction and Cancer Progression. *Antioxidants (Basel Switzerland)* (2018) 7(1):13. doi: 10.3390/antiox7010013
52. Reczek CR, Chandel NS. The Two Faces of Reactive Oxygen Species in Cancer. *Annu Rev Cancer Biol* (2017) 1:79–98. doi: 10.1146/annurev-cancerbio-041916-065808
53. Barrera G. Oxidative Stress and Lipid Peroxidation Products in Cancer Progression and Therapy. *ISRN Oncol* (2012) 2012:137289. doi: 10.5402/2012/137289
54. Gurer-Orhan H, Ince E, Konyar D, Saso L, Suzen S. The Role of Oxidative Stress Modulators in Breast Cancer. *Curr Med Chem* (2018) 25(33):4084–101. doi: 10.2174/0929867324666170711114336
55. Wang Y, Branicky R, Noë A, Hekimi S. Superoxide Dismutases: Dual Roles in Controlling ROS Damage and Regulating ROS Signaling. *J Cell Biol* (2018) 217(6):1915–28. doi: 10.1083/jcb.201708007
56. Poli G, Leonarduzzi G, Biasi F, Chiarpotto E. Oxidative Stress and Cell Signalling. *Curr Med Chem* (2004) 11(9):1163–82. doi: 10.2174/0929867043365323
57. Fruehauf JP, Meyskens FLJr. Reactive Oxygen Species: A Breath of Life or Death? *Clin Cancer Res* (2007) 13(3):789–94. doi: 10.1158/1078-0432.CCR-06-2082
58. Zhang J, Ney PA. Role of BNIP3 and NIX in Cell Death, Autophagy, and Mitophagy. *Cell Death Differ* (2009) 16(7):939–46. doi: 10.1038/cdd.2009.16
59. Novak I. Mitophagy: A Complex Mechanism of Mitochondrial Removal. *Antioxid Redox Signal* (2012) 17(5):794–802. doi: 10.1089/ars.2011.4407
60. Feng D, Liu L, Zhu Y, Chen Q. Molecular Signaling Toward Mitophagy and its Physiological Significance. *Exp Cell Res* (2013) 319(12):1697–705. doi: 10.1016/j.yexcr.2013.03.034
61. Youle RJ, Narendra DP. Mechanisms of Mitophagy. *Nat Rev Mol Cell Biol* (2011) 12(1):9–14. doi: 10.1038/nrm3028
62. Schweers RL, Zhang J, Randall MS, Loyd MR, Li W, Dorsey FC, et al. NIX Is Required for Programmed Mitochondrial Clearance During Reticulocyte Maturation. *Proc Natl Acad Sci USA* (2007) 104(49):19500–5. doi: 10.1073/pnas.0708818104
63. Matsuda N, Sato S, Shiba K, Okatsu K, Saisho K, Gautier CA, et al. PINK1 Stabilized by Mitochondrial Depolarization Recruits Parkin to Damaged Mitochondria and Activates Latent Parkin for Mitophagy. *J Cell Biol* (2010) 189(2):211–21. doi: 10.1083/jcb.200910140
64. Paulsen CE, Carroll KS. Cysteine-Mediated Redox Signaling: Chemistry, Biology, and Tools for Discovery. *Chem Rev* (2013) 113(7):4633–79. doi: 10.1021/cr300163e
65. Li L, Ishdorj G, Gibson SB. Reactive Oxygen Species Regulation of Autophagy in Cancer: Implications for Cancer Treatment. *Free Radical Biol Med* (2012) 53(7):1399–410. doi: 10.1016/j.freeradbiomed.2012.07.011
66. Bauer G. Targeting Extracellular ROS Signaling of Tumor Cells. *Anticancer Res* (2014) 34(4):1467–82.
67. Irani K, Xia Y, Zweier JL, Sollott SJ, Der CJ, Fearon ER, et al. Mitogenic Signaling Mediated by Oxidants in Ras-Transformed Fibroblasts. *Science (New York N Y)* (1997) 275(5306):1649–52. doi: 10.1126/science.275.5306.1649
68. Vafa O, Wade M, Kern S, Beeche M, Pandita TK, Hampton GM, et al. C-Myc Can Induce DNA Damage, Increase Reactive Oxygen Species, and Mitigate P53 Function: A Mechanism for Oncogene-Induced Genetic Instability. *Mol Cell* (2002) 9(5):1031–44. doi: 10.1016/s1097-2765(02)00520-8
69. Du J, Nelson ES, Simons AL, Olney KE, Moser JC, Schrock HE, et al. Regulation of Pancreatic Cancer Growth by Superoxide. *Mol Carcinog* (2013) 52(7):555–67. doi: 10.1002/mc.21891
70. Kim MJ, Woo SJ, Yoon CH, Lee JS, An S, Choi YH, et al. Involvement of Autophagy in Oncogenic K-Ras-Induced Malignant Cell Transformation. *J Biol Chem* (2011) 286(15):12924–32. doi: 10.1074/jbc.M110.138958
71. De Raedt T, Walton Z, Yecies JL, Li D, Chen Y, Malone CF, et al. Exploiting Cancer Cell Vulnerabilities to Develop a Combination Therapy for Ras-Driven Tumors. *Cancer Cell* (2011) 20(3):400–13. doi: 10.1016/j.ccr.2011.08.014
72. Inoki K, Zhu T, Guan KL. TSC2 Mediates Cellular Energy Response to Control Cell Growth and Survival. *Cell* (2003) 115(5):577–90. doi: 10.1016/s0092-8674(03)00929-2
73. Gwinn DM, Shackelford DB, Egan DF, Mihaylova MM, Mery A, Vasquez DS, et al. AMPK Phosphorylation of Raptor Mediates a Metabolic Checkpoint. *Mol Cell* (2008) 30(2):214–26. doi: 10.1016/j.molcel.2008.03.003
74. Choi SL, Kim SJ, Lee KT, Kim J, Mu J, Birnbaum MJ, et al. The Regulation of AMP-Activated Protein Kinase by H(2)O(2). *Biochem Biophys Res Commun* (2001) 287(1):92–7. doi: 10.1006/bbrc.2001.5544
75. Poillet-Perez L, Despouy G, Delage-Mourroux R, Boyer-Guittaut M. Interplay Between ROS and Autophagy in Cancer Cells, From Tumor Initiation to Cancer Therapy. *Redox Biol* (2015) 4:184–92. doi: 10.1016/j.redox.2014.12.003
76. Alexander A, Cai SL, Kim J, Nanez A, Sahin M, MacLean KH, et al. ATM Signals to TSC2 in the Cytoplasm to Regulate Mtorc1 in Response to ROS. *Proc Natl Acad Sci USA* (2010) 107(9):4153–8. doi: 10.1073/pnas.0913860107
77. Chen Y, McMillan-Ward E, Kong J, Israels SJ, Gibson SB. Oxidative Stress Induces Autophagic Cell Death Independent of Apoptosis in Transformed and Cancer Cells. *Cell Death Differ* (2008) 15(1):171–82. doi: 10.1038/sj.cdd.4402233

78. Djavaheri-Mergny M, Amelotti M, Mathieu J, Besançon F, Bauvy C, Souquère S, et al. NF-kappaB Activation Represses Tumor Necrosis Factor-Alpha-Induced Autophagy. *J Biol Chem* (2006) 281(41):30373–82. doi: 10.1074/jbc.M602097200
79. Boyer-Guittaut M, Poillet L, Liang Q, Bôle-Richard E, Ouyang X, Benavides GA, et al. The Role of GABARAPL1/GEC1 in Autophagic Flux and Mitochondrial Quality Control in MDA-MB-436 Breast Cancer Cells. *Autophagy* (2014) 10(6):986–1003. doi: 10.4161/auto.28390
80. Salmeen A, Barford D. Functions and Mechanisms of Redox Regulation of Cysteine-Based Phosphatases. *Antioxid Redox Signal* (2005) 7(5-6):560–77. doi: 10.1089/ars.2005.7.560
81. Leslie NR. The Redox Regulation of PI 3-Kinase-Dependent Signaling. *Antioxid Redox Signal* (2006) 8(9-10):1765–74. doi: 10.1089/ars.2006.8.1765
82. Byun YJ, Kim SK, Kim YM, Chae GT, Jeong SW, Lee SB. Hydrogen Peroxide Induces Autophagic Cell Death in C6 Glioma Cells *via* BNIP3-Mediated Suppression of the mTOR Pathway. *Neurosci Lett* (2009) 461(2):131–5. doi: 10.1016/j.neulet.2009.06.011
83. Zhang H, Kong X, Kang J, Su J, Li Y, Zhong J, et al. Oxidative Stress Induces Parallel Autophagy and Mitochondria Dysfunction in Human Glioma U251 Cells. *Toxicol Sci* (2009) 110(2):376–88. doi: 10.1093/toxsci/kfp101
84. Yu L, Alva A, Su H, Dutt P, Freundt E, Welsh S, et al. Regulation of an ATG7-Beclin 1 Program of Autophagic Cell Death by Caspase-8. *Science (New York N Y)* (2004) 304(5676):1500–2. doi: 10.1126/science.1096645
85. Yu L, Wan F, Dutta S, Welsh S, Liu Z, Freundt E, et al. Autophagic Programmed Cell Death by Selective Catalase Degradation. *Proc Natl Acad Sci USA* (2006) 103(13):4952–7. doi: 10.1073/pnas.0511288103
86. Chen Y, Azad MB, Gibson SB. Superoxide is the Major Reactive Oxygen Species Regulating Autophagy. *Cell Death Differ* (2009) 16(7):1040–52. doi: 10.1038/cdd.2009.49
87. Li L, Tan J, Miao Y, Lei P, Zhang Q. ROS and Autophagy: Interactions and Molecular Regulatory Mechanisms. *Cell Mol Neurobiol* (2015) 35(5):615–21. doi: 10.1007/s10571-015-0166-x
88. Aita VM, Liang XH, Murty VV, Pincus DL, Yu W, Cayanis E, et al. Cloning and Genomic Organization of Beclin 1, a Candidate Tumor Suppressor Gene on Chromosome 17q21. *Genomics* (1999) 59(1):59–65. doi: 10.1006/geno.1999.5851
89. Liang C, Feng P, Ku B, Dotan I, Canaani D, Oh BH, et al. Autophagic and Tumour Suppressor Activity of a Novel Beclin1-Binding Protein UVRAG. *Nat Cell Biol* (2006) 8(7):688–99. doi: 10.1038/ncb1426
90. Qu X, Yu J, Bhagat G, Furuya N, Hibshoosh H, Troxel A, et al. Promotion of Tumorigenesis by Heterozygous Disruption of the Beclin 1 Autophagy Gene. *J Clin Invest* (2003) 112(12):1809–20. doi: 10.1172/JCI20039
91. Yue Z, Jin S, Yang C, Levine AJ, Heintz N. Beclin 1, an Autophagy Gene Essential for Early Embryonic Development, Is a Haploinsufficient Tumor Suppressor. *Proc Natl Acad Sci U S A* (2003) 100(25):15077–82. doi: 10.1073/pnas.2436255100
92. Morselli E, Galluzzi L, Kepp O, Mariño G, Michaud M, Vitale I, et al. Oncosuppressive Functions of Autophagy. *Antioxid Redox Signal* (2011) 14(11):2251–69. doi: 10.1089/ars.2010.3478
93. Imlay JA, Linn S. DNA Damage and Oxygen Radical Toxicity. *Science (New York N Y)* (1988) 240(4857):1302–9. doi: 10.1126/science.3287616
94. Karantza-Wadsworth V, Patel S, Kravchuk O, Chen G, Mathew R, Jin S, et al. Autophagy Mitigates Metabolic Stress and Genome Damage in Mammary Tumorigenesis. *Genes Dev* (2007) 21(13):1621–35. doi: 10.1101/gad.1565707
95. Mathew R, Kongara S, Beaudoin B, Karp CM, Bray K, Degenhardt K, et al. Autophagy Suppresses Tumor Progression by Limiting Chromosomal Instability. *Genes Dev* (2007) 21(11):1367–81. doi: 10.1101/gad.1545107
96. Karin M. NF-kappaB as a Critical Link Between Inflammation and Cancer. *Cold Spring Harb Perspect Biol* (2009) 1(5):a000141. doi: 10.1101/cshperspect.a000141
97. Ghosh S, Mukherjee S, Choudhury S, Gupta P, Adhikary A, Baral R, et al. Reactive Oxygen Species in the Tumor Niche Triggers Altered Activation of Macrophages and Immunosuppression: Role of Fluoxetine. *Cell Signal* (2015) 27(7):1398–412. doi: 10.1016/j.cellsig.2015.03.013
98. Munn LL. Cancer and Inflammation. *Wiley Interdiscip Rev Syst Biol Med* (2017) 9(2):10.1002/wsbm.1370. doi: 10.1002/wsbm.1370
99. Kitamura T, Qian BZ, Pollard JW. Immune Cell Promotion of Metastasis. *Nat Rev Immunol* (2015) 15(2):73–86. doi: 10.1038/nri3789
100. Komohara Y, Jinushi M, Takeya M. Clinical Significance of Macrophage Heterogeneity in Human Malignant Tumors. *Cancer Sci* (2014) 105(1):1–8. doi: 10.1111/cas.12314
101. Bingle L, Brown NJ, Lewis CE. The Role of Tumour-Associated Macrophages in Tumour Progression: Implications for New Anticancer Therapies. *J Pathol* (2002) 196(3):254–65. doi: 10.1002/path.1027
102. Bruna F, Scodeller P. Pro-Tumorigenic Macrophage Infiltration in Oral Squamous Cell Carcinoma and Possible Macrophage-Aimed Therapeutic Interventions. *Front Oncol* (2021) 11:675664. doi: 10.3389/fonc.2021.675664
103. Nasrollahzadeh E, Razi S, Keshavarz-Fathi M, Mazzone M, Rezaei N. Pro-Tumorigenic Functions of Macrophages at the Primary, Invasive and Metastatic Tumor Site. *Cancer Immunol Immunother* (2020) 69(9):1673–97. doi: 10.1007/s00262-020-02616-6
104. Jounai N, Kobiyama K, Takeshita F, Ishii KJ. Recognition of Damage-Associated Molecular Patterns Related to Nucleic Acids During Inflammation and Vaccination. *Front Cell Infect Microbiol* (2013) 2:168. doi: 10.3389/fcimb.2012.00168
105. Hervera A, De Virgiliis F, Palmisano I, Zhou L, Tantardini E, Kong G, et al. Reactive Oxygen Species Regulate Axonal Regeneration Through the Release of Exosomal NADPH Oxidase 2 Complexes Into Injured Axons. *Nat Cell Biol* (2018) 20(3):307–19. doi: 10.1038/s41556-018-0039-x
106. Saitoh T, Fujita N, Jang MH, Uematsu S, Yang BG, Satoh T, et al. Loss of the Autophagy Protein Atg16L1 Enhances Endotoxin-Induced IL-1beta Production. *Nature* (2008) 456(7219):264–8. doi: 10.1038/nature07383
107. Bensaad K, Cheung EC, Vousden KH. Modulation of Intracellular ROS Levels by TIGAR Controls Autophagy. *EMBO J* (2009) 28(19):3015–26. doi: 10.1038/emboj.2009.242
108. Nakahira K, Haspel JA, Rathinam VA, Lee SJ, Dolinay T, Lam HC, et al. Autophagy Proteins Regulate Innate Immune Responses by Inhibiting the Release of Mitochondrial DNA Mediated by the NALP3 Inflammasome. *Nat Immunol* (2011) 12(3):222–30. doi: 10.1038/ni.1980
109. Zhou R, Yazdi AS, Menu P, Tschopp J. A Role for Mitochondria in NLRP3 Inflammasome Activation. *Nature* (2011) 469(7329):221–5. doi: 10.1038/nature09663
110. Roy D, Sarkar S, Felty Q. Levels of IL-1 Beta Control Stimulatory/Inhibitory Growth of Cancer Cells. *Front Biosci* (2006) 11:889–98. doi: 10.2741/1845
111. Thannickal VJ, Fanburg BL. Reactive Oxygen Species in Cell Signaling. *Am J Physiol Lung Cell Mol Physiol* (2000) 279(6):L1005–28. doi: 10.1152/ajplung.2000.279.6.L1005
112. Qian M, Fang X, Wang X. Autophagy and Inflammation. *Clin Trans Med* (2017) 6(1):24. doi: 10.1186/s40169-017-0154-5
113. Aggarwal C. Targeted Therapy for Lung Cancer: Present and Future. *Ann Palliat Med* (2014) 3(3):229–35. doi: 10.3978/j.issn.2224-5820.2014.06.01
114. Tang J, Di J, Cao H, Bai J, Zheng J. P53-Mediated Autophagic Regulation: A Prospective Strategy for Cancer Therapy. *Cancer Lett* (2015) 363(2):101–7. doi: 10.1016/j.canlet.2015.04.014
115. Kenzelmann Broz D, Spano Mello S, Bieging KT, Jiang D, Dusek RL, Brady CA, et al. Global Genomic Profiling Reveals an Extensive P53-Regulated Autophagy Program Contributing to Key P53 Responses. *Genes Dev* (2013) 27(9):1016–31. doi: 10.1101/gad.212282.112
116. Luo XJ, Li LL, Deng QP, Yu XF, Yang LF, Luo FJ, et al. Grifolin, a Potent Antitumour Natural Product Upregulates Death-Associated Protein Kinase 1 DAPK1 *via* P53 in Nasopharyngeal Carcinoma Cells. *Eur J Cancer (Oxford England: 1990)* (2011) 47(2):316–25. doi: 10.1016/j.ejca.2010.09.021
117. Crighton D, Wilkinson S, O'Prey J, Syed N, Smith P, Harrison PR, et al. DRAM, a P53-Induced Modulator of Autophagy, Is Critical for Apoptosis. *Cell* (2006) 126(1):121–34. doi: 10.1016/j.cell.2006.05.034
118. Pattingre S, Tassa A, Qu X, Garuti R, Liang XH, Mizushima N, et al. Bcl-2 Antiapoptotic Proteins Inhibit Beclin 1-Dependent Autophagy. *Cell* (2005) 122(6):927–39. doi: 10.1016/j.cell.2005.07.002
119. Budanov AV, Karin M. P53 Target Genes Sestrin1 and Sestrin2 Connect Genotoxic Stress and mTOR Signaling. *Cell* (2008) 134(3):451–60. doi: 10.1016/j.cell.2008.06.028
120. Feng Z, Zhang H, Levine AJ, Jin S. The Coordinate Regulation of the P53 and mTOR Pathways in Cells. *Proc Natl Acad Sci USA* (2005) 102(23):8204–9. doi: 10.1073/pnas.0502857102

121. Green DR, Kroemer G. Cytoplasmic Functions of the Tumour Suppressor P53. *Nature* (2009) 458(7242):1127–30. doi: 10.1038/nature07986
122. Morselli E, Galluzzi L, Kroemer G. Mechanisms of P53-Mediated Mitochondrial Membrane Permeabilization. *Cell Res* (2008) 18(7):708–10. doi: 10.1038/cr.2008.77
123. Tasdemir E, Maiuri MC, Galluzzi L, Vitale I, Djavaheri-Mergny M, D'Amelio M, et al. Regulation of Autophagy by Cytoplasmic P53. *Nat Cell Biol* (2008) 10(6):676–87. doi: 10.1038/ncb1730
124. Budanov AV, Lee JH, Karin M. Stressin' Sestrins Take an Aging Fight. *EMBO Mol Med* (2010) 2(10):388–400. doi: 10.1002/emmm.201000097
125. Pani G, Galeotti T. Role of MnSOD and P66shc in Mitochondrial Response to P53. *Antioxid Redox Signal* (2011) 15(6):1715–27. doi: 10.1089/ars.2010.3499
126. Hu W, Zhang C, Wu R, Sun Y, Levine A, Feng Z. Glutaminase 2, a Novel P53 Target Gene Regulating Energy Metabolism and Antioxidant Function. *Proc Natl Acad Sci USA* (2010) 107(16):7455–60. doi: 10.1073/pnas.1001006107
127. Suzuki S, Tanaka T, Poyurovsky MV, Nagano H, Mayama T, Ohkubo S, et al. Phosphate-Activated Glutaminase (GLS2), a P53-Inducible Regulator of Glutamine Metabolism and Reactive Oxygen Species. *Proc Natl Acad Sci USA* (2010) 107(16):7461–6. doi: 10.1073/pnas.1002459107
128. Budanov AV. Stress-Responsive Sestrins Link P53 With Redox Regulation and Mammalian Target of Rapamycin Signaling. *Antioxid Redox Signal* (2011) 15(6):1679–90. doi: 10.1089/ars.2010.3530
129. Fan S, Li L, Chen S, Yu Y, Qi M, Tashiro S, et al. Silibinin Induced-Autophagic and Apoptotic Death Is Associated With an Increase in Reactive Oxygen and Nitrogen Species in HeLa Cells. *Free Radical Res* (2011) 45(11-12):1307–24. doi: 10.3109/10715762.2011.618186
130. Fan S, Qi M, Yu Y, Li L, Yao G, Tashiro S, et al. P53 Activation Plays a Crucial Role in Silibinin Induced ROS Generation *via* PUMA and JNK. *Free Radical Res* (2012) 46(3):310–9. doi: 10.3109/10715762.2012.655244
131. Duan WJ, Li QS, Xia MY, Tashiro S, Onodera S, Ikejima T. Silibinin Activated P53 and Induced Autophagic Death in Human Fibrosarcoma HT1080 Cells *via* Reactive Oxygen Species-P38 and C-Jun N-Terminal Kinase Pathways. *Biol Pharm Bull* (2011) 34(1):47–53. doi: 10.1248/bpb.34.47
132. Kimmelman AC. The Dynamic Nature of Autophagy in Cancer. *Genes Dev* (2011) 25(19):1999–2010. doi: 10.1101/gad.17558811
133. Maiuri MC, Zalckvar E, Kimchi A, Kroemer G. Self-Eating and Self-Killing: Crosstalk Between Autophagy and Apoptosis. *Nat Rev Mol Cell Biol* (2007) 8(9):741–52. doi: 10.1038/nrm2239
134. Takamura A, Komatsu M, Hara T, Sakamoto A, Kishi C, Waguri S, et al. Autophagy-Deficient Mice Develop Multiple Liver Tumors. *Genes Dev* (2011) 25(8):795–800. doi: 10.1101/gad.2016211
135. Pérez-Mancera PA, Young AR, Narita M. Inside and Out: The Activities of Senescence in Cancer. *Nat Rev Cancer* (2014) 14(8):547–58. doi: 10.1038/nrc3773
136. Kang C, Xu Q, Martin TD, Li MZ, Demaria M, Aron L, et al. The DNA Damage Response Induces Inflammation and Senescence by Inhibiting Autophagy of GATA4. *Science (New York N Y)* (2015) 349(6255):aaa5612. doi: 10.1126/science.aaa5612
137. Rusten TE, Stenmark H. P62, an Autophagy Hero or Culprit? *Nat Cell Biol* (2010) 12(3):207–9. doi: 10.1038/ncb0310-207
138. Jain A, Lamark T, Sjøttem E, Larsen KB, Awuh JA, Øvervatn A, et al. P62/SQSTM1 Is a Target Gene for Transcription Factor NRF2 and Creates a Positive Feedback Loop by Inducing Antioxidant Response Element-Driven Gene Transcription. *J Biol Chem* (2010) 285(29):22576–91. doi: 10.1074/jbc.M110.118976
139. Komatsu M, Kurokawa H, Waguri S, Taguchi K, Kobayashi A, Ichimura Y, et al. The Selective Autophagy Substrate P62 Activates the Stress Responsive Transcription Factor Nrf2 Through Inactivation of Keap1. *Nat Cell Biol* (2010) 12(3):213–23. doi: 10.1038/ncb2021
140. Yousefi S, Perozzo R, Schmid I, Ziemiecki A, Schaffner T, Scapozza L, et al. Calpain-Mediated Cleavage of Atg5 Switches Autophagy to Apoptosis. *Nat Cell Biol* (2006) 8(10):1124–32. doi: 10.1038/ncb1482
141. Rubinstein AD, Eisenstein M, Ber Y, Bialik S, Kimchi A. The Autophagy Protein Atg12 Associates With Antiapoptotic Bcl-2 Family Members to Promote Mitochondrial Apoptosis. *Mol Cell* (2011) 44(5):698–709. doi: 10.1016/j.molcel.2011.10.014
142. Guo JY, Xia B, White E. Autophagy-Mediated Tumor Promotion. *Cell* (2013) 155(6):1216–9. doi: 10.1016/j.cell.2013.11.019
143. Kuma A, Hatano M, Matsui M, Yamamoto A, Nakaya H, Yoshimori T, et al. The Role of Autophagy During the Early Neonatal Starvation Period. *Nature* (2004) 432(7020):1032–6. doi: 10.1038/nature03029
144. Singh R, Cuervo AM. Autophagy in the Cellular Energetic Balance. *Cell Metab* (2011) 13(5):495–504. doi: 10.1016/j.cmet.2011.04.004
145. Guo JY, Chen HY, Mathew R, Fan J, Strohecker AM, Karsli-Uzunbas G, et al. Activated Ras Requires Autophagy to Maintain Oxidative Metabolism and Tumorigenesis. *Genes Dev* (2011) 25(5):460–70. doi: 10.1101/gad.2016311
146. Masliah-Planchon J, Garinet S, Pasmant E. RAS-MAPK Pathway Epigenetic Activation in Cancer: miRNAs in Action. *Oncotarget* (2016) 7(25):38892–907. doi: 10.18632/oncotarget.6476
147. Zhu D, Zhou J, Zhao J, Jiang G, Zhang X, Zhang Y, et al. ZC3H13 Suppresses Colorectal Cancer Proliferation and Invasion *via* Inactivating Ras-ERK Signaling. *J Cell Physiol* (2019) 234(6):8899–907. doi: 10.1002/jcp.27551
148. Su CC. Tanshinone IIA can Inhibit MiaPaCa-2 Human Pancreatic Cancer Cells by Dual Blockade of the Ras/Raf/MEK/ERK and PI3K/AKT/mTOR Pathways. *Oncol Rep* (2018) 40(5):3102–11. doi: 10.3892/or.2018.6670
149. Gonçalves PR, Rocha-Brito KJ, Fernandes MR, Abrantes JL, Durán N, Ferreira-Halder CV. Violacein Induces Death of RAS-Mutated Metastatic Melanoma by Impairing Autophagy Process. *Tumour Biol* (2016) 37(10):14049–58. doi: 10.1007/s13277-016-5265-x
150. Guo JY, White E. Autophagy Is Required for Mitochondrial Function, Lipid Metabolism, Growth, and Fate of KRAS(G12D)-Driven Lung Tumors. *Autophagy* (2013) 9(10):1636–8. doi: 10.4161/auto.26123
151. Yang ZJ, Chee CE, Huang S, Sinicrope FA. The Role of Autophagy in Cancer: Therapeutic Implications. *Mol Cancer Ther* (2011) 10(9):1533–41. doi: 10.1158/1535-7163.MCT-11-0047
152. Lock R, Roy S, Kenific CM, Su JS, Salas E, Ronen SM, et al. Autophagy Facilitates Glycolysis During Ras-Mediated Oncogenic Transformation. *Mol Biol Cell* (2011) 22(2):165–78. doi: 10.1091/mbc.E10-06-0500
153. Yang S, Wang X, Contino G, Liesa M, Sahin E, Ying H, et al. Pancreatic Cancers Require Autophagy for Tumor Growth. *Genes Dev* (2011) 25(7):717–29. doi: 10.1101/gad.2016111
154. Weinberg F, Hamanaka R, Wheaton WW, Weinberg S, Joseph J, Lopez M, et al. Mitochondrial Metabolism and ROS Generation Are Essential for Kras-Mediated Tumorigenicity. *Proc Natl Acad Sci USA* (2010) 107(19):8788–93. doi: 10.1073/pnas.1003428107
155. Guo JY, Karsli-Uzunbas G, Mathew R, Aisner SC, Kamphorst JJ, Strohecker AM, et al. Autophagy Suppresses Progression of K-Ras-Induced Lung Tumors to Oncocytomas and Maintains Lipid Homeostasis. *Genes Dev* (2013) 27(13):1447–61. doi: 10.1101/gad.219642.113
156. Duran A, Linares JF, Galvez AS, Wikenheiser K, Flores JM, Diaz-Meco MT, et al. The Signaling Adaptor P62 Is an Important NF-kappaB Mediator in Tumorigenesis. *Cancer Cell* (2008) 13(4):343–54. doi: 10.1016/j.ccr.2008.02.001
157. Mathew R, Karp CM, Beaudoin B, Vuong N, Chen G, Chen HY, et al. Autophagy Suppresses Tumorigenesis Through Elimination of P62. *Cell* (2009) 137(6):1062–75. doi: 10.1016/j.cell.2009.03.048
158. Wei H, Wei S, Gan B, Peng X, Zou W, Guan JL. Suppression of Autophagy by FIP200 Deletion Inhibits Mammary Tumorigenesis. *Genes Dev* (2011) 25(14):1510–27. doi: 10.1101/gad.2051011
159. Seyfried TN, Huysentruyt LC. On the Origin of Cancer Metastasis. *Crit Rev Oncog* (2013) 18(1-2):43–73. doi: 10.1615/critrevoncog.v18.i1-2.40
160. Clark AG, Vignjevic DM. Modes of Cancer Cell Invasion and the Role of the Microenvironment. *Curr Opin Cell Biol* (2015) 36:13–22. doi: 10.1016/j.ceb.2015.06.004
161. Lamouille S, Xu J, Derynck R. Molecular Mechanisms of Epithelial-Mesenchymal Transition. *Nat Rev Mol Cell Biol* (2014) 15(3):178–96. doi: 10.1038/nrm3758
162. Kalluri R, Weinberg RA. The Basics of Epithelial-Mesenchymal Transition. *J Clin Invest* (2009) 119(6):1420–8. doi: 10.1172/JCI39104
163. Polyak K, Weinberg RA. Transitions Between Epithelial and Mesenchymal States: Acquisition of Malignant and Stem Cell Traits. *Nat Rev Cancer* (2009) 9(4):265–73. doi: 10.1038/nrc2620
164. Yilmaz M, Christofori G. EMT, the Cytoskeleton, and Cancer Cell Invasion. *Cancer Metastasis Rev* (2009) 28(1-2):15–33. doi: 10.1007/s10555-008-9169-0

165. Avivar-Valderas A, Salas E, Bobrovnikova-Marjon E, Diehl JA, Nagi C, Debnath J, et al. PERK Integrates Autophagy and Oxidative Stress Responses to Promote Survival During Extracellular Matrix Detachment. *Mol Cell Biol* (2011) 31(17):3616–29. doi: 10.1128/MCB.05164-11
166. Fung C, Lock R, Gao S, Salas E, Debnath J. Induction of Autophagy During Extracellular Matrix Detachment Promotes Cell Survival. *Mol Biol Cell* (2008) 19(3):797–806. doi: 10.1091/mbc.e07-10-1092
167. Peng YF, Shi YH, Ding ZB, Ke AW, Gu CY, Hui B, et al. Autophagy Inhibition Suppresses Pulmonary Metastasis of HCC in Mice *via* Impairing Anoikis Resistance and Colonization of HCC Cells. *Autophagy* (2013) 9 (12):2056–68. doi: 10.4161/auto.26398
168. Peng YF, Shi YH, Shen YH, Ding ZB, Ke AW, Zhou J, et al. Promoting Colonization in Metastatic HCC Cells by Modulation of Autophagy. *PLoS One* (2013) 8(9):e74407. doi: 10.1371/journal.pone.0074407
169. Maes H, Kuchnio A, Peric A, Moens S, Nys K, De Bock K, et al. Tumor Vessel Normalization by Chloroquine Independent of Autophagy. *Cancer Cell* (2014) 26(2):190–206. doi: 10.1016/j.ccr.2014.06.025
170. Scherz-Shouval R, Shvets E, Fass E, Shorer H, Gil L, Elazar Z. Reactive Oxygen Species Are Essential for Autophagy and Specifically Regulate the Activity of Atg4. *EMBO J* (2019) 38(10):e101812. doi: 10.15252/embj.2019101812
171. Heldin CH, Vanlandewijck M, Moustakas A. Regulation of EMT by TGFβ in Cancer. *FEBS Lett* (2012) 586(14):1959–70. doi: 10.1016/j.febslet.2012.02.037
172. Tobar N, Villar V, Santibanez JF. ROS-NFkappaB Mediates TGF-Beta1-Induced Expression of Urokinase-Type Plasminogen Activator, Matrix Metalloproteinase-9 and Cell Invasion. *Mol Cell Biochem* (2010) 340(1-2):195–202. doi: 10.1007/s11010-010-0418-5
173. Lam CR, Tan C, Teo Z, Tay CY, Phua T, Wu YL, et al. Loss of TAK1 Increases Cell Traction Force in a ROS-Dependent Manner to Drive Epithelial-Mesenchymal Transition of Cancer Cells. *Cell Death Dis* (2013) 4(10):e848. doi: 10.1038/cddis.2013.339
174. Matsuno Y, Matsuyama M, Kiwamoto T, Morishima Y, Ishii Y, Hizawa N. ROS-Nrf2 Pathway Mediates the Development of TGF-B1-Induced Epithelial-Mesenchymal Transition Through the Interaction With Notch Signaling. In: *B61. Epithelial Cell Biology in Respiratory Disease*. American Thoracic Society International Conference Abstracts (2018). p. A3805–5.
175. Robertson IB, Rifkin DB. Unchaining the Beast; Insights From Structural and Evolutionary Studies on TGFβ Secretion, Sequestration, and Activation. *Cytokine Growth Factor Rev* (2013) 24(4):355–72. doi: 10.1016/j.cytogfr.2013.06.003
176. Rabinowitz JD, White E. Autophagy and Metabolism. *Science (New York N Y)* (2010) 330(6009):1344–8. doi: 10.1126/science.1193497
177. Eng CH, Abraham RT. The Autophagy Conundrum in Cancer: Influence of Tumorigenic Metabolic Reprogramming. *Oncogene* (2011) 30(47):4687–96. doi: 10.1038/onc.2011.220
178. Chang JY, Chiang MF, Lin SR, Lee MH, He H, Chou PY, et al. TIAF1 Self-Aggregation in Peritumor Capsule Formation, Spontaneous Activation of SMAD-Responsive Promoter in P53-Deficient Environment, and Cell Death. *Cell Death Dis* (2012) 3(4):e302. doi: 10.1038/cddis.2012.36
179. Debnath J. The Multifaceted Roles of Autophagy in Tumors-Implications for Breast Cancer. *J Mammary Gland Biol Neoplasia* (2011) 16(3):173–87. doi: 10.1007/s10911-011-9223-3
180. Chandel NS, McClintock DS, Feliciano CE, Wood TM, Melendez JA, Rodriguez AM, et al. Reactive Oxygen Species Generated at Mitochondrial Complex III Stabilize Hypoxia-Inducible Factor-1alpha During Hypoxia: A Mechanism of O_2 Sensing. *J Biol Chem* (2000) 275(33):25130–8. doi: 10.1074/jbc.M001914200
181. Zhang H, Bosch-Marce M, Shimoda LA, Tan YS, Baek JH, Wesley JB, et al. Mitochondrial Autophagy is an HIF-1-Dependent Adaptive Metabolic Response to Hypoxia. *J Biol Chem* (2008) 283(16):10892–903. doi: 10.1074/jbc.M800102200
182. Bellot G, Garcia-Medina R, Gounon P, Chiche J, Roux D, Pouysségur J, et al. Hypoxia-Induced Autophagy Is Mediated Through Hypoxia-Inducible Factor Induction of BNIP3 and BNIP3L *via* Their BH3 Domains. *Mol Cell Biol* (2009) 29(10):2570–81. doi: 10.1128/MCB.00166-09
183. Rouschop KM, Ramaekers CH, Schaaf MB, Keulers TG, Savelkouls KG, Lambin P, et al. Autophagy Is Required During Cycling Hypoxia to Lower Production of Reactive Oxygen Species. *Radiother Oncol* (2009) 92(3):411–6. doi: 10.1016/j.radonc.2009.06.029
184. Brahimi-Horn MC, Bellot G, Pouysségur J. Hypoxia and Energetic Tumour Metabolism. *Curr Opin Genet Dev* (2011) 21(1):67–72. doi: 10.1016/j.gde.2010.10.006
185. Mazure NM, Pouysségur J. Hypoxia-Induced Autophagy: Cell Death or Cell Survival? *Curr Opin Cell Biol* (2010) 22(2):177–80. doi: 10.1016/j.ceb.2009.11.015
186. Papandreou I, Lim AL, Laderoute K, Denko NC. Hypoxia Signals Autophagy in Tumor Cells *via* AMPK Activity, Independent of HIF-1, BNIP3, and BNIP3L. *Cell Death Differ* (2008) 15(10):1572–81. doi: 10.1038/cdd.2008.84
187. Rouschop KM, van den Beucken T, Dubois L, Niessen H, Bussink J, Savelkouls K, et al. The Unfolded Protein Response Protects Human Tumor Cells During Hypoxia Through Regulation of the Autophagy Genes MAP1LC3B and ATG5. *J Clin Invest* (2010) 120(1):127–41. doi: 10.1172/JCI40027
188. Li J, Yang B, Zhou Q, Wu Y, Shang D, Guo Y, et al. Autophagy Promotes Hepatocellular Carcinoma Cell Invasion Through Activation of Epithelial-Mesenchymal Transition. *Carcinogenesis* (2013) 34(6):1343–51. doi: 10.1093/carcin/bgt063
189. Kim YH, Baek SH, Kim EK, Ha JM, Jin SY, Lee HS, et al. Uncoordinated 51-Like Kinase 2 Signaling Pathway Regulates Epithelial-Mesenchymal Transition in A549 Lung Cancer Cells. *FEBS Lett* (2016) 590(9):1365–74. doi: 10.1002/1873-3468.12172
190. Galavotti S, Bartesaghi S, Faccenda D, Shaked-Rabi M, Sanzone S, McEvoy A, et al. The Autophagy-Associated Factors DRAM1 and P62 Regulate Cell Migration and Invasion in Glioblastoma Stem Cells. *Oncogene* (2013) 32 (6):699–712. doi: 10.1038/onc.2012.111
191. Macintosh RL, Timpson P, Thorburn J, Anderson KI, Thorburn A, Ryan KM. Inhibition of Autophagy Impairs Tumor Cell Invasion in an Organotypic Model. *Cell Cycle (Georgetown Tex)* (2012) 11(10):2022–9. doi: 10.4161/cc.20424
192. Catalano M, D'Alessandro G, Lepore F, Corazzari M, Caldarola S, Valacca C, et al. Autophagy Induction Impairs Migration and Invasion by Reversing EMT in Glioblastoma Cells. *Mol Oncol* (2015) 9(8):1612–25. doi: 10.1016/j.molonc.2015.04.016
193. Grassi G, Di Caprio G, Santangelo L, Fimia GM, Cozzolino AM, Komatsu M, et al. Autophagy Regulates Hepatocyte Identity and Epithelial-to-Mesenchymal and Mesenchymal-to-Epithelial Transitions Promoting Snail Degradation. *Cell Death Dis* (2015) 6(9):e1880. doi: 10.1038/cddis.2015.249
194. Zhao Z, Zhao J, Xue J, Zhao X, Liu P. Autophagy Inhibition Promotes Epithelial-Mesenchymal Transition Through ROS/HO-1 Pathway in Ovarian Cancer Cells. *Am J Cancer Res* (2016) 6(10):2162–77.
195. Lv Q, Wang W, Xue J, Hua F, Mu R, Lin H, et al. DEDD Interacts With PI3KC3 to Activate Autophagy and Attenuate Epithelial-Mesenchymal Transition in Human Breast Cancer. *Cancer Res* (2012) 72(13):3238–50. doi: 10.1158/0008-5472.CAN-11-3832
196. Wang MC, Liang X, Liu ZY, Cui J, Liu Y, Jing L, et al. *In Vitro* Synergistic Antitumor Efficacy of Sequentially Combined Chemotherapy/Icotinib in Non-Small Cell Lung Cancer Cell Lines. *Oncol Rep* (2015) 33(1):239–49. doi: 10.3892/or.2014.3583
197. Qiang L, Zhao B, Ming M, Wang N, He TC, Hwang S, et al. Regulation of Cell Proliferation and Migration by P62 Through Stabilization of Twist1. *Proc Natl Acad Sci USA* (2014) 111(25):9241–6. doi: 10.1073/pnas.1322913111
198. Bertrand M, Petit V, Jain A, Amsellem R, Johansen T, Larue L, et al. SQSTM1/p62 Regulates the Expression of Junctional Proteins Through Epithelial-Mesenchymal Transition Factors. *Cell Cycle (Georgetown Tex)* (2015) 14(3):364–74. doi: 10.4161/15384101.2014.987619
199. Kanzawa T, Germano IM, Komata T, Ito H, Kondo Y, Kondo S. Role of Autophagy in Temozolomide-Induced Cytotoxicity for Malignant Glioma Cells. *Cell Death Differ* (2004) 11(4):448–57. doi: 10.1038/sj.cdd.4401359
200. Qadir MA, Kwok B, Dragowska WH, To KH, Le D, Bally MB, et al. Macroautophagy Inhibition Sensitizes Tamoxifen-Resistant Breast Cancer Cells and Enhances Mitochondrial Depolarization. *Breast Cancer Res Treat* (2008) 112(3):389–403. doi: 10.1007/s10549-007-9873-4
201. Carew JS, Nawrocki ST, Kahue CN, Zhang H, Yang C, Chung L, et al. Targeting Autophagy Augments the Anticancer Activity of the Histone

Deacetylase Inhibitor SAHA to Overcome Bcr-Abl-Mediated Drug Resistance. *Blood* (2007) 110(1):313–22. doi: 10.1182/blood-2006-10-050260
202. Abedin MJ, Wang D, McDonnell MA, Lehmann U, Kelekar A. Autophagy Delays Apoptotic Death in Breast Cancer Cells Following DNA Damage. *Cell Death Differ* (2007) 14(3):500–10. doi: 10.1038/sj.cdd.4402039
203. Bellodi C, Lidonnici MR, Hamilton A, Helgason GV, Soliera AR, Ronchetti M, et al. Targeting Autophagy Potentiates Tyrosine Kinase Inhibitor-Induced Cell Death in Philadelphia Chromosome-Positive Cells, Including Primary CML Stem Cells. *J Clin Invest* (2009) 119(5):1109–23. doi: 10.1172/JCI35660
204. Harhaji-Trajkovic L, Vilimanovich U, Kravic-Stevovic T, Bumbasirevic V, Trajkovic V. AMPK-Mediated Autophagy Inhibits Apoptosis in Cisplatin-Treated Tumour Cells. *J Cell Mol Med* (2009) 13(9B):3644–54. doi: 10.1111/j.1582-4934.2009.00663.x
205. White E, DiPaola RS. The Double-Edged Sword of Autophagy Modulation in Cancer. *Clin Cancer Res* (2009) 15(17):5308–16. doi: 10.1158/1078-0432.CCR-07-5023
206. Martin AP, Park MA, Mitchell C, Walker T, Rahmani M, Thorburn A, et al. BCL-2 Family Inhibitors Enhance Histone Deacetylase Inhibitor and Sorafenib Lethality *via* Autophagy and Overcome Blockade of the Extrinsic Pathway to Facilitate Killing. *Mol Pharmacol* (2009) 76(2):327–41. doi: 10.1124/mol.109.056309
207. Zhou H, Shen T, Shang C, Luo Y, Liu L, Yan J, et al. Ciclopirox Induces Autophagy Through Reactive Oxygen Species-Mediated Activation of JNK Signaling Pathway. *Oncotarget* (2014) 5(20):10140–50. doi: 10.18632/oncotarget.2471
208. Hahm ER, Sakao K, Singh SV. Honokiol Activates Reactive Oxygen Species-Mediated Cytoprotective Autophagy in Human Prostate Cancer Cells. *Prostate* (2014) 74(12):1209–21. doi: 10.1002/pros.22837
209. Gonzalez Y, Aryal B, Chehab L, Rao VA. Atg7- and Keap1-Dependent Autophagy Protects Breast Cancer Cell Lines Against Mitoquinone-Induced Oxidative Stress. *Oncotarget* (2014) 5(6):1526–37. doi: 10.18632/oncotarget.1715
210. Kim H, Moon JY, Ahn KS, Cho SK. Quercetin Induces Mitochondrial Mediated Apoptosis and Protective Autophagy in Human Glioblastoma U373MG Cells. *Oxid Med Cell Longev* (2013) 2013:596496. doi: 10.1155/2013/596496
211. Zhang Q, Zhang Y, Zhang P, Chao Z, Xia F, Jiang C, et al. Hexokinase II Inhibitor, 3-BrPA Induced Autophagy by Stimulating ROS Formation in Human Breast Cancer Cells. *Genes Cancer* (2014) 5(3-4):100–12. doi: 10.18632/genesandcancer.9
212. Ganguli A, Choudhury D, Datta S, Bhattacharya S, Chakrabarti G. Inhibition of Autophagy by Chloroquine Potentiates Synergistically Anti-Cancer Property of Artemisinin by Promoting ROS Dependent Apoptosis. *Biochimie* (2014) 107 Pt B:338–49. doi: 10.1016/j.biochi.2014.10.001
213. Al Dhaheri Y, Attoub S, Ramadan G, Arafat K, Bajbouj K, Karuvantevida N, et al. Carnosol Induces ROS-Mediated Beclin1-Independent Autophagy and Apoptosis in Triple Negative Breast Cancer. *PLoS One* (2014) 9(10):e109630. doi: 10.1371/journal.pone.0109630
214. Kondo Y, Kondo S. Autophagy and Cancer Therapy. *Autophagy* (2006) 2 (2):85–90. doi: 10.4161/auto.2.2.2463
215. Kanzawa T, Kondo Y, Ito H, Kondo S, Germano I. Induction of Autophagic Cell Death in Malignant Glioma Cells by Arsenic Trioxide. *Cancer Res* (2003) 63(9):2103–8.
216. Chen Y, Gibson SB. Is Mitochondrial Generation of Reactive Oxygen Species a Trigger for Autophagy? *Autophagy* (2008) 4(2):246–8. doi: 10.4161/auto.5432
217. Sweeney C, Liu G, Yiannoutsos C, Kolesar J, Horvath D, Staab MJ, et al. A Phase II Multicenter, Randomized, Double-Blind, Safety Trial Assessing the Pharmacokinetics, Pharmacodynamics, and Efficacy of Oral 2-Methoxyestradiol Capsules in Hormone-Refractory Prostate Cancer. *Clin Cancer Res* (2005) 11(18):6625–33. doi: 10.1158/1078-0432.CCR-05-0440
218. Nicolau-Galmés F, Asumendi A, Alonso-Tejerina E, Pérez-Yarza G, Jangi SM, Gardeazabal J, et al. Terfenadine Induces Apoptosis and Autophagy in Melanoma Cells Through ROS-Dependent and -Independent Mechanisms. *Apoptosis* (2011) 16(12):1253–67. doi: 10.1007/s10495-011-0640-y
219. Selimovic D, Porzig BB, El-Khattouti A, Badura HE, Ahmad M, Ghanjati F, et al. Bortezomib/proteasome Inhibitor Triggers Both Apoptosis and Autophagy-Dependent Pathways in Melanoma Cells. *Cell Signal* (2013) 25 (1):308–18. doi: 10.1016/j.cellsig.2012.10.004
220. Liang QP, Xu TQ, Liu BL, Lei XP, Hambrook JR, Zhang DM, et al. Sasanquasaponin III From Schima Crenata Korth Induces Autophagy Through Akt/mTOR/p70S6K Pathway and Promotes Apoptosis in Human Melanoma A375 Cells. *Phytomedicine* (2019) 58:152769. doi: 10.1016/j.phymed.2018.11.029
221. Hao W, Zhang X, Zhao W, Chen X. Psoralidin Induces Autophagy Through ROS Generation Which Inhibits the Proliferation of Human Lung Cancer A549 Cells. *PeerJ* (2014) 2:e555. doi: 10.7717/peerj.555
222. Miki H, Uehara N, Kimura A, Sasaki T, Yuri T, Yoshizawa K, et al. Resveratrol Induces Apoptosis *via* ROS-Triggered Autophagy in Human Colon Cancer Cells. *Int J Oncol* (2012) 40(4):1020–8. doi: 10.3892/ijo.2012.1325
223. Giammarioli AM, Gambardella L, Barbati C, Pietraforte D, Tinari A, Alberton M, et al. Differential Effects of the Glycolysis Inhibitor 2-Deoxy-D-Glucose on the Activity of Pro-Apoptotic Agents in Metastatic Melanoma Cells, and Induction of a Cytoprotective Autophagic Response. *Int J Cancer* (2012) 131(4):E337–47. doi: 10.1002/ijc.26420
224. Antunes F, Corazzari M, Pereira G, Fimia GM, Piacentini M, Smaili S. Fasting Boosts Sensitivity of Human Skin Melanoma to Cisplatin-Induced Cell Death. *Biochem Biophys Res Commun* (2017) 485(1):16–22. doi: 10.1016/j.bbrc.2016.09.149
225. Raffoul F, Campla C, Nanjundan M. SnoN/SkiL, a TGFβ Signaling Mediator: A Participant in Autophagy Induced by Arsenic Trioxide. *Autophagy* (2010) 6(7):955–7. doi: 10.4161/auto.6.7.13041
226. Luo Y, Sun X, Huang L, Yan J, Yu BY, Tian J. Artemisinin-Based Smart Nanomedicines With Self-Supply of Ferrous Ion to Enhance Oxidative Stress for Specific and Efficient Cancer Treatment. *ACS Appl Mater Interfaces* (2019) 11(33):29490–7. doi: 10.1021/acsami.9b07390
227. Bailey HH, Mulcahy RT, Tutsch KD, Arzoomanian RZ, Alberti D, Tombes MB, et al. Phase I Clinical Trial of Intravenous L-Buthionine Sulfoximine and Melphalan: An Attempt at Modulation of Glutathione. *J Clin Oncol* (1994) 12(1):194–205. doi: 10.1200/JCO.1994.12.1.194
228. Maeda H, Hori S, Ohizumi H, Segawa T, Kakehi Y, Ogawa O, et al. Effective Treatment of Advanced Solid Tumors by the Combination of Arsenic Trioxide and L-Buthionine-Sulfoximine. *Cell Death Differ* (2004) 11 (7):737–46. doi: 10.1038/sj.cdd.4401389
229. Li Q, Yin X, Wang W, Zhan M, Zhao B, Hou Z, et al. The Effects of Buthionine Sulfoximine on the Proliferation and Apoptosis of Biliary Tract Cancer Cells Induced by Cisplatin and Gemcitabine. *Oncol Lett* (2016) 11 (1):474–80. doi: 10.3892/ol.2015.3879
230. Hollomon MG, Gordon N, Santiago-O'Farrill JM, Kleinerman ES. Knockdown of Autophagy-Related Protein 5, ATG5, Decreases Oxidative Stress and Has an Opposing Effect on Camptothecin-Induced Cytotoxicity in Osteosarcoma Cells. *BMC Cancer* (2013) 13:500. doi: 10.1186/1471-2407-13-500
231. Pardee AB, Li YZ, Li CJ. Cancer Therapy With Beta-Lapachone. *Curr Cancer Drug Targets* (2002) 2(3):227–42. doi: 10.2174/1568009023333854
232. Bey EA, Bentle MS, Reinicke KE, Dong Y, Yang CR, Girard L, et al. An NQO1- and PARP-1-Mediated Cell Death Pathway Induced in Non-Small-Cell Lung Cancer Cells by Beta-Lapachone. *Proc Natl Acad Sci USA* (2007) 104(28):11832–7. doi: 10.1073/pnas.0702176104
233. Park EJ, Choi KS, Kwon TK. β-Lapachone-Induced Reactive Oxygen Species (ROS) Generation Mediates Autophagic Cell Death in Glioma U87 MG Cells. *Chem Biol Interact* (2011) 189(1-2):37–44. doi: 10.1016/j.cbi.2010.10.013
234. Yen CJ, Hung CH, Tsai WM, Cheng HC, Yang HL, Lu YJ, et al. Effect of Exercise Training on Exercise Tolerance and Level of Oxidative Stress for Head and Neck Cancer Patients Following Chemotherapy. *Front Oncol* (2020) 10:3389/fonc.2020.01536. doi: 10.3389/fonc.2020.01536
235. Lin JF, Lin YC, Tsai TF, Chen HE, Chou KY, Hwang TI. Cisplatin Induces Protective Autophagy Through Activation of BECN1 in Human Bladder Cancer Cells. *Drug Des Dev Ther* (2017) 11:1517–33. doi: 10.2147/DDDT.S126464
236. Lee YJ, Kim NY, Suh YA, Lee C. Involvement of ROS in Curcumin-Induced Autophagic Cell Death. *Korean J Physiol Pharmacol* (2011) 15(1):1–7. doi: 10.4196/kjpp.2011.15.1.1

237. Al-Aamri HM, Ku H, Irving HR, Tucci J, Meehan-Andrews T, Bradley C. Time Dependent Response of Daunorubicin on Cytotoxicity, Cell Cycle and DNA Repair in Acute Lymphoblastic Leukaemia. *BMC Cancer* (2019) 19 (1):179. doi: 10.1186/s12885-019-5377-y
238. Han W, Sun J, Feng L, Wang K, Li D, Pan Q, et al. Autophagy Inhibition Enhances Daunorubicin-Induced Apoptosis in K562 Cells. *PLoS One* (2011) 6(12):e28491. doi: 10.1371/journal.pone.0028491
239. Sritharan S, Sivalingam N. A Comprehensive Review on Time-Tested Anticancer Drug Doxorubicin. *Life Sci* (2021) 278:119527. doi: 10.1016/j.lfs.2021.119527
240. Aydinlik S, Erkisa M, Cevatemre B, Sarimahmut M, Dere E, Ari F, et al. Enhanced Cytotoxic Activity of Doxorubicin Through the Inhibition of Autophagy in Triple Negative Breast Cancer Cell Line. *Biochim Biophys Acta Gen Subj* (2017) 1861(2):49–57. doi: 10.1016/j.bbagen.2016.11.013
241. Fang B. Genetic Interactions of STAT3 and Anticancer Drug Development. *Cancers* (2014) 6(1):494–525. doi: 10.3390/cancers6010494
242. Doroshow JH, Juhasz A, Ge Y, Holbeck S, Lu J, Antony S, et al. Antiproliferative Mechanisms of Action of the Flavin Dehydrogenase Inhibitors Diphenylene Iodonium and Di-2-Thienyliodonium Based on Molecular Profiling of the NCI-60 Human Tumor Cell Panel. *Biochem Pharmacol* (2012) 83(9):1195–207. doi: 10.1016/j.bcp.2012.01.022
243. Ligeon LA, Pena-Francesch M, Vanoaica LD, Núñez NG, Talwar D, Dick TP, et al. Oxidation Inhibits Autophagy Protein Deconjugation From Phagosomes to Sustain MHC Class II Restricted Antigen Presentation. *Nat Commun* (2021) 12(1):1508. doi: 10.1038/s41467-021-21829-6
244. Cen D, Gonzalez RI, Buckmeier JA, Kahlon RS, Tohidian NB, Meyskens FLJr. Disulfiram Induces Apoptosis in Human Melanoma Cells: A Redox-Related Process. *Mol Cancer Ther* (2002) 1(3):197–204.
245. Fruehauf JP, Trapp V. Reactive Oxygen Species: An Achilles' Heel of Melanoma? *Expert Rev Anticancer Ther* (2008) 8(11):1751–7. doi: 10.1586/14737140.8.11.1751
246. Wu X, Xue X, Wang L, Wang W, Han J, Sun X, et al. Suppressing Autophagy Enhances Disulfiram/Copper-Induced Apoptosis in Non-Small Cell Lung Cancer. *Eur J Pharmacol* (2018) 827:1–12. doi: 10.1016/j.ejphar.2018.02.039
247. Zhang X, Hu P, Ding SY, Sun T, Liu L, Han S, et al. Induction of Autophagy-Dependent Apoptosis in Cancer Cells Through Activation of ER Stress: An Uncovered Anti-Cancer Mechanism by Anti-Alcoholism Drug Disulfiram. *Am J Cancer Res* (2019) 9(6):1266–81.
248. Hu Y, Qian Y, Wei J, Jin T, Kong X, Cao H, et al. The Disulfiram/Copper Complex Induces Autophagic Cell Death in Colorectal Cancer by Targeting ULK1. *Front Pharmacol* (2021) 12:3389/fphar.2021.752825. doi: 10.3389/fphar.2021.752825
249. Zhang Q, Yang W, Man N, Zheng F, Shen Y, Sun K, et al. Autophagy-Mediated Chemosensitization in Cancer Cells by Fullerene C60 Nanocrystal. *Autophagy* (2009) 5(8):1107–17. doi: 10.4161/auto.5.8.9842
250. Zhang L, Li J, Zong L, Chen X, Chen K, Jiang Z, et al. Reactive Oxygen Species and Targeted Therapy for Pancreatic Cancer. *Oxid Med Cell Longev* (2016) 2016:1616781. doi: 10.1155/2016/1616781
251. Chen M, He M, Song Y, Chen L, Xiao P, Wan X, et al. The Cytoprotective Role of Gemcitabine-Induced Autophagy Associated With Apoptosis Inhibition in Triple-Negative MDA-MB-231 Breast Cancer Cells. *Int J Mol Med* (2014) 34(1):276–82. doi: 10.3892/ijmm.2014.1772
252. Yang MC, Wang HC, Hou YC, Tung HL, Chiu TJ, Shan YS. Blockade of Autophagy Reduces Pancreatic Cancer Stem Cell Activity and Potentiates the Tumoricidal Effect of Gemcitabine. *Mol Cancer* (2015) 14:179. doi: 10.1186/s12943-015-0449-3
253. Yang X, Yin H, Zhang Y, Li X, Tong H, Zeng Y, et al. Hypoxia-Induced Autophagy Promotes Gemcitabine Resistance in Human Bladder Cancer Cells Through Hypoxia-Inducible Factor 1α Activation. *Int J Oncol* (2018) 53(1):215–24. doi: 10.3892/ijo.2018.4376
254. Mizutani H, Shiga C, Imai M, Ikemura K, Kitamura Y, Ohta K, et al. Idarubicin, an Anthracycline, Induces Oxidative DNA Damage in the Presence of Copper (II). *Anticancer Res* (2020) 40(10):5399–404. doi: 10.21873/anticanres.14548
255. Zhang Y, Li Q, Xu D, Li T, Gu Z, Huang P, et al. Idarubicin-Induced Oxidative Stress and Apoptosis in Cardiomyocytes: An *In Vitro* Molecular Approach. *Hum Exp Toxicol* (2021) 40(12_suppl):S553–62. doi: 10.1177/09603271211033774
256. Ristic B, Bosnjak M, Arsikin K, Mircic A, Suzin-Zivkovic V, Bogdanovic A, et al. Idarubicin Induces mTOR-Dependent Cytotoxic Autophagy in Leukemic Cells. *Exp Cell Res* (2014) 326(1):90–102. doi: 10.1016/j.yexcr.2014.05.021
257. Kim SJ, Kim HS, Seo YR. Understanding of ROS-Inducing Strategy in Anticancer Therapy. *Oxid Med Cell Longev* (2019) 2019:5381692. doi: 10.1155/2019/5381692
258. Graczyk-Jarzynka A, Zagozdzon R, Muchowicz A, Siernicka M, Juszczynski P, Firczuk M. New Insights Into Redox Homeostasis as a Therapeutic Target in B-Cell Malignancies. *Curr Opin Hematol* (2017) 24(4):393–401. doi: 10.1097/MOH.0000000000000351
259. Wang W, Dong X, Liu Y, Ni B, Sai N, You L, et al. Itraconazole Exerts Anti-Liver Cancer Potential Through the Wnt, PI3K/AKT/mTOR, and ROS Pathways. *Biomed Pharmacother* (2020) 131:110661. doi: 10.1016/j.biopha.2020.110661
260. Liu R, Li J, Zhang T, Zou L, Chen Y, Wang K, et al. Itraconazole Suppresses the Growth of Glioblastoma Through Induction of Autophagy: Involvement of Abnormal Cholesterol Trafficking. *Autophagy* (2014) 10(7):1241–55. doi: 10.4161/auto.28912
261. Deng H, Huang L, Liao Z, Liu M, Li Q, Xu R. Itraconazole Inhibits the Hedgehog Signaling Pathway Thereby Inducing Autophagy-Mediated Apoptosis of Colon Cancer Cells. *Cell Death Dis* (2020) 11(7):539. doi: 10.1038/s41419-020-02742-0
262. Alexandre J, Nicco C, Chéreau C, Laurent A, Weill B, Goldwasser F, et al. Improvement of the Therapeutic Index of Anticancer Drugs by the Superoxide Dismutase Mimic Mangafodipir. *J Natl Cancer Inst* (2006) 98 (4):236–44. doi: 10.1093/jnci/djj049
263. Khanim FL, Hayden RE, Birtwistle J, Lodi A, Tiziani S, Davies NJ, et al. Combined Bezafibrate and Medroxyprogesterone Acetate: Potential Novel Therapy for Acute Myeloid Leukaemia. *PLoS One* (2009) 4(12):e8147. doi: 10.1371/journal.pone.0008147
264. Elmaci İ, Ozpinar A, Bilir A, Altinoz MA. Medroxyprogesterone Effects on Colony Growth, Autophagy and Mitochondria of C6 Glioma Cells Are Augmented With Tibolone and Temozolomide: Cell Kinetic and Electron Microscopical Studies With a Broad Review of the Literature. *Clin Neurol Neurosurg* (2019) 177:77–85. doi: 10.1016/j.clineuro.2018.12.022
265. Mogavero A, Maiorana MV, Zanutto S, Varinelli L, Bozzi F, Belfiore A, et al. Metformin Transiently Inhibits Colorectal Cancer Cell Proliferation as a Result of Either AMPK Activation or Increased ROS Production. *Sci Rep* (2017) 7(1):15992. doi: 10.1038/s41598-017-16149-z
266. Bharath LP, Agrawal M, McCambridge G, Nicholas DA, Hasturk H, Liu J, et al. Metformin Enhances Autophagy and Normalizes Mitochondrial Function to Alleviate Aging-Associated Inflammation. *Cell Metab* (2020) 32(1):44–55.e6. doi: 10.1016/j.cmet.2020.04.015
267. Gao C, Fang L, Zhang H, Zhang WS, Li XO, Du SY. Metformin Induces Autophagy *via* the AMPK-mTOR Signaling Pathway in Human Hepatocellular Carcinoma Cells. *Cancer Manag Res* (2020) 12:5803–11. doi: 10.2147/CMAR.S257966
268. De Santi M, Baldelli G, Diotallevi A, Galluzzi L, Schiavano GF, Brandi G. Metformin Prevents Cell Tumorigenesis Through Autophagy-Related Cell Death. *Sci Rep* (2019) 9(1):66. doi: 10.1038/s41598-018-37247-6
269. Magda D, Miller RA. Motexafin Gadolinium: A Novel Redox Active Drug for Cancer Therapy. *Semin Cancer Biol* (2006) 16(6):466–76. doi: 10.1016/j.semcancer.2006.09.002
270. Gao M, Yeh PY, Lu YS, Hsu CH, Chen KF, Lee WC, et al. OSU-03012, a Novel Celecoxib Derivative, Induces Reactive Oxygen Species-Related Autophagy in Hepatocellular Carcinoma. *Cancer Res* (2008) 68(22):9348–57. doi: 10.1158/0008-5472.CAN-08-1642
271. Giannopoulou E, Antonacopoulou A, Matsouka P, Kalofonos HP. Autophagy: Novel Action of Panitumumab in Colon Cancer. *Anticancer Res* (2009) 29(12):5077–82.
272. Marino ML, Fais S, Djavaheri-Mergny M, Villa A, Meschini S, Lozupone F, et al. Proton Pump Inhibition Induces Autophagy as a Survival Mechanism Following Oxidative Stress in Human Melanoma Cells. *Cell Death Dis* (2010) 1(10):e87. doi: 10.1038/cddis.2010.67
273. Dolmans DE, Fukumura D, Jain RK. Photodynamic Therapy for Cancer. *Nat Rev Cancer* (2003) 3(5):380–7. doi: 10.1038/nrc1071
274. Brown SB, Brown EA, Walker I. The Present and Future Role of Photodynamic Therapy in Cancer Treatment. *Lancet Oncol* (2004) 5 (8):497–508. doi: 10.1016/S1470-2045(04)01529-3

275. Martins WK, Belotto R, Silva MN, Grasso D, Suriani MD, Lavor TS, et al. Autophagy Regulation and Photodynamic Therapy: Insights to Improve Outcomes of Cancer Treatment. *Front Oncol* (2021) 10:610472. doi: 10.3389/fonc.2020.610472
276. Dewaele M, Martinet W, Rubio N, Verfaillie T, de Witte PA, Piette J, et al. Autophagy Pathways Activated in Response to PDT Contribute to Cell Resistance Against ROS Damage. *J Cell Mol Med* (2011) 15(6):1402–14. doi: 10.1111/j.1582-4934.2010.01118.x
277. Xiong L, Liu Z, Ouyang G, Lin L, Huang H, Kang H, et al. Autophagy Inhibition Enhances Photocytotoxicity of Photosan-II in Human Colorectal Cancer Cells. *Oncotarget* (2017) 8(4):6419–32. doi: 10.18632/oncotarget.14117
278. Saleem MZ, Alshwmi M, Zhang H, Din S, Nisar MA, Khan M, et al. Inhibition of JNK-Mediated Autophagy Promotes Proscillaridin A-Induced Apoptosis *via* ROS Generation, Intracellular Ca^{+2} Oscillation and Inhibiting STAT3 Signaling in Breast Cancer Cells. *Front Pharmacol* (2020) 11:1055. doi: 10.3389/fphar.2020.01055
279. Gdynia G, Keith M, Kopitz J, Bergmann M, Fassl A, Weber AN, et al. Danger Signaling Protein HMGB1 Induces a Distinct Form of Cell Death Accompanied by Formation of Giant Mitochondria. *Cancer Res* (2010) 70 (21):8558–68. doi: 10.1158/0008-5472.CAN-10-0204
280. Sun X, Tang D. HMGB1-Dependent and -Independent Autophagy. *Autophagy* (2014) 10(10):1873–6. doi: 10.4161/auto.32184
281. Tang D, Kang R, Cheh CW, Livesey KM, Liang X, Schapiro NE, et al. HMGB1 Release and Redox Regulates Autophagy and Apoptosis in Cancer Cells. *Oncogene* (2010) 29(38):5299–310. doi: 10.1038/onc.2010.261
282. Tan C, Lai S, Wu S, Hu S, Zhou L, Chen Y, et al. Nuclear Permeable Ruthenium(II) β-Carboline Complexes Induce Autophagy to Antagonize Mitochondrial-Mediated Apoptosis. *J Med Chem* (2010) 53(21):7613–24. doi: 10.1021/jm1009296
283. Jazirehi AR. Regulation of Apoptosis-Associated Genes by Histone Deacetylase Inhibitors: Implications in Cancer Therapy. *Anticancer Drugs* (2010) 21(9):805–13. doi: 10.1097/CAD.0b013e32833dad91
284. Li J, Liu R, Lei Y, Wang K, Lau QC, Xie N, et al. Proteomic Analysis Revealed Association of Aberrant ROS Signaling With Suberoylanilide Hydroxamic Acid-Induced Autophagy in Jurkat T-Leukemia Cells. *Autophagy* (2010) 6 (6):711–24. doi: 10.4161/auto.6.6.12397
285. Naumann P, Fortunato F, Zentgraf H, Büchler MW, Herr I, Werner J. Autophagy and Cell Death Signaling Following Dietary Sulforaphane Act Independently of Each Other and Require Oxidative Stress in Pancreatic Cancer. *Int J Oncol* (2011) 39(1):101–9. doi: 10.3892/ijo.2011.1025
286. Xiao D, Powolny AA, Antosiewicz J, Hahm ER, Bommareddy A, Zeng Y, et al. Cellular Responses to Cancer Chemopreventive Agent D, L-Sulforaphane in Human Prostate Cancer Cells Are Initiated by Mitochondrial Reactive Oxygen Species. *Pharm Res* (2009) 26(7):1729–38. doi: 10.1007/s11095-009-9883-5
287. Rai P, Young JJ, Burton DG, Giribaldi MG, Onder TT, Weinberg RA. Enhanced Elimination of Oxidized Guanine Nucleotides Inhibits Oncogenic RAS-Induced DNA Damage and Premature Senescence. *Oncogene* (2011) 30 (12):1489–96. doi: 10.1038/onc.2010.520
288. Bauvy C, Gane P, Arico S, Codogno P, Ogier-Denis E. Autophagy Delays Sulindac Sulfide-Induced Apoptosis in the Human Intestinal Colon Cancer Cell Line HT-29. *Exp Cell Res* (2001) 268(2):139–49. doi: 10.1006/excr.2001.5285
289. de Medina P, Silvente-Poirot S, Poirot M. Tamoxifen and AEBS Ligands Induced Apoptosis and Autophagy in Breast Cancer Cells Through the Stimulation of Sterol Accumulation. *Autophagy* (2009) 5(7):1066–7. doi: 10.4161/auto.5.7.9820
290. Lin CJ, Lee CC, Shih YL, Lin TY, Wang SH, Lin YF, et al. Resveratrol Enhances the Therapeutic Effect of Temozolomide Against Malignant Glioma *In Vitro* and *In Vivo* by Inhibiting Autophagy. *Free Radical Biol Med* (2012) 52(2):377–91. doi: 10.1016/j.freeradbiomed.2011.10.487
291. Lowndes SA, Adams A, Timms A, Fisher N, Smythe J, Watt SM, et al. Phase I Study of Copper-Binding Agent ATN-224 in Patients With Advanced Solid Tumors. *Clin Cancer Res* (2008) 14(22):7526–34. doi: 10.1158/1078-0432.CCR-08-0315
292. Juarez JC, Manuia M, Burnett ME, Betancourt O, Boivin B, Shaw DE, et al. Superoxide Dismutase 1 (SOD1) Is Essential for H_2O_2-Mediated Oxidation and Inactivation of Phosphatases in Growth Factor Signaling. *Proc Natl Acad Sci USA* (2008) 105(20):7147–52. doi: 10.1073/pnas.0709451105
293. Yu Z, Zhou R, Zhao Y, Pan Y, Liang H, Zhang JS, et al. Blockage of SLC31A1-Dependent Copper Absorption Increases Pancreatic Cancer Cell Autophagy to Resist Cell Death. *Cell Prolif* (2019) 52(2):e12568. doi: 10.1111/cpr.12568
294. Fu J, Shao CJ, Chen FR, Ng HK, Chen ZP. Autophagy Induced by Valproic Acid Is Associated With Oxidative Stress in Glioma Cell Lines. *Neuro Oncol* (2010) 12(4):328–40. doi: 10.1093/neuonc/nop005
295. Perri M, Pingitore A, Cione E, Vilardi E, Perrone V, Genchi G. Proliferative and Anti-Proliferative Effects of Retinoic Acid at Doses Similar to Endogenous Levels in Leydig MLTC-1/R2C/TM-3 Cells. *Biochim Biophys Acta* (2010) 1800(9):993–1001. doi: 10.1016/j.bbagen.2010.06.006
296. Huang P, Feng L, Oldham EA, Keating MJ, Plunkett W. Superoxide Dismutase as a Target for the Selective Killing of Cancer Cells. *Nature* (2000) 407(6802):390–5. doi: 10.1038/35030140
297. Reumann S, Shogren KL, Yaszemski MJ, Maran A. Inhibition of Autophagy Increases 2-Methoxyestradiol-Induced Cytotoxicity in SW1353 Chondrosarcoma Cells. *J Cell Biochem* (2016) 117(3):751–9. doi: 10.1002/jcb.25360
298. Miller CM, O'Sullivan EC, McCarthy FO. Novel 11-Substituted Ellipticines as Potent Anticancer Agents With Divergent Activity Against Cancer Cells. *Pharmaceuticals (Basel Switzerland)* (2019) 12(2):90. doi: 10.3390/ph12020090

Conflict of Interest: The authors declare that the research was conducted in the absence of any commercial or financial relationships that could be construed as a potential conflict of interest.

Publisher's Note: All claims expressed in this article are solely those of the authors and do not necessarily represent those of their affiliated organizations, or those of the publisher, the editors and the reviewers. Any product that may be evaluated in this article, or claim that may be made by its manufacturer, is not guaranteed or endorsed by the publisher.

frontiers in Oncology

ORIGINAL RESEARCH
published: 21 March 2022
doi: 10.3389/fonc.2022.788496

Elaiophylin Inhibits Tumorigenesis of Human Uveal Melanoma by Suppressing Mitophagy and Inducing Oxidative Stress *via* Modulating SIRT1/FoxO3a Signaling

Xue Zhu[1,2†], Wenjun Zou[3†], Xinmin Meng[4,5], Jiali Ji[4], Xun Wang[4], Hong Shu[5], Yuan Chen[1,2], Donghui Pan[1,2], Ke Wang[1,2*] and Fanfan Zhou[6]*

[1] National Health Commission (NHC) Key Laboratory of Nuclear Medicine, Jiangsu Key Laboratory of Molecular Nuclear Medicine, Jiangsu Institute of Nuclear Medicine, Wuxi, China, [2] Department of Radiopharmaceuticals, School of Pharmacy, Nanjing Medical University, Nanjing, China, [3] Department of Ophthalmology, The Affiliated Wuxi No.2 People's Hospital of Nanjing Medical University, Wuxi, China, [4] Department of Respiratory and Critical Care Medicine, The Affiliated Wuxi No.2 People's Hospital of Nanjing Medical University, Wuxi, China, [5] Department of Laboratory Medicine, Cancer Medical College of Guangxi Medical University, Affiliated Tumor Hospital of Guangxi Medical University, Nanning, China, [6] Sydney Pharmacy School, The University of Sydney, Sydney, NSW, Australia

OPEN ACCESS

Edited by:
Junmin Zhang,
Lanzhou University, China

Reviewed by:
Agnieszka Zdzisława Robaszkiewicz,
University of Łódź, Poland
Boel De Paepe,
Ghent University, Belgium

***Correspondence:**
Wenjun Zou
wendyzwj0805@njmu.edu.cn
Ke Wang
wangke@jsinm.org

[†]These authors have contributed equally to this work

Specialty section:
This article was submitted to Pharmacology of Anti-Cancer Drugs, a section of the journal Frontiers in Oncology

Received: *02 October 2021*
Accepted: *28 February 2022*
Published: *21 March 2022*

Citation:
Zhu X, Zou W, Meng X, Ji J, Wang X, Shu H, Chen Y, Pan D, Wang K and Zhou F (2022) Elaiophylin Inhibits Tumorigenesis of Human Uveal Melanoma by Suppressing Mitophagy and Inducing Oxidative Stress via Modulating SIRT1/FoxO3a Signaling. Front. Oncol. 12:788496. doi: 10.3389/fonc.2022.788496

Uveal melanoma (UM) is the most common primary intraocular tumor in adults, which is associated with poor prognosis. Up to 50% of UM patients develop metastasis. Therapeutics that have proven effective in cutaneous melanoma have little success in treating UM, possibly due to its low mutational burden. Therefore, new drug therapies are highly desired for UM. Our *in vitro* studies showed that Elaiophylin, a late-stage autophagy inhibitor, exhibited an outstanding anticancer activity in human UM cell lines and human UM primary cells through suppressing mitophagy, inducing oxidative stress and leading to autophagic cell death. Our mechanistic study revealed that Elaiophylin exerted its effect by down-regulating SIRT1 and thus influencing deacetylation and mitochondrial localization of FoxO3a. In our confirmatory experiments, SRT1720, a SIRT1 specific activator, could attenuate Elaiophylin-induced inhibition of mitophagy and elevation of oxidative stress, and such effects was partly reversed by FoxO3a knockdown. Our further *in vivo* studies showed that Elaiophylin dramatically inhibited tumor growth in the human UM xenograft mouse model, which was accompanied with a decreased SIRT1 expression. Thus, the current study is the first to demonstrate that Elaiophylin has a potent anti-cancer effect against UM, which activity is possibly mediated through regulating SIRT1-FoxO3a signaling axis. And Elaiophylin may be a new and promising drug candidate to treat human UM.

Keywords: uveal melanoma, elaiophylin, mitophagy, oxidative stress, SIRT1/FoxO3a signaling

INTRODUCTION

Although rare, uveal melanoma (UM) is the most common primary ocular cancer in the Caucasian population (1). Both uveal and cutaneous melanomas originate from melanocytes; however, they are significantly different regarding their pathogenesis and clinical behaviors (2). About 85% of ocular melanomas occur in the uveal tract, the vascular layer of the eye (comprising the choroid, ciliary body, and iris) (3). Approximately 50% of patients with primary UM ultimately develop distant metastasis and the median survival was reported to be less than 6 months. The liver metastasis counts up to 90% of cases (2). Overall, UM is a rare but deadly cancer. At present, the most widely used first-line treatment for this malignancy includes resection, radiation therapy and enucleation (4). Although local recurrence is extremely rare, however, it's association with significantly higher risk of systemic metastasis highlights an urgent need of novel systematic therapies to better manage human UM.

Autophagy is an essential homeostatic and catabolic process. It sequesters misfolded proteins, damaged or aged organelles, as well as mutated proteins in double membrane vesicles called autophagosomes that ultimately fuse to lysosomes leading to the degradation of the sequestered components (5). The recycling capacity of autophagy plays a crucial role in both physiological and pathophysiological contexts and its dysregulation is associated with tumorigenesis and tumor-stroma interactions (6). Autophagy is commonly upregulated in UM and there is a strong association between extensive BECN1 overexpression and early metastases/poor prognosis (7). Autophagy inhibition may sensitize GNAQ/11-mutated UM to the MEK1/2 inhibitor, trametinib (8). Mitophagy, a specific form of autophagy, is a particular adaptation of cancer cell metabolism to recycle intracellular components in condition of metabolic stress. Its dysregulation is associated with tumorigenesis and tumor-stroma interactions (6, 9). Mitochondria are known to be the major source of intracellular reactive oxygen species (ROS) (10). The release of ROS upon mitochondrial injury induces mitophagy in order to reduce oxidative damage by eliminating impaired mitochondria and preventing ROS accumulation (11). It plays a pivotal role in reinstating cellular homeostasis in both normal and stress conditions. Increasing evidence has indicated that elevated ROS generation upon inhibiting mitophagy flux can induce lysosomal dysfunction and autophagy suppression, and finally lead to cancer cell death (12–14). Therefore, mitophagy inhibition and oxidative stress induction have been considered as new therapeutic targets in cancer treatment (15).

Elaiophylin, a C2 symmetry 16-member macrodiolide antibiotic isolated from *Streptomyces melanosporus*, is a novel late-stage autophagy inhibitor (16). Elaiophylin and its derivatives exhibit various activities including antimicrobial, anthelmintic, immunosuppressive, anti-inflammatory, antiviral and α-glucosidase inhibitory effects. Previous studies indicated that Elaiophylin exerted moderate cytotoxicity against various cancer cells such as human gastric cancer (SNU-1), hepatocellular carcinoma (SNU-354), vinblastine sensitive epidermoid carcinoma (KB-3-1) and resistant cervical cancer (KB-V1) cell lines (17). In the study of Zhao et al., Elaiophylin showed a potent antitumor efficacy as a single agent or in combination with cisplatin or under hypoxic condition in human ovarian cancer cells. Such effect of Elaiophylin was mediated through suppressing the downstream autophagosome formation (eg. inhibiting autophagosome and lysosome fusion and/or blocking the degradation of autophagic cargo inside autolysosomes) (18). Elaiophylin also exerts antitumor activity against multiple myeloma with mutant TP53 by blocking autophagy flux and subsequently inducing the persistent activation of endoplasmic reticulum stress (19). Recent studies have shown that Elaiophylin is a potent Hsp90/Cdc37 protein interface inhibitor. It interferes the interaction of Cdc37 and the N-terminus of Hsp90, and depletes Gal3, thus selectively decreases K-Ras nanoclustering (20). Hsp90/Cdc37 chaperone complex regulates mitophagy by stabilizing and activating Ulk1, which is required for the phosphorylation and release of Atg13 from Ulk1, and for the recruitment of Atg13 to damaged mitochondria (21). However, the role of Elaiophylin in UM remains unclear. SIRT1 is a member of the sirtuin family of the class III NAD^+-dependent HDACs, which consists of seven enzymes (SIRT1 to SIRT7) that share conserved core catalytic domains but differ in their cellular localization and tissue distribution (22). Forkhead box protein O3a (FoxO3a) is one of the main effectors of cellular stress-activated signal transduction pathways. Its activity is controlled by various post-translational modifications (PTMs), which determine its subcellular localization (23). SIRT1 is known to deacetylate FoxO3a and in turn, promotes mitophagy. In the present study, we are the first to report the anti-cancer effect of Elaiophylin in *in vitro*, *ex vivo* and *in vivo* UM models, which is mediated through mitophagy inhibition, and the modulation of SIRT1-FoxO3a signaling axis.

METHODS

Reagents

Elaiophylin was kindly provided by Prof. Xie (Institute of Medicinal Biotechnology, Chinese Academy of Medical Sciences & Peking Union Medical College, Beijing, China.) (Purity>99%), prepared as a stock solution (50 mM) in dimethyl sulfoxide (DMSO) and stored at -20°C.

Cell Culture and Treatment

The human UM C918 and OCM1A cell lines were obtained from Beijing Beina Chuanglian Biotechnology Research Institute (BeNa Culture Collection, Beijing, China). Uveal melanoma cell line C918, derived from primary uveal melanoma and characterized by Folberg et al. (24). The human UM Mel270 cell line was purchased from BioVector NTCC Inc. (Beijing, China). The human retinal pigment epithelial cell line ARPE-19 was obtained from the National Collection of Authenticated Cell Cultures (Shanghai, China). All cells were cultured in RPMI 1640 medium with 10% (v/v) fetal bovine serum (Thermo Fisher Scientific, Waltham, MA, USA) in a humidified atmosphere of 5% CO_2 at 37°C. Five primary UM cell lines were isolated from

UM patient tumor samples and cultured with the approval from the human research ethics committee of St. Vincent's Hospital (HREC/17/SVH/346). The primary UM cell lines were maintained in RPMI medium containing 20% FBS (v/v), 1% L-glutamine, 1% P/S, 1% ITS and 2% GCT (Thermo Scientific, Lidcombe, NSW, Australia) in a humidified atmosphere of 5% CO_2 at 37°C.

Cell Proliferation Assay

Cell viability was assessed by MTT assay. Briefly, cells were plated in 96-well plates at a density of 1×10^4 cells per well. After 24 h treatment with indicated drugs, cells were incubated with 5 mg/mL MTT solution for 4 h at 37°C. The absorbance was measured at 570 nm using a SpectraMax M5 microplate reader (Molecular Devices, San Jose, CA, USA). Each experiment was performed in sextuples and repeated on three occasions. SPSS 19 was used to estimate IC_{50} values.

Cell Apoptosis Assay

Cell apoptosis was measured with AnnexinV-FITC/PI double staining. Cells were seeded in 6-well plates at a density of 1×10^6 cells per well. After 24 h pre-treatment with Elaiophylin (0, 0.25, 0.5 and 0.75 μM), cells were washed twice with D-PBS, and then incubated in 300 μL binding buffer (containing10 μL AnnexinV-FITC and 10 μL PI) for 15 min in the dark at room temperature. The fluorescence was analyzed by flow cytometry (Becton-Dickinson, CA, USA).

Intracellular ROS Generation Detection

The level of intracellular ROS was determined by DCFH-DA staining. Cells were pretreated with indicated drugs for 2 h. Cells were then harvested and incubated with DCFH-DA (10 μM) for 30 min in the dark at 37°C. After staining, cells were washed twice with D-PBS. The intracellular ROS fluorescence intensity was quantified by flow cytometry and the images were taken by a fluorescence microscope (Olympus IX53; Olympus Corporation, Tokyo, Japan).

Measurement of Mitochondrial Membrane Potential

Mitochondrial membrane potential (MMP) was measured using the lipophilic cation JC-1, which exhibits a potential-dependent amassing in mitochondria. When the mitochondrial membrane potential is high, JC-1 accumulates in the matrix of mitochondria to form polymers (J-aggregates), which can produce red fluorescence; when the mitochondrial membrane potential is low, JC-1 cannot aggregate in the matrix of mitochondria and presents as a monomer that can produce green fluorescence. Therefore, it is very convenient to detect the change of mitochondrial membrane potential through the change of fluorescence colors. The relative ratio of red to green fluorescence is often used to measure the proportion of mitochondrial depolarization. Briefly, cells (1×10^6 cells/mL) were seeded into 6-well plates and treated with indicated drugs for 6 h. After treatment, cells were stained with JC-1 at 37°C for 30 min. The alternation of MMP level was determined by flow cytometry.

Cell Mitochondria Isolation

The cytosol and mitochondrial fractions were isolated using Cell Mitochondria Isolation Kit (C3601, Beyotime, Shanghai, China). Cells were washed with PBS, digested with trypsin EDTA solution and collected with centrifugation (100-200g) at room temperature for 5-10 min. Then mitochondrial separation reagent was added to cells with PMSF, gently suspended the cells and place them in ice bath for 10-15 min. The cell suspension was transferred to a glass homogenizer of appropriate size and homogenize for about 10-30 times. The cell homogenates were centrifuged (600g) at 4°C for 10 min. The isolated cytoplasmic protein was precipitated with centrifugation. The supernatant was carefully transferred to another set of tubes and centrifuged (11,000g) again at 4°C for 10 min. The isolated cell mitochondria were captured in the precipitates.

Western Blot Analysis

Cells were seeded into 6-well plates at 5×10^6 cells per well. After treatment, cells were harvested and lysed in ice-cold RIPA buffer (Beyotime) for 30 min. Then the protein concentration was measured using BCA protein assay kit (Beyotime). A total of 50 μg protein of each sample was loaded on 15% sodium-dodecyl sulfatepoly-acrylamide gel electrophoresis and blotted onto PVDF membranes (Beyotime). The membranes were blocked with 5% non-fat milk for 1 h at room temperature and then incubated with the primary antibodies overnight at 4°C and HRP-conjugated secondary antibody for 2 h at room temperature. The protein bands were visualized using the ECL assay kit (Cat. No: P0018AM; Beyotime). The density of each band was normalized to the expression of GADPH (Cat. No: ab8245, Abcam, Cambridge, USA), VDAC1 (Cat. No: ab15895, Abcam) or Lamin A (Cat. No: ab108595, Abcam). The other primary antibodies used include Cytochrome c (Cat. No: ab13575, Abcam), SIRT1 (Cat. No: ab110304, Abcam), LC3II (Cat. No: ab192890, Abcam), PINK1 (Cat. No: ab23707, Abcam), Parkin (Cat. No: ab77924, Abcam), PGC-1α (Cat. No: ab106814, Abcam), FoxO3a (Cat. No: ab70315, Abcam), and Acetyl-K (Cat. No: ab4729, Abcam).

Co-Immunoprecipitation Assay

Cell lysate was prepared in the immunoprecipitation buffer [1% NP-40, 150 mM NaCl, 50 mM pH7.4 Tris-HCl, 10 mM NaF, 1 mM Na_3VO_4, 10 mM N-ethylamide (NEM) and protease inhibitors (Complete protease inhibitor cocktail; Roche, Lewes, UK)]. For co-immunoprecipitation, 500 μg of total protein was diluted to a 500 μl total volume in lysis buffer and incubated with 10 μl of anti-Acetyl-K antibody overnight at 4°C with rocking. Immuno-complexes were captured with 30 μl of DynaBeads Protein G (Thermo Fisher Scientific, Madison, USA) for 3 h with rocking at 4°C. Protein G bead complexes were washed three times with ice-cold lysis buffer, and boiled with 1× Laemmli buffer and subjected to western blot analysis. The immunoblot was probed with anti-FoxO3a antibody (1:1,000 dilution).

Mito-Keima Mitophagy Analysis

Keima gene stably expresses a natural protein that emits red and green fluorescence under acidic and central conditions

respectively, which can be used for qualitative and quantitative analysis of autophagy and autophagy lysosome. The leading peptide sequence of Cox V III and *Keima* curtain form a fusion gene *mito-Keima*, and the expressed Keima protein is located in the mitochondrial matrix. When the mitochondrial autophagosome is fused with the lysosome, the fluorescence signal of Keima protein changes from green to red, which can reflect the activity of mitochondrial autophagy. Cells were transfected with the mKeima-Red-Mito-7 plasmid using Lipofectamine 3000 for 24 h and then treated with different concentrations of Elaiophylin for another 24 h. The cells were imaged using a fluorescence microscope.

Immunofluorescent Assay

Cells growing on glass coverslips were treated accordingly, fixed with 4% PFA and blocked with 5% BSA containing 0.4% Triton X-100. Subsequently, the cells were incubated with MitoTracker Green and the primary antibodies against LAMP1 or FoxO3a at 4°C overnight and then the fluorescent secondary antibody for 1 h at room temperature. After stained with DAPI for 5 min, the cellular fluorescence was observed with a fluorescence microscope (Olympus IX53).

Small Interfering RNA (SiRNA) Silencing

Cells were transfected with scrambled siRNA duplexes or specific siRNA duplexes targeting FoxO3a (GenePharm, Shanghai, China) using Lipofectamine 3000 according to the manufacturer's protocol. After transfection, the cells were treated with indicated drugs and the protein expression was analysed by western blotting. The scrambled siRNA duplexes were adopted as negative controls with nontargeting sequences. The sequences of siRNAs were as following: FoxO3a siRNA (5′-AAUGUGACA-UGGAGUCCAUUA-3′); the scrambled siRNA (5′-UUCUCCGAACGUGUCA-CGUTT3′).

Nude Mice Tumorigenesis Assay

All animals were kept in a pathogen-free environment and fed ad lib. The procedures for care and use of animals were approved by the Laboratory Animal Ethics Committee of Jiangsu Institute of Nuclear Medicine (JSINM-2020-096) and all applicable institutional and governmental regulations concerning the ethical use of animals were followed. C918 cells (3×10^7) mixed with Matrigel at a 2:1 volume ratio was injected subcutaneously into 5-week-old BALB/c nude mice (ChangZhou Cavens Laboratory Animal Co., Ltd, Changzhou, China). When the tumor volumes reached approximately 100 mm^3, the mice were divided randomly into two groups (n=5 per group): vehicle and Elaiophylin (2 mg/kg). The mice were then administered with vehicle or Elaiophylin by intraperitoneal injection once per day for 14 days. Body weight and tumor volumes were measured every other day. Tumor volumes were calculated as $(a \times b^2)/2$, where a and b were the longest and shortest diameters of the tumors, respectively. At the end of the treatment, the mice were anesthetized by intraperitoneal injection of 5 ml/kg 1% pentobarbital sodium salt. The tumors were removed, weighed, and photographed. The tumor samples were then fixed in 4% paraformaldehyde for pathological examinations.

Preparation of [^{68}Ga]Ga-NOTA-PRGD2

The fresh ^{68}Ga activity was eluted from the ^{68}Ge/^{68}Ga generator (Isotopen Technologien München, Munich, Germany) with 0.05 M HCl at 1.5 mL per fraction into the 1.5 mL polypropylene tubes. The fraction containing the most radioactivity (~5.26 MBq) was added to 93 μL of 1M sodium acetate buffer and 50 μg of NOTA-PRGD2. The mixture was heated at 97°C for 10 min. At the end of the reaction, the activity was loaded onto a C18 column (Agilent, USA) using 10 mL deionized water and then eluted by 0.3 mL 10 mM HCl-containing ethanol.

MicroPET Imaging and Analysis

PET scans were performed using an Inveon microPET scanner (Siemens Medical Solutions, Germany). About 3.7 MBq of 68Ga labeled tracer was administered *via* tail vein injection under isoflurane anesthesia. The dynamic image acquisitions were continued from the beginning to 60 min after the administration. For each scan, regions of interest (ROIs) were drawn using vendor software (ASI Pro 5.2.4.0) on decay-corrected whole-body coronal images. The radioactivity concentrations (accumulation) were obtained from mean pixel values within the multiple ROI volume and then converted to MBq per milliliter. These values were then divided by the administered activity to obtain (assuming a tissue density of 1 g/ml) an image-ROI-derived percent injected dose per gram (% ID/g).

Histology and Immunohistochemistry

Tumor tissues from the vehicle and Elaiophylin groups were embedded in paraffin and cut into 8 μm-thick sections. Then, the sections were stained with H&E. For immunohistochemical staining, the sections were incubated with anti-ki67 and anti-SIRT1 antibodies overnight at 4°C and then with HRP-conjugated secondary antibodies. The sections were visualized using a DAB kit, and the images were observed using a light microscope (Olympus IX53).

Statistical Analysis

All data were presented as the mean ± SD for a minimum of three independent experiments in triplicates. All comparisons were made using Student's t–test or one-way ANOVA followed by Tukey's *post hoc* test. SPSS 19.0 software package was used to analyze the data. A value of $P<0.05$ was considered as statistically significant.

RESULTS

Elaiophylin Inhibits Cell Proliferation and Induces Autophagic Cell Death in C918 Cells

To determine the cytotoxic effect of Elaiophylin (**Figure 1A**) in UM cells, three immortalised UM cell lines (C918 for wildtype,

OCM1A for $BRAF^{V600E}$ mutant, Mel270 for $GNAQ^{Q209L/P}$ mutant) and five primary UM cell lines obtained from UM patient tumors were treated with different concentration of Elaiophylin for 24 h and cell viability was estimated using MTT assay. As shown in **Figures 1B, C**, Elaiophylin exhibited a dose-dependent cytotoxicity in all UM cell lines. In comparison to the human retinal pigment epithelial cell line ARPE-19 (**Figure 1D**), it inhibited C918 cell viability in a dose-dependent manner (IC_{50}: 0.69 μM), with an over 80% cell death observed at 2 μM. However, ARPE-19 cells were more resistant to Elaiophylin treatment (IC_{50}: 32.70 μM). Elaiophylin-incubated C918 cells were stained with Annexin V-FITC/PI and evaluated by FACS. As shown in **Figure 1E**, Elaiophylin significantly induced cell death in a concentration-dependent manner, ranged from 5.02 ± 2.43% (0 μM) to 42.04 ± 3.89% (0.75 μM). It is consistent with the report that this compound is known to be a late-stage autophagy inhibitor (18).

Elaiophylin Induces Oxidative Stress and Mitochondrial Dysfunction in C918 Cells

Oxidative stress-mediated mitochondrial dysfunction is the inductive factor of autophagic cell death. To assess the effect of Elaiophylin on mitochondrial function, the intracellular ROS generation and MMP were evaluated. The intracellular ROS level was evaluated with DCFH-DA fluorescent probe. As shown in **Figure 2A**-ROS level (green), the results indicated that intracellular ROS level was significantly increased in a concentration-dependent manner in C918 cells upon exposure to different concentrations of Elaiophylin. As shown in **Figures 2B, C**, the MMP was significantly reduced upon the treatment of Elaiophylin, in accompany with the releasement on cytochrome *c* from the mitochondria into the cytoplasm. Pre-treatment with 10 μM NAC (N-acetylcysteine, widely used as an antioxidant) for 6 h dramatically attenuated the Elaiophylin-induced mitochondrial dysfunction in C918 cells (**Figure 2D**-ROS level (green), and **Figure 2F**). Taken together, our findings suggested that Elaiophylin-induced autophagic cell death was associated with ROS-mediated mitochondrial dysfunction in C918 cells.

Elaiophylin Inhibits Mitophagy by Down-Regulating SIRT1 in C918 Cells

Mitophagy is an important cell protective mechanism against oxidative stress by cleaning up defective mitochondria. To explore the role of Elaiophylin in mitophagy, C918 cells were transfected with mito-Keima plasmid, a pH-sensitive fluorescent protein located in mitochondria. As shown in **Figure 3A**-Mito-Keima (red), red fluorescence was observed in untreated C918 cytoplasm, indicating the occurrence of mitophagy at physiological level. FCCP, an activator of mitophagy as well as mitochondrial oxidative phosphorylation uncoupling agent, was used as the positive control. Importantly, Elaiophylin significantly suppressed mitophagy in a concentration-dependent manner. In addition, the colocalization of mitochondria with LAMP1 (a lysosome marker shown as red fluorescence), demonstrated mitophagy inhibition by Elaiophylin (**Figure 3B**-Mito Tracker (green), LAMP1 (red), DAPI (blue) and 3C). Furthermore, compared to the control, mitochondrial autophagosome marker light chain 3 (LC3)-II (mito-LC3II) expression was downregulated in response to

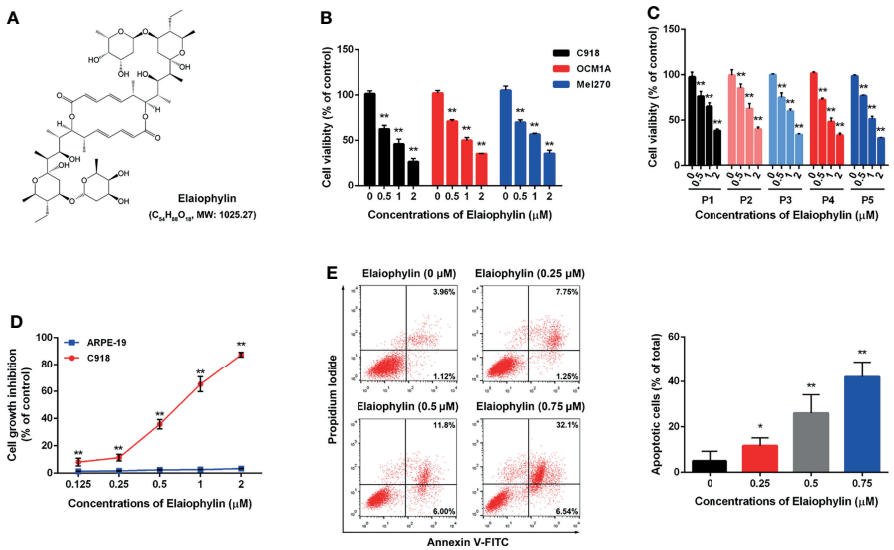

FIGURE 1 | Elaiophylin inhibits cell proliferation and induces autophagic cell death in C918 cells. **(A)** The chemical structure of Elaiophylin; **(B)** C918, OCM1A and Mel270 cells were treated with different concentrations of Elaiophylin (0, 0.5, 1 and 2 μM) for 24 h. Cell viability was determined by MTT assay. **(C)** Five primary UM cells were treated with different concentrations of Elaiophylin (0, 0.5, 1 and 2 μM) for 24 h. Cell viability was determined by MTT assay. **(D)** C918 and ARPE-19 cells were treated with different concentrations of Elaiophylin (ranged from 0 to 2 μM) for 24 h. Cell viability was determined by MTT assay. **(E)** C918 cells were treated with indicated concentrations of Elaiophylin for 24h, and then apoptotic cells stained with Annexin V-FITC/PI were detected with flow cytometry. Apoptotic rates are shown in bars. Data was expressed as mean ± SD of three experiments and each experiment included triplicate repeats. *p<0.05, **p<0.01 *vs.* control.

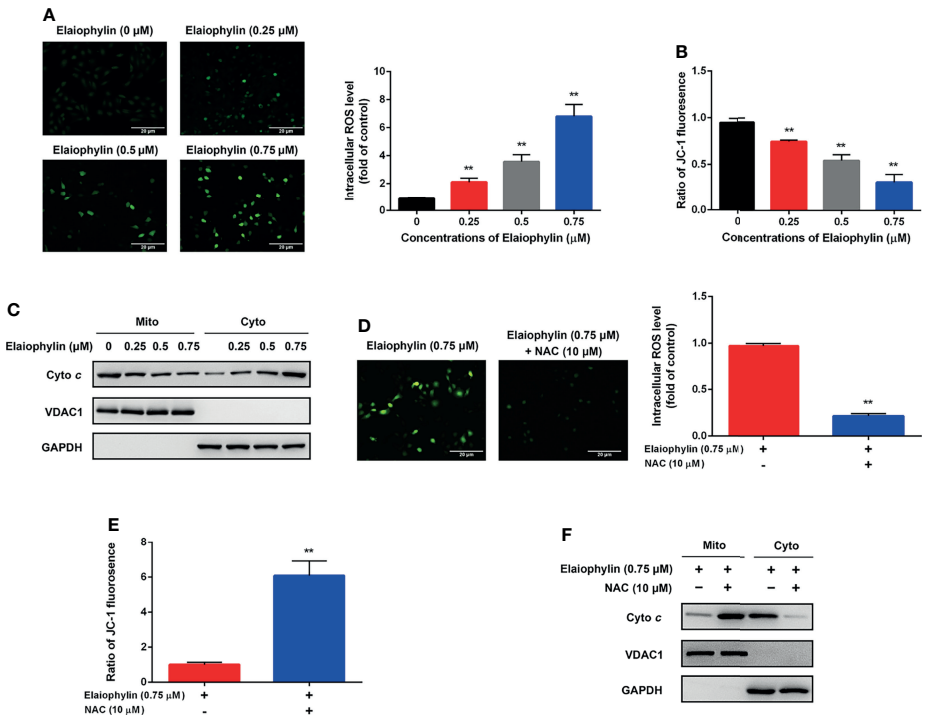

FIGURE 2 | Elaiophylin induces oxidative stress and mitochondrial dysfunction in C918 cells. C918 cells were exposed to indicated concentrations of Elaiophylin, with or without NAC (10 μM) pre-treatment. **(A, D)** The representative images of ROS measurement (green fluorescence) in C918 cells after 2 h exposure to Elaiophylin. Intracellular ROS levels were detected by DCFH-DA fluorescent probe. The representative images of fluorescent probe were shown on the left and the quantitative analysis of ROS level was shown on the right. **(B, E)** The MMP of C918 cells exposed to indicated concentrations of Elaiophylin, with or without NAC. **(C, F)** Lysates of C918 cells exposed to indicated concentrations of Elaiophylin, with or without NAC were separated into cytoplasmic and mitochondrial fractions. Cytochrome *c* translocation was measured by western blotting. GAPDH and VDAC1 were used as loading controls for cytoplasm and mitochondria, respectively. Data was expressed as mean ± SD of three experiments. $^{**}p<0.01$ *vs.* control.

Elaiophylin treatment, as well as that of PINK1 and Parkin, two key factors that regulate mitophagy (**Figure 3D**).

SIRT1 (silent information regulator of transcription 1) is a key regulator of autophagy/mitophagy and mitochondrial function. We found that the expression of SIRT1 and its downstream target PGC-1α (proliferator-activated receptor-γ coactivator α) were both reduced in Elaiophylin-treated C918 cells (**Figure 3C**). SIRT1 activator SRT1720 reduced intracellular ROS generation and restored MMP in Elaiophylin-treated C918 cells [(**Figures 4A–C**)-ROS level (green)]. And the inhibitory effect of Elaiophylin on the fusion of mitochondria and lysosomes was significantly attenuated by SRT1720 [(**Figure 4D**)-Mito Tracker (green), LAMP1 (red), DAPI (blue)]. Moreover, SRT1720 treatment increased the expression of related proteins that downregulated by Elaiophylin (**Figure 4A**). Together, these data indicated that Elaiophylin inhibited mitophagy activity by down-regulating SIRT1 in C918 cells.

Elaiophylin Regulates SIRT1 by Modulating FoxO3a Deacetylation and Mitochondrial Localization in C918 Cells

Elaiophylin First, whether the acetylation of the SIRT1 substrate FoxO3a, could be modulated by Elaiophylin was assessed. To investigate the level of acetylated FoxO3a, co-immunoprecipitation assay was used with Acetyl-K antibody to pull all acetylated proteins down. As shown in **Figure 5A**, Elaiophylin treatment resulted in a concentration-dependent induction of FoxO3a acetylation, while SRT1720 could potently attenuate such effect (**Figure 5B**). To identify the subcellular localization of FoxO3a, cell lysate was separated to nuclear, mitochondrial, or cytosolic fractions. As shown in **Figure 5C**, FoxO3a showed a more prominent localization in the nuclear fraction upon Elaiophylin treatment than that in the cytosol fraction. Interestingly, the activation of SIRT1 significantly increased the accumulation of FoxO3a in the mitochondrial fraction [(**Figures 5C, D**)-Mito Tracker (green), FoxO3a (red), DAPI (blue)]. Our findings showed that Elaiophylin may facilitate FoxO3a leakage into the nucleus, which was dramatically attenuated by SIRT1 activation.

To confirm the role of FoxO3a in SIRT1-mediated mitophagy, FoxO3a knockdown was exerted by siRNA in C918 cells. As shown in **Figure 5E**, FoxO3a knockdown significantly attenuated the SIRT1 activation-enhanced mitophagy-related protein expression, in particular PGC-1α, PINK1 and Parkin, in Elaiophylin-treated C918 cells. The findings indicated that SITR1-mediated FoxO3a deacetylation and mitochondrial translocation play critical roles in the inhibitory effect of Elaiophylin on mitophagy in C918 cells.

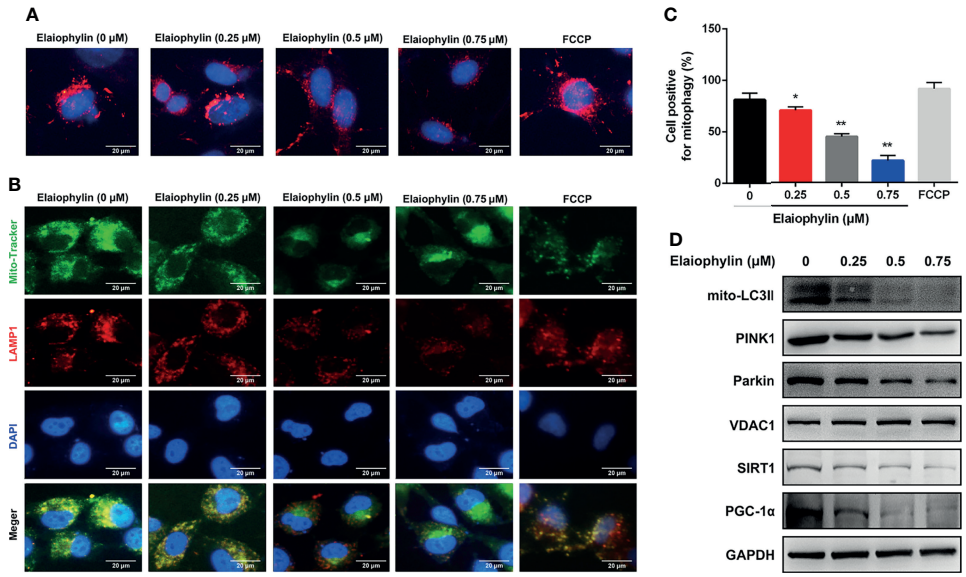

FIGURE 3 | Elaiophylin inhibits mitophagy in C918 cells. **(A)** C918 cells overexpressing Mito-Keima plasmid was treated with Elaiophylin for 24 h. Mito-Keima (red fluorescence) was detected by a fluorescence microscope. FCCP, a mitophagy agonist, was used as positive control. **(B)** Colocalization of mitochondria and lysosomes. Mitochondria were stained with MitoTracker Green (200 nM), and lysosomes were stained with LAMP1 (red fluorescence). The representative images of fluorescent labeling were shown here. **(C)** Quantitative analysis of cellular mitophagy of **(B)** was conducted with Image J software. Five different visual fields of each group were selected for measurement. **(D)** Western blotting was performed to analyze the expression of proteins related to mitophagy. GAPDH and VDAC1 were used as loading controls for cytoplasm and mitochondria, respectively. Data was expressed as mean ± SD of three experiments. *p<0.05, **p<0.01 *vs.* control.

Elaiophylin Suppresses Tumor Growth in a C918-Xenograft Model by Inhibiting SIRT1-Mediated Mitophagy

To determine the *in vivo* anti-UM effect of Elaiophylin, C918 cells were xenografted into immunodeficient nude mice. The xenograft mice received intraperitoneal injections of either vehicle or Elaiophylin (2 mg/kg) every day for 14 days. No significant difference in the mean body weight was observed between the control and Elaiophylin treatment group (**Figure 6A**). Elaiophylin at the current dose was well tolerated in mice with no toxic events encountered throughout the course of treatment, such as agitation, impaired movement and posture, indigestion, or diarrhea. As shown in **Figure 6B**, tumor volume was significantly reduced in Elaiophylin-treated group compared to that of the control. Dynamic PET scanning was also performed after one hour post injection of the radiotracer [^{68}Ga]Ga-NOTA-PRGD$_2$. **Figure 6C**-white arrow showed representative PET images of mice bearing C918 xenograft tumor with or without Elaiophylin treatment. The control group displayed markedly higher uptake of radiotracer in the tumor than the Elaiophylin-treated group. Hematoxylin and eosin (H&E) staining of tumor sections of xenograft mice Elaiophylin demonstrated morphological changes in the treatment group, as indicated by signs of necrosis with infiltration of inflammatory cells and fibrosis (**Figure 6D**). Elaiophylin treatment dramatically increased the numbers of TUNEL-positive cells, which is indicative of apoptosis in the treatment group compared to that of the control group. Additionally, Elaiophylin treatment inhibited the expression of Ki67 (**Figure 6D**). In addition, Elaiophylin treatment significantly decreased the level of SIRT1 in the tumors of xenograft mice. All these findings indicated that Elaiophylin suppressed xenograft UM tumor growth by inhibiting SIRT1-mediated mitophagy.

DISCUSSION

Mitophagy-induced mitochondrial clearance is an important cancer survival mechanism in response to oxidative stress and mitochondrial injury. New agents that can inhibit this process have attracted a lot of attentions in cancer drug development. In this study, we reported for the first time that Elaiophylin, a late-stage autophagy inhibitor, potently inhibits UM cell proliferation by inhibiting mitophagy. Elaiophylin-induced ROS generation and mitochondrial dysfunction cannot be reversed by low-level mitophagy. Additionally, our mechanistic study revealed that SIRT1-medicated FoxO3a deacetylation and mitochondrial translocation play critical roles in the anti-UM effect of Elaiophylin.

Sirtuins are a family of mammalian class III histone deacetylases with a fundamental role in sensing and modulating cellular response to external stress and therefore involved in aging, oxidative stress control, inflammation, differentiation, and cancer development (25). Recent studies indicated that sirtuins' activation contributes to the control of autophagy and mitophagy. During transcriptional and post translational modifications of proteins related to the autophagy and mitophagy machinery, sirtuins

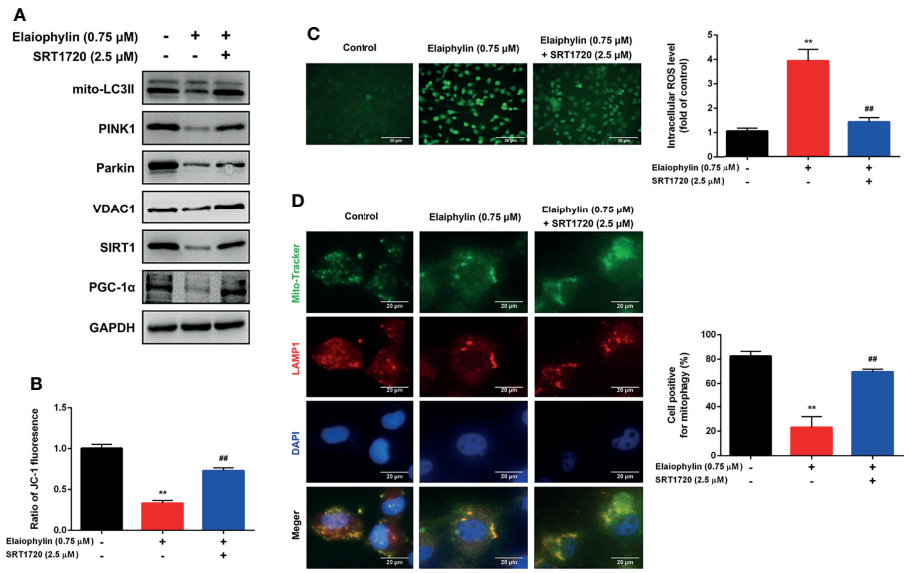

FIGURE 4 | Elaiophylin inhibits mitophagy in C918 cells by regulating SIRT1. After pre-treatment with SRT1720 (a SIRT1 specific activator) for 24 h, C918 cells were incubated with Elaiophylin for another 24 h. **(A)** Western blotting was performed to analyze the proteins related to mitophagy. GAPDH and VDAC1 were used as loading controls for cytoplasm and mitochondria, respectively. **(B)** The membrane potential of C918 cells pre-treatment with or without SRT1720 followed by the incubation with or without Elaiophylin was evaluated by JC-1 fluorescent probe. **(C)** Intracellular ROS level was determined by DCFH-DA fluorescent probe. The representative images of fluorescent probe were shown on the left and the quantitative analysis of ROS level was shown on the right. **(D)** Colocalization of mitochondria and lysosomes. Mitochondria were stained with MitoTracker Green (200 nM), and lysosomes were stained with LAMP1 (red fluorescence). The representative images of fluorescent labeling were shown on the left and the quantitative analysis of cellular mitophagy was shown on the right (Image J was used for quantitative analysis of fluorescence co-localization, and five different visual fields of each group were selected for measurement). Data was expressed as mean ± SD of three experiments. $^{**}p<0.01$ *vs.* control, $^{\#\#}p<0.01$ *vs.* Elaiophylin group.

control ROS production or the major metabolic pathways in cancer cells (26). SIRT1 is the most prominent and extensively studied member of sirtuins. As a primary nuclear protein, SIRT1 greatly influences mitochondrial biogenesis and turnover (26). SIRT1-regulated macro-autophagy has been widely considered as a cellular protective mechanism against stress and death insults (22, 27). Accumulating evidence demonstrated that SIRT1 is involved in oxidative stress and might promote mitophagosome formation through deacetylating key autophagy-related molecules in the form of NAD^+-dependence (28, 29). PINK1 (PTEN induced putative kinase 1) and the E3 ubiquitin ligase Parkin are two critical factors involved in SIRT1-mediated mitophagy in response to oxidative stress (30–32). ROS generation and mitochondrial membrane potential dissipation stabilize PINK1 on the outer mitochondrial membrane (OMM), facilitate the phosphorylation and E3 ligase activity of Parkin, and induce the phosphorylation of ubiquitin molecules at Ser65 on OMM proteins (33, 34). These proteins further recruit autophagy receptors (eg. NBR1, p62, NDP52, OPTN and TAX1BP1) to mitochondria and subsequently engulf into the autophagosomes for degradation (14). In the present study, SIRT1 is down-regulated by Elaiophylin treatment, which in turn, decreases the level of PGC-1α and autophagosome marker light chain 3 (LC3)-II as well as inhibits PINK1/Parkin accumulation in the mitochondria. SIRT1 activator SRT1720 partly attenuates the above effects that influenced by Elaiophylin.

Besides its nuclear localization, the majority of SIRT1's known functions are associated with deacetylation of transcriptional factors, such as FOXO, tumor suppressor p53, and nuclear factor-kappa B (NF-κB) (35, 36). FoxO3a is a member of the forkhead box (FOX) family (class O subfamily), and is a core regulator of cellular homeostasis, stress response and longevity, since it can modulate a variety of stress responses upon nutrient shortage, oxidative stress, hypoxia, heat shock and DNA damage (37, 38). The precise regulation of FoxO3a is likely enacted by an intricate combination of post-translational modifications (PTMs), such as phosphorylation, acetylation, methylation, and ubiquitination, which determine its subcellular localization (23, 39). In particular, FoxO3a PTMs drive FOXO3a towards the nuclear and/or mitochondrial compartment in response to stress stimuli. FoxO3a regulates a set of specific genes involved in the modulation of various cellular processes. In fact, cytoplasmic FoxO3a is inactive and shuttled either to the nucleus or the mitochondria to exert its transcriptional function. Over accumulation of ROS can cause oxidative damage to mitochondria, leading to mitophagy through an SIRT1-dependent mechanism (40). Activated SIRT1 modulates FoxO3a transcriptional activity by specific deacetylation. Deacetylated FoxO3a translocates to mitochondria and inhibits mitochondrial activity by lowering the mtDNA copy number, reducing the expression of mitochondrial genes and directly interacting with PGC-1α (41,

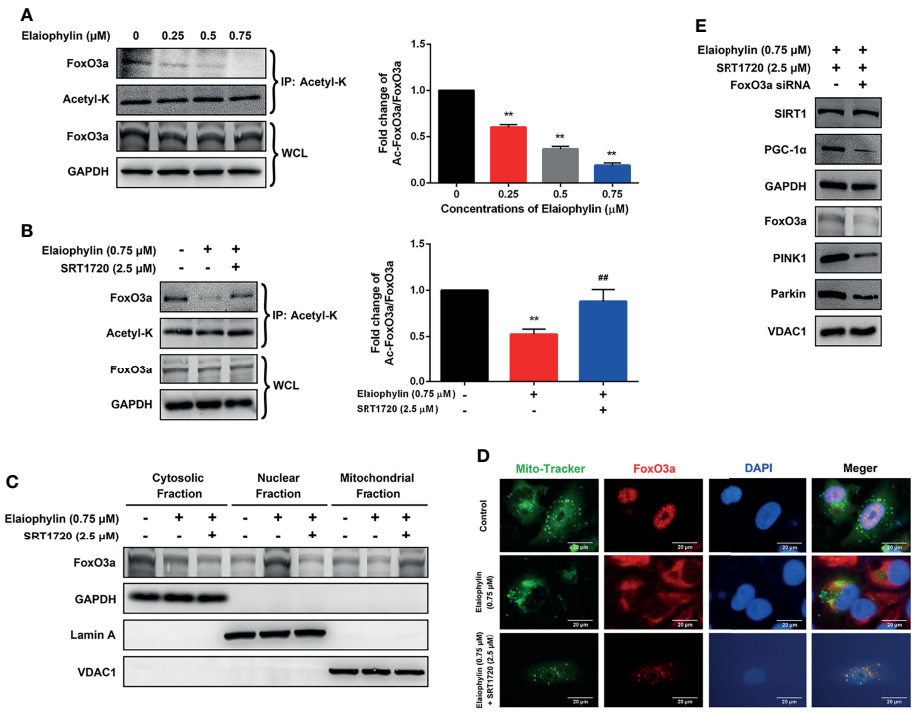

FIGURE 5 | Elaiophylin modulates SIRT1 in C918 cells by manipulating FoxO3a deacetylation and mitochondrial localization. **(A, B)** After treatment with indicated drugs, cells were divided into two groups. A portion of lysate was immunoprecipitated with anti-Acetyl-K antibody and the rest was directly subjected to immunoblotting. The representative images were shown on the left and the densitometry analysis of protein expression was shown on the right. **(C)** Cell lysate fractions (ie. cytosolic, nuclear, and mitochondrial fractions) were prepared and subjected to immunoblotting analysis. GAPDH is the cytosolic marker; LaminA is applied as the nuclear marker; and VDAC1 is adopted as the mitochondrial marker. **(D)** Colocalization of mitochondria with FoxO3a by immunofluorescence **(E)** The expression of typical proteins related to mitophagy. Western blotting was performed to analyze the representative proteins in mitophagy. GAPDH and VDAC1 were used as loading controls for cytoplasm and mitochondria, respectively. Data was expressed as mean ± SD of three experiments. $^{**}p<0.01$ *vs.* control, $^{\#\#}p<0.01$ *vs.* Elaiophylin group.

42). PGC-1α regulates mitochondrial biogenesis but also impacts on mitochondrial quality control machinery including fission, fusion, and mitophagy (43). Sirt1-deacetylated FoxO3a also induces mitophagy by promoting the expression of Bnip3, an atypical BH3-only protein known as a pro-apoptotic factor, which thus protects cells from mitochondrial dysfunction (44). In this study, we observe that Elaiophylin treatment in C918 cells increased FoxO3a acetylation and cytoplasm localization. And the SIRT1 activator SRT1720 potently attenuated such effect by inducing FoxO3a deacetylation and translocation to the mitochondria. FoxO3a knockdown significantly inhibited SIRT1-mediated mitophagy.

Other members of sirtuins have also been linked to the control of autophagy and mitophagy by modulating transcription of autophagy and mitophagy genes, by post translational modification of proteins related to the autophagy and mitophagy machinery, by controlling ROS production or major metabolic pathways such as Krebs cycle or glutamine metabolism. SIRT2 interacts and deacetylates FoxO1 and suppresses its induction of autophagic cell death by un-interacting with ATG7 (45). Downregulation of SIRT2 also increases basal autophagy in colorectal cancer cells protecting them from mitotic catastrophe caused by microtubule inhibitors (46). SIRT3 controlling mitophagy represents an important mechanism to prevent mitochondrial dysfunction and apoptosis in tumor cells under hypoxia. SIRT3 silencing causes a decrease of mitochondriogenesis and an increase of mitochondrial dysfunction and ROS leading to an activation of autophagy and apoptosis. SIRT3 overexpression has been linked to poor survival in many cancer patients, including ER positive breast cancer and colorectal cancer (47). SIRT4 also plays an important role in mitochondrial morphology/quality control and regulation of mitophagy. Moderate overexpression of SIRT4 accompanied by increased levels of the inner-membrane bound long form of the GTPase OPA1 (L-OPA1) promotes mitochondrial fusion, and sensitized cells to mitochondrial stress (48). SIRT5 controls ammonia detoxification by regulating CPS1 in liver mitochondria. Ammonia-induced autophagy and mitophagy are regulated by SIRT5. It upregulates autophagy markers MAP1LC3B, GABARAP, and GABARAPL2, mitophagy markers BNIP3 and the PINK1-PARK2 system (49). SIRT6 has pleiotropic protective actions,

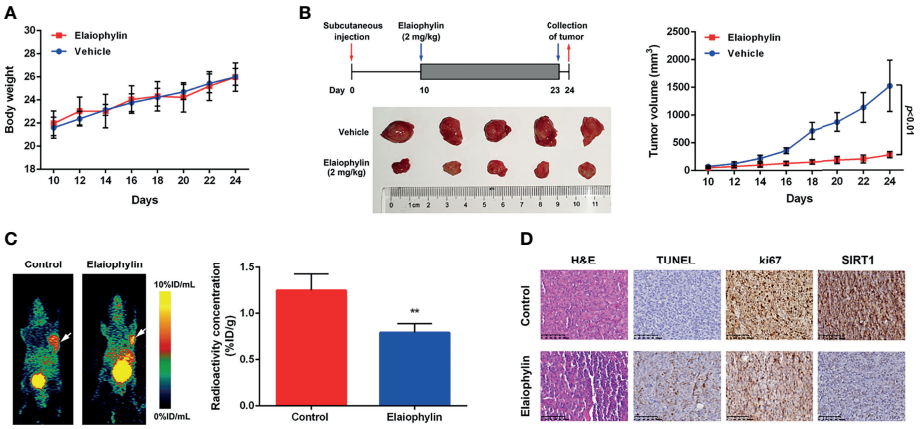

FIGURE 6 | Elaiophylin suppresses tumor growth in the C918-xenograft model by inhibiting SIRT1-mediated mitophagy. **(A)** Body weight of xenograft mice were measured every other day. **(B)** Tumor volumes were measured every other day. At the end of the treatment, the tumors were removed and photographed (n=5). The images of tumors were shown on the left and the tumor growth curve was displayed on the right. **(C)** *In vivo* PET imaging of C918-xenografted mice injected with [^{68}Ga]Ga-NOTA-PRGD$_2$. Tumors are indicated by arrows. ROIs are shown as mean %ID/g ± SD. **(D)** H&E staining of tumor sections of C918-xenograft mice. TUNEL and immunohistochemistry staining of ki67 and SIRT1 were performed. The representative images of staining are shown here. Data was expressed as mean ± SD of three experiments. $^{**}p<0.01$ *vs.* control.

including anti-inflammatory and anti-apoptotic effects, and promotes autophagy in podocytes (50). SIRT7-mediated autophagic response plays a protective role against cell death and the inhibition of SIRT7 has a potential to improve the efficacy of anti-metabolic therapy in non-small cell lung cancer cells (51). The role of each sirtuin member in cancer cells forms the basis of their potential application as adjuvant anti-cancer therapies. Natural and synthetic activators or inhibitors of sirtuins have been developed and these molecules seem to hold promising results against cancers. Further study on the regulatory mechanism of Elaiophylin on sirtuins may lead to new targets to treat relevant tumors.

UM is a rare but deadly cancer. The treatment of the primary tumor has made significant improvement with the introduction of globe-preserving approaches; however, metastatic disease remains a critical issue due to the lack of effective therapeutic strategies. UM is not sensitive to traditional chemotherapeutic drugs and immunotherapies barely have any effect. Despite lower efficacy demonstrated in initial ICI studies, there are a number of ongoing clinical trials investigating novel immunotherapy approaches in UM, including vaccine, adoptive T cells, and combination immunotherapy trials. The induction of autophagy may also benefit tumor cells escape from immune surveillance and result in intrinsic resistance against anti-tumor immunotherapy (52). Therefore, autophagy inhibitor such as Elaiophylin may play a critical role in the combination immunotherapy in UM. The acquired drug resistance of molecular targeted drugs is the primary challenge in treating UM. Cancer cells reutilize their mitochondria to facilitate cancer progression and acquire drug resistance. Oncometabolites, such as fumarate and 2-hydroxyglutarate, may promote resistance by upregulating the nuclear factor erythroid 2-related factor 2 (Nrf2) pathway, inhibiting the anti-tumor immune response, or promoting angiogenesis (53). Therefore, targeting autophagy or mitophagy may be potential and effective UM therapeutics (54). Zhou et al. identified a novel autophagy/mitophagy inhibitor liensinine sensitizes breast cancer cells to chemotherapeutic drugs through DNM1L dephosphorylation and mitochondrial translocation-mediated mitochondrial fission (12). Moreover, microRNA and long noncoding RNAs (lncRNAs) are proved to be critical regulators in numerous cellular processes, including autophagy and mitophagy. MicroRNAs overexpressed in high-risk UM, such as miR-17-5p, miR-21-5p, and miR-151a-3p, target 106 genes involved in the pathways like cell cycle regulation, EGF signaling and EIF2 signaling (55). LncRNA ZNNT1, as a major downstream effector of MTOR, promotes ATG12 transcription and subsequently induces cell death, leading to the suppression of UM tumorigenesis. Cui et al. reported a total of 13 differentially expressed autophagy genes were identified and validated in Gene Expression Omnibus, and 11 autophagy-related lncRNAs were found to be associated with overall survival. Several biological processes and signaling pathways were enriched in the high-risk group, including Toll-like receptor signaling pathway, natural killer cell-mediated cytotoxicity, and B- and T-cell receptor signaling pathway (56). Chen et al. also predicted 6 autophagy-related lncRNAs that are potential molecular biomarkers and treatment targets for UM patients, which were significantly concentrated in the biological pathways related to cytoplasmic component recycling, energy metabolism, and apoptosis (57).

In conclusion, our results suggested that Elaiophylin inhibits UM proliferation and induces apoptosis by increasing oxidative stress. SIRT1-mediated antioxidant regulation is dependent on FoxO3a deacetylation and mitochondrial localization. Elaiophylin can down-regulate the expression of SIRT1, increase FoxO3a

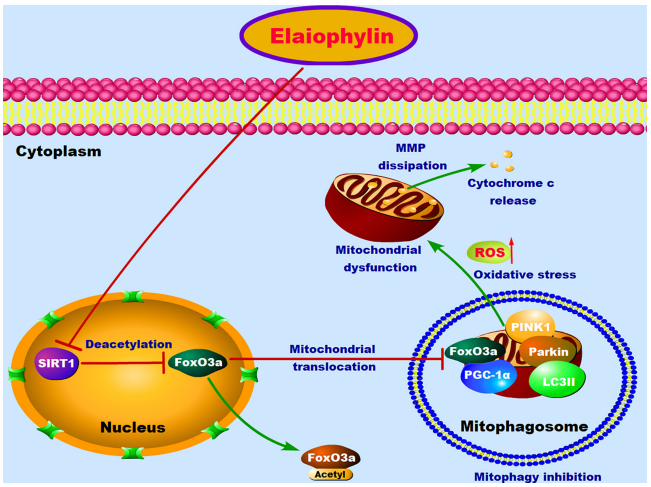

FIGURE 7 | The proposed molecular mechanism of Elaiophylin in killing UM cells. In normal condition, FoxO3a deacetylated by SIRT1 results in its translocation to mitochondria, where deacetylated FoxO3a and PGC-1α form the FoxO3a/PGC-1α complex. Increased formation of FoxO3a/PGC-1α complex triggers ubiquitination and PINK1/Parkin-mediated proteasomal degradation for mitochondrial clearance. Elaiophylin treatment inhibits SIRT1-mediated mitophagy, promotes mitochondrial dysfunction and oxidative stress, which eventually leads to the death of UM cells.

acetylation and cytoplasm localization, as well as suppress mitophagy to clean up damaged mitochondria (**Figure 7**). These novel anti-cancer properties of Elaiophylin may have important clinical implications in developing new therapeutic agents for UM.

DATA AVAILABILITY STATEMENT

The original contributions presented in the study are included in the article/supplementary materials. Further inquiries can be directed to the corresponding authors.

ETHICS STATEMENT

Five primary UM cell lines were isolated and cultured from UM patient tumor samples with the approval from the human research ethics committee of St. Vincent's Hospital (HREC/17/SVH/346). The patients/participants provided their written informed consent to participate in this study. All animals were kept in a pathogen-free environment and fed ad lib. The procedures for care and use of animals were approved by the Laboratory Animal Ethics Committee of Jiangsu Institute of Nuclear Medicine (JSINM-2020-096) and all applicable institutional and governmental regulations concerning the ethical use of animals were followed.

AUTHOR CONTRIBUTIONS

XZ, WZ, and KW designed experiments. XZ, WZ, XM, JJ, YC, DP, and FZ carried out experiments. XZ, WZ, XW, HS, and FZ analyzed experimental results. XZ and WZ wrote the manuscript. WZ and KW finished the final version approval. All authors contributed to the article and approved the submitted version.

FUNDING

This work was supported by Major project of Wuxi Commission of Health (Z202009, Z202014), Six talent peaks project in Jiangsu Province (No. WSW-047), Six-one Scientific Research Project (No. LGY2019087), Young and middle-aged top medical and health talents project of Wuxi Commission of Health (BJ2020031), Postdoctoral Science Foundation funded project of Jiangsu Province (2021K196B).

REFERENCES

1. Amaro A, Gangemi R, Piaggio F, Angelini G, Barisione G, Ferrini S, et al. The Biology of Uveal Melanoma. *Cancer Metastasis Rev* (2017) 36(1):109–40. doi: 10.1007/s10555-017-9663-3
2. Spagnolo F, Caltabiano G, Queirolo P. Uveal Melanoma. *Cancer Treat Rev* (2012) 38(5):549–53. doi: 10.1016/j.ctrv.2012.01.002
3. Singh M, Durairaj P, Yeung J. Uveal Melanoma: A Review of the Literature. *Oncol Ther* (2018) 6(1):87–104. doi: 10.1007/s40487-018-0056-8
4. Álvarez-Rodríguez B, Latorre A, Posch C, Somoza Á. Recent Advances in Uveal Melanoma Treatment. *Med Res Rev* (2017) 37(6):1350–72. doi: 10.1002/med.21460
5. Behrends C, Sowa ME, Gygi SP, Harper JW. Network Organization of the Human Autophagy System. *Nature* (2010) 466(7302):68–76. doi: 10.1038/nature09204
6. Onorati AV, Dyczynski M, Ojha R, Amaravadi RK. Targeting Autophagy in Cancer. *Cancer* (2018) 124(16):3307–18. doi: 10.1002/cncr.31335
7. Giatromanolaki AN, Charitoudis GS, Bechrakis NE, Kozobolis VP, Koukourakis MI, Foerster MH, et al. Autophagy Patterns and Prognosis in

Uveal Melanomas. *Mod Pathol* (2011) 24(8):1036–45. doi: 10.1038/modpathol.2011.63
8. Truong A, Yoo JH, Scherzer MT, Sanchez JMS, Dale KJ, Kinsey CG, et al. Chloroquine Sensitizes GNAQ/11-Mutated Melanoma to MEK1/2 Inhibition. *Clin Cancer Res* (2020) 26(23):6374–86. doi: 10.1158/1078-0432.Ccr-20-1675
9. Ferro F, Servais S, Besson P, Roger S, Dumas JF, Brisson L. Autophagy and Mitophagy in Cancer Metabolic Remodelling. *Semin Cell Dev Biol* (2020) 98:129–38. doi: 10.1016/j.semcdb.2019.05.029
10. Moloney JN, Cotter TG. ROS Signalling in the Biology of Cancer. *Semin Cell Dev Biol* (2018) 80:50–64. doi: 10.1016/j.semcdb.2017.05.023
11. Li L, Tan J, Miao Y, Lei P, Zhang Q. ROS and Autophagy: Interactions and Molecular Regulatory Mechanisms. *Cell Mol Neurobiol* (2015) 35(5):615–21. doi: 10.1007/s10571-015-0166-x
12. Zhou J, Li G, Zheng Y, Shen HM, Hu X, Ming QL, et al. A Novel Autophagy/Mitophagy Inhibitor Liensinine Sensitizes Breast Cancer Cells to Chemotherapy Through DNM1L-Mediated Mitochondrial Fission. *Autophagy* (2015) 11(8):1259–79. doi: 10.1080/15548627.2015.1056970
13. Yao N, Wang C, Hu N, Li Y, Liu M, Lei Y, et al. Inhibition of PINK1/Parkin-Dependent Mitophagy Sensitizes Multidrug-Resistant Cancer Cells to B5G1, a New Betulinic Acid Analog. *Cell Death Dis* (2019) 10(3):232. doi: 10.1038/s41419-019-1470-z
14. Sun H, Ou T, Hu J, Yang Z, Lei Q, Li Y, et al. Nitazoxanide Impairs Mitophagy Flux Through ROS-Mediated Mitophagy Initiation and Lysosomal Dysfunction in Bladder Cancer. *Biochem Pharmacol* (2021) 190:114588. doi: 10.1016/j.bcp.2021.114588
15. Kulikov AV, Luchkina EA, Gogvadze V, Zhivotovsky B. Mitophagy: Link to Cancer Development and Therapy. *Biochem Biophys Res Commun* (2017) 482 (3):432–9. doi: 10.1016/j.bbrc.2016.10.088
16. Fiedler HP, Wörner W, Zähner H, Kaiser HP, Keller-Schierlein W, Müller A. Metabolic Products of Microorganisms. 200 Isolation and Characterization of Niphithricins A, B, and Elaiophylin, Antibiotics Produced by Streptomyces Violaceoniger. *J Antibiot (Tokyo)* (1981) 34(9):1107–18. doi: 10.7164/antibiotics.34.1107
17. Lim HN, Jang JP, Han JM, Jang JH, Ahn JS, Jung HJ. Antiangiogenic Potential of Microbial Metabolite Elaiophylin for Targeting Tumor Angiogenesis. *Molecules* (2018) 23(3):563. doi: 10.3390/molecules23030563
18. Zhao X, Fang Y, Yang Y, Qin Y, Wu P, Wang T, et al. Elaiophylin, a Novel Autophagy Inhibitor, Exerts Antitumor Activity as a Single Agent in Ovarian Cancer Cells. *Autophagy* (2015) 11(10):1849–63. doi: 10.1080/15548627.2015.1017185
19. Wang G, Zhou P, Chen X, Zhao L, Tan J, Yang Y, et al. The Novel Autophagy Inhibitor Elaiophylin Exerts Antitumor Activity Against Multiple Myeloma With Mutant TP53 in Part Through Endoplasmic Reticulum Stress-Induced Apoptosis. *Cancer Biol Ther* (2017) 18(8):584–95. doi: 10.1080/15384047.2017.1345386
20. Siddiqui FA, Vukic V, Salminen TA, Abankwa D. Elaiophylin Is a Potent Hsp90/ Cdc37 Protein Interface Inhibitor With K-Ras Nanocluster Selectivity. *Biomolecules* (2021) 11(6):836. doi: 10.3390/biom11060836
21. Joo JH, Dorsey FC, Joshi A, Hennessy-Walters KM, Rose KL, McCastlain K, et al. Hsp90-Cdc37 Chaperone Complex Regulates Ulk1- and Atg13-Mediated Mitophagy. *Mol Cell* (2011) 43(4):572–85. doi: 10.1016/j.molcel.2011.06.018
22. Salminen A, Kaarniranta K. SIRT1: Regulation of Longevity *via* Autophagy. *Cell Signal* (2009) 21(9):1356–60. doi: 10.1016/j.cellsig.2009.02.014
23. Xie Q, Chen J, Yuan Z. Post-Translational Regulation of FOXO. *Acta Biochim Biophys Sin (Shanghai)* (2012) 44(11):897–901. doi: 10.1093/abbs/gms067
24. Daniels KJ, Boldt HC, Martin JA, Gardner LM, Meyer M, Folberg R. Expression of Type VI Collagen in Uveal Melanoma: Its Role in Pattern Formation and Tumor Progression. *Lab Invest* (1996) 75(1):55–66.
25. Aventaggiato M, Vernucci E, Barreca F, Russo MA, Tafani M. Sirtuins' Control of Autophagy and Mitophagy in Cancer. *Pharmacol Ther* (2021) 221:107748. doi: 10.1016/j.pharmthera.2020.107748
26. Tang BL. Sirt1 and the Mitochondria. *Mol Cells* (2016) 39(2):87–95. doi: 10.14348/molcells.2016.2318
27. Ng F, Tang BL. Sirtuins' Modulation of Autophagy. *J Cell Physiol* (2013) 228 (12):2262–70. doi: 10.1002/jcp.24399
28. Yoshii SR, Mizushima N. Autophagy Machinery in the Context of Mammalian Mitophagy. *Biochim Biophys Acta (BBA) - Mol Cell Res* (2015) 1853(10, Part B):2797–801. doi: 10.1016/j.bbamcr.2015.01.013
29. Liang D, Zhuo Y, Guo Z, He L, Wang X, He Y, et al. SIRT1/PGC-1 Pathway Activation Triggers Autophagy/Mitophagy and Attenuates Oxidative Damage in Intestinal Epithelial Cells. *Biochimie* (2020) 170:10–20. doi: 10.1016/j.biochi.2019.12.001
30. Yao ZQ, Zhang X, Zhen Y, He XY, Zhao S, Li XF, et al. A Novel Small-Molecule Activator of Sirtuin-1 Induces Autophagic Cell Death/Mitophagy as a Potential Therapeutic Strategy in Glioblastoma. *Cell Death Dis* (2018) 9 (7):767. doi: 10.1038/s41419-018-0799-z
31. Xiong H, Chen S, Lai L, Yang H, Xu Y, Pang J, et al. Modulation of miR-34a/SIRT1 Signaling Protects Cochlear Hair Cells Against Oxidative Stress and Delays Age-Related Hearing Loss Through Coordinated Regulation of Mitophagy and Mitochondrial Biogenesis. *Neurobiol Aging* (2019) 79:30–42. doi: 10.1016/j.neurobiolaging.2019.03.013
32. Yi S, Zheng B, Zhu Y, Cai Y, Sun H, Zhou J. Melatonin Ameliorates Excessive PINK1/Parkin-Mediated Mitophagy by Enhancing SIRT1 Expression in Granulosa Cells of PCOS. *Am J Physiol Endocrinol Metab* (2020) 319(1): E91–e101. doi: 10.1152/ajpendo.00006.2020
33. Palmeira CM, Teodoro JS, Amorim JA, Steegborn C, Sinclair DA, Rolo AP. Mitohormesis and Metabolic Health: The Interplay Between ROS, cAMP and Sirtuins. *Free Radic Biol Med* (2019) 141:483–91. doi: 10.1016/j.freeradbiomed.2019.07.017
34. Grasso D, Zampieri LX, Capelôa T, Van de Velde JA, Sonveaux P. Mitochondria in Cancer. *Cell Stress* (2020) 4(6):114–46. doi: 10.15698/cst2020.06.221
35. Finkel T, Deng CX, Mostoslavsky R. Recent Progress in the Biology and Physiology of Sirtuins. *Nature* (2009) 460(7255):587–91. doi: 10.1038/nature08197
36. Haigis MC, Sinclair DA. Mammalian Sirtuins: Biological Insights and Disease Relevance. *Annu Rev Pathol* (2010) 5:253–95. doi: 10.1146/annurev.pathol.4.110807.092250
37. Martins R, Lithgow GJ, Link W. Long Live FOXO: Unraveling the Role of FOXO Proteins in Aging and Longevity. *Aging Cell* (2016) 15(2):196–207. doi: 10.1111/acel.12427
38. Fasano C, Disciglio V, Bertora S, Lepore Signorile M, Simone C. FOXO3a From the Nucleus to the Mitochondria: A Round Trip in Cellular Stress Response. *Cells* (2019) 8(9):1110. doi: 10.3390/cells8091110
39. Wang Z, Yu T, Huang P. Post-Translational Modifications of FOXO Family Proteins (Review). *Mol Med Rep* (2016) 14(6):4931–41. doi: 10.3892/mmr.2016.5867
40. Kobayashi Y, Furukawa-Hibi Y, Chen C, Horio Y, Isobe K, Ikeda K, et al. SIRT1 is Critical Regulator of FOXO-Mediated Transcription in Response to Oxidative Stress. *Int J Mol Med* (2005) 16(2):237–43. doi: 10.3892/ijmm.16.2.237
41. Olmos Y, Valle I, Borniquel S, Tierrez A, Soria E, Lamas S, et al. Mutual Dependence of Foxo3a and PGC-1alpha in the Induction of Oxidative Stress Genes. *J Biol Chem* (2009) 284(21):14476–84. doi: 10.1074/jbc.M807397200
42. Olmos Y, Sánchez-Gómez FJ, Wild B, García-Quintans N, Cabezudo S, Lamas S, et al. SirT1 Regulation of Antioxidant Genes is Dependent on the Formation of a FoxO3a/PGC-1α Complex. *Antioxid Redox Signal* (2013) 19(13):1507–21. doi: 10.1089/ars.2012.4713
43. Halling JF, Pilegaard H. PGC-1α-Mediated Regulation of Mitochondrial Function and Physiological Implications. *Appl Physiol Nutr Metab* (2020) 45(9):927–36. doi: 10.1139/apnm-2020-0005
44. Ney PA. Mitochondrial Autophagy: Origins, Significance, and Role of BNIP3 and NIX. *Biochim Biophys Acta* (2015) 1853(10 Pt B):2775–83. doi: 10.1016/j.bbamcr.2015.02.022
45. Zhao Y, Wang L, Yang J, Zhang P, Ma K, Zhou J, et al. Anti-Neoplastic Activity of the Cytosolic FoxO1 Results From Autophagic Cell Death. *Autophagy* (2010) 6(7):988–90. doi: 10.4161/auto.6.7.13289
46. Inoue T, Nakayama Y, Li Y, Matsumori H, Takahashi H, Kojima H, et al. SIRT2 Knockdown Increases Basal Autophagy and Prevents Postslippage Death by Abnormally Prolonging the Mitotic Arrest That is Induced by Microtubule Inhibitors. *FEBS J* (2014) 281(11):2623–37. doi: 10.1111/febs.12810
47. Torrens-Mas M, Oliver J, Roca P, Sastre-Serra J. SIRT3: Oncogene and Tumor Suppressor in Cancer. *Cancers (Basel)* (2017) 9(7):90. doi: 10.3390/cancers9070090

48. Lang A, Anand R, Altinoluk-Hambüchen S, Ezzahoini H, Stefanski A, Iram A, et al. SIRT4 Interacts With OPA1 and Regulates Mitochondrial Quality Control and Mitophagy. *Aging (Albany NY)* (2017) 9(10):2163–89. doi: 10.18632/aging.101307
49. Polletta L, Vernucci E, Carnevale I, Arcangeli T, Rotili D, Palmerio S, et al. SIRT5 Regulation of Ammonia-Induced Autophagy and Mitophagy. *Autophagy* (2015) 11(2):253–70. doi: 10.1080/15548627.2015.1009778
50. Liu M, Liang K, Zhen J, Zhou M, Wang X, Wang Z, et al. Sirt6 Deficiency Exacerbates Podocyte Injury and Proteinuria Through Targeting Notch Signaling. *Nat Commun* (2017) 8(1):413. doi: 10.1038/s41467-017-00498-4
51. Jiang Y, Han Z, Wang Y, Hao W. Depletion of SIRT7 Sensitizes Human Non-Small Cell Lung Cancer Cells to Gemcitabine Therapy by Inhibiting Autophagy. *Biochem Biophys Res Commun* (2018) 506(1):266–71. doi: 10.1016/j.bbrc.2018.10.089
52. Yamamoto K, Venida A, Yano J, Biancur DE, Kakiuchi M, Gupta S, et al. Autophagy Promotes Immune Evasion of Pancreatic Cancer by Degrading MHC-I. *Nature* (2020) 581(7806):100–5. doi: 10.1038/s41586-020-2229-5
53. Yong C, Stewart GD, Frezza C. Oncometabolites in Renal Cancer. *Nat Rev Nephrol* (2020) 16(3):156–72. doi: 10.1038/s41581-019-0210-z
54. Panigrahi DP, Praharaj PP, Bhol CS, Mahapatra KK, Patra S, Behera BP, et al. The Emerging, Multifaceted Role of Mitophagy in Cancer and Cancer Therapeutics. *Semin Cancer Biol* (2020) 66:45–58. doi: 10.1016/j.semcancer.2019.07.015
55. Smit KN, Chang J, Derks K, Vaarwater J, Brands T, Verdijk RM, et al. Aberrant MicroRNA Expression and Its Implications for Uveal Melanoma Metastasis. *Cancers (Basel)* (2019) 11(6):815. doi: 10.3390/cancers11060815
56. Cui Y, Zheng M, Chen J, Xu N. Autophagy-Related Long Non-Coding RNA Signature as Indicators for the Prognosis of Uveal Melanoma. *Front Genet* (2021) 12:625583. doi: 10.3389/fgene.2021.625583
57. Chen Y, Chen L, Wang J, Tan J, Wang S. Identification of Six Autophagy-Related-lncRNA Prognostic Biomarkers in Uveal Melanoma. *Dis Markers* (2021) 2021:2401617. doi: 10.1155/2021/2401617

Conflict of Interest: The authors declare that the research was conducted in the absence of any commercial or financial relationships that could be construed as a potential conflict of interest.

Publisher's Note: All claims expressed in this article are solely those of the authors and do not necessarily represent those of their affiliated organizations, or those of the publisher, the editors and the reviewers. Any product that may be evaluated in this article, or claim that may be made by its manufacturer, is not guaranteed or endorsed by the publisher.

frontiers | Frontiers in Oncology

ORIGINAL RESEARCH
published: 26 April 2022
doi: 10.3389/fonc.2022.811411

A Phase I Trial to Determine the Safety and Tolerability of Autophagy Inhibition Using Chloroquine or Hydroxychloroquine in Combination With Carboplatin and Gemcitabine in Patients With Advanced Solid Tumors

Nagla Abdel Karim[1], Asad Ullah[1], Imran Ahmad[2], Elmustapha Bahassi[2], Olugbenga Olowokure[2], Ahmed Khaled[3], Harold Davis[2] and John C. Morris[2]*

[1] Division of Hematology/Oncology-Augusta University, Augusta, GA, United States, [2] Division of Hematology/Oncology-The University of Cincinnati, Augusta, GA, United States, [3] GlaxoSmithKline, Division of Solid Tumors-Augusta, Augusta, GA, United States

OPEN ACCESS

Edited by:
Abdelhabib Semlali, Laval University, Canada

Reviewed by:
Kasper Rouschop, Maastricht University, Netherlands
Jean Marie Mulcahy Levy, University of Colorado Denver, United States

***Correspondence:**
Nagla Abdel Karim
nkarim@augusta.edu

Specialty section:
This article was submitted to Cancer Molecular Targets and Therapeutics, a section of the journal Frontiers in Oncology

Received: *08 November 2021*
Accepted: *22 February 2022*
Published: *26 April 2022*

Citation:
Karim NA, Ullah A, Ahmad I, Bahassi E, Olowokure O, Khaled A, Davis H and Morris JC (2022) A Phase I Trial to Determine the Safety and Tolerability of Autophagy Inhibition Using Chloroquine or Hydroxychloroquine in Combination With Carboplatin and Gemcitabine in Patients With Advanced Solid Tumors. Front. Oncol. 12:811411. doi: 10.3389/fonc.2022.811411

Background: Autophagy is a catabolic process that is triggered in cells during periods of metabolic or hypoxic stress, which enables their survival during this challenge. Autophagy may also impart survival advantage to tumors cells undergoing attack from chemotherapy or radiation. Inhibition of early-stage autophagy can rescue cancer cells, while inhibition of late-stage autophagy enhances cell death due to accumulation of damaged organelles. The antiparasitic drugs chloroquine (CQ) and hydroxychloroquine (HCQ) inhibit late-phase autophagy. We assessed the safety, tolerability, and efficacy of combining CQ or HCQ with carboplatin and gemcitabine (CG) in patients with refractory advanced solid tumors.

Methods: This single institution phase 1 dose-escalation study was designed to evaluate the maximum tolerated dose (MTD) of CQ/HCQ, in combination with CG, in patients with advanced solid tumors. Secondary objectives were to determine overall response rate (ORR), progression-free survival (PFS), and overall survival (OS). A starting dose of CQ or HCQ 50 mg was used in conjunction with standard starting doses of CG and increased in increments of 50 mg in each patient dose cohort. Grade 3 or greater toxicity that is treatment related, and was not self-limited, or not controlled in <7 days was considered dose-limiting toxicity (DLT).

Results: Twenty-two patients were enrolled. All patients had at least one prior treatment, and 11 of them had 3 prior regimens. CQ/HCQ 100 mg daily was found to be the MTD in combination with CG with thrombocytopenia and/or neutropenia dose limiting. The median overall (OS) was 11 months, and the 1- and 3-year OS were 30% and 7%, respectively. Median progression-free survival was 5 months, and the 6-, 12-, and 18-month progression-free survivals were 48%, 21%, and 14%, respectively.

Conclusion: The MTD identified for CQ/HCQ was lower than previously reported with concomitant use of chemotherapeutic regimes likely due to the myelosuppressive nature of CG in previously treated patients.

Keywords: lung cancer, autophagy, phase 1, solid tumor, chloroquine

INTRODUCTION

Autophagy, or "self-eating," is a cellular process by which cytoplasmic organelles and proteins are sequestered into autophagic vesicles and delivered to lysosomes for "bulk" degradation and recycling (1, 2). It is a housekeeping process that regulates organelle and cellular protein turnover (3). Autophagy has been shown to become deregulated in certain pathological states including cancer. Under normal circumstances, autophagy is believed to suppress cellular transformation and tumor progression by limiting chromosomal instability. Alternatively, it has been demonstrated that established tumors utilize autophagy to survive periods of metabolic or hypoxic stress (4). Thus, manipulation of autophagy has become a potential area for the development of novel antineoplastic strategies (5). Aminoquinolines such as CQ have been shown to inhibit autophagy by mechanisms distinct from other inhibitors such as 3-methyladenine (3-MA). Whereas 3-MA inhibits early phase autophagy, consequently inhibiting the formation of acidic vesicular organelles (AVOs) that consist predominantly of autophagosomes and autolysosomes, CQ inhibits autophagy in its late phases after cytoplasmic AVOs have been formed. Therefore, CQ-treated cells typically demonstrate accumulation of cytoplasmic AVOs (6). CQ has been identified as a chemotherapy sensitizer when used in combination with certain antineoplastic drugs (7, 8). The lysosomotropic properties of CQ are likely responsible for many of its biological effects. Accumulating lines of evidence suggest that through its lysosomotropic effect, CQ can sensitize cancer cells to the killing effects of and various chemotherapeutic agents and ionizing radiation (9, 10).

In a small, randomized study, Sotelo et al. (5), reported improved survival in patients with glioblastoma treated with four cycles of carmustine with radiation and CQ versus placebo beginning 5 days after surgery.

Amaravadi et al. demonstrated that targeting autophagy with CQ derivatives enhanced the efficacy of chemotherapy (7) HCQ has been extensively studied in combination with several chemotherapeutic agents to assess its clinical safety and activity. Several phase I trials studying HCQ in combination with various antineoplastic agents determined the maximum tolerated dose (MTD) to be 200–1,200 mg daily. HCQ has been studied in combination with temozolomide 150 mg in patients with advanced solid tumors (11). Wolpin et al. reported the safety and antineoplastic activity of HCQ in 20 patients with metastatic pancreatic cancer who did not respond to conventional chemotherapy. In this phase II trial, patients received 400 mg ($n = 10$) or 600 mg ($n = 10$) of HCQ twice daily as a single agent (12).

Five other phase I trials of HCQ involved combination with various chemotherapeutic agents including temozolomide, bortezomib, temsirolimus, vorinostat, or doxorubicin (7, 12, 13). A number of patients with melanoma, colorectal cancer, myeloma, and renal cell carcinoma demonstrated partial responses or stable disease, suggesting antitumor activity. In a phase II study in advanced pancreatic cancer, Karasic et al. showed that HCQ 600 mg daily in combination with gemcitabine and nab-paclitaxel resulted in an improved response rate, making some tumors resectable (14). Based on this rationale and the importance of gemcitabine and carboplatin in treating many types of cancer, our study was designed to investigate if CQ will resensitize use of chemotherapy again in heavily pretreated patients. Patients enrolled in our phase I study were mostly heavily pretreated and were candidates for the systemic therapy with carboplatin and gemcitabine and thus the choice of starting with lower doses of HCQ.

STUDY OBJECTIVES

Primary Objective

This study primarily aims to determine the maximum tolerated dose (MTD) of chloroquine (CQ) or (HCQ) in combination with carboplatin and gemcitabine (CG) in patients with advanced solid tumors.

Secondary Objectives

The secondary objectives were as follows:

1. To estimate the overall response rate (ORR), progression-free survival (PFS), and overall survival (OS) of patients with advanced solid tumors treated with chloroquine (CQ) or (HCQ). HCQ has been used in place of CQ due to the acute shortage in the US and since both has similar chemistry and efficacy.
2. To determine the pharmacokinetics of CQ/HCQ in combination with CG; and
3. To detect effects on autophagy through changes in plasma levels of exosomal microtubule-associated protein 1A/1B light chain 3B (LC3) levels in peripheral blood.

PATIENTS AND METHODS

Human Subjects Protections

Eligible patients were enrolled in this Institutional Review Board (IRB)-approved study through the University of Cincinnati Cancer Institute Clinical Trials Office (CTO). To register a patient, all of the following were obtained: written informed

consent form, Health Insurance Portability and Accountability Act (HIPAA) Authorization form, eligibility screening worksheet, and registration form. The trial was listed in https://clinicaltrials.gov (NCT02071537).

Study Design

This was a single institution phase I dose-escalation study using a 3 + 3 dose-escalation schema. Patients with progressing advanced solid tumors with either no other available standard of care treatment or where carboplatin and gemcitabine were considered an acceptable treatment option, Eastern Cooperative Oncology Group (ECOG) performance status 0–1 were eligible. Sequential CQ/HCQ dose cohorts of three to six patients were treated. The starting dose of CQ was 50 mg p.o. days 1–21 in addition to intravenous carboplatin (AUC 5) and gemcitabine (500 mg/2) day 1 (**Table 1**). Patients in cohort 1 were treated with CQ; however, CQ became unavailable due to an international shortage, so the study continued using HCQ at the cited doses in cohorts 2 and 3 and the expansion cohort with IRB-approval.

Eligibility Criteria

Subjects were required to have histologically or cytologically confirmed metastatic or unresectable cancer for which either standard curative measures do not exist, are no longer effective, or for which the combination of carboplatin and gemcitabine are considered a reasonable treatment option; no other than active malignancy, or chronic systemic immune therapy, and no known G-6-PD deficiency; age ≥18 years; ECOG performance status <2 (Karnofsky >60%); acceptable organ and bone marrow function defined as an absolute neutrophil count ≥1,500/μl, platelet count ≥100,000/μl, total bilirubin <1.5× upper limit of normal (ULN), aspartate aminotransferase (AST) [serum glutamic-oxaloacetic transaminase (SGOT)], or alanine aminotransferase (ALT) [serum glutamic-pyruvic transaminase (SGPT)] <3× ULN; adequate baseline renal function with serum creatinine <1.5× ULN; a life expectancy >3 months; and at least one measurable lesion by RECIST 1.1. Patients with treated and asymptomatic brain metastases were eligible. Women and men of child-bearing potential must have agreed to use adequate contraception for the duration of study, and participants must have the ability to understand and willingness to sign a written informed consent document. Patients receiving other investigational agents, those with untreated brain metastases, history of allergic reactions to CQ/HCQ or other agents used in study, and an uncontrolled intercurrent illness or infection were ineligible.

Treatment

CQ or HCQ was administered at the dose levels, as indicated in **Table 1**, for a total of four 21-day treatment cycles (initially HCQ was used, then due to unavailability of HCQ, patients were switched to CQ). CQ was administered orally daily starting 1 week prior to the start of carboplatin and gemcitabine (CG) chemotherapy (day −7 until day 1) andthroughout the 21-day cycle for a total of four treatment cycles of CG. Additional fifth and sixth cycles of carboplatin and gemcitabine were allowed without the addition of CQ or HCQ in case of continued response or benefit per the decision of the treating investigator. The lower and higher dose groups (N = 6 and 3, respectively) received 50 or 150 mg of CQ or HCQ as a fixed daily oral dose. The first seven patients received CQ 50 mg; 50 mg was given in a suspension form, then 100 mg was given through splitting the 200-mg tablet (where the first patient received only one dose of 50 mg of CQ and was found to be ineligible after dosing on day 1 and was excluded and replaced), and the next three patients received 100 mg of HCQ due to the worldwide shortage and unavailability of CQ. The third cohort received 150 mg of HCQ and the expansion cohort of 10 patients received 100 mg of HCQ. HCQ tablets were split into half to provide the 100-mg dose. This was done by an experienced clinical pharmacist to ensure all patients are getting the same dose. For the dose-limiting toxicity definition and dose escalation, the dose-limiting toxicity (DLT) of HCQ was 150 mg when given in combination with carboplatin and gemcitabine. We believe that the major toxicity though occurred due to the cytotoxic chemotherapy in heavily pre-treated patients. The maximum tolerated dose (MTD) of HCQ was 100 mg when given in combination with carboplatin and gemcitabine.

Evaluation of Safety and Outcome

Adverse event descriptions and grading as described in the revised National Cancer Institute (NCI) Common Terminology Criteria for Adverse Events (CTCAE) version 4.0 were utilized for AE reporting (CTCAE 4.0 was the available criteria used during the evaluation of our studied patients). Primary outcome measures were as follows: CTCAE grade >3 adverse events clearly linked to treatment and was not self-limited or resolved in <7 days. Secondary outcome measures were RECIST 1.1 response criteria: complete response (CR), partial response (PR), stable disease (SD), and progressive disease (PD). The duration of overall response was measured from the time that the measurement criteria are met for CR or PR (whichever is first recorded) until the first date that recurrent

TABLE 1 | Planned dose escalation and MTD cohort expansion.

Dose level	Patients	CQ (first cohort) HCQ (all subsequent patients) (mg/day) Day −7 to day 21	Carboplatin (AUC) Day 1	Gemcitabine (mg/m^2) Day 1 and 8 out of 21-day cycle
1	3–6	CQ 50 mg daily	5	1,250-1,000
2	3–6	HCQ 100 mg daily	5	1,000
3	3–6	HCQ	5	1,000
4	3–6	200	5	1,000
Expansion cohort	10–12	100	5	1,000

or progressive disease was objectively documented. Duration of stable disease is measured from the start of the treatment until criteria for progression are met, taking as reference the smallest RECIST measurements recorded since the treatment began. Progression-free survival (PFS) is defined as the duration of time from start of treatment to time of progression.

Ocular Exam

Due to the potential ocular toxicity of CQ/HCQ, all subjects underwent a baseline ocular/funduscopic exam before the start of CQ/HCQ treatment and a repeat exam at the end of the study to ensure that there was no ocular toxicity.

Statistical Considerations

The primary endpoint was DLT, and they were defined as dichotomous variables in the study. At each dose level, DLT has been summarized using frequency (%).

Secondary endpoints are a dichotomous variable of treatment response (CR or PR); events of progression free (PF) and overall survival (OS) are both censored at 12 months after treatment. The dichotomous variables of response have been summarized in frequency at each follow-up visit. Kaplan–Meier curves were used to summarize the PFS and OS over time. In addition, as exploratory analyses, logistical and Cox proportional hazard models have been used to assess associations of secondary variables to baseline characteristics such as patient's demographics, cancer types and stages, and therapy plans.

Sample Size Justification

Determination of MTD was followed using an algorithm of a maximum of six patients in each cohort. No power analysis was needed as only descriptive statistics are providedfor the primary variables. The analyses of secondary variables were based upon a total of 10 patients in the MDT cohort. Tiered enrollment for each cohort was included according to the standard three to six patients, and it takes up to 28 days to ensure that there are no serious adverse events before moving to the next cohort.

Data and Safety Monitoring

Review of data and patients' outcome was discussed at the time of the initiation of the study, before expanding or moving to the following cohort, and at the end of the study. Progress and adverse events were monitored by the University of Cincinnati Cancer Institute Data Safety Monitoring Board after accrual to each dose cohort before approval of accruing to the next cohort.

CORRELATIVE STUDIES

Quantification of Autophagosomes

From Patients' Plasma

Patients' blood samples were collected at the mentioned time points and span down at 1,500*g* for 15 min. The upper phase (plasma) was collected in new tubes and stored at −80°C until use. Exosome's extraction was done using an exosome extraction reagent (total exosomes precipitation reagent from plasma, Invitrogen by Thermo Fisher Scientific, Ref. 4484451) following the manufacturer's instructions, then suspended in phosphate-buffered saline (PBS) and stored at −80°C.

Pharmacokinetics

Metabolism of Chloroquine/Hydroxychloroquine

CQ/HCQ was 60% bound to plasma proteins and cleared equally by the kidney and liver. Following administration of C, it was rapidly de-alkylated *via* cytochrome p450 (CYP) into active desethylchloroquine and bisdesethylchloroquine with elimination half-lives of 20–60 days. Both parent drug and metabolite can be detected in urine months after a single dose.

CQ/HCQ has a rapid and almost complete absorption, and peak plasma concentrations reached within 1–2 h following oral administration. CQ/HCQ has a long half-life of 3–5 days. For pharmacokinetic analysis, blood samples (5 ml per time point) were collected on day −7 at baseline pre-dose, then at 1, 2, 4, 6, and 24 h on day 1. Trough levels were collected at days 8 and 15. Blood samples were collected at each subsequent cycle (cycles 2–4) on day 1 at 1, 2, 4, 6, 24, 48, and 72 h. Trough levels were collected on days 8 and 15 for cycles 2–4. Blood was collected into B-D vacutainer tubes containing K3-EDTA mixed and centrifuged at 1,500*g* for 10 min at 4°C. Plasma was transferred into a storage tube and maintained on dry ice until stored in a −20°C freezer. Post-dose trough levels for CQ/HCQ were measured on days 8, 15, and 22 (15).

RESULTS

Patients

Twenty-three patients with advanced solid tumors were enrolled between 2014 and 2018. The patient demographic is shown in **Table 2**. Among the 22 eligible treated patients, there were 15 men (68%) and 7 women (32%) with median age of 58 years.

There 15 White (68%), 6 African American (27%), and 1 Asian patient (5%). Regarding ECOG performance status (PS), 5 patients had PS of 0 (22%), 14 had PS of 1 (64%) and 3 had PS of 2 (14%). Tumor histological types were as follows: 5 patients had adenocarcinoma (23%), 4 had squamous cell carcinoma (18%), while 13 had different types (59%) including small cell, urothelial, hepatocellular, and cholangiocarcinoma. The number of regimens received prior to inclusion in this trial was 0 for 3 patients (14%), 1 for 5 patients (22%), 2 for 3 patients (14%), and 3 or more regimens for 11 patients (50%) (**Tables 3**, **4**).

Dose escalation

The first cohort constituted of seven patients, as the first patient was excluded and not treated on day 1 and did not meet the eligibility criterion having a baseline platelet count <100,000/μl. Cohort 1 was expanded to include six patients due to treatment-related neutropenia and thrombocytopenia. It was recommended by the Data Safety Monitoring Board to decrease the dose of gemcitabine from 1,250 to 1,000 mg/m^2. The next three enrolled patients tolerated carboplatin AUC = 5 and gemcitabine 1,000 mg/

TABLE 2 | Patient characteristics.

Cohort/Dose	Tumor Type	Age	Gender	Race	ECOG PS	SAE/AE
1 (CQ) dose level 50 mg	NSCLC-squamous	57	AA	M	1	Neutropenia thrombocytopenia (DLT)
1 dose level 50 mg	NSCLC-adenocarcinoma	41	W	F	2	
1 dose 50 mg	NSCLC	71	W	F	1	
1 dose level 50 mg	GIST	51	W	M	2	Anemia (not DLT)
1 dose level 50 mg	HCC	48	AA	F	1	Diarrhea grade 2
1 dose level 50 mg	Esophageal cancer	55	W	M	1	Anemia (not DLT)
2 (HCQ) dose level 100 mg	HCC	64	AA	F	1	Neutropenia (not DLT)
2 (HCQ) dose level 100 mg	NSCLC-adenocarcinoma	58	W	M	1	
2 dose level 100 mg	HCC	68	AA	F	1	Fatigue (not DLT), nausea, vomiting, thrombocytopenia (grade 2)
3 (HCQ) dose level 150 mg	Urothelial carcinoma	84	Asian	M	0	Fatigue, rash grade I, HTH grade 2
3 (HCQ) dose level 150 mg	Cholangiocarcinoma	68	W	M	1	Neutropenia
3 (HCQ) dose level 150 mg	Refractory SCLC	51	W	M	1	
Expansion (HCQ) dose level 100 mg	NSCLC	61	W	M	2	
Expansion (HCQ) dose level 100 mg	Head and neck cancer	55	W	M	0	
Expansion (HCQ) dose level 100 mg	Metastatic rectal cancer	66	AA	M	1	
Expansion (HCQ) dose level 100 mg	Metastatic colorectal cancer	43	W	M	1	
Expansion (HCQ) Dose Level 100 mg	Other	47	W	F	1	
Expansion (HCQ) dose level 100 mg	Other	65	W	M	0	
Expansion (HCQ) dose level 100 mg	Metastatic adenocarcinoma	57	W	M	0	
Expansion (HCQ) dose level 100 mg	Metastatic adenocarcinoma	61	W	M	0	
Expansion (HCQ) dose level 100 mg	Other	61	W	F	1	
Expansion (HCQ) Dose level 100 mg	Other	57	AA	F	0	

Variable	Number (N)	Percentage %
Age in years (median–range)	**Median**	**Range**
	58	**41–84**
Gender		
Male	15	68
Female	7	32
Race White (W)	15	68
African American (AA)	6	27
Asian (A)	1	5
ECOG PS 0	5	22
1	14	64
2	3	14
Histology		
Non-small cell lung cancer, adenocarcinoma	5	23
Non-small cell lung cancer, squamous cell carcinoma	4	18
Other (small cell, urothelial, hepatocellular, and cholangiocarcinoma)	13	59
Number of prior regimens		
0	3	14
1	5	22
2	3	14
≥3	11	50

TABLE 3 | Clinical outcome.

Outcome	Number of patients (N)	Percentage (%)
Response rate		
PR	1	
SD	15	5
PD	6	68
		27
Disease control		
Rate		
>6 months		48
>12 months		21
>18 months		14

TABLE 4 | Table of adverse events.

Event	Grade 2	Grade 3	Grade 4	Grade 5	Total all grades (N)
Fatigue	1	1			2
Rash	1				1
Dehydration		1			1
Leucopenia (Persistent > 7 days)	1 (Baseline)	3			4
Neutropenia (persistent >7days)	1 (Baseline)	3	5		9
Anemia (persistent >7 days)		3	1		4
Thrombocytopenia (persistent >7 days)		2	1		3
Elevated transaminases		2			2
Elevated serum creatinine		1			1
Hyponatremia		1			1
Pain		4 (Unrelated)			4
Weakness		1			1

m^2 days 1 and 8 in addition to CQ 50 mg with no DLT. HCQ replaced CQ due to an international shortage of CQ at that time. The second cohort included three patients who were treated with HCQ 100 mg daily with no DLT. The first two cohorts of that study thus showed no DLTs at doses of 50 and 100 mg of CQ and HCQ subsequently. The third patient cohort included three patients treated with HCQ 150 mg daily, and two of them experienced DLT due to grade 4 thrombocytopenia and grade 3 neutropenia of more than 7 days duration. The patient with neutropenia did not receive growth factor support. There were no protocol-related deaths.

One DLT occurred in two patients treated with HCQ 150 mg qd group, and the MTD for this combination was determined to be HCQ 100 mg daily. Subsequently, 10 patients were enrolled in the expansion cohort at HCQ 100 mg with carboplatin and gemcitabine.

Efficacy

While assessing the response rate (RR) for various patients included in this study, 1 patient achieved partial response (PR) (5%), 15 patients had stable disease (SD) (68%), while 6 patients had progressive disease (PD) (27%). Nevertheless, the disease control rate (DCR) was 48% for more than 6 months duration, 21% for more than 12 months, and 14% for more than 18 months. In the univariate analysis of predictors of all-cause mortality and predictors of disease progression, neither age, gender, nor number of cycles was statistically significant. Overall, the response rate was 71%. PFS was 48% at 6 months. The DCR was 68% at 6 months, and median overall survival (OS) was 30% at 1 year (**Figure 1**).

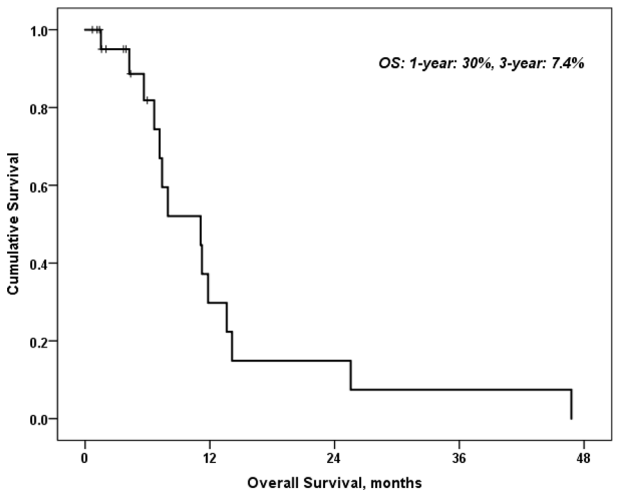

FIGURE 1 | Overall survival of patients with HCQ and carboplatin and gemcitabine.

Efficacy of Subsequent Therapies

Interestingly, we observed that patients receiving subsequent immunotherapy after progressing on this clinical trial had excellent clinical outcomes. One patient with squamous cell carcinoma of the lung (cohort 1) had prolonged stable disease of 11 months on carboplatin and gemcitabine + HCQ. Similarly, prolonged stable disease was noted in a patient with small cell lung cancer in cohort 3 who experienced disease progression on this protocol but then benefited from subsequent nivolumab therapy with a partial remission and improvement of performance status from ECOG 2 to 0. This patient had an ongoing response following 15 cycles of the PDL-1 inhibitor. Another elderly patient in cohort 3 with progressive urothelial cancer tolerated the protocol treatment well with no serious adverse events. This patient achieved disease control with subsequent atezolizumab therapy (**Figure 2**).

LABORATORY CORRELATES

To assess the effects of treatment on the autophagy pathway, we developed a panel of relevant assays.

Quantification of Autophagosomes

Study Population

This study included 24 patients who were recruited in 4 cohorts, namely, cohort 1 (n=6), cohort 2 (n=3), cohort 3 (n=3), and extension cohort (n=8). All patients were histologically diagnosed with advanced solid. All subjects provided a written informed consent before treatment in accordance with the Declaration of Helsinki, and the study protocol was approved by the Institutional Review Board of the University of Cincinnati

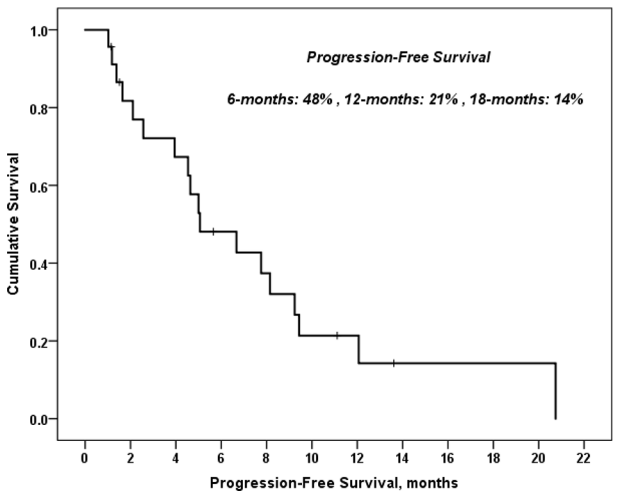

FIGURE 2 | Progression free survival of patients with HCQ and carboplatin and gemcitabine.

Hospital. The subjects enrolled have failed their previous lines of treatment, and the proposed chemotherapy regimen (carboplatin/gemcitabine) was considered a standard of care

Exosome extraction

From Patients Plasma

Patients' blood samples were collected at the mentioned time points and span down at 1,500*g* for 15 min. The upper phase (plasma) was collected in new tubes and stored at −80°C until use. Exosome's extraction was done using an exosome extraction reagent (total exosomes precipitation reagent from plasma, Invitrogen by Thermo Fisher Scientific, Ref: 4484451) following the manufacturer's instructions, then suspended in PBS and stored at −80°C.

Western blotting

Detection of LC3b expression in the isolated exosomes was done using Western blotting following standard protocols. LI-COR detection was used to scan the membranes. LC3B protein detection was achieved by anti-LC3B rabbit monoclonal antibody (Cell Signaling Inc., catalogue #2775, USA). CD9 was used as a loading control and was blotted using rabbit monoclonal antibody (#3700) from Cell Signaling Technology Inc. All Western blots were run on 4–15% gradient gels after estimating and unifying sample protein content by bicinchoninic acid (BCA).

LC-3B conversion from LC-3B I to II has been used as an indicator for autophagy, since it measures the dynamicity of the process by reflecting the turnover of autophagosome fusion with lysosomes (16). However, increased expression of both isoforms is used to measure the activity of both autophagy inducers and inhibitors (17, 18).

This methodology is simple and cost effective, which may track stimulus effect on autophagy by interpretation of Western blotting compared to well-known controls.

PHARMACOKINETICS

Metabolism of Chloroquine/ Hydroxychloroquine

CQ/HCQ was 60% bound to plasma proteins and cleared equally by the kidney and liver. Following administration of C, it was rapidly de-alkylated *via* cytochrome p450 (CYP) into active desethylchloroquine and bisdesethylchloroquine with elimination half-lives of 20–60 days. Both parent drug and metabolite can be detected in urine months after a single dose.

CQ/HCQ has a rapid and almost complete absorption and peak plasma concentrations reached within 1–2 h following oral administration. CQ/HCQ has a long half-life of 3–5 days. For pharmacokinetic analysis, blood samples (5 ml per time point) were collected on day −7 at baseline pre-dose, then at 1, 2, 4, 6, and 24 h on day 1. Trough levels were collected at days 8 and 15. Blood samples were collected at each subsequent cycle (cycles 2–4) on day 1 at 1, 2, 4, 6, 24, 48, and 72 h. Trough levels were collected on days 8 and 15 for cycles 2–4. Blood was collected into B-D vacutainer tubes containing K3-EDTA mixed and centrifuged at 1,500*g* for 10 min at 4°C. Plasma will be transferred into a storage tube and maintained on dry ice until stored in a −20°C freezer. Post-dose trough levels for CQ/HCQ were measured on days 8, 15, and 22 (15).

Pharmacokinetic (PK) estimates were determined using drug concentrations measured at each time point after HCQ dosing. The maximum plasma concentration (Cmax), time to maximum concentration (Tmax), and area under the concentration–time curve from 0 to 360 h post-dose (AUC0-360h) were determined for the subject following an oral dose. AUC0-360h was calculated using the trapezoidal rule with the linear trapezoidal linear interpolation method. The terminal elimination half-life for each participant was calculated using the last three data points.

For analysis of plasma HCQ, 100 ml of each sample was placed in a low-retention microcentrifuge tube (Thermo Fisher) and spiked with 500 ng of D4-hydroxychloroquine (D4-HCQ; Cayman Chemicals, Ann Arbor, MI). Acetonitrile (300 ml) was added, and the samples were agitated using a vortex mixer for 1 min. The samples were then centrifuged at 10,000*g* for 5 min at 440°C, and 250 ml of the supernatant was transferred to glass high-performance liquid chromatography (HPLC) tubes for mass spectroscopic analysis. Mass spectroscopic acquisition was performed with an ABSciex TripleTOF 5600 (ABSciex, Foster City, CA, USA) equipped with an electrospray interface with a 50-mm i.d. capillary and coupled to an Eksigent µUHPLC (Eksigent, Redwood City, CA, USA). Analyst TF 1.7 software was used to control the instrument and for data processing and acquisition. The optimized MRM parameters were used to monitor HCQ and D4-HCQ. HCQ, the parent ion, was 337.2, and the selected MRM MS/MS ion was 248.15. For D4-HCQ, the parent ion was 341.2, and the selected MRM MS/MS ion was 252.12. Separation was performed on a reversed-phase ACE C18 50 mm × 0.5 mm column, which was maintained at 450°C. Samples were injected by loop overfilling into a 2-ml loop. For the 2.5-min LC gradient, the mobile phase consisted of solvent A (0.1% v/v formic acid in water) and solvent B (0.1% v/v formic acid in acetonitrile) at

a flowrate of 40 ml/min. Gradient started from 95:5 A:B. Data integration and quantification were performed with MultiQuant software (ABSciex) using the area under the curve (**Tables 5**, **6**).

DISCUSSION

Our study determined an MTD for HCQ that was very close to the dose determined in a study using CQ in addition to the standard therapy for patients with glioblastoma multiforme (5).

One limitation of our study is that we used HCQ instead of CQ for the continuation of the study due to the acute shortage of CQ in the US and the inability of our institution to obtain CQ.

Our study used CQ or HCQ combined with carboplatin and gemcitabine (CG) in a heavily pretreated patient population with various advanced solid tumors. As a result, the MTD appeared to be much lower than the MTD dose of CQ or HCQ in reported other studies (19). The highest-dose cohort in the current study included patients who were heavily pretreated and experienced >7 days of either neutropenia or thrombocytopenia. No on-study deaths occurred. Other trials that incorporated either CQ or HCQ were able to deliver higher doses of these agents given that these studies included agents that are not usually myelosuppressive (19) or in chemotherapy-naive subjects (20).

Subsequent responses to immunotherapeutic agents such as PD-1 or PD-L1 inhibitors may be considered in the future. Autophagymodifying agents combined with evolving immunotherapy as a potential new treatment option may offer an interesting area for additional studies, both in the laboratory and clinic. Autophagy is involved in the processing of tumor antigens and their presentation to the immune system and thus may be considered as a line of defense against cancer.

Autophagic pathways induced by hypoxia in the tumor microenvironment can impair antitumor immune responses mediated by cytotoxic T-lymphocytes (CTL) and natural killer (NK) cells and has also been shown to enhance the immunosuppressive properties of myeloid-derived suppressor cells (MDSCs) (20). In response to hypoxia, the hypoxia-inducible family of transcription factors (HIFs) does not become ubiquitinated, thus evading degradation by the ubiquitin–proteasome system. As a result, they accumulate in the cytoplasm and are transported to the cell nucleus leading to the activation of about 300 genes involved in many biological processes, including angiogenesis, enhanced cell survival, metastasis, induction of a stem cell-like phenotype, and immune escape (20). Targeting HIF-2α decreases PD-L1 expression, whereas HIF-2α overexpression increases both PD-L1 mRNA and protein expression in renal cancer cells (21).

In his study, Wolpin et al. used HCQ as monotherapy for previously treated metastatic pancreatic cancer, and he achieved much lower median PFS and OS (46.5 and 69.0 days, respectively) while using higher doses or HCQ (400 and 600

TABLE 5 | Pharmacokinetics of patients 9–13 in cycle 1.

	Cycle 1							
Time	9	10	11	12	13	Mean	SD	SEM
D-7	0.0	0.0	102.1	0.0	0.0	20.4	45.7	20.5
D1 1h	206.0	46.2	82.6	161.2	123.4	123.9	63.0	28.2
D1 2h	263.5	75.4		172.1	150.8	165.5	77.4	38.7
D1 4h	320.5	70.7	224.6	183.3	174.5	194.7	90.3	40.5
D1 6h	229.0	57.1	235.7	192.4	116.4	166.1	77.2	34.6
D1 24h	160.5	22.1		78.6	126.7	97.0	60.2	30.1
D1 48h			58.2			58.2		0.0
D1 72h								
D8	101.0	38.3	119.6	175.2	32.1	93.2	59.7	26.7
D15	57.0	7.5		93.4	0.0	39.5	43.9	22.0

SD, Standard deviation, SED, Standard error of mean.

TABLE 6 | Pharmacokinetics of patients 9–13 in cycle 2.

	Cycle 2							
Time	**9**	**10**	**11**	**12**	**13**	**Mean**	**SD**	**SEM**
D-7								
D1 1h		60.3	29.7	220.6		103.6	102.5	59.3
D1 2h		109.6	37.8	250.7		132.7	108.3	62.6
D1 4h		88.9	25.7			57.3	44.7	31.7
D1 6h		105.3	22.7	239.4		122.4	109.4	63.2
D1 24h		97.2	20.5	50.2		56.0	38.7	22.4
D1 48h			71.9	224.8		148.3	108.1	76.7
D1 72h			49.2	380.7		214.9	234.4	166.3
D8		64.1	58.9	122.6		81.9	35.4	20.4
D15			44.9	53.7		49.3	6.2	4.4

SD, Standard deviation, SED, Standard error of mean.

mg twice daily dose) (22). In addition, Malhotra et al. used chemotherapy [carboplatin, paclitaxel (and bevacizumab if meeting criteria)] in addition to HCQ (twice daily dose of 200–600 mg) in newly diagnosed non-small cell lung cancer (NSCLC) patients achieving a PFS of 3.7 months, thus demonstrating an improved response with addition of HCQ even with lower doses to the CG chemotherapy regimen (23).

Barbeau et al. (24) concluded that for increased survival, early or advanced stages are dependent on autophagy. The high metabolic demand and increased resistance to chemotherapeutic agents are dependent on autophagy *via* genetic mutations, such as *EGFR*, *EGFRvIII*, and *BRAFv600E*. Compter et al. (25) have described the role of autophagy in glioblastoma cells expressing *EGFRvIII*. The maximum tolerated dose of CQ was 200 mg. The median overall survival time was 16 months. The median survival of patients with *EGFRvIII*– was 11.5 months and that of patients with *EGFRvIII*+ was 20 months. In their study, a total of 44 adverse events were related to CQ with QT prolongation and blurring of vision along with nausea and vomiting. In our study, the overall median survival was 11 months, and the MTD was 100 mg, with neutropenia and thrombocytopenia as the limiting factors. Levy et al. suggested a role for the molecular mechanisms by which autophagy affects the tumor microenvironment (26).

CONCLUSION

The results from this study demonstrate that HCQ opens a new era for heavily treated HCQ-naive patients to receive HCQ in addition to chemotherapy, thus improving both PFS and overall survival. These are still ambitious hypotheses that need further research, and that is why we need to expand our trial to phase II.

The switch from CQ to HCQ had to occur due to the acute shortage of CQ supply during the time of the phase I clinical trial, which might be a limitation to our study.

DATA AVAILABILITY STATEMENT

The original contributions presented in the study are included in the article/supplementary material. Further inquiries can be directed to the corresponding author.

ETHICS STATEMENT

The studies involving human participants were reviewed and approved by University of Cincinnati. The patients/participants provided their written informed consent to participate in this study.

AUTHOR CONTRIBUTIONS

All authors listed have made a substantial, direct, and intellectual contribution to the work and approved it for publication.

FUNDING

This trial was funded by the Division of Hematology/Oncology, Department of Internal Medicine, University of Cincinnati. Institutional Support from The University of Cincinnati-Division of Hematology Oncology EXP-1301 clinical trial.

ACKNOWLEDGMENTS

LC-MS/MS was provided by Hugo Gagnon and the team at PhenoSwitch Bioscience—Expert services in mass spectrometry (*via* Science Exchange).

REFERENCES

1. Yang Z, Klionsky DJ. Eaten Alive: A History of Macroautophagy. *Nat Cell Biol* (2010) 12(9):814–22. doi: 10.1038/ncb0910-814
2. Klionsky DJ. Ancient Autophagy. *Autophagy* (2013) 9(4):445–6. doi: 10.4161/auto.23907
3. Viry E, Noman MZ, Arakelian T, Lequeux A, Chouaib S, Berchem G, et al. Hijacker of the Antitumor Immune Response: Autophagy Is Showing Its Worst Facet. *Front Oncol* (2016) 6:246. doi: 10.3389/fonc.2016.00246
4. Mathew R, Karantza-Wadsworth V, White E. Role of Autophagy in Cancer. *Nat Rev Cancer* (2007) 7(12):961–7. doi: 10.1038/nrc2254
5. Sotelo J, Briceño E, López-González MA. Adding Chloroquine to Conventional Treatment for Glioblastoma Multiforme: A Randomized, Double-Blind, Placebo-Controlled Trial. *Ann Internal Med* (2006) 144 (5):337–43. doi: 10.7326/0003-4819-144-5-200603070-00008
6. Tasdemir E, Galluzzi L, Maiuri MC, Criollo A, Vitale I, Hangen E, et al. Methods for Assessing Autophagy and Autophagic Cell Death. In: *Autophagosome and Phagosome*. Clifton NJ: Humana Press (2008). p. 29–76.
7. Amaravadi RK, Thompson CB. The Roles of Therapy-Induced Autophagy and Necrosis in Cancer Treatment. *Clin Cancer Res* (2007) 13(24):7271–9. doi: 10.1158/1078-0432.CCR-07-1595
8. Solomon VR, Lee H. Chloroquine and its Analogs: A New Promise of an Old Drug for Effective and Safe Cancer Therapies. *Eur J Pharmacol* (2009) 625(1-3):220–33. doi: 10.1016/j.ejphar.2009.06.063
9. Hu C, Solomon VR, Ulibarri G, Lee H. The Efficacy and Selectivity of Tumor Cell Killing by Akt Inhibitors Are Substantially Increased by Chloroquine. *Bioorg Med Chem* (2008) 16(17):7888–93. doi: 10.1016/j.bmc.2008.07.076
10. Chude CI, Amaravadi RK. Targeting Autophagy in Cancer: Update on Clinical Trials and Novel Inhibitors. *Int J Mol Sci* (2017) 18(6):1279. doi: 10.3390/ijms18061279
11. Rangwala R, Leone R, Chang YC, Fecher LA, Schuchter LM, Kramer A, et al. Phase I Trial of Hydroxychloroquine With Dose-Intense Temozolomide in Patients With Advanced Solid Tumors and Melanoma. *Autophagy* (2014) 10 (8):1369–79. doi: 10.4161/auto.29118
12. Vogl DT, Stadtmauer EA, Tan K-S, Heitjan DF, Davis LE, Pontiggia L, et al. Combined Autophagy and Proteasome Inhibition: A Phase 1 Trial of Hydroxychloroquine and Bortezomib in Patients With Relapsed/Refractory Myeloma. *Autophagy* (2014) 10(8):1380–90. doi: 10.4161/auto.29264
13. Tanida I, Ueno T, Kominami E. LC3 and Autophagy. *Methods Mol Biol (Clifton NJ)* (2008) 445:77–88. doi: 10.1007/978-1-59745-157-4_4
14. Karasic TB, O'Hara MH, Loaiza-Bonilla A, Reiss KA, Teitelbaum UR, Borazanci E, et al. Effect of Gemcitabine and Nab-Paclitaxel With or Without Hydroxychloroquine on Patients With Advanced Pancreatic Cancer: A Phase 2 Randomized Clinical Trial. *JAMA Oncol* (2019) 5 (7):993–8. doi: 10.1001/jamaoncol.2019.0684
15. Carew JS, Kelly KR, Nawrocki ST. Autophagy as a Target for Cancer Therapy: New Developments. *Cancer Manage Res* (2012) 4:357. doi: 10.2147/CMAR.S26133

16. Redmann M, Benavides GA, Berryhill TF, Wani WY, Ouyang X, Johnson MS, et al. Inhibition of Autophagy With Bafilomycin and Chloroquine Decreases Mitochondrial Quality and Bioenergetic Function in Primary Neurons. *Redox Biol* (2017) 11:73–81. doi: 10.1016/j.redox.2016.11.004
17. Sharifi MN, Mowers EE, Drake LE, Macleod KF. Measuring Autophagy in Stressed Cells. In: *Stress Responses*. New York, NY: Humana Press (2015). p. 129–50.
18. Goldberg SB, Supko JG, Neal JW, Muzikansky A, Digumarthy S, Fidias P, et al. A Phase I Study of Erlotinib and Hydroxychloroquine in Advanced Non–Small-Cell Lung Cancer. *J Thorac Oncol* (2012) 7(10):1602–8. doi: 10.1097/JTO.0b013e318262de4a
19. ClinicalTrials.gov. *Hydroxychloroquine, Carboplatin, Paclitaxel, and Bevacizumab in Recurrent Advanced Non-Small Cell Lung Cancer*. Clinicaltrials.gov: Identifier: NCT00728845. (2013)
20. Messai Y, Gad S, Noman MZ, Le Teuff G, Couve S, Janji B, et al. Renal Cell Carcinoma Programmed Death-Ligand 1, a New Direct Target of Hypoxia-Inducible Factor-2 Alpha, Is Regulated by Von Hippel–Lindau Gene Mutation Status. *Eur Urol* (2016) 70(4):623–32. doi: 10.1016/j.eururo.2015.11.029
21. Malhotra J, Jabbour S, Orlick M, Riedlinger G, Joshi S, Guo JY, et al. Modulation of Autophagy With Hydroxychloroquine in Patients With Advanced Non-Small Cell Lung Cancer (NSCLC): A Phase Ib Study. *J Clin Onco* (2018) 36(15_suppl): e21138. doi: 10.1200/JCO.2018.36.15_suppl.e21138
22. Wolpin BM, Rubinson DA, Wang X, Chan JA, Cleary JM, Enzinger PC, et al. Phase II and Pharmacodynamic Study of Autophagy Inhibition Using Hydroxychloroquine in Patients With Metastatic Pancreatic Adenocarcinoma. *Oncol* (2014) 19(6):637–8. doi: 10.1634/theoncologist.2014-0086
23. Patel S, Hurez V, Nawrocki ST, Goros M, Michalek J, Sarantopoulos J, et al. Vorinostat and Hydroxychloroquine Improve Immunity and Inhibit Autophagy in Metastatic Colorectal Cancer. *Oncotarget* (2016) 7(37):59087. doi: 10.18632/oncotarget.10824
24. Barbeau LMO, Tom GHK, Rouschop K. Tumors Responsive to Autophagy-Inhibition: Identification and Biomarkers. *Cancers* (2020) 12(9):2463. doi: 10.3390/cancers12092463
25. Compter I, Eekers DBP, Hoeben A, Rouschop KMA, Reymen B, Ackermans L, et al. Chloroquine Combined With Concurrent Radiotherapy and Temozolomide for Newly Diagnosed Glioblastoma: A Phase IB Trial. *Autophagy* (2021) 17(9):2604–12. doi: 10.1080/15548627.2020.1816343
26. Mulcahy L, Jean M, Thorburn A. Autophagy in Cancer: Moving From Understanding Mechanism to Improving Therapy Responses in Patients. *Cell Death Differ* (2020) 27(3):843–57. doi: 10.1038/s41418-019-0474-7

Conflict of Interest: Author AK was employed by GlaxoSmithKline.

The remaining authors declare that the research was conducted in the absence of any commercial or financial relationships that could be construed as a potential conflict of interest.

Publisher's Note: All claims expressed in this article are solely those of the authors and do not necessarily represent those of their affiliated organizations, or those of the publisher, the editors and the reviewers. Any product that may be evaluated in this article, or claim that may be made by its manufacturer, is not guaranteed or endorsed by the publisher.

frontiers | Frontiers in Oncology

ORIGINAL RESEARCH
published: 31 May 2022
doi: 10.3389/fonc.2022.911615

Carnosol Induces p38-Mediated ER Stress Response and Autophagy in Human Breast Cancer Cells

Halima Alsamri[1†], Aysha Alneyadi[1†], Khalid Muhammad[1], Mohammed Akli Ayoub[1], Ali Eid[2] and Rabah Iratni[1]*

[1] Department of Biology, College of Science, United Arab Emirates University, Al Ain, United Arab Emirates, [2] Department of Basic Medical Sciences, College of Medicine, Qatar University Health, Qatar University, Doha, Qatar

We recently reported that carnosol induces ROS-dependent autophagy and apoptosis in breast cancer cells. We also reported that carnosol inhibits breast cancer cell migration, invasion, and *in ovo* tumor growth, as well as targets STAT3, PCAF, and p300 to proteasome degradation. Here, we investigated the molecular mechanisms underlying its anti-malignant activity in breast cancer. We report that carnosol induces a ROS-dependent type I and type II programmed cell death (PCD-I or PCD-II, respectively), which occurred independently of each other. Indeed, chemical inhibition of autophagy had no effect on the induction of apoptosis, evident by the absence of cleaved PARP. Electron microscopy revealed that carnosol-treated cells exhibited enlarged endoplasmic reticulum, characteristic of ER stress. Markers of the three unfolded protein response pathways (PERK, IRE-1 α, and ATF6), namely ATF4, CHOP, phospho-IRE-1α, XBP1S, and cleaved ATF6 were upregulated in a ROS-dependent manner. In addition, carnosol induced a ROS-dependent activation of p38MAPK, increased the overall level of protein polyubiquitination, and targeted mTOR protein to proteasome degradation. Interestingly, inhibition of p38MAPK, by SB202190 and 203580, reduced cell death, selectively blocked the induction of IRE-1α and ATF6 UPR sensors and inhibited autophagy. In addition, inhibition of p38 reduced the carnosol-induced polyubiquitination and rescued mTOR, PCAF, and STAT3 from proteasomal degradation. Importantly, activation of PERK sensors and induction of apoptosis occurred independently of p38 activation. Taken together, our results suggest that ROS-dependent induced-ER stress contributes to carnosol-induced apoptotic and autophagic cell death in breast cancer cells, and further confirm that carnosol is a promising agent for breast cancer therapy.

Keywords: p38MAPK, ER stress, proteasome, breast cancer, ROS, unfolded protein response, autophagy

OPEN ACCESS

Edited by:
Abdelhabib Semlali, Laval University, Canada

Reviewed by:
Tarek Benameur, King Faisal University, Saudi Arabia
Tannaz Jamialahamdi, Mashhad University of Medical Sciences, Iran

***Correspondence:**
Rabah Iratni
R_iratni@uaeu.ac.ae

[†]These authors have contributed equally to this work

Specialty section:
This article was submitted to Cancer Molecular Targets and Therapeutics, a section of the journal Frontiers in Oncology

Received: *02 April 2022*
Accepted: *03 May 2022*
Published: *31 May 2022*

Citation:
Alsamri H, Alneyadi A, Muhammad K, Ayoub MA, Eid A and Iratni R (2022) Carnosol Induces p38-Mediated ER Stress Response and Autophagy in Human Breast Cancer Cells. Front. Oncol. 12:911615. doi: 10.3389/fonc.2022.911615

INTRODUCTION

The endoplasmic reticulum (ER) is a multifunctional organelle that is mainly responsible for protein folding and trafficking, in addition to maintaining other cellular functions. Changes in the protein-folding environment evoke accumulation of unfolded or misfolded proteins in the ER lumen, which profoundly affects several cellular processes and causes ER stress (1). This stress induces a collection

of adaptive signaling pathways called an unfolded protein response (UPR) which involves the restoration of an efficient protein-folding environment and proper re-folding of misfolded protein (2). However, when ER stress is too severe to be rescued, UPR triggers autophagy and/or apoptosis (3, 4).

UPR is a highly regulated cascade system that involves three key sensors located on the ER membrane: protein kinase R-like ER kinase (PERK), transcription factor 6 (ATF6), and inositol requiring enzyme 1α (IRE1α) (2). Upon ER stress, PERK phosphorylates the alpha subunit of the eukaryotic translation initiation factor-2 (eIF2α). This, in turn, rapidly attenuates protein translation and decreases the overload of proteins in the ER lumen. This action also promotes the expression of the UPR transcription factor ATF4, which triggers apoptosis through activating the pro-apoptotic CCAAT/enhancer-binding protein-homologous protein (CHOP) leading to cell arrest or death (5, 6). CHOP can be induced by PERK/ATF4 and ATF6 (7–9), another UPR sensor. Under ER stress, ATF6 is transported to the Golgi apparatus and cleaved into fragments that can function as transcription factors. Activated ATF6 is known to regulate the expression of genes involved in the degradation of misfolded proteins (3). The third UPR sensor is IRE1, a kinase and an endoribonuclease (RNase), which upon activation, catalyzes the splicing of X-box binding protein 1(XBP1) mRNA. XBP1s is a transcription activator of essential genes known to regulate protein folding, trafficking, phospho-lipid biosynthesis, and ER membrane expansion (10, 11).

Accumulated evidence suggests that UPR signaling cascades are activated in response to oxidative stress or reactive oxygen species (ROS) accumulation (12). Abnormal increases in ROS damage cellular lipids, proteins, and DNA, resulting in irreversible oxidative damage, which ultimately leads to cell death and may culminate in pathologies like neurogenerative or cardiovascular disease (13). On the other hand, several studies have suggested the beneficial effects of ROS generation on chemotherapy-induced cell death in cancer cells (14–16). For example, bortezomib (17), apatinib (18), doxorubicin, inostamycin, vinblastin, xanthine oxidase–conjugated polymer, and camptothecin are chemotherapeutic agents that were shown to induce apoptosis by increasing ROS production (19, 20). Since some tumor cells are more sensitive to ROS than normal cells (14), the generation of ROS could be an effective approach for selectively killing cancer cells without causing significant toxicity (21, 22). Finding a new drug that stimulates ROS production and ultimately leads to UPR activation would be an attractive approach in the hunt for new effective therapeutic approaches in the fight against cancer.

A large variety of polyphenolic compounds are found in teas, vegetables, and fruits. These compounds possess different pharmacologic properties, including anticancer effects (23). Most dietary and synthetic polyphenols are known to be safe even at relatively high concentrations. Thus, polyphenols are considered promising candidates for use in developing novel anticancer drugs (24, 25). Some of these compounds exhibit their anticancer activity through ROS production and ER stress (26, 27). Moreover, preclinical studies reveal that bioactive dietary polyphenols exert anticancer effects by inducing ROS-mediated cytotoxicity in cancer cells (28).

Carnosol is a phenolic compound isolated from culinary herbs including sage, oregano, and rosemary. Currently, the interest in carnosol is on the rise due to its health-promoting properties, especially its anticancer activities in the colon (29), breast (30, 31), gastric (32) and prostate (33) cancers. Indeed, we recently showed that carnosol inhibits migration, metastasis, and tumor growth of breast cancer *via* a ROS-dependent proteasome degradation of STAT3 (31). We also reported that carnosol induces ROS-mediated beclin1-independent autophagy and apoptosis in triple-negative breast cancer (30). More recently, we showed that carnosol selectively inhibits the p300 histone acetyl transferase in breast cancer cells (34). Here, we show that carnosol triggers a ROS-dependent ER-stress response through activation of the three ER stress sensor pathways in breast cancer cells. In addition, we show that carnosol induces p38-dependent autophagy and activates the ubiquitin proteasome pathway.

MATERIALS AND METHODS

Cell Culture, Chemicals, and Antibodies

Human breast cancer cells MDA-MB-231(cat. 300275) were purchased from Cell Line Service (CLS)-GmbH, Germany. Cells were cultured in high glucose Gibco Dulbecco's Modified Eagle Medium (DMEM) (cat. 03640, Gibco, Life Technologies, Rockville, UK) supplemented with 10% fetal bovine serum (cat. 02187, Gibco, Life Technologies, Rockville, UK), 100 U./ml penicillin/streptomycin (cat. 01574, Gibco, Life Technologies, Rockville, UK). All Cells were maintained at 37°C under a humidified atmosphere containing 5% CO2. Carnosol (cat. C9617), and N-acetylcysteine (cat. A9165) were obtained from Sigma Aldrich (Saint-Quentin Fallavier, France). Pan-caspase inhibitor (cat. 627601) and 3-methyladenine (cat.189490) were obtained from Millipore (Hayward, CA, USA). SB 203580 (cat. Ab120162), SB 202190 (cat. Ab1206388158), and chloroquine (cat. Ab142116) were obtained from Abcam (Cambridge, UK). Bortezomib (cat. 2204) was obtained from cell signaling technologies (Beverly, MA, USA). Antibodies to phospho-mTOR (cat. 2972), total mTOR (cat. 2972), total IRE-1 (cat. 3294), XBP-1s (cat. 12782), phospho-eIF2α (cat.9721), eIF2α (cat.9722), ATF4 (cat. 11815), CHOP (cat. 2895), PDI (cat. 3501), Ero-1α (cat. 3264), phospho-p38 (cat. 4511), total p38 (cat.8690), LC3 (cat. 1274), STAT3 (cat. 9139) and ubiquitin (cat.3933) were obtained from Cell Signaling (Beverly, MA, USA). Antibodies to phospho-IRE-1 (cat Ab226974) and cleaved PARP (cat. Ab4830) were obtained from Abcam (Cambridge, UK). Antibody to cleaved ATF6 (cat. A12570) was obtained from AB clonal (Woburn, MA, USA). Antibodies to PCAF (cat. Sc13124) antibody, β-actin (Sc-47778), goat anti-mouse IgG-HRP (Cat. # sc-2005), and goat anti-rabbit IgG-HRP antibody (Cat. # sc-2004) were from Santa Cruz Biotechnology Inc (USA).

Cellular Viability

Cells were seeded in triplicate in 12-well plates at a density of 50,000 cells/well and left in culture for 24 hours before treatment with or without carnosol for 24 hours. Cellular viability was measured with the Muse Cell Analyzer (Millipore, Hayward, CA, USA) using the Muse Count and Viability Kit (Millipore, Hayward, CA, USA) which differentially stains viable and dead cells based on their permeability to two DNA binding dyes. Data were presented as proportional viability (%) by comparing the treated vs. the untreated cells, the viability of which is considered to be 100%.

Analysis of the Mitochondrial Membrane Potential

Cells (50,000) grown in 12-well plates for 24 hours were first treated with or without carnosol for 24 h in the presence or absence of the indicated inhibitors, collected by trypsinization, washed, and incubated with the Muse Mitopotential Dye (Muse MitoPotential kit, Millipore), a cationic lipophilic dye, for 20 min in a 37°C CO2 incubator. Cells were then incubated with 7-AAD, a dead cell marker, for an additional 5 min at room temperature. The mitochondrial membrane potential changes were determined using the Muse Cell Analyzer (Millipore).

Transmission Electron Microscopy

Transmission electron microscopy (TEM) was carried out as previously described (REF carnosol paper PLOS one). Briefly, Control and carnosol-treated cells were fixed in fixation buffer (2% paraformaldehyde, 2.5% glutaraldehyde in 0.1 M sodium cacodylate, pH 7.2) overnight at 4°C, before being post-fixed with 1% OsO4 for 1 h. Cells were then dehydrated in a graded ethanol series and embedded in Agar 100 epoxy resin. Ultrathin sections were mounted on Cu grids and stained first with uranyl acetate followed by lead citrate. Sections were observed and photographed under a Philips CM10 Transmission Electron Microscope.

Whole Cell Extract and Western Blotting Analysis

Breast cancer cells (1.8×10^6) were seeded in 10 cm tissue culture dishes and left in culture for 24 hours. Cell s were then treated with or without carnosol in the presence or absence of N-acetylcysteine, SB 203580, or SB202190 for another 24 hours. Cells were washed twice with ice-cold PBS, scraped, and collected by centrifugation at 2000 rpm for 5 min. The pelleted cells were then lysed in RIPA buffer (ThermoFisher Scientific) containing protease inhibitor cocktail (Roche) and phosphatase inhibitor (Roche) followed by incubation for 30 min on ice. Cell lysates were centrifuged at 14,000 rpm for 20 min at 4°C, and the supernatants were collected. Total protein concentration was quantified by a BCA protein assay kit (ThermoFisher Scientific) and the lysates were adjusted with lysis buffer. Aliquots of 20 μg of total cell lysate were loaded and resolved onto 6–15% SDS-PAGE. After electrophoresis, proteins were transferred from the gels to PVDF membranes (Thermo Scientific) and blocked for 1 h at room temperature with 5% non-fat dry milk in TBST (TBS and 0.05% Tween 20). The membranes were immunoblotted with specific primary antibodies in blocking buffer overnight at 4°C and then with horseradish peroxidase-conjugated secondary antibodies against rabbit or mouse IgG. Immunoreactive protein bands were detected, depending on the targeted protein, by ECL chemiluminescent substrate (ThermoFisher Scientific) or SuperSignal™ West Femto Maximum Sensitivity Substrate (ThermoFisher Scientific) and, chemiluminescence was detected using the LiCOR C-DiGit blot scanner (LI-COR Biosciences). Quantification was carried using the ImageJ software.

Statistical Analysis

Data were presented as means ± S.E.M. Differences between groups were analyzed using a Student's t-test for paired or unpaired values. Graphpad prism (v.6.0) software was used for statistical analysis. P- values of <0.05 were considered to be statistically significant. Unless otherwise stated, experiments were repeated at least 3 times.

RESULTS

Autophagic and Apoptotic Cell Death Occurs Independently From Each Other in Carnosol-Treated Breast Cancer Cells

We have previously reported that carnosol induced ROS-dependent autophagy and apoptosis in MDA-MB-231 breast cancer cells (30). While autophagy was triggered as early as 6 h post-treatment, apoptosis was detected later. Because both events are known to induce cell death through PCD-I and PCD-II, respectively, we decided to extend our previous work and investigate the contribution of these two events (apoptosis and autophagy) to the cytotoxic activity of carnosol. We first confirmed, by Western blotting, the ROS-dependent induction of apoptosis and autophagy in carnosol-treated cells (**Figure 1A**). Next, we examined the effect of chloroquine (CQ) and 3-methyadenine (3-MA), two autophagy inhibitors, and Z-VAD-FMK, a pan-caspase inhibitor, on cell viability. As shown in **Figure 1B**, cell viability was modestly but significantly improved when autophagy was inhibited compared to control cells treated with carnosol alone. On the other hand, inhibition of apoptosis by Z-VAD-FMK had almost no effect on cell death when compared to cells treated with carnosol alone (**Figure 1B**). Interestingly, a combination of both inhibitors (3-MA and Z-VAD-FMK), restored cell viability, at 50 μM carnosol, to a level comparable to control cells. A high concentration of carnosol (100 μM) led to only a modest recovery of cell viability (**Figure 1B**). As expected, and as previously reported, inhibition of ROS generation by N-acetylcysteine (NAC) completely abolished the cytotoxic effect of carnosol even at high concentration (**Figure 1B**). The fact that cell death still occurred even when autophagy or apoptosis was inhibited, suggests that these two mechanisms of cell death are independent of each other. This is further confirmed by the detection of cleaved PARP (a marker of apoptosis) in cells where autophagy was inhibited by 3-MA (**Figure 1C**). Similarly, inhibition of autophagy by 3-MA did not affect the carnosol-induced loss of mitochondria membrane potential (**Figure 1D**). Taken together, our data suggest that in carnosol-treated cells, autophagy and apoptosis are independent events and both lead to cell death and that one mechanism may indeed compensate for the other.

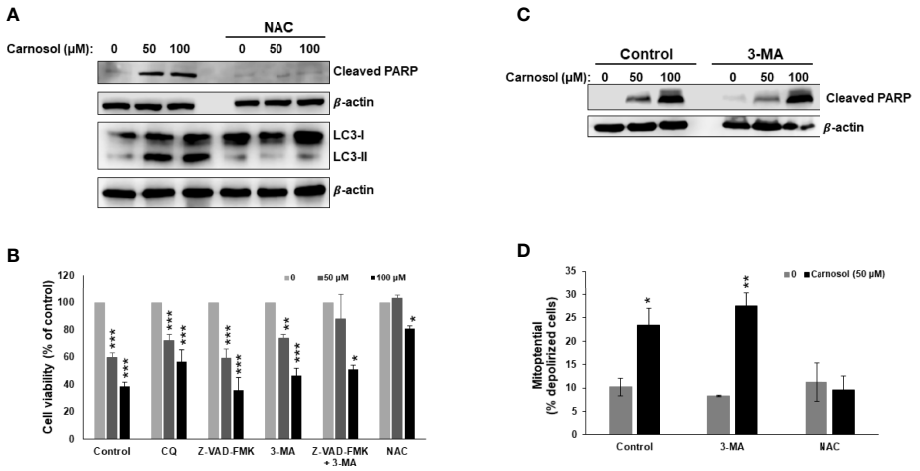

FIGURE 1 | Carnosol induces breast cancer cell death through activation of PCD-I and PCD-II pathways. **(A)** ROS-dependent LC3II accumulation and PARP cleavage in carnosol-treated MDA-MB-231 cells. Cells were pre-treated with the ROS scavenger NAC (10mM) before adding carnosol at the indicated concentrations for 24 hours. Whole cell lysates were analyzed by Western blot for LC3II and cleaved PARP. **(B)** Inhibition of autophagy but not apoptosis reduces carnosol-induced cell death. MDA-MB-231cells were pretreated with the inhibitors of autophagy CQ (50 μM) and 3-MA (10mM), or the pan-caspase inhibitor (Z-VAD-FMK) (50 μM) alone or in combination then treated with carnosol for 24 hours. Cell viability was determined as described in Material and Methods. **(C)** Western blot of cleaved PARP in cells pretreated with and without autophagy inhibitor. **(D)** Inhibition of autophagy failed to restore the carnosol-induced loss of mitochondrial membrane potential in MDA-MB-231 cells. Mitochondrial membrane potential (MMP) of cells pre-treated with 3-MA or NAC, prior to the addition of carnosol for 24 hours, was assessed with the Muse Cell Analyzer using the Muse MitoPotential kit as described in Materials and Methods. Data represent the mean ± SEM of at least 3 independent experiments. Student's t-test was performed to determine the significance (*p<0.05, **p<0.005, and ***p<0.001).

Carnosol Induces Proteasome-Dependent Degradation of mTOR in Breast Cancer Cells

We next examined the effect of carnosol on the mTOR pathway, a major negative regulator of autophagy. This is of particular interest because mTOR signaling is known to be dysregulated in many human cancers, including breast cancer. We first determined the level of phospho-mTOR(ser2448). As shown in **Figure 2A**, carnosol reduced, in a concentration-dependent manner, the level of phosphorylated mTOR, indicating that mTOR pathway is inhibited in treated cells. Strikingly, we also found that carnosol induced a significant decrease in the level of total mTOR (**Figure 2A**). Since carnosol induced autophagy, we

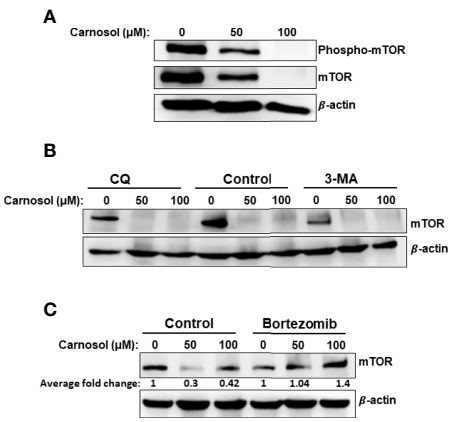

FIGURE 2 | Targeting of mTOR protein to ROS-dependent proteasome degradation. **(A)** Inhibition of mTOR signaling by carnosol in MDA-MB-231 cells. Cells were treated for 24 hours with carnosol (50 and 100 μM) and whole protein lysates were analyzed by Western blot for phosphorylated and total mTOR protein. **(B)** Western blot analysis of mTOR protein level in MDA-MB-231 cells pre-treated with the autophagy inhibitors 3-MA and CQ. Cells were pretreated with or without 3-MA (50 mM) and CQ (50 μM) for 1 h before adding carnosol for 24 hours. **(C)** Carnosol targets mTOR to proteasome degradation. MDA-MB-231 cells were pre-treated for 1 h with or without Bortezomib (25 nM) before treatment with carnosol at the indicated concentrations for 24. Whole protein lysates were resolved on SDS-PAGE and analyzed for mTOR protein.

first sought to determine whether STAT3 was targeted to autophagolysosome degradation. Our interesting results show that blockade of autophagy by 3-MA or CQ did not restore the level of mTOR protein (**Figure 2B**), hence excluding autophagy as a mechanism of degradation of mTOR protein. Next, we tested whether mTOR was a target of proteasomal degradation. We found that bortezomib, a proteasome inhibitor, restored the mTOR protein to a level comparable with that of control cells (**Figure 2C**). This clearly indicates that carnosol targets mTOR to proteasome degradation, ultimately leading to the activation of autophagy.

Carnosol Induces a ROS-Dependent Activation of the UPR and Increase in Protein Polyubiquitination in Breast Cancer Cells

We have previously shown that carnosol induced mitophagy in MDA-MB-231 cells (30). Further examination of ultrastructural changes *via* transmission electron microscopy of carnosol-treated cells revealed many dilated endoplasmic reticula (**Figure 3A**, panel d–f, dashed arrow). In addition, multilamellar ER structures are also observed (**Figure 3A**, panel d, asterisk). Similar to our previous report, damaged mitochondria can also be seen (**Figure 3A**, panel d–f, arrowhead). Several autophagolysosomes could be seen in treated cells (**Figure 2A**, panel d, thin arrow). The large number of swollen ER prompted us to hypothesize that this effect is triggered by carnosol-induced ER stress. To test our hypothesis, we assessed the activation of PERK, ATF6, and IRE-1α pathways. Our results show that carnosol induced phosphorylation of IRE-1 α and EIF2 α, and increased levels of XBP-1s, cleaved ATF6, ATF4, and CHOP (**Figure 3B**). These results suggest that the three UPR pathways were activated by carnosol. We next examined the protein level of protein disulfide isomerase (PDI) and endoplasmic reticulum oxidoreductase 1 (ERO-1α), two enzymes that promote proper protein folding in the ER and are upregulated in several cancers including breast cancer. We found that carnosol caused a dramatic decrease in the level of PDI and ERO-1α enzymes (**Figure 3C**), hence further suggesting an impaired protein folding of the ER.

We have shown that carnosol induces a ROS-dependent cytotoxic effect on MDA-MB-231 cells (**Figure 1A**). Pre-treatment of MDA-MB-231 cells with NAC (**Figure 1A**) a ROS scavenger, abolished the carnosol-mediated cytotoxic effect, thus demonstrating that carnosol exerts its anticancer activity through a ROS-dependent manner. This prompted us to examine whether carnosol-induced ER stress is ROS-dependent. As shown in **Figure 4A**, NAC completely abolished the activation of PERK, IRE1α, and ATF6, strongly suggesting that induction of ER stress is solely dependent upon the carnosol-mediated generation of ROS. Similarly, carnosol failed to decrease the level of PDI and ERO-1α in the presence of NAC (**Figure 4B**), hence arguing in favor of the normal protein folding function of ER when ROS accumulation is inhibited.

It is documented that impaired folding function of ER is associated with increased protein polyubiquitination. Other studies also showed that inhibition of mTOR activity increases the overall protein ubiquitination and degradation by the

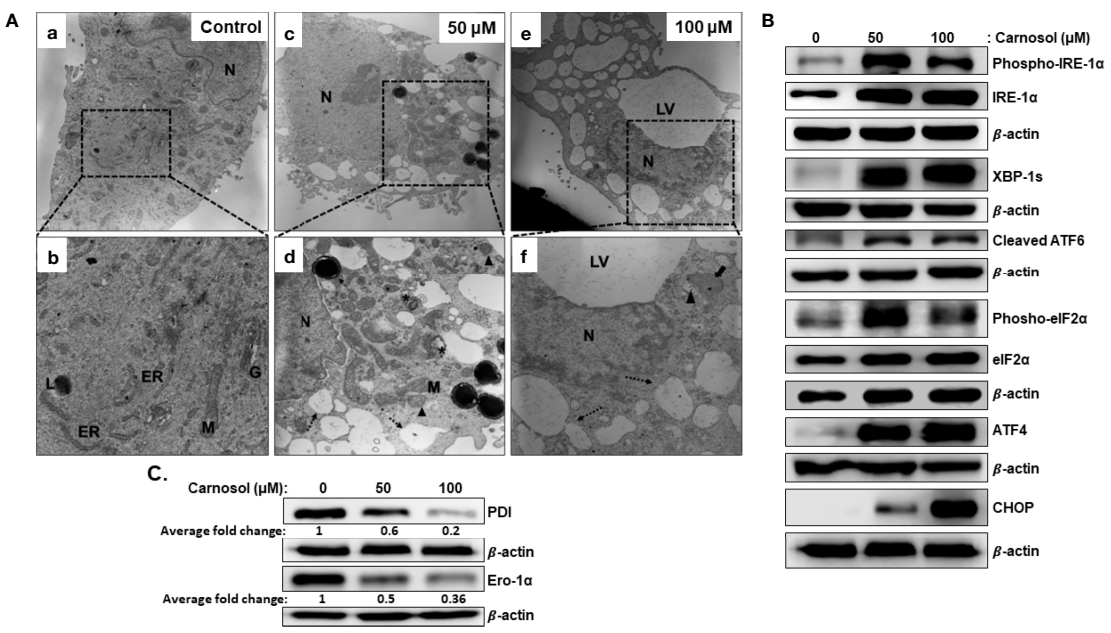

FIGURE 3 | Carnosol induces ER stress in MDA-MB-231 cells. **(A)** Representative electron micrographs of untreated MDA-MB-231 cells **(a–b)** and MDA-MB-231 cells treated with 50 **(c–d)** and 100 μM **(e–f)** carnosol for 24 h. **(B)** Activation of the UPR sensors in carnosol-treated cells. Cells were treated for 24 hours with carnosol (50 and 100 μM) and whole protein lysates were analyzed by Western blot for proteins of the ER stress markers. **(C)** Carnosol disrupts the proper protein folding machinery. Immunoblot of protein folding enzymes PDI and Ero-1α. Protein extract was prepared as described in **(B)**.

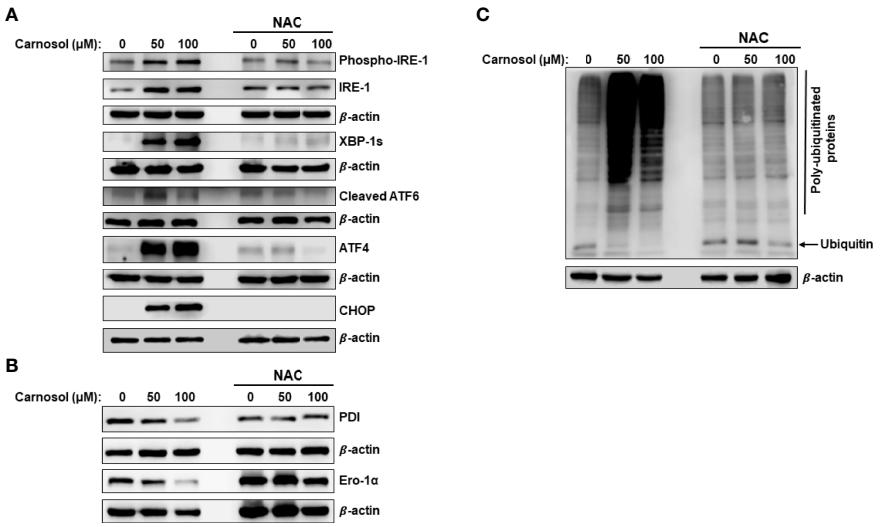

FIGURE 4 | ROS-dependent induction of ER stress and increase in protein ubiquitination. **(A, B)** ROS-dependent activation of UPR sensors in carnosol-treated MDA-MB-231 cells. Cells were pre-treated with the ROS scavenger NAC (10mM) before adding carnosol at the indicated concentrations for 24 hours. Whole cell lysates were analyzed by Western blot for ER stress markers **(A)** and protein folding enzymes **(B)**. **(C)** Carnosol increases the cellular level of polyubiquitinated proteins in MDA-MB-231 cells. Cells were treated with or without carnosol (50 and 100 μM) for 24 h, then whole-cell extracts were subjected to Western blot analysis for ubiquitinated proteins.

ubiquitin proteasome system (UPS) (35). This prompted us to measure the overall level of protein ubiquitination in carnosol-treated cells. As shown in **Figure 4C**, carnosol induced a dramatic increase in the overall level of polyubiquitinated proteins, an effect that was completely abolished by NAC.

Carnosol Induces p38-Dependent Autophagy in Breast Cancer Cell

p38MAPK is involved in ER stress, autophagy, and apoptosis in many types of cancer cells. This prompted us to examine p38 activation in carnosol-treated cells. As shown in **Figure 5A**,

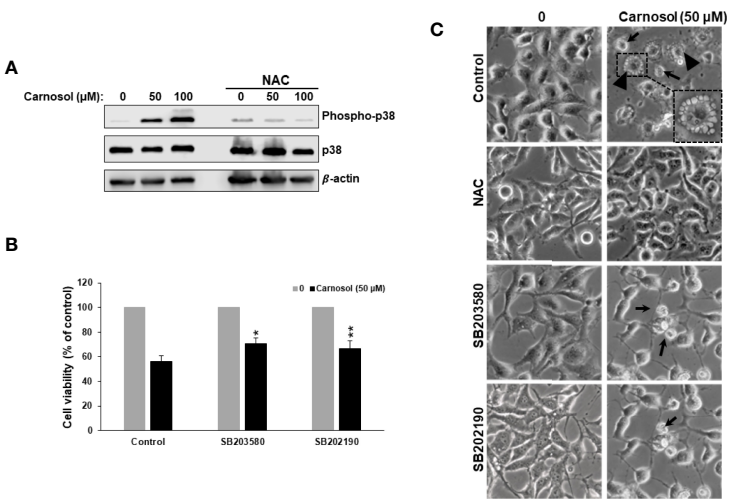

FIGURE 5 | ROS-dependent activation of p38MAPK by carnosol. **(A)** Concentration-dependent increase of phospho-p38 protein in carnosol-treated MDA-MB-231 cells. Cells were pre-treated with the ROS scavenger NAC (10mM) before adding carnosol at the indicated concentrations for 24 hours. Whole cell lysates were analyzed by Western blot for phospho-p38, total p38, and β-actin (loading control). **(B)** Chemical inhibition of p38 activation reduced carnosol-induced cell death. MDA-MB-231 cells were pre-treated for 1 h with or p38 inhibitors, SB203580 (50 μM), or SB202190 (50 μM) before treatment with carnosol (50 μM) for 24 hours. Cell viability was determined as described in Material and Methods. Data represent the mean ± SEM of 3 independent experiments. The student's t-test was performed to determine the significance (*$p<0.05$ and **$p<0.005$). **(C)** Morphological changes in carnosol-treated MDA-MB-231 cells. Cells were observed under EVOS XL Core Cell Imaging System (Life Technologies) at 400X.

carnosol induced a concentration-dependent increase in the level of phosphorylation of p38. Next, we investigated the role of p38 activation in carnosol-mediated ER stress, autophagy, and apoptosis. Toward this, we found that SB203580 and 202190, two p38 inhibitors, significantly promoted cell viability (70% and 67%, respectively) (**Figure 5B**) when compared to control cells treated with carnosol only (56%), thus suggesting that p38MAPK contributes to carnosol-induced cell death. Since both autophagy and apoptosis contribute to carnosol-induced cell death (**Figure 1**), we wanted to examine which mechanism is affected by p38. We first looked at the morphology of MDA-MB-231 cells treated with carnosol alone or in a combination of carnosol and p38 inhibitors. As shown in **Figure 5C**, light microscopy observation of cells treated with carnosol alone revealed cytoplasmic vacuolation, indicative of autophagy, in a subpopulation of treated cells (arrowheads). Also, smaller and rounded cells, characteristic of apoptotic cells were observed (thin arrows). Interestingly, no autophagic vacuoles were seen when in cells treated with both carnosol and p38 inhibitors (**Figure 5C**). However, cells with morphological characteristics of apoptosis were observed (thin arrows) in the presence of p38 inhibitors. As expected, inhibition of ROS generation by NAC completely abolished the morphological changes associated with carnosol treatment (**Figure 5C**). Altogether, these data supported our hypothesis that p38 activation might be involved in the induction of autophagy but not apoptosis.

To confirm this hypothesis, we examined the level of LC3II and cleaved PARP, markers of autophagy and apoptosis, respectively, in cells treated with carnosol in the absence or presence of p38 inhibitors. As shown in **Figure 6A**, inhibition of p38 did not have any effect on the level of cleaved PARP. Similarly, inhibition of p38 did not affect the carnosol-induced loss of mitochondria membrane potential (**Figure 6B**). These results reveal that carnosol-induced apoptosis is p38-independent. On contrary, inhibition of p38 evoked a dramatic decrease in the level of the autophagy marker, LC3II (**Figure 6A**). This finding along with the morphological observation (absence of cytoplasmic autophagic vacuolation) (**Figure 5C**) demonstrates that induction of autophagy is p38-dependent.

Carnosol Activates the IRE1α and ATF6 ER Stress Pathways *via* a p38-Dependent Mechanism

Next, we investigated the role of p38 activation in carnosol-induced ER stress response. We assessed the level of cleaved ATF6, XBP-1s, ATF4, and CHOP in cells treated with carnosol in the absence or presence of SB203580 or SB202190. **Figure 7** reveals that blocking p38 inhibited the activation of ATF6 and the expression of XBP-1s. Interestingly, both inhibitors did not modulate the activity of PERK sensors, ATF4 and CHOP. This indicates that p38 selectively activates the ATF6/IRE1α ER stress pathway.

We have previously reported that ROS generation occurs as early as 1 hour while autophagy and apoptosis occurred at 6 hours and 24 hours post-carnosol treatment, respectively (30). Here, we show that p38 activation also occurred as early as 1 hour post-carnosol treatment (**Figure 7B**). On the other hand, activation of ER stress sensors was observed later starting from 3 hours post-treatment (**Figure 7B**). It is worth mentioning that CHOP expression was delayed, detected at 6 h, compared to its upstream inducer ATF4, detected at 3 hours showed (**Figure 7B**). This result further cements the argument that p38 activation precedes UPR response in carnosol-treated cells.

Next, we determined the time at which protein polyubiquitination and mTOR degradation occurred. An increase in the overall protein polyubiquitination was as well as mTOR degradation was detectable as early as 3 hours post-carnosol treatment (**Figure 7C**). Because we had previously shown that carnosol also induced a proteasome degradation of STAT3 (31)as well as p300 (34)and PCAF (34) histone

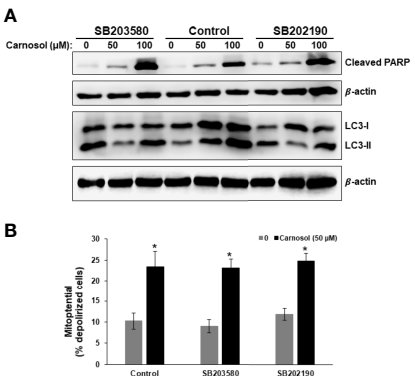

FIGURE 6 | p38-dependent induction of autophagy in carnosol-treated MDA-Mb-231 cells. **(A)** Inhibition of p38 blocks carnosol-induced autophagy in MDA-MB-231 cells. Cells were pre-treated with the p38 inhibitors (SB203580 or SB202190) before adding carnosol (50 and 100 μM) for 24 hours. Whole cell lysates were analyzed by Western blot for the marker of autophagy (LC3II) and apoptosis (cleaved PARP). **(B)** Inhibition of p38 activation failed to restore the carnosol-induced loss of mitochondrial membrane potential in MDA-MB-231 cells. Mitochondrial membrane potential (MMP) of cells pre-treated with p38 inhibitor, prior to the addition of carnosol for 24 hours, was assessed with the Muse Cell Analyzer using the Muse MitoPotential kit as described in Materials and Methods. Data represent the mean ± SEM of at least 3 independent experiments. Student's t-test was performed to determine the significance (*p<0.05).

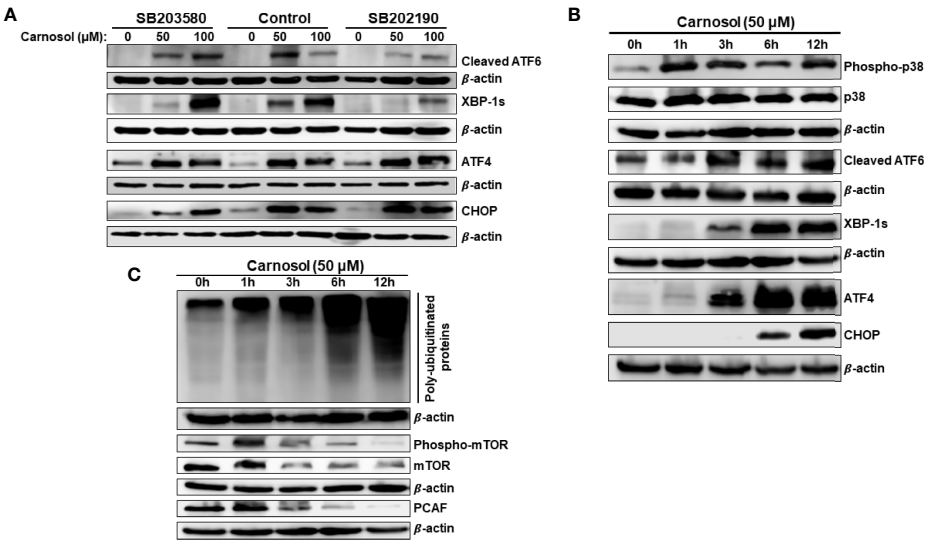

FIGURE 7 | p38MAPK activation of ATF6 and IRE-1α UPR sensors. **(A)** Chemical inhibition of p38 blocked the activation of ATF6 and IRE-1α UPR sensors but did not affect the activation of the PERK sensor. Cells were pre-treated with the p38 inhibitors (SB203580 or SB202190) before adding carnosol (50 μM) for 24 hours. Whole cell lysates were analyzed by Western blot for markers of ER stress (cleaved ATF6, XBP-1s, ATF4, and CHOP). **(B)** Time-course analysis, by Western blotting, of phospho-p38, total p38, cleaved ATF6, XBP-1s, ATF4, and CHOP. Cells were treated with carnosol (50 μM) and proteins were extracted at the indicated time points (0, 1, 3, 6, 12 hours) as described in Materials and Methods. **(C)** Time-course analysis, by Western blotting, of phospho-mTOR, total mTOR, and PCAF.

acetyltransferases, we decided to determine the time at which this degradation occurs. As shown in **Figure 7C**, similar to mTOR's, PCAF degradation was detected as early as 3 hours post-treatment.

Based on these data along with our previous findings, we can stipulate that the sequence of events induced in breast cancer by carnosol is as follows: ROS generation, p38 activation, ER stress concomitant with polyubiquitination and protein degradation, then autophagy followed by apoptosis.

p38 Promotes Protein Degradation in Carnosol-Treated Breast Cancer Cells

We have shown that activation of p38 (**Figure 7B**) precedes protein ubiquitination and protein degradation (**Figure 7C**). Therefore, we next wished to investigate whether these last two events were tied to p38 activation. To this end, we first analyzed the protein ubiquitination level in cells treated with carnosol (50 μM) in the presence or absence of SB202190. Our results show that inhibition of p38 activation dramatically reduced protein ubiquitination (**Figure 8A**), and almost completely rescued mTOR from degradation (**Figure 8B**). Interestingly, the level of phosphorylated mTOR was also restored to a level comparable to that in control untreated cells (**Figure 8B**). These findings are in agreement with the inhibition of autophagy by the p38 inhibitors. Altogether, these results strongly suggest that p38 activation, in response to carnosol-induced ROS generation, induces autophagy by targeting mTOR for proteasomal degradation.

Having shown that inhibition of p38 prevented the proteasomal degradation of mTOR protein, we decided to investigate whether STAT3 and PCAF proteasomal degradation was mediated through a p38-dependent mechanism. Indeed, treatment with SB202190 efficiently prevented STAT3 and PCAF degradation by the proteasome (**Figure 8C**), hence strongly suggesting that p38 activation contributes to the induction of the ubiquitin proteasome system leading to degradation of proteins like mTOR, p300, PCAF, and STAT3.

DISCUSSION

We have previously reported that carnosol induced a ROS-dependent beclin-1 independent autophagy and apoptosis in MDA-MB-231 breast cancer cells (30). However, the relationship between these two events in carnosol-mediated cytotoxicity was not investigated. Here, we extended the work and examined whether these two mechanisms of cell death were linked. Here, we showed that autophagy and apoptosis are triggered *via* ROS-mediated ER stress and that both mechanisms contribute to carnosol-induced cell death independently of each other. Interestingly, we found that autophagy is induced *via* the p38-mediated induction of the IRE-1α and ATF6 pathways, while apoptosis seems to be activated through the PERK-ATF4-CHOP pathway. We also found that activation of p38MAPK leads to an increase in protein polyubiquitination and activation of the ubiquitin proteasome system causing the degradation of several proteins including mTOR, p300, PCAF, and STAT3. Inhibition of p38MAPK reduced carnosol-induced cytotoxicity, inhibited the induction of IRE-1α and ATF6 and autophagy and blocked protein

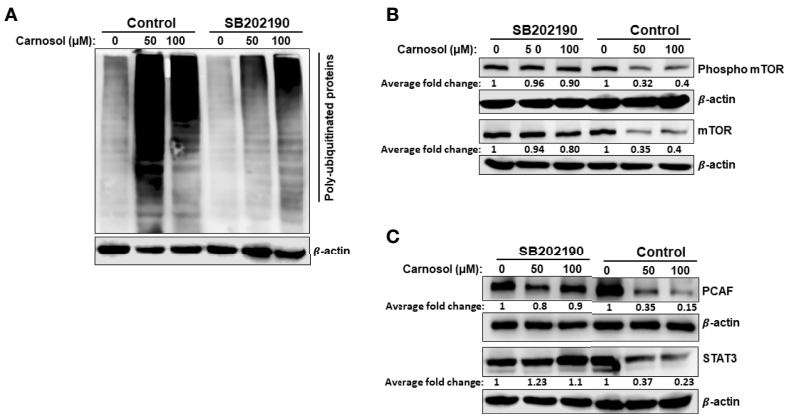

FIGURE 8 | Inhibition of p38MAPK reduces carnosol-mediated protein polyubiquitination and proteasome degradation of mTOR, STAT3, and PCAF. **(A)** Inhibition of p38 reduces the level of polyubiquitinated proteins in MDA-MB-231 cells. Cells were pre-treated for 1 h with or without SB202190 (50 μM) before treatment with carnosol (50 μM). Whole cell lysates were subjected to Western blotting analysis for ubiquitinated proteins. **(B, C)** SB202190 restored mTOR PCAF and STAT3 proteins to a level comparable to control cells. Cells were treated as described in **(A)** and whole protein lysates were subjected to Western blotting analysis for mTOR and phospho-mTOR **(B)** and PCAF and STAT3 **(C)**.

degradation. Further analysis revealed that p38MAPK activation preceded the induction of autophagy and UPS activation in carnosol-treated cells.

PCD-I (Apoptosis) and PCD-II (autophagy) are two different mechanisms of cell death and cross-talk between them exists. It is also very common that autophagy and apoptosis usually occur within the same cell, where autophagy precedes apoptosis. The intricate interplay between these two mechanisms of cell death is a major challenge for cancer treatment. The relationship between autophagy and apoptosis in cancer cells is quite complex and can be divided into synergistic/collaborative, promoting or antagonistic effects depending on the cell type and, nature and duration of the stress (35). Carnosol induced both beclin-1 independent autophagic and apoptotic cell death of breast cancer cells. Inhibition of autophagy had only a very limited effect on carnosol-induced cell death. Also, apoptosis still occurred even when autophagy was inhibited. Moreover, blocking autophagy failed to reduce ROS generation or restore the mitochondrial membrane potential. On the other hand, inhibiting apoptosis did not prevent carnosol-induced cell death. These findings suggest that the two mechanisms are activated concomitantly through different mechanisms and might act collaboratively to promote cell death of breast cancer cells, particularly in response to carnosol-induced cellular damage. Because apoptosis is triggered only 24 hours post-carnosol treatment, while autophagy was detectable as early as 6 hours post-treatment, we believe that cell death through activation of apoptosis comes as a secondary response due to increased intracellular stresses and therefore increased cellular damage due to longer exposure of the cells to carnosol. Like carnosol, an increasing number of anticancer drugs have been reported to induce autophagic and apoptotic cells death of different cancer cell types through synergistic/collaborative effect. For example, dovitinib, a novel multi-target receptor tyrosine kinase inhibitor enrolled in several clinical trials in different cancers, was shown to induce autophagic cell death and apoptosis in several breast cancer cell lines including MDA-MB-231 (36). Dovitinib was shown to mediate its cytotoxic effect through inhibition of STAT3. Interestingly, we have previously shown that carnosol inhibited the STAT3 pathway through targeting STAT3 protein to proteasome degradation. Hence, we cannot exclude that the downregulation of the STAT3 pathway could also account, at least partly, for the induction of PCD-1 and PCD-II in carnosol-treated breast cancer cells. Tetraarsenic hexoxide (As_4O_6) was also shown to induce p38-mediated beclin1-independent autophagic and apoptotic cell death in SW620 colon cancer cells (37). For example, berberine was shown to induce both apoptotic and autophagic death of HepG2 cancer cells (38).

The ER plays many crucial cellular functions such as protein folding and secretion, lipid biosynthesis, and calcium homeostasis. In addition, the ER is also involved in oxygen and nutrient sensing as cells adapt to their microenvironment (39). Disturbance of ER function by various stressors such as oxidative stress, DNA damage, nutrient deficiency, or calcium depletion can lead to ER stress with subsequent accumulation of unfolded or misfolded proteins which ultimately triggers UPR to restore metabolic homeostasis (27, 40). However, under persistent ER stress, components of the UPR pathways, namely ATF4, XBP-1s, and CHOP can also lead to cell death through activation of PCD-I, PCD-II, or both (27).

The increasing number of natural compounds are known to trigger a ROS-dependent ER stress-mediated cell death in several types of cancer including breast cancer cells (26). One such compound, saxifragifolin D (SD) isolated from *Androsace umbellate*, was shown to inhibit breast cancer by inducing ROS-dependent ER stress leading to autophagy and apoptotic cell death (41). SD-induced ER stress was shown to be associated with the

upregulation of IRE-1α expression, and an increase in the level of XBP-1s, BiP and CHOP proteins (41). Another natural compound, γ-tocotrienol and member of the vitamin E, was also shown to promote breast cell death through induction of ER stress, autophagy, and apoptosis (42, 43). Indeed, γ-tocotrienol-induced cell death of MDA-MB-231 and MCF-7 breast cancer cells was partially reduced by inhibition of either autophagy or apoptosis (43). γ-tocotrienol also induced markers of ER stress through modulation of the UPR markers BiP, phospho-PERK, phospho-EIF2α, phsopho-IRE1α, ATF3, ATF4, and CHOP (42, 43). Interestingly, γ-tocotrienol-induced apoptosis might involve the ATF4-ATF3-CHOP pathway (42). Here we showed that carnosol induces a ROS-dependent ER stress through activation of the three main UPR pathways, namely PERK, ATF6, and pIRE-1α. We also showed that both autophagy and apoptosis contribute through an independent mechanism to carnosol-induced cell death. Interestingly, we reported here that only the PERK-ATF4-CHOP pathway of the UPR seems to be responsible for the induction of apoptosis in carnosol-treated cells. Indeed, inhibiting p38, which blocked the activation of ATF6 and pIRE-1α pathways and autophagy, had no effect on the PERK pathway nor the activation of the apoptotic program demonstrated by PARP cleavage. It is well-documented that prolonged activation of the UPR might initiate apoptotic cell death through the upregulation of CHOP, which indeed plays a role in ER stress-mediated apoptosis (44). Although CHOP could be induced by the three UPR pathways, we believe that in the presence of carnosol, only the PERK-ATF4 contributes to CHOP upregulation. This is supported by the observation that the inhibition of ATF6 and IRE1-α pathways, by SB202190 or SB203580, did not affect the upregulation of carnosol-induced CHOP expression. This is strongly indicative that activation of apoptosis depended mainly on the PERK-ATF4-CHOP pathway. It is noteworthy to mention that one mechanism through which CHOP induces apoptosis is *via* downregulation of the expression of the anti-apoptotic proteins BcL2, BcL-xL, and Mc-1 and upregulation of pro-apoptotic proteins such as Bax, Bim and BAK (44). Interestingly, we have previously reported that carnosol downregulated BcL-2 while upregulated Bax protein in MDA-MB-231 breast cancer cells (30).

p38 links extracellular signals to the intracellular machinery that regulates a plethora of cellular processes that including regulation of the cell cycle, induction of cell death, differentiation, and senescence depending on the kinetics of activation and downstream signaling pathways activated (45–47). Recent studies showed that p38MAPK plays a dual role in the unfolded protein response pathway (48, 49). p38MAPK can be activated as a consequence of UPR activation through IRE-1α and PERK oligomerization (49, 50). Furthermore, sustained activation of p38 MAPK induces ER stress and activates the UPR response pathway by regulating the expression of UPR components such as BiP (49, 51), CHOP (52), ATF6 (53) and XBP-1s (54). Studies showed that in the presence of ER stress, p38MAPK can promote cell death by autophagy and/or apoptosis of various types of cancer depending on the type and duration of the stimulus. Here we showed that p38MAPK was not a component of a signaling pathway that led to the activation of apoptosis. Indeed, apoptosis occurred in carnosol-treated cells even when p38 activation was inhibited, hence excluding p38 in the activation of PCD-I. However, our data strongly suggest that p38MAPK activation, by a ROS-dependent mechanism, triggers selective activation of IRE-1α and ATF6 UPR response pathway, followed by stimulation of the ubiquitin proteasome system (UPS) and induction of autophagy. Time course analysis showed that activation of p38, is the first event that occurred in carnosol-treated cells followed by the concomitant activation

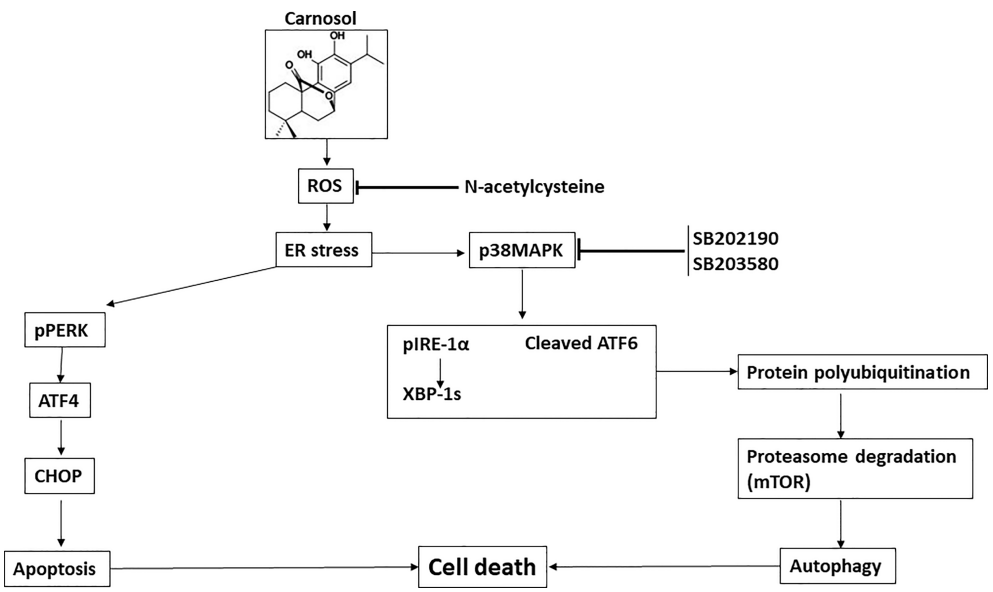

FIGURE 9 | Hypothetic model for the anti-breast cancer effect of carnosol.

of IRE-1α and ATF6 and UPS, and then by autophagy. Inhibition of p38 blocked the carnosol-induced activation of IRE-1α and ATF6 sensors without affecting the CHOP activation, decreased UPS activity and blocked autophagy, as well as attenuated cell death in breast cancer cells. These findings strongly suggest that, under certain stress conditions, p38 plays a stimulatory role in the ubiquitin proteasome system. We also propose that induction of autophagy is probably a consequence, although another mechanism may be involved, of the proteasomal degradation and hence inactivation of the negative regulator of autophagy, mTOR protein. This is supported by the notion that degradation of mTOR, which occurred as early as 3 hours post-carnosol treatment, preceded autophagy which was detectable only after 6 hours. Also, blockade of proteasome activity not only restored total mTOR protein level but also restored phosphorylated mTOR which restored its ability to inhibit autophagy. mTOR inhibition was shown to induce autophagy and stimulate protein breakdown (55). A recent study showed that mTOR inhibition by Torin 1 or rapamycin stimulates and enhances overall protein degradation by the ubiquitin proteasome system as well as by autophagy in HEK 293 cells (56). Another study showed that *Rhus coriaria* ethanolic extract induced autophagy and increased the overall level of protein ubiquitination and the degradation of several proteins including mTOR protein in HT-29 colon cancer cells (57). The mechanism through which inhibition of mTOR stimulates proteasome degradation remains poorly understood. Our current data further confirm the role of mTOR inhibition in stimulating the UPS activity but also incriminates p38 MAPK in this process.

In summary, our current findings further enhance our understanding of the molecular mechanisms through which carnosol exerts its anticancer activity at least in the case of breast cancer. We show for the first time that carnosol induces a ROS-dependent activation of p38 MAPK which in turn activates ER stress response IRE-1a and ATF6 associated with stimulation of the proteasome activity leading to the degradation of the autophagy regulator mTOR. As consequence, autophagy is activated leading to cell death. We also show, that apoptosis is triggered through a p38MAPK-independent pathway, yet to be uncovered. Hence, our data are consistent with the model shown in **Figure 9**. These current findings along with previous reports provide further evidence that carnosol is a good candidate for treating an aggressive form of breast cancer.

DATA AVAILABILITY STATEMENT

The raw data supporting the conclusions of this article will be made available by the authors, without undue reservation.

AUTHOR CONTRIBUTIONS

HA, AA, KM, and MA performed all experiments. AE edited the manuscript. RI designed the project, analyzed the data, and wrote the manuscript. All authors reviewed the manuscript. All authors contributed to the article and approved the submitted version.

FUNDING

This work was supported by Al Jalila Foundation (Grant 21S102-AJF2018007) and by the Zayed Center for Health Sciences (ZCHS) research grant (Grant # 31R086).

REFERENCES

1. Cao SS, Kaufman RJ. Endoplasmic Reticulum Stress and Oxidative Stress in Cell Fate Decision and Human Disease. *Antioxid Redox Signal* (2014) 21 (3):396–413. doi: 10.1089/ars.2014.5851
2. Rutkowski DT, Kaufman RJ. A Trip to the ER: Coping With Stress. *Trends Cell Biol* (2004) 14(1):20–8. doi: 10.1016/j.tcb.2003.11.001
3. Hetz C. The Unfolded Protein Response: Controlling Cell Fate Decisions Under ER Stress and Beyond. *Nat Rev Mol Cell Biol* (2012) 13(2):89–102. doi: 10.1038/nrm3270
4. Mishra RR, Belder N, Ansari SA, Kayhan M, Bal H, Raza U, et al. Reactivation of cAMP Pathway by PDE4D Inhibition Represents a Novel Druggable Axis for Overcoming Tamoxifen Resistance in ER-Positive Breast Cancer. *Clin Cancer Res* (2018) 24(8):1987–2001. doi: 10.1158/1078-0432.CCR-17-2776
5. Zhong F, Xie J, Zhang D, Han Y, Wang C. Polypeptide From Chlamys Farreri Suppresses Ultraviolet-B Irradiation-Induced Apoptosis Through Restoring ER Redox Homeostasis, Scavenging ROS Generation, and Suppressing the PERK-Eif2a-CHOP Pathway in HaCaT Cells. *J Photochem Photobiol B* (2015) 151:10–6. doi: 10.1016/j.jphotobiol.2015.06.016
6. Rozpedek W, Pytel D, Mucha B, Leszczynska H, Diehl JA, Majsterek I. The Role of the PERK/Eif2α/ATF4/CHOP Signaling Pathway in Tumor Progression During Endoplasmic Reticulum Stress. *Curr Mol Med* (2016) 16(6):533–44. doi: 10.2174/1566524016666160523143937
7. Anding AL, Chapman JS, Barnett DW, Curley RW, Clagett-Dame M. The Unhydrolyzable Fenretinide Analogue 4-Hydroxybenzylretinone Induces the Proapoptotic Genes GADD153 (CHOP) and Bcl-2-Binding Component 3 (PUMA) and Apoptosis That is Caspase- Dependent and Independent of the Retinoic Acid Receptor. *Cancer Res* (2007) 67(13):6270–7. doi: 10.1158/0008-5472.CAN-07-0727
8. Scaiewicz V, Nahmias A, Chung RT, Mueller T, Tirosh B, Shibolet O. CCAAT/enhancer-Binding Protein Homologous (CHOP) Protein Promotes Carcinogenesis in the DEN-Induced Hepatocellular Carcinoma Model. *PloS One* (2013) 8(12):e81065. doi: 10.1371/journal.pone.0081065
9. Gaudette BT, Iwakoshi NN, Boise LH. Bcl-xL Protein Protects From C/EBP Homologous Protein (CHOP)-Dependent Apoptosis During Plasma Cell Differentiation. *J Biol Chem* (2014) 289(34):23629–40. doi: 10.1074/jbc.M114.569376
10. Lerner AG, Upton J-P, Praveen PVK, Ghosh R, Nakagawa Y, Igbaria A, et al. Ire1α Induces Thioredoxin-Interacting Protein to Activate the NLRP3 Inflammasome and Promote Programmed Cell Death Under Irremediable ER Stress. *Cell Metab* (2012) 16(2):250–64. doi: 10.1016/j.cmet.2012.07.007
11. Upton J-P, Wang L, Han D, Wang ES, Huskey NE, Lim L, et al. Ire1α Cleaves Select microRNAs During ER Stress to Derepress Translation of Proapoptotic Caspase-2. *Science* (2012) 338(6108):818–22. doi: 10.1126/science.1226191
12. Zeeshan HMA, Lee GH, Kim H-R, Chae H-J. Endoplasmic Reticulum Stress and Associated ROS. *Int J Mol Sci* (2016) 17(3):327. doi: 10.3390/ijms17030327
13. Valko M, Leibfritz D, Moncol J, Cronin MTD, Mazur M, Telser J. Free Radicals and Antioxidants in Normal Physiological Functions and Human Disease. *Int J Biochem Cell Biol* (2007) 39(1):44–84. doi: 10.1016/j.biocel.2006.07.001

14. Schumacker PT. Reactive Oxygen Species in Cancer Cells: Live by the Sword, Die by the Sword. *Cancer Cell* (2006) 10(3):175–6. doi: 10.1016/j.ccr.2006.08.015
15. Fruehauf JP, Meyskens FL. Reactive Oxygen Species: A Breath of Life or Death? *Clin Cancer Res* (2007) 13(3):789–94. doi: 10.1158/1078-0432.CCR-06-2082
16. Rigas B, Sun Y. Induction of Oxidative Stress as a Mechanism of Action of Chemopreventive Agents Against Cancer. *Br J Cancer* (2008) 98(7):1157–60. doi: 10.1038/sj.bjc.6604225
17. Li X, Liang M, Jiang J, He R, Wang M, Guo X, et al. Combined Inhibition of Autophagy and Nrf2 Signaling Augments Bortezomib-Induced Apoptosis by Increasing ROS Production and ER Stress in Pancreatic Cancer Cells. *Int J Biol Sci* (2018) 14(10):1291–305. doi: 10.7150/ijbs.26776
18. Cheng X, Feng H, Wu H, Jin Z, Shen X, Kuang J, et al. Targeting Autophagy Enhances Apatinib-Induced Apoptosis *via* Endoplasmic Reticulum Stress for Human Colorectal Cancer. *Cancer Lett* (2018), 431:105–14. doi: 10.1016/j.canlet.2018.05.046
19. Simizu S, Takada M, Umezawa K, Imoto M. Requirement of Caspase-3(-Like) Protease-Mediated Hydrogen Peroxide Production for Apoptosis Induced by Various Anticancer Drugs. *J Biol Chem* (1998) 273(41):26900–7. doi: 10.1074/jbc.273.41.26900
20. Sawa T, Wu J, Akaike T, Maeda H. Tumor-Targeting Chemotherapy by a Xanthine Oxidase-Polymer Conjugate That Generates Oxygen-Free Radicals in Tumor Tissue. *Cancer Res* (2000) 60(3):666–71.
21. Trachootham D, Zhou Y, Zhang H, Demizu Y, Chen Z, Pelicano H, et al. Selective Killing of Oncogenically Transformed Cells Through a ROS-Mediated Mechanism by Beta-Phenylethyl Isothiocyanate. *Cancer Cell* (2006) 10(3):241–52. doi: 10.1016/j.ccr.2006.08.009
22. Trachootham D, Alexandre J, Huang P. Targeting Cancer Cells by ROS-Mediated Mechanisms: A Radical Therapeutic Approach? *Nat Rev Drug Discovery* (2009) 8(7):579–91. doi: 10.1038/nrd2803
23. Agarwal R. Cell Signaling and Regulators of Cell Cycle as Molecular Targets for Prostate Cancer Prevention by Dietary Agents. *Biochem Pharmacol* (2000) 60(8):1051–9. doi: 10.1016/S0006-2952(00)00385-3
24. Hadi SM, Bhat SH, Azmi AS, Hanif S, Shamim U, Ullah MF. Oxidative Breakage of Cellular DNA by Plant Polyphenols: A Putative Mechanism for Anticancer Properties. *Semin Cancer Biol* (2007) 17(5):370–6. doi: 10.1016/j.semcancer.2007.04.002
25. Colomer R, Sarrats A, Lupu R, Puig T. Natural Polyphenols and Their Synthetic Analogs as Emerging Anticancer Agents. *Curr Drug Targ* (2017) 18(2):147–59. doi: 10.2174/1389450117666160112113930
26. Liu H, Yang J, Li L, Shi W, Yuan X, Wu L. The Natural Occurring Compounds Targeting Endoplasmic Reticulum Stress. *Evid Based Complement Alternat Med* (2016) 2016:7831282. doi: 10.1155/2016/7831282
27. Limonta P, Moretti RM, Marzagalli M, Fontana F, Raimondi M, Montagnani Marelli M. Role of Endoplasmic Reticulum Stress in the Anticancer Activity of Natural Compounds. *Int J Mol Sci* (2019) 20(4):1–24. doi: 10.3390/ijms20040961
28. NavaneethaKrishnan S, Rosales JL, Lee K-Y. ROS-Mediated Cancer Cell Killing Through Dietary Phytochemicals. *Oxid Med Cell Longev* (2019) 2019:9051542. doi: 10.1155/2019/9051542
29. Park K-W, Kundu J, Chae I-G, Kim D-H, Yu M-H, Kundu JK, et al. Carnosol Induces Apoptosis Through Generation of ROS and Inactivation of STAT3 Signaling in Human Colon Cancer HCT116 Cells. *Int J Oncol* (2014) 44 (4):1309–15. doi: 10.3892/ijo.2014.2281
30. Al Dhaheri Y, Attoub S, Ramadan G, Arafat K, Bajbouj K, Karuvantevida N, et al. Carnosol Induces ROS-Mediated Beclin1-Independent Autophagy and Apoptosis in Triple Negative Breast Cancer. *PloS One* (2014) 9(10):e109630. doi: 10.1371/journal.pone.0109630
31. Alsamri H, El Hasasna H, Al Dhaheri Y, Eid AH, Attoub S, Iratni R. Carnosol, a Natural Polyphenol, Inhibits Migration, Metastasis, and Tumor Growth of Breast Cancer *via* a ROS-Dependent Proteasome Degradation of STAT3. *Front Oncol* (2019) 9:743. doi: 10.3389/fonc.2019.00743
32. Wang L, Zhang Y, Liu K, Chen H, Yang R, Ma X, et al. Carnosol Suppresses Patient-Derived Gastric Tumor Growth by Targeting RSK2. *Oncotarget* (2018) 9(76):34200–12. doi: 10.18632/oncotarget.24409
33. Johnson JJ. Carnosol: A Promising Anti-Cancer and Anti-Inflammatory Agent. *Cancer Lett* (2011) 305(1):1–7. doi: 10.1016/j.canlet.2011.02.005
34. Alsamri H, Hasasna HE, Baby B, Alneyadi A, Dhaheri YA, Ayoub MA, et al. Carnosol Is a Novel Inhibitor of P300 Acetyltransferase in Breast Cancer. *Front Oncol* (2021) 11:664403. doi: 10.3389/fonc.2021.664403
35. Xie Q, Liu Y, Li X. The Interaction Mechanism Between Autophagy and Apoptosis in Colon Cancer. *Transl Oncol* (2020) 13(12):100871–1. doi: 10.1016/j.tranon.2020.100871
36. Chiu Y-H, Lee Y-Y, Huang K-C, Liu C-C, Lin C-S. Dovitinib Triggers Apoptosis and Autophagic Cell Death by Targeting SHP-1/P-STAT3 Signaling in Human Breast Cancers. *J Oncol* (2019) 2019:2024648. doi: 10.1155/2019/2024648
37. Nagappan A, Lee WS, Yun JW, Lu JN, Chang S-H, Jeong J-H, et al. Tetraarsenic Hexoxide Induces G2/M Arrest, Apoptosis, and Autophagy *via* PI3K/Akt Suppression and P38 MAPK Activation in SW620 Human Colon Cancer Cells. *PloS One* (2017) 12(3):e0174591. doi: 10.1371/journal.pone.0174591
38. Yu R, Zhang Z, Wang B, Jiang H, Cheng L, Shen L. Berberine-Induced Apoptotic and Autophagic Death of HepG2 Cells Requires AMPK Activation. *Cancer Cell Int* (2014) 14(1):49. doi: 10.1186/1475-2867-14-49
39. Tsai YC, Weissman AM. The Unfolded Protein Response, Degradation From Endoplasmic Reticulum and Cancer. *Genes Cancer* (2010) 1(7):764–78. doi: 10.1177/1947601910383011
40. Clarke HJ, Chambers JE, Liniker E, Marciniak SJ. Endoplasmic Reticulum Stress in Malignancy. *Cancer Cell* (2014) 25(5):563–73. doi: 10.1016/j.ccr.2014.03.015
41. Shi J-M, Bai L-L, Zhang D-M, Yiu A, Yin Z-Q, Han W-L, et al. Saxifragifolin D Induces the Interplay Between Apoptosis and Autophagy in Breast Cancer Cells Through ROS-Dependent Endoplasmic Reticulum Stress. *Biochem Pharmacol* (2013) 85(7):913–26. doi: 10.1016/j.bcp.2013.01.009
42. Patacsil D, Tran AT, Cho YS, Suy S, Saenz F, Malyukova I, et al. Gamma-Tocotrienol Induced Apoptosis is Associated With Unfolded Protein Response in Human Breast Cancer Cells. *J Nutr Biochem* (2012) 23(1):93–100. doi: 10.1016/j.jnutbio.2010.11.012
43. Tiwari RV, Parajuli P, Sylvester PW. γ-Tocotrienol-Induced Endoplasmic Reticulum Stress and Autophagy Act Concurrently to Promote Breast Cancer Cell Death. *Biochem Cell Biol* (2015) 93(4):306–20. doi: 10.1139/bcb-2014-0123
44. Hu H, Tian M, Ding C, Yu S. The C/EBP Homologous Protein (CHOP) Transcription Factor Functions in Endoplasmic Reticulum Stress-Induced Apoptosis and Microbial Infection. *Front Immunol* (2018) 9:3083. doi: 10.3389/fimmu.2018.03083
45. Coulthard LR, White DE, Jones DL, McDermott MF, Burchill SA. P38 (MAPK): Stress Responses From Molecular Mechanisms to Therapeutics. *Trends Mol Med* (2009) 15(8):369–79. doi: 10.1016/j.molmed.2009.06.005
46. Lee J, Sun C, Zhou Y, Lee J, Gokalp D, Herrema H, et al. P38 MAPK–mediated Regulation of Xbp1s is Crucial for Glucose Homeostasis. *Nat Med* (2011) 17 (10):1251–60. doi: 10.1038/nm.2449
47. Darling NJ, Cook SJ. The Role of MAPK Signalling Pathways in the Response to Endoplasmic Reticulum Stress. *Biochim Biophys Acta (BBA) Mol Cell Res* (2014) 1843(10):2150–63. doi: 10.1016/j.bbamcr.2014.01.009
48. Wagner EF, Nebreda ÁR. Signal Integration by JNK and P38 MAPK Pathways in Cancer Development. *Nat Rev Cancer* (2009) 9(8):537–49. doi: 10.1038/nrc2694
49. Koeberle A, Pergola C, Shindou H, Koeberle SC, Shimizu T, Laufer SA, et al. Role of P38 Mitogen-Activated Protein Kinase in Linking Stearoyl-CoA Desaturase-1 Activity With Endoplasmic Reticulum Homeostasis. *FASEB J* (2015) 29(6):2439–49. doi: 10.1096/fj.14-268474
50. Kim I, Xu W, Reed JC. Cell Death and Endoplasmic Reticulum Stress: Disease Relevance and Therapeutic Opportunities. *Nat Rev Drug Discovery* (2008) 7 (12):1013–30. doi: 10.1038/nrd2755
51. Ranganathan AC, Zhang L, Adam AP, Aguirre-Ghiso JA. Functional Coupling of P38-Induced Up-Regulation of BiP and Activation of RNA-Dependent Protein Kinase-Like Endoplasmic Reticulum Kinase to Drug Resistance of Dormant Carcinoma Cells. *Cancer Res* (2006) 66(3):1702–11. doi: 10.1158/0008-5472.CAN-05-3092
52. Wang XZ, Ron D. Stress-Induced Phosphorylation and Activation of the Transcription Factor CHOP (GADD153) by P38 MAP Kinase. *Science* (1996) 272(5266):1347–9. doi: 10.1126/science.272.5266.1347
53. Thuerauf DJ, Arnold ND, Zechner D, Hanford DS, DeMartin KM, McDonough PM, et al. P38 Mitogen-Activated Protein Kinase Mediates the

Transcriptional Induction of the Atrial Natriuretic Factor Gene Through a Serum Response Element. *A Potential Role Transcription Factor ATF6 J Biol Chem* (1998) 273(32):20636–43. doi: 10.1074/jbc.273.32.20636
54. Qu M, Liu Y, Xu K, Wang D. Activation of P38 MAPK Signaling-Mediated Endoplasmic Reticulum Unfolded Protein Response by Nanopolystyrene Particles. *Adv Biosyst* (2019) 3(4):1800325. doi: 10.1002/adbi.201800325
55. Klionsky DJ, Emr SD. Autophagy as a Regulated Pathway of Cellular Degradation. *Science* (2000) 290(5497):1717–21. doi: 10.1126/science.290.5497.1717
56. Zhao J, Zhai B, Gygi SP, Goldberg AL. mTOR Inhibition Activates Overall Protein Degradation by the Ubiquitin Proteasome System as Well as by Autophagy. *PNAS* (2015) 112(52):15790–7. doi: 10.1073/pnas.1521919112
57. Athamneh K, Hasasna HE, Samri HA, Attoub S, Arafat K, Benhalilou N, et al. Rhus Coriaria Increases Protein Ubiquitination, Proteasomal Degradation and Triggers non-Canonical Beclin-1-Independent Autophagy and Apoptotic Cell Death in Colon Cancer Cells. *Sci Rep* (2017) 7(1):11633. doi: 10.1038/s41598-017-11202-3

Conflict of Interest: The authors declare that the research was conducted in the absence of any commercial or financial relationships that could be construed as a potential conflict of interest.

Publisher's Note: All claims expressed in this article are solely those of the authors and do not necessarily represent those of their affiliated organizations, or those of the publisher, the editors and the reviewers. Any product that may be evaluated in this article, or claim that may be made by its manufacturer, is not guaranteed or endorsed by the publisher.

frontiers | Frontiers in Oncology

ORIGINAL RESEARCH
published: 13 July 2022
doi: 10.3389/fonc.2022.923890

BNIP3 Upregulation Characterizes Cancer Cell Subpopulation With Increased Fitness and Proliferation

Yanyan Zhu[1], Bowang Chen[2,3], Junya Yan[1], Wendi Zhao[4], Pengli Dou[5], Na Sun[2], Yaokai Wang[6]* and Xiaoyun Huang[2,3]**

[1] Department of Oncology, Henan Provincial People's Hospital, People's Hospital of Zhengzhou University, School of Clinical Medicine, Henan University, Zhengzhou, China, [2] Department of Computational Oncology, Intelliphecy, Shenzhen, China, [3] Center for Systems Biology, Intelliphecy, Shenzhen, China, [4] Department of Oncology, Henan Provincial People's Hospital, School of Clinical Medicine, Henan University, Zhengzhou, China, [5] Department of Experimental Cancer Modeling, Intelliphecy, Nanjing, China, [6] Department of Gynecology and Obstetrics, The University of Hong Kong-Shenzhen Hospital, Shenzhen, China

OPEN ACCESS

Edited by:
Abdelhabib Semlali, Laval University, Canada

Reviewed by:
Louis-Etienne Lorenzo, Laval University, Canada
Nael Abutaha, King Saud University, Saudi Arabia

***Correspondence:**
Yanyan Zhu
xjtu100@163.com
Yaokai Wang
wangyk@hku-szh.org
Xiaoyun Huang
x.huang@intelliphecy.com

Specialty section:
This article was submitted to Cancer Molecular Targets and Therapeutics, a section of the journal Frontiers in Oncology

Received: *19 April 2022*
Accepted: *09 June 2022*
Published: *13 July 2022*

Citation:
Zhu Y, Chen B, Yan J, Zhao W, Dou P, Sun N, Wang Y and Huang X (2022) BNIP3 Upregulation Characterizes Cancer Cell Subpopulation With Increased Fitness and Proliferation. Front. Oncol. 12:923890. doi: 10.3389/fonc.2022.923890

BNIP3 is a BH3-only protein with both pro-apoptotic and pro-survival roles depending on the cellular context. It remains unclear how BNIP3 RNA level dictates cell fate decisions of cancer cells. Here, we undertook a quantitative analysis of BNIP3 expression and functions in single-cell datasets of various epithelial malignancies. Our results demonstrated that BNIP3 upregulation characterizes cancer cell subpopulations with increased fitness and proliferation. We further validated the upregulation of BNIP3 in liver cancer 3D organoid cultures compared with 2D culture. Taken together, the combination of *in silico* perturbations using public single-cell datasets and experimental cancer modeling using organoids ushered in a new approach to address cancer heterogeneity.

Keywords: BNIP3, ScRNA-seq, mitophagy, systems biology, cancer heterogeneity

INTRODUCTION

The heterogeneity of cancer is a well-known phenomenon that poses a daunting challenge for effective treatment. Cell-to-cell variability in signaling pathways and transcription factor activities render the whole cancer cell population only partially responsive to most drugs (1, 2). The design of a better combination targeting strategy relies on the accurate identification of key genes and pathways that define cancer cell subpopulations with increased cancer hallmarks.

The ability of cancer cells to elicit uncontrolled proliferation and evade apoptosis requires a healthy mitochondrial network maintained through coordinated fission and mitophagy (3). BNIP3 is involved in cellular responses to a multitude of different stresses through either apoptotic or non-apoptotic cell death (4). BNIP3 also serves as an autophagy receptor that plays crucial roles in the removal of damaged mitochondria *via* interaction with ATG8. We have previously shown that phosphorylation of S17 and S24 in the LC3 interacting domains dictates whether BNIP3 signals apoptosis or pro-survival mitophagy (5). However, it is still unclear how the RNA expression level of BNIP3 dictates cell fate decisions of cancer cells at the single-cell level.

Single-cell RNA sequencing (scRNA-seq) has been harnessed to gain important insights into cancer heterogeneity and resulted in overwhelmingly rich datasets (6). Almost all solid tumors and hematological malignancies have been investigated with scRNA-seq. Those datasets enabled the possibility to perform *in silico* perturbation experiments with single-cell resolution to investigate the functional significance of genes of interest (7).

Here, we undertook a comprehensive analysis of BNIP3 expression and functions in single-cell datasets and The Cancer Genome Atlas (TCGA) datasets. We identified a cancer cell subpopulation characterized by upregulated BNIP3 in most epithelial malignancies. We also interrogated the pathway alterations in cancer cells with upregulated BNIP3 expression with a quantitative pathway enrichment approach using gene set variation analysis (GSVA) (8). Our study underscored the power to combine computational and experimental approach to address gene-centered cancer heterogeneity.

RESULTS

BNIP3 expression was first investigated in the tumor and normal samples from the TCGA and the Genotype-Tissue Expression (GTEx) projects. Using transcripts per million reads normalization, BNIP3 expression was investigated in cancer samples and paired normal samples across different cancer types (**Supplementary Figure 1A**). The highest BNIP3 expression was found in Kidney Renal Clear Cell Carcinoma (KIRC), while significant patient-to-patient variability in BNIP3 was noted. Those population averaged measurements were incapable of capturing the intratumoral heterogeneity reflected by cell-to-cell variability of cancer cells and the complex tumor ecosystem. Single-cell transcriptomic datasets were used to determine the heterogeneous BNIP3 expression in cancer cells. Due to the inherent technical constrains of scRNA-seq, dropouts (zero UMI detected) were common. Considering the technical dropouts, cancer cells were stratified based on whether at least one UMI is detected whenever UMI count datasets were available. BNIP3 positivity actually might reflect BNIP3 upregulation. In almost all patients, scRNA-seq data revealed a cancer cell subpopulation with BNIP3 positivity.

The survival analysis was performed with all cancer types in the TCGA project (**Figure 1A**), suggesting BNIP3 mRNA expression as a worse prognostic factor also for cervical squamous cell carcinoma and endocervical adenocarcinoma (CESC), cholangiocarcinoma (CHOL), and sarcoma (SARC). However, BNIP3 upregulation appeared to be a better prognosis indicator in kidney renal clear cell carcinoma (KIRC) and low-grade glioma (LGG).

The functional significance of BNIP3 in cancer cells was first investigated using a single-cell dataset derived from head and neck cancer (9). Cancer cells were stratified by BNIP3 RNA expression. The differentially expressed genes between BNIP3-positive and BNIP3-negative cancer cells were shown (**Figure 1B**). The top pathways enriched for BNIP3 upregulated genes included formation of the cornified envelope, Nuclear factor erythroid 2-related factor 2 (NRF2) pathway, and response to wounding (**Figure 1C**). NRF2 is a transcription factor associated with antioxidant responses in cells. Interestingly, the top transcription factor regulating BNIP3 upregulated was HIF1A (**Figure 1D**), in agreement with the involvement of BNIP3 in cellular response to hypoxia. Using BNIP3 upregulated genes, protein–protein interaction network was constructed and analyzed for core modules. NRF2 pathway and metabolic reprogramming were among the enriched core modules, suggesting that cancer cells with higher expression of BNIP3 might have achieved increased fitness by multiple pathways (**Figure 1E**).

To gain a quantitative insight into BNIP3-associated pathways, we employed GSVA to investigate the differential pathway activity of BNIP3-positive and -negative cancer cells (**Figure 2A**). BNIP3-positive cancer cells have an upregulated activity in reactive oxygen species pathway, oxidative phosphorylation, as well as MYC targets. The high ROS burden within BNIP3-positive cancer cells might explain the feedback activation of antioxidant transcription factor NRF2. Cell cycle phase at the single-cell level was inferred using single-cell RNA, suggesting that the percentage of cells in S phase is higher in BNIP3-positive cells (**Figure 2B**). BNIP3-positive cancer cell subpopulation was also detected in lung cancer (**Supplementary Figure 1B**). Next, a lung cancer dataset with 42 patients was integrated with CCA or harmony algorithm and employed to obtain BNIP3 altered gene lists and pathways. The differentially expressed genes with p-value < 0.05 and detection rate higher than 25% were identified with Wilcoxon test. Interestingly, BNIP3 upregulated genes were enriched for response to hypoxia, response to oxygen levels, response to decreased oxygen levels, and response to oxidative stress after CCA integration (**Figure 2C**). Response to oxidative stress was also among the top pathways enriched after harmony integration (**Figure 2D**).

Next, we investigated BNIP3 expression in a cervical cancer single-cell atlas. BNIP3-positive cervical cancer cells displayed a shifted transcriptional signature (**Figure 3A**). Cervical cancer patients with high BNIP3 expression in the TCGA cohort had a significantly decreased overall survival as compared with those with low BNIP3 expression (**Figure 3B**). The top 3 pathways enriched for BNIP3 upregulated genes were HIF1 TF pathway, response to wounding, and Vitamin D receptor pathway (**Figure 3C**). The top 3 transcription factors regulating the upregulated genes were HIF1A, SP1, and RELA (**Figure 3D**). The proportion of BNIP3-positive cells is higher in breast cancer cells as compared to normal breast epithelial cells (**Figure 3E**). HER2-positive and triple-negative breast cancers seemed to have an increased proportion of BNIP3-positive cancer cells as compared with ER-positive breast cancers (**Supplementary Figure 1C**). Of note, BNIP3 is mostly expressed by epithelial cells, but not immune cells in the tumor microenvironment (**Figure 3F**). The prognostic significance of BNIP3 in breast cancer patients was also investigated in the TCGA breast cancer cohort. Patients with high BNIP3 expression had a significantly worse prognosis compared with patients with low BNIP3 expression (**Figure 3G**).

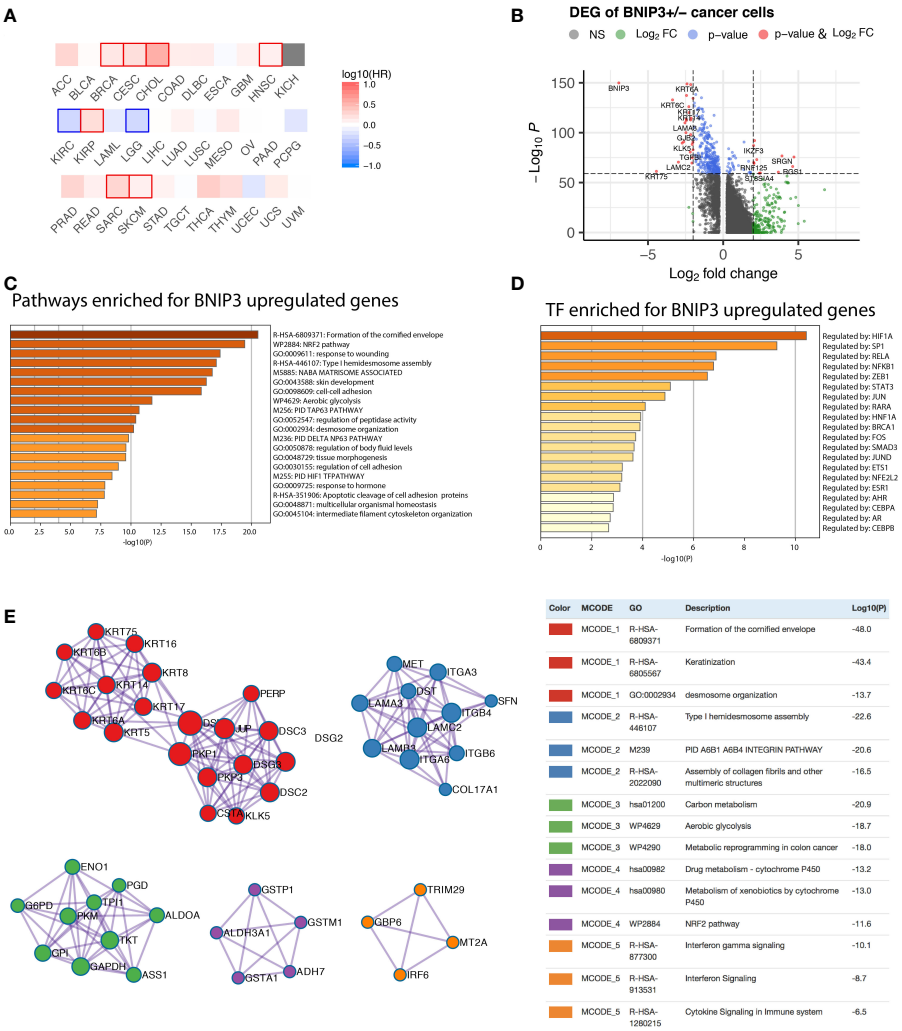

FIGURE 1 | **(A)** Prognostic significance of BNIP3 in the TCGA cohort. Highlighted squares indicate *p*-value smaller than 0.1. **(B)** Volcano plot showing the differentially expressed genes between BNIP3-positive and -negative cancer cells. **(C)** Top pathways enriched for BNIP3 upregulated genes shown as barplot. **(D)** The top transcription factors enriched for BNIP3 upregulated genes. **(E)** Top protein–protein interaction modules enriched for BNIP3 upregulated genes.

The expression of BNIP3 was also investigated in a normal liver cell atlas. BNIP3 was mostly expressed by hepatocytes in the liver, but not by immune cells or stromal cells (**Figures 4A, B**). BNIP3-positive hepatocytes appeared to have a more active cycling feature, as evidenced by an increased proportion of hepatocytes in S and G2M phase (**Figure 4C**). In the TCGA liver cancer cohort, we did observe that liver cancer patients with high expression of HIF1A or NRF2 (NFE2L2) tend to have a worse prognosis (p-value < 0.1) (**Figures 4D, E**). The expression of HIF1A and NRF2 was highly correlated in liver cancer samples from the TCGA cohort (**Figure 4F**).

Cancer cells cultured as organoids could better represent cancer cells grown *in vivo* and were shown to harbor increased stemness compared with cancer cells in 2D culture. We hypothesized that cancer cells might upregulate BNIP3 as a means to increase fitness when monolayer cell lines were converted into organoid lines. To validate this hypothesis, the HepG2 cell line was used as a parental cell line to establish a liver cancer organoid line (**Figure 5A**). HepG2 2D culture and organoid culture were subjected to bulk RNA-seq. The similarity matrix derived from RNA-seq data indicated a global change of transcriptome from 2D culture to 3D organoid culture (**Figure 5B**). Both oxidative phosphorylation and reactive oxygen species pathway increased in HepG2 organoids compared with HepG2 2D culture (**Figure 5C**). The expression of BNIP3 was significantly upregulated in the 3D culture of HepG2 as compared with 2D culture (p < 0.05). This upregulation was not observed for BCL2 Interacting Protein 3 Like (BNIP3L). Interestingly, liver cancer cells cultured as organoids have a significantly upregulated CD24 expression (p < 0.05), which played important roles in evasion from phagocytosis of cancer cells from macrophages (**Figure 5D**).

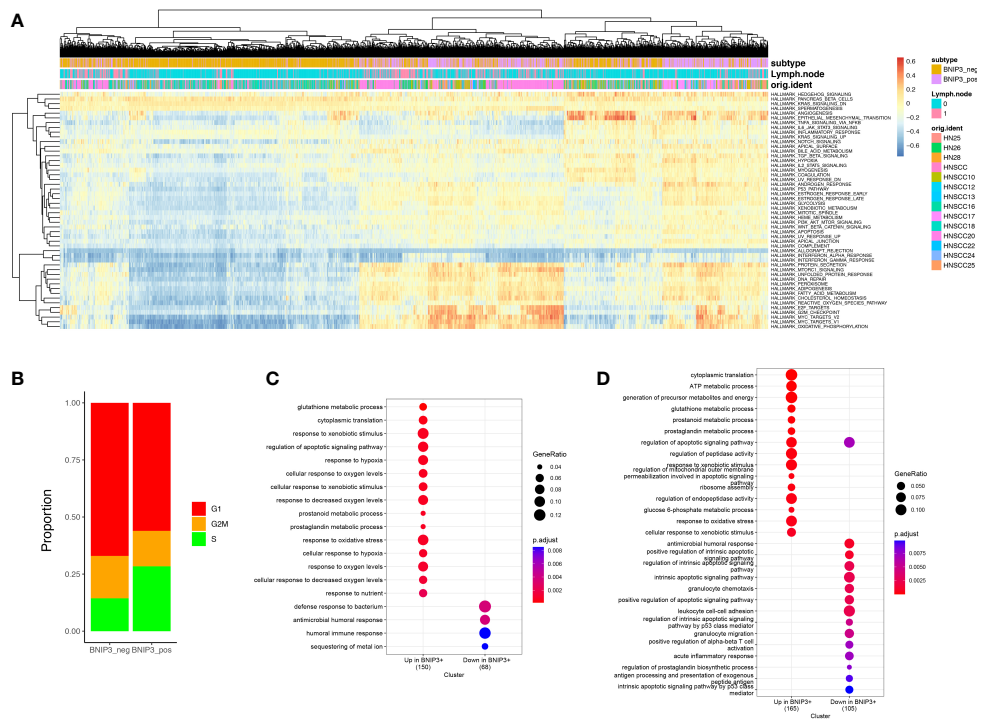

FIGURE 2 | **(A)** Heatmap of the hallmark pathways at the single-cell level. Each row represents one pathway and each column represents one cell. **(B)** Distribution of cell cycle phases for BNIP3-positive and BNIP3-negative cancer cells. **(C)** Pathway enrichment for BNIP3 upregulated and downregulated genes in lung cancer, using CCA integration. **(D)** Pathway enrichment for BNIP3 upregulated and downregulated genes in lung cancer, using harmony integration.

DISCUSSION

As carcinogenesis progresses, cancer cells are making important decisions of life and death constantly. Cancer cells have unlocked the secret of phenotypic plasticity represented by distinct subpopulations with genetic or epigenetic variability. Identification of key genes and pathways that serve as master regulators of cancer cell fate decisions is key for the design of optimal treatment strategy. Our study unraveled BNIP3 upregulation as a hallmark characterizing cancer cell subpopulation with increased fitness and proliferation.

Single-cell RNA sequencing has been applied by the research community to gain insights into cancer heterogeneity and cellular ecosystem. The enormous datasets generated so far would serve as a gold mine to identify key regulators of cancer cell fate decisions if carefully reanalyzed and integrated.

Interestingly, the cancer type with the highest BNIP3 expression is clear cell renal cell carcinoma (ccRCC). This is in agreement with the fact that HIF is no longer degradable due to the loss of tumor suppressor VHL in ccRCC (10). It has been demonstrated *in vitro* that siRNA-mediated downregulation of BNIP3 very effectively reduced the colony-forming capacity of RCC cells (11). BNIP3 overexpression has also been shown to enhance tumor growth for lung cancer (12) and liver cancer (13). In liver cancer cells, BNIP3 was proposed to be a therapeutic target for cancer metastasis as BNIP3 upregulation enhanced anoikis resistance of HCC cells.

Controversial results have been reported regarding the role of BNIP3 in breast cancer. BNIP3 deletion in triple-negative breast cancer promoted the metastasis of disease by deregulating mitophagy (14). On the contrary, it has been demonstrated that BNIP3 promoted the malignant phenotypes of breast cancer cells under hypoxia (15). Other studies made a distinction between ductal carcinoma *in situ* (DCIS) and invasive carcinoma, suggesting that BNIP3 upregulation was correlated with higher risk of relapse and shorter disease-free survival only in DCIS (16).

Cancer cells have harnessed the built-in cellular programs to adapt to hypoxia, which is a common feature of tumor microenvironment. The hypoxic niches typically render chemotherapy (17) or radiation therapy (18) ineffective. Targeting HIF-2a with belzutifan (MK-6482) has been quite successful in a recent phase II trial, achieving a 49% objective response rate in patients with renal cell carcinoma (19). Another key transcription factor, NRF2, underlying BNIP3 upregulated cancer cell subpopulation has also recently been indirectly targeted with a chemical proteomic approach (20).

Our study suggested that BNIP3 might be involved in the enhanced tumorigenicity of liver cancer cells. This is consistent with a previous report that BNIP3 protects HepG2 cells against etoposide-induced cell death under hypoxia (21). Furthermore, BNIP3 upregulated cancer cells might be armed with immune evasion arsenals. Our results have demonstrated that CD24, a

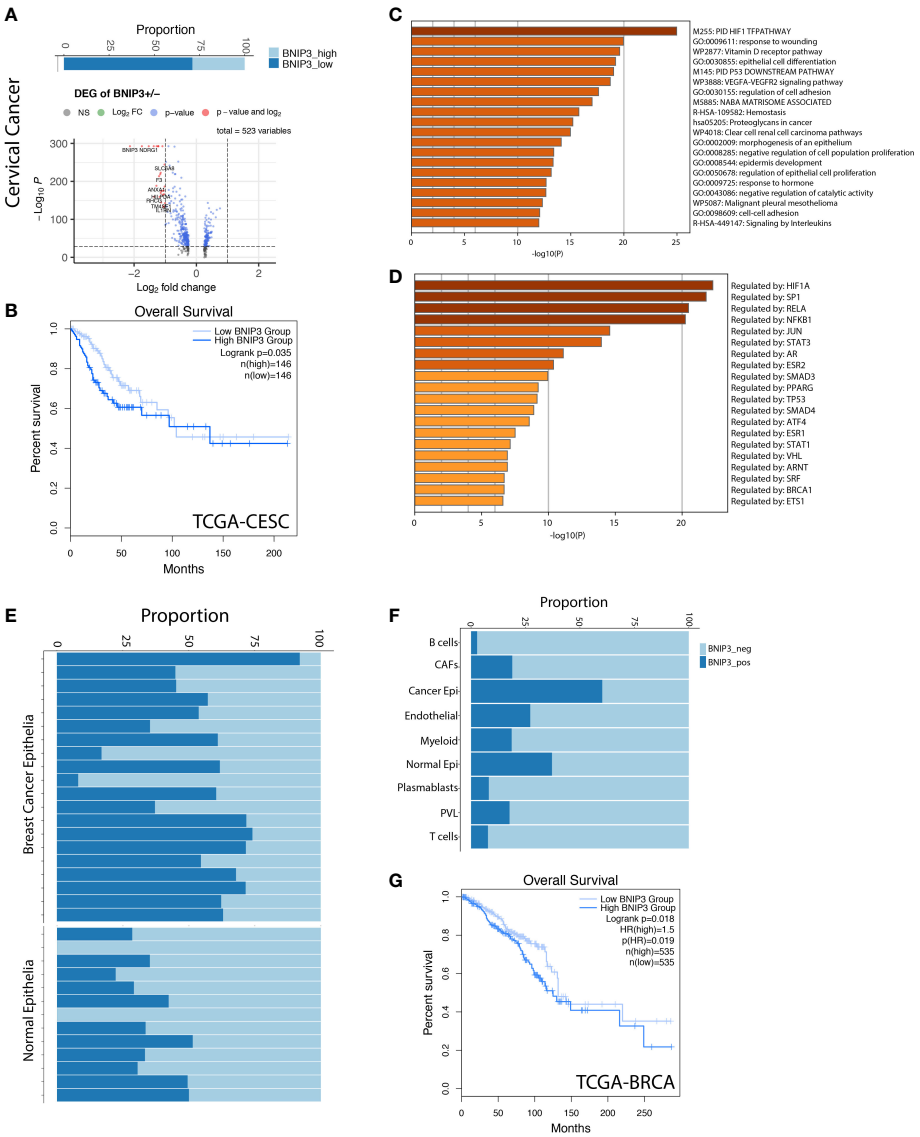

FIGURE 3 | **(A)** The percentage of BNIP3 high and low cancer cells in cervical cancer and the volcano plot visualizing the differentially expressed genes between BNIP3 high and low cervical cancer cells. **(B)** Survival curve for cervical cancer patients in the TCGA cohort, stratified by BNIP3 mRNA expression. **(C)** Top pathways enriched for BNIP3 upregulated genes shown as barplot. **(D)** The top transcription factors enriched for BNIP3 upregulated genes. **(E)** Proportion of BNIP3-positive and -negative cells in cancer epithelia and normal epithelia of the breast shown visualized as stacked barplot. Each bar indicates one individual. **(F)** Proportion of BNIP3-positive cells and negative cells in major cell types in the breast cancer cell atlas. **(G)** Survival curve for breast cancer patients in the TCGA cohort, stratified by BNIP3 mRNA expression.

"don't eat me" signal, has been upregulated in liver cancer organoids together with BNIP3. It has also been shown that a hypoxia-inducible factor elevated the expression of PD-L1 in ccRCC cells (22).

Taken together, the systems biology approach marrying *in silico* perturbations using public single-cell datasets and experimental cancer modeling using organoids in our study unraveled a cancer cell subpopulation characterized by BNIP3 upregulation and revealed the potential druggable master regulators of enhanced fitness and proliferation.

METHODS

Processing of Single-Cell Datasets

For single-cell datasets, annotations (meta data) from the original publications were used whenever possible. For GSE131907, "Malignant cells" as defined by original researchers were considered as cancer cells and used in our analysis. For GSE168652, cells with the number of detected genes (nFeature_RNA) between 500 and 7,500 were retained. The upper limit of total UMI count was set as 50,000 to remove

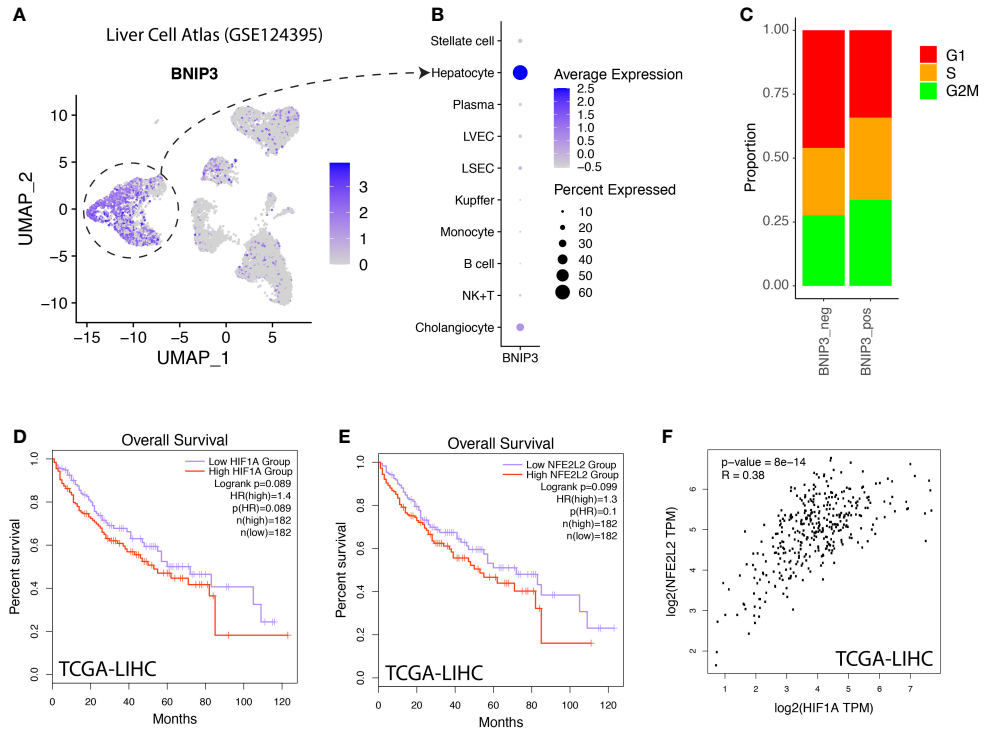

FIGURE 4 | **(A)** Liver cell atlas visualized in UMAP plot, the intensity of color indicating expression of BNIP3. **(B)** Dotplot visualization of BNIP3 in major cell types within the liver. **(C)** Distribution of cell cycle phases for BNIP3-positive and BNIP3-negative hepatocytes. **(D)** Survival analysis of hepatocellular carcinoma patients in the TCGA cohort, stratified by mRNA expression of HIF1A. **(E)** Survival analysis of hepatocellular carcinoma patients in the TCGA cohort, stratified by mRNA expression of NFE2L2. **(F)** Correlation between the expression of HIF1A and NFE2L2 in liver cancers in the TCGA cohort.

potential doublets and multiplets. Cells with more than 20% of mitochondrial RNA detected were also removed from our analysis. For datasets without meta data, quality control and unsupervised clustering were performed with Seurat. The count data were normalized using the "LogNormalize" method with a scaling factor of 10,000. The top 2,000 most variable genes were selected using the "vst" method. For cancer cell grouping based on BNIP3 expression, cancer cells with at least one UMI detected for BNIP3 were considered as BNIP3-positive.

Identification of Differentially Expressed Genes

Upregulated genes in each cell cluster were identified using the "FindMarkers" function with the statistical test method "wilcox". Only genes expressed in more than 25% of cells and altered with log2FC higher than 0.25 were retained for further analysis.

Inference of Cell Cycle Phase From Single-Cell Data

Cell cycle scoring with single-cell transcriptomic data was performed with the "CellCycleScoring" function in Seurat. Each cell is assigned a score based on expression of G2/M markers and S phase markers. Cell cycle phase was predicted based on the respective cell cycle scores (G1, S, and G2M). The genes used for cell cycle scoring can be found in cc.genes.updated.2019 originally derived from a melanoma study (23).

Gene List Analysis

Differentially expressed genes with |log2FC| higher than 1 and *p*-value smaller than 0.05 were subjected to gene list analysis using metascape (24), including pathway enrichment, analysis of protein–protein interaction, and inference of transcription factors. Default parameters were used for implementation.

Gene Set Variation Analysis

GSVA was implemented with the GSVA package in R. The hallmark pathways and KEGG pathways were retrieved from MSigDB. For transcript per million reads (TPM) expression data, "Gaussian" was used as the kernel for the non-parametric estimation of the cumulative distribution function of expression levels. For single-cell datasets, the normalized data slot from the RNA assay was used as input for GSVA implemented also using "Gaussian" as the kernel for the non-parametric estimation of the cumulative distribution function of expression levels.

SCENIC Analysis

SCENIC (25) was implemented with pySCENIC software. Transcription factors and corresponding target genes (regulon) were inferred based on co-expression of genes across cells. In brief, SCENIC infers TFs and their target genes from correlations between the expression of genes across cells. A TF and its target genes are defined as a regulon. The regulons are then refined by

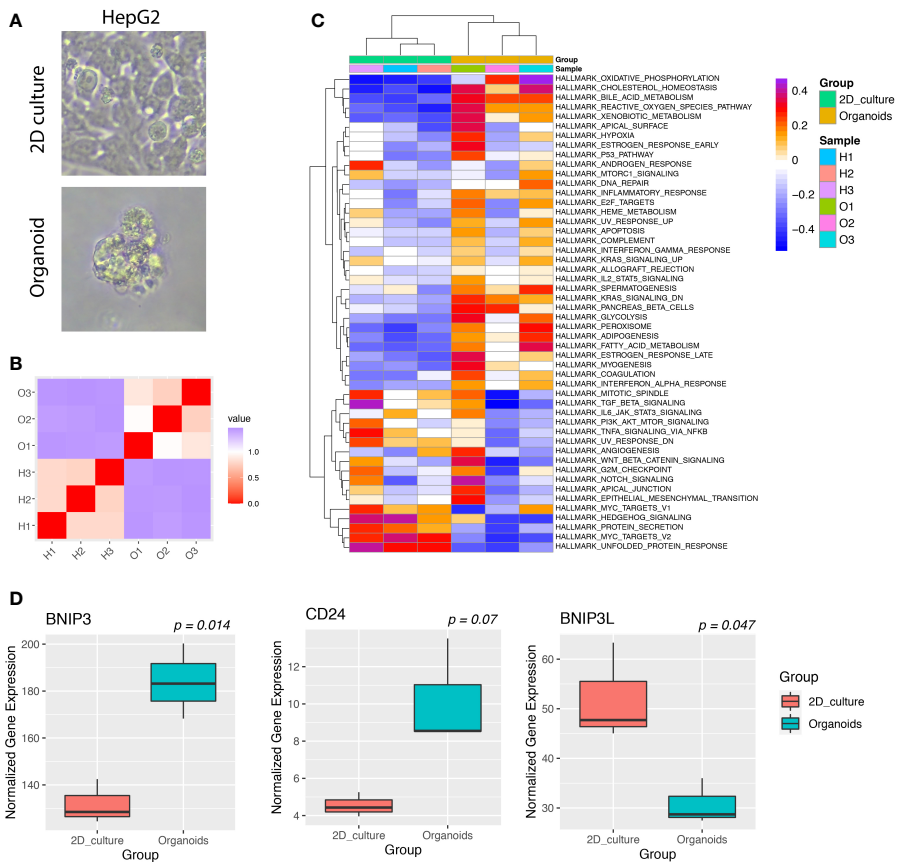

FIGURE 5 | **(A)** Images of HepG2 cancer cells cultured in 2D culture or organoid culture. **(B)** Heatmap of the correlation matrix between individual cancer transcriptomes derived from 2D culture or organoid culture. **(C)** GSVA of hallmark pathways for individual cancer samples. Each row represents one hallmark pathway and each column represents one sample. Both rows and columns were arranged by hierarchical clustering. **(D)** Boxplots showing the expression of indicated genes for HepG2 cultured in 2D or organoids.

pruning targets based on enriched motifs. Finally, the activity of a regulon is measured by an AUCell value in each single cell. A high AUCell value indicates high activity and enrichment of a regulon in a cell.

Transcription Factor Scoring

The bulk RNA-seq data from HepG2 2D culture and organoid culture were analyzed by a method previously developed for global transcription factor activity scoring (26). For each transcription factor, the target genes with known regulation modes were extracted from the TTRUST database (27), resulting in a list of genes activated by the transcription factor and a list of genes repressed by the transcription factor. The ratio between the median expression level of an activated target gene and the median expression level of a repressed target gene was calculated for each transcription factor and log2 transformed to obtain a final transcription factor score.

TCGA/GTEx Data Mining

Investigation of BNIP3 expression in cancer samples and normal samples from TCGA or GTEx consortium was performed with GEPIA2 (http://gepia2.cancer-pku.cn/) (28). For survival map analysis, the significance level of 0.05 was used and the median expression was used to stratify patients into a high-expression group and a low-expression group. In total, 33 different cancer types from the TCGA project were investigated.

Cell Culture

HepG2 cells were seeded in a 10-cm culture dish and maintained in DMEM medium (L110KJ, BasalMedia) supplemented with 10% FBS. Medium was renewed every 2 days. For derivation of organoid line, HepG2 cells were centrifuged at 500 g for 5 min at 4°C. The cell pellet was resuspended in Matrigel (R&D, 3533-005-02). For one well of a 24-well plate, 50 µl of cell suspension with 10,000 cells was seeded for the Matrigel to solidify. After Matrigel solidification, 1 ml of medium was added to each well. The organoid medium A contained 1% PS, 1% Glutamax, 10 mM HEPES, B27 (1:50), N2 (1:100), 1.25 mM n-Acetyl-L-cysteine, 10 mM nicotinamide, 10 nM recombinant human Gastrin I, 50 ng/ml recombinant human EGF, 100 ng/ml recombinant human FGF10, 25 ng/ml recombinant human HGF, 10 µM Forskolin, 5 µM A8301, 10 µM Y27632, and 3 nM dexamethasone. The

organoid medium B contained 1% PS, 1% Glutamax, 10 mM HEPES, B27 (1:50), N2 (1:100), 1.25 mM n-Acetyl-L-cysteine, 10% Rspo-1 supernatant, 10 mM nicotinamide, 10 nM recombinant human Gastrin I, 50 ng/ml recombinant human EGF, 100 ng/ml recombinant human FGF10, 25 ng/ml recombinant human HGF, 10 μM Forskolin, and 5 μM A8301.

RNA Sequencing

HepG2 cultures were subjected to RNA extraction. After quality control with gel electrophoresis and Agilent 2100, mRNA were captured with beads coupled with oligo(dT) and fragmented before priming with random hexamers. First-strand and second-strand cDNA were synthesized and purified. The purified double-stranded cDNA were subjected to end repairing, A-tailing, and adapter ligation. The products were purified and size-selected before final PCR amplification. The PCR products were purified to obtain the final libraries, which were sequenced with Nova-seq 6000 to obtain 6G data for each sample. The raw reads were pre-processed and filtered before alignment to hg38 reference genome. Stringtie was employed to derive TPM expression matrix (29).

Statistical Analysis

All statistical analyses were performed with R. No statistical analysis was employed to estimate the sample size for desired statistical power. The identification of markers distinguishing different clusters of cells was performed with "wilcox" test, with 0.05 set as the cutoff for statistical significance. Multiple tests were corrected with the "BH" method. The statistical difference between survival curves for different patient groups stratified by BNIP3 expression level was tested with log-rank test, with 0.05 set as the cutoff for statistical significance. The difference in gene expression between 2D and 3D HepG2 cultures was tested with *t*-test, using 0.05 as the significance level.

DATA AVAILABILITY STATEMENT

The data presented in the study are deposited in the Zenodo repository, accession number 6481921. The single cell datasets analyzed in this study can be accessed from GEO repository with the following accession numbers: head and neck cancer (GSE103322) (9), lung cancer (GSE131907) (30), lung cancer (GSE148071) (31), breast cancer (GSE176078) (32), cervical cancer (GSE168652) (33), normal liver (GSE124395) (34).

AUTHOR CONTRIBUTIONS

YZ, YW, and XH designed and supervised the study. YZ, BC, JY, WZ, NS, YW, and XH performed data analysis and result interpretation. PD performed the experiments. YZ, YW, and XH wrote the manuscript. All authors participated in discussion and manuscript editing. All authors contributed to the article and approved the submitted version.

FUNDING

This study is supported by the National Science Foundation (Grant ID: 81903106).

ACKNOWLEDGMENTS

We thank Yantao Du for providing the HepG2 cell line used in our study. We also thank all the members of Center for Systems Biology (Intelliphecy) for discussion and input. We acknowledge the publication of a preprint by bioRxiv (35).

SUPPLEMENTARY MATERIAL

The Supplementary Material for this article can be found online at: https://www.frontiersin.org/articles/10.3389/fonc.2022.923890/full#supplementary-material

Supplementary Figure 1 | (A). The expression of BNIP3 quantified as TPM was shown for BNIP3 in cancer samples and paired normal samples in the TCGA datasets. **(B)**. The proportion of BNIP3 positive cancer cells in individual lung cancer sample. **(C)**. The proportion of BNIP3 positive cancer cells for three subtypes of breast cancers.

REFERENCES

1. Paek AL, Liu JC, Loewer A, and Forrester WC, Lahav G. Cell-To-Cell Variation in P53 Dynamics Leads to Fractional Killing. *Cell* (2016) 165 (3):631–42. doi: 10.1016/j.cell.2016.03.025
2. Spencer SL, Gaudet S, Albeck JG, Burke JM, Sorger PK. Non-Genetic Origins of Cell-to-Cell Variability in TRAIL-Induced Apoptosis. *Nature* (2009) 459 (7245):428–32. doi: 10.1038/nature08012
3. Ma Y, Wang L, Jia R. The Role of Mitochondrial Dynamics in Human Cancers. *Am J Cancer Res* (2020) 10(5):1278–93.
4. Chinnadurai G, Vijayalingam S, Gibson SB. *BNIP3 Subfamily BH3-Only Proteins: Mitochondrial Stress Sensors in Normal and Pathological Functions. Oncogene* (2008) 27 Suppl 1:S114–27. doi: 10.1038/onc.2009.49
5. Zhu Y, Massen S, Terenzio M, Lang V, Chen-Lindner S, Eils R, et al. Modulation of Serines 17 and 24 in the LC3-Interacting Region of Bnip3 Determines Pro-Survival Mitophagy Versus Apoptosis. *J Biol Chem* (2013) 288(2):1099–113. doi: 10.1074/jbc.M112.399345
6. Gonzalez-Silva L, Quevedo L, Varela I. Tumor Functional Heterogeneity Unraveled by scRNA-Seq Technologies. *Trends Cancer* (2020) 6(1):13–9. doi: 10.1016/j.trecan.2019.11.010
7. Tanay A, Regev A. Scaling Single-Cell Genomics From Phenomenology to Mechanism. *Nature* (2017) 541(7637):331–8. doi: 10.1038/nature21350
8. Hanzelmann S, Castelo R, Guinney J. GSVA: Gene Set Variation Analysis for Microarray and RNA-Seq Data. *BMC Bioinf* (2013) 14:7. doi: 10.1186/1471-2105-14-7
9. Puram SV, Tirosh I, Parikh AS, Patel AP, Yizhak K, Gillespie S, et al. Single-Cell Transcriptomic Analysis of Primary and Metastatic Tumor Ecosystems in Head and Neck Cancer. *Cell* (2017) 171(7):1611–24. doi: 10.1016/j.cell.2017.10.044
10. Kaelin WGJr. The Von Hippel-Lindau Tumor Suppressor Gene and Kidney Cancer. *Clin Cancer Res*. (2004) 10:6290S-6295S. doi: 10.1158/1078-0432.CCR-sup-040025

11. Xu Q, Junttila S, Scherer A, Giri KR, Kivela O, Skovorodkin I, et al. Renal Carcinoma/Kidney Progenitor Cell Chimera Organoid as a Novel Tumorigenesis Gene Discovery Model. *Dis Model Mech* (2017) 10 (12):1503–15. doi: 10.1242/dmm.028332
12. Vijayalingam S, Pillai SG, Rashmi R, Subramanian T, and Sagartz JE, Chinnadurai G. Overexpression of BH3-Only Protein BNIP3 Leads to Enhanced Tumor Growth. *Genes Cancer* (2010) 1(9):964–71. doi: 10.1177/1947601910386110
13. Sun L, Li T, Wei Q, Zhang Y, Jia X, Wan Z, et al. Upregulation of BNIP3 Mediated by ERK/HIF-1alpha Pathway Induces Autophagy and Contributes to Anoikis Resistance of Hepatocellular Carcinoma Cells. *Future Oncol* (2014) 10(8):1387–98. doi: 10.2217/fon.14.70
14. Chourasia AH, Tracy K, Frankenberger C, Boland ML, Sharifi MN, Drake LE, et al. Mitophagy Defects Arising From BNip3 Loss Promote Mammary Tumor Progression to Metastasis. *EMBO Rep* (2015) 16(9):1145–63. doi: 10.15252/embr.201540759
15. Zhang G, Xu Z, Yu M, Gao H. Bcl-2 Interacting Protein 3 (BNIP3) Promotes Tumor Growth in Breast Cancer Under Hypoxic Conditions Through an Autophagy-Dependent Pathway. *Bioengineered* (2022) 13(3):6280–92. doi: 10.1080/21655979.2022.2036399
16. Tan EY, et al. BNIP3 as a Progression Marker in Primary Human Breast Cancer; Opposing Functions in in Situ Versus Invasive Cancer. *Clin Cancer Res* (2007) 13(2 Pt 1):467–74. doi: 10.1158/1078-0432.CCR-06-1466
17. Cosse JP, Michiels C. Tumour Hypoxia Affects the Responsiveness of Cancer Cells to Chemotherapy and Promotes Cancer Progression. *Anticancer Agents Med Chem* (2008) 8(7):790–7. doi: 10.2174/187152008785914798
18. Rockwell S, Dobrucki IT, Kim EY, and Marrison ST, Vu VT. Hypoxia and Radiation Therapy: Past History, Ongoing Research, and Future Promise. *Curr Mol Med* (2009) 9(4):442–58. doi: 10.2174/156652409788167087
19. Jonasch E, Donskov F, Iliopoulos O, Rathmell WK, Narayan VK, Maughan BL, et al. Belzutifan for Renal Cell Carcinoma in Von Hippel-Lindau Disease. *N Engl J Med* (2021) 385(22):2036–46. doi: 10.1056/NEJMoa2103425
20. Bar-Peled L, Kemper EK, Suciu RM, Vinogradova EV, Backus KM, Horning BD, et al. Chemical Proteomics Identifies Druggable Vulnerabilities in a Genetically Defined Cancer. *Cell* (2017) 171(3):696–709.e23. doi: 10.1016/j.cell.2017.08.051
21. Cosse JP, Rommelaere G, Ninane N, and Arnould T, Michiels C. BNIP3 Protects HepG2 Cells Against Etoposide-Induced Cell Death Under Hypoxia by an Autophagy-Independent Pathway. *Biochem Pharmacol* (2010) 80 (8):1160–9. doi: 10.1016/j.bcp.2010.07.009
22. Ruf M, Moch H, Schraml P. PD-L1 Expression is Regulated by Hypoxia Inducible Factor in Clear Cell Renal Cell Carcinoma. *Int J Cancer* (2016) 139 (2):396–403. doi: 10.1002/ijc.30077
23. Tirosh I, Izar B, Prakadan SM, Wadsworth MH 2nd, Treacy D, Trombetta JJ, et al. Dissecting the Multicellular Ecosystem of Metastatic Melanoma by Single-Cell RNA-Seq. *Science* (2016) 352(6282):189–96. doi: 10.1158/1078-0432.CCR-sup-040025
24. Zhou Y, Zhou B, Pache L, Chang M, Khodabakhshi AH, Tanaseichuk O, et al. Metascape Provides a Biologist-Oriented Resource for the Analysis of Systems-Level Datasets. *Nat Commun* (2019) 10(1):1523. doi: 10.1038/s41467-019-09234-6
25. Aibar S, Gonzalez-Blas CB, Moerman T, Huynh-Thu VA, Imrichova H, Hulselmans G, et al. SCENIC: Single-Cell Regulatory Network Inference and Clustering. *Nat Methods* (2017) 14(11):1083–6. doi: 10.1038/nmeth.4463
26. Zhu Y, Cang S, Chen B, Gu Y, Jiang M, Yan J, et al. Patient Stratification of Clear Cell Renal Cell Carcinoma Using the Global Transcription Factor Activity Landscape Derived From RNA-Seq Data. *Front Oncol* (2020) 10:526577. doi: 10.3389/fonc.2020.526577
27. Han H, Cho JW, Lee S, Yun A, Kim H, Bae D, et al. TRRUST V2: An Expanded Reference Database of Human and Mouse Transcriptional Regulatory Interactions. *Nucleic Acids Res* (2018) 46(D1):D380–6. doi: 10.1093/nar/gkx1013
28. Tang Z, Kang B, Li C, and Chen T, Zhang Z. GEPIA2: An Enhanced Web Server for Large-Scale Expression Profiling and Interactive Analysis. *Nucleic Acids Res* (2019) 47(W1):W556–60. doi: 10.1093/nar/gkz430
29. Pertea M, Pertea GM, Antonescu CM, Chang TC, and Mendell JT, Salzberg SL. StringTie Enables Improved Reconstruction of a Transcriptome From RNA-Seq Reads. *Nat Biotechnol* (2015) 33(3):290–5. doi: 10.1038/nbt.3122
30. Kim N, et al. Single-Cell RNA Sequencing Demonstrates the Molecular and Cellular Reprogramming of Metastatic Lung Adenocarcinoma. *Nat Commun* (2020) 11(1):2285. doi: 10.1038/s41467-020-16164-1
31. Wu F, et al. Single-Cell Profiling of Tumor Heterogeneity and the Microenvironment in Advanced non-Small Cell Lung Cancer. *Nat Commun* (2021) 12(1):2540. doi: 10.1158/1078-0432.CCR-sup-040025
32. Wu SZ, et al. A Single-Cell and Spatially Resolved Atlas of Human Breast Cancers. *Nat Genet* (2021) 53(9):1334–47.
33. Li C, et al. Single-Cell Transcriptomics Reveals the Landscape of Intra-Tumoral Heterogeneity and Transcriptional Activities of ECs in CC. *Mol Ther Nucleic Acids* (2021) 24:682–94. doi: 10.1016/j.omtn.2021.03.017
34. Aizarani N, Sagar Saviano A, Mailly L, Durand S, Herman JS, et al. A Human Liver Cell Atlas Reveals Heterogeneity and Epithelial Progenitors. *Nature* (2019) 572(7768):199–204. doi: 10.1038/s41586-019-1373-2
35. Zhu Y, Chen B, Yan J, Zhao W, Dou P, Sun N, et al. BNIP3 upregulation characterizes cancer cell subpopulation with increased fitness and proliferation. *bioRxiv* (2022) 03(21):485237. doi: 10.1101/2022.03.21.485237

Conflict of Interest: XH, BC, PD, and NS were employed by Intelliphecy.

The remaining authors declare that the research was conducted in the absence of any commercial or financial relationships that could be construed as a potential conflict of interest.

Publisher's Note: All claims expressed in this article are solely those of the authors and do not necessarily represent those of their affiliated organizations, or those of the publisher, the editors and the reviewers. Any product that may be evaluated in this article, or claim that may be made by its manufacturer, is not guaranteed or endorsed by the publisher.

frontiers | Frontiers in Oncology

TYPE Original Research
PUBLISHED 01 August 2022
DOI 10.3389/fonc.2022.937444

OPEN ACCESS

EDITED BY
Junmin Zhang,
Lanzhou University, China

REVIEWED BY
Shigeo Ohba,
Fujita Health University, Japan
Xuan Yuan,
The Affiliated Hospital of Qingdao University, China

*CORRESPONDENCE
Jinyue Hu
2018050703@usc.edu.cn

SPECIALTY SECTION
This article was submitted to Pharmacology of Anti-Cancer Drugs, a section of the journal Frontiers in Oncology

RECEIVED 06 May 2022
ACCEPTED 11 July 2022
PUBLISHED 01 August 2022

CITATION
Ling M, Liu Q, Wang Y, Liu X, Jiang M and Hu J (2022) LCS-1 inhibition of superoxide dismutase 1 induces ROS-dependent death of glioma cells and degradates PARP and BRCA1. *Front. Oncol.* 12:937444. doi: 10.3389/fonc.2022.937444

LCS-1 inhibition of superoxide dismutase 1 induces ROS-dependent death of glioma cells and degradates PARP and BRCA1

Min Ling[1], Qing Liu[1], Yufei Wang[2,3], Xueting Liu[3], Manli Jiang[3] and Jinyue Hu[3]*

[1]Department of Neurosurgery, Xiangya Hospital, Central South University, Changsha, China, [2]Department of Clinical Laboratory, Changsha Central Hospital, Hengyang Medical School, University of South China, Changsha, China, [3]Medical Research Center, Changsha Central Hospital, Hengyang Medical School, University of South China, Changsha, China

Gliomas are characterized by high morbidity and mortality, and have only slightly increased survival with recent considerable improvements for treatment. An innovative therapeutic strategy had been developed *via* inducing ROS-dependent cell death by targeting antioxidant proteins. In this study, we found that glioma tissues expressed high levels of superoxide dismutase 1 (SOD1). The expression of SOD1 was upregulated in glioma grade III and V tissues compared with that in normal brain tissues or glioma grade I tissues. U251 and U87 glioma cells expressed high levels of SOD1, low levels of SOD2 and very low levels of SOD3. LCS-1, an inhibitor of SOD1, increased the expression SOD1 at both mRNA and protein levels slightly but significantly. As expected, LCS-1 caused ROS production in a dose- and time-dependent manner. SOD1 inhibition also induced the gene expression of HO-1, GCLC, GCLM and NQO1 which are targeting genes of nuclear factor erythroid 2-related factor 2, suggesting the activation of ROS signal pathway. Importantly, LCS-1 induced death of U251 and U87 cells dose- and time-dependently. The cell death was reversed by the pretreatment of cells with ROS scavenges NAC or GSH. Furthermore, LCS-1 decreased the growth of xenograft tumors formed by U87 glioma cells in nude mice. Mechanistically, the inhibition of P53, caspases did not reverse LCS-1-induced cell death, indicating the failure of these molecules involving in cell death. Moreover, we found that LCS-1 treatment induced the degradation of both PARP and BRCA1 simultaneously, suggesting that LCS-1-induced cell death may be associated with the failure of DNA damage repair. Taking together, these results suggest that the degradation of both PARP and BRCA1 may contribute to cell death induced by SOD1 inhibition, and SOD1 may be a target for glioma therapy.

KEYWORDS

glioma, LCS-1, SOD1, ROS, PARP, BRCA1, cell death

Introduction

Owing to the localization and the often locally invasive growth, central nervous system tumors are characterized by high morbidity and mortality (1). Gliomas are the most common types of primary brain tumors, accounting for almost 30% of all primary brain tumors, and 80% of all malignant types, and are responsible for the majority of deaths from primary brain tumors (1). Conventional treatment strategies of gliomas provide a gross total removal of tumors, which are associated with several cycles of radiotherapy and chemotherapy (1). Though considerable improvements in terms of surgical approaches including operative microscopes and image guided surgery have been reached, patients have only slightly increased survival (1). So optimal therapeutic strategy is required to improve the therapeutic effects and increase patient survival.

Reactive oxygen species (ROS) are oxygen-containing free radicals which are derived from the partial reduction of oxygen (2). ROS have dual roles in cell metabolism. At low to moderate levels, ROS act as signal transducers to activate cell proliferation, migration, invasion, and angiogenesis. In contrast, high levels of ROS cause damage to proteins, nucleic acids, lipids, membranes, and organelles, leading to cell death (3). Typically, cancer cells exhibit high levels of ROS compared with normal cells as a result of an imbalance between oxidants and antioxidants (3). Anticancer therapeutic strategies have been developed by manipulating ROS levels *via* inducing more oxidants and/or targeting antioxidants (3). By modulating ROS, a number of natural or synthesized compounds have been used for cancer therapy (4–9).

Superoxide Dismutases (SOD) are highly conserved enzymes, which play fundamental roles in protecting cells from oxidative stress by catalyzing the dismutation of the superoxide radical (10). There are three forms of SOD that incorporate different covalently bound substances (Mn, Zn, Cu, Fe), and inactivate both intra- and extra-cellular superoxides (10). SOD1 (Cu/Zn SOD), which contains copper and zinc, localizes in the cytoplasm, nuclei, lysosomes and peroxisomes, and also in mitochondrial intermembrane space (10). SOD2 (Mn SOD) contains manganese and is predominantly observed in the mitochondrial matrix (10). The third one, SOD3 (Cu/Zn extracellular SOD), also contains copper and zinc but is secreted to the extracellular space (10). SOD1 is a 15.9 kDa homodimer which is held by hydrophobic contacts that reduce solvent accessibility and increase its stability. Each monomer contains a copper and a zinc ion, which together have either a structural or catalytic function. Beside its enzymatic activity to dismutae superoxide radical, SOD1 translocates nuclei as a transcription factor to regulate the expression of oxidative resistance and repair genes in response to high levels of hydrogen peroxide (11).

In cancer cells, the dysfunction of SOD1 causes ROS-dependent cell damage which should benefit for cancer therapy. Early, SOD1 inhibitor ATN-224 has been reported to attenuate angiogenesis and tumor cell proliferation (12). ATN-224 has also been reported to induce cell death in various NSCLC cells, including those harboring KRAS mutations (13). Another samll molecular LCS-1 (lung cancer screen 1, 4,5-Dichloro-2-(3-methylphenyl)-3(2H)-pyridazinone) is screened as an inhibitor of SOD1 and inhibits the growth of lung adenocarcinoma cell lines (14), and has been reported to induce death of colorectal cancer cells and breast cancer cells (15–17). However, the effect of SOD1 inhibition on glioma therapy is not understood. Especially, the detailed mechanism of cell death induced by SOD1 inhibition remains elusive in cancer cells.

In this study, we found that clinical glioma expressed increased SOD1. LCS-1 inhibition of SOD1 induced ROS-dependent cell death in glioma cells, and decreased glioma growth *in vivo*. Mechanistically, LCS-1-induced cell death was not associated with P53 and caspase. But it may be associated with PARP and BRCA1, because PARP inhibitors induce anti-cancer effect in BRCA1-mutant cancer types, and LCS-1 induced the degradation of both PARP and BRCA1 simultaneously.

Materials and methods

Cell lines

Hunan glioma cell line U87 was purchased from ATCC (Manassas, VA, USA). U251 is a human glioma cell line as well (18). Cells were grown in DMEM, containing 10% FCS, 100 units/ml penicillin, and 100 mg/ml streptomycin. All cells were cultured in a humidified atmosphere with 5% CO_2 at 37°C.

Animals

Female BALB/c nude mice (6–8 weeks old) were purchased from SLAC Laboratory Animal Center (Shanghai, China). All animal studies were carried out in accordance with the Guidelines for the Care and Use of Laboratory Animals issued by the National Institutes of Health and approved by the Animal Ethics Committee of the Changsha Central Hospital, University

Abbreviations: BRCA1, breast cancer gene 1; EJ, end-joining; FITC, fluorescein isothiocyanate; GAPDH, glyceraldehyde-3-phosphate dehydrogenase; GCLC, γ-glutamyl cysteine ligase catalytic subunits; GCLM, γ-glutamyl cysteine ligase modulatory subunits; GSH, reduced glutathione; HO-1, heme oxygenase-1; HR, homologous recombination; IHC, immunohistochemistry; LCS-1, lung cancer screen 1; NAC, N-acetyl-L-cysteine; NPC, nasopharyngeal carcinoma; NQO1, NAD(P)H dehydrogenase quinone 1; NSCLC, non-small-cell lung cancer; PARP, poly (ADP-ribose) polymerase; PI, propidium iodide; qRT-PCR, quantitative reverse transcriptional-polymerase chain reaction; RIP1, receptor-interacting protein 1; ROS, Reactive oxygen species; SOD1, superoxide dismutase 1.

of South China (No. CCH-AEC-2020-02). Animals were maintained with standard rodent chow and free access to water under controlled conditions with a 12-h light and 12-h dark cycle and a temperature of 24 ± 2°C.

Reagents

Mouse monoclonal anti-human SOD1 (sc-101523), SOD2 (sc-137254), BRCA1 (sc-6954) and BRCA2 (sc-518154) were purchased from Santa Cruz Biotechnology (Santa Cruz, CA, USA). Rabbit anti-human caspase 3 (9662), PARP (9532), HO-1 (5853) antibodies were purchased from Cell Signaling Technology (Beverly, MA, USA). ROS scavengers N-acetyl cysteine (NAC, ST1546) and reduced glutathione (GSH, S0073), DCF ROS assay kit (S0033), pan-caspase inhibitor Z-vad-FMK (C1202), and a mouse monoclonal anti-human GAPDH antibody (AF5009) were purchased from Beyotime (Shanghai, China). PARP inhibitor PJ34 (3255), were purchased from Tocris (Ellisville, MO, USA). SOD1 inhibitor LCS-1 (567417) was purchased from Merck (Darmstadt, Germany). Recombinant human EGF (AF-100-15), IL-6 (200-06) were purchased from PeproTech (Rocky Hill, NJ, USA).

Immunoblot

1 – 2 × 10^6 cells were lysed in 200 ml lysis buffer (20 mM Tris, pH 7.5, 150 mM NaCl, 1% Triton X-100, 1 mM EDTA, 1 mM β-glycerophosphate, 1 mM sodium pyrophosphate, 1 mM Na_3VO_4, 1 mg/ml leupeptin). The cell lysate was centrifuged at 12,000 g for 5 min at 4°C. Proteins were electrophoresed on 8-10% SDS-PAGE gels, and transferred onto Immobilon P membranes (Millipore, Billerica, MA, USA). The membranes were blocked by incubation in 3% nonfat dry milk at room temperature for 1 h and then incubated with primary antibodies in PBS containing 0.01% Tween 20 at 4°C overnight. After incubation with a horseradish peroxidase-conjugated secondary antibody, the protein bands were detected with SuperSignal chemiluminescent substrate-stable peroxide solution (Pierce Rockford, IL, USA) and BIOMAX-MR film (Eastman Kodak Co., Rochester, NY, USA). When necessary, the membranes were stripped with Restore Western Blot Stripping Buffer (Pierce) and re-probed with antibodies against various cellular proteins.

Quantitative reverse transcriptional-polymerase chain reaction (qRT-PCR)

The qRT-PCR was performed as described by Sun et al. (19). Briefly, total RNA was extracted from 1 - 2 × 10^6 cells by use of TRIzol (Invitrogen, Carlsbad, CA, USA) as described by the manufacturer. mRNA was reverse transcribed with RevertAid (MBI Fermentas, Burlington Ontario, Canada) at 42°C for 60 min. cDNA was amplified by use of TaqMan Universal PCR master mix (Roche Applied Science) and a LightCycle 96 detection system (Roche Applied Science). The amplification of the target genes was normalized by use of the amplification levels of glyceraldehyde-3-phosphate dehydrogenase (GAPDH) as an endogenous control. The efficiency of the PCR was tested by amplification of the target from serially diluted cDNA generated from the reverse transcription of a stock set of human RNA. The data analysis and calculations were performed using the $2^{-\Delta\Delta CT}$ comparative method, as described by the manufacturer. Gene expression is shown as the fold induction of a gene measured in LCS-1-treated samples relative to samples cultured with medium. The forward and reverse primer pairs are listed (5' to 3') as follows:

BCL2-S: CGTTTGGCAGTGCAATGGT,
BCL2-A: TTCTTGATTGAGCGAGCCTT;
GAPDH-S, AATCCCATCACCATCTTCCA,
GAPDH-A, CCTGCTTCACCACCTTCTTG;
GCLC-S: ATCCTCCAGTTCCTGCACAT,
GCLC-A: TTTTCGCATGTTGGCCTCAA;
GCLM-S: TCCTTGGAGCATTTACAGCC,
GCLM-A: AGAGCTTCTTGGAAACTTGCT;
HO-1-S: CCAGTCTTCGCCCCTGTC,
HO-1-A: GGGCTTTCTGGGCAATCTTT;
MDM2-S: TTCGTGAGAATTGGCTTCC,
MDM2-A: GGCAGGGCTTATTCCTTTTCT;
Noxa-S: CCAAACTCTTCTGCTCAGGAA,
Noxa-A: ATCACAGGTCATCTCCCTTCA;
NQO1-S: GTCGGACCTCTATGCCATGA,
NQO1-A: GGGTCCTTTGTCATACATGGC;
SOD1-S: AGGGCATCATCAATTTCGAGC,
SOD1-A: TGATGCAATGGTCTCCTGAG;
SOD2-S: ACATCAACGCGCAGATCATG,
SOD2-A: CAACAGATGCAGCCGTCAG;
SOD3-S: CCACCATCCTTCCATCCTGA,
SOD3-A: GAAACAGCTGAAGACGCGG;

DCF staining assay for measurement of ROS

Intracellular ROS levels were measured by DCF ROS assay according to the manufacturers' standard protocols. Briefly, 1 – 2 × 10^6 cells were cultured in FCS-free medium with 10 μM dichlorofluorescein diacetate (DCFH-DA) at 37°C for 30 min, and then washed with FCS-free medium trice, followed by the treatment with various reagents described in figure legends. ROS in the cells causes the oxidation of DCFH-DA, yielding the fluorescent product 2′,7′-dichlorofluorescein (DCF). The fluorescence of DCF was measured using a FACScan (BD Bioscience, San Jose, CA). For each analysis, 10,000 events were recorded.

Flow cytometric analysis

Cell death was detected by propidium iodide (PI)/fluorescein isothiocyanate (FITC)-annexin V staining. Briefly, 1 - 2 × 10^6 cells were washed twice with PBS and then labeled with FITC-annexin V and PI in binding buffer according to manufacturer's instructions. The fluorescence signals were detected on a FACScan (BD Bioscience, San Jose, CA). The log of FITC-annexin V–fluorescence was displayed on the x-axis, and the log of PI fluorescence was displayed on the y-axis. For each analysis, 10,000 events were recorded.

For protein detection, cells were cultured in 6 well plates for 24 h, and harvested and washed with fluorescence-activated cell sorting buffer (5 mmol/L EDTA, 0.1% NaN 3, and 1% FCS in Dulbecco's PBS). After incubation with an antibody against human SOD1 or SOD2 for 30 min on ice, the cells were stained with a FITC-labeled secondary antibody and protein expression was examined by flow cytometry (BD Bioscience, San Jose, CA).

Tissue microarray and immunohistochemistry

For immunohistochemistry, a tissue microarray (78 samples) was purchased from Bioaitech company (F1081301, Xian, China), which contained four samples of brain normal tissue, 10 samples of glioma adjacent tissue, 64 samples of glioma. The use of the human tissue microarrays was approved by the ethics committee of Changsha Central Hospital, University of South China. Immunohistochemistry was performed to detect SOD1 expression as described in a previous study (20). Positive staining was evaluated in random four fields (100 cells) under microscope at 400× magnification. The staining intensity was scored as follows: 0 = no expression, 1 + = weak expression, 2 + = moderate expression, 3 + = strong expression, and 4 + = very strong expression. The final scores were expressed as immunohistochemical staining scores (IHC scores) obtained by multiplying the percentage of positive cells with the staining intensity (21).

Implantation of cervical cancer cells in nude mice

Female BALB/c nude mice (6 – 8 weeks old) from SLAC Laboratory Animal Center (Shanghai, China) were used in all experiments. 1× 10^7 U87 glioma cells in 200 µl PBS were implanted by s.c. injection into the right flanks of the mice. At day 15 after initial implantation, 10 mice were divided into two groups. In experimental group, five mice were injected i.p. with LCS-1 (400 nmol per mouse) every two days for 14 times beginning at day 15. Five mice were injected with vehicle as control. The growth of implanted tumors was examined every two days. Tumor sizes were calculated by the formula $LW^2/2$, where L is the length of the tumors in centimeters and W is the width of the tumors in centimeters. At day 45, all mice were euthanized, and the weight of tumors and mouse bodies was measured. Animal care was provided in accordance with the Guide for the Care and Use of Laboratory Animals.

Statistical analysis

All experiments were performed at least three times, and the representative results were shown. The results were expressed as the mean ± S.D. Differences between groups were examined for statistical significance using two tailed Student's *t* test, and *P* values equal to or < 0.05 were considered statistically significant (n = 3 for each qRT-PCR and ELISA test).

Results

The expression of SOD1 was up-regulated in glioma tissues

Emerging evidences indicate that SOD1 is overexpressed in cancers and is essential to maintain cellular redox homeostasis under the condition with excessive ROS derived from the aberrant metabolism (22, 23). However, the expression of SOD1 in gliomas is still unknown. In this study, SOD1 expression was first detected in glioma tissue microassay (78 samples) which included four samples of brain normal tissues, 10 samples of glioma adjacent tissues, 12 samples of glioma grade I tissues, 12 samples of glioma grade II tissues, 22 samples of glioma grade III tissues, and 18 samples of glioma grade IV tissues (Bioaitech). The expression levels of SOD1 were evaluated by use of immunohistochemical (IHC) scores. The results showed that SOD1 IHC scores were 224 ± 57, 294 ± 51, 238 ± 85, 281 ± 78, 308 ± 55, 314 ± 42 for normal tissues, glioma adjacent tissues, glioma grade I, II, III and IV tissues respectively (Figure 1A). Statistical results showed that the expression scores of SOD1 in glioma grade III and IV tissues were significantly higher than that in brain normal tissues and glioma grade I tissues ($P < 0.05$) (Figure 1A). In brain normal tissues, non-sample was SOD1 negative staining (scores: 0-80), two samples were SOD1 weak staining (scores: 81-200), two samples were SOD1 moderate staining (scores: 201-300) and non-sample was SOD1 strong staining (301–400) (Figure 1B). In glioma adjacent tissues, non-sample was SOD1 negative staining, one sample was SOD1 weak staining, five samples were SOD1 moderate staining, and four samples were SOD1 strong staining (Figure 1B). In glioma grade I tissues, non-sample was SOD1 negative staining, three samples were SOD1 weak staining, six samples were SOD1 moderate staining, and three samples were SOD1 strong staining

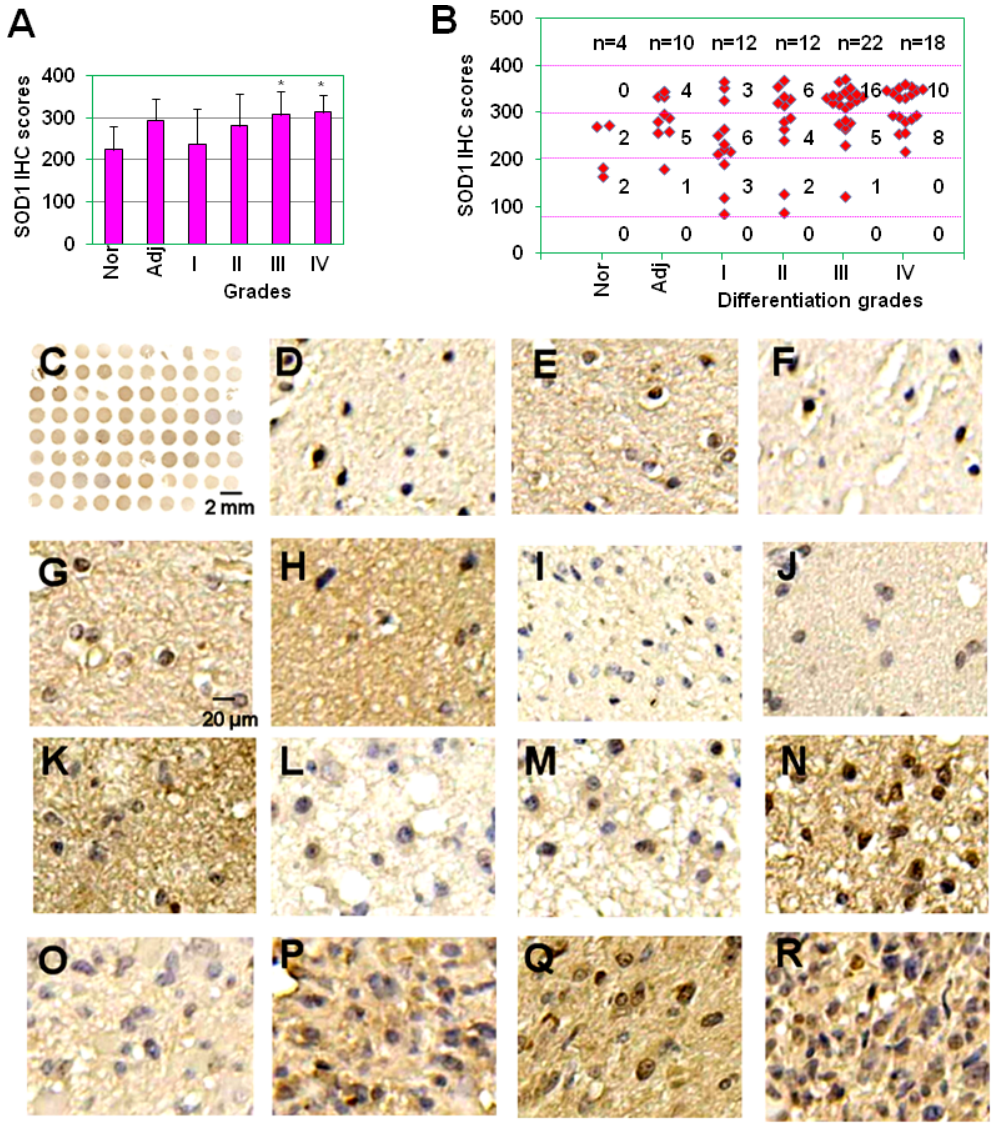

FIGURE 1
The expression of SOD1 in glioma tissues. **(A)** SOD1 IHC scores of normal brain tissues, tumor adjacent tissues and glioma grade I, II, III and IV tissues. * $P < 0.05$ compared with the normal brain tissue (Nor) or glioma grade I tissues. **(B)** Staining intensity of glioma with different histopathological types. Staining intensity was scored using a four-tier scale and defined as follows: negative staining (0-80); weak staining (80-200); moderate staining (200-300); strong staining (300-400). Nor, normal brain tissue; Adj, glioma adjacent tissues; I, well differentiated glioma; II, moderately differentiated glioma; III, poorly differentiated glioma; and IV, non-differentiated glioma. **(C)** SOD1 IHC staining for full glioma microarray. **(D-E)** Representative SOD1 weak **(D)**, moderate staining **(E)** in normal brain tissues. **(F-H)** Representative SOD1 weak **(F)**, moderate **(G)**, strong staining **(H)** in glioma adjacent tissues. **(I-K)** Representative SOD1 weak **(I)**, moderate **(J)**, strong staining **(K)** in glioma grade I tissues. **(L, M)** Representative SOD1 weak **(L)**, moderate **(M)**, strong staining **(N)** in glioma grade II tissues. **(O-Q)** Representative SOD1 weak **(O)**, moderate **(P)**, strong staining **(Q)** in glioma grade III tissues. **(R)** Representative SOD1 strong staining in glioma grade IV tissues.

(Figure 1B). In glioma grade II tissues, non-sample was SOD1 negative staining, two samples were SOD1 weak staining, four samples were SOD1 moderate staining and 6 samples were SOD1 strong staining (Figure 1B). In glioma grade III tissues, non-sample was SOD1 negative staining, one sample was SOD1 weak staining, five samples were SOD1 moderate staining and 16 samples were SOD1 strong staining (Figure 1B). In glioma grade IV tissues, non-sample was SOD1 negative staining, non-sample was SOD1 weak staining, 8 samples were SOD1 moderate staining and 10 samples were SOD1 strong staining (Figure 1B). Figure 1C showed the immunohistochemical (IHC) staining of SOD1 in the full tissue microarray. Figures 1D, E showed the representative SOD1 weak,

moderate staining in normal brain tissues. Figures 1F-H showed the representative SOD1 weak, moderate, strong staining in glioma adjacent tissues. Figures 1I-K showed the representative SOD1 weak, moderate, strong staining in glioma grade I tissues. Figures 1L-N showed the representative SOD1 weak, moderate, strong staining in glioma grade II tissues. Figures 1O-Q showed the representative SOD1 weak, moderate, strong staining in glioma grade III tissues. Figure 1R showed the representative SOD1 strong staining in glioma grade IV tissues. These results indicate that SOD1 expression is increased in clinical gliomas.

The expression of SOD1 in glioma cell lines

Before the testing of SOD1 inhibitor on cell survival in glioma, the expression of SOD1, SOD2 and SOD3 in U251 and U87 glioma cell lines was measured. qRT-PCR results showed that these two glioma cell lines expressed higher levels of SOD1, lower levels of SOD2, and very low levels of SOD3 (Figures 2A, B). FACS results showed that U251 and U87 cells expressed SOD1 and SOD2 proteins (Figure 2C). When SOD1 was inhibited by LCS-1, qRT-PCR results showed that SOD1 mRNA levels were slightly but significantly up-regulated (Figures 2D, E). Meanwhile, western blot results showed that LCS-1 treatment of U251 and U87 cells increased the protein levels slightly but significantly (Figures 2F-I). These results indicate that glioma cells expressed SOD1 and SOD2, and LCS-1 up-regulated SOD1.

LCS-1 mediates ROS production

The inhibition of SOD1 elicits the accumulation of ROS (22). To test the effect of SOD1 inhibitor LCS-1 on the production of ROS in U251 and U87 cells, DCF staining assay was used to detect the ROS levels in cells treated with LCS-1. FACS results showed that LCS-1 up-regulated ROS levels in a dose- and time-dependent manner (Figure 3A), suggest that SOD1 inhibition induced ROS production. To further test the activity of ROS induced by LCS-1, qRT-PCR was used to measure the expression of the targeting genes regulated by ROS pathways. The results showed that the mRNA levels of heme oxygenase-1 (HO-1), γ-glutamyl cysteine ligase modulatory and catalytic subunits GCLM and GCLC, NAD(P)H dehydrogenase quinone 1 (NQO1) were significantly increased in a dose- and time-

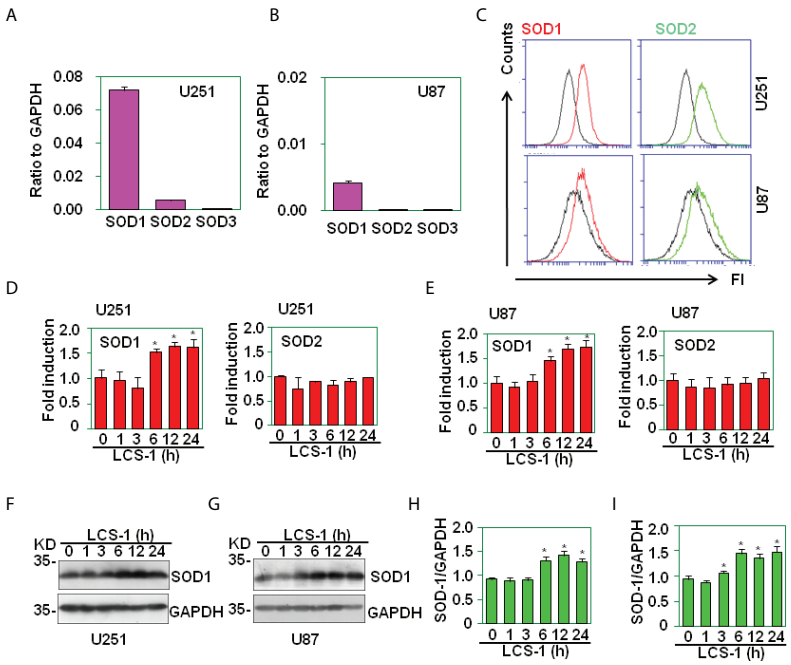

FIGURE 2
The expression of SOD1, SOD2 and SOD3 in glioma cell lines. **(A)** qRT-PCR analysis of SOD1, SOD2 and SOD3 mRNA levels in U251 cells. **(B)** qRT-PCR analysis of SOD1, SOD2 and SOD3 mRNA levels in U87 cells. **(C)** FACS analysis of SOD1 and SOD2 protein levels in U251 and U87 cells. **(D)** qRT-PCR analysis of SOD1 and 2 mRNA levels in U251 cells treated with 10 μM LCS-1 for the indicated time periods. * $P < 0.05$ compared with the medium groups. **(E)** qRT-PCR analysis of SOD1, SOD2 and SOD3 mRNA levels in U87 cells treated with 10 μM LCS-1 for the indicated time periods. * $P < 0.05$ compared with the medium groups. **(F, G)** Western blot analysis of the protein levels of SOD1 in U251 **(F)** and U87 **(G)** cells. **(H, I)** The quantitative data from F **(H)** and G **(I)** respectively. * $P < 0.05$ compared with the medium groups.

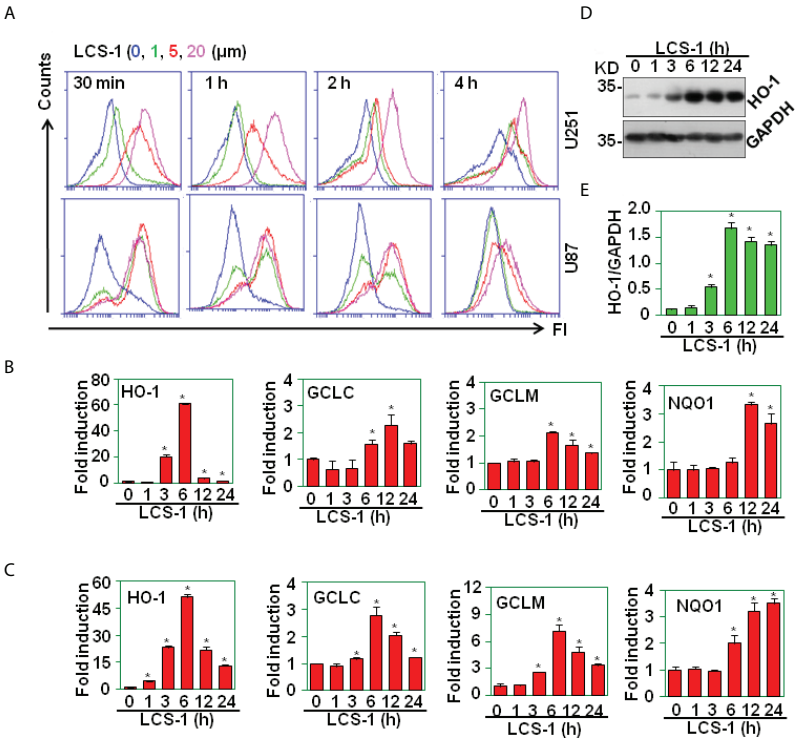

FIGURE 3
LCS-1 induces the production of ROS. **(A)** DCF staining analysis of ROS levels in U251 and U87 cells treated with the indicated doses of LCS-1 for the indicated time periods. **(B)** qRT-PCR analysis of the mRNA levels of NRF2-targeted genes in U251 cells treated with 10 μM LCS-1 for the indicated time periods. * $P < 0.05$ compared with the control groups. **(C)** qRT-PCR analysis of the mRNA levels of NRF2-targeted genes in U87 cells treated with 10 μM LCS-1 for the indicated time periods. * $P < 0.05$ compared with the control groups. **(D)** Western blot analysis of the protein levels of HO-1 in U87 cells treated with 10 μM LCS-1 for the indicated time periods. **(E)** Quantitative data from **(D)** * $P < 0.05$ compared with the medium groups.

dependent manner (Figures 3B, C). Meanwhile, western blot results showed that the treatment of U87 cells with LCS-1 significantly up-regulated the protein levels of HO-1 in U87 cells (Figures 3D, E). These results indicate that LCS-1 inhibition of SOD1 induces the production of ROS, and activates the ROS signaling pathways in glioma cell lines.

SOD1 inhibitor LCS-1 induces cell death

It is reported that SOD1 inhibitor LD100 promotes cancer cell apoptosis *via* regulating ROS signal pathway (23). In this study, SOD1 inhibitor LCS-1 induced ROS production, activated ROS signal pathway in glioma cells, indicating that LCS-1 may induce cell death in gliomas. By use of PI/FITC-Annexin V staining and FACS, we detected the effect of LCS-1 on the cell survival in U251 and U87 cells. The results showed that LCS-1 significantly induced cell death in both U251 and U87 cells in a dose- and time-dependent manner (Figures 4A-H). These results suggest that SOD1 inhibitor LCS-1 is an effective chemical for the induction of cell death in glioma cells.

ROS scavengers reverse LCS-1-induced cell death

To determine that LCS-1-induced cell death is related to the production of ROS, U251 and U87 cells were pretreated with ROS scavengers N-acetyl-L-cysteine (NAC) and reduced glutathione (GSH), and retreated with LCS-1, then cell death was measured. The results showed that in both U251 and U87 cells, NAC and GSH significantly reversed the cell death induced by LCS-1 in a dose-dependent manner (Figures 5A-H). These results indicate that LCS-1-induced cell death is ROS-dependent.

LCS-1 inhibits glioma growth in nude mice model

To determine the effect of LCS-1 on glioma growth *in vivo*, U87 glioma cells were implanted s.c. into the flanks of nude mice (n = 10). At day 15 after implantation, the mice (n = 5) in the experimental group were treated with LCS-1, and the mice (n = 5) in the control group were injected with vehicle.

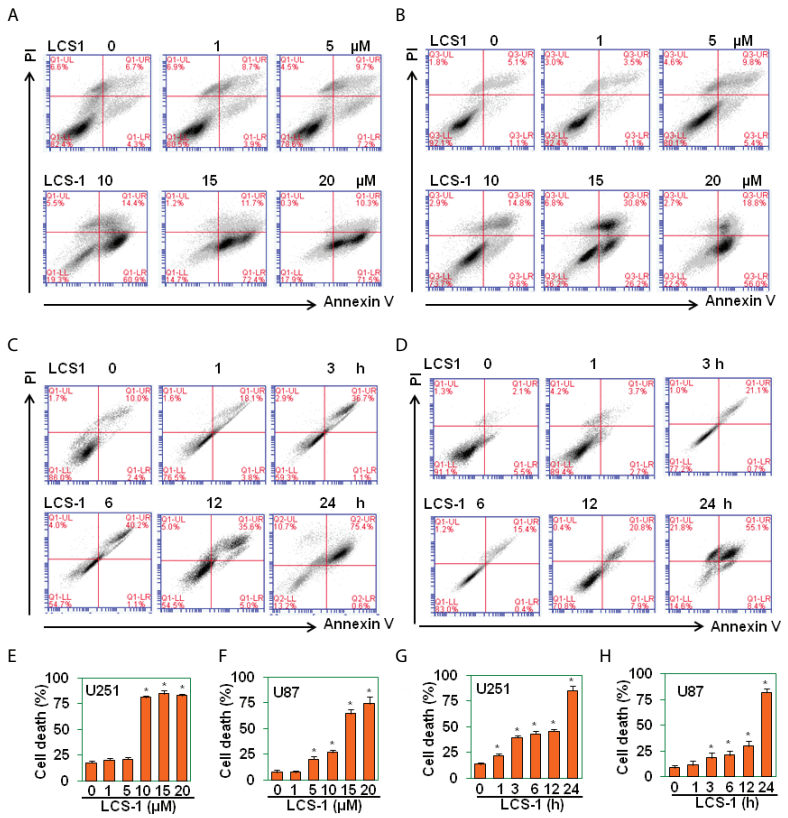

FIGURE 4
LCS-1 induces cell death in glioma cells. **(A-B)** PI/FITC-Annexin V staining of death of U251 **(A)** and U87 **(B)** cells treated with the indicated doses of LCS-1 for 24 h **(C, D)** PI/FITC-Annexin V staining of death of U251 **(C)** and U87 **(D)** cells treated with 20 μM LCS-1 for the indicated time periods. **(E-H)** Quantitative data from **A (E), B (F), C (G)** and **D (H)** respectively. * $P < 0.05$ compared with the control groups.

Tumors in LCS-1-treated mice grew more slowly than those in control mice (Figure 6A), as shown by the photographs in Figure 6B, as well as the weight of tumors shown in Figure 6C. However, there was no difference in the mouse body weight between LCS-1-treated and control groups (Figure 6D). These results suggest that LCS-1 inhibits glioma growth *in vivo* without causing side effects in mice.

LCS-1-induced cell death is P53-independent

It has been reported that ROS activates P53 signaling pathway (24–26). To determine whether LCS-1-induced cell death is associated with P53 activation, P53-targeted genes including Bcl-2, MDM2, Noxa were measured by qRT-PCR. The results showed that the treatment of U87 cells with LCS-1 did not down-regulate the mRNA levels of Bcl-2, only slightly up-regulated the mRNA of MDM2 and Noxa (Figures 7A, B), indicating that P53 did not involve in LCS-1-induced cell death. Furthermore, U87 cells were pretreated with P53 inhibitor Pifithrin-α (PFT-α), and retreated with LCS-1, then cell death was measured. The results showed that Pifithrin-α did not reverse LCS-1-induced cell death (Figures 7C-F). These results indicate that LCS-1-induced cell death is P53-independent.

LCS-1-induced cell death is caspase-independent

It has been reported that ROS induces caspase-dependent cell death in breast cancer cells and in hepatocellular carcinoma (27, 28). To determine where LCS-1-induced cell death is associated with caspase activation, western blot was used to measure the activation of caspase 3. The results showed that LCS-1 treatment of U251 and U87 cells did not activate caspase 3, the cleaved fragments p19 and p17 were not observed (Figure 8A). As a control, staurosprine induced the activation of caspase 3, cleaved p19 and p17 were detected by western blot (Figure 8A). Meanwhile, when U251 and U87 cells were pretreated with caspase paninhibitor Z-vad-FMK, and then retreated with LCS-1, LCS-1-induced cell death was not

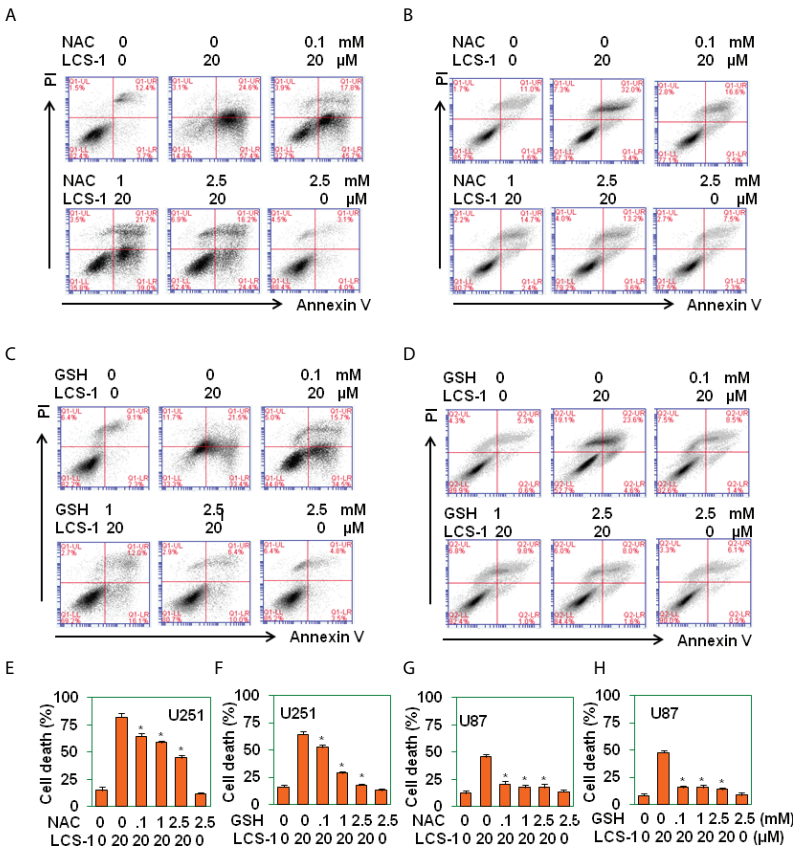

FIGURE 5
ROS scavenges reverse LCS-1-induces cell death. **(A-D)** PI/FITC-Annexin V staining of death of U251glioma cells pretreated with the indicated doses of NAC **(A)**, or GSH **(B)** for 1 h and re-treated with 20 μM LCS-1 for 24 h, and U87 cells pretreated with indicated doses of NAC **(C)**, or GSH **(D)** for 1h and retreated with 20 μM LCS-1 for 24 h **(E-H)** Quantitative data from **A (E), B (F), C (G)** and **D (H)** respectively. * $P < 0.05$ compared with LCS-1-treated alone groups.

reversed (Figures 8B-D). These results suggest that LCS-1-induced cell death is caspase-independent.

LCS-1 induces degradation of PARP and BRCA1

Parthanatos is a poly(ADP-ribose) polymerase (PARP)-dependent programed cell death (29, 30), and ROS may elicit Parthanatos (31). To determine LCS-1-induced cell death is associated with parthanatos, U251 and U87 cells were pretreated with PARP-1 inhibitor PJ34, and retreated with LCS-1, and cell death was measured. The results showed that PJ34 did not reverse LCS-1-induced cell death (Figures 9A-D). On the contrary, PJ34 treatment increased LCS-1-induced cell death slightly but significantly (Figures 9A-D). Considering that PARP inhibitors can elicit cell death in BRCA1 or BRCA2 mutant breast cancer cells (32), we speculated that LCS-1 may induce cell death *via* degrading PARP and BRCA1. This hypothesis was confirmed by the observation that LCS-1 treatment induced the degradation of PARP and BRCA1 dose- and time-dependent in both U251 and U87 cells (Figures 9E-H). However, LCS-1 did not induce the decrease of the mRNA levels of PARP and BRCA1 (Figure 9I). Meanwhile, LCS-1 treatment increased the phosphorylated levels of H2AX, which is a maker for DNA damage (Figure 9J). Moreover, EGF increased the expression of PARP, but IL-6 decreased the expression of PARP (Figure 9K). Expectedly, EGF decreased the cell death induced by LCS-1, and IL-6 increased cell death induced by LCS-1 (Figures 9L, M). These results suggest that LCS-1-induced cell death is not associated with parthanatos, but may be associated with the degradation of PARP and BRCA1.

Discussion

In normal cells, SOD1 localizes in the cytoplasm, the inter-membrane space of the mitochondria and the nucleus (33).

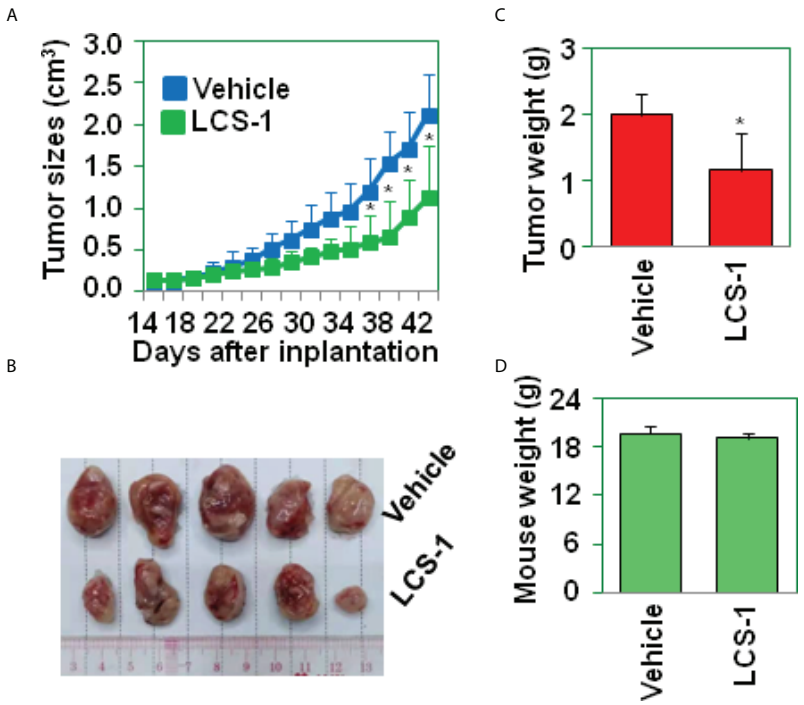

FIGURE 6
LCS-1 decreases tumor growth in nude mice. **(A)** Tumor growth curve from nude mice implanted with U87 cells and treated with or without LCS-1. * $P < 0.05$ compared with the vehicle groups. **(B)** Tumors from nude mice implanted with U87 cells and treated with or without LCS-1. **(C)** The weights of tumors from nude mice implanted with U87 cells and treated with or without LCS-1. * $P < 0.05$ compared with the vehicle group. **(D)** The weights of mice implanted with U87 cells and treated with or without LCS-1.

Observed evidences from several groups indicate that SOD1 is upregulated in cancers and is essential to maintain cellular redox balance under the condition with excessive ROS derived from the aberrant metabolism (33, 34). The SOD activities in normal and tumor breast tissues are determined, and each donor has a higher SOD activity in cancer than in normal tissue samples (35). In cisplatin resistant human ovarian cancer cells, the SOD1 expression is higher than that in cisplatin-sensitive human ovarian cancer cells (36). In breast cancer, no difference is found in SOD1 levels between matched plasma and nipple aspirate fluid (NAF) from cancer patients, whereas SOD1 levels in no-cancer NAF are significantly higher compared with matched plasma (37). In lung cancer patients, erythrocyte SOD1 activities are significantly higher than those in normal controls (38). In bronchial epithelium adjacent to invasive cancer, the expression of cytoplasmic or nuclear SOD1 is significantly lower compared with its expression in the uninvolved bronchial epithelium away from cancer (39). In breast cancer cells, SOD2 to SOD1 switch is found, resulting in the SOD2 down-regulation, and SOD1 upregulation, and SOD1 functions to maintain the integrity of the organelle (16). A significant upregulation of SOD1 in nasopharyngeal carcinoma (NPC) tissue is observed and high SOD1 expression is a predictor of poor prognosis and is correlated with poor outcome, indicating that SOD1 is a potential prognostic biomarker and a promising target for NPC therapy (40). However, less evidence is reported about the expression of SOD1 in gliomas. In this study, SOD1 moderate staining was observed in normal brain tissues, glioma adjacent tissues, glioma grade I and II tissues, whereas SOD1 strong staining was found in glioma grade III, IV tissues. The higher expression of SOD1 in glioma tissue may be due to the higher levels of ROS, which are derived from the aberrant metabolism. In glioma cell lines, SOD1 inhibitor induced ROS production, activated ROS signaling, and increased SOD1 expression. So we consider that the upregulation of SOD1 in glioma may be associated with the high levels of ROS.

SOD function to catalyze superoxide anion into oxygen and hydrogen peroxide, to decrease ROS levels, to maintain cellular redox homeostasis. SOD dysfunction leads to excessive increase of ROS, blocks redox balance, and results in tissue and cell damage. However, in cancer cells, the cell damage induced by SOD dysfunction should benefit to cancer therapy. Early evidences show that SOD1 inhibitor ATN-224 inhibits endothelial cell proliferation *in vitro*, and attenuates angiogenesis *in vivo* (12). The effects of ATN-224 on endothelial and tumor cells could be substantially reversed using a catalytic small-molecule SOD mimetic (12). Other evidences show that inhibition of SOD1 by

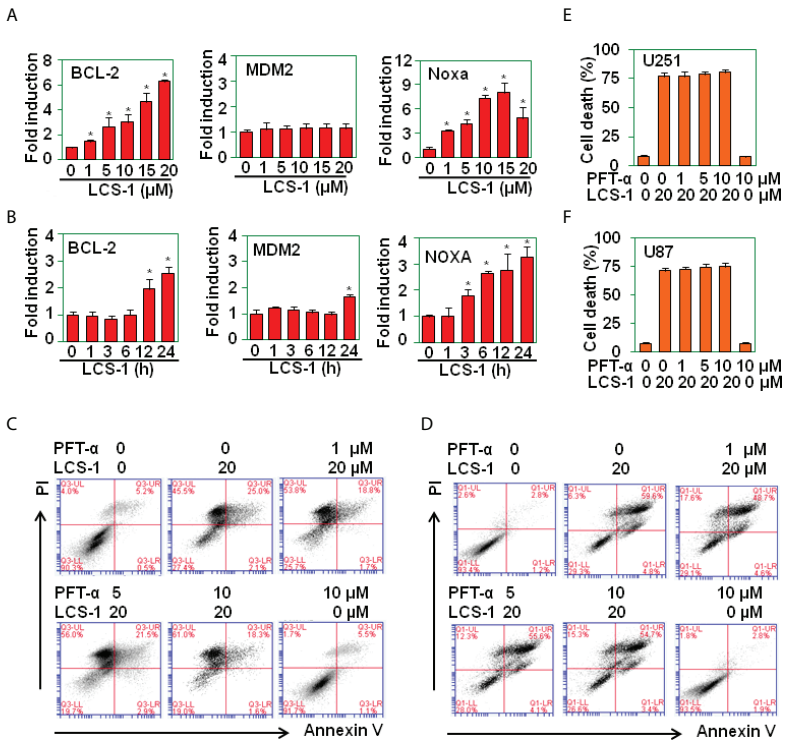

FIGURE 7
LCS-1-induced cell death is P53 in-dependent. **(A)** qRT-PCR analysis of the mRNA levels of P53-targeted genes in U251 cells treated with the indicated doses of LCS-1 for 12 h. * $P < 0.05$ compared with the medium groups. **(B)** qRT-PCR analysis of the mRNA levels of P53-targeted genes in U87 cells treated with 10 μM LCS-1 for the indicated time periods. * $P < 0.05$ compared with the medium groups. **(C, D)** PI/FITC-Annexin V staining of death of U251 **(C)** and U87 **(D)** cells pretreated with the indicated doses of P53 inhibitor Pifithrin-α (PFT-α) for 1 h and retreated with 20 μM LCS-1 for 24 h. **(E, F)** Quantitative data from **C (E)** and **D (F)**. * $P < 0.05$ compared with LCS-1-treated alone groups.

ATN-224 induces cell death in various non–small-cell lung cancer (NSCLC) cells, including those harboring KRAS mutations (13). ATN-224 inhibition of SOD1 increases superoxide, which diminishes enzyme activity of the antioxidant glutathione peroxidase, leading to an increase in intracellular hydrogen peroxide levels (13). By combining affinity proteomics and gene expression analysis, a small molecule, referred to as lung cancer screen 1 (LCS-1) is identified as SOD1 inhibitor and reduces the growth of lung adenocarcinoma cell lines (14). Overexpression of SOD1 increases proliferation of lung cancer cells and reduces sensitivity of these cells to LCS-1 (14). Chebulinic acid (CA), a polyphenol derived from the fruits of various medicinal plants, downregulates the expression of SOD1, reduces its enzyme activity, elicits cell oxidative stress, inhibits cell proliferation and promotes cell apoptosis in breast cancer cells (41). In this study, SOD1 inhibitor LCS-1 induced time- and dose-dependent cell death in glioma cells. And LCS-1 reduced growth of glioma *in vivo*. These observations suggest that targeting SOD1 may be a strategy for glioma therapy.

Several natural or synthetical compounds have been reported to induce anti-glioma effect *via* ROS-dependent mechanism. WIN 55,212-2, a cannabinoid analogue, dose-dependently inhibits glioma cell proliferation, migration, and invasion *in vitro*, effectively suppresses glioma spheroids growth *ex vivo* (42). WIN 55,212-2 also induces significant apoptosis, and causes dysfunction of VEGF-AKT/FAK signaling (42). The effects of WIN 55,212-2 are ROS-dependent, ROS inhibition effectively attenuates dysfunction of VEGF-AKT/FAK signaling and eventually improves glioma cell proliferation, migration, and invasion (42). Osthole, a coumarin derivative, is found to trigger glioma cell necroptosis accompanied with ROS production (43).. Osthole treatment decreases the expression of necroptosis inhibitor caspase-8, and the levels of necroptosis proteins receptor-interacting protein 1 (RIP1), RIP3 and mixed lineage kinase domain-like protein (43). The pretreatment with RIP1 inhibitor necrostatin-1 attenuates both osthole-induced necroptosis and the production of ROS in glioma cells (43). Natural borneol has been reported to sensitize human glioma cells to cisplatin-induced apoptosis by triggering ROS-mediated oxidative damage and regulating MAPK and PI3K/AKT signaling (44). Paris polyphyllins are monomers extracted from rhizome of Paris polyphylla var. yunnanensis. Polyphyllin VII promotes apoptosis and autophagic cell death *via* ROS-inhibited AKT activity, and sensitizes glioma cells to

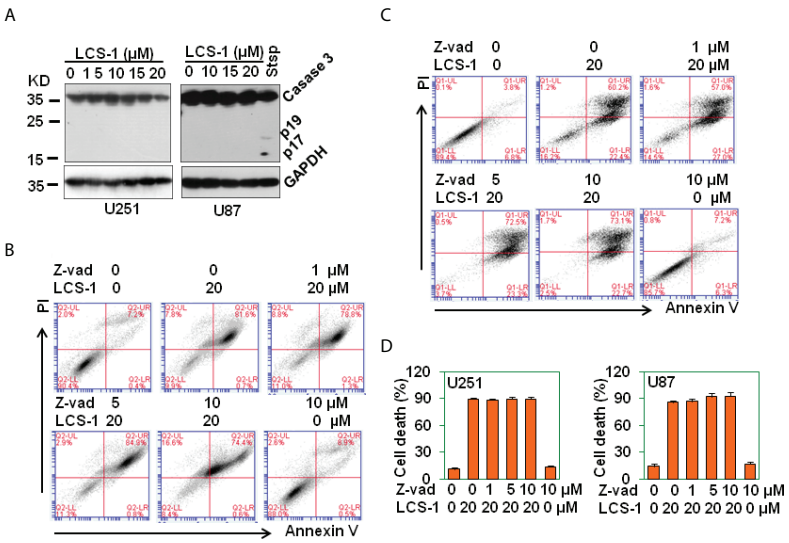

FIGURE 8
LCS-1-induced cell death is Caspase in-dependent. **(A)** Western blot analysis of caspase 3 activation in U251 and U87 cells treated with the indicated doses of LCS-1 for 24 h. U87 cells treated with 1 μM Staurosporine (Stsp) for 24 h as positive controls. GAPDH protein levels were measured as loading controls. **(B)** PI/FITC-Annexin V staining of death of U251 glioma cells pretreated with the indicated doses of pan-caspase inhibitor Z-vad-FMK (Z-vad) for 1 h, and retreated with 20 μM LCS-1 for 24 h **(C)** PI/FITC-Annexin V staining of death of U87 glioma cells pretreated with the indicated doses of pan-caspase inhibitor Z-vad-FMK (Z-vad) for 1 h. and retreated with 20 μM LCS-1 for 24 h **(D)** Quantitative data from B and C respectively.

temozolomide (45). Ampelopsin, an effective component of the traditional Chinese herb of Ampelopsis grossedentata, inhibits human glioma through inducing apoptosis and autophagy dependent on ROS generation and JNK pathway (46). Fucoxanthin, a natural carotenoid derived from algae, induces apoptosis in human glioma cells *via* triggering of ROS-mediated oxidative damage and regulation of MAPKs and PI3K-AKT pathways (47). In this study, LCS-1 induces ROS production, activates ROS signaling. ROS scavengers reversed LCS-1-induced cell death. These results suggest that LCS-1 induced cell death *via* ROS-dependent pathway.

Multiple evidences show that ROS induced by various factors elicit cell differentiation, cell death, and inhibit tumor growth *via* P53 pathway (24–26). In this study, we found that LCS-1 has less effect on P53-targeted genes, indicating that LCS-1 did not activate P53. Meanwhile, P53 inhibitor did not reverse LCS-1-induced cell death, suggesting that LCS-1-induced cell death is P53-independent.

ROS have been reported to induce tissue damage, to elicit anti-tumor immune response, to cause cell death *via* caspase 1, 3 and 8 pathways (27, 28). However, in this study, we found that LCS-1 did not activate caspase 3. Meanwhile, caspase pan-inhibitor did not reverse LCS-1-induced cell death. These results suggest that LCS-1-induced cell death is caspase-independent.

PARP has been reported to involve in inflammatory response and cell death induced by ROS (48). In this study, we found that SOD1 inhibitor LCS-1 induced ROS-dependent cell death. But PARP inhibitor did not reverse LCS-1-induced cell death, suggesting that LCS-1-induced cell death is not asssociated with PARP activation.

ROS induces DNA damage and activates DNA damage responses (49). There are three ways to repair DNA damage: the PARylation-mediated repair, the homologous recombination (HR)-mediated repair, and end-joining (EJ)-mediated repair (32). Upon DNA damage, PARP is rapidly recruited to single-strand breaks (SSBs) and double-strand breaks (DSBs) where it PARylates itself and other proteins resulting in the recruitment of downstream DNA repair factors (32). In BRCA-proficient cells, HR enables the error-free repair of DNA damage (32). By contrast, BRCA1/2-deficient cells are HR-deficient and are therefore reliant upon error-prone DNA end-joining pathway, in which PARP is necessary (32, 50). Therefore, the treatment of BRCA1/2-deficient cells with PARP inhibitors blocks all three DNA damage repair pathways, leading to the induction of cell death, and these inhibitors have been used as cancer therapeutic strategies (51–53).

The results presented in this study are compatible with the model outlined in Figure 10. The treatment of glioma cells with LCS-1 inhibits SOD1, resulting in the accumulation of ROS, leading to DNA damage. Meanwhile, LCS-1 induces the degradation of PARP, which cause the dysfunction of PARylation-mediated repair and EJ-mediated repair, and the degradation of BRCA1, which causes the blocking of HR-

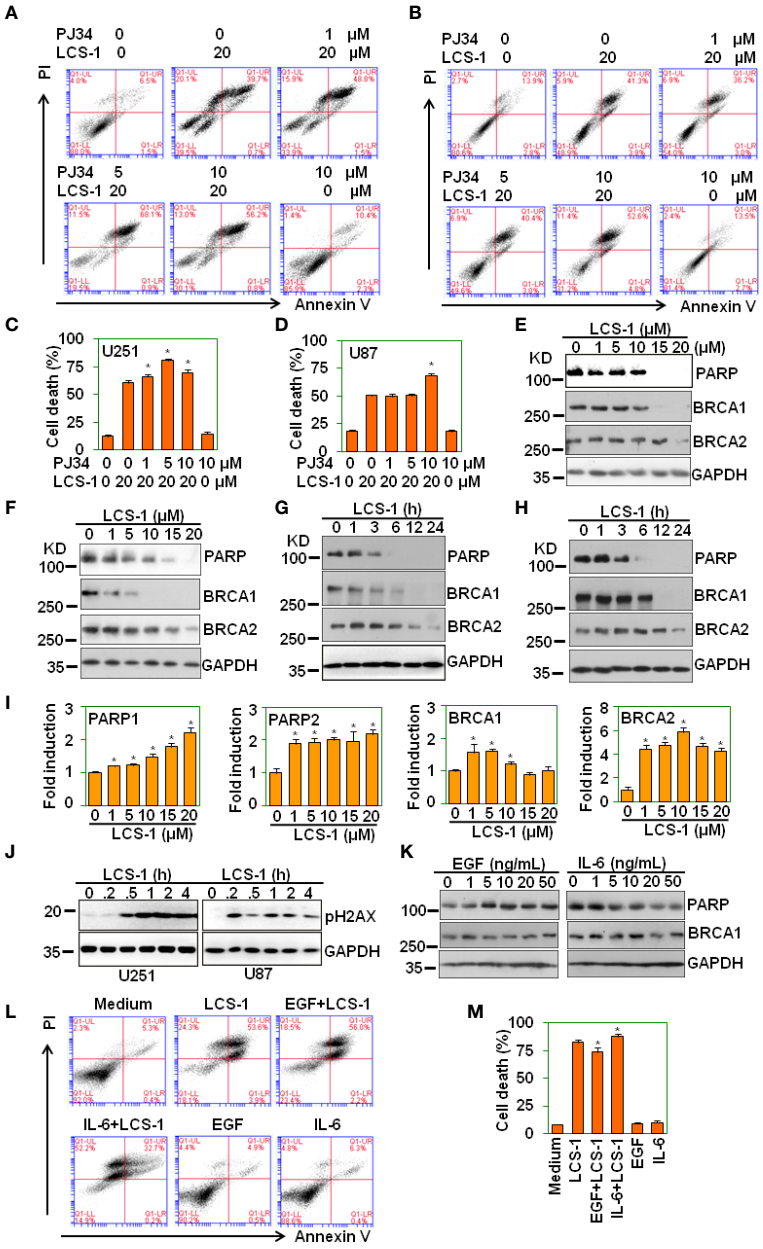

FIGURE 9
LCS-1 induces degradation of both PARP and BRCA1. **(A)** PI/FITC-Annexin V staining of death of U251 glioma cells pretreated with the indicated doses of PARP inhibitor PJ34 for 1 h. and retreated with 20 μM LCS-1 for 24 h **(B)** PI/FITC-Annexin V staining of death of U87 glioma cells pretreated with the indicated doses of PARP inhibitor PJ34 for 1 h. and retreated with 20 μM LCS-1 for 24 h. **(C, D)** Quantitative data of **A (C)** and B **(D)** respectively. * $P < 0.05$ compared with LCS-1-treated alone groups. **(E, F)** Western blot analysis of the protein levels of PARP, BRCA1 and BRCA2 in U251 **(E)** and U87 **(F)** cells treated with the indicated doses of LCS-1 for 24 h. GAPDH protein levels were measured as loading controls. **(G, H)** Western blot analysis of the protein levels of PARP, BRCA1 and BRCA2 in U251 **(G)** and U87 **(H)** cells treated with 20 μM LCS-1 for the indicated time periods. GAPDH protein levels were measured as loading controls. **(I)** qRT-PCR analysis of the mRNA levels of PARP1, PARP2, BRCA1 and BRCA2 in U251 cells treated with the indicated doses of LCS-1 for 12 h. * $P < 0.05$ compared with the control groups. **(J)** Western blot analysis of the phosphorylated levels of H2AX in U251 and U87 cells treated with 20 μM LCS-1 for the indicated time periods. GAPDH protein levels were measured as loading controls. **(K)** Western blot analysis of the protein levels of PARP, BRCA1 in U87 cells treated with the indicated doses of EGF, or IL-6 for 24 h. GAPDH protein levels were measured as loading controls. **(L)** PI/FITC-Annexin V staining of death of U87 glioma cells pretreated with 20 ng/mL EGF, or 20 ng/mL IL-6 for 24 h. and retreated with 20 μM LCS-1 for 24 h. **(M)** Quantitative data from L. * $P < 0.05$ compared with LCS-1-treated alone group.

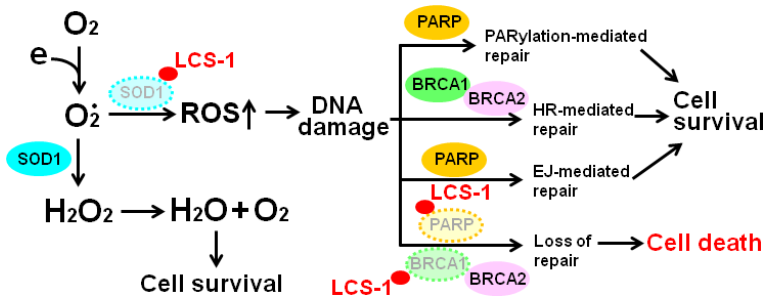

FIGURE 10
Model of the mechanism by which LCS-1 induces cell death. LCS-1 inhibited the enzyme activity of SOD1, resulting in the accumulation of ROS, leading to the induction of DNA damage. Meanwhile, LCS-1 induces the degradation of PARP. The dysfunction of PARP inhibits DNA damage repair *via* blocking both PARylation-mediated and EJ-mediated pathways. Furthermore, LCS-1 induces the degradation of BRCA1, eliciting the block of HR-mediated pathway. The inhibition of these three repair pathways results in death of glioma cells.

mediated repair. Combining these effects of LCS-1 in glioma cells, it induces death of glioma cells through the similar mechanism compared to that PARP inhibitors induce cell death in BRCA1/2 deficient cells.

Data availability statement

The raw data supporting the conclusions of this article will be made available by the authors, without undue reservation.

Ethics statement

The studies involving human participants were reviewed and approved by the ethics committee of Changsha Central Hospital, University of South China. The patients/participants provided their written informed consent to participate in this study. The animal study was reviewed and approved by the Animal Ethics Committee of the Changsha Central Hospital, University of South China.

Author contributions

JH conceived and designed the study. ML, QL, YW, XL, MJ, and JH collected and analyzed the data.

ML and QL completed the experimental cell manipulation. YW completed immunohistochemistry of SOD1 and immunohistochemical scoring. ML and XL completed western blot analysis. ML and MJ completed qRT-PCR analysis. JH wrote the manuscript. All authors revised the manuscript and read and approved the submitted version.

Funding

This study was supported by the National Natural Science Foundation of China (81172042).

Conflict of interest

The authors declare that the research was conducted in the absence of any commercial or financial relationships that could be construed as a potential conflict of interest.

Publisher's note

All claims expressed in this article are solely those of the authors and do not necessarily represent those of their affiliated organizations, or those of the publisher, the editors and the reviewers. Any product that may be evaluated in this article, or claim that may be made by its manufacturer, is not guaranteed or endorsed by the publisher.

Supplementary material

The Supplementary Material for this article can be found online at: https://www.frontiersin.org/articles/10.3389/fonc.2022.937444/full#supplementary-material

References

1. Weller M, Wick W, Aldape K, Brada M, Berger M, Pfister S, et al. Glioma. *Nat Rev Dis Primers* (2015) 1:15017. doi: 10.1038/nrdp.2015.17

2. Schieber M, Chandel NS. ROS function in redox signaling and oxidative stress. *Curr Biol* (2014) 24:R453–462. doi: 10.1016/j.cub.2014.03.034

3. Nakamura H, Takada K. Reactive oxygen species in cancer: Current findings and future directions. *Cancer Sci* (2021) 112:3945–52. doi: 10.1111/cas.15068

4. Ruiz-Torres V, Rodríguez-Pérez C, Herranz-López M, Martín-García B, Gómez-Caravaca AM, Arráez-Román D, et al. Marine invertebrate extracts induce colon cancer cell death *via* ROS-mediated DNA oxidative damage and mitochondrial impairment. *Biomolecules* (2019) 9:771. doi: 10.3390/biom9120771

5. Sunilkumar D, Drishya G, Chandrasekharan A, Shaji SK, Bose C, Jossart J, et al. Oxyresveratrol drives caspase-independent apoptosis-like cell death in MDA-MB-231 breast cancer cells through the induction of ROS. *Biochem Pharmacol* (2020) 173:113724. doi: 10.1016/j.bcp.2019.113724

6. Lin X, Jia Y, Dong X, Shen J, Jin Y, Li Y, et al. Diplatin, a novel and low-toxicity anti-lung cancer platinum complex, activation of cell death in tumors *via* a ROS/JNK/p53-dependent pathway, and a low rate of acquired treatment resistance. *Front Pharmacol* (2019) 10:982. doi: 10.3389/fphar.2019.00982

7. Teng JF, Qin DL, Mei QB, Qiu WQ, Pan R, Xiong R, et al. Polyphyllin VI, a saponin from trillium tschonoskii maxim. induces apoptotic and autophagic cell death *via* the ROS triggered mTOR signaling pathway in non-small cell lung cancer. *Pharmacol Res* (2019) 147:104396. doi: 10.1016/j.phrs.2019.104396

8. Zhang T, Zheng P, Shen X, Shao R, Wang B, Shen H, et al. Curcuminoid WZ26, a TrxR1 inhibitor, effectively inhibits colon cancer cell growth and enhances cisplatin-induced cell death through the induction of ROS. *Free Radic Biol Med* (2019) 141:93–102. doi: 10.1016/j.freeradbiomed.2019.06.005

9. Li Y, Tian X, Liu X, Gong P. Bufalin inhibits human breast cancer tumorigenesis by inducing cell death through the ROS-mediated RIP1/RIP3/PARP-1 pathways. *Carcinogenesis* (2018) 39:700–7. doi: 10.1093/carcin/bgy039

10. Altobelli GG, Van Noorden S, Balato A, Cimini V. Copper/Zinc superoxide dismutase in human skin: Current knowledge. *Front Med (Lausanne)* (2020) 7:183. doi: 10.3389/fmed.2020.00183

11. Tsang CK, Liu Y, Thomas J, Zhang Y, Zheng XF. Superoxide dismutase 1 acts as a nuclear transcription factor to regulate oxidative stress resistance. *Nat Commun* (2014) 5:3446. doi: 10.1038/ncomms4446

12. Juarez JC, Betancourt O Jr., Pirie-Shepherd SR, Guan X, Price ML, Shaw DE, et al. Copper binding by tetrathiomolybdate attenuates angiogenesis and tumor cell proliferation through the inhibition of superoxide dismutase 1. *Clin Cancer Res* 2006, 12:4974-82. doi: 10.1158/1078-0432.CCR-06-0171

13. Glasauer A, Sena LA, Diebold LP, Mazar AP, Chandel NS. Targeting SOD1 reduces experimental non–small-cell lung cancer. *J Clin Invest* (2014) 124:117–28. doi: 10.1172/jci71714

14. Somwar R, Erdjument-Bromage H, Larsson E, Shum D, Lockwood WW, Yang G, et al. Superoxide dismutase 1 (SOD1) is a target for a small molecule identified in a screen for inhibitors of the growth of lung adenocarcinoma cell lines. *Proc Natl Acad Sci U.S.A.* (2011) 108:16375–80. doi: 10.1073/pnas.1113554108

15. Sajesh BV, McManus KJ. Targeting SOD1 induces synthetic lethal killing in BLM- and CHEK2-deficient colorectal cancer cells. *Oncotarget* (2015) 6:27907–22. doi: 10.18632/oncotarget.4875

16. Papa L, Hahn M, Marsh EL, Evans BS, Germain D. SOD2 to SOD1 switch in breast cancer. *J Biol Chem* (2014) 289:5412–6. doi: 10.1074/jbc.C113.526475

17. McAndrew EN, Lepage CC, McManus KJ. The synthetic lethal killing of RAD54B-deficient colorectal cancer cells by PARP1 inhibition is enhanced with SOD1 inhibition. *Oncotarget* (2016) 7:87417–30. doi: 10.18632/oncotarget.13654

18. Hu J, Shi B, Liu X, Jiang M, Yuan C, Jiang B, et al. The activation of toll-like receptor 4 reverses tumor differentiation in human glioma U251 cells *via* notch pathway. *Int Immunopharmacol* (2018) 64:33–41. doi: 10.1016/j.intimp.2018.08.019

19. Sun R, Zhang Y, Lv Q, Liu B, Jin M, Zhang W, et al. Toll-like receptor 3 (TLR3) induces apoptosis *via* death receptors and mitochondria by up-regulating the transactivating p63 isoform alpha (TAP63alpha). *J Biol Chem* (2011) 286:15918–28. doi: 10.1074/jbc.M110.178798

20. Hu J, Deng X, Bian X, Li G, Tong Y, Li Y, et al. The expression of functional chemokine receptor CXCR4 is associated with the metastatic potential of human nasopharyngeal carcinoma. *Clin Cancer Res* (2005) 11:4658–65. doi: 10.1158/1078-0432.ccr-04-1798

21. Xia Y, Wang G, Jiang M, Liu X, Zhao Y, Song Y, et al. A novel biological activity of the STAT3 inhibitor stattic in inhibiting glutathione reductase and suppressing the tumorigenicity of human cervical cancer cells *via* a ROS-dependent pathway. *Onco Targets Ther* (2021) 14:4047–60. doi: 10.2147/ott.s313507

22. Wang L, Xu J, Liu H, Li J, Hao H. PM2.5 inhibits SOD1 expression by up-regulating microRNA-206 and promotes ROS accumulation and disease progression in asthmatic mice. *Int Immunopharmacol* (2019) 76:105871. doi: 10.1016/j.intimp.2019.105871

23. Li X, Chen Y, Zhao J, Shi J, Wang M, Qiu S, et al. The specific inhibition of SOD1 selectively promotes apoptosis of cancer cells *via* regulation of the ROS signaling network. *Oxid Med Cell Longev* (2019) 2019:9706792. doi: 10.1155/2019/9706792

24. Yang Z, Li H, Luo P, Yan D, Yang N, Zhang Y, et al. UNC5B promotes vascular endothelial cell senescence *via* the ROS-mediated P53 pathway. *Oxid Med Cell Longev* (2021) 2021:5546711. doi: 10.1155/2021/5546711

25. Ye Z, Chen D, Zheng R, Chen H, Xu T, Wang C, et al. Curcumin induced G2/M cycle arrest in SK-N-SH neuroblastoma cells through the ROS-mediated p53 signaling pathway. *J Food Biochem* (2021) 45:e13888. doi: 10.1111/jfbc.13888

26. Zhang C, Li Z, Wang J, Jiang X, Xia M, Lu S, et al. Ethanol extracts of solanum lyratum thunb regulate ovarian cancer cell proliferation, apoptosis, and epithelial-to-Mesenchymal transition (EMT) *via* the ROS-mediated p53 pathway. *J Immunol Res* (2021) 2021:5569354. doi: 10.1155/2021/5569354

27. An H, Heo JS, Kim P, Lian Z, Lee S, Park J, et al. Tetraarsenic hexoxide enhances generation of mitochondrial ROS to promote pyroptosis by inducing the activation of caspase-3/GSDME in triple-negative breast cancer cells. *Cell Death Dis* (2021) 12:159. doi: 10.1038/s41419-021-03454-9

28. Mu W, Cheng X, Zhang X, Liu Y, Lv Q, Liu G, et al. Hinokiflavone induces apoptosis *via* activating mitochondrial ROS/JNK/caspase pathway and inhibiting NF-κB activity in hepatocellular carcinoma. *J Cell Mol Med* (2020) 24:8151–65. doi: 10.1111/jcmm.15474

29. Wang X, Ge P. Parthanatos in the pathogenesis of nervous system diseases. *Neuroscience* (2020) 449:241–50. doi: 10.1016/j.neuroscience.2020.09.049

30. Zhou Y, Liu L, Tao S, Yao Y, Wang Y, Wei Q, et al. Parthanatos and its associated components: Promising therapeutic targets for cancer. *Pharmacol Res* (2021) 163:105299. doi: 10.1016/j.phrs.2020.105299

31. Li D, Kou Y, Gao Y, Liu S, Yang P, Hasegawa T, et al. Oxaliplatin induces the PARP1-mediated parthanatos in oral squamous cell carcinoma by increasing production of ROS. *Aging (Albany NY)* (2021) 13:4242–57. doi: 10.18632/aging.202386

32. Dias M, Moser S, Ganesan S, Jonkers J. Understanding and overcoming resistance to PARP inhibitors in cancer therapy. *Nat Rev Clin Oncol* (2021) 18:773–91. doi: 10.1038/s41571-021-00532-x

33. Papa L, Manfredi G, Germain D. SOD1, an unexpected novel target for cancer therapy. *Genes Cancer* (2014) 5:15–21. doi: 10.18632/genesandcancer.4

34. Damiano S, Sozio C, La Rosa G, Guida B, Faraonio R, Santillo M, et al. Metabolism regulation and redox state: Insight into the role of superoxide dismutase 1. *Int J Mol Sci* (2020) 21:6606. doi: 10.3390/ijms21186606

35. Bianchi MS, Bianchi NO, Bolzán AD. Superoxide dismutase activity and superoxide dismutase-1 gene methylation in normal and tumoral human breast tissues. *Cancer Genet Cytogenet* (1992) 59:26–9. doi: 10.1016/0165-4608(92)90152-x

36. Kim JW, Nie B, Sahm H, Brown DP, Tegeler T, You JS, et al. Targeted quantitative analysis of superoxide dismutase 1 in cisplatin-sensitive and cisplatin-resistant human ovarian cancer cells. *J Chromatogr B Analyt Technol BioMed Life Sci* (2010) 878:700–4. doi: 10.1016/j.jchromb.2010.01.013

37. Mannello F, Tonti GA, Pederzoli A, Simone P, Smaniotto A, Medda V. Detection of superoxide dismutase-1 in nipple aspirate fluids: a reactive oxygen species-regulating enzyme in the breast cancer microenvironment. *Clin Breast Cancer* (2010) 10:238–45. doi: 10.3816/CBC.2010.n.032

38. Kaynar H, Meral M, Turhan H, Keles M, Celik G, Akcay F. Glutathione peroxidase, glutathione-s-transferase, catalase, xanthine oxidase, Cu-zn superoxide dismutase activities, total glutathione, nitric oxide, and malondialdehyde levels in erythrocytes of patients with small cell and non-small cell lung cancer. *Cancer Lett* (2005) 227:133–9. doi: 10.1016/j.canlet.2004.12.005

39. Piyathilake CJ, Bell WC, Oelschlager DK, Heimburger DC, Grizzle WE. The pattern of expression of Mn and Cu-zn superoxide dismutase varies among squamous cell cancers of the lung, larynx, and oral cavity. *Head Neck* (2002) 24:859–67. doi: 10.1002/hed.10135

40. Li S, Fu L, Tian T, Deng L, Li H, Xia W, et al. Disrupting SOD1 activity inhibits cell growth and enhances lipid accumulation in nasopharyngeal carcinoma. *Cell Commun Signal* (2018) 16:28. doi: 10.1186/s12964-018-0240-3

41. Sharma A, Mishra T, Thacker G, Mishra M, Narender T, Trivedi AK. Chebulinic acid inhibits MDA-MB-231 breast cancer metastasis and promotes cell death through down regulation of SOD1 and induction of autophagy. *Cell Biol Int* (2020) 44:2553–69. doi: 10.1002/cbin.11463

42. Wang K, Wang Q, Li Q, Zhang Z, Gao J, Fan C, et al. Cannabinoid WIN 55,212-2 inhibits human glioma cell growth by triggering ROS-mediated signal pathways. *BioMed Res Int* (2021) 2021:6612592. doi: 10.1155/2021/6612592

43. Huangfu M, Wei R, Wang J, Qin J, Yu D, Guan X, et al. Osthole induces necroptosis *via* ROS overproduction in glioma cells. *FEBS Open Bio* (2021) 11:456–67. doi: 10.1002/2211-5463.13069

44. Cao WQ, Zhai XQ, Ma JW, Fu XQ, Zhao BS, Zhang P, et al. Natural borneol sensitizes human glioma cells to cisplatin-induced apoptosis by triggering ROS-mediated oxidative damage and regulation of MAPKs and PI3K/AKT pathway. *Pharm Biol* (2020) 58:72–9. doi: 10.1080/13880209.2019.1703756

45. Pang D, Li C, Yang C, Zou Y, Feng B, Li L, et al. Polyphyllin VII promotes apoptosis and autophagic cell death *via* ROS-inhibited AKT activity, and sensitizes glioma cells to temozolomide. *Oxid Med Cell Longev* (2019) 2019:1805635. doi: 10.1155/2019/1805635

46. Guo Z, Guozhang H, Wang H, Li Z, Liu N. Ampelopsin inhibits human glioma through inducing apoptosis and autophagy dependent on ROS generation and JNK pathway. *BioMed Pharmacother* (2019) 116:108524. doi: 10.1016/j.biopha.2018.12.136

47. Wu HL, Fu XY, Cao WQ, Xiang WZ, Hou YJ, Ma JK, et al. Induction of apoptosis in human glioma cells by fucoxanthin *via* triggering of ROS-mediated oxidative damage and regulation of MAPKs and PI3K-AKT pathways. *J Agric Food Chem* (2019) 67:2212–9. doi: 10.1021/acs.jafc.8b07126

48. Chiu LY, Wu NL, Hung CF, Bai P, Dai YS, Lin WW. PARP-1 involves in UVB-induced inflammatory response in keratinocytes and skin injury *via* regulation of ROS-dependent EGFR transactivation and p38 signaling. *FASEB J* (2021) 35:e21393. doi: 10.1096/fj.202002285RR

49. Srinivas U, Tan B, Vellayappan B, Jeyasekharan A. ROS and the DNA damage response in cancer. *Redox Biol* (2019) 25:101084. doi: 10.1016/j.redox.2018.101084

50. Wei H, Yu X. Functions of PARylation in DNA damage repair pathways. *Genomics Proteomics Bioinf* (2016) 14:131–9. doi: 10.1016/j.gpb.2016.05.001

51. Verma P, Zhou Y, Cao Z, Deraska P, Deb M, Arai E, et al. ALC1 links chromatin accessibility to PARP inhibitor response in homologous recombination-deficient cells. *Nat Cell Biol* (2021) 23:160–71. doi: 10.1038/s41556-020-00624-3

52. Yap T, Kristeleit R, Michalarea V, Pettitt S, Lim J, Carreira S, et al. BRCA1/2Phase I trial of the PARP inhibitor olaparib and AKT inhibitor capivasertib in patients with - and non–mutant cancers. *Cancer Discovery* (2020) 10:1528–43. doi: 10.1158/2159-8290.cd-20-0163

53. Lin K, Harrell M, Oza A, Oaknin A, Ray-Coquard I, Tinker A, et al. BRCA reversion mutations in circulating tumor DNA predict primary and acquired resistance to the PARP inhibitor rucaparib in high-grade ovarian carcinoma. *Cancer Discovery* (2019) 9:210–9. doi: 10.1158/2159-8290.cd-18-0715

frontiers | Frontiers in Oncology

TYPE Review
PUBLISHED 12 September 2022
DOI 10.3389/fonc.2022.957373

OPEN ACCESS

EDITED BY
Shing Yau Tam,
Hong Kong Polytechnic University,
Hong Kong SAR, China

REVIEWED BY
David A. Gewirtz,
Virginia Commonwealth University,
United States
Elisa Helena Farias Jandrey,
Institute of Biosciences, University of São Paulo, Brazil

*CORRESPONDENCE
Amrita Roy
amrita@uic.edu;
dr_amritaroy@yahoo.com
Soumen Bera
sbera@uic.edu;
bera.sls@crescent.education
Bilikere S. Dwarakanath
dwarakanath@sriramachandra.edu.in;
dwarakanathdrbs@gmail.com

†PRESENT ADDRESS
Amrita Roy,
Department of Medicine, Division of Hematology and Oncology, University of Illinois at Chicago, Chicago, IL, United States

‡These authors have contributed equally to this work and share first authorship

SPECIALTY SECTION
This article was submitted to Cancer Molecular Targets and Therapeutics, a section of the journal Frontiers in Oncology

RECEIVED 31 May 2022
ACCEPTED 15 August 2022
PUBLISHED 12 September 2022

CITATION
Roy A, Bera S, Saso L and Dwarakanath BS (2022) Role of autophagy in tumor response to radiation: Implications for improving radiotherapy. *Front. Oncol.* 12:957373. doi: 10.3389/fonc.2022.957373

Role of autophagy in tumor response to radiation: Implications for improving radiotherapy

Amrita Roy[1*†‡], Soumen Bera[2,3*‡], Luciano Saso[4] and Bilikere S. Dwarakanath[5*]

[1]Department of Biotechnology, Indian Academy Degree College (Autonomous), Bengaluru, Karnataka, India, [2]B. S. Abdur Rahman Crescent Institute of Science and Technology, Chennai, India, [3]Department of Pathology, University of Illinois at Chicago, Chicago, IL, United States, [4]Department of Physiology and Pharmacology "Vittorio Erspamer", Sapienza University, Rome, Italy, [5]Central Research Facility, Sri Ramachandra Institute of Higher Education and Research Institute, Chennai, India

Autophagy is an evolutionary conserved, lysosome-involved cellular process that facilitates the recycling of damaged macromolecules, cellular structures, and organelles, thereby generating precursors for macromolecular biosynthesis through the salvage pathway. It plays an important role in mediating biological responses toward various stress, including those caused by ionizing radiation at the cellular, tissue, and systemic levels thereby implying an instrumental role in shaping the tumor responses to radiotherapy. While a successful execution of autophagy appears to facilitate cell survival, abortive or interruptions in the completion of autophagy drive cell death in a context-dependent manner. Pre-clinical studies establishing its ubiquitous role in cells and tissues, and the systemic response to focal irradiation of tumors have prompted the initiation of clinical trials using pharmacologic modifiers of autophagy for enhancing the efficacy of radiotherapy. However, the outcome from the Phase I/II trials in many human malignancies has so far been equivocal. Such observations have not only precluded the advancement of these autophagy modifiers in the Phase III trial but have also raised concerns regarding their introduction as an adjuvant to radiotherapy. This warrants a thorough understanding of the biology of the cancer cells, including its spatio-temporal context, as well as its microenvironment all of which might be the crucial factors that determine the success of an autophagy modifier as an anticancer agent. This review captures the current understanding of the interplay between radiation induced autophagy and the biological responses to radiation damage as well as provides insight into the potentials and limitations of targeting autophagy for improving the radiotherapy of tumors.

KEYWORDS

autophagy, radiotherapy, cell death, tumor microenvironment, DNA damage repair

1 Introduction

Since its discovery in 1898, ionizing radiation exposure has been used to eradicate cancer cells by inflicting DNA damage (1). Present-day radiation therapy (RT), along with chemotherapy, immunotherapy, hormone therapy, and surgery has established itself as one of the principal therapeutic modalities employed for the treatment of cancer. It is often combined with other therapeutic modalities like surgery, chemotherapy, and immunotherapy as this approach has been found to provide better tumor control in many human malignancies (2–4). The RT regimen—comprising of the total dose and the fractionation schedule, including dose per fraction— is designed based on several factors that include the histopathological type and anatomical location of the malignancy (5, 6), while the genetic profile (viz. status of p53, VEGF, EGF, etc.) and the physiological status (7) play a crucial role in determining the outcome of RT. The biological responses of RT at the cellular, tissue, and systemic levels depend on the type and quality of radiation, the nature of macromolecular lesions induced as well as the molecular responses elicited, which are a set of interconnected signaling pathways regulated by the genomic and proteomic status of cells—all these cumulatively drive the irradiated cells to either towards death or survival (8).

Autophagy, meaning "self-eating" in Greek, can be defined as the cellular phenomenon through which senescent, damaged, or malfunctioning biomolecules and organelles are targeted for lysosomal degradation. It is an evolutionarily conserved cellular process that is activated in response to a multitude of intrinsic and extrinsic stressors like depletion of nutrients or growth factors, infection, or hypoxia (9, 10). Under such conditions, autophagy acts predominantly as a survival response by eliminating the damaged organelles or toxic aggregates whose presence otherwise would have triggered the apoptotic response. Simultaneously, lysosomal degradation of the redundant cellular components generates valuable raw materials and nutrients that can be reused to reconstruct important biomolecules.

Though initially conceived as a pathway employed to dispose of damaged or degraded cellular organelles and biomolecules, autophagy have emerged as one of the key mechanisms involved in the modulation of several cellular processes like metabolic homeostasis (11), apoptosis (12), and the development and differentiation (9, 13). Deregulation of the autophagic process is observed in numerous diseases like neurodegenerative disorders and cancer. As such targeting autophagy, besides other response like senescence and various death pathways has recently gained interest as an approach to improve the efficacy of anticancer therapies (14). The role of autophagy in the radiation response at the cellular and tissue levels is emerging wherein the facilitation of survival or progression to death has been observed, besides contributing to tissue responses as well. This review discusses the interplay between autophagy and tumor responses to ionizing radiation and emphasizes on the clinical responses of the cancer cells towards a combination therapy of radiation with autophagy modulators.

Abbreviations: ATG, Autophagy; ATM, Ataxia,telangiectasia; BRCA, Breast cancer gene; cGAS, Cyclic GMP AMP synthase; CHK1 & 2, Checkpoint kinase 1 & 2; CDK – Cyclin,dependent kinase; CSC – Cancer stem cells; DAMP, Damage associated molecular patterns; DDR, DNA damage repair; DSB, Double, strand breaks; EMT, Epithelial mesenchyme transformation; HIF, 1 – Hypoxia, inducible factor 1; HR, Homologous recombination; IR, Ionizing radiation; LET, Linear Energy Transfer; NHEJ , Nonhomologous end, joining; NTE, Non, target effects; RIBE, Radiation,induced bystander effects; RT, Radiotherapy; SBRT – Stereotactic body radiotherapy; STING, Stimulator of interferon genes; TGF, Transforming growth factor; TME, Tumor microenvironment; VEGF, Vascular endothelial growth factor.

2 Radiation response of tumors

Radiotherapy (RT) is one of the major armamentariums of cancer therapy that employs either photon based low LET (Linear Transfer of Energy—i.e. the amount of energy that is transferred by the radiation beam per unit distance it travels through the biological matter) radiation like X-rays and gamma-ray photons or/and high LET particles like proton, carbon ion, etc. Several forms of external beam irradiation and internally delivered radiation are currently employed depending on the nature of the malignancy and anatomical location of the tumor (15, 16). Despite significant advancements in RT technology providing a differential dose distribution between the tumor and the adjoining normal tissues (or organs at risk; OAR), acute and/or late toxicity in the non-target normal tissues or organs do compromises the clinical efficacy of radiotherapy (17).

2.1 Molecular and cellular responses of cancer cells towards IR

At the cellular level the effect of Ionizing radiation (IR) can be both direct and indirect. The direct interaction of radiation with the macromolecules (particularly DNA) and their subsequent damage is referred to as the direct effect, while the indirect effect is brought about by the interaction between the macromolecules with the highly reactive molecular species generated due to radiation (18). Low LET radiations (X-rays and gamma-ray photons) causes damage majorly through the indirect effect, thereby are subject to the environmental conditions of the cell (particularly the oxygen level), while damages induction by high LET or particle radiations (protons, carbon, α particles, and neutron)are determined mainly by the track structures and are influenced little by the

environment (19). The short-lived and highly reactive oxygen and nitrogen species generated from the ionization of cellular water react with macromolecules in the vicinity (DNA, RNA, lipids, and proteins) to generate DNA strand breaks (both single and double), lipid peroxides, and oxidized proteins. Accumulating evidences also suggest that complex DNA damage in the form of a cluster of damages comprising DNA strand breaks and a variety of non-break types of DNA damage viz. base damages play a critical role in determining the cellular and tissue responses to both low and high LET IR (20). Thus, DNA damage (particularly DNA double-strand breaks) and non-DNA damages in the form of membrane damage and imbalances in the cellular metabolism collectively determine the fate of an irradiated cell. The DNA damage response (DDR) comprises of the hierarchically regulated pathways of DNA repair, pro-survival signaling, perturbations in cell cycle progression, various cell death processes (interphase as well as mitotic), alterations in antioxidant and metabolic pathways, induction of senescence, autophagy, stem cell phenotype, bystander responses, and immune signals (Figure 1). A spatiotemporal competition between these pathways determine the fate of the irradiated tumor and non-malignant cells that translates into the therapeutic benefit (21) of radiotherapy. Additionally, the tumor microenvironment (consisting of stromal cells, immune cells, endothelial cells, and adipocytes), cancer stem cells, and the immunological responses of the host also contribute to the radiosensitivity of the cancer cell in determining the efficacy of radiotherapy.

The DNA damage response pathway is a multi-gene-multistep process and is greatly influenced by the post-translational modifications of several regulatory proteins that sense, transduce, and orchestrates (effectors) the dynamic interplay between, DNA repair, cell cycle arrest, mitotic death, interphase death, autophagy and senescence (22) thereby determines the survival or death of the irradiated cells (23). Ataxia-telangiectasia mutated (ATM) and the MRN complex (Mre11-Rad50-Nbs1) are two important members among the sensor proteins of DSB that play an important role in initiating DNA repair. They phosphorylate the histone variant, H2AX (gamma H2AX; γH2AX) creating a platform (template) for the progress of the repair and other events viz. cell cycle arrest in a p53 dependent and independent manner, involving other proteins like CHK1, CHK2, GADD45, CDK1, etc. DNA double-strand breaks (DSB) caused by IR primarily activates non-homologous end joining (NHEJ) and/or homologous recombination (HR) repair pathways in a context-dependent manner that like cell type, and proliferation status (24, 25). The DNA-dependent protein kinase (DNA-PK) and the RAD50 complex play a predominant role in the G1/early S phase cells, while the homology dependent HR requiring the RAD52 complex acts mainly in the late S/G2 phase, or the breast cancer predisposition genes BRCA1/2 complex, in the S phase

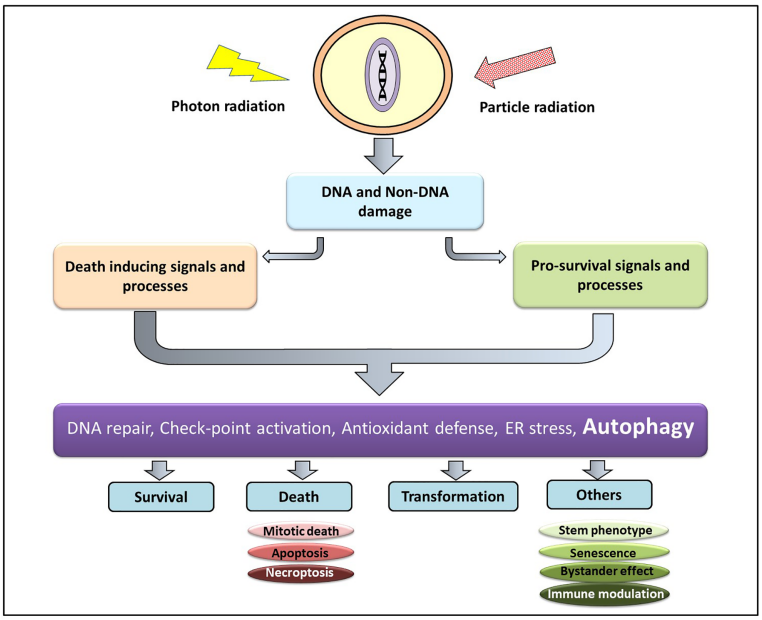

FIGURE 1
Cellular responses to radiation damage. Radiation induced macromolecular damage (DNA and non-DNA) activates pro-survival and death processes regulated by several proteins (ATM, p53, ATF6, Atg, NFκβ etc) whose level and activity are regulated majorly by post-translational modifications (which can be targeted for therapeutic benefit). This results in survival, death, and transformation of the irradiated cells, besides other responses.

of the cell cycle (26). Inhibitors of the DNA repair pathway and CHK1 inhibitors which sensitize cancer cells to ionizing radiation are currently under evaluation in different phases of clinical trials (22).

Although DNA damage response (DDR) plays the major role in the cellular responses to IR, non-DNA damage like membrane damage and damage to other organelles also contributes to the ultimate IR response. Ceramides generated from membrane damage induce apoptosis (8) that add to or synergize with the DNA damage-dependent apoptosis in determining the extent of cell death. Necroptosis, a regulated form of necrosis orchestrated by receptor interacting proteins (RIPK1 and RIPK3) and mixed lineage kinase like (LIKE) protein is also induced by IR and has recently been found to be involved in the activation of antitumor immunity (27). IR also enhances the unfolding of proteins due to the damage caused by radiation-induced ROS, leading to an unfolded protein response (UPR) in endoplasmic reticulum (ER) (28), which triggers the release of calcium stored in ER to the cytoplasm and causing the activation of ER stress mediated by UPR response (28, 29). A strong correlation exists between UPR response and autophagy, thus suggesting an association between radiation-induced ROS, ER stress, intracellular calcium level and autophagy (30). In addition to these many non-coding RNAs viz. the micro RNAs, long non-coding RNAs, and circular RNAs that regulate several DDR and other damaged molecular pathways, have also been shown to play crucial role in the cellular responses towards radiation which (31).

2.2 Systemic responses of cancer cells towards IR

Besides its effect on the irradiated cells or tissue, IR has also been found to affect the distant, un-irradiated cells or tissues in an organism in a manner that mimic the response of an irradiated cell or tissue. This phenomenon is known to as the non-target effects (NTE). NTE in a given tissue (or cells in a 2D or 3D cell culture) is widely referred to as the radiation-induced bystander effect or RIBE.

RIBE is often mediated by intercellular interactions (through gap junctions and associated proteins),secretory factors related to the radiation-induced damage called the “damage-associated molecular patterns (DAMP)” as well as others like exosomes that could contain a cocktail of microRNAs (32). As demonstrated by a variety of paradigms, phenomenologically, the RIBE can elicits several responses in the non-target cells (that are similar to the responses in irradiated cells) including autophagy, albeit to a lesser extent generally (20, 33) and has been linked to many hallmarks of cancer, including autophagy and enhanced radioresistance of observed in irradiated tumors (34).

Focal irradiation of the tumor can cause both cytotoxic and cytostatic effects on the irradiated cells thus leads to varying extents of local tumor control (18). Irradiation of the tumor also elicits a response at the systemic level that primarily arises from the alterations in the functional status of various components of the tumor microenvironment (TME) like endothelial cells, stromal cells, adipocytes, immune cells, etc. which could either enhance the resistance or result in the regrowth of the tumor (35). One of the interesting NTEs of tumor irradiation is the abscopal effect defined as the response to IR observed on a metastatic lesion located distally to the irradiated tumor. Focal irradiation of normal (non-malignant) tissues also elicits an abscopal effect including autophagy that involves the release of soluble factors from the irradiated tissue that contains microRNA (36, 37).

One of the important contributing factors to the systemic effects of radiation is the induction of inflammatory response initiated by damage suffered by the irradiated tissue. Increased expression of cell adhesion molecules from the endothelial cells related to vascular cell adhesion (VCAM-1 and E-selectin) as well as intercellular adhesion, (ICAM-1) that occurs as a response to irradiation, elicit inflammatory and immunological responses (38). Concurrently, HIF-1 (hypoxia-inducible factor 1) signaling, VEGF (vascular endothelial growth factor), and the chemokine CXCL12 stimulate pro-angiogenic signals, leading to angiogenesis and survival of the irradiated cells (26). Cancer-associated fibroblast also secrets modifiers of extracellular matrix and cytokines, while TGF-β signaling down-regulates the anti-tumor T cells and dendritic cells’ immunogenicity (39). Concurrently, radiation enhances the proliferative capacity and functionality of the Regulatory T cells (T_{reg}) resulting in immunosuppression and tumor relapse. Interestingly, stereotactic radiotherapy (SBRT) has been suggested to increase the functionality of Tregs in the tumor microenvironment, in a TGF-β and IL33 independent manner pointing out the existence of multiple mechanisms involved in T_{regs} linked radioresistance (40). More recently, radiation-induced DNA damage (including fragments of chromatin found in the cytoplasm) well as micronuclei expressed in the daughter cells as a consequence of unrepaired or mis-repair DNA strand breaks has been shown to stimulate the cGAS-STING pathway leading to the activation of CD8+ T cells thereby enhancing the antitumor immunity and enhanced tumor response (41, 42). Interestingly, this pathway is negatively regulated as autophagy-deficient cells secrete higher amounts of IFNγ that can be suppressed with the knockdown of cGAS or STING (35).

Irradiation of the tumor is also known to induce the generation of the cancer stem cells (CSCs) which are relatively radio-resistant compared to the bulk of the tumor cells and responsible for increased tumor resistance to RT (43). Therefore, targeting CSCs or suppressing the induction of CSC has been considered to be a promising approach for improving RT. Several mechanisms underlie the radioresistance of CSC that include high anti-oxidant capacity, efficient DNA damage repair, reprogramming of metabolism, and induction of EMT as well as

developmental signaling (43). Awakening of the quiescent CSCs following RT has been recently shown to result in tumor relapse and metastasis of oral cancers (44). More recently, the persistence of induced senescence has been shown to result in the development of CSC leading to therapeutic resistance (45).

3 Autophagy: Initiation, progression, and execution; micro, mini and macro-autophagy; mitophagy

The term Autophagy was coined by Christian de Duve in the early 60s (10) to describe the lysosome mediated degradation of redundant cellular organelles and since then autophagy has emerged predominantly as a survival response in the eukaryotic system, triggered in response to a hoard of intrinsic and extrinsic stressors like nutritional deprivation, oxidative or radiological stress. Studies conducted in the last 30 years have identified three major classes of autophagy occurring in the eukaryotic system, namely i) microautophagy, ii) chaperone-mediated autophagy, and iii) macroautophagy.

3.1 Microautophagy

Microautophagy is a local process that occurs on the surface of the lysosome. During this process, the lysosomal membrane invaginates forming a cup-shaped depression that eventually engulfs a damaged protein or organelle and release the cargo is within the lysosomal matrix for degradation (46). Although an entire organelle can be engulfed by the microautophagy process, the uptake of cargo is essentially limited by the range of the lysosomal outer membrane (Figure 2A).

3.2 Chaperone-mediated Autophagy

The chaperone-mediated autophagy (CMA) specifically targets the targets proteins bearing the KFERQ pentapeptide motif (47) which encompass nearly 30% of all cytosolic proteins like the glycolytic enzymes, proteasomal subunit proteins, several transcription factors, and their inhibitors, calcium, and lipid-binding proteins, and proteins involved in vesicular transport. CMA is induced by stressors like oxidative stress, prolonged nutritional deprivation, and several protein-degrading toxins. During the process, the target protein is identified and delivered on the lysosomal surface through the interaction between HSP8 (heat shock protein 8) and the KFERQ motif of the target protein. Presence of target protein initiates the aggregation of LAMP2A lysosomal-associated membrane protein 2A) on the membrane surface which is stabilized by interaction with HSP90 on the luminal side of the lysosomal membrane. HASP8 unfolds target protein and delivers it through the translocation channel formed by the LAMP2A aggregate into the lysosomal lumen (46) (Figure 2B).

3.3 Macroautophagy

Macroautophagy is the most common and hence the most widely studied mechanism among the autophagy processes. Unlike the microautophagy and the CMA process, macroautophagy is initiated away from the lysosomal membrane in a specific cytosolic location. In yeast, this initiation site is known as the Phagophore Assembly Site or PAS (10, 48), although the mammalian counterpart of the PAS is yet to be established. However, during starvation-induced autophagy in the mammalian system, a certain subdomain of the ER known as the "omegasome" serve as the site for the initiation process (48). Once triggered, autophagy proceeds through four stages— initiation or nucleation, elongation, maturation, and culminates in the fusion of the autophagosome and the lysosome (49). The entire process is orchestrated by a family of conserved proteins known as the autophagy-related proteins or the Atg proteins (50).

In mammalian cells, the initiation complex is made up of either ULK1 or 2 (Unc-51 like kinase family), ATG13, and RB1CC1 (RB1 inducible Coiled-coil 1, also known as FIP200) proteins. The ULK1/2-ATG13-RB1CC1 complex is highly stable and exists within the cell even in absence of any stressors. The complex remains bound to the mTORC1 complex which phosphorylates and maintain the complex in a dormant state. However, prolonged nutrient stress dissociates the ULK1/2-ATG13-RB1CC1 complex from the mTORC1. This leads to the dephosphorylation and subsequent activation of the former and initiates the "nucleation" process (51, 52).

In both yeast and mammalian systems PIP3 generated by a novel Atg14 containing class III PI3K complex plays a crucial role in the nucleation process (46). Subsequently, PI3K forms a complex with the Beclin1 and UVRAG—an association that is crucial in the induction of macroautophagy. Several regulatory proteins are known to interact with the PI3K-Beclin1-UVRAG complex, thereby regulate the macroautophagy process. For example, Bcl2 or Rubicon is known to prevent the Beclin1 from interacting with the PI3K (53, 54) or with the PI3K-UVRAG complex (55, 56) and thereby suppress autophagy. Similarly, AMBRA1 and SH3BLG1 positively regulate the PI3K system by directly (*via* AMBRA1) (57) or indirectly (*via* UVRAG) (58) interacting with Beclin1.

3.3.1 The elongation

The nucleation of the autophagy process leads to the formation of an isolated membrane structure that elongates

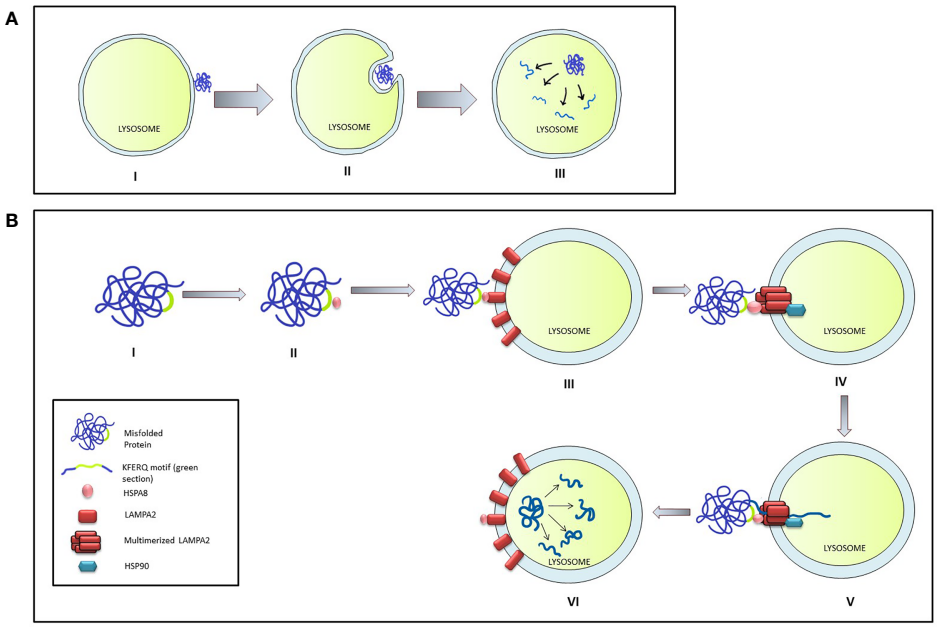

FIGURE 2
Micro-autophagy and Chaperone mediated autophagy in mammalian cells. **(A)** The stages of Micro-autophagy. I: Unfolded or damaged proteins present near the lysosomal surface triggers micro-autophagy. II: Invagination of lysosomal membrane into a cup shaped depression engulfs and degrades the damaged protein. III: Release of the cargo in the lysosome leads to its degradation. **(B)** Chaperone mediated autophagy (CMA): I & II: HSPA8 binds to the mis-folded protein by interacting through the KFERQ motif. III & IV: HSPA8 delivers the cargo on the lysosomal membrane by interacting with LAMPA2. Multimerization of LAMPA2, also mediated through HSPA2, creates a channel which is stabilized by interaction with HSP90. V & VI: HSPA8 mediates the unfolding of the protein and its translocation to the lysosomal matrix, where the cargo is degraded.

into a cup-like phagophore which expands and after encircling the damaged cellular components forms a double membrane sphere known as the autophagosome. The expansion of the membrane structure is mediated by a couple of conjugation systems recognized as UBL (Ubiquitine-like) complexes such as Atg5, Atg12, and Atg16 or the Atg8/LC3 system. A dimer of Atg12-Atg5-Atg16 complex (formed by the covalent linking of Atg16 to Atg5-Atg12 complex) is required for the expansion of the membrane system (59).

The multimeric Atg12-Atg5-Atg16 complex, once formed, mediates the formation of the Atg8/LC3 system which is also essential for the elongation of the phagophore. Atg8 is initially cleaved by Atg4, exposing a Gly residue at its C terminal end, followed by activation by the sequential interaction with Atg3 and Atg7. The activation of Atg4 is stringently controlled by the phosphorylation by ULK1 complex (60) or by the ROS level of the cell (61). The exposure of the Gly residue is a critical step in the activation process of Atg8 as this residue is required to link the Atg8 complex with the phosphatidylethanolamine moieties of the growing phagophore membrane. This interaction is believed to be mediated by the Atg12-Atg5-Atg16 dimers (62, 63) (Figure 3).

The membrane components essential for the elongation of the autophagosome is usually sequestered from the peripheral membrane systems—a process mediated by Atg9. Under normal physiological conditions Atg9 resides in the trans-Golgi and endosomal region. However, during nutritional stress, Atg9 reportedly migrates to the nucleation sit following an ULK1-PI3K signaling axis and shuttles between the growing phagophore and the peripheral biomembranes (64, 65). The interaction between Atg9 and Atg17 is required for the successful recruitment of the Atg9 on the autophagosome and this interaction is mediated by Atg1 complex (66). On the surface of the developing autophagosome, ATG9 is stabilized by the direct physical interaction with LC3 through specific docking domains (Ubiquitin-interacting motifs in ATG9 and UIM docking site on LC3) (67) (Figure 4).

The elongation/curvature of the growing autophagosome is a direct function of the Atg14 dependent class III PI3K activity. The C terminal domain of the Atg4 bears a BATS (Barkor/Atg14 autophagosome-targeting sequence) domain that facilitates its interaction with the PI3P in the lipid bilayer of the autophagosome. PI3P is responsible for a higher degree of membrane curvature (68) and it can be surmised that Atg14 acts as an indicator for membrane curvature of a budding autophagosome.

3.3.2 Maturation and fusion of the autophagosome with the lysosome

In the final steps, the developing phagophore expand and close its double-membrane structure to create the

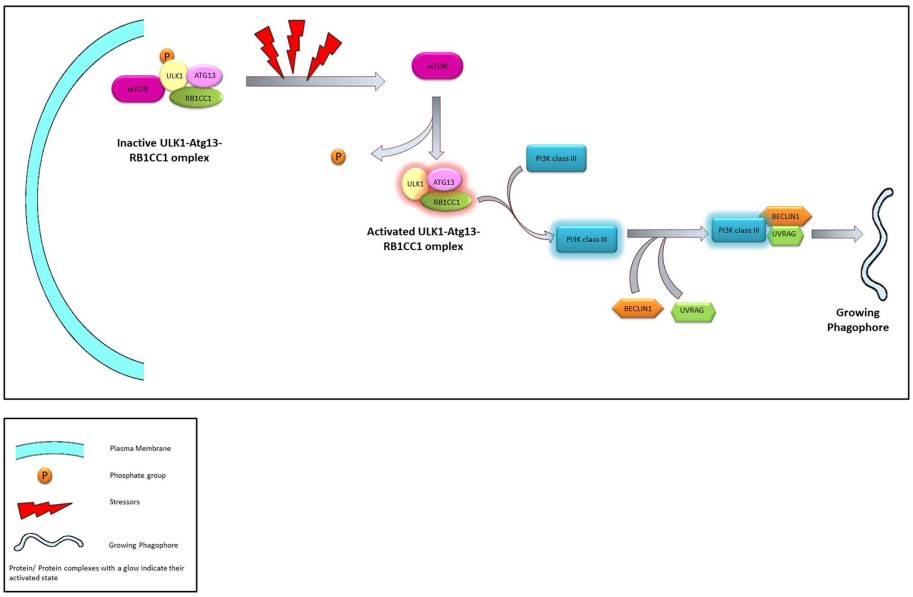

FIGURE 3
The Process of Nucleation. Under normal conditions ULK1-Atg13-RB1CC1 is maintained in an inactivated state through phosphorylation promoted by interaction with mTOR. In presence of stressors ULK1-Atg13-RB1CC1 complex is activated following dissociation from mTOR and dephosphorylation. ULK1 complex activates class III PI3K which in turn associates with Beclin1 and UVRAG leading to the initiation of phagophore.

autophagosome which undergoes "maturation" before its fusion with the lysosome. The maturation process is characterized by the gradual removal of the membrane-bound Atg proteins associated with the nucleation and elongation steps and the simultaneous incorporation of proteins belonging to the SNARE machinery like the VAM7, VAM9, syntaxin17, and SNAP29 (69, 70), proteins that are considered integral for membrane fusion. On completion of the maturation process, the autophagosome travels to the lysosome assisted by the microtubule system (71) and fused with the lysosome to form the phagosome.

3.4 Mitophagy

The name mitophagy was coined by Lemasters to describe autophagic machinery that selectively degrades mitochondria (72). Based upon the molecular machinery, mitophagy can be either PINK1/Perkin mediated, or receptor mediated both of which proceeds through initiation, priming of the damaged organelle, formation of autophagosome which fuses with the lysosome.

3.4.1 The PINK1/Perkin mediated mitophagy

PINK1 is a Ser/Thr kinase whose localization on the mitochondrial membrane varies according to the changes in the membrane potential of the organelle ($\Delta\Psi_m$). Under normal physiological conditions, PINK1 is localized in the inner mitochondrial membrane. However, disruption of $\Delta\Psi_m$ (73, 74) or excessive accumulation of misfolded proteins (75) trigger the relocation of PINK to the outer membrane of the damaged mitochondria and its subsequent activation through autophosphorylation. Phosphorylated PINK triggers the localization of ubiquitin and Perkin on mitochondrial surface generating an "eat-me" signal that promote polyubiquitination thereby targeting the damaged mitochondrial for autophagy (76–78). In a Perkin independent pathway that involve interaction with ubiquitin chains, PINK can also mediate the accumulation of autophagy adaptors like p62, NDP52, optineurin, and ULK1 on the mitochondrial surface (78). These adaptor proteins bear LC3 domain and forms "mitophagosom" (78). Phosphorylation of opintoneurin post recruitment also feed forward the process (79).

3.4.2 Receptor-mediated mitophagy

The inner and outer membrane of mitochondria houses several receptor proteins like FUNDC1, BNIP3L, FKBP8, prohibitin2, and cardiolipin (80). The localization of these receptor proteins across the inner and outer mitochondrial membrane depends on the stressor level of the cell and is essential in priming a damaged mitochondrion for elimination through different autophagic machinery. For example FKBP38, prohibitin2, and cardiolipin are known to bear LC3 domain and

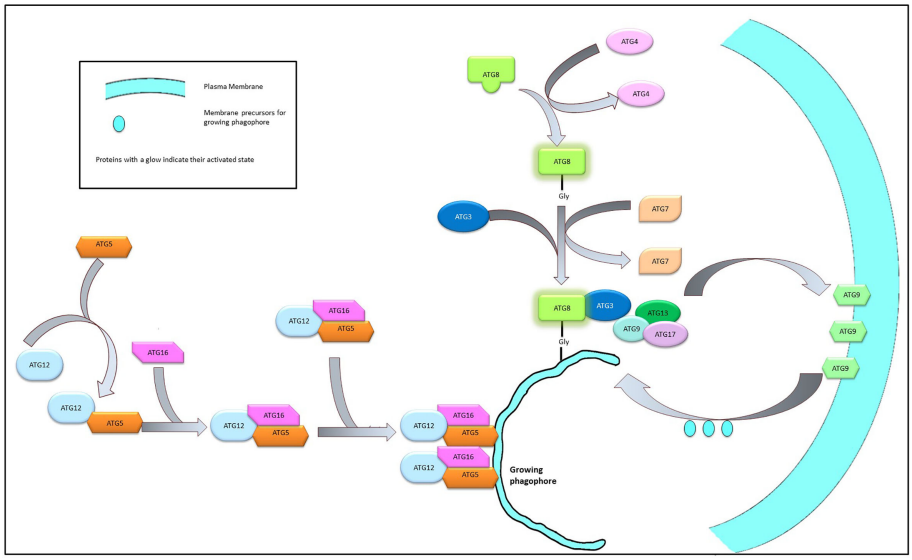

FIGURE 4
Elongation of phagophore membrane. Dimerization of the Atg12-Atg5-Atg16 complex on the surface of the growing phagophore membrane promote the recruitment of Atg8 and Atg9 complex on the growing membrane. Atg9 imports membrane components from the neighboring bio-membranes to the growing phagophore to facilitate elongation.

can promote the formation of autophagosome around a damaged mitochondria (81). Prohibitn2 also promote localization of Perkin on the mitochondrial membrane, thus interlinking different branches of mitophagy (82). Similarly translocation of cardiolipin from the inner to the outer mitochondrial membrane in response to stressors generates a potent "eat-me" signal (83) and its release from the outer mitochondrila membrane acts as a strong inducer of apoptosis (84).

These receptors are also known to mediate PINK1-Perkin independent mitophagy in high energy demanding tissues like brain (85). Under normoxic conditions, FUNDC1 phosphorylation promotes mitochondrial fusion as well as prevents mitophagy (86), whereas under hypoxic conditions, dephosphorylation of FUNDC1 by specific mitochondria-based phosphatases initiate mitochondrial fragmentation (87) and mitophagy (86, 88).

The BNIP3/NIX axis, that interlinks the mitophagy machinery with that of the general autophagy ones, is often deregulated in cancer (89). Under hypoxic conditions the BNIP3 and NIX are overexpressed [through a HIF1α mediated pathway (90)] and undergo phosphorylation. Phosphorylated BNIP3 and NIX interacts with LC3 (91, 92) and channelize the organelle for macroautophagy based elimination. BNIP3 also stabilizes that the PINK1-Perkin machinery (93), thereby not only links mitophagy with a major macroautophagy machinery, they effectively target the damaged mitochondrion for degradation and thereby suppress the production of excess amount of mtROS under hypoxic conditions (94, 95).

In addition to mitophagy several forms of autophagy have been identified dedicated to the selective elimination of specific challenges like pathogens (xenophagy), protein aggregates (aggrephagy), or damaged ER (reticulophagy). Protein aggregates —formed by the aberrant interaction of misfolded proteins— are eliminated through receptor-mediated autophagic machinery (96). Simultaneously, excessive accumulation of misfolded proteins in the ER lumen trigger reticulophagy or ER-phagy. The amelioration of ER stress is known to have significant survival implications. Moreover, autophagy processes like ferritinophagy (the receptor-mediated lysosomal degradation of ferritin that takes place under iron deprivation) (97), glycophagy (degradation of glycogen molecule by lysosomal α-glucosidase) (98), or lipophagy (lysosomal degradation of lipid droplets and lipoproteins) (99) are crucial for nutrient homeostasis and cell survival.

4 Influence of autophagy on radiation response of tumors

Radiotherapy although being a frontline approach for cancer treatment, often meets with failures. This is due to the radio-resistance that a growing tumor acquires through deregulation of stress responses, like the DNA damage and repair mechanisms that promote autophagy and leads to nutrient recycling. In addition to the damaged proteins, various intermediate molecules and their complexes and damaged organelles like mitochondria and micronuclei do serve as cargo for autophagy

(49). Recent studies have bestowed both pro and anti survival nature to the autophagic pathways and cancer cells are known to exploit this dual nature of autophagic pathways to survive in a metabolically challenged microenvironment, to escape the host-immune responses, to evade apoptosis, and to metastasize (100, 101).

4.1 Effect of autophagy on IR induced DNA damage and repair

Irradiation of tumor cells ionizing radiation initiates a series of events ranging from DNA damage, ROS induction, cell death, and cell senescence with intricate crosstalk amongst themselves. It is widely acknowledged that DNA double-strand breaks that results in are majorly responsible for the initiation of the cell death that are instrumental in regulating local tumor growth. Along with the inducement of DNA damage the DNA damage response (DDR) acts pro-actively and seamlessly to prevent the accumulation of DNA damages (arising due to any stress). Once the DDR commences and the extent of the DNA damage is assessed, autophagy plays a pivotal role in deciding the ultimate fate of the cell.

Ataxia-telangiectasia mutated (ATM) and ATM/Rad 3-related (ATR) are cell cycle checkpoint regulators that also act as DNA damage sensors and are involved in activating the DDR pathways (102). ATM is involved in multiple cellular phenomena like cycle arrest, apoptosis, and autophagy and hence considered as a tumor suppressor protein (103). Moreover cancer cells are known to employ myriad pathways—like upregulation of miRNA18a (104) and WIP1 phosphatase (105)—to suppress ATM activity leading to induction of autophagy through deregulations of glucose metabolism and energy deprivation (106). However growing evidences also suggest that ATM is also involved in promoting chemo- and radio-resistance (107–109) to cancer cells which might in turn be the reflection of the dual nature of the autophagic processes that the protein initiates. Activation of autophagic pathway, through ATM-CHK2-BECN1 axis, is also observed in irradiated tumor cells exhibiting high level of oxidative stress.

4.2 Effect of autophagy on IR induced cell death

The radiosensitivity of the tumor cells are often mediated through suppression of the autophagic machinery. The nuclear translocation of Beclin1 is often observed in response to IR exposure which in turn leads to G2/M cell cycle arrest (110). ATG5-driven autophagy is also known to promotes the radio-sensitivity of prostate cancer cells under nutrient-starved or glutamine depleted conditions or with the silencing of MYC (111). Hence silencing the Belcin1 or ATG5 expression had been shown to reduce the IR sensitivity of the cancer cells. Similarly suppression of ATG7 by long non-coding RNA (lncRNA) HOTAIR—which significantly overexpresses in irradiated prostate cancer cell lines in response to irradiation—is associated with radioresistance in irradiated cells (112).

The association between IR and autophagic pathways is further emphasized by the observation that in breast cancer cells, which are inherently resistant to apoptosis, IR exposure results in enhanced autophagic phenotypes resulting in increased iron accumulation, which coupled with the subsequent ROS generation, oxidative stress, and DNA damage, can result in the induction of cell death through ferroptosis (113, 114). Consequently, in recent years combining autophagic inducers along with IR is emerging as an interesting approach to increase the radiosensitivity of the cancer cells (105, 106). In a similar approach, treatment of Non-small cell lung carcinoma (NSCLC) cells with rapamycin and histone deacetylase inhibitor was found to promote radiosensitization (115). This combination has dual effects of enhancing autophagy along with the inhibition of the DNA damage repair machinery and the effect was observed both in the cultured cells and in the tumor xenograft mice models.

However, the effect of autophagy on the survival of cancer cells are function of multiple aspects and as a result, autophagy can act as a promoter as well as an antagonist towards radio-sensitization. In fact, different cancer cell types have been found to benefit from enhancing autophagy as their survival strategy. For example, in presence of autophagy inhibitors, otherwise radio-resistant bladder cancer cells developed sensitivity towards chemotherapy (116). Similarly, inhibition of autophagy through ATG5 silencing is known to increase the IR-induced cell death in nasopharyngeal carcinoma (117). The autophagy inhibitors when combined with IR have emerged as one of the principal factor that influence the bystander and abscopal effects (as discussed in the later sections) observed after chemo and radiotherapy (118).

4.3 Effect of autophagy on cancer stem cells and IR response

Autophagy plays an important role in maintaining the ‘stem-ness’ of the CSCs. The majority of the tumors activate the epithelial-mesenchymal transition (EMT) program to attain the stem cell-like properties and to promote their growth, invasion, and metastasis. The autophagy-related genes, especially ATG5 play a critical role in the EMT process as indicated by a study on cervical cancer cells (119). In radio-resistant cancer cells, like pancreatic ductal adenocarcinoma cells and NSCLC stem cells, autophagy has found to be essential in promoting tumor growth and invasiveness (120) as well as maintaining the stem cell-like properties (121) of the cells. as a result autophagy inhibitors, either individually or with combination with other traditional

methods of cancer therapy, have been able to block proliferation, colony and, spheroid formation (in pancreatic CSC populations) in cancer cells (122). Similarly, silencing of prominent autophagic genes like Atg5 was able to induce radio sensitivity within radio-resistant cancer stem cell populations (prostate CSCs) (111).

4.4 Effect of autophagy on Radiation Induced Bystander Effect (RIBE) and Abscopal Effect

IR-exposed cancer cells secrete hoard of signaling molecules in their microenvironment that modulate the biology of the neighboring non-transformed cells leading to what is now recognized as the Radiation induced Bystander Effect (RIBE). RIBE is one of the principal factor that is considered to modulate the cytotoxic effects of radiation in the irradiated tumor targets (34). Usually the bystander cells responds to the challenge by secreting a number of cytokines like IL6 (123), IL1, TNFα, IL18 (124), colony-stimulating factor 2 (CSF2)/JAK2/STAT3 (125), as well as microRNAs such as microRNA-7 (36), microRNA-7-5P (33), and ROS (126). All these molecules significantly influence the crosstalk between cancer and the neighboring non-irradiated cells that often translates in altered autophagy (33). RIBE have often been mediated by regulation of autophagy that exhibit spatial and temporal differences. The exosomal miRNAs like miR17-5p that are secreted by the irradiated cancer cells are known to induce autophagy in non-irradiated bystander cells while suppress the same within themselves (33). In irradiated HeLa cell culture, the bystander cells have been shown to exhibit enhanced autophagy, providing nutrient supplies to the nutrient-deficient cancer cells (123) while in irradiated glioma cells higher level of miR17-5p or miR273 results in pronounced antitumor effect through suppression of autophagy (127, 128). Exosomes containing miR7-5-p are known to induce autophagy in neighboring non-irradiated cells through suppression of the EGRF-Akt-mTOR axis resulting in radiation induced tissue damage (129).

Apart from systemic level, autophagy appears to be a crucial mediator of RIBE/tumor response to radiation at the organelle level. Mitophagy is often induced in irradiated cancer cells through which the mitochondria, damaged by the excess mtROS produced due to radiation, renew themselves (130). However, the dichotomous nature of autophagy is also reflected in such cases as well. In the bystander HepG2 cells, increase in the level of ROS production reflects in higher expression level of autophagic proteins LC3II/I and Beclin 1, suggesting that ROS level might be a critical determinant between the cytotoxic and cytoprotective nature of autophagy (126).

5 Impact of autophagy modifiers on radiation response of tumors: pre-clinical studies

Autophagy is considered as one of the very first cellular processes activated in response to radiation onslaught and although Consequently autophagy modifiers have immense importance in radiation therapy considering the dual role of autophagy in tumor formation, aggression, and metastasis (101). However, the role autophagy on cancer cells changes with the stage and progression of the tumor mass. In the initial stages of a tumor, autophagy plays a predominantly tumor suppressor role (131) while in the established tumor, where autophagy protects (cytoprotective autophagy) the cancerous cells against different stresses, helps them survive, and gain therapy-resistant phenotypes (132). Consequently, the inclusion of autophagy inducers in the treatment regimen might have a cancer-suppressing effect during the early stages of malignancy, but an autophagy inhibitor may have better radio-sensitizing efficacy in the later stages of the disease. Hence—in spite of their promises—application of the autophagy modifiers in cancer therapy, are considered to be strategically challenging and are yet to gain favor as a therapeutic modality. In this section, a broad overview of the different types of autophagy modifiers, with their reported applications in the preclinical models of cancers, has been discussed (Table 1) to elucidate the complex role of autophagy in determining the success of RT.

The autophagy inducers are usually the nutrient or ER stress inducers, or antagonists of the mTOR blocker rapamycin (and its derivatives). ER stress induction is accompanied by the downstream activation of autophagy and the appearance of autophagolysosomes. Hence an induction of the autophagic flux was observed when EC109 esophageal cancer cell line is treated tunicamycin (a ER stress inducer) (154). However, when irradiated EC109 cells were treated with tunicamycin along with 3-methyladenine (3-MA), and autophagy inhibitor, an increased apoptosis was observed in the treated cells, suggesting the involvement of autophagy in rescuing irradiated cells from apoptotic cell death (154).

The PI3K/Akt/mTOR pathway is known to suppress the ER-induced autophagy pathways and consequently mTOR—a serine/threonine kinase and an integral part of the PI3K/Akt/mTOR signaling pathway—have been targeted in many *in vitro* and *in vivo* studies to regulate the outcome of RT. Rapamycin and its derivatives everolimus, temsirolimus, deferolimus, zotarolimus, etc. are well-known TOR kinase inhibitors that have been employed in combination treatments to increase both chemo-therapeutic and radio-therapeutic efficacies. Rapamycin has been demonstrated to increase the efficacy of fractionated radiation against glioma xenograft models (133). In glioblastoma cells, rapamycin pretreatment has increased radiosensitivity with reduced expression of surviving and

TABLE 1 Preclinical studies involving Autophagy modulators, the molecular mechanism they employ and, their effect on response to RT.

Autophagy modifier	Mechanisms reported in the study	Response to IR	Pre-clinical model	Reference
Autophagy Induction				
Rapamycin	mTOR inhibition, downregulation of Survivin expression; Reduced clonogenicity	Radiosensitization	Glioma cell line and mouse xenograft	(133, 134)
	mTOR inhibition, impaired DNA damage repair	Radiosensitization	Breast cancer cell line	(135)
	mTOR inhibition	Radioresistance	C57BL/6 Mice	(136)
Rapamycin + ABT-737	Apoptosis induction	Radiosensitization	Non-small cell lung carcinoma and mouse xenograft	(137)
Temsirolimus	mTOR inhibition	Radiosensitization	Renal cancer cell line	(138)
Everolimus	mTOR inhibition	Radiosensitization	Prostate cancer cell lines	(139)
M867 + Everolimus	mTOR inhibition and apoptosis inhibition	Radiosensitization	Lung cancer cells	(140)
PCI-5002	Apoptosis inhibition	Radiosensitization	Lung cancer cells and mouse xenograft	(141)
BEZ235 + PI103	PI3K/mTOR inhibition, cell cycle arrest, apoptosis induction	Radiosensitization	Prostate cancer cell lines	(142, 143)
NVP-BEZ235 + AZD6244	Inhibition of mTOR and MAP Kinase pathway	Radioresistance	Lung and glioma cell lines	(144)
Pevonedistat/MLN4924	Inhibition of NEDDylation	Radiosensitization	Liver cancer cell lines	(145, 146)
Autophagy Inhibition				
NVP-BEZ235 + 3MA or Chloroquine	Inhibition of PI3K/mTOR, apoptosis induction	Radiosensitization	Head and neck carcinoma and glioblastoma cells	(147)
Chloroquine	Apoptosis induction	Radiosensitization	C57BL/6 Mice	(136)
Chloroquine	Apoptosis induction	Radiosensitization	Colorectal cells	(148)
Chloroquine + Temsirolimus	Inhibition of mTOR, induction of apoptosis	Radiosensitization	Colorectal cells	(149)
Everolimus + Chloroquine	Inhibition of mTOR, induction of apoptosis	Radiosensitization	Neuroendocrine cells	(150)
Hydroxychloroquine	Apoptosis induction	Radiosensitization	Colon cancer cells	(151)
3-MA	PI3K inhibition and apoptosis induction	Radiosensitization	Esophageal cancer cells and mouse xenograft model	(152, 153)
Tunicamycin + 3-MA	ER stress induction and apoptosis	Radiosensitization	Esophageal cancer cell	(154)
Core-shell copper selenide-coated gold nanoparticles	Lysosomal alkalization, impaired DNA damage repair	Radiosensitization	Glioblastoma cells	(155)

Autophagic modulators, generating radioresistance are indicated in red highlighted box.

clonogenic potential (134). One of the major pathways involved in rapamycin-induced autophagy induction (*via* mTOR inhibition) and subsequent radio-sensitization is by impairing the DNA damage responses, specifically the homologous recombination and the non-homologous end-joining mechanisms (135). Rapamycin blocks the recruitment of BRCA1 and Rad51 to the damaged DNA thereby inhibiting the downstream pathways of homologous recombination.

Although rapamycin has been successfully used in *in vitro* cell cultures its low solubility in an aqueous system limits its application as a potential therapeutic agent. Hence its analogs, with better water solubilities, are currently used in cancer therapeutics. In renal cancer cell lines which are deficient in the VHL (von Hippel-Lindau) tumor suppressor gene, inhibition of the late-stage autophagy by small molecule inhibitor, STF-62247 or temsirolimus (the first FDA-approved mTOR inhibitor) has better radiosensitization effects than the individual treatments (138). Everolimus, another rapamycin analog, enhanced the radiosensitivity of the prostate cancer cell lines, PC3 and DU145, in a PTEN (phosphatase and tensin homolog) dependent manner (139) with PTEN-deficient PC3 cells exhibiting higher susceptibility to radiation with significant autophagy induction. Moreover, blocking apoptotic pathways in these cells had increased radiation-induced autophagic cell death.

PTEN is a tumor suppressor and metabolic regulator which has a profound role in cell division and proliferation by negatively regulating the PI3K/Akt/mTOR pathway and it is frequently mutated or inactivated in tumors. Loss of PTEN induces radioresistance in cancer cells by the downregulation of radiation-induced autophagic cell death which has been observed to be overcome by treating the cells with mTOR inhibitors. In non-small-cell lung cancer cell line HCC827, which are refractory to gefitinib, an EGFR tyrosine kinase inhibitor (TKI) possibly due to PTEN deficiency has been radiosensitized by treating with mTOR inhibitors with activation of autophagic flux (156).

Application of dual PI3K/mTOR inhibitors, BEZ235 and PI103, in combination with IR, had shown superior anticancer efficacies and enhanced radiosensitization characterized by reduced colony-formation, G2/M cell cycle arrest, increased DNA damage, apoptosis, autophagic flux in the radioresistant prostate cancer cells (128). In prostate cancer radioresistance is largely modulated by the PI3K/Akt/mTOR activation in association with an epithelial-mesenchymal transition (EMT)/cancer stem cell-like phenotype. Treating these cells with the dual inhibitor BEZ235 induced apoptotic cell death which helped to overcome the radioresistance suggesting BEZ235 to be a promising candidate for combination therapy in prostate cancers therapeutics (142). Similarly NVP-BEZ235—another a novel PI3K/mTOR inhibitor—had exhibited promising autophagy induction and enhanced radiosensitivity and apoptosis in human glioma stem cells (157) through blocking the DNA damage repairing pathway. However, when combined with temozolomide, an alkylating agent, NVP-BEZ235 has been shown to downregulate PI3K/mTOR pathways, in glioma cells (158) but in combination with AZD6244, a MAP kinase inhibitor, NVP-BEZ235 significantly reduced radiosensitization of irradiated lung cancer and glioma cells (144). One of the reasons for the contradictory behavior of NVP-BEZ235 could be the different mechanisms through which it enhances radiosensitization and induces autophagy as suggested by Cerniglia et al. (147). Although autophagy was induced by NVP-BEZ235 in cancer cells but using the autophagy inhibitors 3MA or CQ in NVP-BEZ235-treated and IR exposed cells, had increased the level of cytotoxicity.

Emerging evidence indicates improved radiosensitization of cancer cells when combined with NEDDylation inhibitor MLN4924 (also known as Pevonedistat) with augmented autophagy induction associated with DNA damage, apoptosis, and senescence (145, 146, 159). NEDDylation (conjugation of NEDD8 moiety to protein substrates) which is tightly regulated in normal cells, targets crucial tumor suppressor proteins towards degradation and is highly active in cancer cells (160); hence, NEDDylation inhibitors are conspicuous contenders in anticancer therapeutics. Although it has been predicted that the mode of autophagy induced by Pevonedistat is protective and promotes tumor drug resistance but the inclusion of autophagy inhibitor along with it showed promising antitumor effects (161). With significant successes in the preclinical studies, Pevonedistat is currently under clinical phase I/II trials (162) even though investigational studies on it as radiosensitizer is limited.

Interestingly, induction of autophagy by modulating the apoptotic signaling cascade has been studied in some preclinical models. The lung cancer cells had turned radiosensitive when treated with zinc ionophore PCI-5002 (141) or with apoptosis inhibitor, M867 in combination with everolimus (140). On the other hand, rapamycin along with ABT-737, an apoptosis inducer, enhances the radiotherapy response of the non-small cell lung cancer cells (NSCLC), both in *in vitro* and *in vivo* xenograft mice models with an almost 6-fold induction in the autophagic flux compared to the radiation only group (137). One reason for the synergistic effect could be the application of ABT-737 which induces apoptosis in a Bax/Bak-dependent pathway. The NSCLC cells are Bax deficient due to the overexpression of Bax inhibitor-1 protein (163), which could be compensated by the upregulation in Bax expression brought about by the rapamycin treatment, thereby enhancing the ABT-737 mediated apoptosis (164).

In a very recent approach core-shell Copper selenide coated gold nanoparticle was used to improve the response of the glioblastoma cells towards RT. The nanoparticles impaired the autophagic machinery by alkylating lysosomes leading to inactivation of the lysosomal enzymes within. Simultaneously the nanoparticles increased the ubiquitination and protosomal degradation of the DNA repair protein Rad51, thereby compromised the repair of the DNA strands damaged by irradiation. The cumulative effect of these were able to significantly improve the response of the glioblastoma cells toward RT (155).

Cytoprotective autophagy induction by IR is largely contributed by ROS and ER stress determining the radiotherapy outcomes. The elevated ROS in irradiated cells generate oxidative damages to DNA, protein, and lipid causing ER stress and unfolded-protein response which in turn stimulate autophagy to eliminate the damaged cellular macromolecules. Attempts has continuously been made to develop a combination therapy involving autophagy inhibitors and IR to enhance radiosensitization of tumors through induction of apoptotic cell death. Combining IR with autophagy inhibitors 3-MA or bafilomycinA1 (BafA1) restricts cell growth and proliferation whereas adding autophagy inducer rapamycin in the IR treatment regimen has induced cell proliferation, clearly demonstrating the differential response of the irradiated cells to autophagy modifiers. Similarly, in *in vivo* studies in whole-body irradiated mice models, rapamycin increased survival rates whereas chloroquine (CQ), an autophagy inhibitor, has lowered the survivability of the animals (136). HT29 colorectal cells which were p53 deficient have been radiosensitized after CQ treatment and autophagy inhibition (148). Interestingly, when combined with the mTOR inhibitor temsirolimus, CQ induced radiosensitization and apoptotic cell death in colorectal cancer cell lines (149). IR-induced activation of mTOR signaling was blocked by temsirolimus with autophagy induction whereas CQ inhibited the autophagy as evidenced by p62 and LC3-II expression levels. When combined, both mTOR signaling and autophagy were suppressed with concomitant induction of apoptosis in the IR-exposed cells. In a similar approach, everolimus and other PI3K/mTOR inhibitors in combination with CQ have shown increased anticancer effect where inhibition of mTOR downstream signaling accompanied by CQ mediated autophagy inhibition induces apoptosis in

neuroendocrine tumor cell line BON1 (150). At low cytotoxic dosages, CQ was found to radio-sensitize bladder cancer cells, both *in vitro* and xenografted mouse models (165). CQ blocks the IR-induced DNA damage repair and activated apoptosis in the irradiated tumor cells by inhibiting autophagy. Autophagy inhibition by chloroquine enhances the radio-sensitivity of the cells with concomitant apoptosis induction associated with G1/G0 cell cycle arrest and reduction in cancer-initiating cell populations (166). Hydroxychloroquine (HCQ)-loaded mesoporous silica nanoparticles with enhanced cellular permeability and intracellular accumulation resulted in autophagy (cytoprotective) inhibition and a marked increase in IR-induced cell death in HCT116 colon cancer cells (167). Tumor xenograft mice models exhibit better tumor targeting of the HCQ-loaded nanoparticles. 3-MA which is a potent inhibitor of PI3K signaling has been found to inhibit radiation-induced autophagy and sensitize the esophageal cancer cells to IR with increased apoptosis and slower cell growth (152, 153). Moreover, the synergistic effect was observed in mice xenograft models with regression of tumor volume and reduction in the vasculature.

The available pre-clinical reports with both the autophagy activators and inhibitors indicated that combining these autophagy modifiers with IR has immense potential in avoiding radioresistance as well as in aggravating cytotoxic effects. However, due to the double edged effect of autophagy on the cancer cells, the effect of autophagic modulators on their survival becomes the function of the disease progression. Hence, while formulating a treatment regimen for clinical studies involving autophagic modulators, caution must be taken and information regarding the site and stage of the tumor mass, along with its genetic profile should be carefully considered.

6 Autophagy and radiation response of tumors: Clinical studies

Prompted by the compelling evidence from preclinical studies that suggested a role for autophagy in the radiation response of tumor cells and the effects of various modifiers of autophagy on the radiation response of tumors, clinical trials were initiated nearly two decades ago to validate these findings in different human malignancies. These studies have focused on the correlation between various regulators of autophagy and the response of tumors to radiotherapy and chemoradiotherapy, as well as the effects of different modifiers of autophagy on the response to radiotherapy and chemoradiotherapy. Although Pevonedistat, a NEDD8 Activating Enzyme inhibitor, and activator of protective autophagy has been extensively investigated either as a monotherapeutic or as part of a combined modality with chemotherapeutic drugs and immune modifiers (168), it has not been investigated so far in combination with radiotherapy.

6.1 Regulators of autophagy and tumor response to various therapies

The influence of various regulators of autophagy on the response of the tumor towards RT and CRT (Chemo-radiotherapy) evaluated in some of the human malignancies has shown an inverse relationship between the levels of these regulators and clinical response to RT or CRT. In nasopharyngeal carcinoma a high Beclin1 level correlated with poor response to CRT (169, 170). Similarly, elevated levels of ATG4B and LC3B were associated with poor response to the standard of care (RT and TMZ) in glioblastoma (171) and in prostate cancers, with high LC3A and low LAMP2 levels, were found to be resistant to RT (172). Table 2 summarizes the outcome of clinical studies that investigated the relationship between the different autophagy regulators and tumor response toward RT or CRT.

6.2 Targeting autophagy for improving the RT of tumors

Many small molecules, subdivided into seven different functional groups and targeting different regulators of autophagy, have been considered as potential adjuvants to RT and chemotherapy of cancer (174, 175). Of these, repurposing of the drug chloroquine (CQ) and its derivative hydroxyl chloroquine (HCQ), originally approved for the treatment of malaria and are known to disrupt the autophagosome formation, have been extensively investigated as mono-therapeutic as well as an adjuvant to radio and chemotherapies (176), although limited clinical trials have evaluated the efficacy of the other classes of autophagy targeting drugs.

A double-blind placebo-controlled trial with (CQ as an adjuvant to chemo-radiotherapy (RT+TMZ) demonstrated a significant improvement in the median survival of patients with glioblastoma as compared to the control (RT+TMZ) arm (177). Likewise, CQ was found to enhance the response of brain metastasis to whole-brain irradiation, without significant toxicity (178). Unfortunately, a Phase I/II clinical trial in stage IV small cell lung cancer evaluating the efficacy of a combination of CRT and CQ had to be terminated due to poor accrual (179).

Due to its lesser toxicity level the CQ derivative HCQ (180), has been extensively investigated in clinical trials both as a mono-therapeutic as well as in combination with chemo- and radiotherapy. Although inhibition of autophagy is clinically feasible with HCQ and also enhances the efficacy of chemo-

TABLE 2 Clinical studies examining the relationship between regulators of autophagy and tumor response to radiotherapy and chemoradiotherapy.

Autophagy regulator	Tumors	Therapy	Findings	References
Beclin1	Nasopharyngeal carcinoma	Floxuridine + carboplatin and RT	High Beclin1 expression correlated with poor overall, progression-free, and distant metastasis-free survival	(147)
pATG4B and LC3B	Glioblastoma multiforme	TMZ and RT	Survival inversely correlated with pATG4B and LC3B	(173)
High LC3A/low LAMP2A	Prostate cancer	RT	Associated with resistance against RT	(170)

and radiotherapy of many human malignancies, dose-limiting toxicity, mainly in the form of retinopathy has limited the efficacy and its utility as an adjuvant to radiotherapy of tumors (181, 182). A Phase II clinical trial was initiated in 2007 in pancreatic cancer (NCT01494155) that evaluated the toxicity and efficacy of a combination of short course chemo-radiotherapy (SCRT; gemcitabine and photon/proton RT) and HCQ. However, a long-term follow-up has revealed that although the combined treatment of HCQ and SCRT was well tolerated, significant improvement in terms of survival benefit was not observed (183). Unfortunately, till date, no information is available in the public domain regarding the outcome or status of many clinical trials initiated in recent years to evaluate the feasibility, toxicity, and efficacy of combining CQ or HCQ with radiotherapy or chemoradiotherapy for the treatment of different solid tumors.

The mTOR inhibitors Temsirolimus and Everolimus are known to inhibit the initial events of autophagy. No significant improvement in terms of patient survival was observed when glioblastoma patients were treated with a therapeutic regime combining Temsirolimus and Everolimus with chemoradiotherapy (184, 185). Interestingly, Nelfinavir; a PI3K/Akt inhibitor has been found to provide moderate survival benefits without severe grade 3/4 toxicity in LAPC (Locally advanced pancreatic cancer) and NSCLC (186–189) patients.

An overview of the clinical trials that target the autophagy machinery is presented in Table 3. Through the course of these trials many limitations of the existing autophagy targeting drugs

TABLE 3 Overview of the clinical trials targeting autophagy for improving radiotherapy of tumors.

Autophagy targeting drugs	Tumors	Trial	Therapy	Findings	References
Autophagosome (formation) Inhibitor					
Hydroxychloroquine (HCQ)	Glioblastoma multiforme	I/II	Conventional RT with TMZ	Dose-limiting toxicity and no significant improvement in survival	(181) NCT02738582
	Pancreatic cancer	I/II	CRT with Photon or Proton therapy	Well tolerated, but no significant survival benefit	(180) NCT01494155
Chloroquine (CQ)	Recurrent glioblastoma	I/II	Conventional RT with TMZ	Feasibility established	(176)
	Glioblastoma multiforme	III	Conventional RT with TMZ	Improvement in survival and reduced death rate	(177) NCT00224978
	Brain metastasis	II	Whole-brain irradiation	Enhanced tumor response without toxicity	(178)
	Stage IV Small Cell Lung Cancer	I/II	Chemoradiotherapy	Terminated due to poor accrual	(179) NCT01575782
mTOR inhibitors					
Temsirolimus	Recurrent glioblastoma	I/II	Conventional RT with TMZ	Clinical benefit in 335 patients	(184)
Everolimus		II		No significant survival benefit	(185)
PI3/Akt inhibitors					

(Continued)

TABLE 3 Continued

Autophagy targeting drugs	Tumors	Trial	Therapy	Findings	References
Nelfinavir (HIV protease inhibitor)	Locally advanced pancreatic cancer	I/II	Chemoradiotherapy	Moderately improved tumor response, but Grade 3 & 4 GI toxicity	(186)
		I/II	Stereotactic body radiotherapy (SBRT)	MTD identified	(187)
	Non-small cell lung cancer	I/II	Chemoradiotherapy	Median survival of 12 months and progression-free survival of 41 months, without grade 3/4 toxicity	(188, 189)

The NCI identifier numbers of the clinical trials are mentioned along with reference to the literature.

have been identified that compromise the efficacy of the therapeutic regimen that involves them. Toxicity, attenuated efficacy in the acidic milieu of TME, and inability to reliably monitor the autophagic flux are among a few. Since most, if not all, modifiers of autophagy investigated clinically so far do not exclusively alter autophagy, but affect other signaling pathways of radiation response, it is reasonable to expect heterogeneity in the response of tumors to a combined regimen of RT and autophagy targeting drugs. Since most of the autophagy regulating genes have moonlighting properties where they have other functions, the therapeutic benefit of combined therapies involving autophagy modifiers may be obscured by their effects on other targets. Thus, therapies combining autophagy targeting drugs with radiation and/or chemotherapeutic agents have not elicited encouraging response either due to the lack of proper selection of patients (which should have been done based on a complete understanding of the biological behavior of the tumor) and/or our inability to adopt the best approach for manipulating autophagy in individual patients. This is particularly relevant when combining RT with modifiers of autophagy as radiation-induced autophagy can be either pro-survival or promote death in a context-dependent manner (49). This limitation can be overcome to a very large extent by complete characterization of tumors for their biological behavior particularly related to the status of regulators of various signaling pathways triggered by radiation damage, especially the status of the autophagy regulators.

7 Summary

Current understanding implicates autophagy in several cellular events including biological responses to stress caused by ionizing radiation and a variety of other therapeutic agents. Autophagy appears to be largely pro-survival while promoting death under certain circumstances in a context-dependent manner. Its emerging role in tissue, as well as its effects in systemic level following focal irradiation of tumors, suggests its ubiquitous impact in therapeutic responses to RT, which has prompted several clinical studies to target autophagy for improving the efficacy of therapy. However, encouraging clinical responses have yet not emerged from the Phase I/II of the clinical trials conducted so far which, unfortunately, has precluded a therapeutic regime consisting of an autophagy modifies as the principal component or adjuvant to RT/CRT to proceed towards the Phase III of clinical trials.

Author contributions

AR, SB, and BD worked in conceptualizing, designing, and preparing the manuscript. All authors contributed to the article and approved the submitted version.

Acknowledgments

The authors wish to thank Dr. Madhuri Chaurasia, Weizmann Institute of Science, Rehovot, Israel for the helpful discussions in preparing the manuscript.

Conflict of interest

The authors declare that the research was conducted in the absence of any commercial or financial relationships that could be construed as a potential conflict of interest.

Publisher's note

References

1. Jean-Claude R, Nüsslin F. Marie Curie's contribution to medical physics. *Physica Med* (2013) 29(5):423–5. doi: 10.1016/j.ejmp.2013.08.001

2. Ejaz A, Spolverato G, Kim Y, Squires MH, Poultsides G, Fields R, et al. Impact of external-beam radiation therapy on outcomes among patients with resected gastric cancer: A multi-institutional analysis. *Ann Surg Oncol* (2014) 21(11):3412–21. doi: 10.1245/s10434-014-3776-5

3. Palata O, Hradilova Podzimkova N, Nedvedova E, Umprecht A, Sadilkova L, Palova Jelinkova L, et al. Radiotherapy in combination with cytokine treatment. *Front Oncol* (2019) 9:367. doi: 10.3389/fonc.2019.00367

4. Hodge JW, Guha C, Neefjes J, Gulley JL. Synergizing radiation therapy and immunotherapy for curing incurable cancers. opportunities and challenges. *Oncol (Williston Park N.Y.)* (2008) 22(9):1064–70.

5. Perri F, Pacelli R, Della Vittoria Scarpati G, Cella L, Giuliano M, Caponigro F, et al. Radioresistance in head and neck squamous cell carcinoma: Biological bases and therapeutic implications. *Head Neck* (2015) 37(5):763–70. doi: 10.1002/hed.23837

6. Mohan G, Ayisha Hamna TP, Jijo AJ, Sardaha Devi KM, Narayanasamy A, Vellingiri B. Recent advances in radiotherapy and its associated side effects in cancer–a review. *J Basic Appl Zoology* (2019) 80(1):14. doi: 10.1186/s41936-019-0083-5

7. Rabinovitch R, Grant B, Berkey BA, Raben D, Ang KK, Fu KK. Group, rImpact of nutrition support on treatment outcome in patients with locally advanced head and neck squamous cell cancer treated with definitive radiotherapy: a secondary analysis of RTOG trial 90-03. *T. O.Head Neck* (2006) 28(4):287–96.

8. Kolesnick R, Fuks Z. Radiation and ceramide-induced apoptosis. *Oncogene* (2003) 22(37):5897–906. doi: 10.1038/sj.onc.1206702

9. Mizushima N, Komatsu M. Autophagy: renovation of cells and tissues. *Cell* (2011) 147(4):728–41. doi: 10.1016/j.cell.2011.10.026

10. Dikic I, Elazar Z. Mechanism and medical implications of mammalian autophagy. *Nat Rev Mol Cell Biol* (2018) 19(6):349–64. doi: 10.1038/s41580-018-0003-4

11. Rocchi A, He C. Emerging roles of autophagy in metabolism and metabolic disorders. *Front Biol* (2015) 10(2):154–64. doi: 10.1007/s11515-015-1354-2

12. Su M, Mei Y, Sinha S. Role of the crosstalk between autophagy and apoptosis in cancer. *Journal of oncology. 2013* (2013):e102735. doi: 10.1155/2013/102735

13. Mizushima N, Levine B. Autophagy in mammalian development and differentiation. *Nat Cell Biol* (2010) 12(9):823–30. doi: 10.1038/ncb0910-823

14. Patel NH, Sohal SS, Manjili MH, Harrell JC, Gewirtz DA. The roles of autophagy and senescence in the tumor cell response to radiation. *Radiat Res* (2020) 194(2):103–15. doi: 10.1667/RADE-20-00009

15. Shirato H, Le Q-T, Kobashi K, Prayongrat A, Takao S, Shimizu S, et al. Selection of external beam radiotherapy approaches for precise and accurate cancer treatment. *J Radiat Res* (2018) 59(Suppl 1):i2–i10. doi: 10.1093/jrr/rrx092

16. Tam S, Amit M, Boonsripitayanon M, Cabanillas ME, Busaidy NL, Gunn GB, et al. Adjuvant external beam radiotherapy in locally advanced differentiated thyroid cancer. *JAMA otolaryngology– Head Neck Surg* (2017) 143(12):1244–51. doi: 10.1001/jamaoto.2017.2077

17. Dilalla V, Chaput G, Williams T, Sultanem K. Radiotherapy side effects: integrating a survivorship clinical lens to better serve patients. *Curr Oncol (Toronto Ont.)* (2020) 27(2):107–12. doi: 10.3747/co.27.6233

18. Hall EJ, Giaccia AJ. *Radiobiology for the radiobiologist (8th ed.)*. Philadelphia: PA: Lippincott Williams and Wilkins (2018).

19. Ward JF. DNA Damage produced by ionizing radiation in mammalian cells: identities, mechanisms of formation, and reparability. *Prog Nucleic Acid Res Mol Biol* (1988) 35:95–125. doi: 10.1016/s0079-6603(08)60611-x

20. Mavragani IV, Nikitaki Z, Kalospyros SA, Georgakilas AG. Ionizing radiation and complex DNA damage: From prediction to detection challenges and biological significance. *Cancers* (2019) 11(11):1789. doi: 10.3390/cancers11111789

21. Hendrickson EA. Cell-cycle regulation of mammalian DNA double-Strand-Break repair. *Am J Hum Genet* (1997) 61(4):795–800. doi: 10.1086/514895

22. Huang R-X, Zhou P-K. DNA Damage response signaling pathways and targets for radiotherapy sensitization in cancer. *Signal Transduction Targeted Ther* (2020) 5(1):1–27. doi: 10.1038/s41392-020-0150-x

23. Morgan MA, Lawrence TS. Molecular pathways: Overcoming radiation resistance by targeting DNA damage response pathways. *Clin Cancer research : an Off J Am Assoc Cancer Res* (2015) 21(13):2898–904. doi: 10.1158/1078-0432.CCR-13-3229

24. Iliakis G. The role of DNA double strand breaks in ionizing radiation-induced killing of eukaryotic cells. *BioEssays: News Rev Molecular Cell Dev Biol* (1991) 13(12):641–8. doi: 10.1002/bies.950131204

25. Czornak K, Chughtai S, Chrzanowska KH. Mystery of DNA repair: the role of the MRN complex and ATM kinase in DNA damage repair. *J Appl Genet* (2008) 49(4):383–96. doi: 10.1007/BF03195638

26. Semenza GL. The hypoxic tumor microenvironment: A driving force for breast cancer progression. *Biochim Biophys Acta* (2016) 1863(3):382–91. doi: 10.1016/j.bbamcr.2015.05.036

27. Yang Y, Wu M, Cao D, Yang C, Jin J, Wu L. Deng, l. (2021). ZBP1-MLKL necroptotic signaling potentiates radiation-induced antitumor immunity *via* intratumoral STING pathway activation. *Sci Adv* 7(41):eabf6290. doi: 10.1126/sciadv.abf6290

28. Scriven P, Brown NJ, Pockley AG, Wyld L. The unfolded protein response and cancer: a brighter future unfolding? *J Mol Med (Berlin Germany)* (2007) 85 (4):331–41. doi: 10.1007/s00109-006-0150-5

29. Farrukh MR, Nissar UA, Afnan Q, Rafiq RA, Sharma L, Amin S, et al. Oxidative stress mediated Ca(2+) release manifests endoplasmic reticulum stress leading to unfolded protein response in UV-b irradiated human skin cells. *J Dermatol Sci* (2014) 75(1):24–35. doi: 10.1016/j.jdermsci.2014.03.005

30. Li T, Su L, Zhong N, Hao X, Zhong D, Singhal S, et al. Salinomycin induces cell death with autophagy through activation of endoplasmic reticulum stress in human cancer cells. *Autophagy* (2013) 9(7):1057–68. doi: 10.4161/auto.24632

31. Cui C, Yang J, Li X, Liu D, Fu L, Wang X. Functions and mechanisms of circular RNAs in cancer radiotherapy and chemotherapy resistance. *Mol Cancer* (2020) 19(1):58. doi: 10.1186/s12943-020-01180-y

32. Du Y, Du S, Liu L, Gan F, Jiang X, Wangrao K. Yao, y. (2020). radiation-induced bystander effect can be transmitted through exosomes using miRNAs as effector molecules. *Radiat Res* 194(1):89–100. doi: 10.1667/RADE-20-00019.1

33. Song M, Wang Y, Shang Z-F, Liu X-D, Xie D-F, Wang Q, et al. Bystander autophagy mediated by radiation-induced exosomal miR-7-5p in non-targeted human bronchial epithelial cells. *Sci Rep* (2016) 6:30165. doi: 10.1038/srep30165

34. Heeran AB, Berrigan HP, O'Sullivan J. The radiation-induced bystander effect (RIBE) and its connections with the hallmarks of cancer. *Radiat Res* (2019) 192(6):668–79. doi: 10.1667/RR15489.1

35. Yamazaki T, Kirchmair A, Sato A, Buqué A, Rybstein M, Petroni G. Galluzzi, l. (2020). mitochondrial DNA drives abscopal responses to radiation that are inhibited by autophagy. *Nat Immunol* 21(10):1160–71. doi: 10.1038/s41590-020-0751-0

36. Cai S, Shi G-S, Cheng H-Y, Zeng Y-N, Li G, Zhang M. Chen, Q. (2017). exosomal miR-7 mediates bystander autophagy in lung after focal brain irradiation in mice. *Int J Biol Sci* 13(10):1287–96. doi: 10.7150/ijbs.18890

37. Gao Y, Ma H, Lv C, Lan F, Wang Y, Deng Y. Exosomes and exosomal microRNA in non-targeted radiation bystander and abscopal effects in the central nervous system. *Cancer letters. 499* (2021), 73–84. doi: 10.1016/j.canlet.2020.10.049

38. Rodriguez-Ruiz ME, Garasa S, Rodriguez I, Solorzano JL, Barbes B, Yanguas A, et al. Intercellular adhesion molecule-1 and vascular cell adhesion molecule are induced by ionizing radiation on lymphatic endothelium. *Int J Radiat Oncology Biology Phys* (2017) 97(2):389–400. doi: 10.1016/j.ijrobp.2016.10.043

39. Cives M, Pelle' E, Quaresmini D, Rizzo FM, Tucci M, Silvestris F. The tumor microenvironment in neuroendocrine tumors: Biology and therapeutic implications. *Neuroendocrinology* (2019) 109(2):83–99. doi: 10.1159/000497355

40. Muroyama Y, Nirschl TR, Kochel CM, Lopez-Bujanda Z, Theodros D, Mao W, et al. Stereotactic radiotherapy increases functionally suppressive regulatory T cells in the tumor microenvironment. *Cancer Immunol Res* (2017) 5(11):992–1004. doi: 10.1158/2326-6066.CIR-17-0040

41. Storozynsky Q, Hitt MM. The impact of radiation-induced DNA damage on cGAS-STING-Mediated immune responses to cancer. *Int J Mol Sci* (2020) 21 (22):8877. doi: 10.3390/ijms21228877

42. Harding SM, Benci JL, Irianto J, Discher DE, Minn AJ, Greenberg RA. Mitotic progression following DNA damage enables pattern recognition within micronuclei. *Nature* (2017) 548(7668):466–70. doi: 10.1038/nature23470

43. Arnold CR, Mangesius J, Skvortsova I-I, Ganswindt U. The role of cancer stem cells in radiation resistance. *Frontiers in oncology. 10* (2020) 164:164. doi: 10.3389/fonc.2020.00164

44. Liu Y, Yang M, Luo J, Zhou H. Radiotherapy targeting cancer stem cells "awakens" them to induce tumour relapse and metastasis in oral cancer. *Int J Oral Sci* (2020) 12:19. doi: 10.1038/s41368-020-00087-0

45. Milanovic M, Fan DNY, Belenki D, Däbritz JHM, Zhao Z, Yu Y, et al. Senescence-associated reprogramming promotes cancer stemness. *Nature* (2018) 553(7686):96–100. doi: 10.1038/nature25167

46. Parzych KR, Klionsky DJ. An overview of autophagy: Morphology, mechanism, and regulation. *Antioxidants Redox Signaling* (2014) 20(3):460–73. doi: 10.1089/ars.2013.5371

47. Dice JF. Peptide sequences that target cytosolic proteins for lysosomal proteolysis. *Trends Biochem Sci* (1990) 15(8):305–9. doi: 10.1016/0968-0004(90)90019-8

48. Itakura E, Mizushima N. Characterization of autophagosome formation site by a hierarchical analysis of mammalian atg proteins. *Autophagy* (2010) 6(6):764–76. doi: 10.4161/auto.6.6.12709

49. Chaurasia M, Bhatt AN, Das A, Dwarakanath BS, Sharma K. Radiation-induced autophagy: mechanisms and consequences. *Free Radical Res* (2016) 50 (3):273–90. doi: 10.3109/10715762.2015.1129534

50. Longatti A, Tooze SA. Vesicular trafficking and autophagosome formation. *Cell Death Differentiation* (2009) 16(7):956–65. doi: 10.1038/cdd.2009.39

51. Hosokawa N, Hara T, Kaizuka T, Kishi C, Takamura A, Miura Y, et al. Nutrient-dependent mTORC1 association with the ULK1-Atg13-FIP200 complex required for autophagy. *Mol Biol Cell* (2009) 20(7):1981–91. doi: 10.1091/mbc.e08-12-1248

52. Jung CH, Jun CB, Ro S-H, Kim Y-M, Otto NM, Cao J. Kim, D.-h. (2009). ULK-Atg13-FIP200 complexes mediate mTOR signaling to the autophagy machinery. *Mol Biol Cell* 20(7):1992–2003. doi: 10.1091/mbc.e08-12-1249

53. Pattingre S, Tassa A, Qu X, Garuti R, Liang XH, Mizushima N, et al. Bcl-2 antiapoptotic proteins inhibit beclin 1-dependent autophagy. *Cell* (2005) 122 (6):927–39. doi: 10.1016/j.cell.2005.07.002

54. Liang XH, Kleeman LK, Jiang HH, Gordon G, Goldman JE, Berry G, et al. Protection against fatal sindbis virus encephalitis by beclin, a novel bcl-2-interacting protein. *J Virol* (1998) 72(11):8586–96. doi: 10.1128/JVI.72.11.8586-8596.1998

55. Matsunaga K, Saitoh T, Tabata K, Omori H, Satoh T, Kurotori N, et al. Two beclin 1-binding proteins, Atg14L and Rubicon, reciprocally regulate autophagy at different stages. *Nat Cell Biol* (2009) 11(4):385–96. doi: 10.1038/ncb1846

56. Zhong Y, Wang QJ, Li X, Yan Y, Backer JM, Chait BT, et al. Distinct regulation of autophagic activity by Atg14L and Rubicon associated with beclin 1-phosphatidylinositol-3-kinase complex. *Nat Cell Biol* (2009) 11(4):468–76. doi: 10.1038/ncb1854

57. Fimia GM, Stoykova A, Romagnoli A, Giunta L, Di Bartolomeo S, Nardacci R, et al. Ambra1 regulates autophagy and development of the nervous system. *Nature* (2007) 447(7148):1121–5. doi: 10.1038/nature05925

58. Takahashi Y, Coppola D, Matsushita N, Cualing HD, Sun M, Sato Y, et al. Bif-1 interacts with beclin 1 through UVRAG and regulates autophagy and tumorigenesis. *Nat Cell Biol* (2007) 9(10):1142–51. doi: 10.1038/ncb1634

59. Kuma A, Mizushima N, Ishihara N, Ohsumi Y. Formation of the 350-kDa Apg12-Apg5· Apg16 multimeric complex, mediated by Apg16 oligomerization, is essential for autophagy in yeast. *J Biol Chem* (2002) 277(21):18619–25.

60. Pengo N, Agrotis A, Prak K, Jones J, Ketteler R. A reversible phospho-switch mediated by ULK1 regulates the activity of autophagy protease ATG4B. *Nat Commun* (2017) 8(1):294. doi: 10.1038/s41467-017-00303-2

61. Scherz-Shouval R, Shvets E, Fass E, Shorer H, Gil L, Elazar Z. Reactive oxygen species are essential for autophagy and specifically regulate the activity of Atg4. *EMBO J* (2007) 26(7):1749–60. doi: 10.1038/sj.emboj.7601623

62. Fujita N, Itoh T, Omori H, Fukuda M, Noda T, Yoshimori T. The Atg16L complex specifies the site of LC3 lipidation for membrane biogenesis in autophagy. *Mol Biol Cell* (2008) 19(5):2092–100. doi: 10.1091/mbc.e07-12-1257

63. Hanada T, Noda NN, Satomi Y, Ichimura Y, Fujioka Y, Takao T, et al. The Atg12-Atg5 conjugate has a novel E3-like activity for protein lipidation in autophagy. *J Biol Chem* (2007) 282(52):37298–302. doi: 10.1074/jbc.C700195200

64. Young ARJ, Chan EYW, Hu XW, Köchl R, Crawshaw SG, High S, et al. Starvation and ULK1-dependent cycling of mammalian Atg9 between the TGN and endosomes. *J Cell Sci* (2006) 119(Pt 18):3888–900. doi: 10.1242/jcs.03172

65. Webber JL, Tooze SA. Coordinated regulation of autophagy by p38alpha MAPK through mAtg9 and p38IP. *EMBO J* (2010) 29(1):27–40. doi: 10.1038/emboj.2009.321

66. Sekito T, Kawamata T, Ichikawa R, Suzuki K, Ohsumi Y. Atg17 recruits Atg9 to organize the pre-autophagosomal structure. *Genes to Cells: Devoted to Mol Cell Mech* (2009) 14(5):525–38. doi: 10.1111/j.1365-2443.2009.01299.x

67. Zhang T, Guo L, Yang Y. Mammalian ATG9s drive the autophagosome formation by binding to LC3. *bioRxiv* (2020). doi: 10.1101/2020.05.12.091637

68. Obara K, Ohsumi Y. Atg14: a key player in orchestrating autophagy. *Int J Cell Biol* (2011) 2011:713435. doi: 10.1155/2011/713435

69. Fader CM, Sánchez DG, Mestre MB, Colombo MI. TI-VAMP/VAMP7 and VAMP3/cellubrevin: two v-SNARE proteins involved in specific steps of the autophagy/multivesicular body pathways. *Biochim Et Biophys Acta* (2009) 1793 (12):1901–16. doi: 10.1016/j.bbamcr.2009.09.011

70. Furuta N, Fujita N, Noda T, Yoshimori T, Amano A. Combinational soluble n-ethylmaleimide-sensitive factor attachment protein receptor proteins VAMP8 and Vti1b mediate fusion of antimicrobial and canonical autophagosomes with lysosomes. *Mol Biol Cell* (2010) 21(6):1001–10. doi: 10.1091/mbc.e09-08-0693

71. Monastyrska I, Rieter E, Klionsky DJ, Reggiori F. Multiple roles of the cytoskeleton in autophagy. *Biol Rev Cambridge Philos Soc* (2009) 84(3):431–48. doi: 10.1111/j.1469-185X.2009.00082.x

72. Lemasters JJ. Selective mitochondrial autophagy, or mitophagy, as a targeted defense against oxidative stress, mitochondrial dysfunction, and aging. *Rejuvenation Res* (2005) 8(1):3–5. doi: 10.1089/rej.2005.8.3

73. Sekine S, Youle RJ. PINK1 import regulation; a fine system to convey mitochondrial stress to the cytosol. *BMC Biol* (2018) 16(1):2. doi: 10.1186/s12915-017-0470-7

74. Becker D, Richter J, Tocilescu MA, Przedborski S, Voos W. Pink1 kinase and its membrane potential (Δψ)-dependent cleavage product both localize to outer mitochondrial membrane by unique targeting mode*. *J Biol Chem* (2012) 287 (27):22969–87. doi: 10.1074/jbc.M112.365700

75. Jin SM, Youle RJ. The accumulation of misfolded proteins in the mitochondrial matrix is sensed by PINK1 to induce PARK2/Parkin-mediated mitophagy of polarized mitochondria. *Autophagy* (2013) 9(11):1750–7. doi: 10.4161/auto.26122

76. Ordureau A, Sarraf SA, Duda DM, Heo J-M, Jedrychowski MP, Sviderskiy VO, et al. Quantitative proteomics reveal a feedforward mechanism for mitochondrial PARKIN translocation and ubiquitin chain synthesis. *Mol Cell* (2014) 56(3):360–75. doi: 10.1016/j.molcel.2014.09.007

77. Wauer T, Swatek KN, Wagstaff JL, Gladkova C, Pruneda JN, Michel MA. Komander, d. (2015). ubiquitin Ser65 phosphorylation affects ubiquitin structure, chain assembly and hydrolysis. *EMBO J* 34(3):307–25. doi: 10.15252/embj.201489847

78. Lazarou M, Sliter DA, Kane LA, Sarraf SA, Wang C, Burman JL, et al. The ubiquitin kinase PINK1 recruits autophagy receptors to induce mitophagy. *Nature* (2015) 524(7565):309–14. doi: 10.1038/nature14893

79. Richter B, Sliter DA, Herhaus L, Stolz A, Wang C, Beli P, et al. Phosphorylation of OPTN by TBK1 enhances its binding to ub chains and promotes selective autophagy of damaged mitochondria. *Proc Natl Acad Sci* (2016) 113(15):4039–44. doi: 10.1073/pnas.1523926113

80. Zuo Z, Jing K, Wu H, Wang S, Ye L, Li Z, et al. Mechanisms and functions of mitophagy and potential roles in renal disease. *Front Physiol* (2020) 11:935. doi: 10.3389/fphys.2020.00935

81. Bhujabal Z, Birgisdottir Å.B, Sjøttem E, Brenne HB, Øvervatn A, Habisov S, et al. FKBP8 recruits LC3A to mediate parkin-independent mitophagy. *EMBO Rep* (2017) 18(6):947–61. doi: 10.15252/embr.201643147

82. Yan C, Gong L, Chen L, Xu M, Abou-Hamdan H, Tang M, et al. PHB2 (prohibitin 2) promotes PINK1-PRKN/Parkin-dependent mitophagy by the PARL-PGAM5-PINK1 axis. *Autophagy* (2020) 16(3):419–34. doi: 10.1080/15548627.2019.1628520

83. Kagan VE, Jiang J, Huang Z, Tyurina YY, Desbourdes C, Cottet-Rousselle C, et al. NDPK-d (NM23-H4)-mediated externalization of cardiolipin enables elimination of depolarized mitochondria by mitophagy. *Cell Death Differentiation* (2016) 23(7):1140–51. doi: 10.1038/cdd.2015.160

84. Kagan VE, Tyurin VA, Jiang J, Tyurina YY, Ritov VB, Amoscato AA, et al. Cytochrome c acts as a cardiolipin oxygenase required for release of proapoptotic factors. *Nat Chem Biol* (2005) 1(4):223–32. doi: 10.1038/nchembio727

85. McWilliams TG, Prescott AR, Montava-Garriga L, Ball G, Singh F, Barini E, et al. Basal mitophagy occurs independently of PINK1 in mouse tissues of high metabolic demand. *Cell Metab* (2018). doi: 10.1016/j.cmet.2017.12.008

86. Chen G, Han Z, Feng D, Chen Y, Chen L, Wu H, et al. A regulatory signaling loop comprising the PGAM5 phosphatase and CK2 controls receptor-mediated mitophagy. *Mol Cell* (2014) 54(3):362–77. doi: 10.1016/j.molcel.2014.02.034

87. Wu W, Lin C, Wu K, Jiang L, Wang X, Li W, et al. FUNDC1 regulates mitochondrial dynamics at the ER-mitochondrial contact site under hypoxic conditions. *EMBO J* (2016) 35(13):1368–84. doi: 10.15252/embj.201593102

88. Kuang Y, Ma K, Zhou C, Ding P, Zhu Y, Chen Q, et al. Structural basis for the phosphorylation of FUNDC1 LIR as a molecular switch of mitophagy. *Autophagy* (2016) 12(12):2363–73. doi: 10.1080/15548627.2016.1238552

89. Li Y, Zheng W, Lu Y, Zheng Y, Pan L, Wu X, et al. BNIP3L/NIX-mediated mitophagy: molecular mechanisms and implications for human disease. *Cell Death Dis* (2021) 13(1):1–11. doi: 10.1038/s41419-021-04469-y

90. Lee HJ, Jung YH, Choi GE, Ko SH, Lee S-J, Lee SH, et al. BNIP3 induction by hypoxia stimulates FASN-dependent free fatty acid production enhancing therapeutic potential of umbilical cord blood-derived human mesenchymal stem cells. *Redox Biol* (2017) 13:426–43. doi: 10.1016/j.redox.2017.07.004

91. Zhu L, Yuan Y, Yuan L, Li L, Liu F, Liu J, et al. Activation of TFEB-mediated autophagy by trehalose attenuates mitochondrial dysfunction in cisplatin-induced acute kidney injury. *Theranostics* (2020) 10(13):5829–44. doi: 10.7150/thno.44051

92. Rogov VV, Suzuki H, Marinković M, Lang V, Kato R, Kawasaki M, et al. Phosphorylation of the mitochondrial autophagy receptor nix enhances its interaction with LC3 proteins. *Sci Rep* (20171131) 7(1). doi: 10.1038/s41598-017-01258-6

93. Zhang T, Xue L, Li L, Tang C, Wan Z, Wang R, et al. BNIP3 protein suppresses PINK1 kinase proteolytic cleavage to promote mitophagy. *J Biol Chem* (2016) 291(41):21616–29. doi: 10.1074/jbc.M116.733410

94. Ding W-X, Ni H-M, Li M, Liao Y, Chen X, Stolz DB, et al. Nix is critical to two distinct phases of mitophagy, reactive oxygen species-mediated autophagy induction and parkin-ubiquitin-p62-mediated mitochondrial priming. *J Biol Chem* (2010) 285(36):27879–90. doi: 10.1074/jbc.M110.119537

95. Lee Y, Lee H-Y, Hanna RA, Gustafsson Å.B. Mitochondrial autophagy by Bnip3 involves Drp1-mediated mitochondrial fission and recruitment of parkin in cardiac myocytes. *Am J Physiol Heart Circulatory Physiol* (2011) 301(5):H1924–1931. doi: 10.1152/ajpheart.00368.2011

96. Lu K, Psakhye I, Jentsch S. Autophagic clearance of PolyQ proteins mediated by ubiquitin-Atg8 adaptors of the conserved CUET protein family. *Cell* (2014) 158(3):549–63. doi: 10.1016/j.cell.2014.05.048

97. Mancias JD, Wang X, Gygi SP, Harper JW, Kimmelman AC. Quantitative proteomics identifies NCOA4 as the cargo receptor mediating ferritinophagy. *Nature* (2014) 509(7498):105–9. doi: 10.1038/nature13148

98. Zhao H, Tang M, Liu M, Chen L. Glycophagy: An emerging target in pathology. *Clinica chimica acta. 484* (2018), 298–303. doi: 10.1016/j.cca.2018.06.014

99. Shin DW. Lipophagy: Molecular mechanisms and implications in metabolic disorders. *Molecules Cells* (2020) 43(8):686–93. doi: 10.14348/molcells.2020.0046

100. Yun CW, Lee SH. The roles of autophagy in cancer. *Int J Mol Sci* (2018) 19 (11):3466. doi: 10.3390/ijms19113466

101. Singh SS, Vats S, Chia AY-Q, Tan TZ, Deng S, Ong MS, et al. Dual role of autophagy in hallmarks of cancer. *Oncogene* (2018) 37(9):1142–58. doi: 10.1038/s41388-017-0046-6

102. Galati S, Boni C, Gerra MC, Lazzaretti M, Buschini A. Autophagy: A player in response to oxidative stress and DNA damage. *Oxid Med Cell Longevity* (2019). doi: 10.1155/2019/5692958

103. Phan LM, Rezaeian A-H. ATM: Main features, signaling pathways, and its diverse roles in DNA damage response, tumor suppression, and cancer development. *Genes* (2021) 12(6):845. doi: 10.3390/genes12060845

104. Song L, Lin C, Wu Z, Gong H, Zeng Y, Wu J, et al. miR-18a impairs DNA damage response through downregulation of ataxia telangiectasia mutated (ATM) kinase. *PloS One* (2011) 6(9):e25454. doi: 10.1371/journal.pone.0025454

105. Le Guezennec X, Bulavin DV. WIP1 phosphatase at the crossroads of cancer and aging. *Trends Biochem Sci* (2010) 35(2):109–14. doi: 10.1016/j.tibs.2009.09.005

106. Duan X, Ponomareva L, Veeranki S, Choubey D. IFI16 induction by glucose restriction in human fibroblasts contributes to autophagy through activation of the ATM/AMPK/p53 pathway. *PloS One* (2011) 6(5):e19532. doi: 10.1371/journal.pone.0019532

107. Antonelli M, Strappazzon F, Arisi I, Brandi R, D'Onofrio M, Sambucci M, et al. ATM Kinase sustains breast cancer stem-like cells by promoting ATG4C expression and autophagy. *Oncotarget* (2017) 8(13):21692–709. doi: 10.18632/oncotarget.15537

108. Cremona CA, Behrens A. ATM Signalling and cancer. *Oncogene* (2014) 33 (26):3351–60. doi: 10.1038/onc.2013.275

109. Palmieri D, Valentino T, D'Angelo D, De Martino I, Postiglione I, Pacelli R, et al. HMGA proteins promote ATM expression and enhance cancer cell resistance to genotoxic agents. *Oncogene* (2011) 30(27):3024–35. doi: 10.1038/onc.2011.21

110. Ma S, Fu X, Liu L, Liu Y, Feng H, Jiang H, et al. Iron-dependent autophagic cell death induced by radiation in MDA-MB-231 breast cancer cells. *Front Cell Dev Biol* (2021) 9:723801:723801. doi: 10.3389/fcell.2021.723801

111. Mukha A, Kahya U, Linge A, Chen O, Löck S, Lukiyanchuk V, et al. GLS-driven glutamine catabolism contributes to prostate cancer radiosensitivity by regulating the redox state, stemness and ATG5-mediated autophagy. *Theranostics* (2021) 11(16):7844–68. doi: 10.7150/thno.58655

112. Wu C, Yang L, Qi X, Wang T, Li M, Xu K. Inhibition of long non-coding RNA HOTAIR enhances radiosensitivity *via* regulating autophagy in pancreatic cancer. *Cancer Manage Res* (2018) 10:5261–71. doi: 10.2147/CMAR.S174066

113. Lei G, Zhang Y, Koppula P, Liu X, Zhang J, Lin SH, et al. The role of ferroptosis in ionizing radiation-induced cell death and tumor suppression. *Cell Res* (2020) 30(2):146–62. doi: 10.1038/s41422-019-0263-3

114. Chen X, Kang R, Kroemer G, Tang D. Broadening horizons: the role of ferroptosis in cancer. *Nat Rev Clin Oncol* (2021) 18(5):280–96. doi: 10.1038/s41571-020-00462-0

115. Wang Y, Liu F, Fang C, Xu L, Chen L, Xu Z, et al. Combination of rapamycin and SAHA enhanced radiosensitization by inducing autophagy and acetylation in NSCLC. *Aging* (2021) 13(14):18223–37. doi: 10.18632/aging.203226

116. Ma X, Mao G, Chang R, Wang F, Zhang X, Kong Z. Down-regulation of autophagy-associated protein increased acquired radio-resistance bladder cancer cells sensitivity to taxol. *Int J Radiat Biol* (2021) 97(4):507–16. doi: 10.1080/09553002.2021.1872812

117. Mo N, Lu Y-K, Xie W-M, Liu Y, Zhou W-X, Wang H-X, et al. Inhibition of autophagy enhances the radiosensitivity of nasopharyngeal carcinoma by reducing Rad51 expression. *Oncol Rep* (2014) 32(5):1905–12. doi: 10.3892/or.2014.3427

118. Prise KM, O'Sullivan JM. Radiation-induced bystander signalling in cancer therapy. *Nat Rev Cancer* (2009) 9(5):351–60. doi: 10.1038/nrc2603

119. Zhou S, Wang X, Ding J, Yang H, Xie Y. Increased ATG5 expression predicts poor prognosis and promotes EMT in cervical carcinoma. *Frontiers in cell and developmental biology. 9* (2021) 757184:757184. doi: 10.3389/fcell.2021.757184

120. Pustovalova M, Alhaddad L, Blokhina T, Smetanina N, Chigasova A, Chuprov-Netochin R, et al. The CD44high subpopulation of multifraction irradiation-surviving NSCLC cells exhibits partial EMT-program activation and DNA damage response depending on their p53 status. *Int J Mol Sci* (20212369) 22 (5). doi: 10.3390/ijms22052369

121. Yazal T, Bailleul J, Ruan Y, Sung D, Chu F-I, Palomera D. Vlashi, e. (2022). radiosensitizing pancreatic cancer *via* effective autophagy inhibition. *Mol Cancer Ther* 21(1):79–88. doi: 10.1158/1535-7163.MCT-20-1103

122. Sai S, Kim EH, Koom WS, Vares G, Suzuki M, Yamada S, et al. Carbon-ion beam irradiation and the miR-200c mimic effectively eradicate pancreatic cancer stem cells under *in vitro* and *in vivo* conditions. *OncoTargets and therapy*. (2021) 14:4749–60. doi: 10.2147/OTT.S311567

123. Kong EY, Cheng SH, Yu KN. Induction of autophagy and interleukin 6 secretion in bystander cells: metabolic cooperation for radiation-induced rescue effect? *J Radiat Res* (2018) 59(2):129–40. doi: 10.1093/jrr/rrx101

124. Kyrkanides S, Moore AH, Olschowka JA, Daeschner JC, Williams JP, Hansen JT, et al. Cyclooxygenase-2 modulates brain inflammation-related gene expression in central nervous system radiation injury. *Brain Res Mol Brain Res* (2002) 104(2):159–69. doi: 10.1016/s0169-328x(02)00353-4

125. Huang Y-H, Yang P-M, Chuah Q-Y, Lee Y-J, Hsieh Y-F, Peng C-W, et al. Autophagy promotes radiation-induced senescence but inhibits bystander effects in human breast cancer cells. *Autophagy* (2014) 10(7):1212–28. doi: 10.4161/auto.28772

126. Wang X, Zhang J, Fu J, Wang J, Ye S, Liu W, et al. Role of ROS-mediated autophagy in radiation-induced bystander effect of hepatoma cells. *Int J Radiat Biol* (2015) 91(5):452–8. doi: 10.3109/09553002.2015.1012308

127. Hou W, Song L, Zhao Y, Liu Q, Zhang S. Inhibition of beclin-1-Mediated autophagy by MicroRNA-17-5p enhanced the radiosensitivity of glioma cells. *Oncol Res* (2017) 25(1):43–53. doi: 10.3727/096504016X14719078133285

128. Chang JH, Hwang YH, Lee DJ, Kim DH, Park JM, Wu H-G, et al. MicroRNA-203 modulates the radiation sensitivity of human malignant glioma cells. *Int J Radiat Oncology Biology Phys* (2016) 94(2):412–20. doi: 10.1016/j.ijrobp.2015.10.001

129. Song M, Wang Y, Shang Z-F, Liu X-D, Xie D-F, Wang Q. Zhou, p.-k. (2016). bystander autophagy mediated by radiation-induced exosomal miR-7-5p in non-targeted human bronchial epithelial cells. *Sci Rep* 6(1):30165. doi: 10.1038/srep30165

130. Poole LP, Macleod KF. Mitophagy in tumorigenesis and metastasis. *Cell Mol Life sciences: CMLS* (2021) 78(8):3817–51. doi: 10.1007/s00018-021-03774-1

131. Russo M, Russo GL. Autophagy inducers in cancer. *Biochemical pharmacology. 153* (2018), 51–61. doi: 10.1016/j.bcp.2018.02.007

132. Kocaturk NM, Akkoc Y, Kig C, Bayraktar O, Gozuacik D, Kutlu O. Autophagy as a molecular target for cancer treatment. *European journal of pharmaceutical sciences: Official journal of the European federation for pharmaceutical sciences. 134* (2019), 116–37. doi: 10.1016/j.ejps.2019.04.011

133. Pang X-L, He G, Liu Y-B, Wang Y, Zhang B. Endoplasmic reticulum stress sensitizes human esophageal cancer cell to radiation. *World J Gastroenterol* (2013) 19(11):1736–48. doi: 10.3748/wjg.v19.i11.1736

134. Weppler SA, Krause M, Zyromska A, Lambin P, Baumann M, Wouters BG. Response of U87 glioma xenografts treated with concurrent rapamycin and fractionated radiotherapy: possible role for thrombosis. *Radiotherapy Oncology: J Eur Soc Ther Radiol Oncol* (2007) 82(1):96–104. doi: 10.1016/j.radonc.2006.11.004

135. Anandharaj A, Cinghu S, Park W-Y. Rapamycin-mediated mTOR inhibition attenuates survivin and sensitizes glioblastoma cells to radiation therapy. *Acta Biochim Et Biophys Sin* (2011) 43(4):292–300. doi: 10.1093/abbs/gmr012

136. Chen H, Ma Z, Vanderwaal RP, Feng Z, Gonzalez-Suarez I, Wang S, et al. The mTOR inhibitor rapamycin suppresses DNA double-strand break repair. *Radiat Res* (2011) 175(2):214–24. doi: 10.1667/rr2323.1

137. Anbalagan S, Pires IM, Blick C, Hill MA, Ferguson DJP, Chan DA, et al. Radiosensitization of renal cell carcinoma *in vitro* through the induction of autophagy. *Radiotherapy Oncology: J Eur Soc Ther Radiol Oncol* (2012) 103 (3):388–93. doi: 10.1016/j.radonc.2012.04.001

138. Cao C, Subhawong T, Albert JM, Kim KW, Geng L, Sekhar KR, et al. Inhibition of mammalian target of rapamycin or apoptotic pathway induces

autophagy and radiosensitizes PTEN null prostate cancer cells. *Cancer Res* (2006) 66(20):10040–7. doi: 10.1158/0008-5472.CAN-06-0802

139. Kim EJ, Jeong J-H, Bae S, Kang S, Kim CH, Lim Y-B. mTOR inhibitors radiosensitize PTEN-deficient non-small-cell lung cancer cells harboring an EGFR activating mutation by inducing autophagy. *J Cell Biochem* (2013) 114(6):1248–56. doi: 10.1002/jcb.24465

140. Chang L, Graham PH, Hao J, Ni J, Bucci J, Cozzi PJ, et al. Acquisition of epithelial-mesenchymal transition and cancer stem cell phenotypes is associated with activation of the PI3K/Akt/mTOR pathway in prostate cancer radioresistance. *Cell Death Dis* (2013) 4:e875. doi: 10.1038/cddis.2013.407

141. Wang W, Long L, Yang N, Zhang Q, Ji W, Zhao J, et al. NVP-BEZ235, a novel dual PI3K/mTOR inhibitor, enhances the radiosensitivity of human glioma stem cells *in vitro*. *Acta Pharmacologica Sin* (2013) 34(5):681–90. doi: 10.1038/aps.2013.22

142. Yu Z, Xie G, Zhou G, Cheng Y, Zhang G, Yao G, et al. NVP-BEZ235, a novel dual PI3K-mTOR inhibitor displays anti-glioma activity and reduces chemoresistance to temozolomide in human glioma cells. *Cancer Lett* (2015) 367 (1):58–68. doi: 10.1016/j.canlet.2015.07.007

143. Kuger S, Flentje M, Djuzenova CS. Simultaneous perturbation of the MAPK and the PI3K/mTOR pathways does not lead to increased radiosensitization. *Radiation oncology (London, england). 10* (2015) 214. doi: 10.1186/s13014-015-0514-5

144. Cerniglia GJ, Karar J, Tyagi S, Christofidou-Solomidou M, Rengan R, Koumenis C, et al. Inhibition of autophagy as a strategy to augment radiosensitization by the dual phosphatidylinositol 3-kinase/mammalian target of rapamycin inhibitor NVP-BEZ235. *Mol Pharmacol* (2012) 82(6):1230–40. doi: 10.1124/mol.112.080408

145. Wei D, Li H, Yu J, Sebolt JT, Zhao L, Lawrence TS, et al. Radiosensitization of human pancreatic cancer cells by MLN4924, an investigational NEDD8-activating enzyme inhibitor. *Cancer Res* (2012) 72(1):282–93. doi: 10.1158/0008-5472.CAN-11-2866

146. Wan J, Zhu J, Li G, Zhang Z. Radiosensitization of human colorectal cancer cells by MLN4924: An inhibitor of NEDD8-activating enzyme. *Technol Cancer Res Treat* (2016) 15(4):527–34. doi: 10.1177/1533034615588197

147. Zhou L, Zhang W, Sun Y, Jia L. Protein neddylation and its alterations in human cancers for targeted therapy. *Cell Signalling* (2018) 44:92–102. doi: 10.1016/j.cellsig.2018.01.009

148. Zhou L, Jiang Y, Luo Q, Li L, Jia L. Neddylation: a novel modulator of the tumor microenvironment. *Mol Cancer* (2019) 18(1):77. doi: 10.1186/s12943-019-0979-1

149. Chen P, Hu T, Liang Y, Jiang Y, Pan Y, Li C, et al. Synergistic inhibition of autophagy and neddylation pathways as a novel therapeutic approach for targeting liver cancer. *Oncotarget* (2015) 6(11):9002–17. doi: 10.18632/oncotarget.3282

150. Sarantopoulos J, Shapiro GI, Cohen RB, Clark JW, Kauh JS, Weiss GJ, et al. Phase I study of the investigational NEDD8-activating enzyme inhibitor pevonedistat (TAK-924/MLN4924) in patients with advanced solid tumors. *Clin Cancer Research: Off J Am Assoc Cancer Res* (2016) 22(4):847–57. doi: 10.1158/1078-0432.CCR-15-1338

151. Kim KW, Speirs CK, Jung DK, Lu B. The zinc ionophore PCI-5002 radiosensitizes non-small cell lung cancer cells by enhancing autophagic cell death. *J Thorac Oncology: Off Publ Int Assoc Study Lung Cancer* (2011) 6 (9):1542–52. doi: 10.1097/JTO.0b013e3182208fac

152. Kim KW, Hwang M, Moretti L, Jaboin JJ, Cha YI, Lu B. Autophagy upregulation by inhibitors of caspase-3 and mTOR enhances radiotherapy in a mouse model of lung cancer. *Autophagy* (2008) 4(5):659–68. doi: 10.4161/auto.6058

153. Kim KW, Moretti L, Mitchell LR, Jung DK, Lu B. Combined bcl-2/mammalian target of rapamycin inhibition leads to enhanced radiosensitization *via* induction of apoptosis and autophagy in non-small cell lung tumor xenograft model. *Clin Cancer Research: Off J Am Assoc Cancer Res* (2009) 15(19):6096–105. doi: 10.1158/1078-0432.CCR-09-0589

154. Lu B, Li Y, Li H, Zhang Y, Xu J, Ren L, et al. Bax inhibitor-1 is overexpressed in non-small cell lung cancer and promotes its progression and metastasis. *Int J Clin Exp Pathol* (2015) 8(2):1411–8.

155. Gardner EE, Connis N, Poirier JT, Cope L, Dobromilskaya I, Gallia GL, et al. Rapamycin rescues ABT-737 efficacy in small cell lung cancer. *Cancer Res* (2014) 74(10):2846–56. doi: 10.1158/0008-5472.CAN-13-3460

156. Xu Q, Zhang H, Liu H, Han Y, Qiu W, Li Z. Inhibiting autophagy flux and DNA repair of tumor cells to boost radiotherapy of orthotopic glioblastoma. *Biomaterials* (2022) 280:121287. doi: 10.1016/j.biomaterials.2021.121287

157. Chaurasia M, Gupta S, Das A, Dwarakanath BS, Simonsen A, Sharma K. Radiation induces EIF2AK3/PERK and ERN1/IRE1 mediated pro-survival autophagy. *Autophagy* (2019) 15(8):1391–406. doi: 10.1080/15548627.2019.1582973

158. Schonewolf CA, Mehta M, Schiff D, Wu H, Haffty BG, Karantza V, et al. Autophagy inhibition by chloroquine sensitizes HT-29 colorectal cancer cells to concurrent chemoradiation. *World J Gastrointestinal Oncol* (2014) 6(3):74–82. doi: 10.4251/wjgo.v6.i3.74

159. Shiratori H, Kawai K, Hata K, Tanaka T, Nishikawa T, Otani K, et al. The combination of temsirolimus and chloroquine increases radiosensitivity in colorectal cancer cells. *Oncol Rep* (2019) 42(1):377–85. doi: 10.3892/or.2019.7134

160. Avniel-Polak S, Leibowitz G, Riahi Y, Glaser B, Gross DJ, Grozinsky-Glasberg S. Abrogation of autophagy by chloroquine alone or in combination with mTOR inhibitors induces apoptosis in neuroendocrine tumor cells. *Neuroendocrinology* (2016) 103(6):724–37. doi: 10.1159/000442589

161. Wang F, Tang J, Li P, Si S, Yu H, Yang X, et al. Chloroquine enhances the radiosensitivity of bladder cancer cells by inhibiting autophagy and activating apoptosis. *Cell Physiol Biochemistry: Int J Exp Cell Physiology Biochemistry Pharmacol* (2018) 45(1):54–66. doi: 10.1159/000486222

162. Ye H, Chen M, Cao F, Huang H, Zhan R, Zheng X. Chloroquine, an autophagy inhibitor, potentiates the radiosensitivity of glioma initiating cells by inhibiting autophagy and activating apoptosis. *BMC Neurol* (2016) 16(1):178. doi: 10.1186/s12883-016-0700-6

163. Li Y, Cho MH, Lee SS, Lee D-E, Cheong H, Choi Y. Hydroxychloroquine-loaded hollow mesoporous silica nanoparticles for enhanced autophagy inhibition and radiation therapy. *J Controlled Release: Off J Controlled Release Soc* (2020) 325:100–10. doi: 10.1016/j.jconrel.2020.06.025

164. Chen Y, Li X, Guo L, Wu X, He C, Zhang S, et al. Combining radiation with autophagy inhibition enhances suppression of tumor growth and angiogenesis in esophageal cancer. *Mol Med Rep* (2015) 12(2):1645–52. doi: 10.3892/mmr.2015.3623

165. Chen YS, Song HX, Lu Y, Li X, Chen T, Zhang Y, et al. Autophagy inhibition contributes to radiation sensitization of esophageal squamous carcinoma cells. *Dis Esophagus: Off J Int Soc Dis Esophagus* (2011) 24(6):437–43. doi: 10.1111/j.1442-2050.2010.01156.x

166. Mohsen S, Sobash PT, Algwaiz GF, Nasef N, Al-Zeidaneen SA, Karim NA. Autophagy agents in clinical trials for cancer therapy: A brief review. *Curr Oncol* (2022) 29(3):1695–708. doi: 10.3390/curroncol29030141

167. Wan X-B, Fan X-J, Chen M-Y, Xiang J, Huang P-Y, Guo L, et al. Elevated beclin 1 expression is correlated with HIF-1α in predicting poor prognosis of nasopharyngeal carcinoma. *Autophagy* (2010) 6(3):395–404. doi: 10.4161/auto.6.3.11303

168. Huang M-L, Qi C-L, Zou Y, Yang R, Jiang Y, Sheng J-F, et al. Plac8-mediated autophagy regulates nasopharyngeal carcinoma cell function *via* AKT/mTOR pathway. *J Cell Mol Med* (2020) 24(14):7778–88. doi: 10.1111/jcmm.15409

169. Huang R-X, Zhou P-K. And targets for radiotherapy sensitization in cancer. *Signal Transduction Targeted Ther* (2020) 5(1):1–27. doi: 10.1038/s41392-020-0150-x

170. Koukourakis MI, Kalamida D, Giatromanolaki A, Zois CE, Sivridis E, Pouliliou S, et al. Autophagosome proteins LC3A, LC3B and LC3C have distinct subcellular distribution kinetics and expression in cancer cell lines. *PloS One* (2015) 10(9):e0137675. doi: 10.1371/journal.pone.0137675

171. Ozpolat B, Benbrook DM. Targeting autophagy in cancer management – strategies and developments. *Cancer Manage Res* (2015) 7:291–9. doi: 10.2147/CMAR.S34859

172. Kondapuram SK, Sarvagalla S, Coumar MS. Targeting autophagy with small molecules for cancer therapy. *J Cancer Metastasis Treat* (2019) 5:32. doi: 10.20517/2394-4722.2018.105

173. Bilger A, Bittner M-I, Grosu A-L, Wiedenmann N, Meyer PT, Firat E, et al. FET-PET-based reirradiation and chloroquine in patients with recurrent glioblastoma. *Strahlentherapie und Onkologie* (2014) 190(10):957–61. doi: 10.1007/s00066-014-0693-2

174. Sotelo J, Briceño E, López-González MA. Adding chloroquine to conventional treatment for glioblastoma multiforme: a randomized, double-blind, placebo-controlled trial. *Ann Internal Med* (2006) 144(5):337–43. doi: 10.7326/0003-4819-144-5-200603070-00008

175. Rojas-Puentes LL, Gonzalez-Pinedo M, Crismatt A, Ortega-Gomez A, Gamboa-Vignolle C, Nuñez-Gomez R, et al. Phase II randomized, double-blind, placebo-controlled study of whole-brain irradiation with concomitant chloroquine for brain metastases. *Radiat Oncol* (2013) 8:209. doi: 10.1186/1748-717X-8-209

176. Varisli L, Cen O, Vlahopoulos S. Dissecting pharmacological effects of chloroquine in cancer treatment: interference with inflammatory signaling pathways. *Immunology* (2020) 159(3):257–78. doi: 10.1111/imm.13160

177. Manic G, Obrist F, Kroemer G, Vitale I, Galluzzi L. Chloroquine and hydroxychloroquine for cancer therapy. *Mol Cell Oncol* (2014) 1(1):e29911. doi: 10.4161/mco.29911

178. Rosenfeld MR, Ye X, Supko JG, Desideri S, Grossman SA, Brem S, et al. A phase I/II trial of hydroxychloroquine in conjunction with radiation therapy and concurrent and adjuvant temozolomide in patients with newly diagnosed glioblastoma multiforme. *Autophagy* (2014) 10(8):1359–68. doi: 10.4161/auto.28984

179. Shi T-T, Yu X-X, Yan L-J, Xiao H-T. Research progress of hydroxychloroquine and autophagy inhibitors on cancer. *Cancer Chemotherapy Pharmacol* (2017) 79(2):287–94. doi: 10.1007/s00280-016-3197-1

180. Hong TS, Lennerz JK, Wo JY, Ulysse C, Yeap BY, Clark JW, et al. Long term follow-up of a phase II study of autophagy inhibition with hydroxychloroquine (HCQ) and preoperative (Preop) short course chemoradiation (SCRT) followed by early surgery for resectable ductal adenocarcinoma of the head of pancreas (PDAC). *Int J Radiat Oncology Biology Phys* (2020) 108(3):S151. doi: 10.1016/j.ijrobp.2020.07.903

181. Galanis E, Buckner JC, Maurer MJ, Kreisberg JI, Ballman K, Boni J, et al. Phase II trial of temsirolimus (CCI-779) in recurrent glioblastoma multiforme: A north central cancer treatment group study. *J Clin Oncol* (2005) 23(23):5294–304. doi: 10.1200/JCO.2005.23.622

182. Ma DJ, Galanis E, Anderson SK, Schiff D, Kaufmann TJ, Peller PJ, et al. A phase II trial of everolimus, temozolomide, and radiotherapy in patients with newly diagnosed glioblastoma: NCCTG N057K. *Neuro-Oncology* (2015) 17(9):1261–9. doi: 10.1093/neuonc/nou328

183. Brunner TB, Geiger M, Grabenbauer GG, Lang-Welzenbach M, Mantoni TS, Cavallaro A, et al. Phase I trial of the human immunodeficiency virus protease inhibitor nelfinavir and chemoradiation for locally advanced pancreatic cancer. *J Clin Oncology: Off J Am Soc Clin Oncol* (2008) 26(16):2699–706. doi: 10.1200/JCO.2007.15.2355

184. Lin C, Verma V, Ly QP, Lazenby A, Sasson A, Schwarz JK, et al. Phase I trial of concurrent stereotactic body radiotherapy and nelfinavir for locally advanced borderline or unresectable pancreatic adenocarcinoma. *Radiotherapy Oncology: J Eur Soc Ther Radiol Oncol* (2019) 132:55–62. doi: 10.1016/j.radonc.2018.11.002

185. Rengan R, Mick R, Pryma DA, Lin LL, Christodouleas J, Plastaras JP, et al. Clinical outcomes of the HIV protease inhibitor nelfinavir with concurrent chemoradiotherapy for unresectable stage IIIA/IIIB non-small cell lung cancer: A phase 1/2 trial. *JAMA Oncol* (2019) 5(10):1464–72. doi: 10.1001/jamaoncol.2019.2095

186. Rengan R, Mick R, Pryma D, Rosen MA, Lin LL, Maity AM, et al. A phase I trial of the HIV protease inhibitor nelfinavir with concurrent chemoradiotherapy for unresectable stage IIIA/IIIB non-small cell lung cancer: a report of toxicities and clinical response. *J Thorac Oncology: Off Publ Int Assoc Study Lung Cancer* (2012) 7(4):709–15. doi: 10.1097/JTO.0b013e3182435aa6

187. Chang L, Graham PH, Hao J, Ni J, Bucci J, Cozzi PJ, et al. PI3K/Akt/mTOR pathway inhibitors enhance radiosensitivity in radioresistant prostate cancer cells through inducing apoptosis, reducing autophagy, suppressing NHEJ and HR repair pathways. *Cell Death Dis* (2014) 5:e1437. doi: 10.1038/cddis.2014.415

188. Ferguson JL, DeSanto LW. Total pharyngolaryngectomy and cervical esophagectomy with jejunal autotransplant reconstruction: complications and results. *Laryngoscope* (1988) 98(9):911–4. doi: 10.1288/00005537-198809000-00001

189. Huang T, Kim CK, Alvarez AA, Pangeni RP, Wan X, Song X, et al. MST4 phosphorylation of ATG4B regulates autophagic activity, tumorigenicity, and radioresistance in glioblastoma. *Cancer Cell* (2017) 32(6):840–855.e8. doi: 10.1016/j.ccell.2017.11.005

frontiers | Frontiers in Oncology

TYPE Original Research
PUBLISHED 15 September 2022
DOI 10.3389/fonc.2022.873447

OPEN ACCESS

EDITED BY
Maria Felice Brizzi,
University of Turin, Italy

REVIEWED BY
Maria Salazar-Roa,
Faculty of Chemistry, Complutense University of Madrid, Spain
Ying Han,
Peking University Hospital of Stomatology, China

*CORRESPONDENCE
Abdelhabib Semlali
abdelhabib.semlali@greb.ulaval.ca

SPECIALTY SECTION
This article was submitted to Cancer Molecular Targets and Therapeutics, a section of the journal Frontiers in Oncology

RECEIVED 10 February 2022
ACCEPTED 06 July 2022
PUBLISHED 15 September 2022

CITATION
Semlali A, Papadakos S, Contant C, Zouaoui I and Rouabhia M (2022) Rapamycin inhibits oral cancer cell growth by promoting oxidative stress and suppressing ERK1/2, NF-κB and beta-catenin pathways. *Front. Oncol.* 12:873447. doi: 10.3389/fonc.2022.873447

Rapamycin inhibits oral cancer cell growth by promoting oxidative stress and suppressing ERK1/2, NF-κB and beta-catenin pathways

Abdelhabib Semlali*, Sofia Papadakos, Camille Contant, Ikram Zouaoui and Mahmoud Rouabhia

Groupe de recherche en écologie buccale, Faculté de médecine dentaire, Université Laval, Québec, QC, Canada

Treatment of oral cancer is based exclusively on surgery combined with or without chemotherapy. However, it has several side effects. Targeting a new, more effective therapy has become an urgent matter. The purpose of this study was to evaluate the anti-tumor activity of rapamycin in oral cancer and its mechanism of action. Human gingival carcinoma cells were stimulated with different concentrations of rapamycin to assess proliferation, colony formation, cell migration, as well as apoptosis, and autophagy. The expression of proteins involved in the cell cycle (cyclin D1, p15, p21, p27) and autophagy, as well as that of oncogenes and tumor suppressor genes, were determined by quantitative PCR. The signaling pathways were evaluated by Western blotting. Our results show that rapamycin has a selective effect at a low dose on cancer cell growth/survival. This was confirmed by low colony formation and the inhibition of cell migration, while increasing cell apoptosis by activating caspase-9 and -3. Rapamycin promoted cell autophagy and increased mitochondrial oxidative stress by being involved in DNA damage in the exposed cells. Finally, rapamycin exhibits potent anti-oral cancer properties through inhibition of several cancer-promoting pathways (MAPK, NF-κB, and Wnt/beta-catenin). These results indicate that rapamycin could be a potential agent for the treatment of oral cancer and for a prevention strategy.

KEYWORDS

rapamycin, oral cancer, apoptosis, autophagy, oxidative stress, MAPK, Wnt pathway

Introduction

Oral cancer is the sixth most malignant disease in the world (1). It can be caused by an alteration in epigenetic, genetic, or environmental factors (1). The conventional treatment for cancer is a combination of surgery with radiation therapy or chemotherapy (1). But this has several adverse effects such as fatigue, vomiting, appetite loss and pain, which may vary for each person in terms of severity (2). Cisplatin is the drug used for chemotherapy treatment as it is the most effective agent against cancer (3). However, this molecule causes negative effects as it tags cancerous and healthy cells (2). Therefore, it is urgent to develop a new therapeutic strategy against oral cancer. Several studies have sought alternative treatments by targeting the inhibition of many signaling pathways in cancer. The mechanistic target of rapamycin (mTOR) is an evolutionary conserved serine-threonine kinase present in multiple cancers. This protein kinase controls a wide variety of cellular functions involved in cell growth and proliferation (4, 5). Rapamycin has antimicrobial and immunosuppressive properties (1; 6–8). More recently, rapamycin was considered as an anti-cancer molecule (9). The mTOR signaling pathway often becomes poorly activated during tumor progression and contributes to tumorigenesis by deregulating cancer cell proliferation. By targeting mTOR signaling, rapamycin shows promise for inhibiting the growth of tumors (1). Rapamycin inhibits cancer cell growth, inducing cancer cell apoptosis, and suppressing tumor angiogenesis (10). This anti-tumor property of rapamycin has been studied with endometrial (11) and breast cancer (12). However, no studies have been made regarding rapamycin and oral cancer. The objective of this study was to *in vitro* evaluate the effect of rapamycin on human gingival carcinoma cell proliferation, apoptosis, and autophagy.

Methods and materials

Cells

The human gingival epithelial carcinoma cell line Ca9-22 was purchased from RIKEN BioResource Research Center (Tsukuba, Japan). The culture of the Ca9-22 was in RPMI-1640 supplemented with 5% fetal bovine serum (FBS). We also included in this study human polyclonal oral epithelial cell line (GMSM-K) provided by Dr. Grenier (Université Laval). The GMSM-K cell line was constructed by Gilchrist et al. (2000) who transfected oral epithelial cells with the shuttle vector plasmid, pZ189, containing the T Antigen Coding Region and Replication Origin from the simian virus 40 (SV40). This cell line was grown in Dulbecco's Modified Eagle's Medium (DMEM) supplemented with 5% FBS and 1% penicillin-streptomycin solution (Sigma Aldrich, St. Louis, MO, USA) both cell lines were maintained in culture at 37°C in a 5% CO_2 atmosphere.

Reagents

Rapamycin was purchased from MedChemExpress LLC (NJ 08540, USA). MTT, protease and phosphatase inhibitors were from Sigma-Aldrich (Oakville, Ontario, Canada). LDH-Cytotoxicity Colorimetric Assay Kit II was purchased from BioVision (Milpitas, California, USA), while Annexin V-FITC/PI Kit was from BD Bioscience. (Mississauga, ON, Canada). Autophagy Assay, Red (Cat. #9156), Intracellular Total ROS Activity Assay (Cat. #9144) and Intracellular GSH Assay (Cat. #9137) were purchased from ImmunoChemistry Technologies (Davis, CA, USA). Autophagy Inhibitor, 3-MA (Cat. #189490) and N-acetylcysteine (NAC) were from Sigma. ECL system was acquired from EMD Millipore (Billerica, MA, USA). The primary antibodies as procaspase 3 (sc-56046), procaspase 9 (sc-17784), NF-κB (sc-8008) and β-catenin (sc-59737) were purchased from Santa Cruz Biotechnology (Santa Cruz, CA, USA), E-cadherin (8834), pERK1/2 (4370), ERK1/2 (4695), pp38 (4631), p38 (9212), cleaved caspase-3 (9664S), cleaved caspase-9 (20750S) were from Cell Signaling Technology (Danvers, MA, USA), LC3B (2775) and p62 (39,749) were all from Cell Signaling Technology (Danvers, MA, USA)and β-actin (A5441) was from Sigma-Aldrich (Oakville, ON, Canada). The secondary goat anti-mouse (554002) and anti-rabbit (554021) were from BD Pharmingen (Mississauga, ON, Canada). VersaDoc™ MP 5000 system was from Bio-Rad (Mississauga, ON, Canada).

Cell viability assay and nucleus staining

Cell proliferation was evaluated using MTT assay as well as nucleus staining. Briefly, Ca9-22 and GMSM-K cells were seeded into 12-well plates at the density of 3 x 10^5 cells/well, cultured overnight and then exposed to different concentrations of rapamycin (from 0.1 to 100 μM) for 24 h. After incubation, the culture medium was replaced with a new one containing MTT solution of 5 mg/ml in PBS for 3 h at 37°C in the dark, as described by Semlali and al. previously (13, 14). The cells were incubated for 15 min in 1 ml HCl 0.05 N-isopropanol solution to lyse the cells and release the formed formazan. The solution was transferred to 96-well microplate with 200 μl per well, and the absorbance was measured at 550 nm by an iMark reader (Bio-Rad). Percentage of viable proliferating cells was determined by using the following formula: % of cell viability = [($OD_{550\ nm}$ (treated cell) − OD (blank)/(OD (control cell) − OD (blank))] × 100. The IC50 of rapamycin was obtained by plotting the percentage inhibition of

cell proliferation against rapamycin concentration. The experiment was repeated eight times.

For nucleus staining, oral cancer cells (Ca9-22) at 10^5 were seeded into sterile glass slides immersed in RPMI-1640 medium supplemented or not with different concentrations of rapamycin (0, 0.1, 1, 10, or 20 and 100 µM). The cells were cultured for 24 h at 37°C in a 5% CO_2 incubator. After 24h the cells were fixed with 4% paraformaldehyde for 60 min at room temperature before Hoechst staining (10 µg/ml) for 15 min. Finally, the slides were washed three times with the phosphate buffered saline (PBS), observed under an epifluorescence microscope (Nikon Optiphot) and photographed with a digital camera (Nikon COOLPIX 995). The experiment was repeated three times.

Cell cytotoxicity by LDH assay

Cellular toxicity was determined by the LDH-Cytotoxicity Detection Kit from BioVision, which allows to directly quantify cell death in culture, based on the measurement of lactate dehydrogenase (LDH) released into growth media (15). Briefly, 3.10^5 cells per well were to be seeded into six-well plates and incubated for 24h, before being exposed to different concentrations of rapamycin for an extra 24 h. Afterward, 50 µl of each supernatant was transferred in triplicates to a 96-well plate and supplemented with 50 µl reconstituted substrate mix. Then, the plates were incubated for 30 min at room temperature in the dark until the yellow color developed, before reading at 490 nm with a xMark microplate absorbance spectrophotometer (Bio-Rad, Mississauga, ON, Canada). Triton X-100 (1%) was used as a positive control for LDH and the negative one was obtained with untreated cells. LDH release was calculated using the following formula: % of LDH activity = [rapamycin (absorbance) − negative control (absorbance)] × 100)/[positive control (absorbance) − negative control (absorbance)]. The experiment was repeated four times.

Clonogenic assay

Ca9-22 cells were seeded into 6-well plates at the density of 2000 cells per well for 24 h. They were then stimulated with different concentrations of rapamycin, ranging from 0 to 100 µM. The cells were incubated for two weeks at 37°C in 5% CO_2. The culture medium was changed every 2 or 3 days. The colonies were fixed with 100% ethanol and then stained with 0.5% crystal violet solution, as described by our previous works (13, 14). The colonies were subsequently washed twice with deionized water, dried at room temperature, observed under an optical microscope, and finally photographed. The experiment was repeated three times.

Cell apoptosis detected by flow cytometry with Annexin/PI protocol

The cells were cultured and stimulated with different concentrations of rapamycin for 24 h at 37°C and 5% CO_2. They were then detached with a solution of 0.05% trypsin and 0.01% EDTA, incubated with Annexin V-FITC and propidium iodide at room temperature for 30 min in the dark. Finally, cells were resuspended in 300 µl of the phosphate buffered saline (PBS), to perform a flow cytometry, using either BD LSR II or BD FACSCanto II cytometer (BD Bioscience) equipped with FACSDiva Software v. 6.1.3. The experiment was repeated four times.

Wound-healing assay

Cell migration assay was performed as described previously by Semlali and al. (13, 14). Ca9-22 cells were seeded into 6-well plates and cultured until they reached 100% confluence. Cell monolayers were subjected to a scratch in the shape of a cross with a sterile pipette tip. The cells were then stimulated with different concentrations of rapamycin, ranging from 0 to 100 µM and incubated at 37°C in a humid atmosphere containing 5% CO_2. Photographs were taken of each well with an inverted microscope after 0, 6, 12 and 24 h after the scratch was made. The cell migration was analyzed by image processing software that was able to measure the distance between opposite edges of the scratch at each time point. Each well was then compared, based on their percentage of closure. The experiment was repeated three times.

Quantification of cellular autophagy

To evaluate the effect of rapamycin on autophagy in Ca9-22 cells, we used flow cytometry analyses as described previously (13, 14). Briefly, Ca9-22 cells were seeded into 60 mm Petri dishes for adhesion overnight. Afterward, cells were treated with controls of vehicle alone (0.2% of DMSO) or with 10 and 20 µM of rapamycin for 24 h. Following the rapamycin treatment, cells were resuspended in 500 µl of culture medium containing 1/5 Red staining solution. Cells were incubated for 60 minutes at 37° C in the dark and then collected by low centrifugation. The cell pellet was washed with 500 µl of the 1X Assay Buffer three times and suspended in 500 µl fresh 1X Assay Buffer before analyzing it with the green (FL1) channel of a flow cytometer using BD LSR II or BD FACSCanto II system (BD Bioscience) equipped with FACSDiva Software v. 6.1.3. The experiment was repeated four times.

Determination of ROS levels by flow cytometry

Oxidative stress was assessed by flow cytometry using ROS marker protocol from ImmunoChemistry Technologies. After stimulation with rapamycin at (0, 10 and 20 µM) for 24 h, cells were detached with trypsin, washed with PBS, and were then resuspended in 490 µl of culture medium supplemented with 10 µl Green ROS stain solution and incubated in the dark for 1 h at 37°C. Fluorescent intensity of labeled cells was analyzed by flow cytometry at 488 nm using BD LSR II or BD FACSCanto II cytometer (BD Bioscience). The percentage of positive results was calculated in living cells with FACSDiva Software v. 6.1.3. This experiment was repeated four times.

Measurement of mitochondrial superoxide

Generation of mitochondria-mediated ROS was evaluated by using the MitoSOX-Red Mitochondrial Superoxide Indicator (Invitrogen). Firstly, Ca9-22 cells were treated with different concentrations of rapamycin (10 and 20 µM) for 24h. Subsequently, cells were harvested, washed twice in PBS and incubated with 5 mmol/l of mitochondrial dye (MitoSOX Red; Molecular Probes, Invitrogen) for 30 min at 37°C in the dark, followed by analysis on a flow cytometer to calculate the percentage of MitoSox-positive cells. This experiment was repeated four times.

Assessment of DNA damage by flow cytometry

As described by our previous studies (13, 14, 16), to evaluate the effect of rapamycin on damage to oral cancer cells, a H2A.X flow cytometry was performed. In addition, after treating Ca9-22 cells with the studied concentrations of rapamycin, they were trypsinized and then fixed with 75% ethanol for 15 min. The centrifugation of the samples was carried out to eliminate the fixative solution. Afterward, a permeabilization solution containing 1% BSA/0.2% Triton/1X PBS was added to the cells and they were then incubated in the dark at 4°C overnight with the first phospho-histone H2A.X (Ser139) monoclonal antibody from Santa Cruz Biotechnology at a dilution 1/100, washed twice with PBS and incubated with the secondary antibody conjugated to Alexa Fluor 488 from Santa Cruz Biotechnology in a 1:100 ratio for 1h before analyzing them with the BD flow cytometry system (BD FACS Canto II) and the percentage of positive cells was calculated. This experiment was repeated three times.

Real-time reverse transcription PCR (qPCR) analysis for gene expression studies

Total RNA was extracted from treated and untreated cells by using the RNeasy Mini Kit from Qiagen (Toronto, Ontario, Canada). An amount of 1 µg total RNA was reverse-transcribed into a cDNA copy with the High-Capacity cDNA Reverse Transcription Kit from Applied Biosystems (Thermo Fisher Scientific, USA) according to the manufacturer's instructions, as described by our previous works (17–19). The RNA concentration and purity were determined by using a Nanodrop 8000 spectrophotometer (Thermo Fisher Scientific, USA). The qPCR protocol was performed with a 7500 Real-Time PCR System (Applied Biosystems). The reaction volume for each sample consisted of 12.5 µl SYBR Green Master Mix 2X, 0.5 µl primer (Forward and Reverse) (See Table 1), 7 µl distilled water, and 5 µl cDNA. The conditions for the PCR hold were 95°C for 5 min, followed by 40 cycles at 95°C for 15 sec, 60°C for 30 minutes and 30 sec at 72°C. The results were then analyzed using the Livak method for relative expression. The experiment was repeated three times.

Western blot

Ca9-22 cells at the density of 10^6 were harvested for extraction by a lysis buffer. A Bradford protein assay was then conducted to determine the protein concentrations of each sample. An amount varying between 20 µg and 60 µg of proteins were separated by SDS-PAGE with 8–15% of acrylamide, electro transferred onto nitrocellulose membrane. The membrane was blocked in a 5% milk solution at room temperature for 1 h and then incubated overnight with the specific primary antibodies. The membrane was then left in the secondary antibody solution for 1 h before being rinsed four times with washing solution. Detection of proteins was carried out with an enhanced chemiluminescence (ECL) Western Blotting Kit according to the manufacturer's instructions and revelation by Versa Doc™ MP 5000 system (Bio-Rad, Mississauga, ON, Canada).

Statistical analysis

The significant difference between experimental (treated) groups and controls (untreated) was evaluated by Student's *t*-test in GraphPad Prism 7 Software. Error bar represented mean ± SEM. **P*- value < 0.05 was statistically significant.

TABLE 1 Primer sequences used for the qRT-PCR.

Gene	Primer sequences	Product length size (pb)
Cyclin D1	**F : 5'**-AGCTGTGCATCTACACCGAC-**3'** **R : 5'**GAAATCGTGCGGGGTCATTG-**3'**	**113**
p21 (**CDKN1A**)	**F :5'**-TGCCGAAGTCAGTTCCTTGT-**3'** **R :5'**CATTAGCGCATCACAGTCGC-**3'**	**190**
p15 (**CDKN2B**)	**F :5'**-TTTACGGCCAACGGTGGATT-**3'** **R:5'**CATCATCATGACCTGGATCGC-**3'**	**220**
p27	**F :5'**- TTGCGCAATTAGGTTTTTCC-**3'** **R :5'**-AAAGGAATTCAAGCCTTCC-**3'**	**64**
LC3B	**F :5'**-TCAGGTTCACAAAACCCGCC-**3'** **R :5'**GCGTTTGTGCCAACTGTGAT-**3'**	**140**
p62	**F :5'**-GCCATTGCGGAGCCTCATCT-**3'** **R :5'**CAGCCATCGCAGATCACATTG-**3'**	**322**
GAPDH	**F :5'**-GGTATCGTGGAAGGACTCATGAC-**3'** **R :5'**ATGCCAGTGAGCTTCCCGTTCAGC-**3'**	**188**

Results

Rapamycin at a low dose selectively inhibits the proliferation of Ca9-22 cells

We first investigate the effect of rapamycin on the proliferation of human gingival epithelial carcinoma cells (Ca9-22) and human polyclonal oral epithelial cells (GMSM-K). As shown in Figure 1A, rapamycin inhibited the proliferation of Ca9-22 cells in a dose-dependent manner. The half-maximal inhibitory concentration (IC_{50}) value was around 15 μM of rapamycin (Figure 1A). In addition, only the high concentration of rapamycin (100 μM) affects the proliferation of normal gingival epithelial cells (GMSM-K). These results were confirmed with the nucleus staining assay. Figure 1B shows that the number of nuclei in cancer cells dramatically decreases in the presence of rapamycin, while no effect was seen with GMSM-K cells (Figure 1B). The anti-proliferation effect of rapamycin evaluated by MTT was confirmed by LDH assay. As shown in Figure 1C, rapamycin increased the LDH activity of Ca9-22 cells in a dose-dependent manner. The median inhibitory concentration was also calculated and was around 15 μM. For GMSM-K, rapamycin induced cell toxicity only for 100 μM; the same effect was observed by MTT assay for this cell type (Figure 1C). These results show that a high dose of rapamycin non-selectively inhibits the viability of human oral cancer and normal cells. However, when the cells were treated with lower concentrations of rapamycin (non-cytotoxic to normal oral cells), we witnessed a significant inhibitory effect on oral cancer cell proliferation. We next investigated whether rapamycin affected the cell morphology.

Differences in cell morphology were observed between rapamycin-treated oral cancer cells and controls (treated with DMSO) under light microscopy (Data not shown), the most dramatic morphology changes were seen with rapamycin-treated cells at low concentrations of rapamycin (10, 20 μM) and high concentration (100 μM) in Ca9-22 cells, but only at 100 μM for normal oral cells. These morphology changes are manifested by cell shrinkage, cells became round and lost their integrity to promote cancer progression as well as their number was significantly reduced, and there was an extensive detachment from the cell culture substratum compared with the vehicle. The morphology changes observed in Ca9-22 cells are probably characteristics of oral cancer cell death and apoptosis.

The mechanism by which rapamycin inhibits oral cancer cell proliferation is probably through the cell cycle. This was confirmed by studying the effect of rapamycin on cell-cycle inhibitors. As shown in Figure 1D, rapamycin at 20 μM (a concentration close to the IC_{50} value) was inhibiting cell proliferation by induction of cell-cycle inhibitors such as p21, p15 and p27 and the repression of cyclin D1 expression. Therefore, rapamycin inhibits proliferation by blocking the cell cycle.

Rapamycin selectively suppresses oral cancer cell growth/survival by inhibition of colony-forming cells

As shown in Figure 2, rapamycin inhibits colony formation in a dose-dependent manner compared with controls, especially in oral cancer cells. No effect was seen in normal cells for the low concentrations (≤ 20 μM), only at the high concentration of rapamycin (100 μM) (Figures 2A, B). These results obtained with the clonogenic assay were consistent with MTT and LDH assays. For the rest of the study, we used 10 and 20 μM as an average of the IC_{50}. With these two concentrations, we next investigated whether the inhibition of oral cancer cell growth/

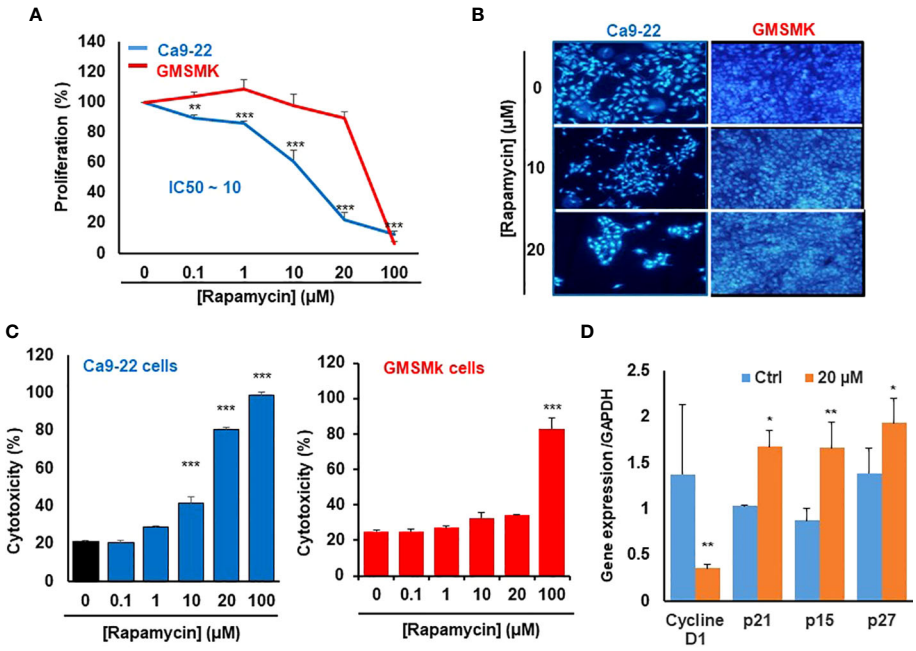

FIGURE 1
Rapamycin at a low dose selectively inhibits the proliferation of Ca9-22 cells. **(A)** Cell growth was measured by MTT assay. Ca9-22 cells were stimulated by rapamycin concentration, from 0.1 to 100 µM for 24h. Results are expressed as mean percentage of proliferation ± SD. The untreated cells represent 100% of proliferation. (n = 8 for Ca9-22 and n = 6 for GMSM-K cells). **(B)** Nucleus staining, Ca9-22 and GMSM-K cells were seeded into sterile glass slides immersed in culture medium. After 24h of rapamycin treatment, cells were fixed with 4% paraformaldehyde before Hoechst staining (10 µg/ml). The experiment was repeated three times. **(C)** Cytotoxicity was assessed by LDH assay. Cells were stimulated by the same rapamycin concentrations for 24h. The LDH activity was presented as mean percentage of cytotoxicity ± SD. *P*-value was considered as significant when it was < 0.05 (comparison between untreated and rapamycin-treated cells). **(D)** Rapamycin inhibits proliferation by blocking the cell cycle in Ca9-22 cells. They were treated with 20 µM of rapamycin for 24h. After, total RNA was extracted, and reverse-transcribed into a cDNA. By using qPCR, we evaluated the expression of cell-cycle inhibitors such as p21, p15, p27 and cyclin D1 (n = 3). $^{*}P < 0.05$, $^{**}p < 0.005$, or $^{***}p < 0.0005$.

survival was accompanied by induction of their apoptosis through rapamycin treatment.

Rapamycin promotes Ca9-22 apoptosis by triggering the intrinsic pathway

As shown in Figure 3A, the stimulation of cancer cells with 10 and 20 µM of rapamycin was causing an increase in cell death and a decrease in living cells. The percentage of the apoptosis cells in untreated cells was 13%, representing necrotic and early and late apoptosis cells. When Ca9-22 cells were exposed to 20 µM of rapamycin, the level of apoptotic cells increased to 41.8% (Figure 3). To further confirm the effect of rapamycin on cell apoptosis in more detail, we investigated the effects of 20 µM rapamycin on inactive and cleaved caspase-3 and -9. Figure 10 shows a decrease in the expression of procaspase 3 and 9 with an increasing concentration of rapamycin. Also, the cleaved forms of caspase-3 and -9 increased following Ca9-22 treatment with rapamycin. Overall, rapamycin promotes cancer cell death through caspases-3 and -9 signaling pathways.

Rapamycin induces autophagy in Ca9-22 cells

It was clearly reported that, mTOR is one of the key autophagy inhibitors and rapamycin is one of the best characterized autophagy inducers, we investigated whether rapamycin-induced cell death occurred *via* induction of autophagy. As shown in Figure 4A, rapamycin increased the percentage of Ca9-22 cells undergoing autophagy. However, that at basal level was 0.9%. Rapamycin treatment for 24 h significantly increased the percentage of Ca9-22 cells autophagic death from 0.9% with the control to 3.1% with 10 µM, and 82.2% with 20 µM. These results were confirmed by the study of *LC3* and *p62* gene expression study Figure 4B. As shown in Figure 4C, rapamycin at 20 µM caused an increase in the expression of both genes *LC3B-II* and *p62*. Thus, rapamycin is a promotor of cancer cell autophagy. The autophagosome accumulation induced by rapamycin measured by flux cytometry is probably linked to an increase in autophagy due to increased autophagosome formation. In addition, Figure 7B shows that rapamycin at 20µM increases autophagy to 32.9% in

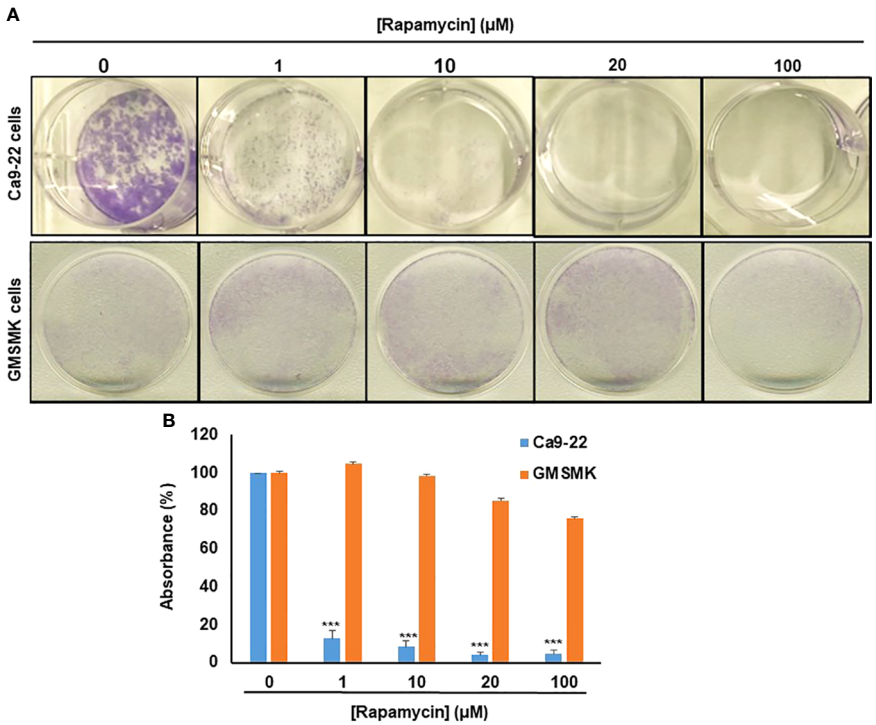

FIGURE 2
Rapamycin selectively suppresses oral cancer cell growth/survival by inhibition of colony-forming cells. **(A)** Colony formation of Ca9-22 and GMSM-K cells after treatment with rapamycin (0, 1, 10, 20 and 100 µM). Cell survival was evaluated by the clonogenic assay using crystal violet staining. **(B)** Histogram showing the percentage of absorbance at 470 nm. (100% represents the absorbance at 470 nm for untreated cells. (n = 3). ***$p < 0.0005$.

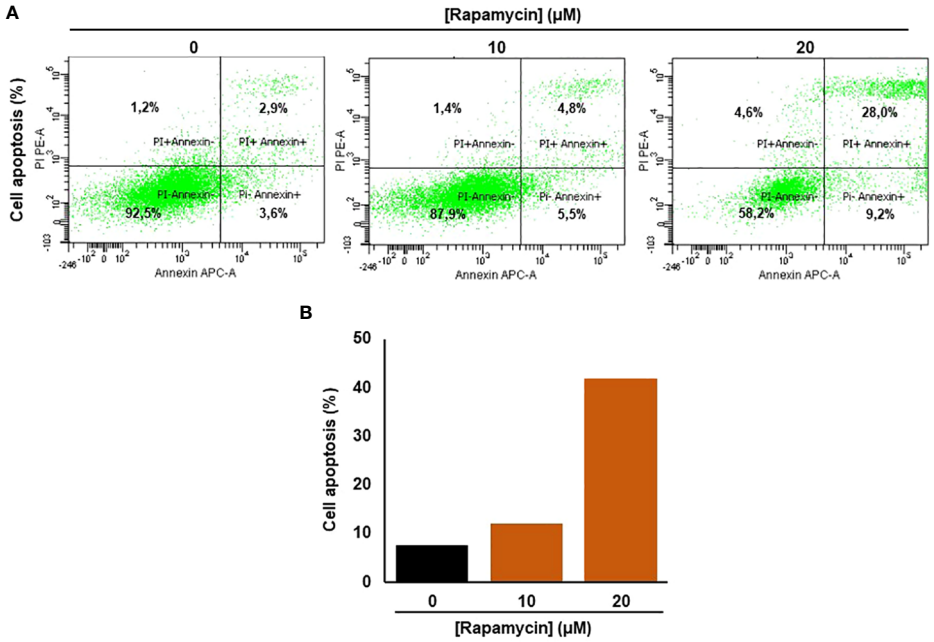

FIGURE 3
Rapamycin promotes Ca9-22 apoptosis. **(A)** Flow cytometry assay using Annexin/Pi. To measure oral cancer cell apoptotic/cell death after different rapamycin treatments (10 and 20 µM). **(B)** The percentage of cell apoptosis obtained from four individual experiments.

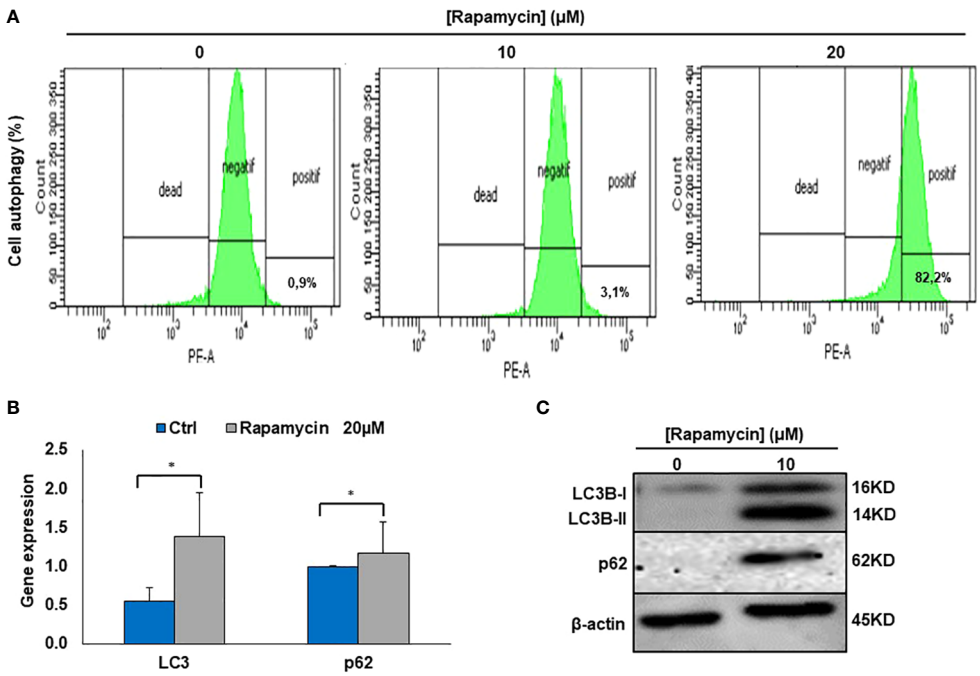

FIGURE 4
Rapamycin induces autophagy in Ca9-22 cells. **(A)** Flow cytometry analysis (n = 4). To evaluate the effect of rapamycin on autophagy in Ca9-22 cells, the percentage of cellular autophagy was determined using flow cytometry using the Autophagy Red Assay. After 24h of treatment, Ca9-22 cells were stained with the autophagy probe before analyzing them with the green (FL1) channel of a flow cytometer. The results were expressed as means (% autophagy) and are considered significant when $*p < 0.05$. (n = 4). **(B)** mRNA level of LC3B and p62 by RT-PCR (n=3). **(C)** Protein level of LC3B and p62 by western blotting (n=3).

ca9-22 compared to 5.9% in untreated cells. However, a pre-treatment with 50μM of 3-MA decreases the percentage of cell autophagic to 13.7%. This autophagy appears to be associated with oxidative stress. In addition, a pre-treatment with 10 mM of NAC also decreases the percentage of cell autophagic from 32.9% in cells treated with 20 μM of rapamycin to 7.6% when the cells were treated by NAC and rapamycin (Figure 7B).

Rapamycin induces oral cancer mitochondrial oxidative stress

As shown in Figure 5A there was a significant induction of ROS in Ca9-22 cells being treated with rapamycin compared to cells untreated. The percentage of ROS increased to 57.9% and 66.1% respectively when the cells were treated with 10 and 20 μM of rapamycin compared to 17.6% in controls (with the vehicle). The generation of mitochondrial ROS in rapamycin-treated Ca9-22 cells for 24h was also assessed by flow cytometry using MitoSOX staining. The percentage of MitoSOX-positive cells also increased with rapamycin concentration. Figure 5B shows an increase from 5.5% in untreated cells to 10.3% with 10 μM, and 25.1% with 20 μM of rapamycin. Overall, these results suggest that rapamycin-mediated oral cancer cell apoptosis by mitochondrial-derived ROS production, which occurred upstream of the mitochondrial apoptosis.

Rapamycin induces oral cancer cell death through oxidative stress and cell autophagy

ROS generation has been recognized to induce stress-mediated cell death in a variety of cancer types. Our hypothesis was that rapamycin triggers cell death *via* ROS production. As shown in Figures 6 and 7, the toxicity rate significantly increased with rapamycin concentration. The inhibition of oxidative stress by 10 mM of N-acetylcysteine (NAC) dramatically reversed the effect of rapamycin. In addition, the percentage of toxicity cutoff in cells decreased from 73.08% ± 12.57% with 20 μM of rapamycin to 41.18% ± 1.18% with the same concentration but having a pretreatment with 10 mM of NAC for 60 min. Similar results were observed for autophagy inhibition, a pretreatment of Ca9-22 cells was carried out with 50 μM of 3-methyladenine (3-MA); this inhibitor decreased the above percentage from 73.08% ± 12.57% with 20 μM of rapamycin to 24.96% ± 4.51% when cells were

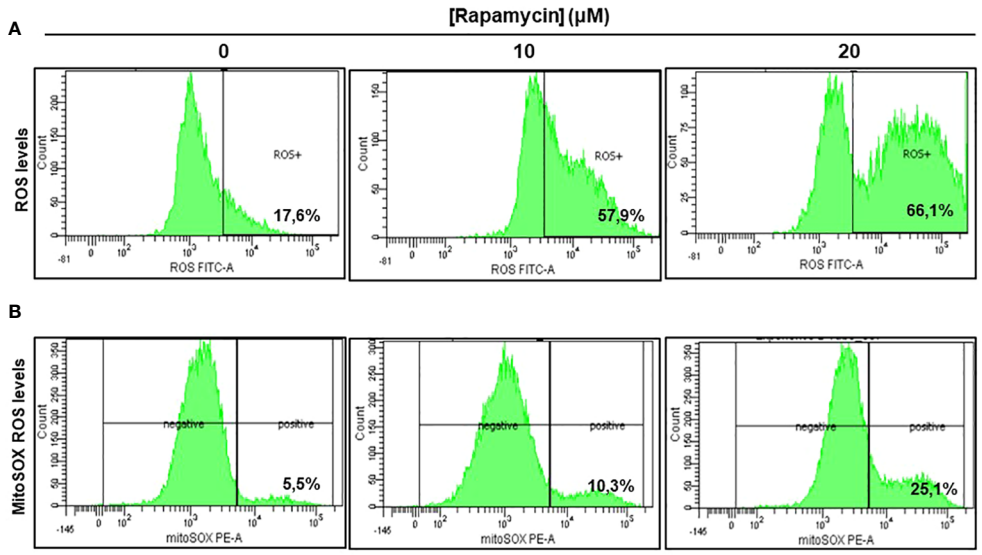

FIGURE 5
Rapamycin induces oral cancer mitochondrial oxidative stress. **(A)** Rapamycin induces ROS expression in oral cancer cells. ROS levels were measured by flow cytometry using ROS marker protocol. After stimulation with rapamycin at (0, 10 and 20 µM) for 24h, cells were exposed to ROS Green working solution before analyzing them by flow cytometry at 488 nm using BD LSR II or BD FACSCanto II cytometer (BD Bioscience). The percentage of positive cells was calculated in living cells with FACSDiva Software v. 6.1.3. This experiment was repeated four times. **(B)** Measurement of mitochondrial superoxide. The generation of mitochondrial reactive oxygen species (ROS) in rapamycin-treated Ca9-22 cells for 24h was also assessed by flow cytometry using MitoSOX staining, highly selective to detect superoxide in mitochondria of living cells. The results were expressed in percentages of MitoSOX-positive cells (n = 4).

pretreated with 3-methyladenine for 60 min and then stimulated by 20 µM of rapamycin (Figure 6). Inhibition of oxidative stress or autophagy also reversed rapamycin-induced apoptosis. As shown in Figure 7, the percentage of apoptotic cells increased with rapamycin concentrations, particularly with 20 µM (28.2%). This induction of apoptosis was inhibited up to 9.3% and 10% when cells were pretreated respectively with NAC and 3-MA.

Rapamycin-induced DNA damage through g-H2AX- expression

Figure 8 shows the effect of rapamycin on the expression of g-H2AX by Ca9-22. The percentage of g-H2AX-positive cells increased significantly following exposure of oral cancer cells to rapamycin. Indeed, the percentage of g-H2AX-positive ranged from 11.6% in control cells to 75% with 10 µM, to 96% with 20 µM of rapamycin (Figure 8).

Rapamycin suppresses cell migration and invasion in Ca9-22 cells

The effect of rapamycin on cell migration was determined by the scratch method. Non-stimulated cells were compared to Ca9-22 stimulated with concentrations of 1, 10, 20, and 100 µM of rapamycin. As shown in Figure 9. the wound-healing assay demonstrated that rapamycin inhibited the Ca9-22 cell migration and invasion. Non-stimulated cells migrated over the scratch made. However, migration of rapamycin-treated cells was inhibited in a dose-dependent manner.

Rapamycin inhibits MAPK, NF-κB and β-catenin signaling pathways and activates caspase pathways

To investigate what signaling pathways related to cancer progression were targeted by rapamycin in oral cancer cells, we analyzed β-catenin, NF-κB, MAP kinase (ERK1/2 and p38) and that of caspases. As shown in Figure 10, there is a decrease in the expression of β-catenin, a pathway involved in cell adhesion as well as for NF-κB a pathway implicated in inflammation. Also, rapamycin decreased the activation of ERK1/2 and p38 pathways but was not affecting the total ERK1/2 and p38. Unlike proliferation pathways, rapamycin is thus activating two key pathways involved in apoptosis, particularly cleaved caspase-3 and cleaved caspase-9 pathways, confirming the results presented in (Figure 10).

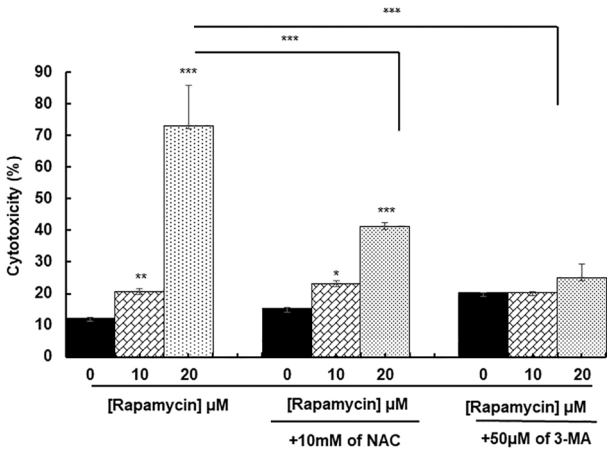

FIGURE 6
Rapamycin induces oral cancer cell death through oxidative stress and autophagy. Ca9-22 cells were firstly pretreated with or without 10 mM of NAC or 50 µM of 3-MA for 60 min, and then stimulated or not by 10 and 20 µM of rapamycin. After 24 h of rapamycin treatment, LDH assay was performed, and the toxicity rate was calculated with the use of Triton as 100% in cytotoxicity (n = 3). *$p < 0.05$, **$p < 0.005$ or ***$p < 0.0005$.

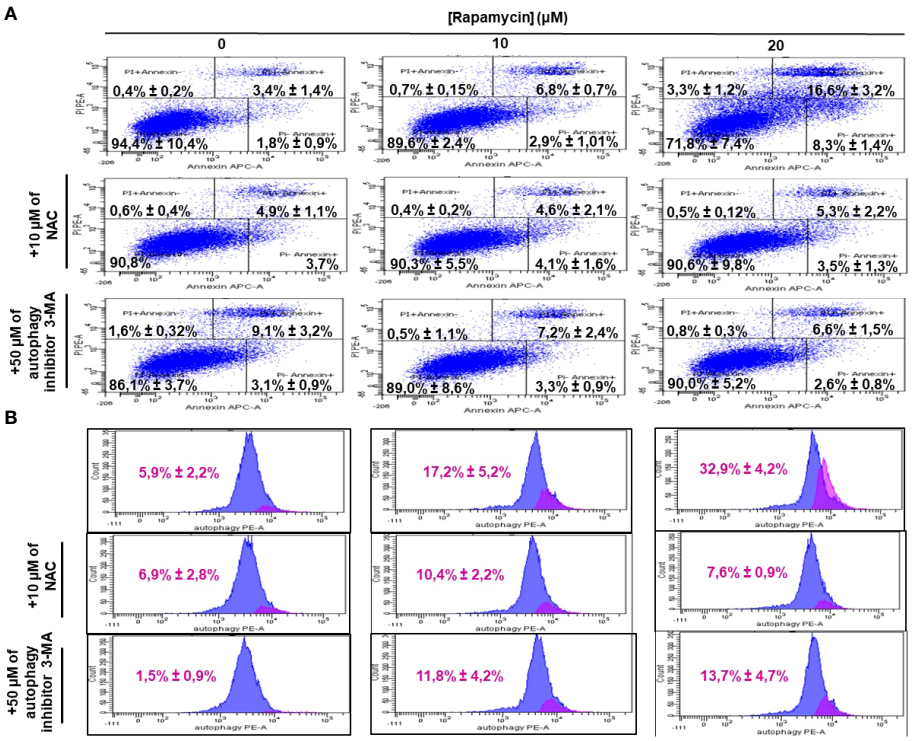

FIGURE 7
Inhibition of oxidative stress and autophagy reverses rapamycin-induced apoptosis. Ca9-22 cells were firstly pretreated with or without 10 mM of NAC or 50 µM of 3-MA for 60 min, and then stimulated or not by 10 and 20 µM of rapamycin. After 24 h of rapamycin treatment, Annexin V/PI assay for evaluating the percentage of apoptotic cells was performed in **(A)** and the percentage of autophagic cells was evaluated in **(B)** (n = 3).

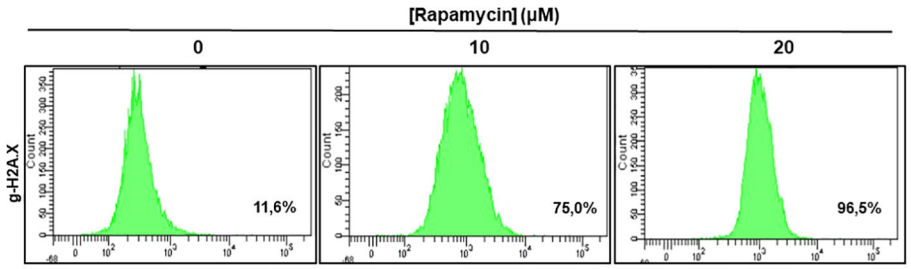

FIGURE 8
Rapamycin-induced DNA damage in Ca9-22 cells: The DNA damage was determined by g-H2AX-based flow cytometry. Ca9-22 cells were treated with 10 and 20 µM of rapamycin for 24h and the damage was evaluated by flow cytometry using g-H2AX antibody (n = 3).

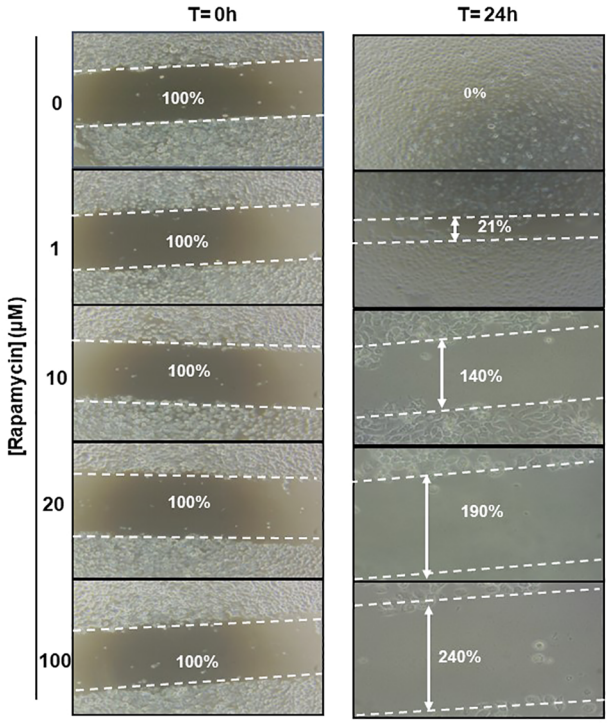

FIGURE 9
Rapamycin suppresses cell migration and invasion in Ca9-22 cells. Wound-healing assay. The effect of rapamycin on cell migration was determined by the scratch method. Non-stimulated cells were compared to Ca9-22 stimulated with concentrations of 1, 10, 20 and 100 µM of rapamycin. The cell migration was analyzed by image processing software that was able to measure the distance between opposite edges of the scratch at each time point. Each well was then compared, based on their percentage of closure.

Discussion

The goal of the current study was to investigate the inhibitory role of rapamycin on oral cancer progression and its potential use as an alternative or complementary agent to the conventional cancer treatment. We demonstrated that a low dosage of rapamycin shows a selective effect on cell growth/survival in oral cancer, with the cell cycle likely blocked by CDKs inhibitors, being crucial for the orderly initiation and progression of the cell-division cycle. It involves modulating the synthesis of CDK inhibitors, such as p21, p15 and p27, found in quiescent cells at high levels, but they are downregulated by

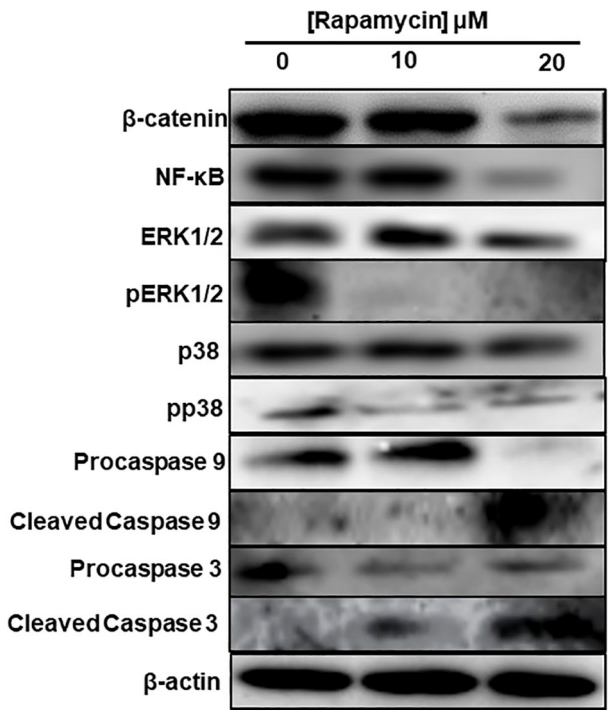

FIGURE 10
Rapamycin inhibits MAPK, Wnt/β-catenin signaling pathways and activates caspase pathways. An amount of each protein varying between 20 µg and 60 µg was needed for Western blotting analysis. We used specific primary antibodies to β-catenin, Wnt/beta catenin, MAP kinase (ERK1/2 and p38) and that of caspases. (n = 3).

mitogenic stimulation (20, 21), and by inhibition of cyclin D1 expression, both are rate-limiting for entry into S phase. Rapamycin increases levels of CDK inhibitors such as $p27^{Kip1}$. These results are consistent with the data published by other groups reporting that rapamycin has multiple biological functions, including anticancer activity (22, 23), and it is considered as one of the key potential chemopreventive agents in therapy causing suppression, or inversion of carcinogenesis (24, 25). Several studies have reported that rapamycin alone or in combination with chemotherapeutic agents inhibits the proliferation of various tumor cells (26, 27). It also inhibits the cell cycle progression, particularly the G1/S transition by targeting mTOR, and cell growth effectors S6K1, 4E-BP1, and cyclin D1 (28, 29).

Importantly, another anticancer property of rapamycin is its ability to promote cancer cell apoptosis. Indeed, we demonstrated that rapamycin promoted Ca9-22 cell apoptosis through the activation of caspase-9 and -3. The effect rapamycin may induce oral cancer cell apoptosis directly by suppressing 4E-BP1 phosphorylation through mTORC1 and indirectly by inactivating eIF4E. Therefore, these data indicate that inhibition of mTOR by rapamycin is closely linked to cell growth and apoptotic processes due to the inactivation of the mTOR pathway and its downstream target genes. These results are consistent with those previously published studies (30–32). Recently, Jun Yao etal. (31) have reported that 0.2 µM and 0.4 µM of rapamycin increased the number of apoptotic cells and the cell cycle of retinoblastoma cells was basically stopped in S phase and consequently, the expression levels of Bcl-2, PI3K and AKT declined with rapamycin stimulation at 0.2 µM and 0.4 µM (31). On the other hand, we have shown that rapamycin induces significantly oral cancer cells undergoing autophagy by increasing the LC3 and p62 expression. Data in concordance with these same recent studies, which reported that targeting the induction of autophagy may be an excellent emerging strategy for cancer therapy (33); (34). In addition, it was demonstrated that rapamycin inhibits cell proliferation and induces autophagy in human neuroblastoma cell lines by suppressing the mTOR signaling pathway through increasing gene expression of LC3-II/LC3-I and Beclin (35). We strongly believe that the induction of autophagy by rapamycin in oral cancer cells is due to its ability to specifically, inhibit mTORC1. It was clearly reported that rapamycin is considered as an allosteric mTORC1 inhibitor (36–38). However, these same research groups reported that mTORC1 is inhibiting the autophagy-initiating kinase UNC-5 like autophagy activating kinase 1 (ULK1) complex by

phosphorylation of complex components, including autophagy-related 13 (ATG13) and ULK1/2 genes (39–42).

Rapamycin could have anti-tumor activity through mitochondrial-derived ROS and DNA damage. We showed that rapamycin increased the accumulation of ROS in cancer cells, as previously reported (22, 43–46). Moreover, we have demonstrated that rapamycin dramatically induces DNA damage in oral cancer cells as measured by histone H2AX phosphorylation, one of the highly sensitive and general markers induced by chemotherapy (47). The consequent accumulation of damaged DNA in Ca9-22 cells is probably due to the ability of rapamycin to promote oral cancer cell cycle disruption, which is closely associated with further increased replication stress (42). However, it is known that replication stress is considered as a key cause of DNA damage and high genomic instability, two main features of cancer cells. Oral cancers are characterized by the invasion/migration capacity of malignant cells, often accompanied by disruption of the extracellular matrix (ECM). Our results show that rapamycin suppressed cell migration and invasion in Ca9-22 cells at the epithelial-to-mesenchymal transition (vimentin and E-cadherin) (data not shown). The same observations were found in our previous studies using a natural product (16), or with the analog of curcumin (14) on oral cancer cells. Song et al. (48) have reported that rapamycin treatment leads to growth arrest and inhibition of invasion in human chondrosarcoma cells (48). Recently, Sahu et al. (49) showed that bladder cancer invasion was closely mediated by mammalian target of rapamycin (49). The rapamycin inhibitory effect of cancer cell proliferation could be related to the expression level of proteolytic enzymes such as plasminogen activator (PAs) and matrix metalloproteinases (MMPs) known to be key factors involved in the tumor cell invasion and metastasis (12). MMPs, like MMP-2 and MMP-9, play a role in ECM degradation and are highly expressed in carcinomas to promote tumor angiogenesis and consequent cancer cell invasion and metastases. Inhibiting MMP represents a real-world new therapeutic strategy for several cancer treatments, thus various MMP inhibitors are currently being assessed for clinical applications. In this study, Ca9-22 cells treated with rapamycin were not enabling the activation of MAP kinases (in particular, ERK1/2) and NF-κB, which are involved in the transcriptional regulation of proteolytic enzymes. The overactivation of ERK1/2 has been reported to be involved in cancer progression (50–52). In addition, NF-κB pathway is shown to induce inflammation and cancer cell invasion *via* increasing MMPs. In fact, several evidences support that rapamycin inhibits NF-κB (53). These results suggest that the inhibitory effect of rapamycin on the motility of Ca9-22 cells might be associated with its ability to inhibit the activation of MAP kinases, beta-catenin, and NF-κB.

In conclusion, when cancer cells are stimulated with increasing concentrations of rapamycin, it is possible to observe an increase in cell death and autophagy, as well as an inhibition of the cell proliferation, colony formation, cell adhesion, inflammation, and cell migration. As shown in (Figure 11), rapamycin has an anti-cancer effect by inducing DNA damage to Ca9-22 cells and inducing their oxidative stress, which, in turn, induces Ca9-22 cell autophagy and apoptosis and inhibits their proliferation (Figure 11). These findings show that rapamycin is a potential agent that could be used in the treatment of oral cancer.

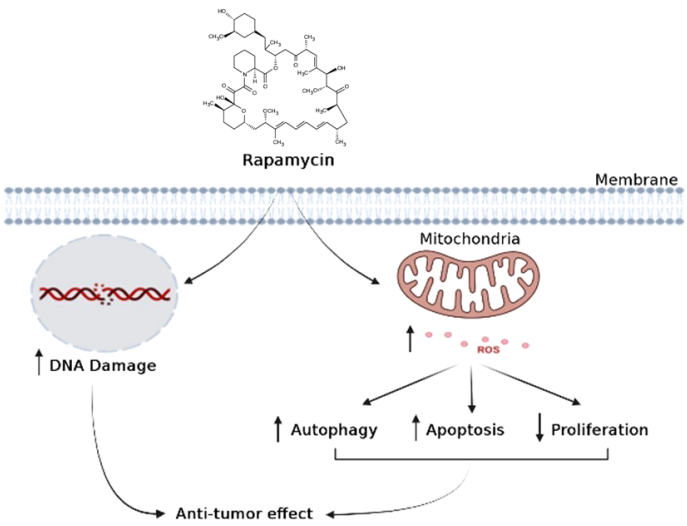

FIGURE 11
Schematic model proposed for the mechanism of action of rapamycin in oral cancer cells.

Data availability statement

The original contributions presented in the study are included in the article/supplementary material. Further inquiries can be directed to the corresponding author.

Author contributions

AS, conceptualization, conducted experiments, and writing - original draft. SP, CC, and IZ, conducted Western blotting and flux cytometry experiments. MR, critical revision of the article, supervision, review, and editing. All authors contributed to the article and approved the submitted version.

Funding

This work was supported by a grant (FO131038) from the "Fonds Émile-Beaulieu" at Laval University and by grant (FO130688) from Network for Canadian Oral Health and Research.

Acknowledgments

The authors are thankful to RSBO (Réseau de Recherche en Santé Buccodentaire et Osseuse) for providing financial support.

Conflict of interest

The authors declare that the research was conducted in the absence of any commercial or financial relationships that could be construed as a potential conflict of interest.

Publisher's note

References

1. Law BK. Rapamycin: An anti-cancer immunosuppressant? *Crit Rev Oncol Hematol* (2005) 56:47–60. doi: 10.1016/j.critrevonc.2004.09.009

2. Society, C. C. *Effets secondaires de la chimiothérapie*. Quebec:Société canadienne du cancer (2021).

3. Klaunig JE. Oxidative stress and cancer. *Curr Pharm Des* (2018) 24:4771–8. doi: 10.2174/1381612825666190215121712

4. Pallet N, Thervet E, Legendre C, Anglicheau D. Sirolimus early graft nephrotoxicity: Clinical and experimental data. *Curr Drug Saf* (2006) 1:179–87. doi: 10.2174/157488606776930580

5. Dreyer CEC. Voies de signalisation de la PI3K et de mTOR: Perspectives de l'utilisation de la rapamycine et de ses dérivés en thérapie antitumorale ciblée. *Bull du Cancer* (2006), 93:31–40.

6. Liu Y, Yang F, Zou S, Qu L. Rapamycin: A bacteria-derived immunosuppressant that has anti-atherosclerotic effects and its clinical application. *Front Pharmacol* (2018) 9:1520. doi: 10.3389/fphar.2018.01520

7. Husain S, Singh N. The impact of novel immunosuppressive agents on infections in organ transplant recipients and the interactions of these agents with antimicrobials. *Clin Infect Dis* (2002) 35:53–61. doi: 10.1086/340867

8. Kim WS, Xu L, Souw D, Fang A, Demain AL. An unexpected inhibitory effect of rapamycin against germination of spores of bacillus brevis strain nagano. *J Antibiot. (Tokyo)* (2002) 55:650–4. doi: 10.7164/antibiotics.55.650

9. Neuzillet Y KG, Lechevallier E, Kleinclauss FComité Transplatation De L'association Francaise D'urologie. MTOR inhibitors: from transplantation to oncology. *J l'association Francaise. d'urologie la Société Francaise. d'urologie* (2007) 17:928–33. doi: 10.1016/s1166-7087(07)92390-8

10. Coutte L, Dreyer C, Sablin MP, Faivre S, Raymond E. PI3K-AKT-mTOR pathway and cancer. *Bull Cancer* (2012) 99:173–80. doi: 10.1684/bdc.2011.1384

11. Zhou C, Gehrig PA, Whang YE, Boggess JF. Rapamycin inhibits telomerase activity by decreasing the hTERT mRNA level in endometrial cancer cells. *Mol Cancer Ther* (2003) 2:789–95.

12. Mignatti P, Rifkin DB. Biology and biochemistry of proteinases in tumor invasion. *Physiol Rev* (1993) 73:161–95. doi: 10.1152/physrev.1993.73.1.161

13. Semlali A, Beji S, Ajala I, Rouabhia M. Effects of tetrahydrocannabinols on human oral cancer cell proliferation, apoptosis, autophagy, oxidative stress, and DNA damage. *Arch Oral Biol* (2021) 129:105200. doi: 10.1016/j.archoralbio.2021.105200

14. Semlali A, Contant C, Al-Otaibi B, Al-Jammaz I, Chandad F. The curcumin analog (PAC) suppressed cell survival and induced apoptosis and autophagy in oral cancer cells. *Sci Rep* (2021) 11:11701. doi: 10.1038/s41598-021-90754-x

15. Semlali A, Chakir J, Rouabhia M. Effects of whole cigarette smoke on human gingival fibroblast adhesion, growth, and migration. *J Toxicol Environ Health A* (2011), 74(13):848–62. doi: 10.1080/15287394.2011.570230

16. Contant C, Rouabhia M, Loubaki L, Chandad F, Semlali A. Anethole induces anti-oral cancer activity by triggering apoptosis, autophagy and oxidative stress and by modulation of multiple signaling pathways. *Sci Rep* (2021) 11:13087. doi: 10.1038/s41598-021-92456-w

17. Semlali A, Almutairi M, Pathan AAK, Azzi A, Parine NR, Alamri A, et al. Toll-like receptor 6 expression, sequence variants, and their association with colorectal cancer risk. *J Cancer* (2019) 10:2969–81. doi: 10.7150/jca.31011

18. Semlali A, Reddy Parine N, Arafah M, Mansour L, Azzi A, Al Shahrani O, et al. Expression and polymorphism of toll-like receptor 4 and effect on NF-kappaB mediated inflammation in colon cancer patients. *PloS One* (2016) 11:e0146333. doi: 10.1371/journal.pone.0146333

19. Semlali A, Witoled C, Alanazi M, Rouabhia M. Whole cigarette smoke increased the expression of TLRs, HBDs, and proinflammory cytokines by human gingival epithelial cells through different signaling pathways. *PloS One* (2012) 7: e52614. doi: 10.1371/journal.pone.0052614

20. Kato JY, Matsuoka M, Strom DK, Sherr CJ. Regulation of cyclin d-dependent kinase 4 (cdk4) by cdk4-activating kinase. *Mol Cell Biol* (1994) 14:2713–21. doi: 10.1128/mcb.14.4.2713-2721.1994

21. Nourse J, Firpo E, Flanagan WM, Coats S, Polyak K, Lee MH, et al. Interleukin-2-Mediated elimination of the P27(Kip1) cyclin-dependent kinase inhibitor prevented by rapamycin. *Nature* (1994) 372:570–3. doi: 10.1038/372570a0

22. He X, Song W, Liu C, Chen S, Hua J. Rapamycin inhibits acrolein-induced apoptosis by alleviating ROS-driven mitochondrial dysfunction in male germ cells. *Cell Prolif.* (2014) 47:161–71. doi: 10.1111/cpr.12091

23. Li J, Kim SG, blenis J. Rapamycin: One drug, many effects. *Cell Metab* (2014) 19:373–9. doi: 10.1016/j.cmet.2014.01.001

24. Xie LX, Sun FF, He BF, Zhan XF, Song J, Chen SS, et al. Rapamycin inhibited the function of lung CSCs *via* SOX2. *Tumour. Biol* (2016) 37:4929–37. doi: 10.1007/s13277-015-4341-y

25. Chen W, Zou P, Zhao Z, Chen X, Fan X, Vinothkumar R, et al. Synergistic antitumor activity of rapamycin and EF24 *via* increasing ROS for the treatment of gastric cancer. *Redox Biol* (2016) 10:78–89. doi: 10.1016/j.redox.2016.09.006

26. Yao C, Liu J, Shao L. Rapamycin inhibits the proliferation and apoptosis of gastric cancer cells by down regulating the expression of survivin. *Hepatogastroenterology* (2011) 58:1075–80.

27. Varma S, Khandelwal RL. Effects of rapamycin on cell proliferation and phosphorylation of mTOR and p70(S6K) in HepG2 and HepG2 cells overexpressing constitutively active Akt/PKB. *Biochim Biophys Acta* (2007) 1770:71–8. doi: 10.1016/j.bbagen.2006.07.016

28. Fingar DC, Richardson CJ, Tee AR, Cheatham L, Tsou C, Blenis J. mTOR controls cell cycle progression through its cell growth effectors S6K1 and 4E-BP1/eukaryotic translation initiation factor 4E. *Mol Cell Biol* (2004) 24:200–16. doi: 10.1128/MCB.24.1.200-216.2004

29. Hashemolhosseini S, Nagamine Y, Morley SJ, Desrivieres S, Mercep L, Ferrari S. Rapamycin inhibition of the G1 to s transition is mediated by effects on cyclin D1 mRNA and protein stability. *J Biol Chem* (1998) 273:14424–9. doi: 10.1074/jbc.273.23.14424

30. Yellen P, Saqcena M, Salloum D, Feng J, Preda A, Xu L, et al. High-dose rapamycin induces apoptosis in human cancer cells by dissociating mTOR complex 1 and suppressing phosphorylation of 4E-BP1. *Cell Cycle* (2011) 10:3948–56. doi: 10.4161/cc.10.22.18124

31. Yao J, Xu M, Liu Z. Rapamycin inhibits proliferation and apoptosis of retinoblastoma cells through PI3K/AKT signaling pathway. *Oncol Lett* (2020) 19:2950–6. doi: 10.3892/ol.2020.11363

32. Stavrou M, Philip B, Traynor-White C, Davis CG, Onuoha S, Cordoba S, et al. A rapamycin-activated caspase 9-based suicide gene. *Mol Ther* (2018) 26:1266–76. doi: 10.1016/j.ymthe.2018.03.001

33. Rebecca VW, Amaravadi RK. Emerging strategies to effectively target autophagy in cancer. *Oncogene* (2016) 35:1–11. doi: 10.1038/onc.2015.99

34. Hoyer-Hansen M, Jaattela M. Autophagy: An emerging target for cancer therapy. *Autophagy* (2008) 4:574–80. doi: 10.4161/auto.5921

35. Lin X, Han L, Weng J, Wang K, Chen T. Rapamycin inhibits proliferation and induces autophagy in human neuroblastoma cells. *Biosci Rep* (2018) 38(6). doi: 10.1042/BSR20181822

36. Evangelisti C, Ricci F, Tazzari P, Tabellini G, Battistelli M, Falcieri E, et al. Targeted inhibition of mTORC1 and mTORC2 by active-site mTOR inhibitors has cytotoxic effects in T-cell acute lymphoblastic leukemia. *Leukemia* (2011) 25:781–91. doi: 10.1038/leu.2011.20

37. Hassan B, Akcakanat A, Sangai T, Evans KW, Adkins F, Eterovic AK, et al. Catalytic mTOR inhibitors can overcome intrinsic and acquired resistance to allosteric mTOR inhibitors. *Oncotarget* (2014) 5:8544–57. doi: 10.18632/oncotarget.2337

38. Jung CH, Ro SH, Cao J, Otto NM, Kim DH. mTOR regulation of autophagy. *FEBS Lett* (2010) 584:1287–95. doi: 10.1016/j.febslet.2010.01.017

39. Ganley IG, Lam Du H, Wang J, Ding X, Chen S, Jiang X. ULK1.ATG13.FIP200 complex mediates mTOR signaling and is essential for autophagy. *J Biol Chem* (2009) 284:12297–305. doi: 10.1074/jbc.M900573200

40. Shimodahira M, Fujimoto S, Mukai E, Nakamura Y, Nishi Y, Sasaki M, et al. Rapamycin impairs metabolism-secretion coupling in rat pancreatic islets by suppressing carbohydrate metabolism. *J Endocrinol* (2010) 204:37–46. doi: 10.1677/JOE-09-0216

41. Jung CH, Jun CB, Ro SH, Kim YM, Otto NM, Cao J, et al. ULK-Atg13-FIP200 complexes mediate mTOR signaling to the autophagy machinery. *Mol Biol Cell* (2009) 20:1992–2003. doi: 10.1091/mbc.e08-12-1249

42. Xu L, Wu T, Lu S, Hao X, Qin J, Wang J, et al. Mitochondrial superoxide contributes to oxidative stress exacerbated by DNA damage response in RAD51-depleted ovarian cancer cells. *Redox Biol* (2020) 36:101604. doi: 10.1016/j.redox.2020.101604

43. Perez-Perez ME, Florencio FJ, Crespo JL. Inhibition of target of rapamycin signaling and stress activate autophagy in chlamydomonas reinhardtii. *Plant Physiol* (2010) 152:1874–88. doi: 10.1104/pp.109.152520

44. Martinez-Cisuelo V, Gomez J, Garcia-Junceda I, Naudi A, Cabre R, Mota-Martorell N, et al. Rapamycin reverses age-related increases in mitochondrial ROS production at complex I, oxidative stress, accumulation of mtDNA fragments inside nuclear DNA, and lipofuscin level, and increases autophagy, in the liver of middle-aged mice. *Exp Gerontol* (2016) 83:130–8. doi: 10.1016/j.exger.2016.08.002

45. Woo Y, Lee HJ, Kim J, Kang SG, Moon S, Han JA, et al. Rapamycin promotes ROS-mediated cell death *via* functional inhibition of xCT expression in melanoma under gamma-irradiation. *Front Oncol* (2021) 11:665420. doi: 10.3389/fonc.2021.665420

46. Habib SL. Mechanism of activation of AMPK and upregulation of OGG1 by rapamycin in cancer cells. *Oncotarget* (2011) 2:958–9. doi: 10.18632/oncotarget.381

47. Clingen PH, Wu JY, Miller J, Mistry N, Chin F, Wynne P, et al. Histone H2AX phosphorylation as a molecular pharmacological marker for DNA interstrand crosslink cancer chemotherapy. *Biochem Pharmacol* (2008) 76:19–27. doi: 10.1016/j.bcp.2008.03.025

48. Song J, Wang X, Zhu J, Liu J. Rapamycin causes growth arrest and inhibition of invasion in human chondrosarcoma cells. *J BUON.* (2016) 21:244–51.

49. Sahu D, Huan J, Wang H, Sahoo D, Casteel DE, Klemke RL, et al. Bladder cancer invasion is mediated by mammalian target of rapamycin complex 2-driven regulation of nitric oxide and invadopodia formation. *Am J Pathol* (2021) 191:2203–18. doi: 10.1016/j.ajpath.2021.08.002

50. Jia H, Xu M, Bo Y, Li W, Zhou R. Ras-ERK1/2 signaling accelerates the progression of colorectal cancer *via* mediation of H2BK5ac. *Life Sci* (2019) 230:89–96. doi: 10.1016/j.lfs.2019.05.060

51. Xiao GY, Mohanakrishnan A, Schmid SL. Role for ERK1/2-dependent activation of FCHSD2 in cancer cell-selective regulation of clathrin-mediated endocytosis. *Proc Natl Acad Sci U S A* (2018) 115:E9570–9. doi: 10.1073/pnas.1810209115

52. Yang L, Zheng L, Chng WJ, Ding JL. Comprehensive analysis of ERK1/2 substrates for potential combination immunotherapies. *Trends Pharmacol Sci* (2019) 40:897–910. doi: 10.1016/j.tips.2019.09.005

53. Giordano A, Avellino R, Ferraro P, Romano S, Corcione N, Romano MF. Rapamycin antagonizes NF-kappaB nuclear translocation activated by TNF-alpha in primary vascular smooth muscle cells and enhances apoptosis. *Am J Physiol Heart Circ Physiol* (2006) 290:H2459–65. doi: 10.1152/ajpheart.00750.2005

Frontiers in Oncology

Advances knowledge of carcinogenesis and tumor progression for better treatment and management

The third most-cited oncology journal, which highlights research in carcinogenesis and tumor progression, bridging the gap between basic research and applications to imrpove diagnosis, therapeutics and management strategies.

Discover the latest Research Topics

See more →

Frontiers

Avenue du Tribunal-Fédéral 34
1005 Lausanne, Switzerland
frontiersin.org

Contact us

+41 (0)21 510 17 00
frontiersin.org/about/contact